Texas Water Development Board Report

Final Report: Groundwater Availability Model for the Central Portion of the Sparta, Queen City, and Carrizo-Wilcox Aquifers

by
Steven Young PhD, PE, PG, INTERA Incorporated
Marius Jigmond, INTERA Incorporated
Toya Jones, PG, INTERA Incorporated
Tom Ewing PhD, PE, Frontera Exploration Consultants

Contributors:
Sorab Panday, PhD, GSI Environmental Inc.
RW Harden, RW Harden & Associates
Daniel Lupton, INTERA Incorporated

September 2018

This page is intentionally blank.

Geoscientist and Engineering Seal

Dr. Steven Young was the project manager and was primarily responsible for developing the approach for constructing and calibrating the groundwater model. He supervised the development and application of PEST for model calibration and the analysis of the aquifer pumping test.

September 14, 2018
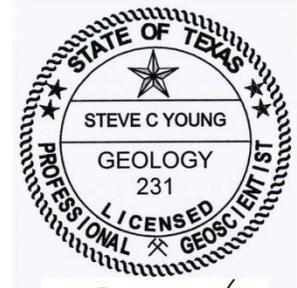
Ms. Toya Jones was primarily responsible for assembling the data used for developing the annual estimates of historical groundwater pumpage from 1930 to 2010, for assembling the historical water levels, and for constructing the well database used to help spatially assign historical pumping to locations. In addition, Ms. Jones guided the construction of the geodatabase for the project.

September 14, 2018

Dr. Thomas Ewing was responsible for analyzing geophysical logs in order to map the location of faults associated with the Milano Fault Zone. The mapping included resolving the Milano Fault Zone into one complex (Kovar Complex) and four grabens (the Paige Graben, the Tanglewood Graben, the Calvert Graben, and the South Kosse Graben). Dr. Ewing also estimated the vertical offsets associated with each fault.

September 14, 2018

This page is intentionally blank.

Final Report: Groundwater Availability Model for the Central Portion
of the Carrizo-Wilcox, Queen City, and Sparta Aquifers

TABLE OF CONTENTS
VOLUME 1

LIST OF FIGURES

LIST OF TABLES

1   Executive Summary

This report documents the construction and calibration of an update to the groundwater availability model for the central portion of the Carrizo-Wilcox, Queen City, and Sparta aquifers. The numerical model was developed as part of the Texas Water Development Board's Groundwater Availability Modeling Program. The model's purpose is to provide a tool for groundwater planning and management in the state of Texas. The project work included updates to both the conceptual and numerical models.

The update to the conceptual model included revisions to fault locations and characteristics in the Milano Fault Zone, historical pumping, recharge, and modeling surface water-groundwater interaction. The update to the numerical model included converting the previous groundwater availability model into MODFLOW-USG, adding model layers, refining the grid mesh in select locations, calibrating the model to steady-state conditions, and extending the transient model calibration period from 1930 to 2010.

Using previously mapped fault traces as a guide, we interpreted geophysical logs to characterize and map the Milano Fault Zone as a series of connected grabens. The conductance associated with each fault was based on the vertical offset assigned to the fault. The importance of the faults to groundwater flow was validated by analyzing 113 aquifer pumping tests in and near the Milano Fault Zone. Our analyses identified lines of evidence that indicated faults were acting as zones of low transmissivity. We validated our findings by reproducing the observed effects in drawdown data from the aquifer pumping tests using analytical models.

We developed the historical pumping dataset to cover an 80-year period from 1930 to 2010. As part of this effort, we developed a well database and associated well owners with pumping entities to help assign historical pumping. Assigning pumping to the model grid cells was a two-part process. First, a dataset of annual pumping by water user groups (for example, cities, water supply companies, industries, irrigation, livestock) and for rural domestic pumping was created. Second, a well dataset was created to guide placement of the pumping spatially as well as temporally.

Our update of the conceptual model for recharge is similar to previous work that used hydrograph separation methods to calculate base flow values from river gages. Recharge rates were then estimated by dividing the base flow value by the drainage area associated with the river gage. However, a distinguishing aspect of our approach was that the recharges rates were adjusted to account for two effects. The first effect was the impact of surface geology on the spatial distribution of recharge. The second effect was the impact of bank flow on base flow. Bank flow is groundwater from bank storage that leaves the alluvium adjacent to a stream to become streamflow. For steady-state conditions, the revised approach generates an average recharge rate of 2 inches per year from precipitation for the entire model domain.

To improve the groundwater availability model's ability to simulate surface water-groundwater interaction, we incorporated two additional model layers. One layer is located near ground surface to represent a shallow groundwater system. This model layer extends across the entire outcrop area associated with the simulated hydrogeologic units. The second layer was

constructed on top of the shallow groundwater flow system layer to represent the Colorado and Brazos rivers alluvium.

In the vicinity of the Colorado River and its major tributaries, the grid cells in the updated model were reduced from 1 mile by 1 mile to 0.25 mile by 0.25 mile. In the vicinity of the Brazos River and its major tributaries, the grid cells were reduced from 1 mile by 1 mile to 0.5 mile by 0.5 mile. Refinement of the grid cells improves the model's ability to represent the location of the pumping wells and streams. In addition, the increased refinement provides for improved resolution for representing horizontal hydraulic gradients between streams and the hydrogeologic units.

The code used to implement the update to the groundwater availability model for the central portion of the Carrizo-Wilcox, Queen City, and Sparta aquifers is MODFLOW-USG. MODFLOW-USG supports an unstructured grid, which allows users to refine the grid locally without adjusting the grid size away from the area of interest. This option was used along select rivers and streams in the model. Because the updated model was developed using MODFLOW-USG, the grid cells are no longer referred to by row and column but rather by unique node numbers. Each model layer represents a different hydrogeologic unit and different areal coverages.

The revised model has 10 layers. Model layer 1 represents the Colorado and Brazos rivers alluvium. Model layer 2 represents the outcrop area in the model and is comprised of the hydrogeologic units which make up model layers 3 through 10. The purpose of model layer 2 is to represent the shallow groundwater flow system in the outcrop area. From youngest to oldest sediments, the remaining model layers represent the Sparta Aquifer, the Weches Formation, the Queen City Aquifer, the Reklaw Formation, the Carrizo Aquifer, the Calvert Bluff Formation, the Simsboro Formation, and the Hooper Formation. These latter three formations comprise the Wilcox Aquifer.

A total of 522 observed hydraulic heads with a range of 400 feet were used for steady-state calibration targets. The steady-state calibration produced a mean error, mean absolute error, and a root-mean square error of 1.9, 18.9, and 24.3 feet, respectively. Out of the 522 values, 190 of the observed hydraulic heads are from wells in the Groundwater Management Area 12. For the 190 observed hydraulic head values in Groundwater Management Area 12, which have a range of 348 feet, the state-state calibration produced a mean error, mean absolute error, and a root-mean square error of 6.3, 19.3, and 24.1 feet, respectively. For the entire model domain, 11,378 observed hydraulic heads from 647 wells were used to calibrate the transient model over the time period from 1930 to 2010. For the 11,378 observed hydraulic heads, which have a range of 845 feet, the transient calibration produced a mean error, mean absolute error, and a root-mean square error of -4.6, 14.7, and 22.6 feet, respectively. Out of the 11,378 values, 4,767 observed hydraulic heads are from wells in the Groundwater Management Area 12. For these 4,767 observed hydraulic heads, which have a range of 473 feet, the transient calibration produced a mean error, mean absolute error, and a root-mean square error of -4.6, 12.1, and 17.4 feet, respectively.

Twenty-four parameters were varied for the steady-state sensitivity analysis and 20 were varied for the transient sensitivity analysis. Sensitivity of the steady-state model was assessed for the metrics average hydraulic head in each hydrogeologic unit, hydraulic boundary fluxes, number of additional flooded cells, and model calibration statistics. Sensitivity of the transient model was assessed for the metrics drawdown in the Sparta, Queen City, and Carrizo aquifers and the Simsboro Formation, river and drain boundary fluxes, and model calibration statistics. To distill the results into a meaningful understanding of model sensitivity, a systematic methodology was developed based on ranking the impact on the metrics as a result of the change in parameter value. For the steady-state model, all metrics are most sensitive to changes in recharge and are also sensitive to the horizontal hydraulic conductivity of the Queen City Aquifer. For the transient model, all metrics are sensitive to the pumping and horizontal hydraulic conductivity of the Carrizo Aquifer.

This page is intentionally blank.

2   Introduction

The Groundwater Availability Modeling Program of the Texas Water Development Board
(TWDB) provides tools for assessing groundwater availability for the major and minor aquifers
in Texas (Figures 2.0a and 2.0b). Groundwater availability models are fundamental tools for
helping to manage groundwater resources. House Bill 1763 (79th Legislature) developed a joint-
planning process whereby groundwater management areas, with input from local groundwater
conservation districts, determine desired future conditions for aquifers. The Groundwater
Availability Modeling Program uses the groundwater availability models to determine the
modeled available groundwater in the aquifer, which guides management of long-term
groundwater production to achieve the desired future conditions.
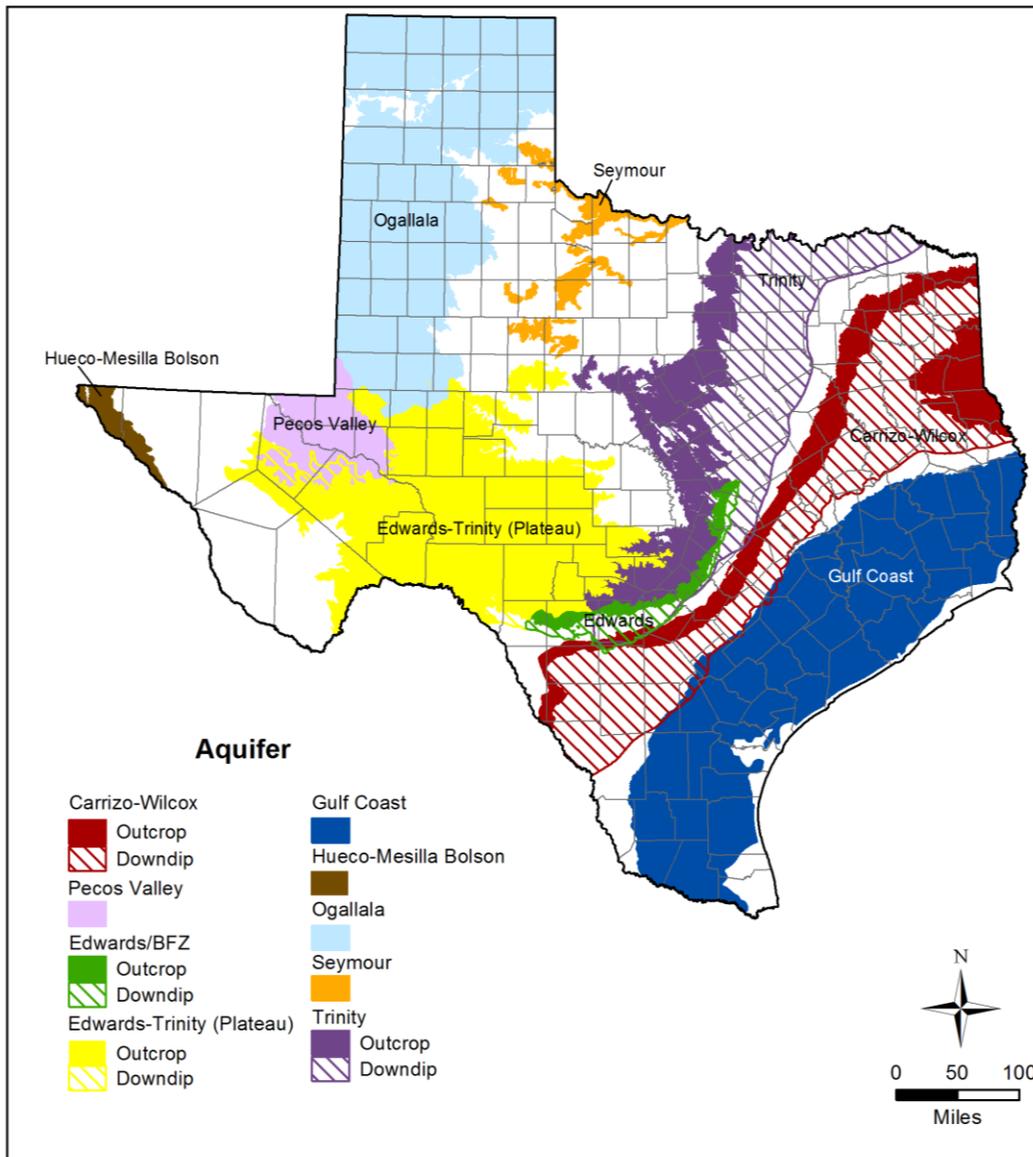
Figure 2.0a.   **Major Texas aquifers (TWDB, 2006).**

Note: BFZ = Balcones Fault Zone
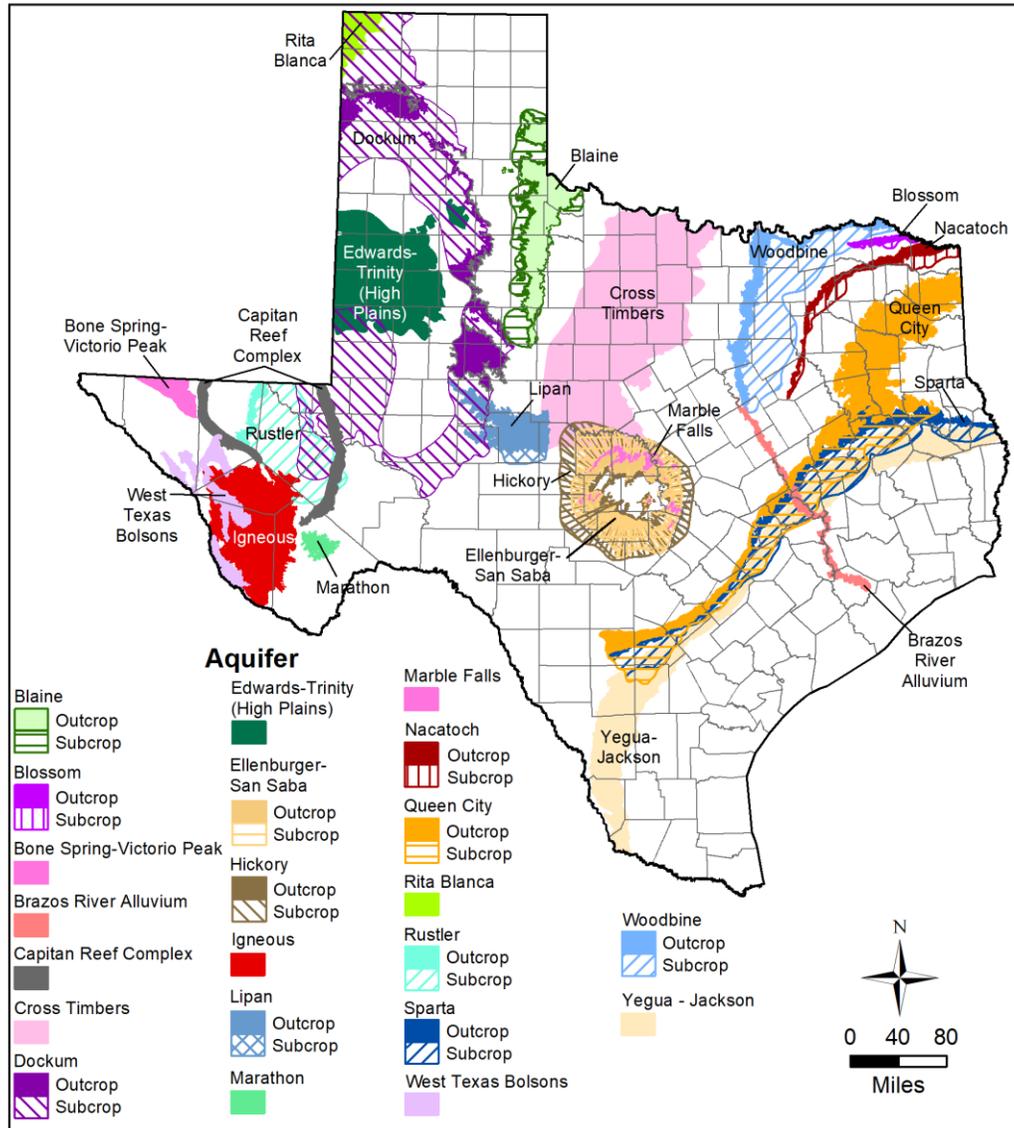
Figure 2.0b.   Minor Texas aquifers (TWDB, 2017a).

2.1 Background

Under the TWDB's Groundwater Availability Modeling Program, groundwater availability models of the northern, central, and southern portions of the Carrizo-Wilcox Aquifer were completed in 2003. The northern and southern models (Fryar and others, 2003; Deeds and others, 2003, respectively) and the central model (Dutton and others, 2003) were developed by two different contractors.

In 2004, Kelly and others (2004) developed three groundwater availability models for the Queen City and Sparta aquifers (northern, central, and southern), which included the underlying Carrizo-Wilcox Aquifer. The Kelly and others (2004) models addressed several inconsistences between the three Carrizo-Wilcox Aquifer groundwater availability models developed in 2003. The 2004 models are now the TWDB-accepted water planning tools for evaluating groundwater resources in the Carrizo-Wilcox Aquifer as well as the Queen City and Sparta aquifers.

In 2009, the 81st Legislature directed the Texas Commission on Environmental Quality to conduct a study of the characteristics and impacts of groundwater planning in the Carrizo-Wilcox Aquifer. That study, which also evaluated the three groundwater availability models for the Carrizo-Wilcox, Queen City, and Sparta aquifers, identified two critical issues: (1) whether the central portion of the aquifer should include faults as barriers to flow and (2) the evaluation of the location of those faults. Although the degree to which faults in the central model are sealing has a minor effect on the model calibration, it has a major impact on predicted future drawdowns because future pumping is anticipated in the vicinity of the faults. Therefore, appropriate representation of fault locations and hydraulic properties in the central model is important for future water planning purposes.

This report provides an update to the groundwater availability model for the central portion of the Carrizo-Wilcox, Queen City and Sparta aquifers. Funding sources for the model update include the TWDB's Groundwater Availability Modeling Program and Environmental Flow Program; the Lower Colorado River Authority, the Brazos River Authority, and the groundwater conservation districts in Groundwater Management Area 12, within which is the boundary for the central Carrizo-Wilcox, Queen City, and Sparta aquifers groundwater availability model.

The major reasons for updating the groundwater availability model for the central portion of the Carrizo-Wilcox, Queen City and Sparta aquifers were to (1) investigate the faults in the central Carrizo-Wilcox Aquifer, specifically those in the Milano Fault Zone, and provide an appropriate method for representing those faults in the model; (2) update the model with historical pumping through 2010 and extend the calibration period to 2010, (3) upgrade the model structure from MODFLOW-96 (Harbaugh and McDonald, 1996) to MODFLOW-USG (Panday and others, 2015) and provide local refinement of the numerical mesh around the Colorado and Brazos rivers and their tributaries; and (4) conduct a comparison of the framework of the existing model to the results of a TWDB geophysical study (http://www.twdb.texas.gov/ innovativewater/ bracs/studies/UCP/index.asp) and update the model as applicable.

2.2   Study Area

The active model area for the central portion of the Carrizo-Wilcox, Queen City, and Sparta aquifers groundwater availability model, as well as the location of Groundwater Management Area 12 and its comprising counties, is shown in Figure 2.2a. The active model boundary extends from the updip limit of the Carrizo-Wilcox Aquifer outcrop to the northwest; the updip limit of the Wilcox growth fault zone, which is located past the extent of fresh water in the Carrizo-Wilcox, Queen City, and Sparta aquifers, to the southeast; approximately the San Antonio River to the southwest; and Cherokee and Nacogdoches counties to the northeast. The model area includes all or part of 46 counties, of which 14 are in Groundwater Management Area 12.

Major cultural features (cities, towns, and major roads) and streams, lakes and river basins in the study area are shown in Figures 2.2b and 2.2c, respectively. The active model area encompasses all or part of five groundwater management areas and eight regional water planning areas (Figure 2.2d) and 19 groundwater conservation districts (Figure 2.2e).
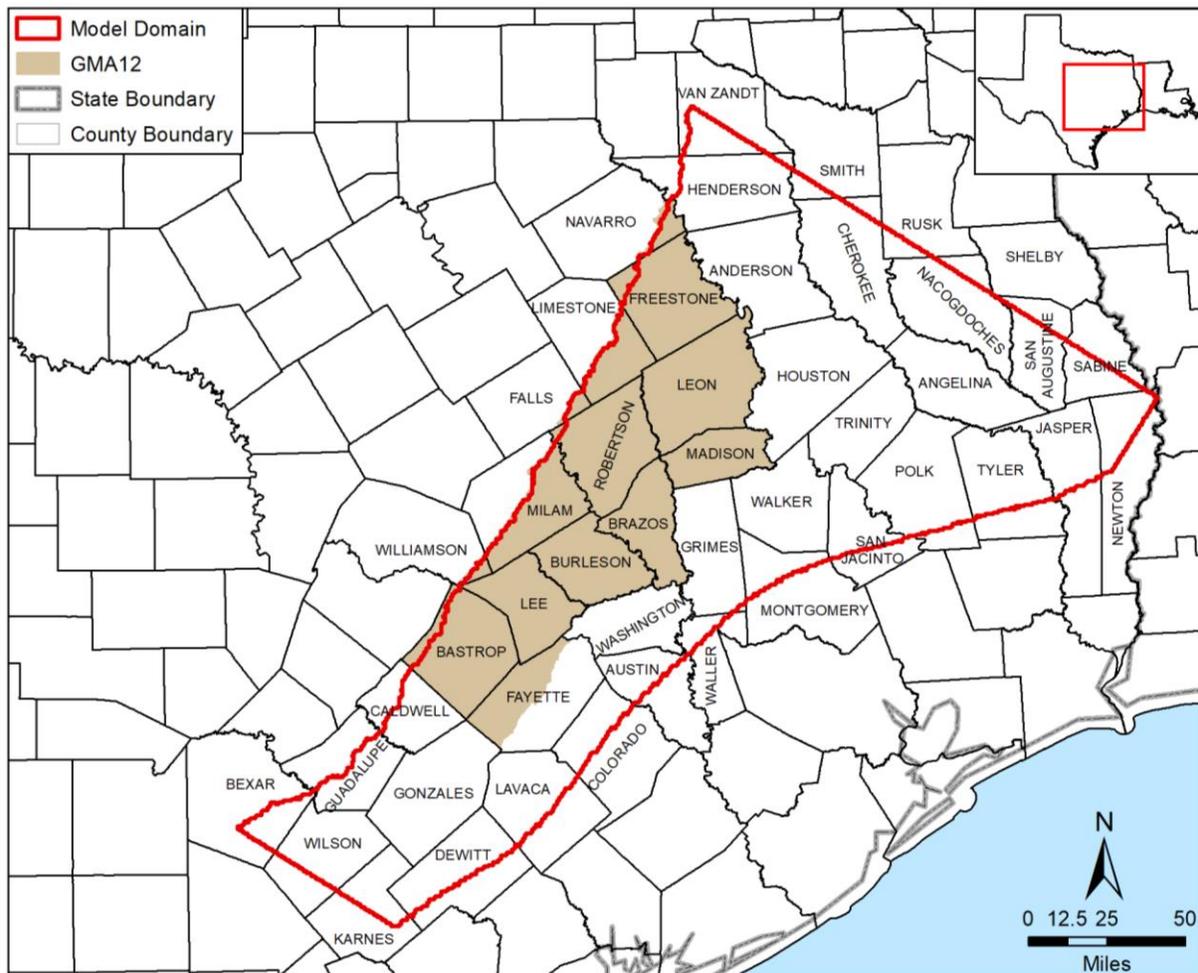
Figure 2.2a.   **Location of the active model area for the groundwater availability model for the central portion of the Carrizo-Wilcox, Queen City, and Sparta aquifers (Kelley and others, 2004) and Groundwater Management Area (GMA) 12 (TWDB, 2014a).**
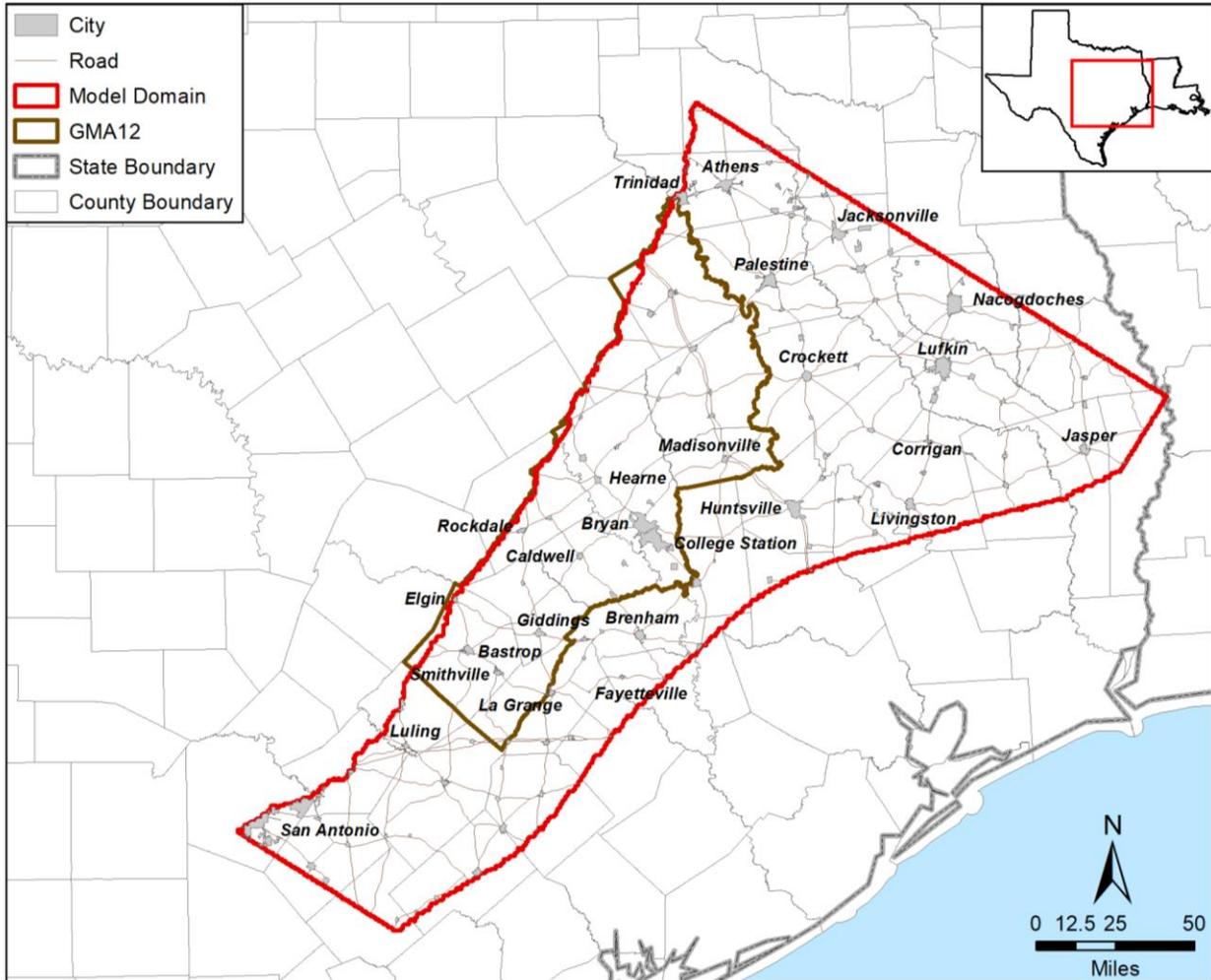
Figure 2.2b. **Cities, towns and major roads in the active model area (Texas Natural Resources Information System, 2016, 2017).**

Note: GMA = Groundwater Management Area
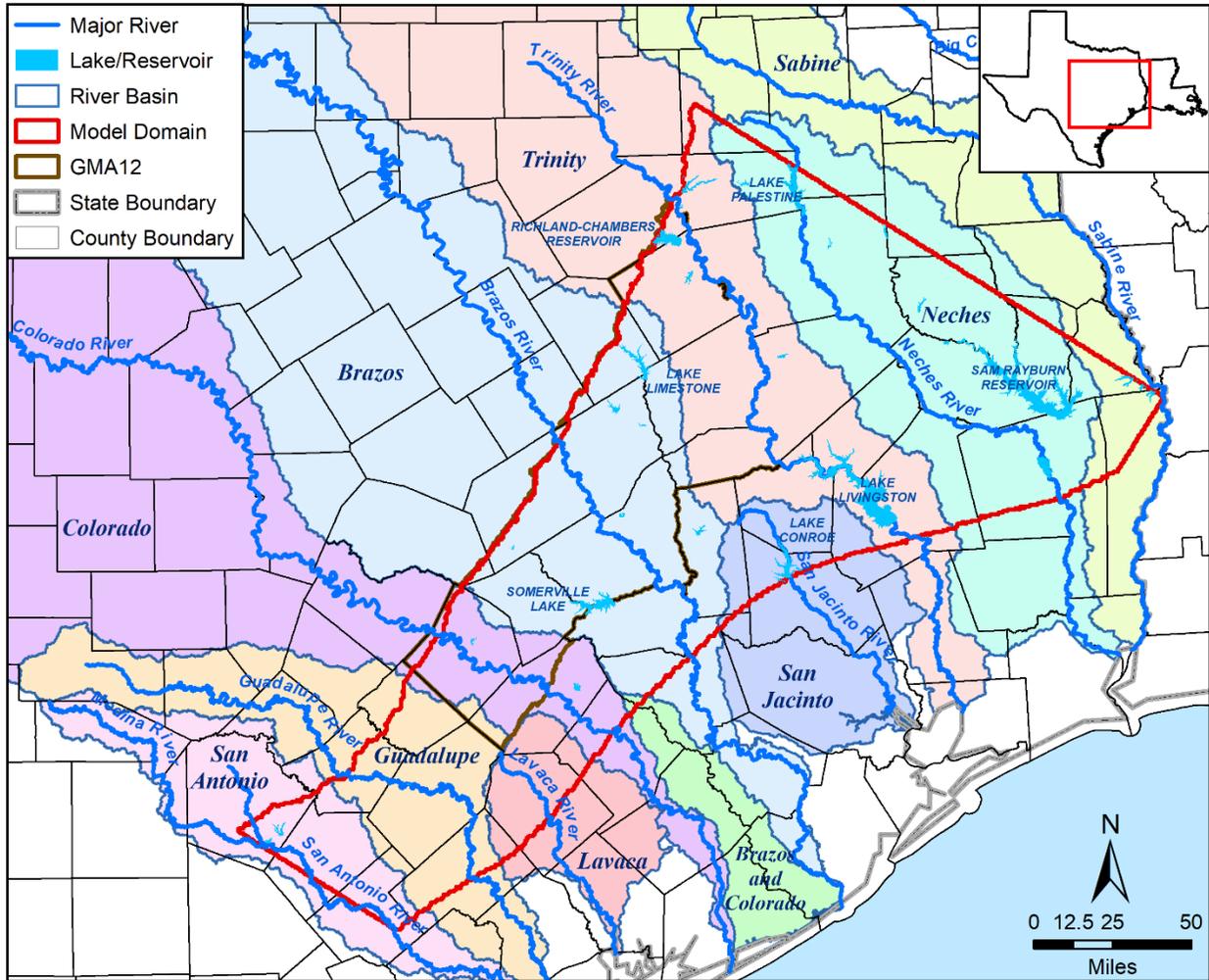
Figure 2.2c. **Rivers, lakes, reservoirs, and river basins in the active model area (TWDB, 2009; TWDB, 2014b, c).**

Note: GMA = Groundwater Management Area
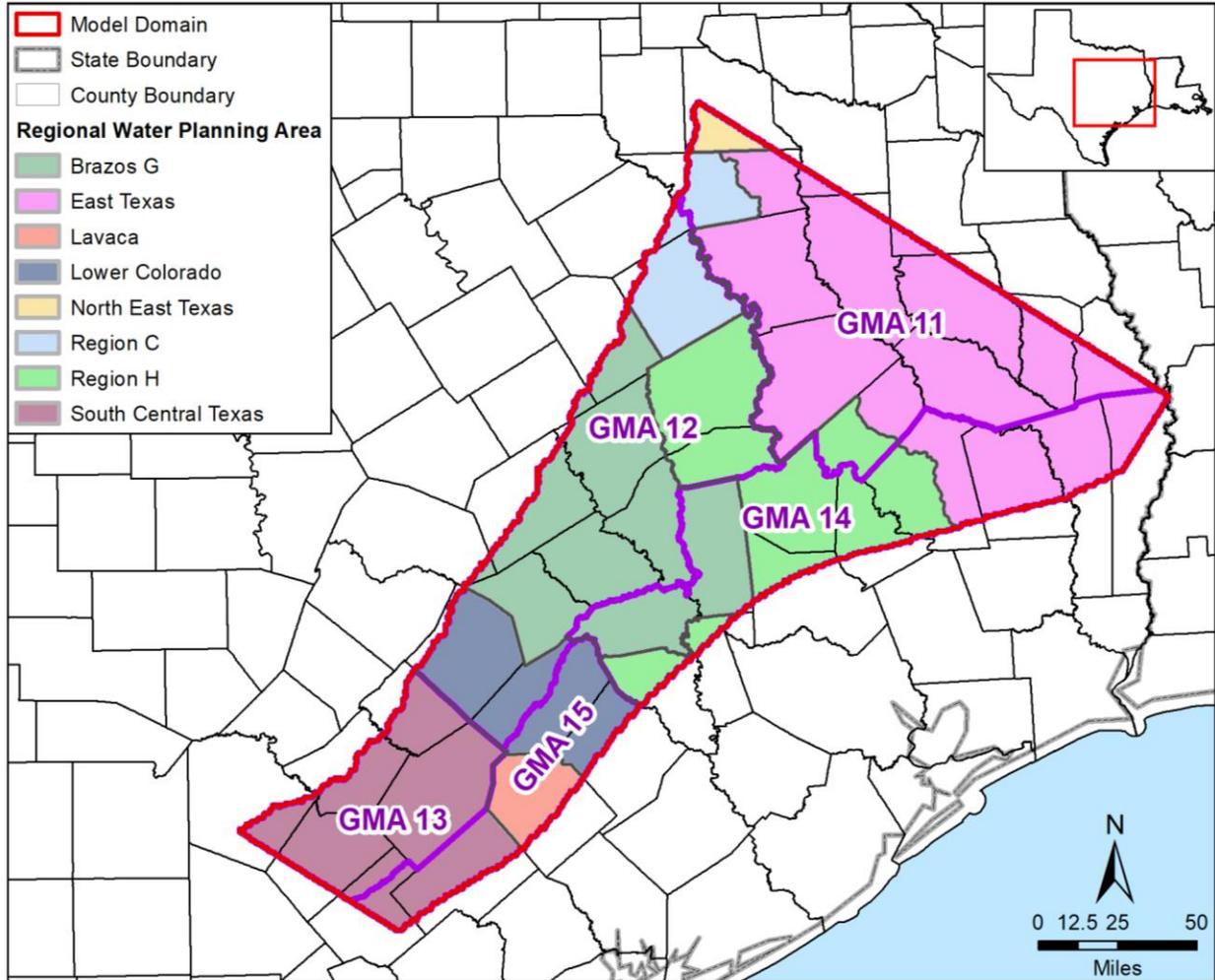
Figure 2.2d.   **Groundwater management areas (GMAs) and regional water planning areas in the active model area (TWDB, 2014a).**
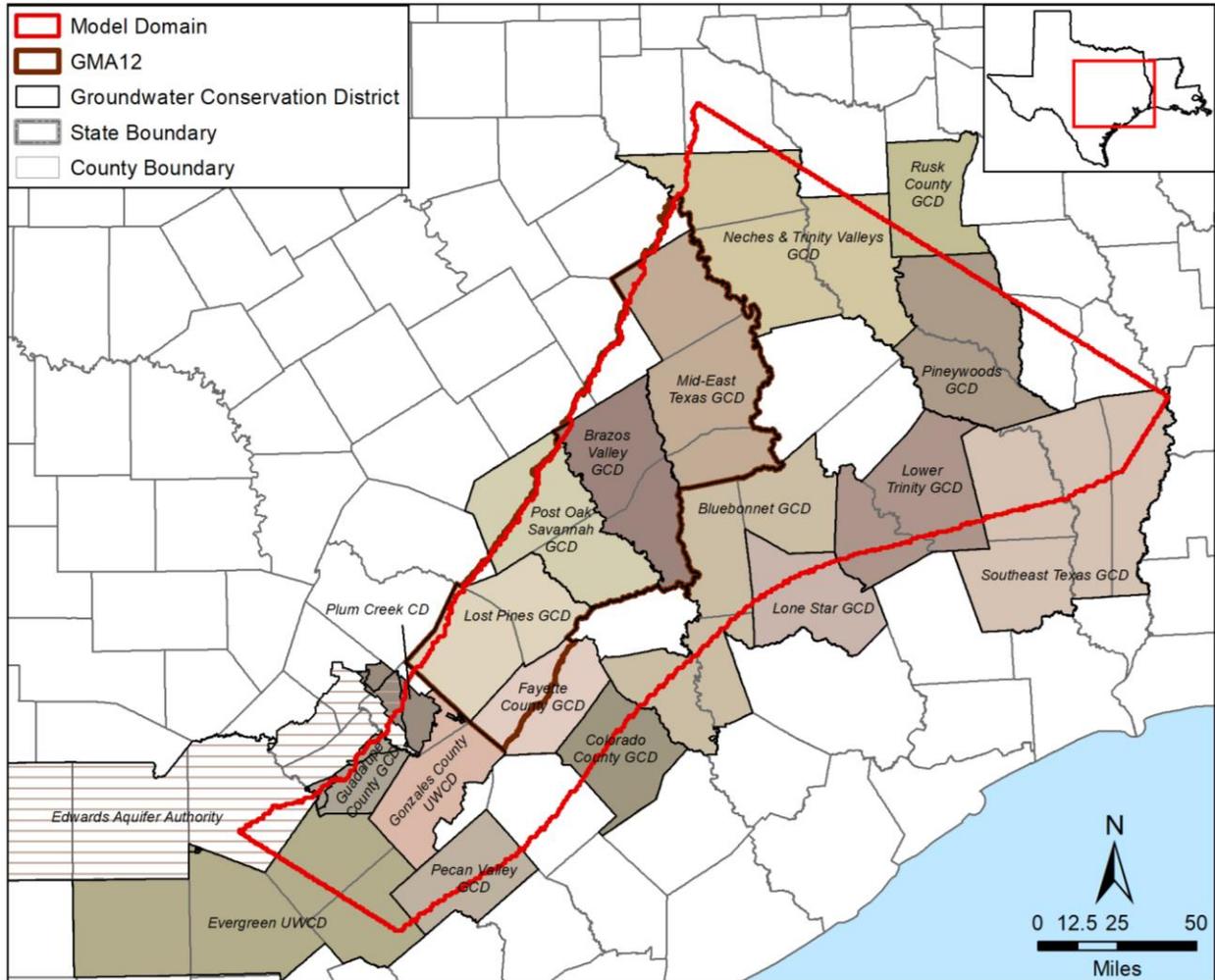
Figure 2.2e. **Groundwater conservation districts (GCDs) in the active model area (TWDB, 2017b).**

Note: GMA = Groundwater Management Area; UWCD = Underground Water Conservation District

2.3   Topography and Climate

Figure 2.3a provides a topographic map of the study area. Ground surface elevation varies from about 45 feet above sea level in river valleys to about 800 feet above sea level in the southwest. The gentle gulfward decrease in ground surface elevation is interrupted by resistant Tertiary sandstone outcrops. River valleys are broadly incised with terraced valleys that are hundreds of feet lower than the surface basin divide elevations.

Most of the study area has a subtropical humid climate dominated by the onshore flow of humid tropical air from the Gulf of Mexico. The amount of moisture decreases as it flows from the east to the west and as continental air masses intrude from the north. Historical average annual precipitation in the study area for the 30-year period from 1981 to 2010 ranges from a low of about 27 inches per year in Wilson County to the southwest to a high of 57 inches per year in Jasper County to the northeast (Figure 2.3b). Lake pan evaporation varies from about 46 to 59 inches per year (Figure 2.3c).
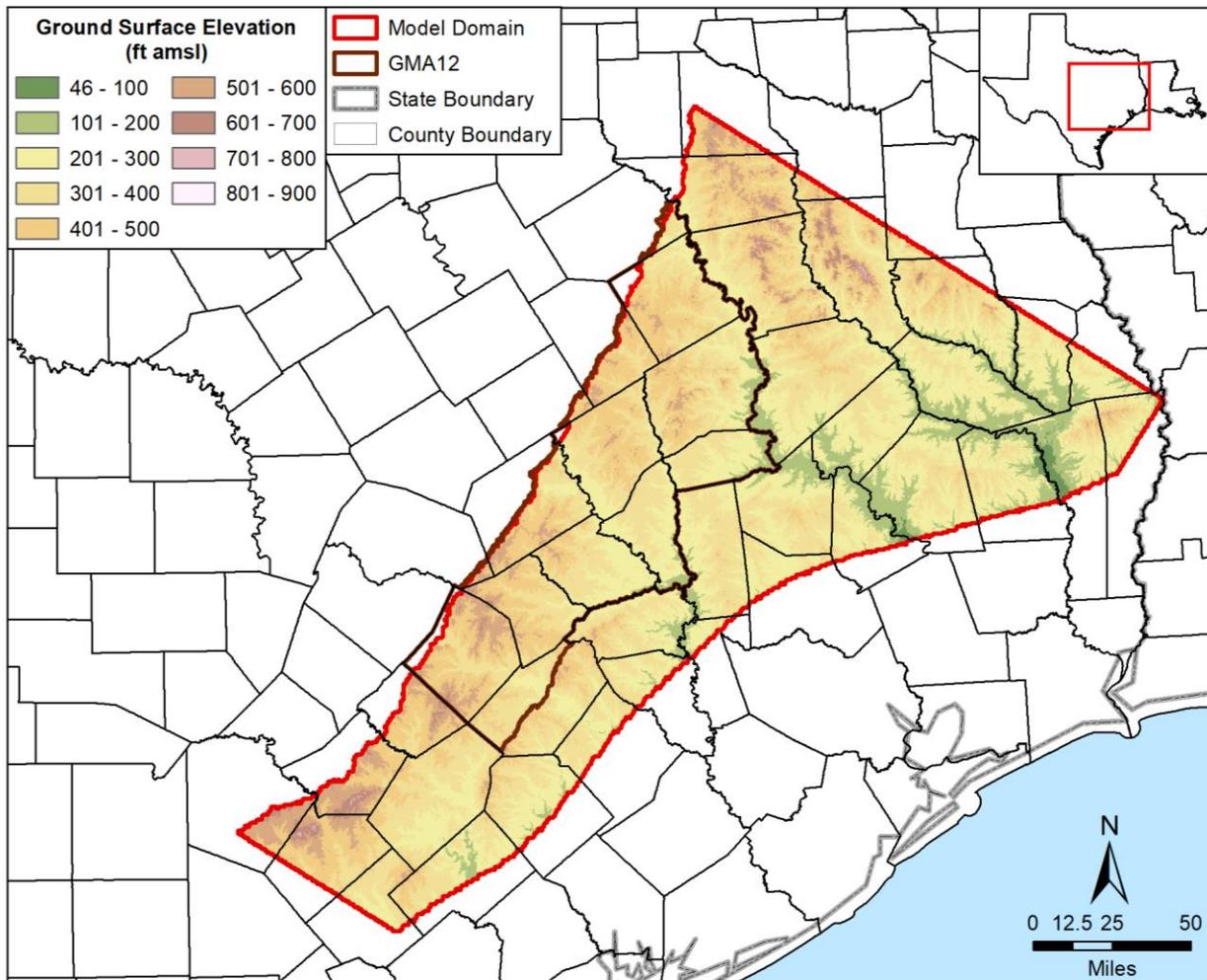
Figure 2.3a.   **Topographic map of the active model area (United States Geological Survey, 2014).**

Note: GMA = Groundwater Management Area, ft amsl = feet above mean sea level
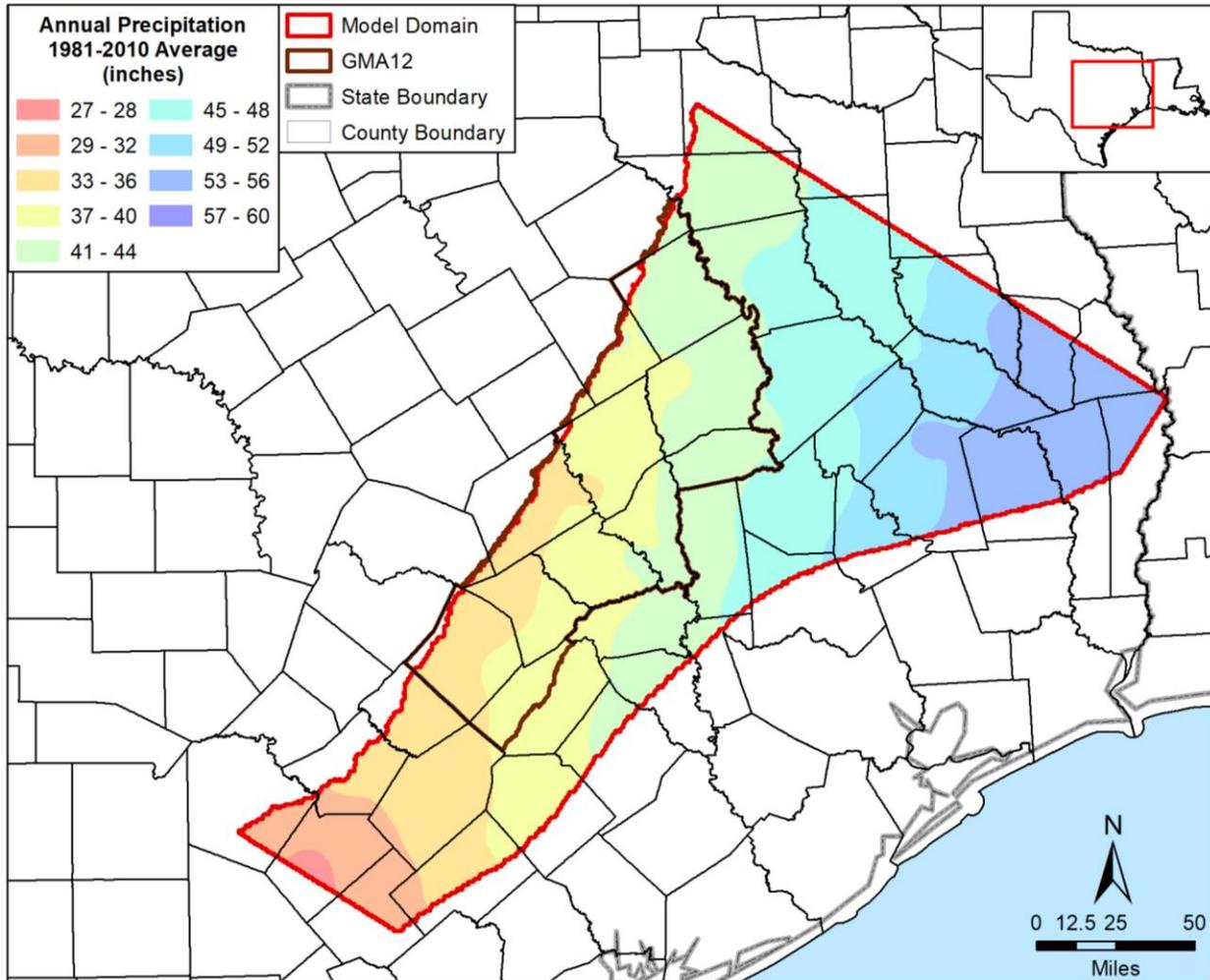
Figure 2.3b.   **Average annual precipitation (1981 to 2010) in the study area in inches per year (PRISM Climate Group, 2015).**

Note: GMA = Groundwater Management Area
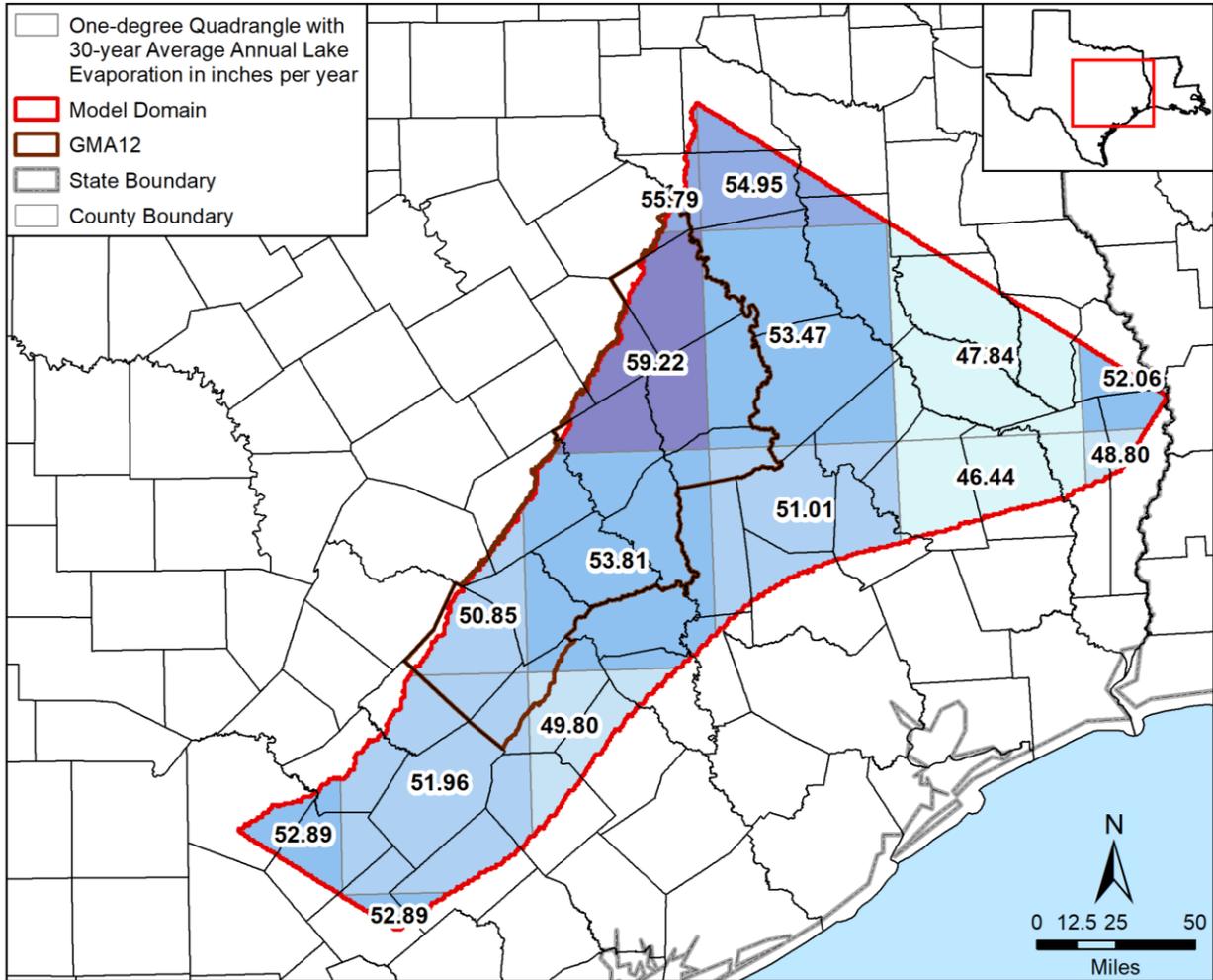
Figure 2.3c. **Average annual lake pan evaporation (1981 to 2010) in the study area in inches per year (TWDB, 2018).**

Note: GMA = Groundwater Management Area

2.4 Geology

The structural setting for the active model area is shown in Figure 2.4a. Except for the Milano Fault Zone, the fault traces were modified from Ewing and others (1990); other structural features were modified from Guevara and Garcia (1972), Galloway (1982), and Galloway and others (2000). A map of the surface geology in the model area is shown in Figure 2.4b. The surface geology shows that the general outcrop pattern is from southwest to northeast, coincident with depositional strike and the Balcones Fault Zone and normal to basin subsidence.

There are several regional fault zones within and adjacent to the active model area, including the Wilcox Fault Zone at the downdip limit of the model, the Milano Fault Zone in the model area, and the Balcones Fault Zone at the updip limit of the model (Figure 2.4a). The Wilcox Fault Zone is a series of growth faults caused by sediment progradation into marine clays and resulting in basinward slippage and subsidence, and the Balcones Fault Zone is a series of normal faults formed at the perimeter of the Gulf Coast Basin.

The sediments that form the hydrogeologic units in the model area are part of a gulf-ward thickening wedge of Cenozoic sediments deposited in the Houston Embayment of the northwest Gulf Coast Basin. Deposition has been influenced by regional crust subsidence, episodes of sediment inflow from areas outside the Gulf Coastal Plain, and eustatic sea-level change (Grubb, 1997). The primary depositional sequences in ascending stratigraphic order are the Wilcox Group; the Carrizo, Queen City, Sparta, Yegua, and Cook Mountain formations of the Claiborne Group; and the Jackson Group (Table 2.4a). Each of these depositional sequences is bounded by marine shales and finer-grained sediments representing transgressions (Reklaw and Weches formations of the Claiborne Group). Thick marine clays of the Midway Group represent the bottom of the stratigraphic column of interest (Table 2.4a). The sequences explicitly modeled in the updated groundwater availability model include the Wilcox Group and the Carrizo Formation, which constitute the Carrizo-Wilcox Aquifer, and the Queen City and Sparta formations, which constitute the Queen City and Sparta aquifers, respectively.

Table 2.4a.   **Generalized stratigraphic section for the model area and corresponding aquifers.**

Series	Group	Formation	Aquifer
Eocene	Jackson	-	Yegua-Jackson
	Claiborne	Yegua	Yegua-Jackson
		Cook Mountain	
		Sparta	Sparta
		Weches	
		Queen City	Queen City
		Reklaw	
		Carrizo	Carrizo-Wilcox
	Wilcox	Calvert Bluff	Carrizo-Wilcox
		Simsboro	
Paleocene		Hooper	
	Midway	-	
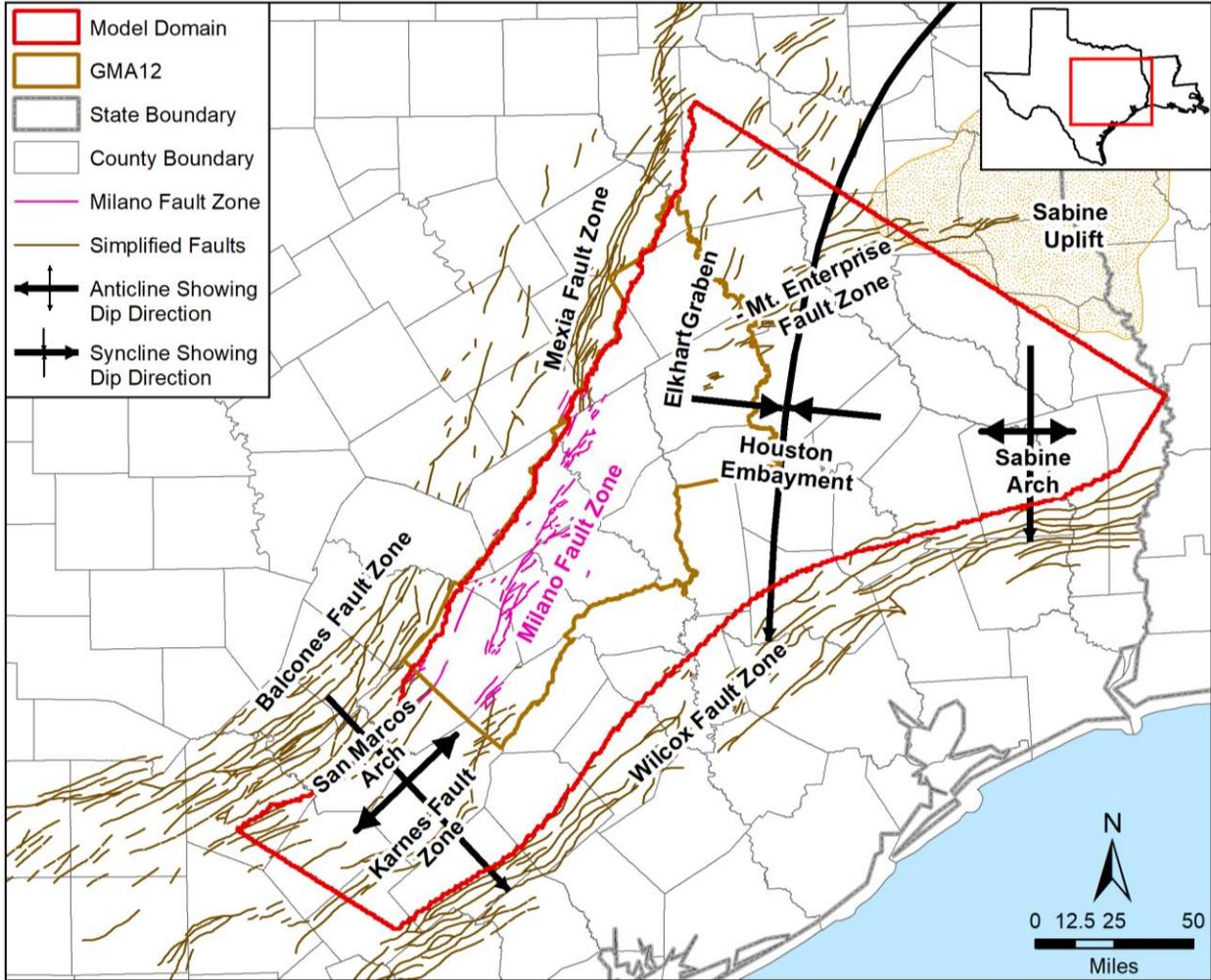
Figure 2.4a. **Map of major faults and structural features in the vicinity of the model area. Wilcox and Balcones Fault Zones modified from Ewing and others (1990), Milano Fault Zone developed by this study; and structural axes modified from Guevara and Garcia (1972), Galloway (1982), and Galloway and others (2000).**

Note: GMA = Groundwater Management Area
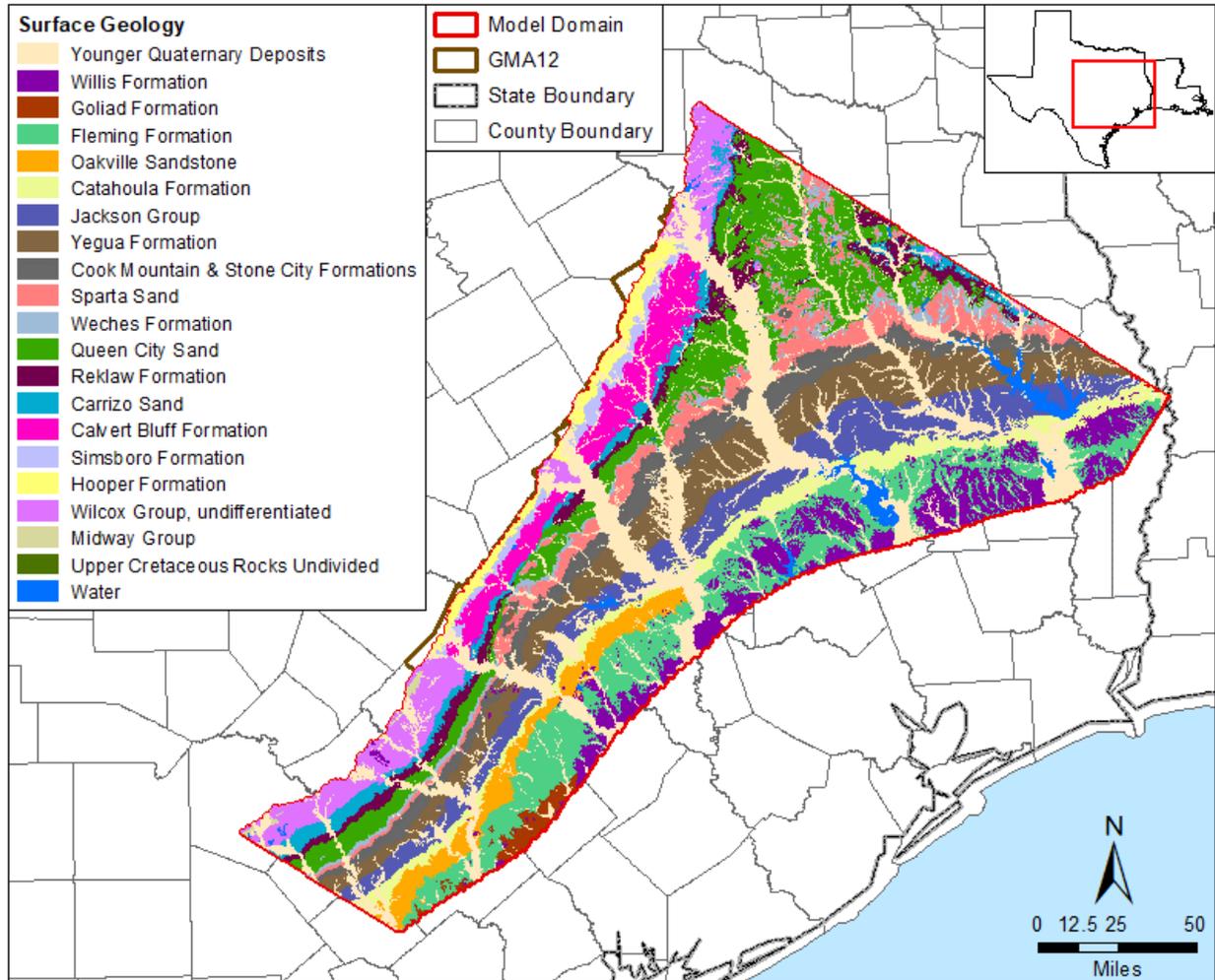
Figure 2.4b. **Surface geology of the model area from the Geologic Atlas of Texas (Barnes, 1970, 1979, 1981; Stoeser and others, 2007).**

Note: GMA = Groundwater Management Area

2.5   Report Organization

This report is provided in two volumes, with Sections 1 through 11 in Volume 1 and Sections 12 through 34 in Volume 2. Updates to the conceptual model are described in Section 3. An overview of the model and the model packages are presented in Section 4. Steady-state and transient calibration of the model and calibration results are discussed in Section 5. Section 6 presents the sensitivity analyses for the steady-state and transient models. Limitations to the model are given in Section 7. Section 8 provides a summary and conclusions. Future model implementation improvements are provided in Section 9. Acknowledgments and references are in Sections 10 and 11, respectively.

The appendices for the report are contained in Volume 2. Appendices A through C and E (Sections 12 through 14 and 16) provide supporting data for the analyses of aquifer pumping tests discussed in Section 3.1. Appendix D (Section 15) contains bar charts of pumping developed for the counties located outside of Groundwater Management Area 12. Tabulated and graphical summaries of pumping in the model can be found in Appendices F and G (Sections 17 and 18). Descriptions of the attributes for electronic files containing information on the drain, general-head boundary, river, and evapotranspiration cells in the model can be found in Appendices H through K (Sections 19 through 22). Appendix L (Section 23) contains histograms of residuals for the transient model, and Appendix M (Section 24) contains hydrograph plots of observed and model results for all transient calibration targets. Tables of water budgets for the steady-state model are provided in Appendices N through Q (Sections 25 through 28) and Appendices R through U (Sections 29 through 32) contain figures of water budgets for the transient model. Responses to comments on the draft fault report provided to the TWDB in 2017 can be found in Appendix V (Section 33). Responses to comments on the draft version of this report can be found in Appendix W (Section 34).

This page is intentionally blank.

3 Updates to the Conceptual Model

The conceptual groundwater availability model for the central portion of the Carrizo-Wilcox, Queen City, and Sparta aquifers is based on the conceptual models provided by Kelley and others (2004) and Dutton and others (2003). These two reports describe the hydrologic setting, the water levels and regional groundwater flow, estimates of recharge, interaction of surface water and groundwater, and aquifer hydraulic properties for the central portion of the Carrizo-Wilcox, Queen City, and Sparta aquifers.

The following subsections provide updates to the conceptual models presented by Kelley and others (2004) and Dutton and others (2003) with respect to the following:

- The Milano Fault Zone
- Historical pumping
- Recharge
- Surface water and groundwater interaction

3.1 The Milano Fault Zone

3.1.1 Previous Studies of the Milano Fault Zone

Work characterizing the geometry of peripheral fault grabens in the Gulf Coast of Texas is primarily represented by the reports *Fault Tectonics of the East Texas Basin* (Jackson, 1982), *Tectonic Map of Texas* (Ewing and others, 1990), and *Salt-Related Fault Families and Fault Welds in the Northern Gulf of Mexico* (Jackson and others, 2003). Other contributors to the location and stratigraphic/structural impacts of these faults on the Wilcox Group are Ayers and Lewis (1985), who drew faults at the top of the Simsboro Formation when creating contour maps of structure and thickness of the Wilcox Group and its member units, and Barnes (1970, 1979, 1981), whose surface mapping shows that these peripheral fault grabens are still active in some areas.

Figure 3.1.1a shows faults digitized from georeferenced portable document format copies of Ayers and Lewis (1985) in their study of lignite in the Wilcox Group. The locations of these faults were generally drawn on the base of the Wilcox Group/top of the Midway Group. Figure 3.1.1b shows faults taken from the digitized Geographic Information System version of the *Tectonic Map of Texas* (Ewing and others, 1990). The fault locations were based on GEOMAP, a commercial mapping service, and drawn on the top of the Austin Chalk, a fairly recognizable pick on geophysical logs. Figure 3.1.1c shows faults at surface from the Geographic Information System version of the *Geologic Atlas of Texas* (Stoeser and others, 2007).
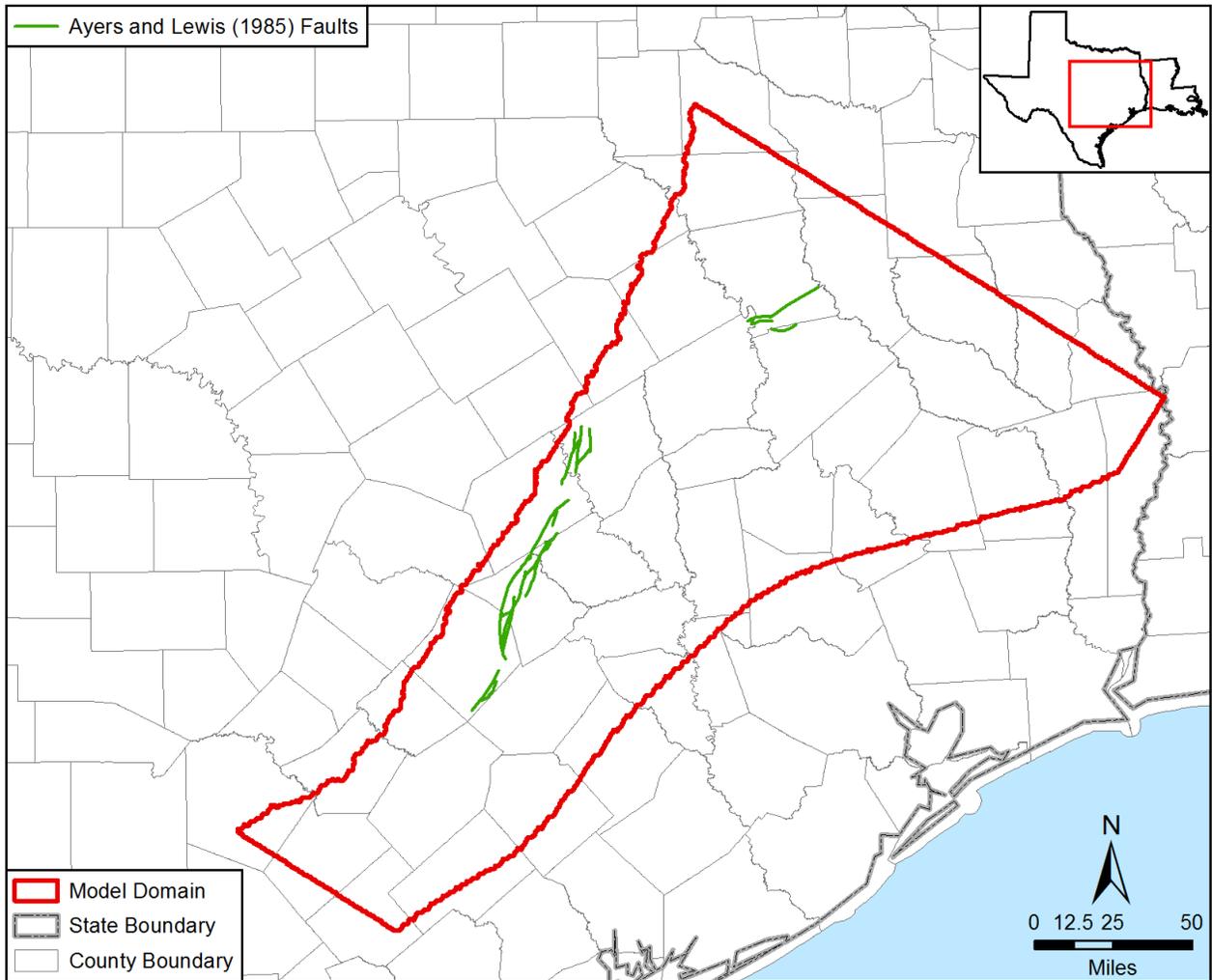
Figure 3.1.1a. **Faults identified by Ayers and Lewis (1985) located in the model domain for the groundwater availability model for the central portion of the Carrizo-Wilcox, Queen City, and Sparta aquifers.**
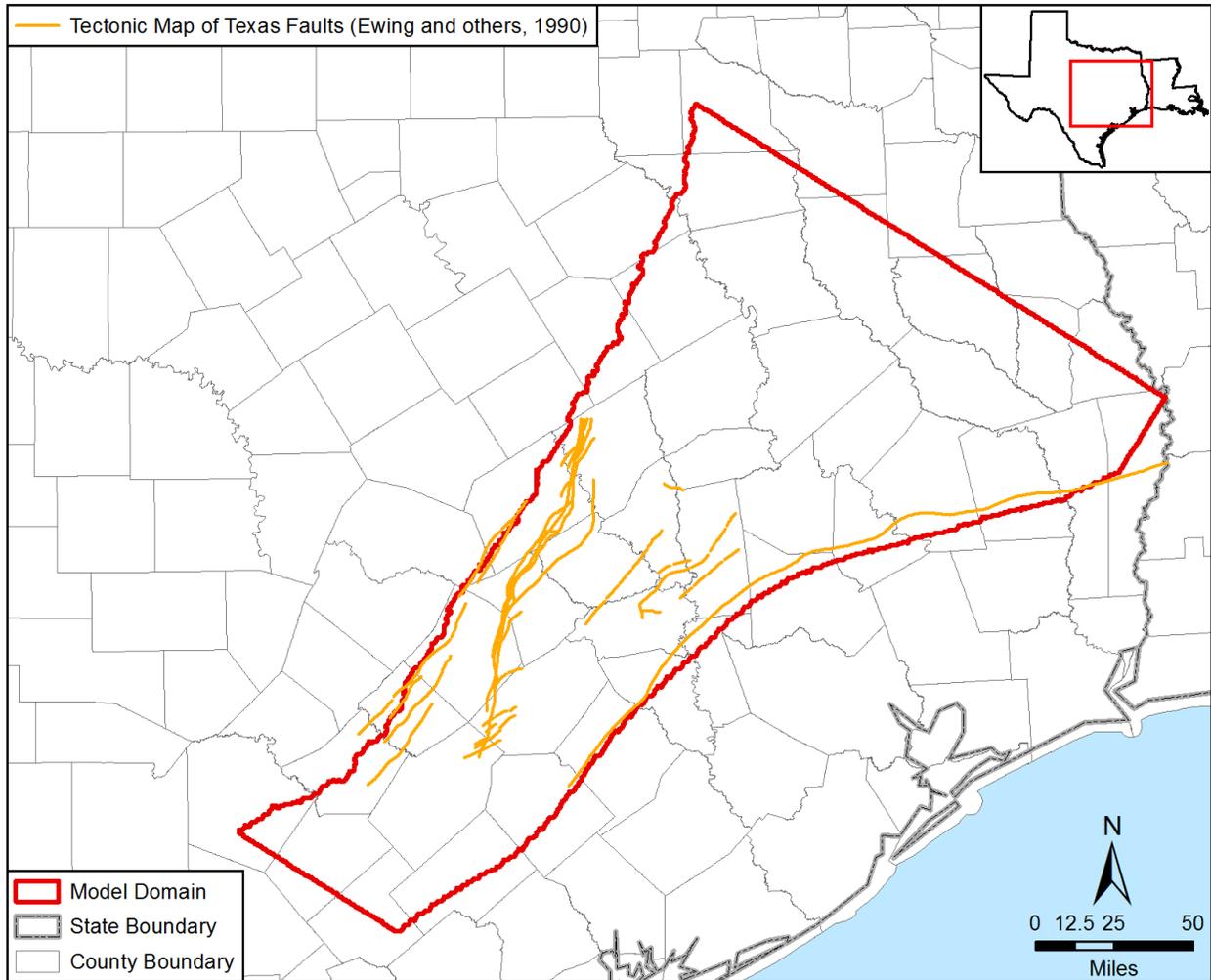
Figure 3.1.1b. **Faults identified by Ewing and others (1990) located in the model domain for the groundwater availability model for the central portion of the Carrizo-Wilcox, Queen City, and Sparta aquifers.**
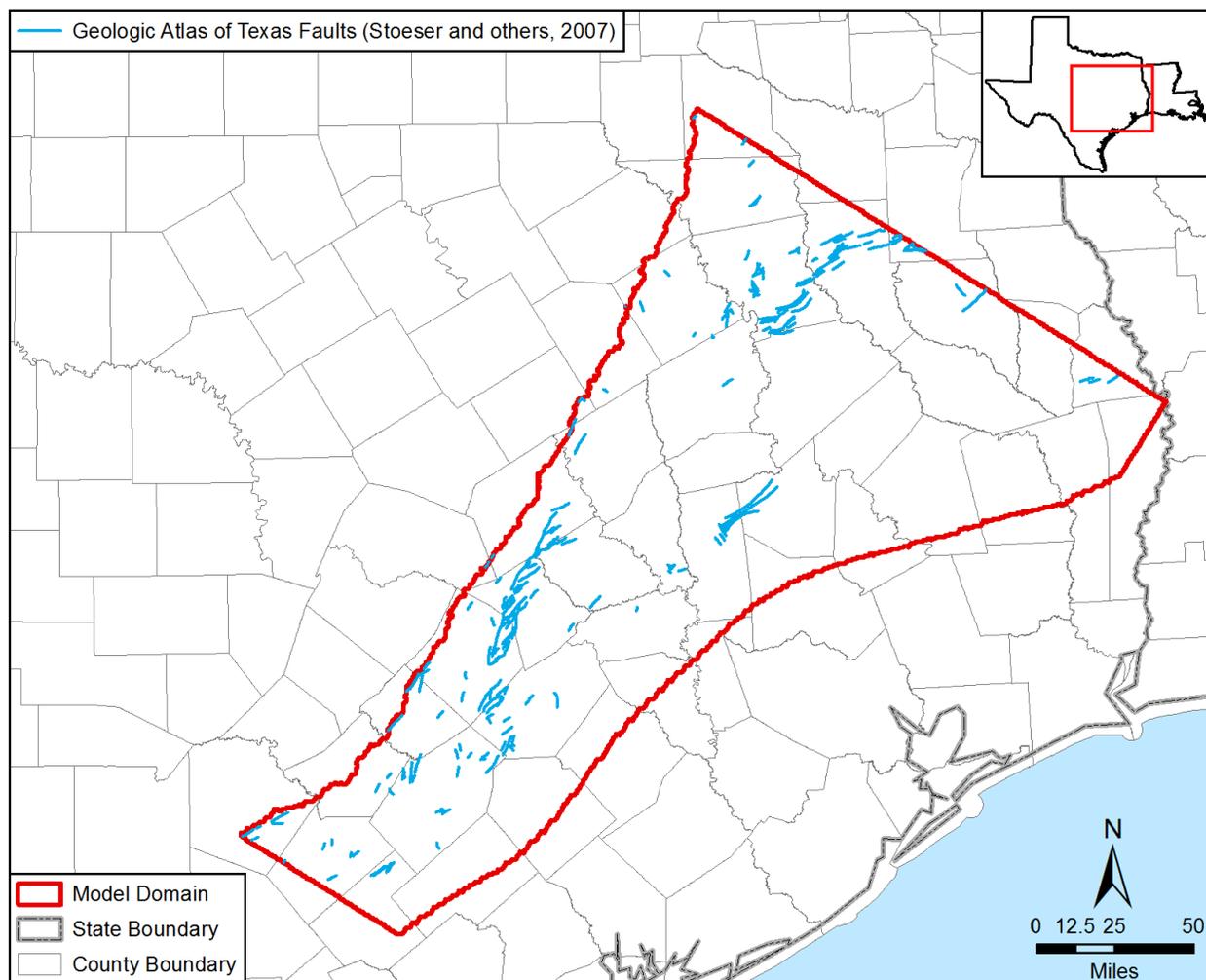
Figure 3.1.1c. **Faults identified from the Geologic Atlas of Texas (Stoeser and others, 2007) located in the model domain for the groundwater availability model for the central portion of the Carrizo-Wilcox, Queen City, and Sparta aquifers.**

3.1.2 Characterization of the Milano Fault Zone

Faults in the Milano Fault Zone were initially mapped using locations from Ayers and Lewis (1985), the *Tectonic Map of Texas* (Ewing and others, 1990), and the *Geologic Atlas of Texas* sheets (Barnes, 1970, 1979, 1981). In the Milano Fault Zone, evidence of faulting was primarily based on picks for the top of the Navarro Group, which is approximately 2,000 feet below the top of the Simsboro Aquifer.

The Navarro Group pick offers several advantages over picks for the formations in the Carrizo-Wilcox Aquifer. One advantage is that the Navarro Group is a marine clay with interbedded sands that produces a distinct geophysical signature on both spontaneous potential and resistivity logs when compared to the unconformably overlying the Midway Group (Figure 3.1.2a). Picks from the Carrizo Formation and Wilcox Group are much more problematic because the Milano Fault Zone is in the updip extent, where flooding surfaces pinch out/transition into their terrestrial equivalent and erosional processes are most prevalent. Thus, the picks within the

Wilcox Group (such as for the Simsboro and Hooper formations) can be inconsistent and irregular on any but the most local basis, showing as much as 200 to 400 feet of variability over several miles. These picks are traditionally made on the top and base of a sand-rich section that contains fresh water (characteristically high resistivity values), but there are fresh-water sands in both the overlying Calvert Bluff Formation and the underlying Hooper Formation that amalgamate and can potentially be recognized as the Simsboro Formation. In addition, log coverage in the Navarro Group is much better than in the updip extent of the Wilcox Group.

Picks on top of the Navarro Group were made for the geophysical logs shown in Figure 3.1.2b and used to create a generalized fault-free map of the top of the Navarro Group. Comparison of the Navarro Group picks with the fault-free surface, analysis of logs that intersect a fault, and faults identified on the *Geologic Atlas of Texas* sheets (Barnes, 1970, 1979, 1981) were used to locate and estimate fault offsets.

In Figure 3.1.2b, several "fault cut" logs are visible. A fault cut occurs when a log intersects a fault, and the geophysical log is a combination of the upthrown and downthrown side of the fault. These scenarios are termed fault cuts because a section of formation has been shifted and, therefore, not represented in the geophysical log. Figure 3.1.2c shows a schematic of a fault-cut log. Figure 3.1.2d shows digitized logs for six of the 16 fault cut wells identified in Figure 3.1.2b.

Once the geometry and displacement of faults on the top of the Navarro Group were determined, the fault segments were projected up to the top of the Simsboro horizon. Picks for the Simsboro Formation were made on 470 logs in the vicinity of the projected faults to check the fault location and offset. Figure 3.1.2e shows the locations of faults in the Navarro Group and Simsboro Formation. Because of the fuzzy and inconsistent nature of the picks for the top of the Simsboro Formation due to sand on sand, some difference in the fault displacements relative to the top of the Simsboro Formation are inconsistent with known displacement at the top of the Navarro Group.

Our picks for the Simsboro Formation and the Simsboro Formation picks from the TWDB geophysical database study (http://www.twdb.texas.gov/innovativewater/bracs/studies/UCP/index.asp) were compared to the surfaces for the Simsboro Formation in the groundwater availability model of Kelley and others (2004). For our picks and the TWDB picks, the majority were within 100 feet of the elevation in the 2004 model. Similar comparisons were performed for the TWDB geophysical database picks for the Sparta Aquifer, Queen City Aquifer, Carrizo Aquifer, Calvert Bluff Formation, and Hooper Formation. For all five of these hydrogeological units, the majority of the TWDB picks were within 100 feet of the surface elevations in the 2004 model. The comparisons were limited to an area southwest of Lee County, because the TWDB study did not cover any counties northeast of Lee County.

As a check on the final placement of the faults in the Simsboro Formation, Figure 3.1.2f shows the faults from this study plotted with faults mapped by Ayers and Lewis (1985) and the *Geologic Atlas of Texas* sheets (Barnes, 1970, 1979, 1981) as digitally provided in Stoeser and others, 2007). The comparisons show good agreement between the faults identified as part of this

study and those mapped by Barnes (1970, 1979, 1981) and moderate to good agreement with the
faults mapped by Ayers and Lewis (1985).

For this study, the Milano Fault Zone was divided into one complex and four grabens
(Figure 3.1.2g). These areas are named, from south to north, the Kovar Complex, the Paige
Graben, the Tanglewood Graben, the Calvert Graben, and the South Kosse Graben. For each of
these areas, a comment regarding the results of the geophysical analysis is provided, along with a
cross-section(s) through the area.
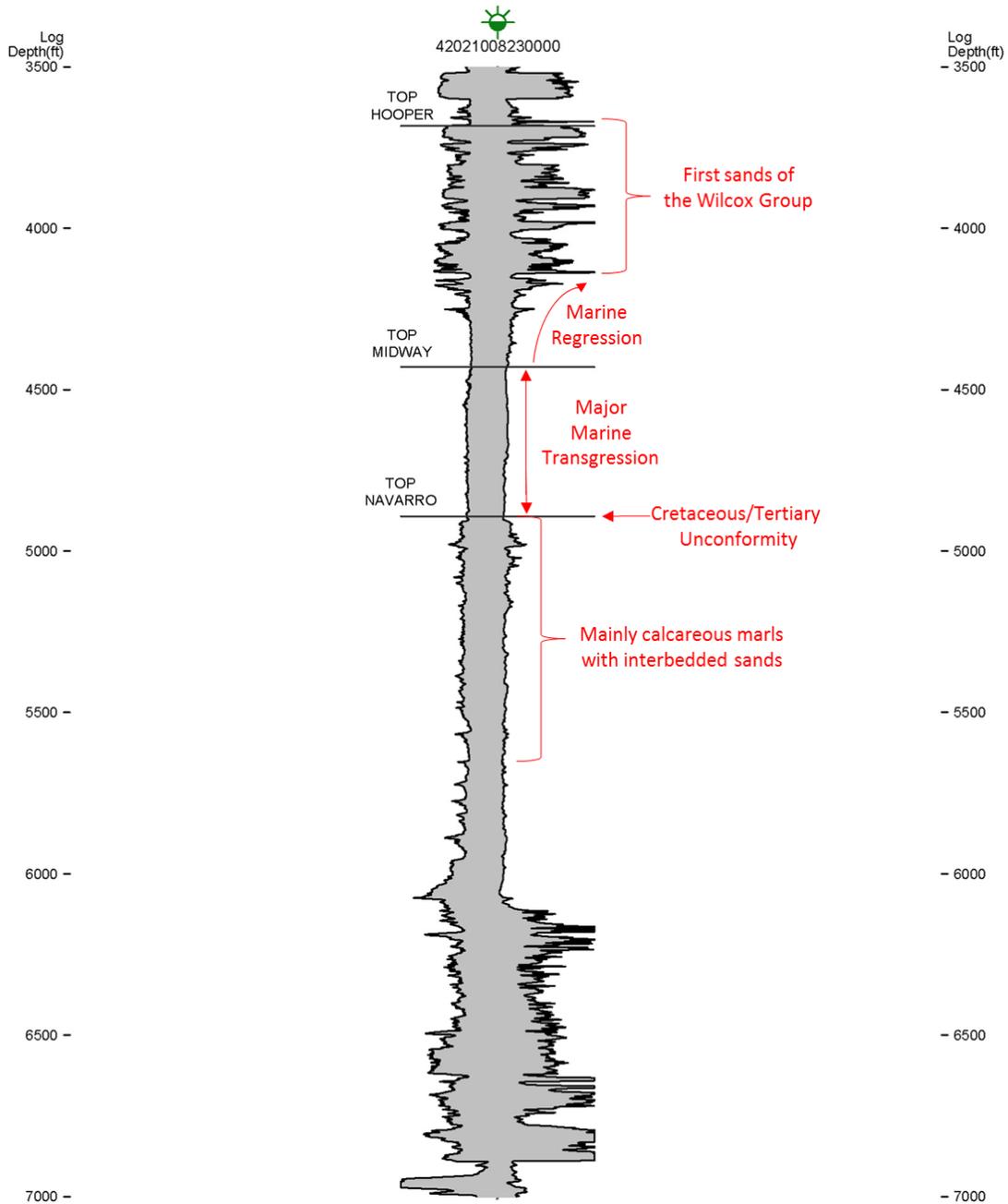
Figure 3.1.2a. **Geophysical signature of the Navarro Group on both the spontaneous potential and resistivity logs.**
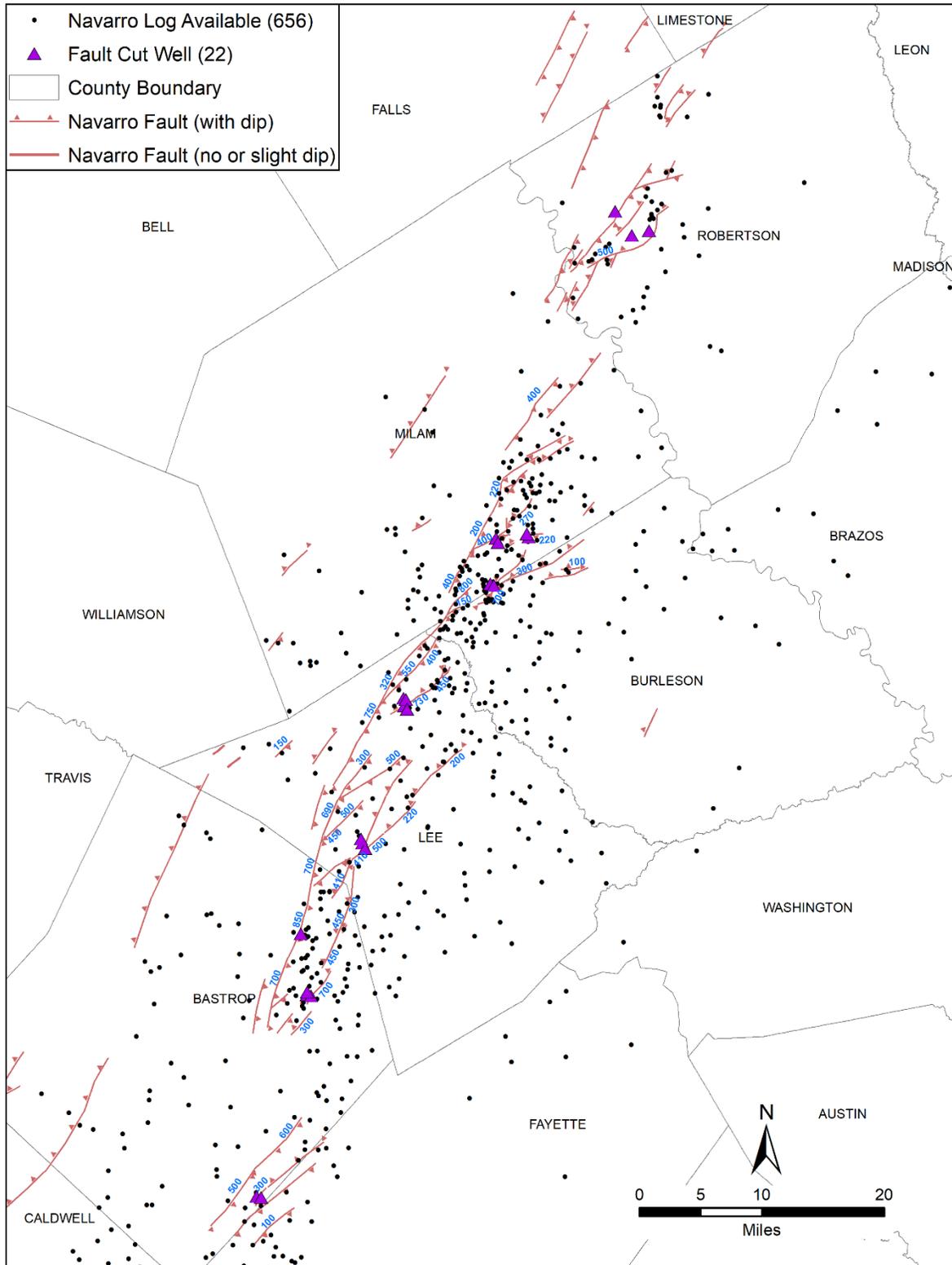
Figure 3.1.2b. Faults mapped onto the top of the Navarro Group determined primarily from the top of the Navarro Group picks from 656 geophysical logs with fault traces mapped on Geologic Atlas of Texas sheets (Barnes, 1970, 1979, 1981). Fault arrows point to the down-thrown side of the fault. Numerical values indicate fault offset in feet.
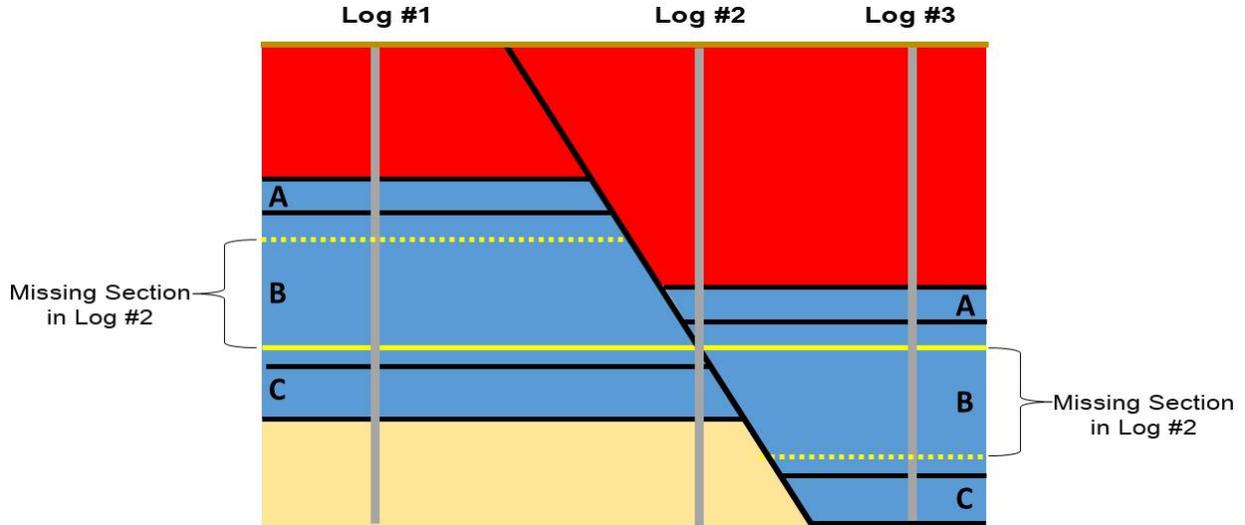
Figure 3.1.2c.　**Schematic representation of how fault-cut logs are identified. Log #1 intersects all three portions of Sections A, B and C. Log #2 intersects all of Section A, the top part of Section B on the down-thrown side and the bottom part of Section B on the up-thrown side, and all of Section C. Log #3 intersects all three portions of Sections A, B, and C. Using all three of these logs together, geologists can piece together missing sections within geologic units. The amount of missing section is referred to as a fault cut and can be used as a quantitative way to characterize the offset associated with faults.**
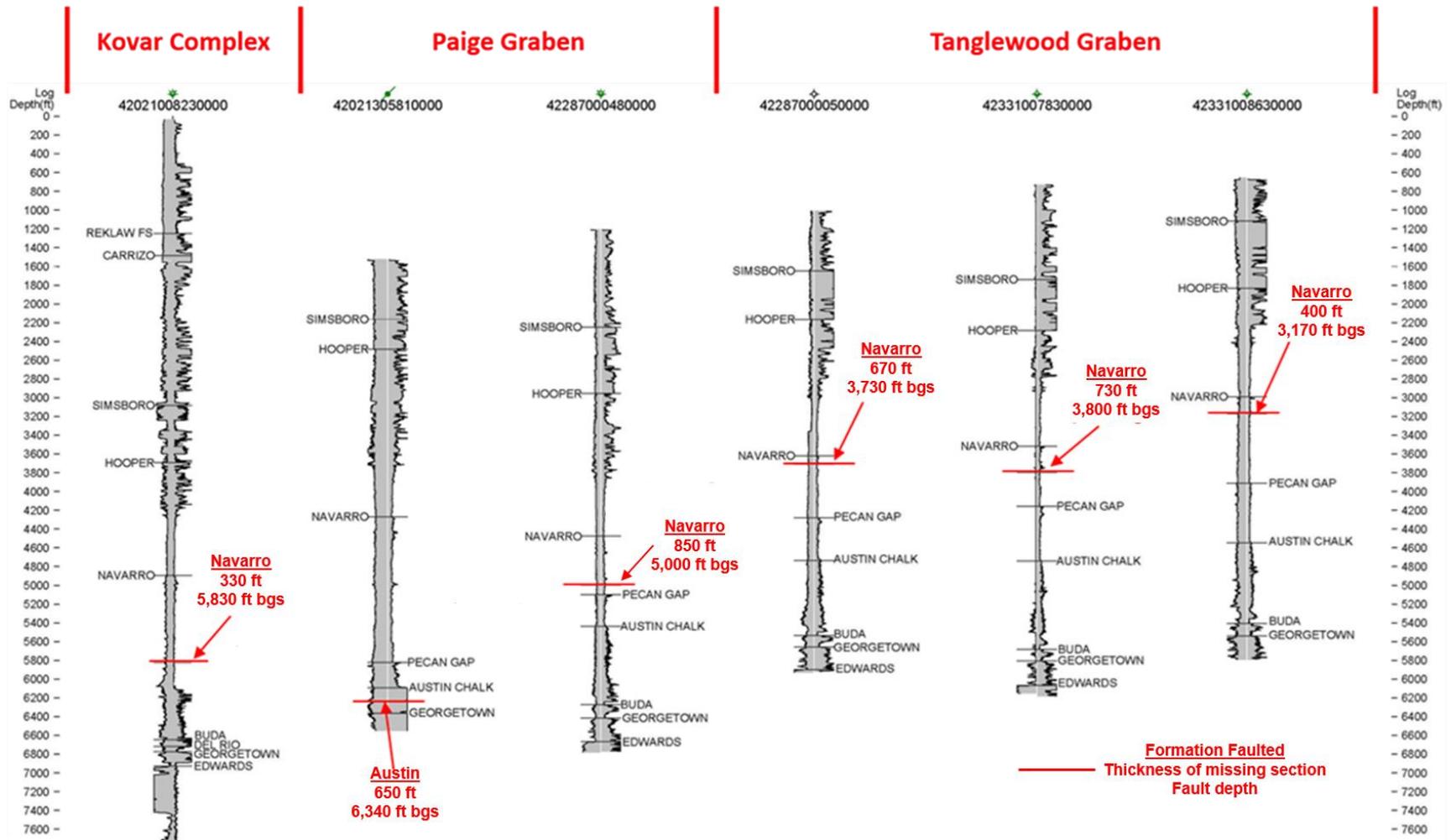
Figure 3.1.2d. Six logs containing fault cuts. Location of logs are shown in Figure 3.1.2g.

Note: ft = feet; bgs = below ground surface
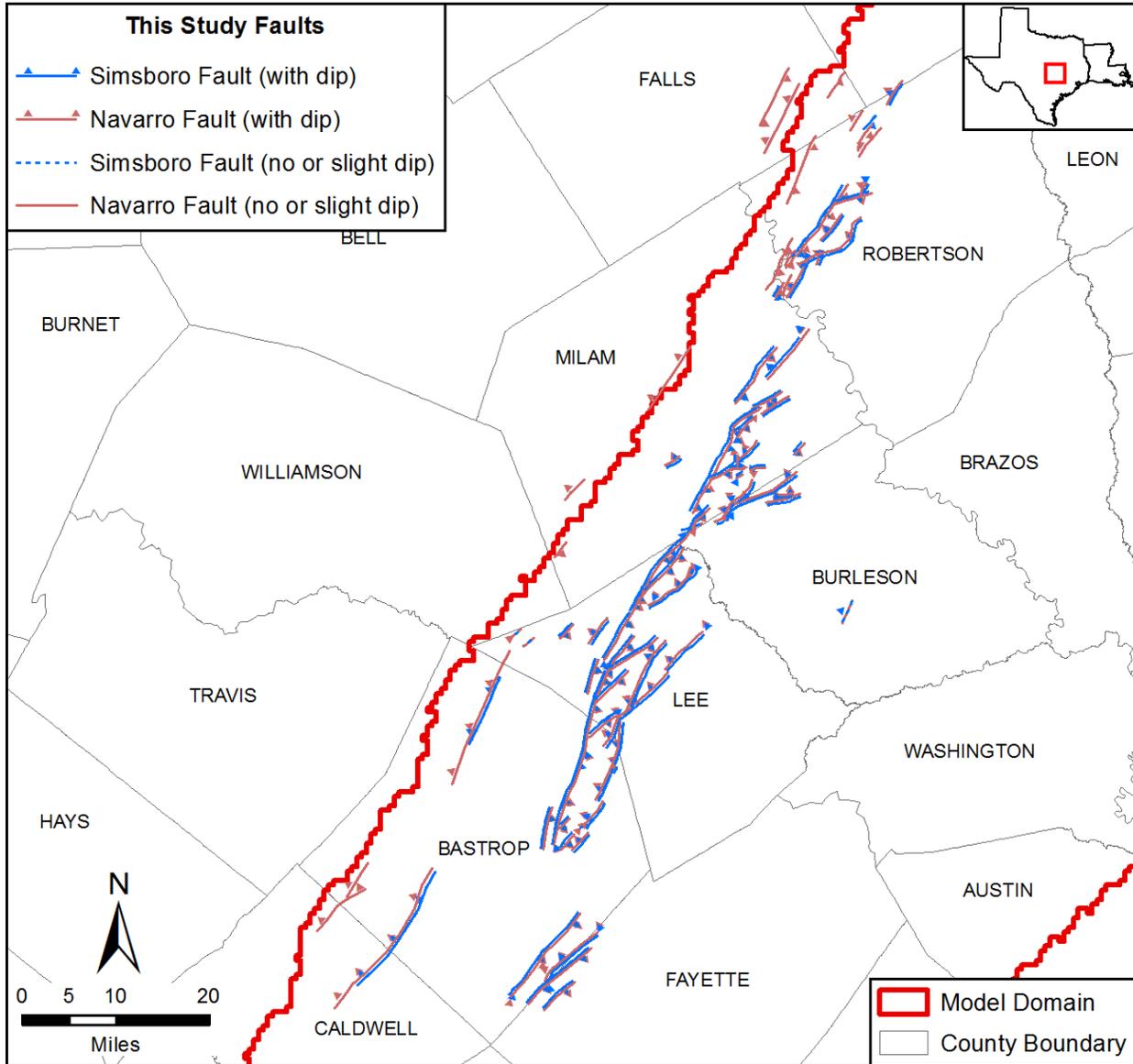
Figure 3.1.2e. **Navarro Group and Simsboro Formation faults mapped by this study. Arrows on fault lines point to the down-thrown side of the fault.**
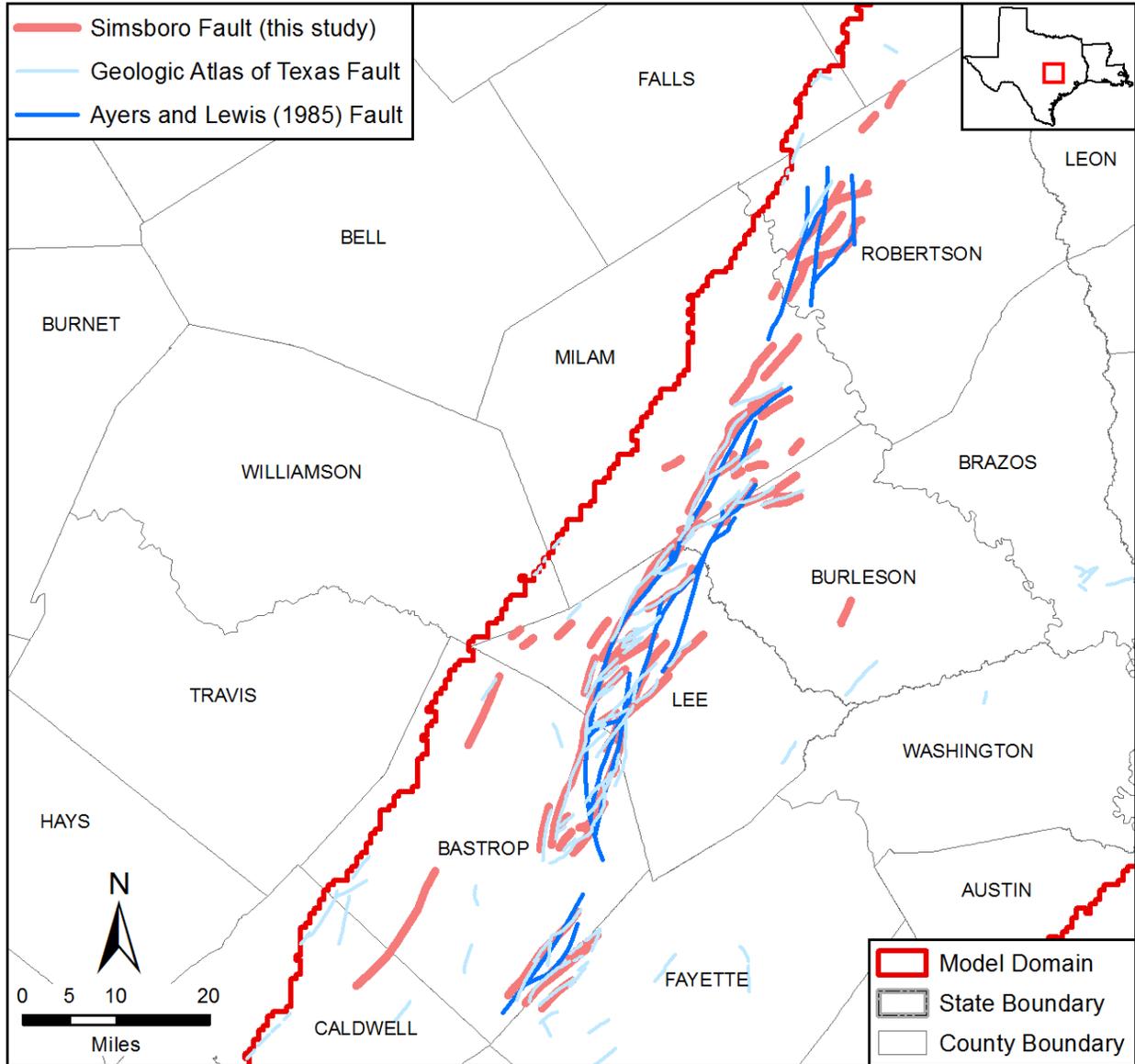
Figure 3.1.2f. **Simsboro Formation faults from this study mapped with faults from Ayers and Lewis (1985) and from the Geologic Atlas of Texas sheets of Barnes (1970, 1979, 1981) as presented by Stoeser and others (2007).**
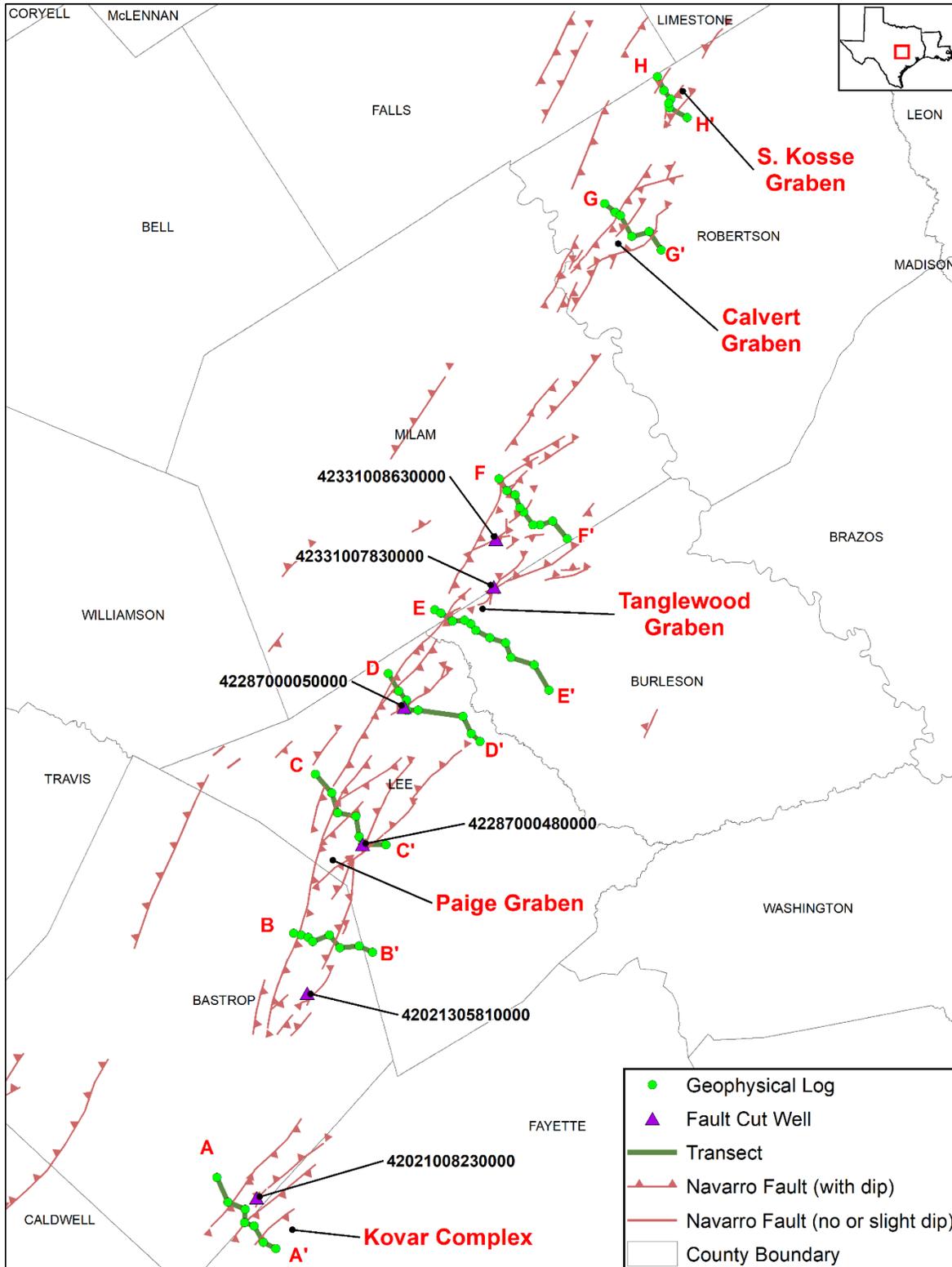
Figure 3.1.2g.   **Plan view map of the Milano Fault Zone showing the five named major areas of faulting, locations of cross-sections that transect the fault zone, and locations of fault cut wells shown in Figure 3.1.2d.**

3.1.2.1 Kovar Complex

In southern Bastrop and western Fayette counties, there is an area containing mainly southeast-down faults, which has been called the Kovar Complex (Figure 3.1.2g), named after the settlement of Kovar. The area is about 10 miles long and 5 miles wide, and the top of the Navarro Group lies at about 4,000 feet below sea level. The log control is insufficient to reliably map the faults, but they appear to strike north 50 degrees east. One fault appears to be northwest-down and bounding a graben. Fault displacements range from 100 to 500 feet. The faulting dies out to the northeast, where wells show no apparent offsets of strata. Similar faults are reported to the south into Gonzales County, as part of an en echelon segment of the peripheral graben system. Additional faults exist in western Bastrop County but are part of the Luling Fault Zone, and for the most part, do not affect the formations in the Wilcox Group.

Figure 3.1.2.1a shows the location of cross-section A-A′ through the Kovar Complex. Figure 3.1.2.1b shows formation tops and the relative locations of faults that were determined from the interpretation of logs in and near cross-section A-A′. Two main faults are represented in this section, with throw being to the south (normal).

Two wells appear to have intersected the same antithetic fault within the Kovar Complex:

- Well 4202100823 has 330 feet of missing section at a structural elevation of -5,416 feet below sea level in the Navarro Formation.
- Well 4202100824 has 230 feet of missing section at a structural elevation of -1,770 feet below sea level in the Calvert Bluff Formation.
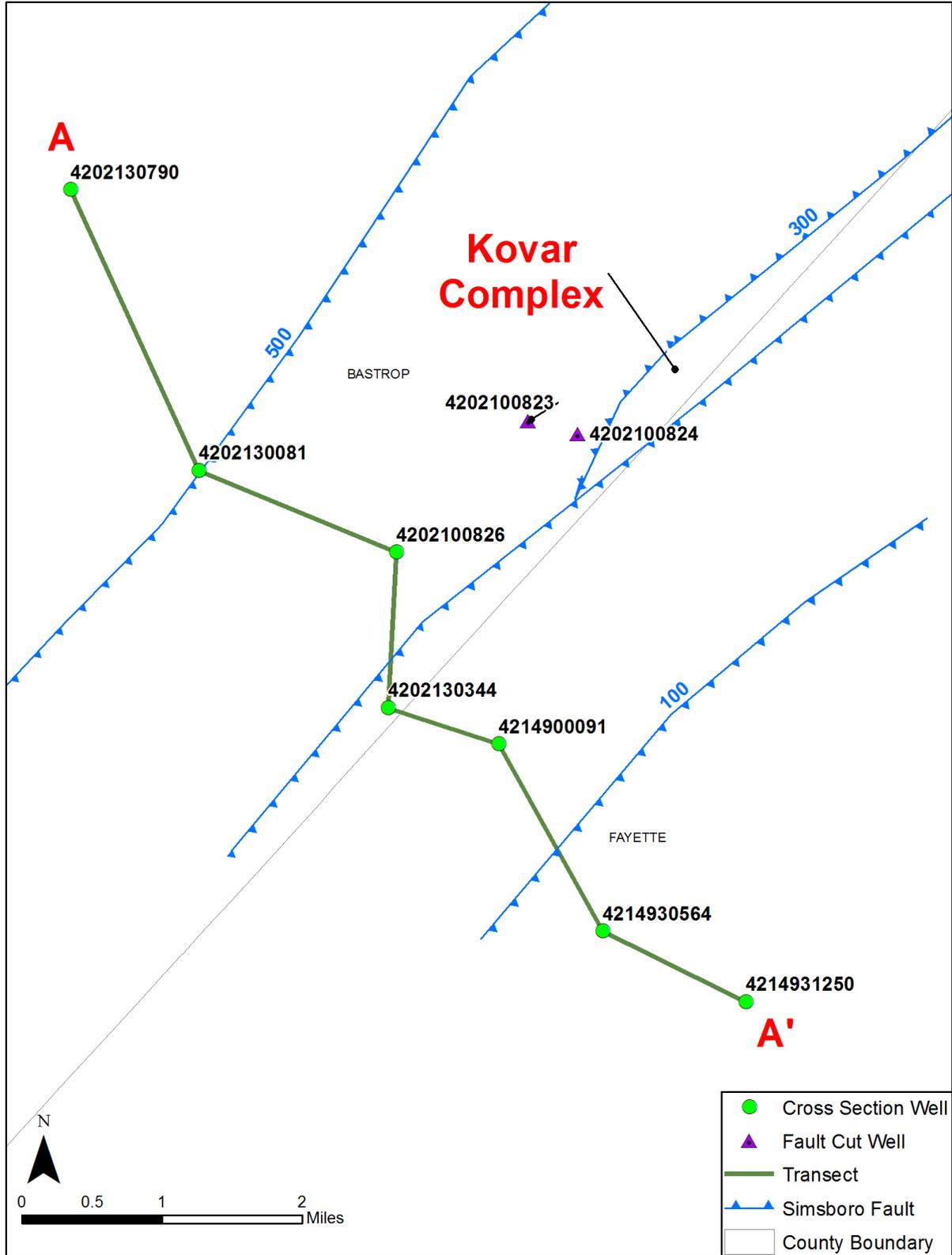
Figure 3.1.2.1a. Simsboro Formation faults and estimated fault offset (in feet) in the Kovar Complex in Bastrop and Fayette counties. Fault arrows point to the down-thrown side of the fault. The wells are labeled with their American Petroleum Institute number.
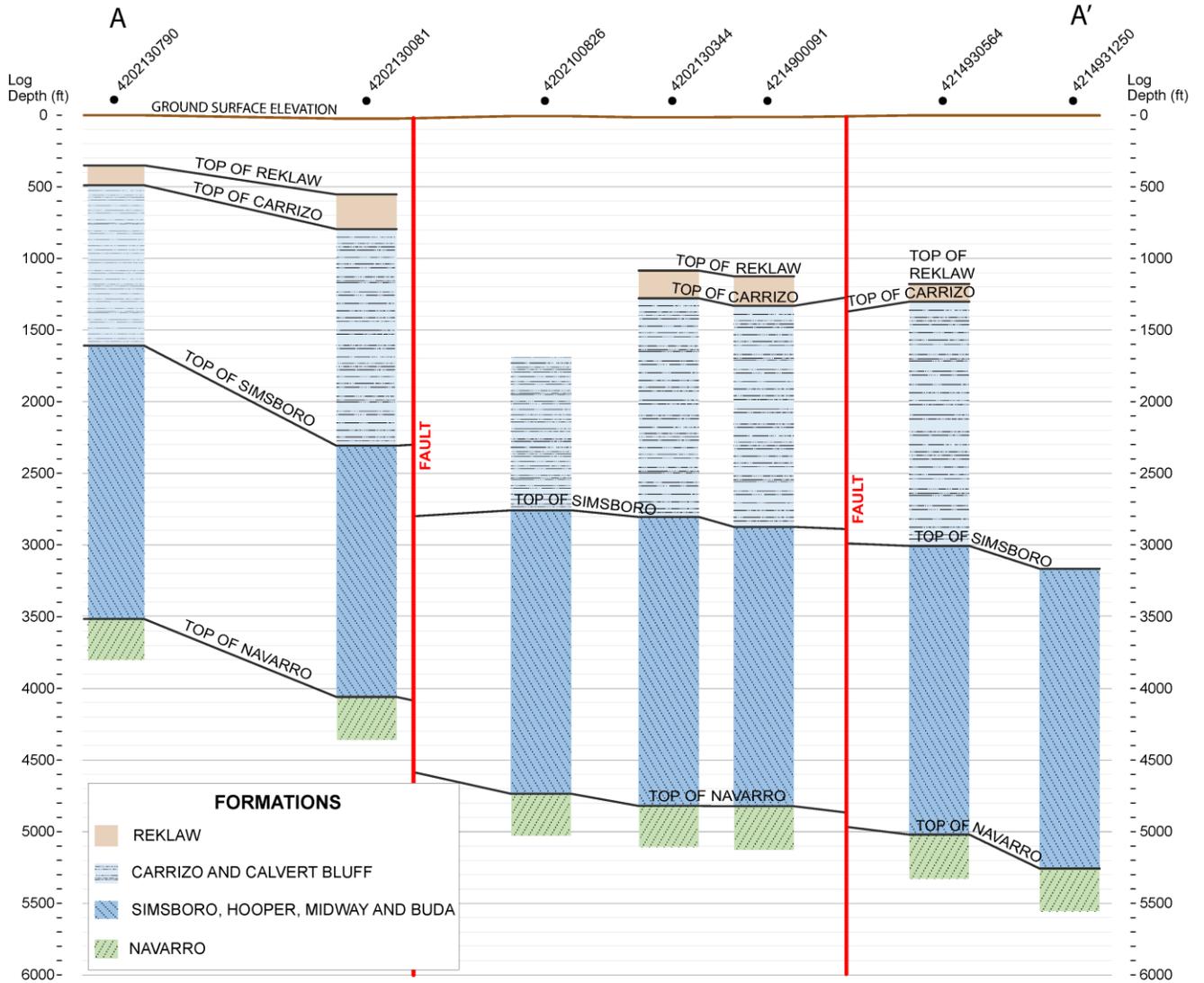
Figure 3.1.2.1b. **Cross-section A-A′ through the Kovar Complex showing the top surface of selected formations and mapped fault locations based on interpretation of geophysical logs in and near cross-section A-A′.**

Note: ft = feet

3.1.2.2 Paige Graben

In northeastern Bastrop and western Lee counties, the Paige Graben complex (Figure 3.1.2g), named after the settlement of Paige, is well defined by the data and is also evident on surface geologic maps. The graben is 24 miles long and 3.7 miles wide, trending north 20 degrees east. The top of Cretaceous-age sediments lies about 3,500 feet below sea level in this graben. The northwestern, southeast-down fault is well marked and very continuous, showing 690 to 700 feet of displacement at the top of the Navarro Group. The eastern, northeast-down faults are less continuous but generally show 450 to 700 feet of displacement. The details of fault relationships here are not well determined from well control. It appears that there are internal faults within the graben and some that cross from one side to another. The faults toward the northeast end of the graben become more easterly trending (north 37 degrees east). The northwest fault appears to feather out into a series of smaller faults, and the displacement steps northwest into the western boundary fault of the next graben to the north; however, well control is not adequate to map this fully.

Figure 3.1.2.2a shows the location of cross-sections B-B′ and C-C′ through the Paige Graben. Figure 3.1.2.2b shows the formation tops and the location of faults that were determined from the interpretation of logs near and in cross-section B-B′. This section shows the northwestern (southeast-down) fault within the Graben and clearly shows more than 700 feet of throw. Further downdip on the cross-section, between wells 4202131558 and 4202131041, the southwestern extent of the graben system is intersected.

Figure 3.1.2.2c shows the top surfaces of formations and the location of faults that were determined from the interpretation of logs near and in cross-section C-C′. This section transects both bounding graben faults between wells 4228700098 and 4228700101 in the updip (throw to the southeast) and wells 4228700048 and 4228731157 in the downdip, where throw is up away from the Gulf of Mexico. Two localities within the Paige Graben have designated fault-cut wells:

East Bounding Fault in Bastrop County Locality

- Well 4202130581 has 650 feet of missing section at an elevation of -5,820 feet below sea level in the Austin Chalk.
- Well 4202100143 has 550 feet of missing section at an elevation of -4,709 feet below sea level in the Taylor Marl and shows an apparent dip of 41 degrees.
- Well 4202100144 has 700 feet of missing section at an elevation of -3,630 feet below sea level, faulting out the Midway and Navarro groups. The fault has an apparent dip of 42 degrees.

Lee County Part of the Graben

- Well 4228731293 has 750 feet of missing section at a structural elevation of -5,254 feet below sea level in the Austin Chalk.
- Well 4228700048 has 850 feet of missing section at a structural elevation of -4,600 feet below sea level in the Navarro Group.
- Well 4228700050 has 400 feet of missing section at a structural elevation of -2,000 feet below sea level in the Simsboro Formation, giving an apparent fault dip of 36 degrees.
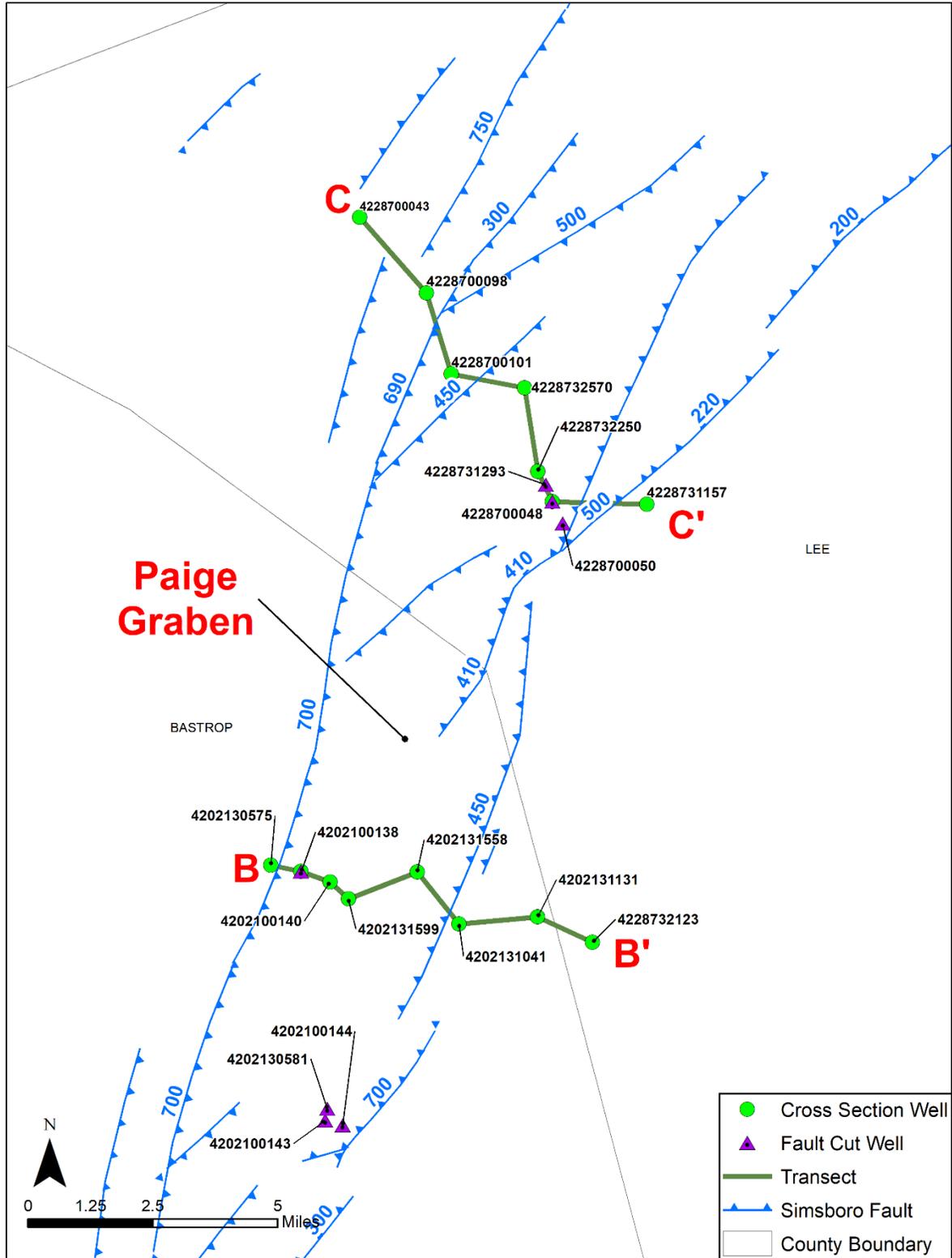
Figure 3.1.2.2a. Simsboro Formation faults and estimated fault offset (in feet) in the Paige Graben in Bastrop and Lee counties. Fault arrows point to the down-thrown side of the fault. The wells are labeled with their American Petroleum Institute number.
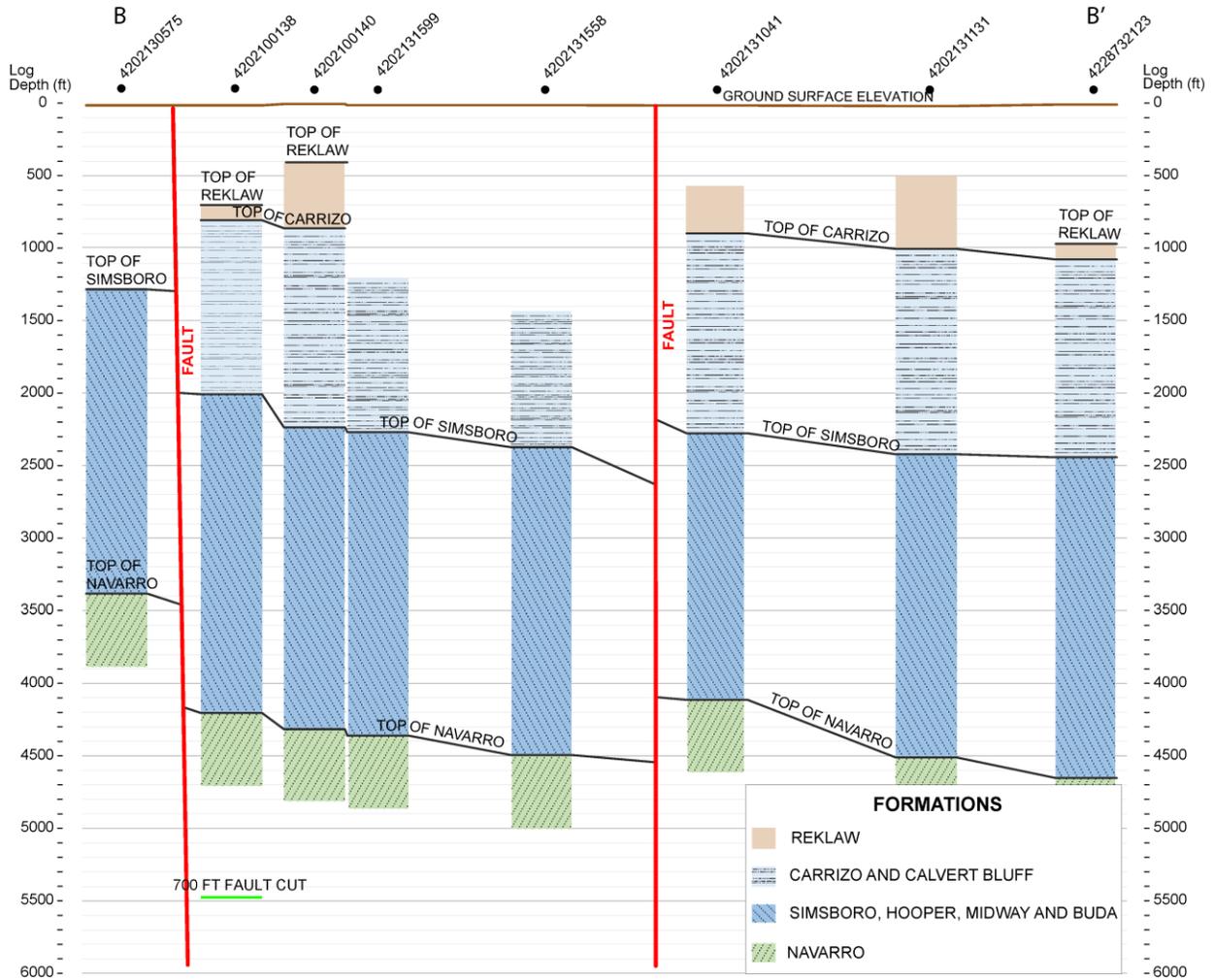
Figure 3.1.2.2b. **Cross-section B-B′ through the southern portion of the Paige Graben showing the top surface of selected formations and mapped fault locations based on interpretation of geophysical logs in and near cross-section B-B′.**

Note: ft = feet
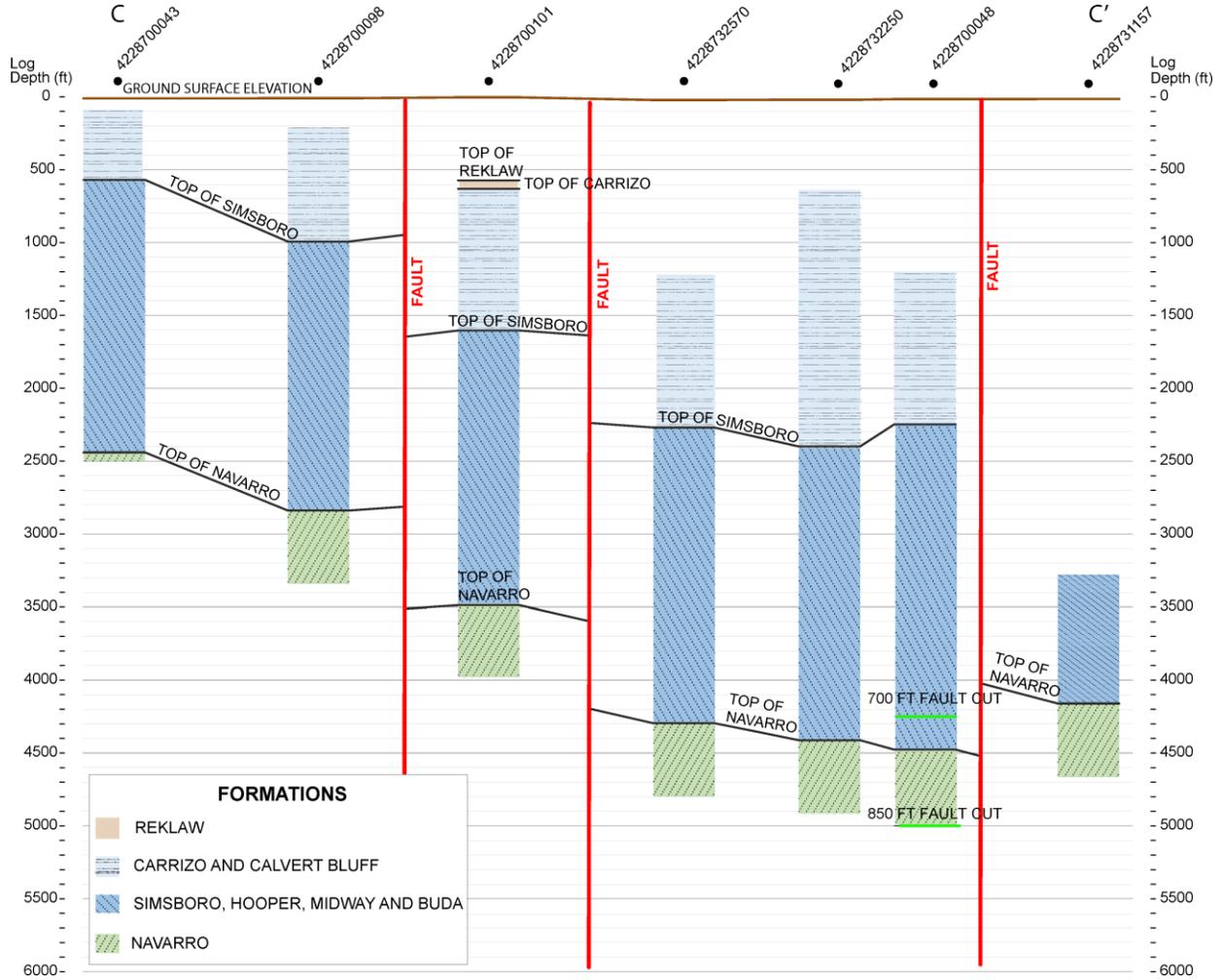
Figure 3.1.2.2c. **Cross-section C-C′ through the northeastern portion of the Paige Graben showing the top surface of selected formations and mapped fault locations based on interpretation of geophysical logs in and near cross-section C-C′.**

Note: ft = feet

3.1.2.3 Tanglewood Graben

The Tanglewood Graben lies in northern Lee, western Burleson and southeastern Milam counties (Figure 3.1.2g). This graben is more complicated than the Paige Graben, but abundant well control allows a fairly reliable interpretation. The main graben system is 21 miles long and 3 miles wide, trending north 47 degrees east. The top of Cretaceous-age sediments lies about 3,000 feet below sea level in this graben. The graben consists of two segments, one in northern Lee County and the other along the Milam-Burleson counties border, separated by a small left-stepping displacement. The northwestern boundary faults are well defined and typically have 700 to 750 feet of displacement. In northern Lee County, this fault appears to splinter into two faults with lesser displacement; however, well control was not adequate to make any concrete interpretations. The southeastern bounding faults are discontinuous and complicated.

In northern Lee County, the faults show around 450 to 730 feet of displacement, and, to the north along the county line, displacements are from 100 to 700 feet. An area between these two faults shows no evident faulting, but a reversal of regional dip. It is possible that there may be smaller, more distributed faults in this area. Northeastward into Milam County, the fault pattern becomes less regular. Faults with 200 to 400 feet of displacement form two or more small grabens. The northwestern bounding fault, trending north 31 degrees east, is the most continuous. This fault, with 200 feet of throw at the top of Navarro Group, has a surface expression in the city of Milano. Faulting continues into eastern Milam County, but the well control is not sufficient to map it in this area. Faults in this area, if present, are either small or closely spaced.

Figure 3.1.2.3a shows the location of cross-sections D-D′, E-E′, and F-F′ through the Tanglewood Graben. Figures 3.1.2.3b, 3.1.2.3c, and 3.1.2.3d show the formation tops and the location of faults that were determined from the interpretation of logs near and in cross-sections D-D′, E-E′, and F-F′, respectively. Based on these cross-sections and nearby geophysical logs, the following observations have been made:

Northern Lee County

- The southernmost well in the graben system, 4228730366, penetrated a fault with about 450 feet of displacement at a structural elevation of -270 feet below sea level in the Calvert Bluff Formation.
- To the northwest, well 4228700005 has 670 feet of missing section at an elevation of -3,323 feet below sea level in the Navarro Group. A fault dip of 57 degrees was calculated.
- Well 4228700013, which is oblique to fault strike, has a displacement of 750 feet at a structural elevation of -4,320 feet below sea level in the Taylor Marl.
- A similar displacement is observed in well 4228700012 in the Austin Chalk to the northwest.

Southeastern Milam County

- The southeastern well 4233100783 has 730 feet of missing section at a structural elevation of -3,310 feet below sea level in the Navarro Group.

- Well 4233100782 has 690 feet of missing section at a structural elevation of -4,900 feet below sea level in the Austin Chalk. The apparent dip of the fault is 44 degrees.

Northern Fringe of the Tanglewood Graben

- Well 4233100863 has 400 feet of missing section at a structural elevation of -2,670 feet below sea level in the Navarro Group.
- Well 4233132745 has 400 feet of missing section at a structural elevation of -4,700 feet below sea level in the Austin Chalk. Apparent fault dip is 45 degrees.
- Well 4233130170 has 240 feet of missing section at a structural elevation of -3,030 feet below sea level in the Taylor Group.
- Well 4233130197 shows 200 feet of missing section at a structural elevation of -348 feet below sea level in the Calvert Bluff Formation. Apparent fault dip is 60 degrees.
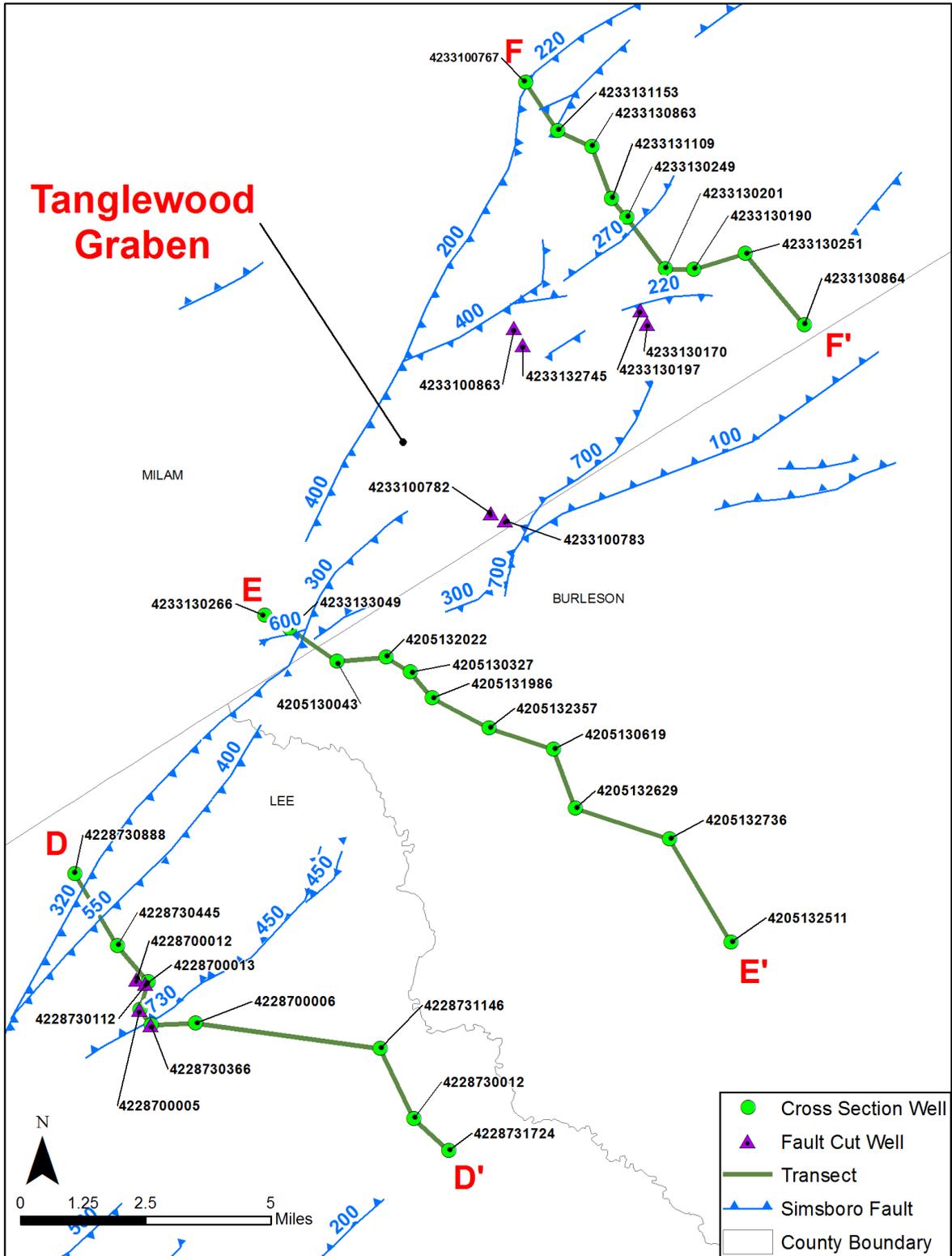
Figure 3.1.2.3a. **Simsboro Formation faults and estimated fault offset (in feet) in the Tanglewood Graben in Lee, Milam and Burleson counties. Fault arrows point to the down-thrown side of the fault. The wells are labeled with their American Petroleum Institute number.**
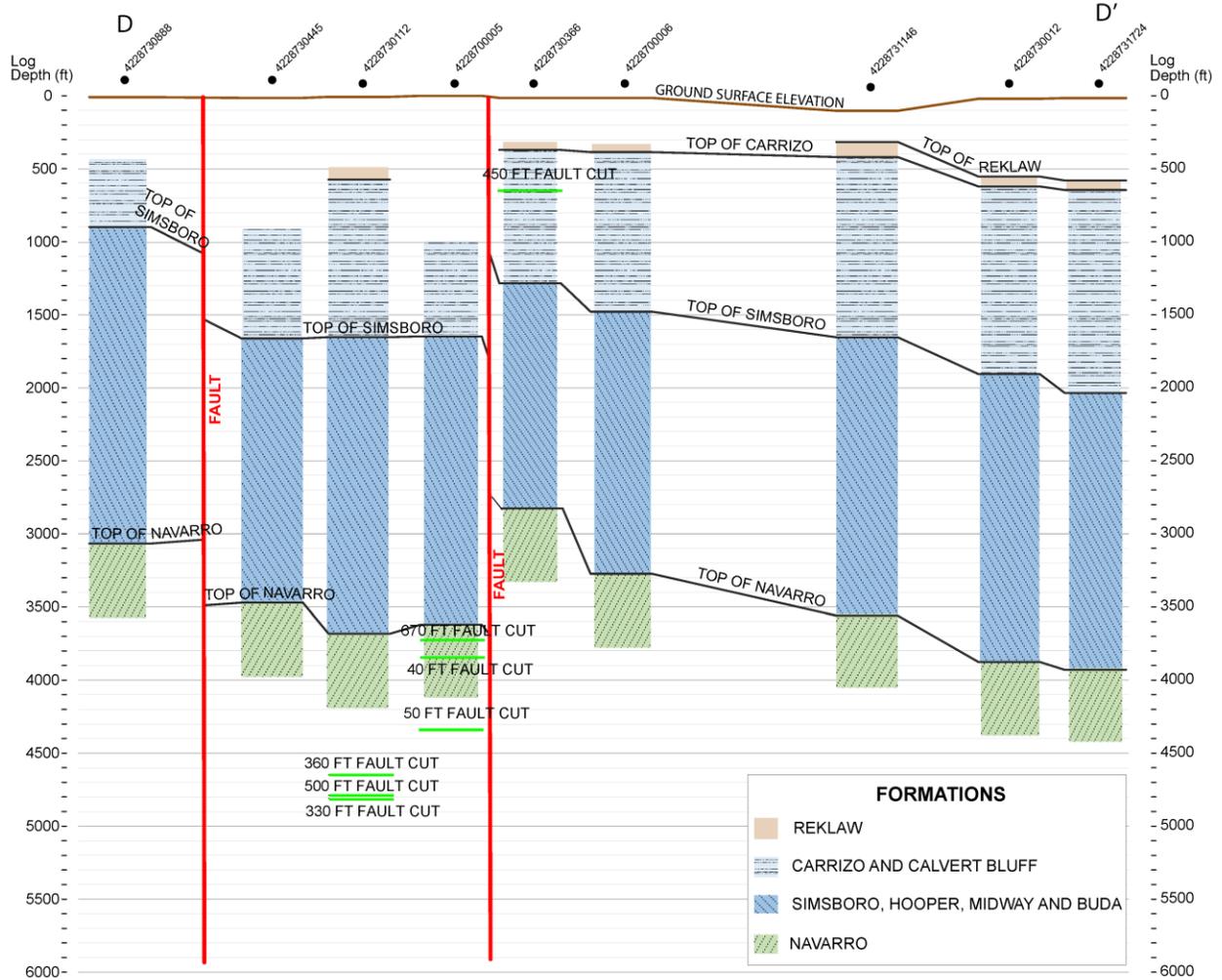
Figure 3.1.2.3b. Cross-section D-D′ through the southern portion of the Tanglewood Graben showing the top surface of selected formations and mapped fault locations based on interpretation of geophysical logs in and near cross-section D-D′.

Note: ft = feet
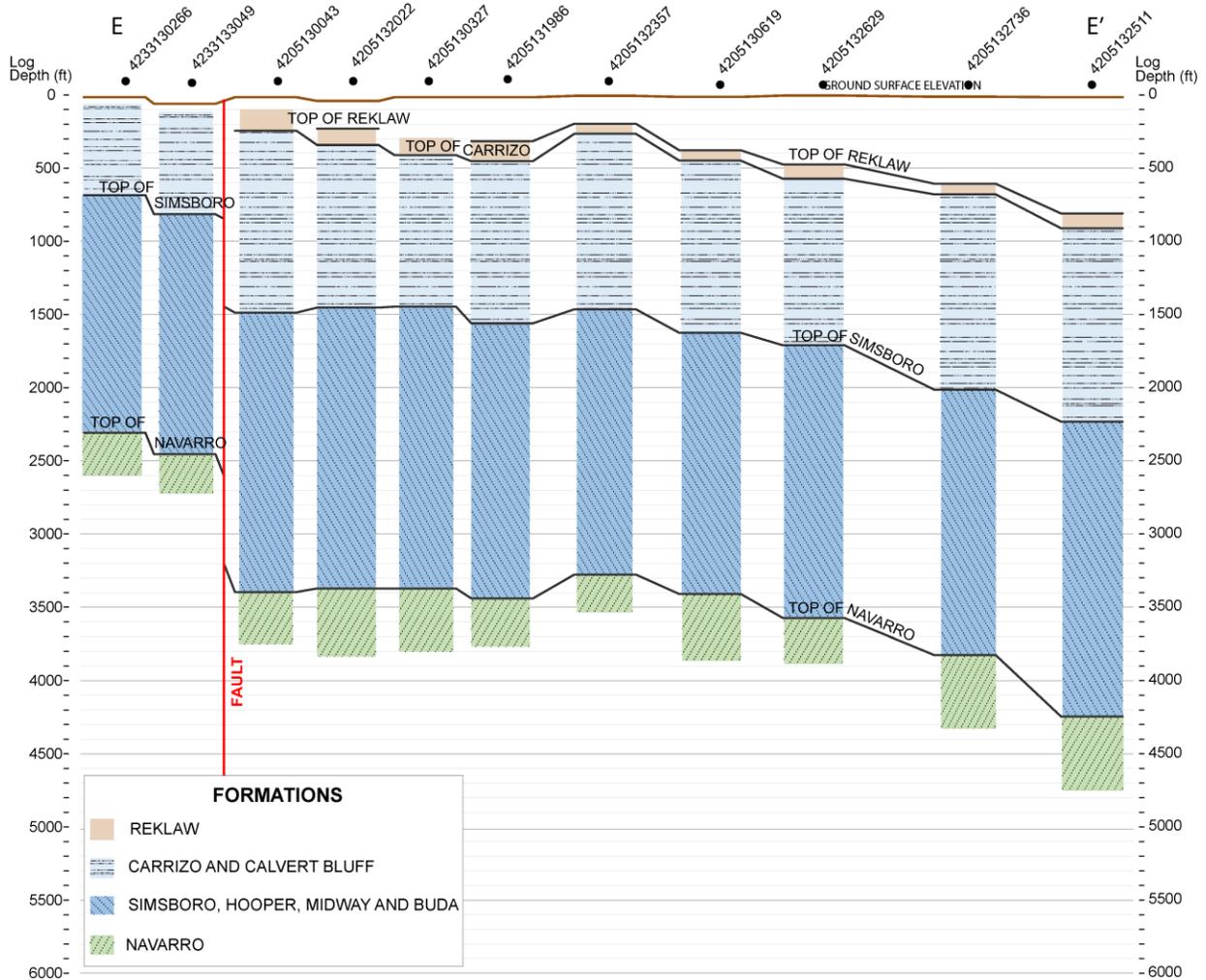
Figure 3.1.2.3c.   **Cross-section E-E′ through the middle portion of the Tanglewood Graben showing the top surface of selected formations and mapped fault locations based on interpretation of geophysical logs in and near cross-section E-E′.**

Note: ft = feet
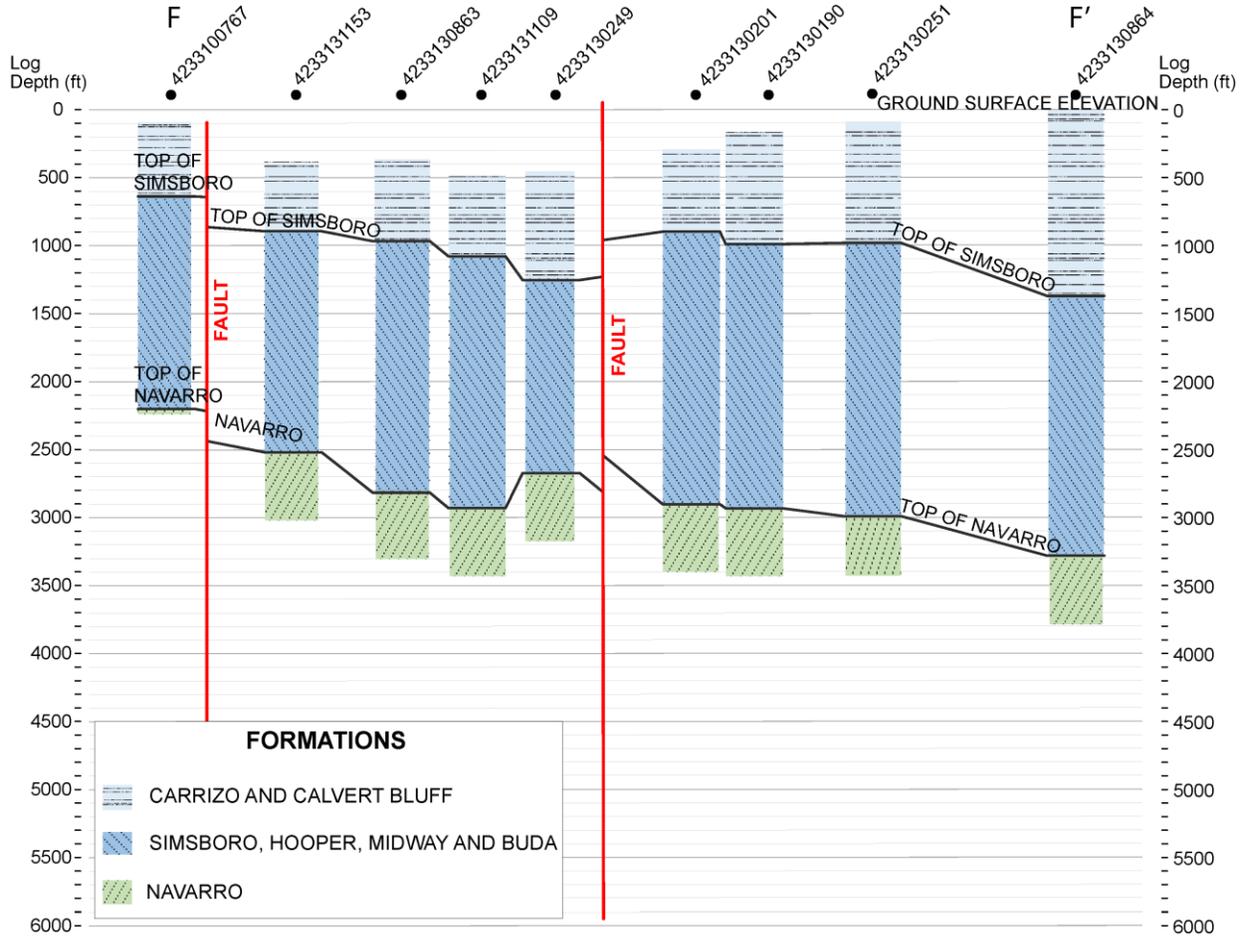
Figure 3.1.2.3d. Cross-section F-F′ through the northeastern portion of the Tanglewood Graben showing the top surface of selected formations and mapped fault locations based on interpretation of geophysical logs in and near cross-section F-F′.

Note: ft = feet

3.1.2.4   Calvert Graben and South Kosse Graben

Calvert Graben lies in western Robertson County (Figure 3.1.2g). Figure 3.1.2.4a shows the location of cross-section G-G′, which crosses through the Calvert Graben. Figure 3.1.2.4b shows the formation tops and the location of faults that were determined from the interpretation of logs near and in cross-section G-G′. This graben has little expression at surface, probably because surface rocks are the Calvert Bluff Formation, which does not yield reliable mapping horizons. The graben is 15 miles long and 2.5 to 3.0 miles wide, trending north 42 degrees east. The top of the Navarro Group lies at a structural elevation of -1,800 feet below sea level in this graben. The deeper eastern part of the graben is bounded by a southeast-down fault on the northwest with 480 to 500 feet of displacement. The northwest-down faults on the southeast show 150 and 820 feet of displacement, varying fairly rapidly along strike. To the south, smaller faults outline two or more grabens with 100 to 270 feet of displacement. Faulting of this magnitude exists at the northeastern end but isn't well resolved by the log control.

A set of faults called the South Kosse Graben (Figure 3.1.2g) is identified in northernmost Robertson, eastern Falls, and southern Limestone counties. Figure 3.1.2.4a shows the location of cross-section H-H′, which crosses through the South Kosse Graben. Figure 3.1.2.4c shows the formation tops and the location of faults that were determined from the interpretation of logs near and in cross-section H-H′. Within the area mapped, the well control only suffices to map a few faults, but some have 600 feet of displacement. The top of Cretaceous-age sediments lies at a structural elevation of only -1,000 feet below sea level here, and the Simsboro Formation is exposed at the surface or absent by erosion. Faulting continues northwest into Falls County and north into Limestone County, where it becomes well organized into a graben complex at Kosse. This is the southernmost portion of the Mexia Fault Zone, which continues northward to Corsicana. The surface geology is well mapped as surficial rocks here are pre-Wilcox Group in age (mainly Midway Group).
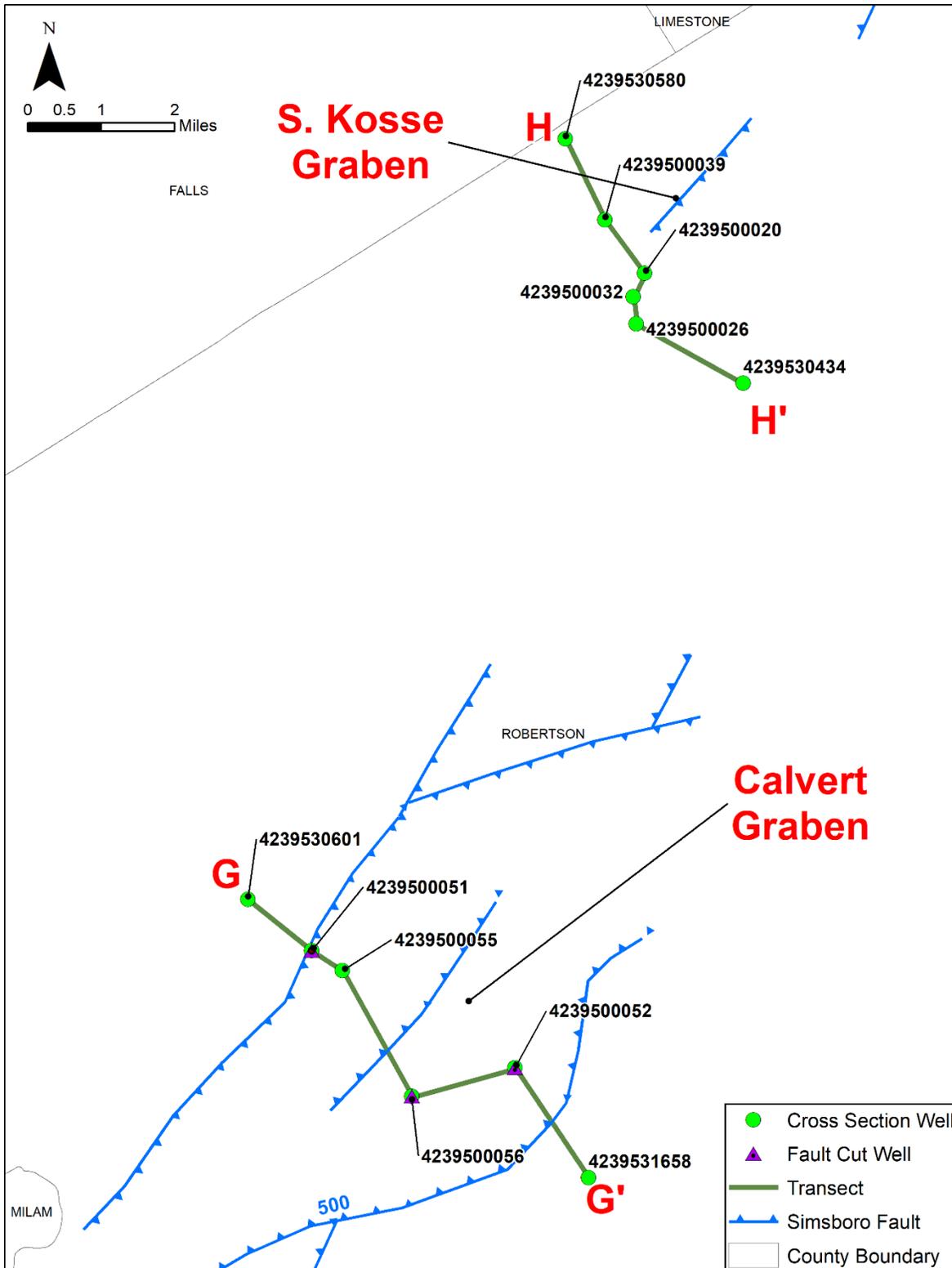
Figure 3.1.2.4a. Simsboro Formation faults and estimated fault offset (in feet) in the South (S.) Kosse and Calvert Grabens in Robertson County. Fault arrows point to the down-thrown side of the fault. The wells are labeled with their American Petroleum Institute number.
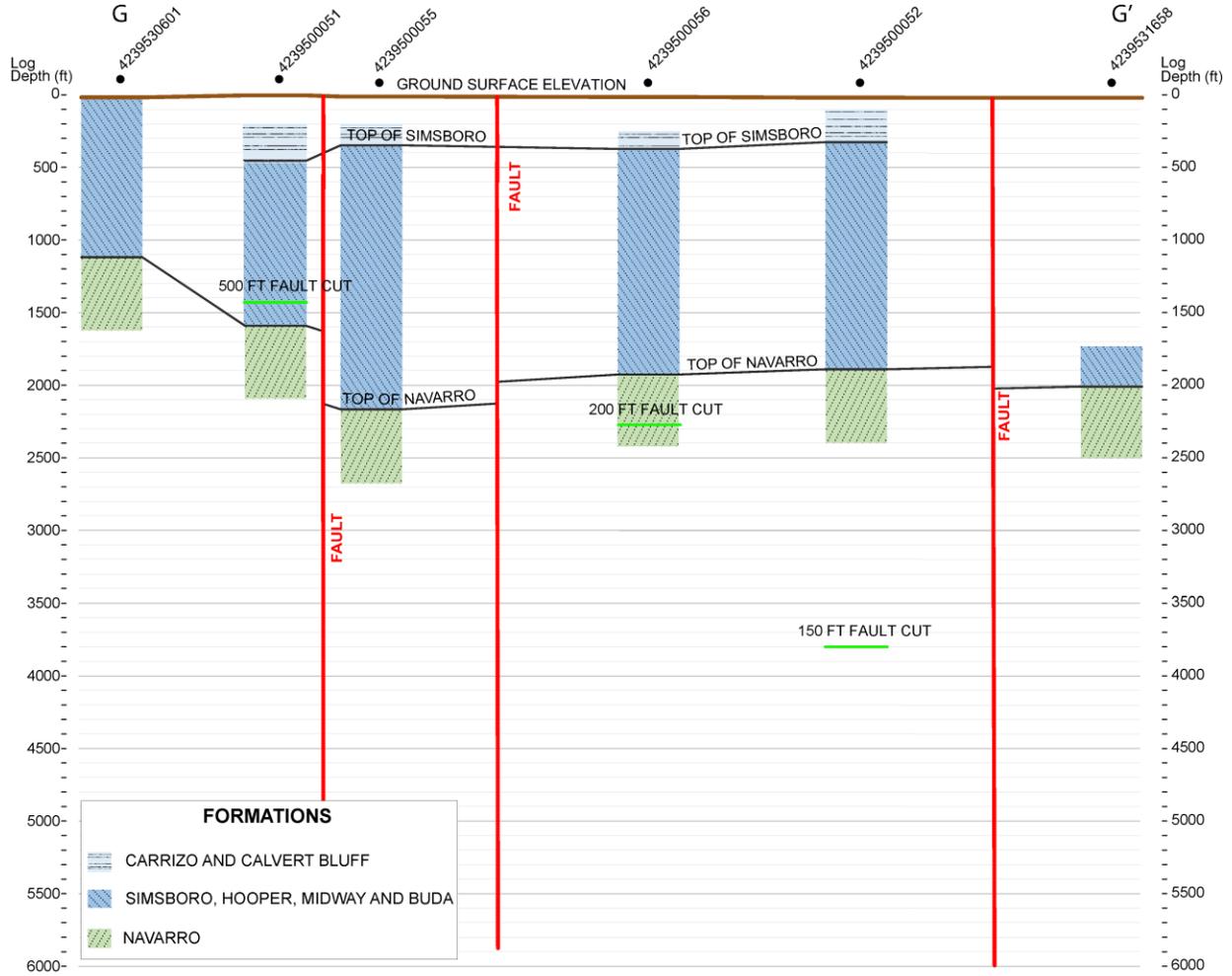
Figure 3.1.2.4b. **Cross-section G-G′ through the Calvert Graben showing the top surface of selected formations and mapped fault locations based on interpretation of geophysical logs in and near cross-section G-G′.**

Note: ft = feet
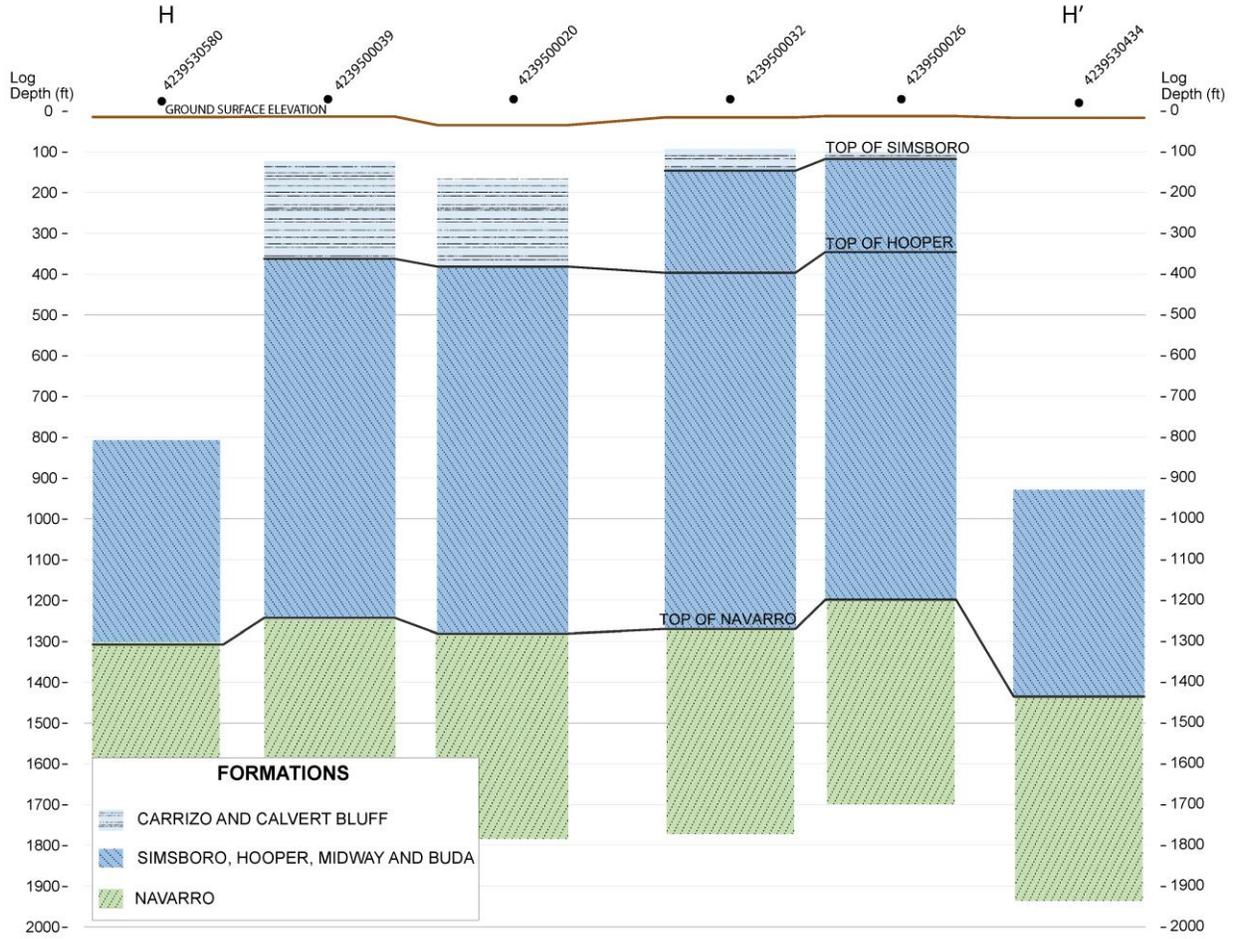
Figure 3.1.2.4c. **Cross-section H-H′ through the South Kosse Graben showing the top surface of selected formations and mapped fault locations based on interpretation of geophysical logs in and near cross-section H-H′.**

Note: ft = feet

3.1.3 Representation of the Milano Fault Zone in the Groundwater Model

The previous groundwater availability models for the central portion of the Carrizo-Wilcox
Aquifer (Kelley and others, 2004; Dutton and others, 2003) represented the Milano Fault Zone
using the Horizontal Flow Barrier package (Hsieh and Freckleton, 1993) developed by the
United States Geological Survey for the MODFLOW family of groundwater codes. This package
provides the ability to cite and parameterize faults in a manner consistent with the impact on
aquifer transmissivity and groundwater flow associated with faults.

The faults identified in Section 3.1.2 were placed on the grid for the groundwater availability
model for the central portion of the Carrizo-Wilcox, Queen City, and Sparta aquifers. To
accomplish this, the fault locations were adjusted and manipulated to be compatible with the
numerical grid. Figure 3.1.3a shows the adjusted fault locations in the Simsboro Formation, as
determined by this study, as a series of straight-line segments that match the boundaries of the
square grid cells in the groundwater availability model. Each fault segment is characterized by a
vertical offset for the fault estimated from the interpretation of the geophysical logs. The faults
are grouped into three categories: (1) offset greater than 500 feet, (2) offset greater than 200 feet
but less than 500 feet, and (3) offset less than 200 feet.

Also shown in Figure 3.1.3a are the sealing faults from the 2004 groundwater availability model
for the central portion of the Carrizo-Wilcox, Queen City, and Sparta aquifers. These sealing
faults are represented by thick lines to simplify the comparison between the two sets of faults.
Such a comparison indicates that the faults identified in this study cover considerably less area
than the set of faults in the 2004 groundwater availability model. This implies that the area
potentially affected by faulting is considerably smaller than the fault representation in the current
groundwater availability model.

Our review of geophysical logs indicates that the Milano Fault Zone consists of a series of
connected grabens. This contrasts with the long, continuous faults, some of which are 100 miles
in length, in Kelly and others' (2004) groundwater availability model. Our reconceptualization of
the character of the faults in the Milano Fault Zone provides for "windows" and "gates" that
allow groundwater to flow more freely perpendicular to the strike of the faults, flow that is not
possible with the system of faults in the 2004 groundwater availability model. In addition,
estimation of offset provides a method for assigning different conductance values to the faults
identified with this study based on differences in offset.

Regardless of how the conductance values were assigned to this study's new network of faults,
the updated location of faults differs significantly from the 2004 model. This study identified no
faults in two areas where the 2004 groundwater availability model has considerable faults:
northern Burleson County, where an over 50-mile long fault in the 2004 model has been
removed, and Robertson County, where a single continuous fault that divides the county has
been removed.
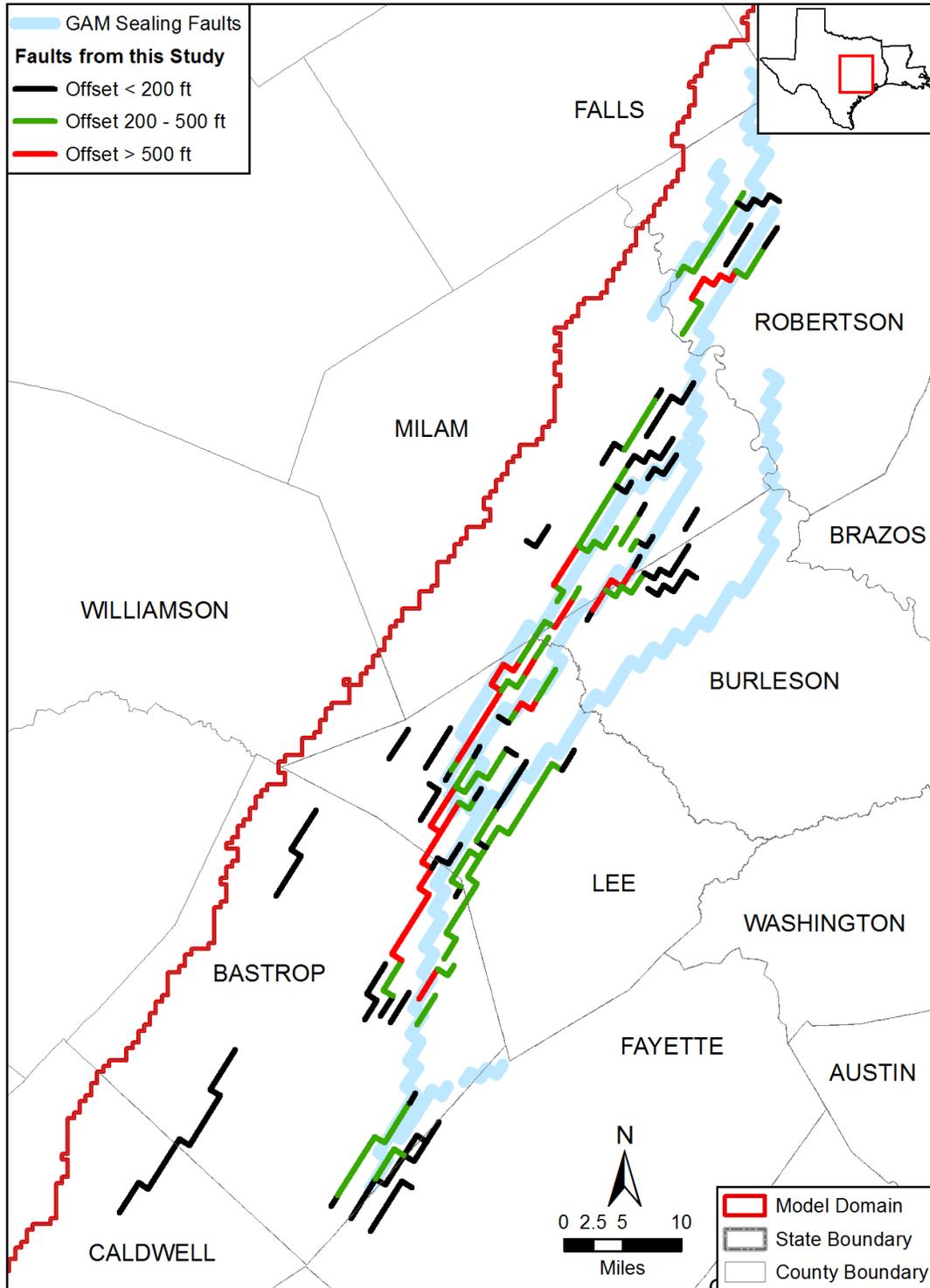
Figure 3.1.3a. Sealing faults in the groundwater availability model (GAM) for the central portion of the Carrizo-Wilcox, Queen City, and Sparta aquifers and the Simsboro Formation faults from this study sampled onto the groundwater availability model grid and color-coded based on the amount of offset between the Simsboro Formation updip and downdip of the fault.

Note: ft = feet

3.1.4   Assessment of Milano Fault Zone on Aquifer Transmissivity

This section evaluates the results of aquifer pumping tests performed near and away from the of the Milano Fault Zone to determine whether there is evidence that some of the faults affect groundwater flow. Such an effect should be detected in the measured drawdown, and this effect should be manifested as if the location of the fault represents a region of low transmissivity.

The analysis of the aquifer pumping tests proceeded on two paths. The first path looked for differences in the behavior between the early-time and late-time drawdown data during the pumping tests. The second path used groundwater models to simulate several of the pumping tests with and without accounting for faults located near the pumping well.

3.1.4.1   Comparison of Early- and Late-Time Transmissivity Values from Aquifer Pumping Tests

Time-drawdown data from aquifer pumping tests performed at 113 wells were assembled from the Texas Commission on Environmental Quality and from hydrogeologic consulting reports. Figure 3.1.4.1a shows the location of the wells and the faults from this study. Appendix A provides the following information for each well: identification number, longitude, latitude, county, well and test data source, well depth, depth to the top of the uppermost screen, depth to the bottom of the lowermost screen, length of screen from the top of the uppermost screen to the base of the lowermost screen, screen length open to the aquifer, and model layer in which the majority of the screen is located.

For each of the aquifer pumping tests, the drawdown data were analyzed using the Cooper-Jacob approximation to the Theis nonequilibrium well equation (Cooper and Jacob, 1946). This analysis method involves fitting a logarithmic model to the elapsed-time/drawdown data for the test, selecting drawdown points one log cycle apart, and applying the equation:

$$T = \frac{35.3Q}{\Delta s} \qquad \text{(Equation 3-1)}$$

where:

T = Transmissivity in square feet per day
Q = Flow in gallons per minute
Δs = Change in drawdown in feet over one log cycle

A Cooper-Jacob analysis relies on the fact that the slope of a semi-log plot of time-drawdown data for a constant-rate pumping test can be used to calculate aquifer transmissivity if the pumping rate is known (Cooper and Jacob, 1946). Butler (1990), Streltsova (1988), and Young (1998) show that the Cooper Jacobs analysis method is robust and can be used to analyze different time periods of a time-drawdown curve to determine whether the aquifer's transmissivity field away from the pumping well is different than the aquifer's transmissivity field close to the pumping well.

Each of the 113 aquifer pumping tests were analyzed by the Cooper-Jacob approximation using software to fit a straight-line through the drawdown values for the first 48 hours of the test. For aquifer tests where the slope, Δs, of the time-drawdown curve changes more than 15 percent, a second slope and transmissivity were calculated. Where two transmissivity values were

calculated for the same aquifer pumping test data, the transmissivity values were designated as an early-time transmissivity and the late-time transmissivity. For each aquifer pumping test, the ratio of the late-time transmissivity to the early-time transmissivity was used to indicate whether the aquifer transmissivity changed with the radial distance from the pumping well based on the categories listed in Table 3.1.4.1a. Figure 3.1.4.1b shows one example of aquifer pumping test data for each of these four categories.

Table 3.1.4.1a.   Transmissivity categories used to classify wells based on the results of the Cooper Jacob analysis.

Transmissivity Category	Criteria for Grouping Based on the Ratio of T_{late}/T_{early}
No change in Transmissivity	> 0.85 and < 1.15
Small decrease in Transmissivity	>0.65 and < 0.85
Large decrease in Transmissivity	<0.65
Increase in Transmissivity	> 1.15

Note: T_{late} = late-time transmissivity; T_{early} = early-time transmissivity; $>$ = greater than, $<$ = less than.

Figures 3.1.4.1c through 3.1.4.1e show the Cooper-Jacob analysis for select wells located in the Milano Fault Zone in Milam, Lee, and Bastrop counties. The Cooper-Jacob analysis for all aquifer pumping tests are provided in Appendix B, along with an explanation of the symbology associated with the plots. The wells shown in Figures 3.1.4.1c to 3.1.4.1e are close to faults and have values for late-time transmissivity that are lower than for early-time transmissivity.

In northwestern Burleson County, the 2004 groundwater availability model includes a sealing fault that was not identified with this study (see Figure 3.1.3a). None of three aquifer tests located near this sealing fault (Figure 3.1.4.1f) have observed data with a ratio of late- to early-time transmissivity less than 0.65. In fact, all three aquifer tests have late- to early-time transmissivity ratios greater than or equal to 1. Hence, our analysis of the data does not indicate the presence of sealing faults hindering groundwater flow in the vicinity of these three pumping tests located in northwestern Burleson County.

Figure 3.1.4.1g shows locations of aquifer pumping test wells color-coded based on their late- to early-time transmissivity ratio value and the location of faults identified as part of this study. All of the wells shown in this figure pump the Carrizo-Wilcox Aquifer. Figure 3.1.4.1g indicates that aquifer pumping tests are more likely to have a late- to early-time transmissivity ratio less than 0.85 if the test is located near the faults of the Milano Fault Zone identified by this study. The only such wells not within the Milano Fault Zone are those located close to faults of the updip Luling and/or Balcones Fault Zones. Wells not in a fault zone do not show a strong decrease in transmissivity with time.

To test the validity of this observation, a statistical analysis of the pattern of late- to early-time transmissivity ratios is presented in Table 3.1.4.1b. This table presents a statistical snapshot of late- to early-time transmissivity ratios for well groupings based on the radial distance between

Figure 3.1.4.1a. Location of wells with aquifer pumping test data and the faults identified by this study mapped to the numerical grid of the groundwater availability model for the central portion of the Carrizo-Wilcox, Queen City, and Sparta aquifers.

Note: ft = feet
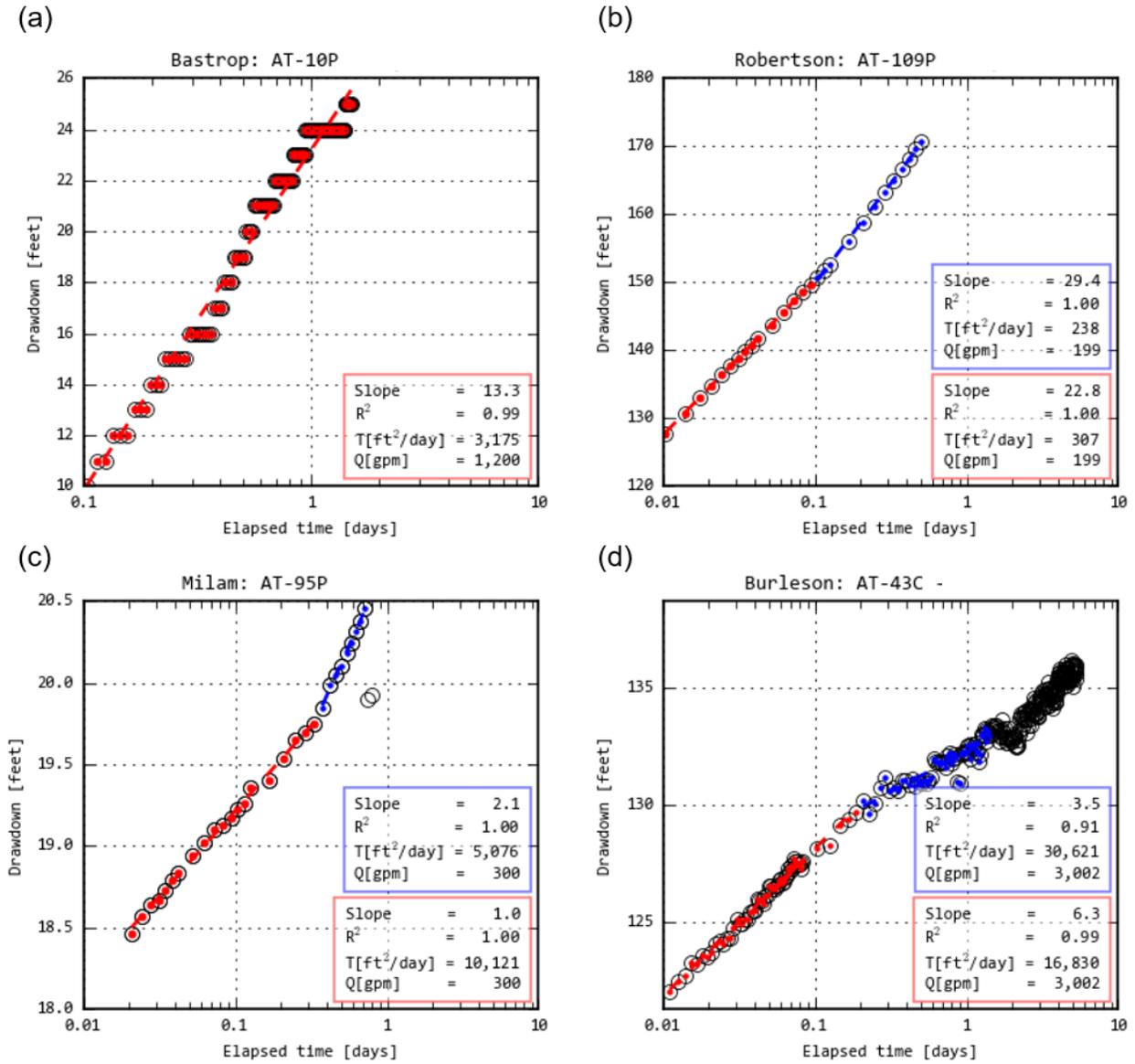
Figure 3.1.4.1b. **Four example applications of the Cooper-Jacob analysis to calculate transmissivity for aquifer test classified as (a) "no change," (b) "small decrease," (c) "large decrease," and (d) "increase" in calculated transmissivity values over time.**

Note: R^2 = coefficient of determination; T = transmissivity; ft^2/day = square feet per day; Q = flow rate of the aquifer test; gpm = gallons per minute
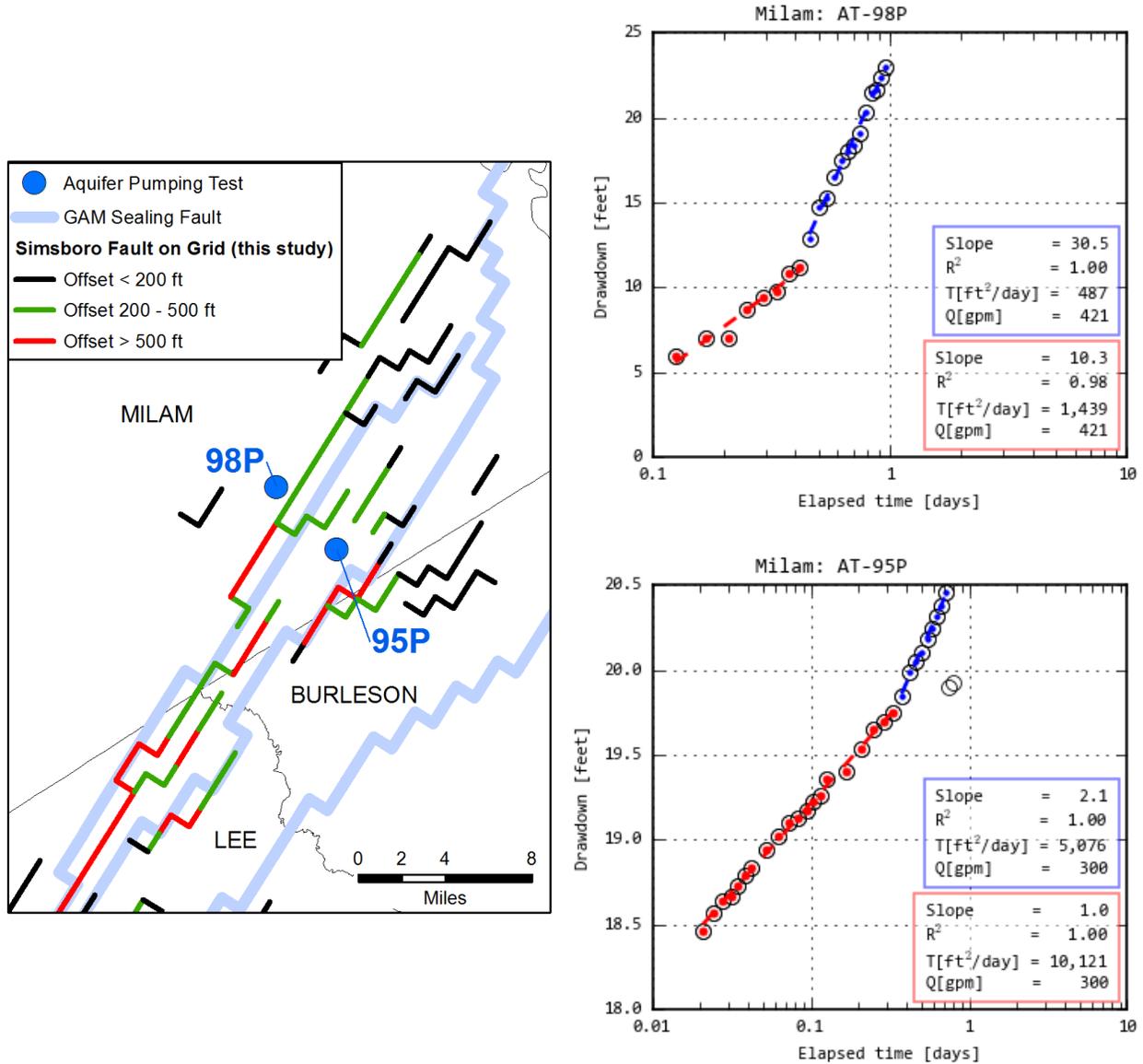
Figure 3.1.4.1c. **Location of aquifer pumping tests near faults in Milam County that produced a CJSL-calculated late-time transmissivity value less than the early-time transmissivity value, which provides a line of evidence that faults could be affecting groundwater flow. For aquifer tests AT-98P and AT-95P, the values for the late-to early-time transmissivity ratio are 0.33 and 0.50, respectively.**

Note: GAM = 2004 groundwater availability model; ft = feet, CSJL = Cooper-Jacob straight line; R^2 = coefficient of determination; T = transmissivity; ft²/day = square feet per day; Q = flow rate of the aquifer test; gpm = gallons per minute
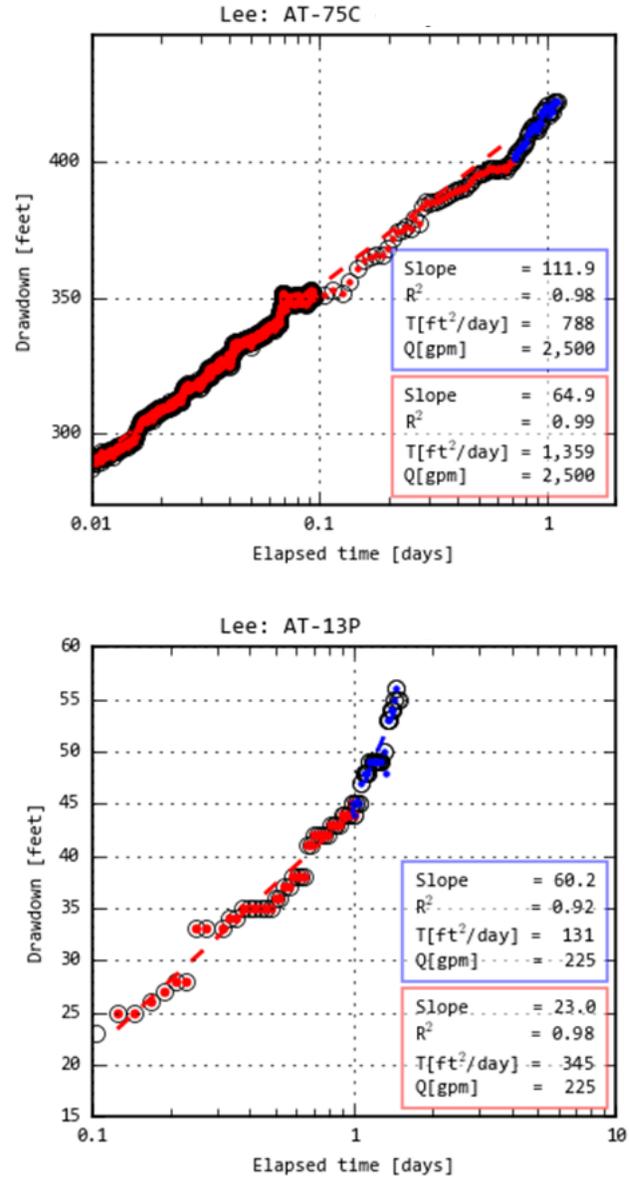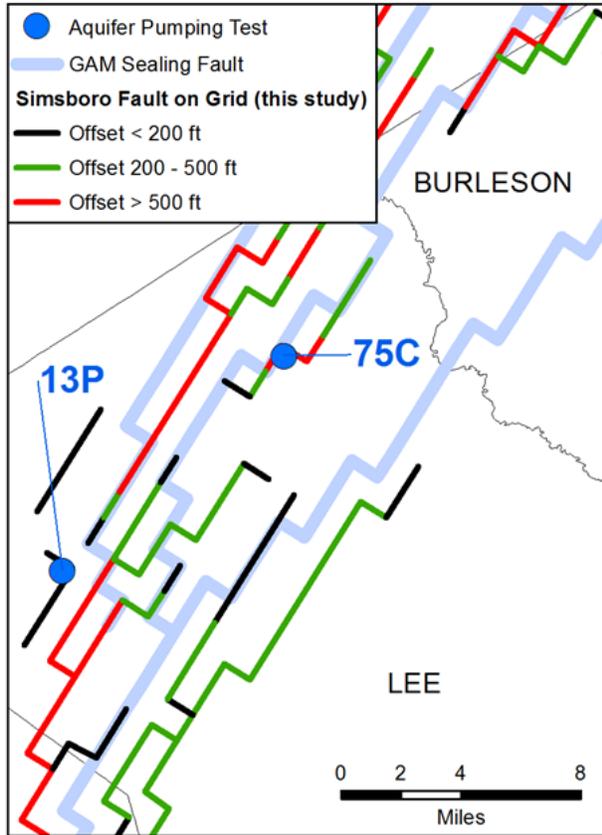
Figure 3.1.4.1d. **Location of aquifer pumping tests near faults in Lee County that produced a CJSL-calculated late-time transmissivity value less than the early-time transmissivity value, which provides a line of evidence that faults could be affecting groundwater flow. For aquifer tests AT-75C and AT-13P, the values for the late-to early-time transmissivity ratio are 0.58 and 0.38, respectively.**

Note: GAM = 2004 groundwater availability model; ft = feet, CSJL = Cooper-Jacob straight line; R^2 = coefficient of determination; T = transmissivity; ft^2/day = square feet per day; Q = flow rate of the aquifer test; gpm = gallons per minute
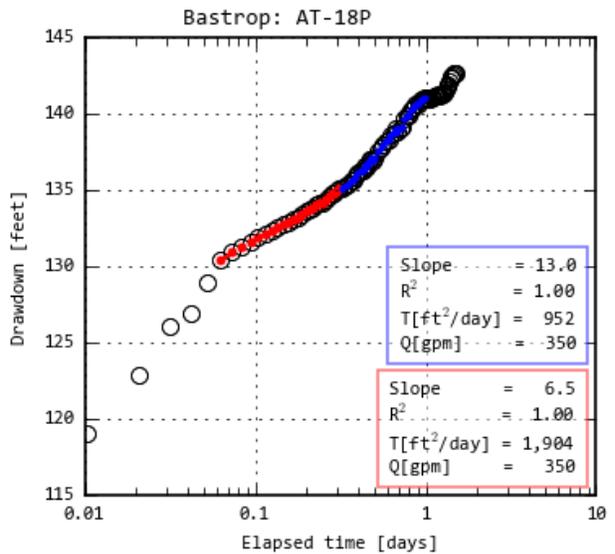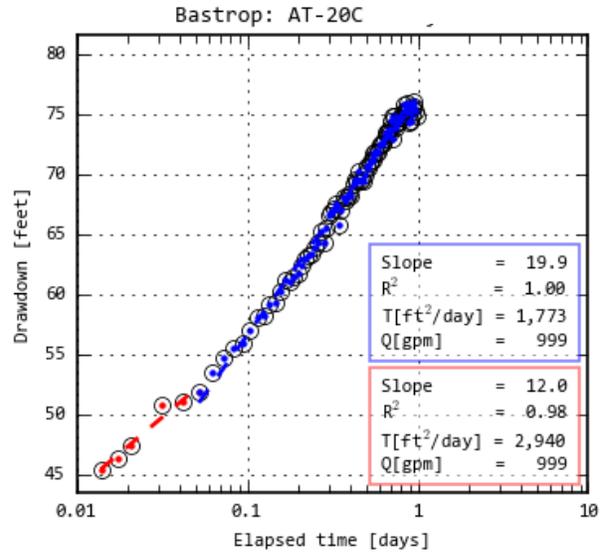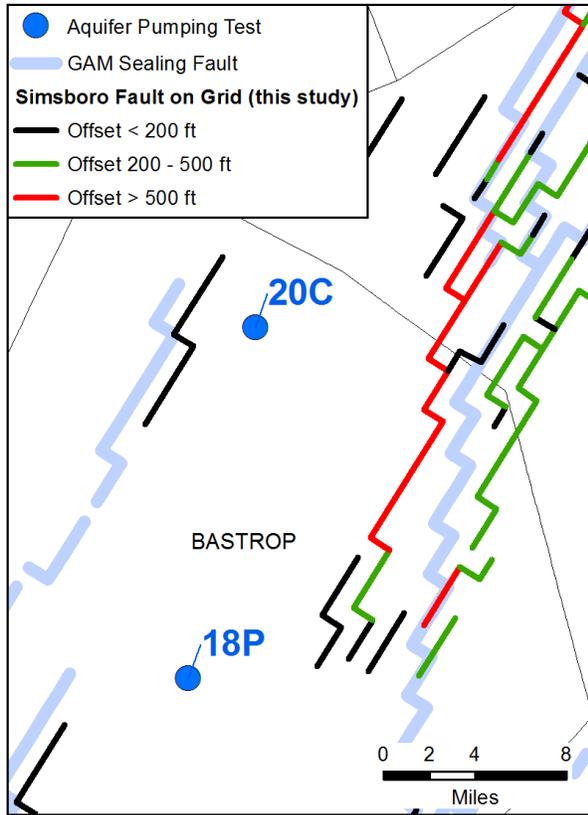
Figure 3.1.4.1e. Location of aquifer pumping tests near faults in Bastrop County that produced a CJSL-calculated late-time transmissivity value less than the early-time transmissivity value, which provides a line of evidence that faults could be affecting groundwater flow. For aquifer tests AT-20C and AT-18P, the values for the late-to early-time transmissivity ratio are 0.60 and 0.50, respectively.

Note: GAM = 2004 groundwater availability model; ft = feet, CSJL = Cooper-Jacob straight line; R^2 = coefficient of determination; T = transmissivity; ft^2/day = square feet per day; Q = flow rate of the aquifer test; gpm = gallons per minute
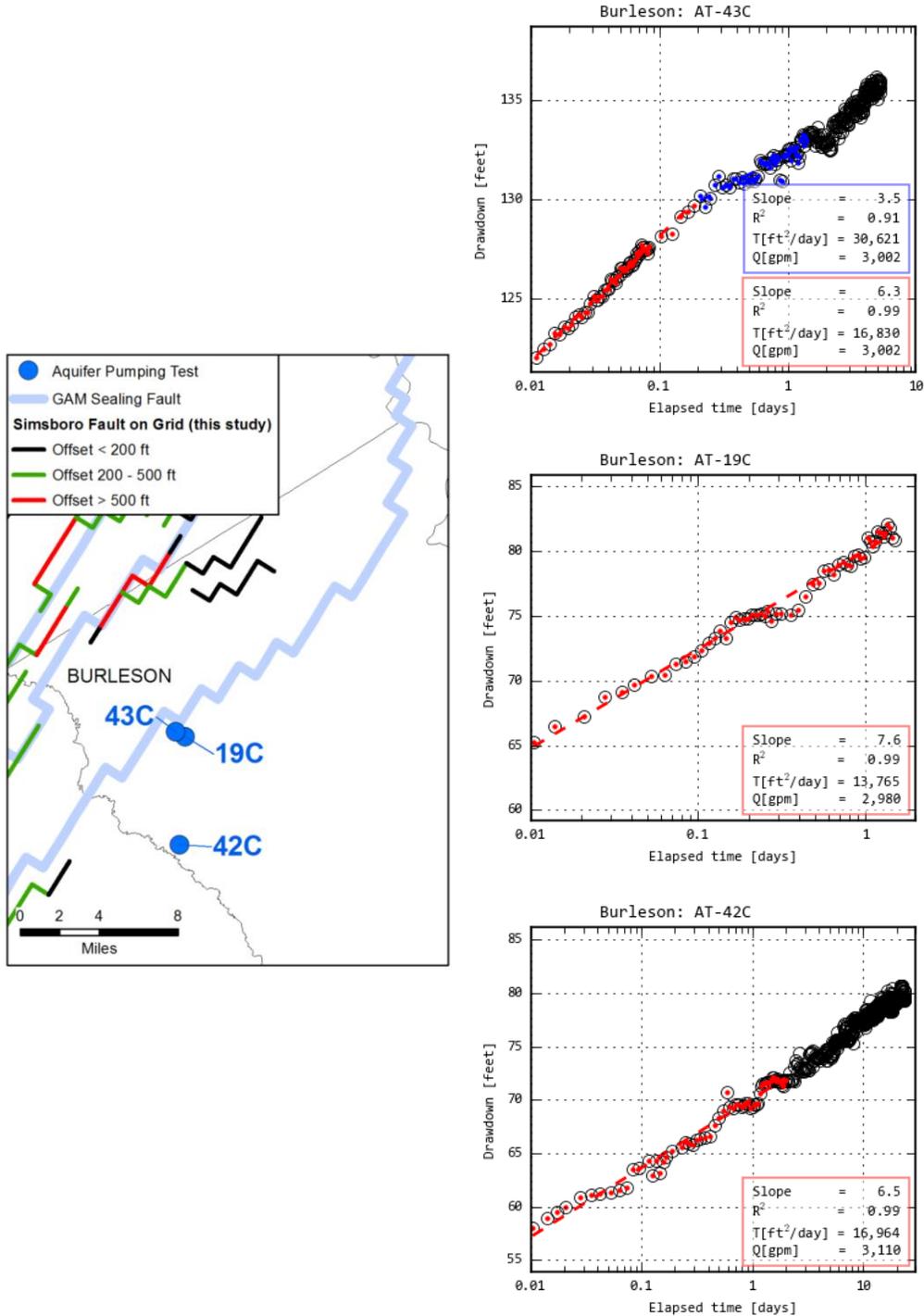
Figure 3.1.4.1f. **Location of aquifer pumping tests near faults in Burleson County that produced a CJSL-calculated late-time transmissivity value equal to or greater than the early-time transmissivity value, which provides little evidence that faults could be affecting groundwater flow. For aquifer tests AT-43C, AT-19C, and AT-42C, the values for the late- to early-time transmissivity ratio are 1.82, 1.0, and 1.0, respectively.**

Note: GAM = 2004 groundwater availability model; ft = feet, CSJL = Cooper-Jacob straight line; R^2 = coefficient of determination; T = transmissivity; ft²/day = square feet per day; Q = flow rate of the aquifer test; gpm = gallons per minute
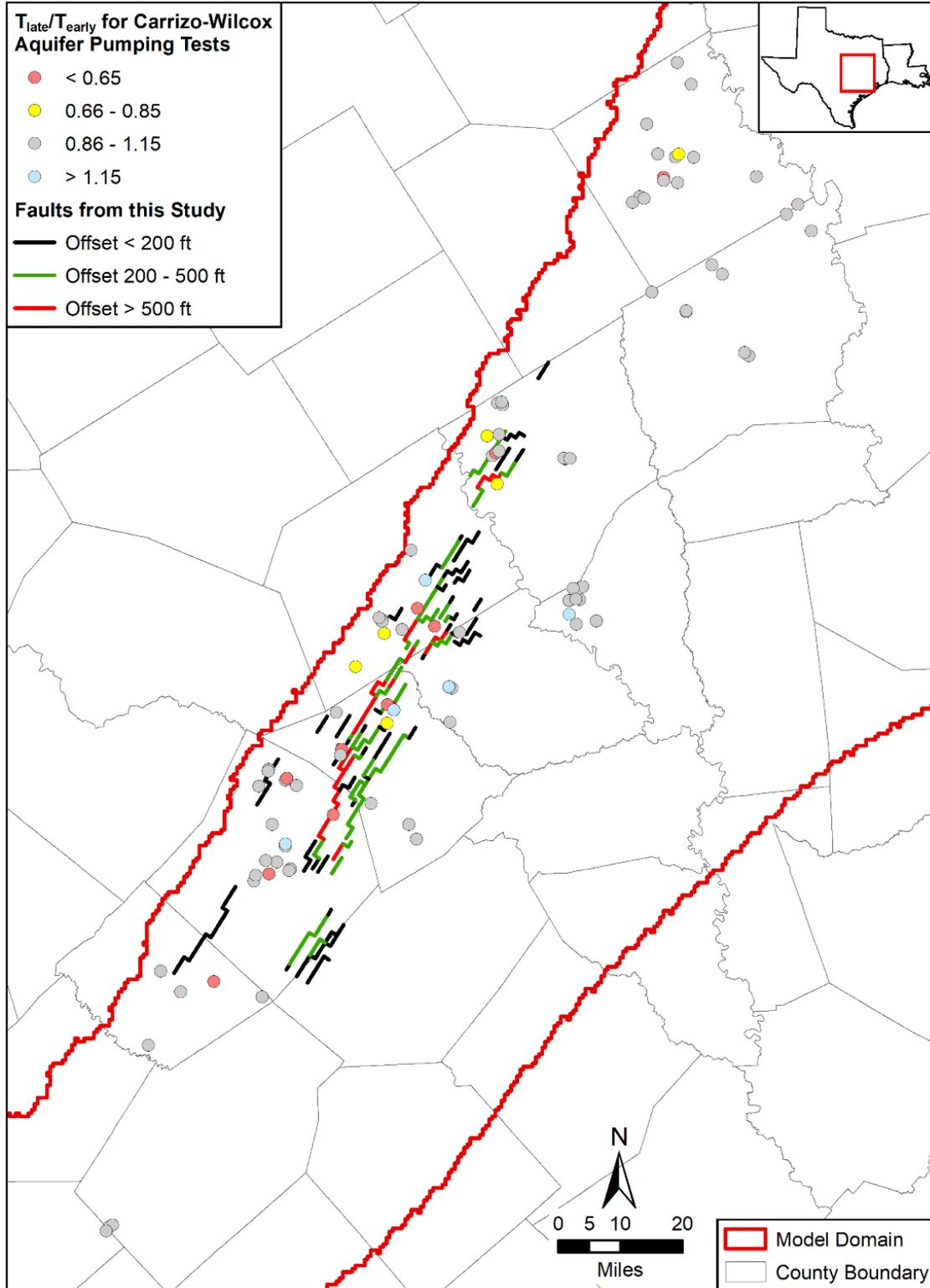
Figure 3.1.4.1g.   Spatial distribution of aquifer tests performed in the Carrizo-Wilcox Aquifer categorized based on the late-to early-time transmissivity ratio.

Note: T_{late} = late-time transmissivity; T_{early} = early-time transmissivity; ft = feet

3.1.4.2   Simulation of the Effects of Faults on the Drawdown Response During an Aquifer Pumping Test

To further demonstrate that low values of the late- to early-time transmissivity ratio are evidence that faults impede groundwater flow, groundwater modeling was performed to simulate several of the aquifer pumping tests. The Cooper-Jacob analysis was then used to interpret the simulated time-drawdown data. Simulated time-drawdown data were generated for seven of the aquifer pumping tests assuming (1) no faults and (2) the presence of the nearby mapped fault of the Milano Fault Zone as determined by this study. If the "fault" simulations produced time-drawdown data that mimicked the type of slope changes observed in the field data, then the modeling results strongly indicate that the low values of the late- to early-time transmissivity ratio are evidence that faults impede groundwater flow.

The groundwater modeling was performed using the analytical element code TTim (Bakker, 2013). TTim (Bakker, 2013) is a three-dimensional analytical element model capable of simulating groundwater flow through a multi-layer aquifer system that can contain simple inhomogeneities that can be approximated using cylinders and planes. For our application, TTim was used to determine whether the simulation of an aquifer test (using a relatively simple two-dimensional aquifer model of uniform transmissivity that contains the faults) could produce results similar to the observed drawdown response.

TTim simulations were performed to generate time-drawdown data for seven aquifer pumping tests (AT-95P, AT-73C, AT-76C, AT-112C, AT-105P, AT-43C, and AT-42C) using two assumptions for faults (no faults and the presence of faults). The locations of these tests are shown in Figure 3.1.4.2a. Each model simulation used the well screen length as the aquifer thickness, the transmissivity calculated from the aquifer pumping test provided in Appendix B, and the specific storage coefficient from the 2004 groundwater availability model for the central portion of the Carrizo-Wilcox, Queen City, and Sparta aquifers at the well location. The fault locations were those determined by this study (Figure 3.1.4.2a). The faults were represented using two values for conductance based on the vertical offset. Faults with an offset greater than 500 feet were assigned a conductance of 1×10^{-4} day^{-1}, and faults with an offset between 200 and 500 feet were assigned a conductance of 1×10^{-3} day^{-1}.

Appendix C shows the TTim simulated aquifer responses (time-drawdown data) and the transmissivity values calculated from the Cooper-Jacob analysis of these data. Table 3.1.4.2a compares the values for the late- to early-time transmissivity ratio calculated from the observed and TTim-generated drawdown data for these seven aquifer pumping tests. This table shows a favorable comparison between the late- to early-time transmissivity ratio for the observed and TTim-generated time-drawdown data. This favorable comparison confirms that the faults identified in this study are a primary cause of the low late- to early-time transmissivity ratio values calculated from the 113 aquifer pumping tests.

Table 3.1.4.2a. **Comparison of T_{late}/T_{early} values from Cooper-Jacob analysis of observed and TTim-generated time-drawdown data for seven aquifer pumping tests.**

Test ID	From Interpretation of Observed Data	From Interpretation of TTim-Generated Data Using This Study's Faults
	T_{late}/T_{early}	T_{late}/T_{early}
AT-95P	0.50	0.60
AT-73C	0.72	0.73
AT-76C	0.59	0.86
AT-112C	0.82	0.76
AT-105P	0.50	0.68
AT-43C	1.00	1.00
AT-42C	1.00	0.91

Note: ID = identification; T_{late} = late-time transmissivity; T_{early} = early-time transmissivity
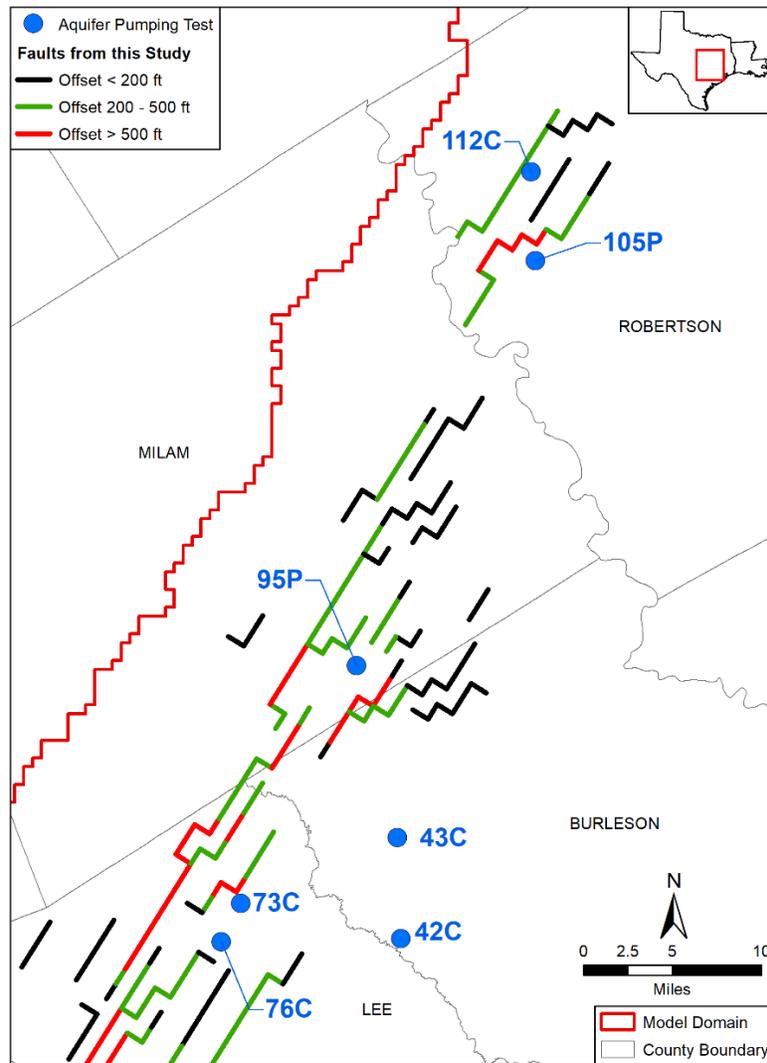
Figure 3.1.4.2a **Location of aquifer pumping tests for which TTim-generated time-drawdown data were analyzed using the Cooper-Jacob method.**

Note: ft = feet

3.1.5 Summary and Recommendations for the Milano Fault Zone

Several investigations were conducted to (1) characterize faults in the Milano Fault Zone and their effect on groundwater flow and (2) investigate the sensitivity of water levels simulated using the groundwater availability model to the conceptualization of faults in the Milano Fault Zone. The first study involved a geologic investigation of the Milano Fault Zone to map its associated faults. That investigation relied on several sources of information. The top surface of the Navarro Group was picked based on interpretation of 656 geophysical logs. Those picks, evaluated in conjunction with faults mapped at ground surface by Barnes (1970, 1979, 1981), were used to develop a network of faults in the Milano Fault Zone. Fault offsets were estimated through analysis of logs that intersect faults.

An important aspect of the geologic investigation was deconstruction of the Milano Fault Zone into four grabens and one complex (Figure 3.1.2g). These are named, from south to north, the Kovar Complex, the Paige Graben, the Tanglewood Graben, the Calvert Graben, and the South Kosse Graben. Cross-section(s) through each of the four grabens and the complex show the offset across faults for select stratigraphic picks including the top of the Simsboro and Navarro formations. The fault footprint resulting from this study is considerably smaller in Burleson and Robertson counties than the faults in the 2004 groundwater availability model and does not include several long continuous, sealing faults, some of which are 100 miles in length, in the 2004 groundwater availability model.

The reconceptualization of the fault zone into a series of connected grabens provides for "windows" and "gates" in the fault zone that allow groundwater to flow more freely perpendicular to the strike of the faults than does the conceptualization of faults in the 2004 groundwater availability model. In addition, the assessment indicates different vertical offsets, which were used to assign different conductance values to the faults. More groundwater flow is likely to occur in areas where fault offset is less and less likely to occur in areas where fault offset is greater.

Faults in the updated model differ significantly from the 2004 groundwater availability model in two areas. In northern Burleson County, the over 50-mile long fault segment in the 2004 groundwater availability model was removed because the geologic investigation conducted for this study does not support the presence of a fault in this area. Likewise, evidence of the single continuous fault that divides Robertson County in the 2004 groundwater availability model was not seen in our investigation, and this fault was also removed from the updated model.

Aquifer pumping test data were obtained from the Texas Commission on Environmental Quality and from hydrogeologic consulting reports. Our review of these data produced a dataset of 113 tests, of which 71 involved pumping of the Carrizo Aquifer, Simsboro Formation, or Hooper Formation. The Cooper-Jacobs Straight Line method was used to analyze the semi-log slope of the time-drawdown data for these tests to determine if the transmissivity of the aquifer changes with distance from the pumping well. The transmissivity based on the semi-log slope calculated at early time is called the early-time transmissivity and the transmissivity based on the semi-log slope calculated at late time is called the late-time transmissivity. For tests with two slopes, the value of the late- to early-time transmissivity ratio was considered a potentially useful indicator

of whether the aquifer transmissivity changes with distance from the well. If the analyses for tests in wells located near faults yield a late-time transmissivity value lower than the early-time transmissivity value, that provides a line of evidence that faults were affecting groundwater flow to the pumping well during the test.

A statistical analysis of the transmissivities interpreted from the aquifer pumping tests demonstrated that, the closer a well is located to one of the faults identified by this study, the more likely the aquifer pumping test data indicate a region of low transmissivity located near the well. For the 16 wells located within 4 miles of a fault from this study with an offset of 500 feet or more, 63 percent have a late-time transmissivity value that is lower than the early-time transmissivity value. For the 58 wells located more than 8 miles from a fault identified by this study with an offset of 500 feet or more, only 5 percent have a late-time transmissivity value that is lower than the early-time transmissivity value. These results demonstrate that the faults from this study with 500 feet of offset are affecting groundwater flow.

Modeling of the drawdown for aquifer pumping tests demonstrated that the conductance assigned to this study's faults based on vertical offset were justified and reasonable. Assignment of conductance values of 10^{-4} and 10^{-3} day^{-1} to faults based on a fault's offset produced simulated time-drawdown plots that were consistent and in good agreement with field results based on the assumptions and uncertainty associated with the model results.

Based on the findings from this study, the conceptualization of the Milano Fault Zone in the 2004 groundwater availability model for the central portion of the Carrizo-Wilcox, Queen City, and Sparta aquifers is not consistent with geologic and hydrogeologic conditions in the fault zone. In the 2004 groundwater availability model, faults are typically represented as long and continuous lines of sealing faults that extend across multiple counties. Our geological work does not support this conceptualization, nor do the results from our analysis and modeling of aquifer pumping tests. As a result of our investigation of faults, we recommended that the conceptualization of the Milano Fault Zone in the 2004 groundwater availability model be abandoned and an updated model be developed using the faults determined by this study. The TWDB agreed with this recommendation, resulting in an update of the groundwater availability model for the central portion of the Carrizo-Wilcox, Queen City, and Sparta aquifers with a revised representation of the Milano Fault Zone. This updated model with the new conceptualization of the Milano Fault Zone is commensurate with the lines of evidence identified by our investigations and will provide an improved groundwater management tool to serve the needs of the TWDB, Groundwater Management Area 12, the member districts of Groundwater Management Area 12, and the public good.

3.2   Historical Pumping

The 2004 groundwater availability model for the central portion of the Carrizo-Wilcox, Queen City, and Sparta aquifers (Kelley and others, 2004) was calibrated using water levels and historical pumping applied from 1980 through 1999. That model did not include a predevelopment steady-state solution. The updated model presented here includes a predevelopment steady-state solution followed by a transient solution from 1930 through 2010.

The historical pumping data prior to 1980 was developed using data and information from historical reports and data downloaded from the TWDB website (TWDB. 2016a). After 1980, the majority of the pumping data was obtained from the TWDB (2016a, 2016b). Additional pumping data were gathered by contacting groundwater conservation districts and municipalities. Pumping data were developed for the Carrizo-Wilcox, Queen City, and Sparta aquifers as well as the alluvium associated with the Colorado River. Development of historical pumping for many counties that overlap with the groundwater availability model for the southern portion of the Carrizo-Wilcox, Queen City, and Sparta aquifers was done by the Lost Pines Groundwater Conservation District (2017). These include Bexar, Caldwell, Gonzales, Guadalupe, Karnes, Lavaca, and Wilson counties.

Pumping for the Brazos River Alluvium Aquifer was taken from the well package for the groundwater availability model developed by Ewing and Jigmond (2016) for that aquifer. The conceptualization of pumping for the Brazos River Alluvium Aquifer can be found in Section 4.6.2 of Ewing and others (2016) and a description of the well package for the numerical model can be found in Section 2.4 of Ewing and Jigmond (2016).

Assigning pumping to the model grid cells was a two-part process. The first part was creation of a dataset of annual pumping by water user groups (for example, cities, water supply companies, industries, irrigation, livestock) and for rural domestic pumping. The second part was creation of a well dataset to guide the placement of pumping spatially as well as temporally. Integration of these two parts consisted of assigning the pumping to model grid cells, discussed in Section 3.2.4. Figure 3.2a is a flow chart showing the data sources and analyses used to assign historical pumping to the model grid.
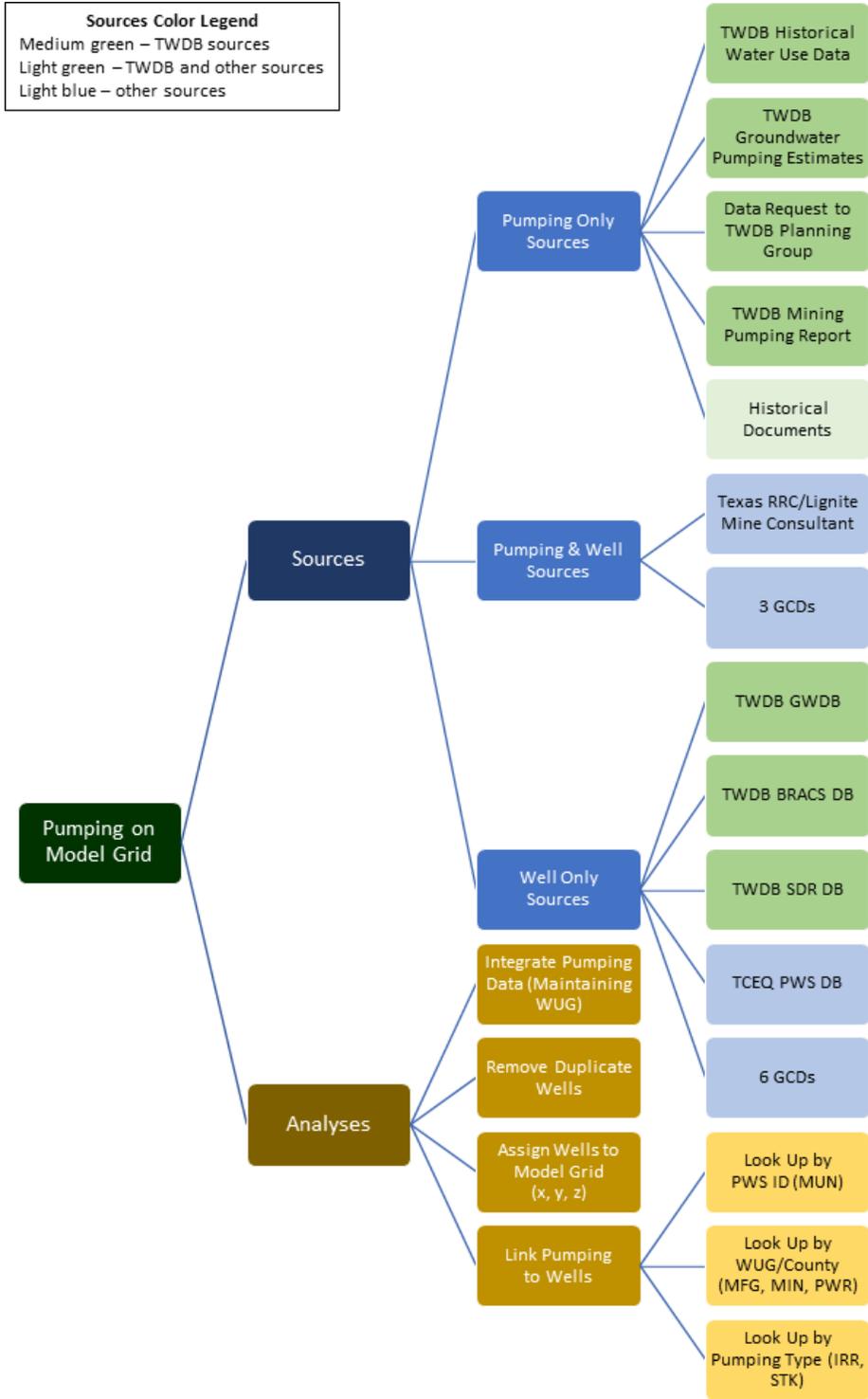
Figure 3.2a. Flow chart showing the data sources and analyses used to assign historical pumping to the model grid.

3.2.1 Development of Pumping Dataset

Development of the pumping dataset for municipal, manufacturing, mining, power, irrigation, and livestock water uses was based on the following objectives:

- Collect data from the start of aquifer development through 2010
- Develop pumping on an annual basis
- Collect and integrate data from all available sources
- Maintain water user group specific pumping data when available
- Include information to match pumping to wells

The sources reviewed in development of pumping for these water use types are described in Section 3.2.1.1. How the data from the various sources were used and integrated to develop pumping by use type is discussed in Section 3.2.1.2. Development of pumping for rural domestic use is described in Section 3.2.1.3.

3.2.1.1 Historical Pumping Data Sources

Updated historical pumping for municipal, manufacturing, mining, power, irrigation, and livestock uses was developed through review and integration of data from:

- Historical documents
- The TWDB website
- Lignite mining documents at the Texas Railroad Commission
- Groundwater conservation districts
- Select municipal water providers

Table 3.2.1.1a lists the data sources that provided the most useful information for developing a record of historical pumping.

Table 3.2.1.1a.   Summary of historical pumping data sources.

Source Type	Source Citation	Data Location	Data Period of Record	Aquifer(s)	Use Type(s)
Historical Report	Guyton & Associates (1970)	Angelina and Nacogdoches Counties	1935-1970	Carrizo-Wilcox	MUN, MFG
Historical Report	Turner (1938)	Brazos County	1911	Carrizo-Wilcox	MUN
Historical Report	Follett (1970)	Bastrop County	1942, 1955-1966	all	MUN (by city)
Historical Report	Follett (1970)	Bastrop County	1962-1966	all	MUN, MFG, IRR, combined RD and STK
Historical Report	Follett (1974)	Brazos and Burleson Counties	1958, 1963-1964, 1969	all, excluding GMA12	MUN, MFG, combined RD and STK
Historical Report	Follett (1974)	Brazos and Burleson Counties	1958, 1963-1964, 1969	GMA12	IRR

Final Report: Groundwater Availability Model for the Central Portion
of the Carrizo-Wilcox, Queen City, and Sparta Aquifers

Source Type	Source Citation	Data Location	Data Period of Record	Aquifer(s)	Use Type(s)
Historical Report	Follett (1974)	Brazos and Burleson Counties	1940-1970	all, excluding GMA12	MUN (by entity)
Historical Report	Thompson (1966)	Lee County	1963	all	MUN, IRR, RD, STK
Historical Report	Thompson (1966)	Lee County	1943, 1955-1963	all	MUN (by city), RD
Historical Report	Peckham (1965)	Leon County	1960	Carrizo-Wilcox	MUN (by city), IRR
Historical Report	Peckham (1965)	Leon County	1960	Queen City	MUN (by city)
Historical Report	Rettman (1987)	Limestone Cunty	1955, 1965, 1970, 1975, 1980	all	MUN, MFG, IRR, combined RD and STK
Historical Report	Rogers (1967)	Fayette County	1964	all	MUN, MFG, IRR, RD, STK
Historical Report	Rogers (1967)	Fayette County	1955-1964	all	MUN (by city)
Historical Report	Guyton & Associates (1972)	Anderson, Freestone, and Henderson Counties	1969	all	MUN, MFG, IRR, combined RD and STK
Historical Report	Baker and others (1974)	Grimes County	1970	GMA12	IRR
Historical Report	Tarver (1966)	Houston County	1955-1963	all	MUN (by entity)
Historical Report	Follett (1966)	Caldwell County	1961-1963	all	MUN, IRR, combined RD and STK
Historical Report	Shafer (1965)	Gonzales County	1962	Carrizo-Wilcox, Queen City and Sparta combined, other	MUN, IRR, RD, STK, MISC
Historical Report	Sundstrom and others (1948)	various counties of interest	1940-1943	all	MUN (by city)
Historical Report	Broadhurst and others (1950)	various counties of interest	1940-1945	all	MUN (by city)
Historical Report	Nicot and others (2011)	various counties of interest	2008-2010	all	MIN
Historical Report	TWDB (2001)	all counties of interest	1958, 1964, 1969, 1974, 1979, 1984, 1989, 1994, 2000	all	IRR

Final Report: Groundwater Availability Model for the Central Portion
of the Carrizo-Wilcox, Queen City, and Sparta Aquifers

| Source Type	Source Citation	Data Location	Data Period of Record	Aquifer(s)	Use Type(s)
GCD Correspondence	Day (2016)	Brazos and Robertson Counties	2008-2010	all	MUN, MFG, PWR
PWS Correspondence	Jones (2014) and Proske (2016)	Brazos and Lee Counties	1992-2005	Carrizo-Wilcox	MUN
TWDB Historical Water Use Estimates, Historical Surveyed Municipal Water Intake, by Water Planning Region	TWDB (2016a)	all counties of interest	1955-2010	all	MUN
TWDB Historical Water Use Estimates, Historical Surveyed Industrial Water Intake, by Water Planning Region	TWDB (2016a)	all counties of interest	1955-2010	all	MFG
TWDB Historical Groundwater Pumpage, Historical Groundwater Pumpage Estimates	TWDB (2016b)	all counties of interest	1980, 1984-2010	all	MUN, MFG, MIN, PWR, IRR, STK
TWDB Historical Groundwater Pumpage, Pumpage Detail, 2000 and Later	TWDB (2016b)	all counties of interest	2000-2010	all	MUN, MFG, MIN, PWR, IRR, STK
Surface Mining Records	na	Bastrop, Freestone, Lee, Leon, Milam, and Robertson Counties	1988-2010	Carrizo-Wilcox	MIN
Consultant Data	Harden and Associates (2016a)	Robertson	1993-1999	Carrizo-Wilcox	MIN
Historical Pumping for the Southern Counties	Lost Pines GCD (2017)	Bexar, Caldwell, Gonzales, Guadalupe, Karnes, Lavaca, and Wilson Counties)		all	MUN, MFG, MIN, PWR, IRR, STK
Model Well Package	Ewing and Jigmond (2016)	Brazos River Alluvium	1950 to 2010	Brazos River Alluvium	IRR

IRR = irrigation, MFG = manufacturing, MIN = mining, MISC = miscellaneous, MUN = municipal, PWR = power, RD = rural domestic, STK = livestock, GCD = groundwater conservation district

3.2.1.2 Historical Reports

The historical reports reviewed in development of the pumping dataset included:

- Public water supply surveys conducted by the United States Geological Survey in the 1940s, which provide:
    - Both specific and anecdotal information related to when suppliers began using groundwater for public supply purposes.
    - Measured or estimated pumping volumes for some public water suppliers for the year in which the supplier was surveyed by the authors.
- Investigations of water supplies conducted by predecessor agencies of the TWDB requested by a public water supplier.
    - These reports typically provide anecdotal information related to when the supplier began using groundwater.
- Investigations of groundwater resources by county conducted by the TWDB and its predecessor agencies, which
    - Typically provide estimates of pumping for select years, which is sometime aquifer and/or water use type specific.
    - Occasionally provide pumping for individual cities for select years.
- The TWDB irrigation surveys report, which provides groundwater used for irrigation purposes by county for select years.
- Estimates of water use by the mining and oil and gas industries for 2008 through 2010 by county developed by the University of Texas at Austin, Bureau of Economic Geology.

3.2.1.3 Texas Railroad Commission and Lignite Mine Consultant

Dewatering and depressurization pumping conducted in association with lignite mining was obtained from surface mining records at the Texas Railroad Commission and from Harden and Associates (2016a) (Table 3.2.1.3a). In general, individual wells used for depressurization pumping are identified in the records. At some mines, groundwater enters the open pits via flow from the Calvert Bluff Formation, resulting in the need to dewater the pits. Therefore, dewatering pumping actually occurs in the pits and not in wells. Because this water is sourced from the Calvert Bluff Formation, it was considered groundwater pumping in the updated model.

Table 3.2.1.3a.   Summary of lignite mine pumping sources.

Mine	Years		Source[a]
	Calvert Bluff Dewatering Pumping	Simsboro Depressurization Pumping	
Sandow	1993-2000	1988-2010	RRC and Harden
Three Oaks	none	2006-2010	RRC
Big Brown	2001-2010	2001-2010	RRC
Calvert (Walnut Creek)	none	2000-2010	RRC and Harden
Jewett[b]	2006-2010		RRC
Jewett E/F[b]	2004-2010		RRC

[a] RRC = Railroad Commission Surface Mining Records, Harden = R.W. Harden and Associates (2016a)
[b] pumping not distinguished between dewatering and depressurization; however, the majority of pumping was from the Calvert Bluff Formation for dewatering purposes

3.2.1.4   TWDB Data

The TWDB collects and generates annual water use estimates for application to water resource planning. Historical municipal and industrial water intake data by organization (that is, public water supplier, industry name) are available on the TWDB website through reports by regional water planning area (TWDB, 2016a). These data were downloaded for Regional Water Planning Areas C, Brazos (G), H, East Texas (I), K, South Central Texas (L), and P, all of which intersect the active boundary for the updated groundwater availability model for the central portion of the Carrizo-Wilcox, Queen City, and Sparta aquifers. These reports typically include data dating back to 1955. Only self-supplied groundwater intake data sourced by counties in the active model area were used in development of the pumping dataset.

Also available from the TWDB website are reports by county of historical groundwater pumping estimates (TWDB, 2016b). These reports include county-wide pumping estimates by water use types municipal, manufacturing, mining, power, irrigation, and livestock by aquifer for years 1980, 1984, and later, and include entity (or organization) specific pumping estimates for year 2000 and later. These reports were carefully reviewed and compiled to ensure inclusion of all available data without any duplication. Water user group-specific pumping was totaled by county and subtracted from the county-wide estimates by water use type to avoid duplicating pumping in the model.

3.2.1.5   Groundwater Conservation Districts and Public Water Providers

Metered pumping data were obtained from the Brazos Valley Groundwater Conservation District for the years 2008 through 2015 and from the Lost Pines Groundwater Conservation District for the years 2000 through 2010. Water use reporting data for the years 1998 through 2016 were obtained from the Gonzales County Underground Water Conservation District. These data provide well-specific pumping by year for predominately municipal wells but also some manufacturing, irrigation, livestock, and domestic wells. The well-specific data supplied by the Districts were included in development of the pumping dataset.

An effort was made to contact several of the large public water providers located in the active model area with the objectives of asking for:

- Their review of the data we obtained from the TWDB for consistency with their records.
- Data they had in additional to that obtained from the TWDB.

Correspondence consisted of calling the water supplier and following up with an email. Most suppliers did not respond; however, we talked with a few who reviewed the data we provided to them and provided us with additional data. Table 3.2.1.5a summarizes communication efforts with the water suppliers.

Table 3.2.1.5a.   Summary of communication efforts with municipal water suppliers.

County	Water Provider	INTERA Action	Provider Action
Bastrop	Aqua WSC	called and left message	no response
	City of Elgin	called and left message	no response
Brazos	City of Bryan	called and spoke with provider, and sent plot of pumping data	no response to email
	City of College Station	called and spoke with provider, and sent plot of pumping data	no response to email
	Texas A&M University	called and spoke with provider	provided pumping for 1992-1998 and 2005-2016 (Texas A&M University, 2016)
	Wellborn SUD	called and left message, and sent plot of pumping data	no response
	Wickson Creek SUD	called and left message	no response
Lee	Manville WSC	called and left message, and sent plot of pumping data	no response
	City of Giddings	called and spoke with provider, and sent plot of pumping data	provided total annual production for 1993 - 2015 (City of Giddings, 2016)
Limestone	Bristone Municipal WSD	called and spoke with provider, and set plot of pumping data	provided total annual production for 2005 - 2013 (Bristone Municipal WSD, 2016)
Madison	City of Madisonville	called and spoke with provider, and sent plot of pumping data	no response

3.2.2 Development of Pumping by Type

This section summarizes how the final pumping dataset was developed by pumping type. For years with no pumping data from any source, linear interpolation was used to calculate the pumping for those gap years. This method to fill gap years was used for all pumping types.

3.2.2.1 Municipal Pumping

Pre-1980. The sources of data for municipal pumping prior to 1980 were historical reports and historical surveyed municipal water intake data downloaded from the TWDB (TWDB, 2016a). Specific and anecdotal information in the historical reports provided a good estimate of the year in which pumping began for several public water suppliers. Municipal pumping estimates provided by county reports typically represent a combined value of pumping from all aquifers (Table 3.2.1.1a). To estimate how reported pumping was distributed among aquifers, we used the aquifer distribution split in municipal pumping for the year 1980, based on the TWDB historical groundwater pumpage data (TWDB, 2016b), for the year(s) with data in the county reports. Aquifer-specific pumping reported in a historical report was used when available. For years that had data in the county reports and data from the TWDB, the latter data were retained for the pumping dataset. For this reason, data from county reports for several counties, for example Freestone and Henderson counties, are not part of the dataset.

1980 through 2010. The source of data for municipal pumping from 1980 through 2010 were groundwater pumping estimates available from the TWDB website (TWDB, 2016a, 2016b). These data were integrated and consolidated, and entity-specific pumping estimates were subtracted from the county total to avoid duplication in the model. Pumping estimate data were

then compared to data received from groundwater conservation districts and water suppliers. The latter data were retained over the TWDB data in instances of duplicate water suppliers and years.

3.2.2.2 Manufacturing Pumping

Pre-1980. The sources of data for manufacturing pumping prior to 1980 were historical county reports on groundwater resources and historical surveyed industrial water intake data available from the TWDB (TWDB, 2016a). The historical county reports provide a county-wide estimate for manufacturing pumping for select years (Table 3.2.1.1a). To estimate how reported pumping was distributed among aquifers, we used the aquifer distribution split in manufacturing pumping for the year 1980, based on the TWDB historical groundwater pumpage data (TWDB, 2016b), for the year(s) with data in the county reports. For years that had data in the county reports and data from TWDB (2016a), the latter data were retained for the pumping dataset. For this reason, data from county reports for several counties are not part of the dataset.

1980 through 2010. The sources of data for manufacturing pumping from 1980 to 2010 were the TWDB historical groundwater pumpage data (TWDB, 2016a, b) and the Brazos Valley Groundwater Conservation District. The data from the two TWDB sources were consolidated, and duplicate pumping estimates were removed. In addition, entity-specific pumping was subtracted from county total pumping. The data from the Brazos Valley Groundwater Conservation District coincided with the TWDB data for some entities and years. In several instances, the data from the two sources differed, and the data from the Brazos Valley Groundwater Conservation District were retained for the pumping dataset.

3.2.2.3 Power Pumping

Pre-1980. The source of data for power pumping prior to 1980 was historical surveyed industrial water intake data available from the TWDB (TWDB, 2016a).

1980 through 2010. The sources of data for power pumping from 1980 to 2010 were the TWDB historical groundwater pumpage data (TWDB, 2016a, b) and the Brazos Valley Groundwater Conservation District. The data from the two TWDB sources were consolidated, duplicate pumping estimates were removed, and entity-specific pumping was subtracted from county total estimates. The data from the Brazos Valley Groundwater Conservation District coincided with the TWDB data for some entities and years. In several instances, the data from the two sources differed, and the data from the Brazos Valley Groundwater Conservation District were retained for the pumping dataset.

3.2.2.4 Mining Pumping

Pre-1980. The source of data for mining pumping prior to 1990 was historical surveyed industrial water intake data available from the TWDB (TWDB, 2016a). The water intake data for industrial use indicate that the water is used for "sand" or "metal ore" mining for several entities. In development of the dataset, this pumping was assumed to fall under the mining category rather than the manufacturing category.

1980 through 2010. The sources of data for mining pumping from 1980 to 2010 were Nicot and others' (2011) historical report on pumping related to mining in the oil and gas industry, the TWDB (2016a, b) historical groundwater pumpage data, Texas Railroad Commission files, and

Harden and Associates (2016a). Data from the TWDB were consolidated, duplicate pumping estimates were removed, and entity-specific pumping estimates were subtracted from county totals.

Nicot and others (2011) provide county-wide estimates for the split between use of surface water and groundwater for mining purposes, as well as county-wide estimates of water use for several mining types. For most mining types, Nicot and others (2011) provide a value for 2008 and projected values for 2010, 2020, 2030, 2040, 2050, and 2060.

Table 3.2.2.4a summarizes the mining types and years for which Nicot and others (2011) provide water use estimates. Water use values for 2008 and 2010 were multiplied by the groundwater/surface water split values (Nicot and others, 2011) to estimate groundwater pumping for mining purposes for these two years. For counties with no groundwater/surface water split, all water use for mining was assumed to be sourced by groundwater. To estimate mining pumping for 2009, the 2008 and 2010 values were averaged. Although Nicot and others (2011) provide an estimate of fresh-water use for enhanced oil recovery operations in 1995, those data were not considered in development of mining pumping. Instead, aquifer-specific estimates of mining pumping in 1995 available from the TWDB were used.

Table 3.2.2.4a.   **Summary of mining data obtained from Nicot and others (2011).**

Mining Type[a]	Years with Water Use Data[b]	Nicot and others (2011) Table(s) Number
Tight Formation Completion	2008	14
Fresh-Water Use in Enhanced Oil Recovery Operations	1995	16
Fresh-Water Use for Waterfloods	2008 & 2010	22
	2010	63
Drilling Water Use	2008	25
Crushed-Stone and Sand & Gravel Water Use	2008	37
Crushed-Stone Water Use	2008 & 2010	67
Sand and Gravel Water Use	2008 & 2010	68
Industrial Sand-Water Consumption	2010	38 & 70
Water Use in the Eagle Ford Shale	2010	55
Water Use in East Texas Tight-Gas Plays	2010	59
Water Use in the South Gulf Coast Basin Tight-Gas Plays	2010	61
Freshwater Use for Drilling	2010	64
Freshwater Pumping for Lignite-Mine Water Use	2010	65
Total Mining Water Use	2008	73
Total Mining Water Use	2010	74

[a] Table lists only types found in the counties within the active model area
[b] 2010 values are Nicot and others (2011) projected values

Estimates of well-specific groundwater pumping from the Simsboro Formation of the Wilcox Aquifer for lignite mining purposes are available from the Texas Railroad Commission and were also obtained from a consultant that has worked for the Sandow and Calvert (Walnut Creek) mines (Harden and Associates, 2016a). The Texas Railroad Commission and Harden and Associates (2016) also provide estimates of dewatering pumping from lignite-mine pits for specified pit areas. The source of water to the pits is the Calvert Bluff Formation of the Wilcox Aquifer. Therefore, this pumping was assumed to be groundwater pumping for the purposes of the model.

Except for pumping associated with lignite mining, TWDB estimates of pumping for mining purposes were used for the years 1980 through 2007. A comparison of the historical pumping estimates from the TWDB for years 2008 through 2010 and the estimated groundwater pumping based on data in Nicot and others (2011) showed the two to be consistent in most instances, and the estimates based on the data in Nicot and others (2011) were retained in the pumping dataset. For counties with lignite mining, only the estimates of pumping for other mining purposes were taken from Nicot and others (2011), and the lignite mining pumping was taken from the Texas Railroad Commission and Harden and Associates (2016a) data. If data from the TWDB were for a specific aquifer, those data where used for these three years rather than the estimates from Nicot and others (2011).

3.2.2.5   Irrigation Pumping

Pre-1980. The sources of data for irrigation pumping prior to 1980 were historical county reports on groundwater resources and the TWDB (2001) irrigation survey report. The county, years and aquifers for which these data are available can be found in Table 3.2.1.1a. In the county report, irrigation pumping is specific to an aquifer(s) for some counties and represents the total for all aquifers in other counties. To estimate irrigation pumping by aquifer in the latter counties, we used the aquifer distribution split in irrigation pumping for the year 1980, based on the TWDB historical groundwater pumpage data (TWDB, 2016b).

The TWDB irrigation survey report provides the volume of irrigation water supplied by groundwater for every county in the state but does not specify the aquifer. TWDB (2001) also includes the volume of irrigation water supplied by combined groundwater and surface water sources along with the percentage from surface water. Using this information, the amount of the combined source supplied by groundwater was calculated. The split in irrigation pumping by aquifer in 1980 based on the TWDB (2016b) data was also used to estimate the distribution of irrigation pumping from TWDB (2001) between the aquifers in the county.

TWDB (2001) provides estimates of pumping for irrigation purposes for about 5-year increments from 1958 through 1979. When data were available from a county report for the same year, the data from the county report was retained in the pumping dataset. After merging irrigation pumping from all historical reports for all available years, irrigation pumping was assumed to change linearly between years with data.

1980 through 2010. The sources of data for irrigation pumping from 1980 to 2010 were the TWDB historical groundwater pumpage data (TWDB, 2016b), the TWDB (2001) irrigation survey report, and data from the Brazos Valley and Lost Pines groundwater conservation districts

and the Gonzales County Underground Water Conservation District. The data from TWDB (2016b) consists of county-wide estimates by aquifer, while the groundwater conservation district data are well-specific. For years with data from both TWDB (2016b) and a groundwater conservation district, the sum of the well-specific data from the District was subtracted from the county total in TWDB (2016b) to avoid double assignment of irrigation pumping. The irrigation pumping estimates from TWDB (2001) and TWDB (2016b) were compared and the source with the highest values was used for the pumping dataset. The values in the irrigation survey report (TWDB, 2001), which are available for years 1984, 1989, 1994, and 2000, are greater than those in the historical groundwater pumping data (TWDB, 2016b) only for Caldwell County.

3.2.2.6 Livestock Pumping

Pre-1980. The sources of data for livestock pumping prior to 1980 were historical county reports on groundwater resources. The counties, years, and aquifers for which these data are available can be found in Table 3.2.1.1a. The livestock pumping in the county reports is combined for all aquifers. To estimate livestock pumping by aquifer in these counties, the split in livestock pumping between aquifers in the year 1980 from the historical groundwater pumpage data provided by TWDB (2016b) was assumed.

1980 through 2010. The sources of data for livestock pumping from 1980 to 2010 are the TWDB historical groundwater pumping data (TWDB, 2016b) and data from the Gonzales County Underground Water Conservation District. The data from TWDB (2016b) consists of county-wide estimates by aquifer, while the District data are well-specific. For years with data from both TWDB (2016b) and the Gonzales County Underground Water Conservation District, the sum of the well-specific data from the District was subtracted from the county total in TWDB (2016b) to avoid double assignment of irrigation pumping.

3.2.2.7 Pumping Data Summary for the Carrizo-Wilcox, Queen City, and Sparta Aquifers

Figures 3.2.2.7a through 3.2.2.7g show bar charts of combined pumping from the Carrizo-Wilcox, Queen City, and Sparta aquifers, as reported by the pumping source, by type for the counties in Groundwater Management Area 12. On these charts, umping is summed for 10-year intervals from 1930 through 1949 and 5-year intervals for 1950 through 2010. Similar charts for all other counties in the model can be found in Appendix D. Total pumping for all Groundwater Management Area 12 counties is shown in Figure 3.2.2.7h. Tables 3.2.2.7a through 3.2.2.7g provide total, municipal, manufacturing, mining, power, irrigation, and livestock pumping, respectively, for the combined Carrizo-Wilcox, Queen City, and Sparta aquifers, as reported by the pumping source, for years 1980, 1985, 1990, 1995, 2000, 2005, and 2010. A similar table for rural domestic pumping, which is discussed in Section 3.2.4.1 and included in the total pumping table, is provided in Table 3.2.2.7h.

Table 3.2.2.7a.   Summary of combined total pumping in acre-feet from the Carrizo-Wilcox, Queen City, and Sparta aquifers by county for the years 1980, 1985, 1990, 1995, 2000, 2005, and 2010.

County	1980	1985	1990	1995	2000	2005	2010
Anderson	7,132	7,983	8,315	10,217	12,525	11,427	11,561
Angelina	29,661	28,311	23,509	22,050	25,330	13,659	11,019
Bastrop	7,838	7,604	8,992	9,844	12,510	13,938	19,836
Bexar	4,825	2,699	3,431	5,254	2,746	1,326	1,967
Brazos	21,674	24,571	25,248	26,959	31,941	46,252	41,321
Burleson	2,110	2,431	2,241	2,582	3,288	3,249	3,154
Caldwell	2,679	2,847	3,387	3,065	3,459	1,983	2,842
Cherokee	8,349	8,212	8,803	9,033	9,464	9,273	9,782
Falls	175	160	145	83	80	37	514
Fayette	166	101	95	165	137	194	179
Freestone	3,100	3,419	3,370	3,735	4,499	7,323	5,795
Gonzales	4,468	3,000	4,996	3,191	7,376	9,539	11,889
Grimes	2	2	4	6	6	6	11
Guadalupe	2,637	2,666	2,901	2,274	2,312	2,750	2,976
Henderson	5,425	7,237	6,796	7,043	8,207	8,136	8,615
Houston	2,131	2,502	2,301	2,439	2,928	2,613	2,865
Karnes	350	421	500	278	54	42	107
Lee	2,953	3,312	3,818	8,632	13,830	14,646	11,757
Leon	3,152	4,308	4,566	5,540	5,578	4,897	5,167
Limestone	1,304	1,983	4,885	4,114	4,301	3,964	2,520
Madison	1,982	2,473	2,229	2,102	2,654	2,518	3,162
Milam	4,719	5,150	16,000	29,823	27,154	29,026	13,708
Nacogdoches	8,939	9,067	10,036	12,001	10,276	10,127	8,328
Navarro	46	118	112	110	61	64	130
Robertson	5,860	5,469	7,331	16,587	17,548	18,854	21,194
Rusk	383	383	276	239	250	263	269
Sabine	33	0	29	52	87	157	0
San Augustine	205	178	198	193	231	259	215
Smith	2,946	6,850	6,369	7,587	9,194	10,078	11,125
Van Zandt	885	1,008	1,194	1,199	1,272	1,601	1,497
Walker	0	0	0	0	26	19	26
Washington	0	0	0	0	0	0	0
Williamson	33	36	40	52	77	103	231
Wilson	10,565	10,724	17,005	15,013	22,408	21,549	22,258
Total	**146,725**	**155,226**	**179,119**	**211,463**	**241,809**	**249,870**	**236,017**

Table 3.2.2.7b. **Summary of combined municipal pumping in acre-feet from the Carrizo-Wilcox, Queen City, and Sparta aquifers by county for the years 1980, 1985, 1990, 1995, 2000, 2005, and 2010.**

County	1980	1985	1990	1995	2000	2005	2010
Anderson	3,426	4,891	5,511	6,993	9,485	9,299	9,176
Angelina	8,544	8,596	8,622	9,304	13,118	12,992	10,954
Bastrop	3,963	5,531	6,635	7,154	9,195	11,012	10,843
Bexar	814	779	886	1,061	1,150	35	734
Brazos	20,694	23,679	24,983	26,684	31,683	41,593	36,902
Burleson	1,486	1,825	1,638	1,866	2,435	2,421	2,270
Caldwell	2,061	2,199	2,271	2,217	2,568	1,017	1,424
Cherokee	5,284	5,075	5,215	5,843	6,659	6,917	7,307
Falls	96	67	63	0	0	0	476
Fayette	62	38	59	110	41	20	76
Freestone	1,755	1,885	1,926	2,212	2,986	2,851	2,434
Gonzales	1,658	1,392	2,146	1,983	3,014	3,004	3,804
Grimes	2	2	4	6	6	6	11
Guadalupe	538	553	413	1,086	1,054	1,154	948
Henderson	2,926	3,893	3,559	4,064	5,317	5,411	6,042
Houston	1,375	1,548	1,355	1,432	1,527	1,628	2,227
Karnes	71	90	224	123	30	42	0
Lee	1,891	2,508	2,850	2,831	3,419	3,576	4,706
Leon	1,408	1,816	1,976	1,820	2,475	2,791	2,784
Limestone	550	454	1,393	1,452	2,210	2,327	808
Madison	1,715	2,068	1,905	1,675	2,173	2,217	2,670
Milam	2,656	2,513	2,760	2,723	3,560	3,683	3,917
Navarro	6,762	6,972	7,573	8,663	7,805	8,097	6,230
Nacogdoches	7	11	11	0	0	0	56
Robertson	3,007	2,491	2,728	2,770	3,145	3,043	3,027
Rusk	76	124	142	114	133	155	170
Sabine	25	0	29	52	87	157	
San Augustine	105	68	78	72	108	134	88
Smith	2,693	6,572	6,065	7,294	8,911	9,805	10,861
Van Zandt	352	422	555	480	474	722	538
Walker	0	0	0	0	0	0	0
Washington	0	0	0	0	0	0	0
Williamson	0	0	0	0	8	11	116
Wilson	2,504	2,944	3,775	4,084	4,884	5,737	6,092
Total	**78,508**	**91,007**	**97,348**	**106,168**	**129,659**	**141,858**	**137,692**

Table 3.2.2.7c. **Summary of combined manufacturing pumping in acre-feet from the Carrizo-Wilcox, Queen City, and Sparta aquifers by county for the years 1980, 1985, 1990, 1995, 2000, 2005, and 2010.**

County	1980	1985	1990	1995	2000	2005	2010
Anderson	350	303	0	25	340	0	0
Angelina	20,666	19,289	14,760	12,582	12,015	610	0
Bastrop	152	128	65	65	87	51	68
Bexar	0	0	0	0	0	0	0
Brazos	7	9	0	15	14	4,051	3,035
Burleson	82	93	96	97	110	111	111
Caldwell	1	1	0	1	1	0	182
Cherokee	414	337	468	133	132	124	121
Falls	0	0	0	0	0	0	0
Fayette	0	0	0	0	0	0	33
Freestone	18	19	20	0	0	0	0
Gonzales	0	0	0	167	1,024	836	604
Grimes	0	0	0	0	0	0	0
Guadalupe	19	0	173	0	0	3	0
Henderson	266	597	351	444	374	574	364
Houston	0	4	0	0	0	0	0
Karnes	221	220	120	5	3	0	0
Lee	0	0	0	0	0	0	0
Leon	161	162	162	278	545	766	544
Limestone	0	2	0	0	0	0	642
Madison	0	69	70	148	183	204	201
Milam	0	88	0	0	0	0	0
Navarro	0	0	0	0	0	0	0
Nacogdoches	0	0	0	0	0	0	0
Robertson	28	14	24	18	8	25	51
Rusk	195	135	0	0	0	0	0
Sabine	8	0	0	0	0	0	0
San Augustine	0	0	0	0	0	0	0
Smith	0	0	0	0	0	0	0
Van Zandt	0	0	0	0	0	0	0
Walker	0	0	0	0	0	0	0
Washington	0	0	0	0	0	0	0
Williamson	0	0	0	0	0	0	0
Wilson	175	141	42	0	5	5	37
Total	**22,763**	**21,615**	**16,351**	**13,977**	**14,843**	**7,358**	**5,994**

Table 3.2.2.7d. **Summary of combined mining pumping in acre-feet from the Carrizo-Wilcox, Queen City, and Sparta aquifers by county for the years 1980, 1985, 1990, 1995, 2000, 2005, and 2010.**

County	1980	1985	1990	1995	2000	2005	2010
Anderson	1,345	405	303	430	0	0	0
Angelina	0	0	0	22	0	0	0
Bastrop	0	10	11	22	0	0	239
Bexar	0	207	147	168	0	0	0
Brazos	115	24	21	25	13	5	1
Burleson	0	0	0	0	0	0	0
Caldwell	0	21	21	10	0	0	0
Cherokee	81	120	53	81	0	0	0
Falls	0	0	0	0	0	0	0
Fayette	0	0	0	0	0	0	0
Freestone	0	16	16	30	7	3,338	2,097
Gonzales	0	18	22	15	0	0	0
Grimes	0	0	0	0	0	0	0
Guadalupe	0	14	8	157	0	0	0
Henderson	39	309	97	31	0	0	0
Houston	0	33	27	37	0	0	0
Karnes	1	65	110	128	0	0	0
Lee	2	8	15	4,471	9,010	9,552	4,625
Leon	26	85	146	1,005	164	91	812
Limestone	398	333	366	807	645	642	0
Madison	0	0	0	0	0	0	0
Milam	968	1,252	11,932	25,553	22,020	21,846	7,681
Navarro	0	0	0	0	0	0	0
Nacogdoches	0	63	56	59	0	0	0
Robertson	0	24	20	8,399	7,905	7,659	7,438
Rusk	0	0	0	0	0	0	0
Sabine	0	0	0	0	0	0	0
San Augustine	0	0	0	0	0	0	0
Smith	0	0	0	0	0	0	0
Van Zandt	0	0	0	0	0	0	0
Walker	0	0	0	0	0	0	0
Washington	0	0	0	0	0	0	0
Williamson	0	0	0	0	0	0	0
Wilson	228	309	281	277	0	0	0
Total	**3,203**	**3,316**	**13,651**	**41,727**	**39,764**	**43,133**	**22,893**

Table 3.2.2.7e. **Summary of combined power pumping in acre-feet from the Carrizo-Wilcox, Queen City, and Sparta aquifers by county for the years 1980, 1985, 1990, 1995, 2000, 2005, and 2010.**

County	1980	1985	1990	1995	2000	2005	2010
Anderson	0	0	0	0	0	0	0
Angelina	0	0	0	0	0	0	0
Bastrop	0	0	0	0	0	0	0
Bexar	0	0	0	0	0	0	0
Brazos	755	641	58	89	58	177	69
Burleson	0	0	0	0	0	0	0
Caldwell	0	0	0	0	0	0	0
Cherokee	333	218	343	133	132	124	121
Falls	0	0	0	0	0	0	0
Fayette	0	0	0	0	0	0	0
Freestone	101	144	163	105	91	110	135
Gonzales	0	0	0	0	0	0	0
Grimes	0	0	0	0	0	0	0
Guadalupe	0	0	0	0	0	0	0
Henderson	0	0	0	1	0	0	0
Houston	0	0	0	0	0	0	0
Karnes	0	0	0	0	0	0	0
Lee	0	0	0	0	0	0	0
Leon	0	0	0	0	0	0	0
Limestone	0	779	2,584	1,425	1,014	649	711
Madison	0	0	0	0	0	0	0
Milam	0	0	0	0	0	0	0
Navarro	0	0	0	0	0	0	0
Nacogdoches	0	0	0	0	0	0	0
Robertson	0	0	1,528	3,346	4,458	3,620	5,059
Rusk	0	0	0	0	0	0	0
Sabine	0	0	0	0	0	0	0
San Augustine	0	0	0	0	0	0	0
Smith	0	0	0	0	0	0	0
Van Zandt	0	0	0	0	0	0	0
Walker	0	0	0	0	0	0	0
Washington	0	0	0	0	0	0	0
Williamson	0	0	0	0	0	0	0
Wilson	0	0	0	0	0	0	0
Total	**1,189**	**1,783**	**4,676**	**5,098**	**5,752**	**4,681**	**6,095**

Table 3.2.2.7f. **Summary of combined irrigation pumping in acre-feet from the Carrizo-Wilcox, Queen City, and Sparta aquifers by county for the years 1980, 1985, 1990, 1995, 2000, 2005, and 2010.**

County	1980	1985	1990	1995	2000	2005	2010
Anderson	23	125	23	183	96	56	259
Angelina	372	297	0	0	0	0	0
Bastrop	1,474	103	317	443	886	620	6,299
Bexar	3,385	1,018	1,644	3,358	1,004	798	766
Brazos	0	0	0	0	53	265	1,180
Burleson	0	0	0	0	110	126	139
Caldwell	50	130	554	220	183	156	373
Cherokee	50	72	100	29	31	50	193
Falls	0	0	0	0	0	0	0
Fayette	89	51	24	41	83	150	42
Freestone	0	100	25	17	20	35	216
Gonzales	600	940	2,125	241	1,880	2,661	4,685
Grimes	0	0	0	0	0	0	0
Guadalupe	1,249	1,251	1,376	6	157	144	250
Henderson	100	70	21	20	14	41	133
Houston	0	24	39	125	576	496	144
Karnes	0	0	0	0	0	0	107
Lee	250	53	156	336	545	520	1,625
Leon	53	69	183	362	542	285	31
Limestone	0	0	0	0	0	0	0
Madison	22	18	16	18	11	7	211
Milam	7	30	54	261	334	2,376	960
Navarro	0	39	140	1,016	186	206	141
Nacogdoches	0	0	0	0	0	0	0
Robertson	1,700	1,638	1,807	602	816	3,380	4,311
Rusk	0	0	0	0	0	0	0
Sabine	0	0	0	0	0	0	0
San Augustine	0	0	0	0	0	0	0
Smith	0	0	0	0	0	0	0
Van Zandt	0	0	0	0	0	0	0
Walker	0	0	0	0	0	0	0
Washington	0	0	0	0	0	0	0
Williamson	0	0	0	0	0	0	0
Wilson	6,499	6,174	11,642	9,300	16,171	13,727	13,553
Total	**15,922**	**12,202**	**20,246**	**16,578**	**23,697**	**26,099**	**35,618**

Table 3.2.2.7g. **Summary of combined livestock pumping in acre-feet from the Carrizo-Wilcox, Queen City, and Sparta aquifers by county for the years 1980, 1985, 1990, 1995, 2000, 2005, and 2010.**

County	1980	1985	1990	1995	2000	2005	2010
Anderson	490	610	679	717	665	62	46
Angelina	47	94	88	102	155	14	20
Bastrop	998	456	463	485	494	235	193
Bexar	29	38	38	29	33	13	66
Brazos	102	218	186	146	120	160	134
Burleson	336	286	259	353	348	288	312
Caldwell	127	12	13	15	30	58	37
Cherokee	584	626	701	906	618	181	178
Falls	50	62	48	48	44		
Fayette	14	9	10	12	11	21	24
Freestone	501	456	350	524	571	187	134
Gonzales	1,966	382	410	483	1,147	2,717	2,465
Grimes	0	0	0	0	0	0	0
Guadalupe	119	64	76	84	74	337	580
Henderson	651	780	1,037	777	820	455	446
Houston	472	581	541	498	471	127	125
Karnes	57	46	46	22	21	0	0
Lee	518	422	447	618	452	568	345
Leon	864	1,473	1,332	1,273	1,014	90	86
Limestone	108	143	244	119	107	8	7
Madison	245	318	238	261	286	90	80
Milam	548	673	606	626	569	438	456
Navarro	738	473	596	600	568	113	251
Nacogdoches	13	15	13	11	12	6	8
Robertson	569	691	558	777	531	432	604
Rusk	0	0	0	0	0	0	0
Sabine	0	0	0	0	0	0	0
San Augustine	0	0	0	0	0	0	0
Smith	0	0	0	0	0	0	0
Van Zandt	0	0	0	0	0	0	0
Walker	0	0	0	0	26	19	26
Washington	0	0	0	0	0	0	0
Williamson	0	0	0	0	6	17	28
Wilson	255	162	180	207	143	815	1,251
Total	**10,401**	**9,090**	**9,159**	**9,693**	**9,336**	**7,451**	**7,902**

Table 3.2.2.7h. **Summary of combined rural domestic pumping in acre-feet from the Carrizo-Wilcox, Queen City, and Sparta aquifers by county for the years 1980, 1985, 1990, 1995, 2000, 2005, and 2010.**

County	1980	1985	1990	1995	2000	2005	2010
Anderson	1,499	1,649	1,799	1,869	1,939	2,010	2,080
Angelina	32	35	38	40	41	43	45
Bastrop	1,251	1,376	1,501	1,674	1,847	2,020	2,194
Bexar	597	657	716	638	559	480	401
Brazos	0	0	0	0	0	0	0
Burleson	206	227	247	266	285	304	322
Caldwell	440	484	528	602	677	752	827
Cherokee	1,603	1,763	1,923	1,908	1,892	1,877	1,861
Falls	29	31	34	35	36	37	38
Fayette	1	1	1	2	2	3	4
Freestone	726	798	871	848	825	802	779
Gonzales	244	268	293	302	312	321	330
Grimes	0	0	0	0	0	0	0
Guadalupe	712	784	855	941	1,027	1,112	1,198
Henderson	1,443	1,587	1,732	1,706	1,681	1,655	1,629
Houston	283	311	340	347	354	362	369
Karnes	0	0	0	0	0	0	0
Lee	292	321	350	377	403	429	456
Leon	639	703	767	803	838	874	909
Limestone	248	273	298	311	324	338	351
Madison	0	0	0	0	0	0	0
Milam	540	594	648	660	671	683	694
Navarro	1,439	1,583	1,727	1,722	1,717	1,711	1,706
Nacogdoches	26	29	32	40	49	58	66
Robertson	556	611	667	676	685	695	704
Rusk	112	123	134	125	117	108	99
Sabine	0	0	0	0	0	0	0
San Augustine	100	110	120	121	123	125	126
Smith	253	278	304	294	284	273	263
Van Zandt	532	585	639	719	799	879	958
Walker	0	0	0	0	0	0	0
Washington	0	0	0	0	0	0	0
Williamson	33	36	40	52	63	75	87
Wilson	904	994	1,085	1,145	1,205	1,265	1,326
Total	**14,739**	**16,213**	**17,687**	**18,221**	**18,756**	**19,290**	**19,824**
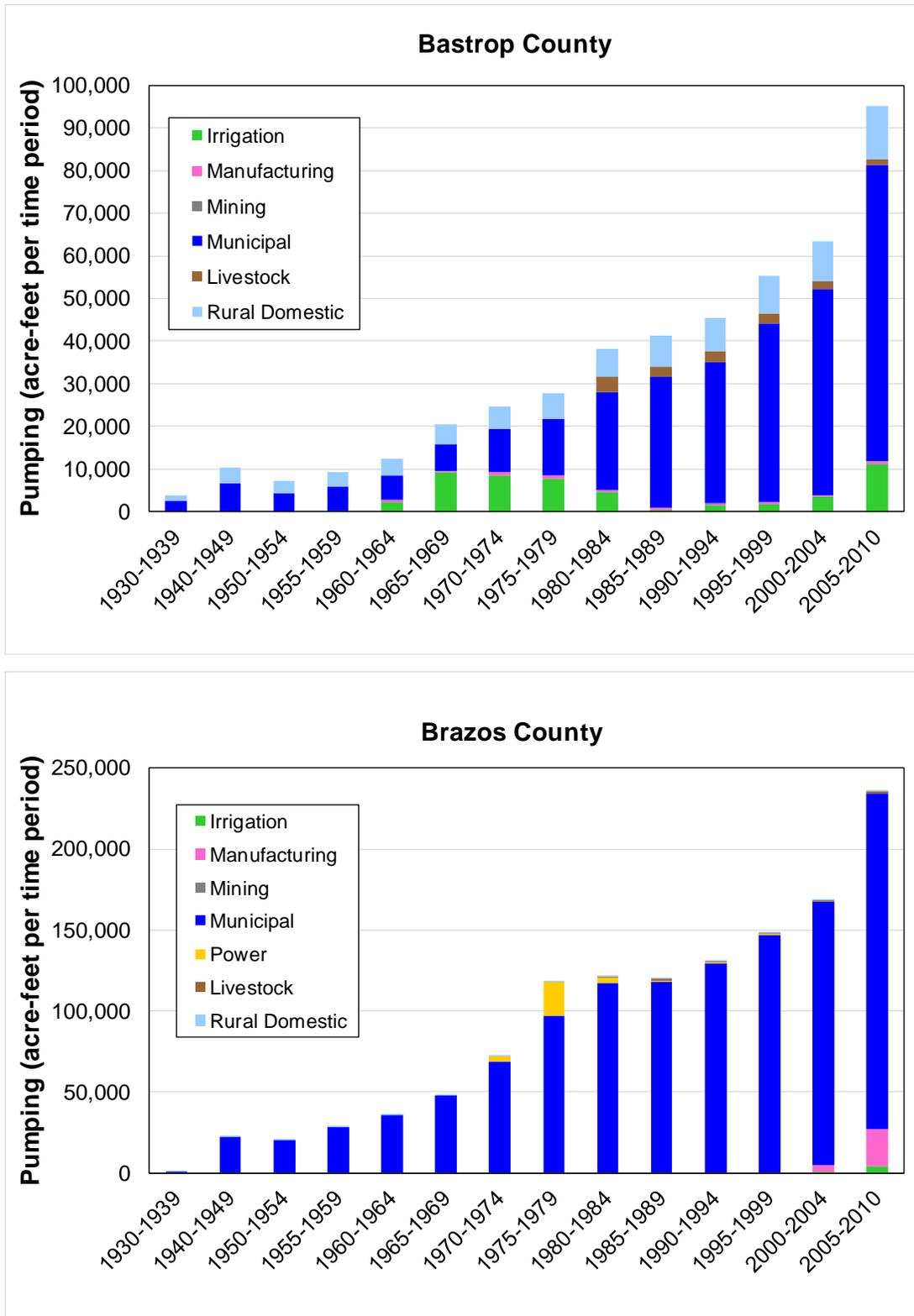
Figure 3.2.2.7a. **Bar chart of combined pumping from the Carrizo-Wilcox, Queen City, and Sparta aquifers by type for 10-year intervals from 1930 through 1949 and 5-year intervals from 1950 through 2010 for (a) Bastrop and (b) Brazos counties.**
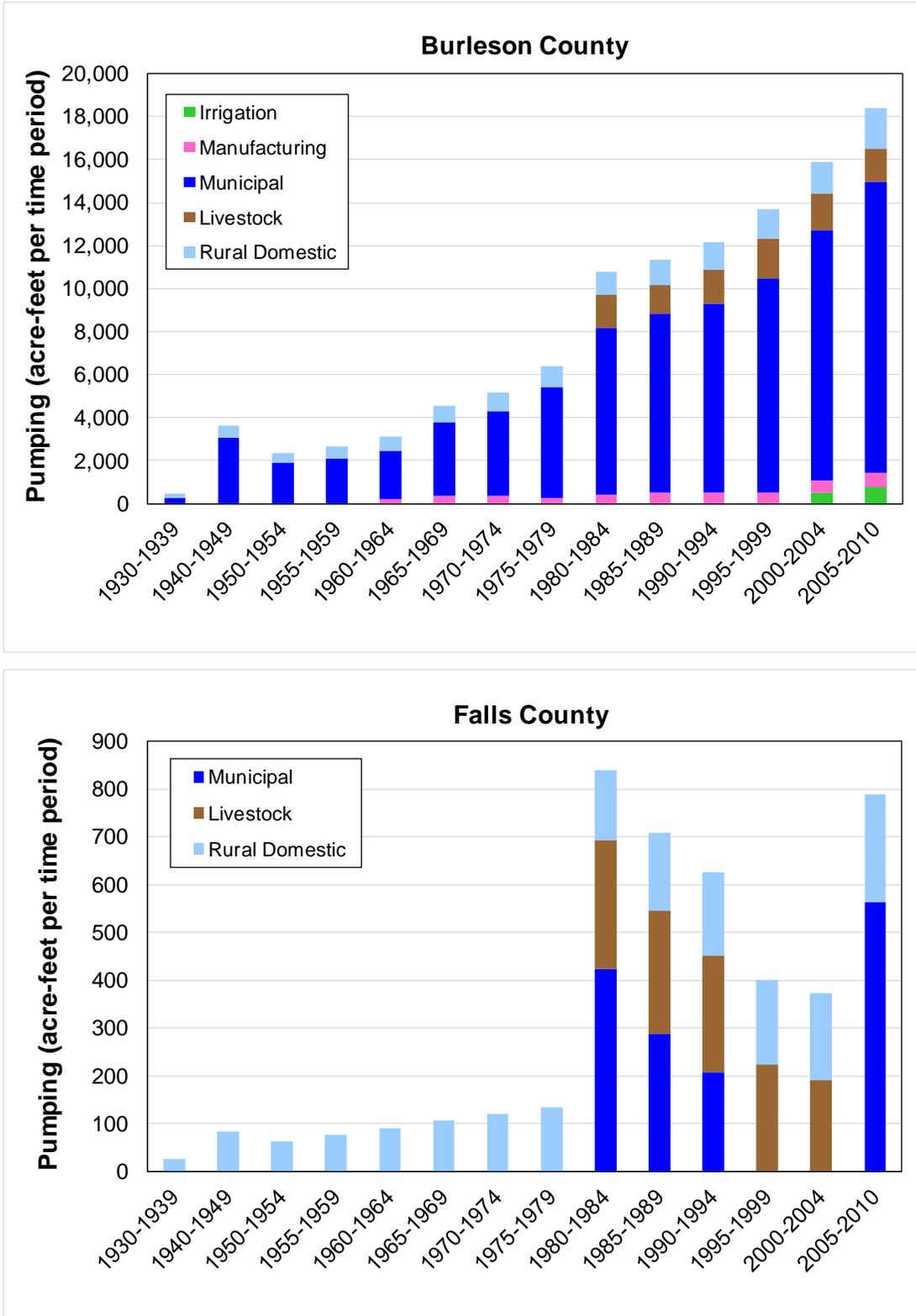
Figure 3.2.2.7b. Bar chart of combined pumping from the Carrizo-Wilcox, Queen City, and Sparta aquifers by type for 10-year intervals from 1930 through 1949 and 5-year intervals from 1950 through 2010 for (a) Burleson and (b) Falls counties.
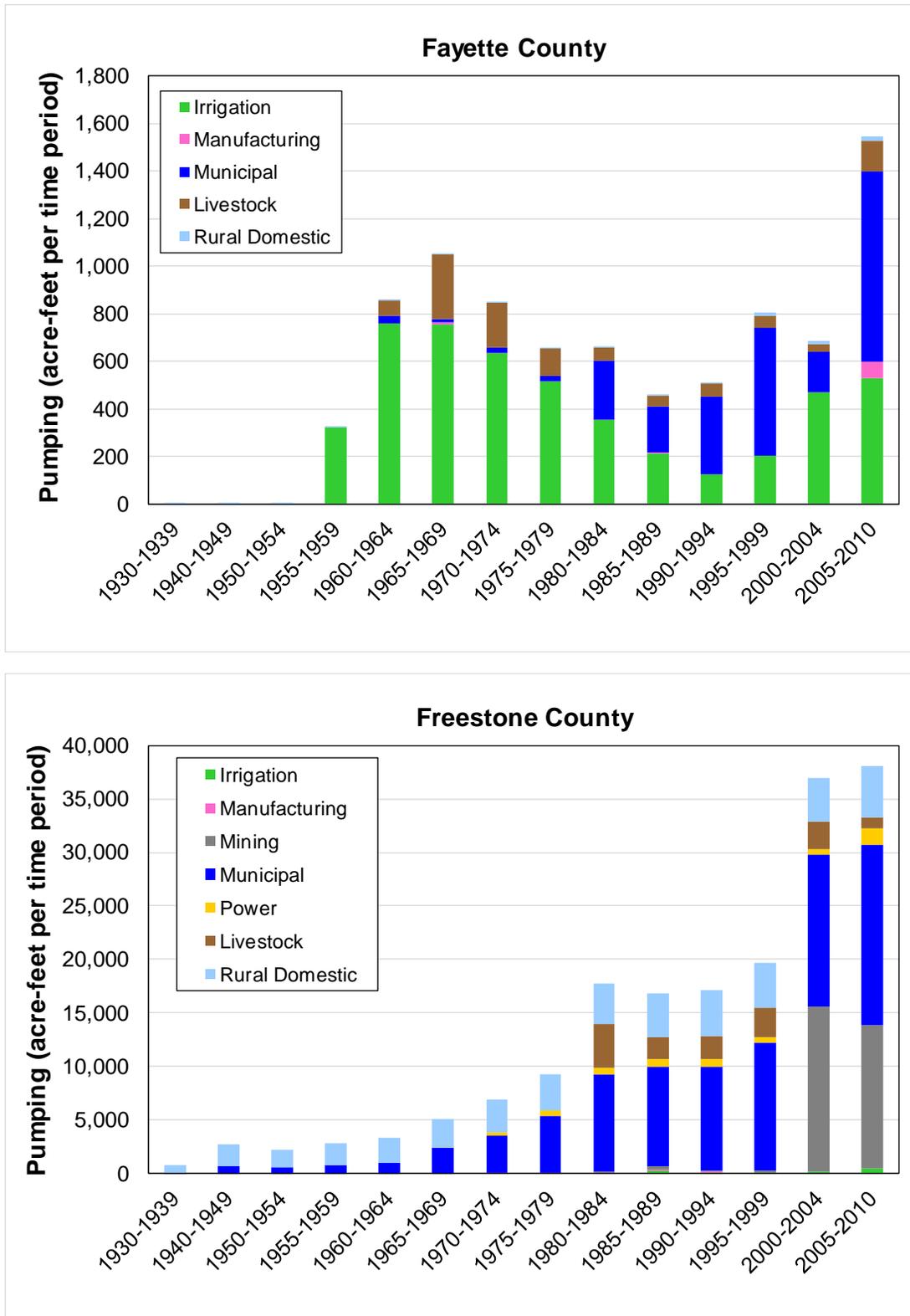
Figure 3.2.2.7c. Bar chart of combined pumping from the Carrizo-Wilcox, Queen City, and Sparta aquifers by type for 10-year intervals from 1930 through 1949 and 5-year intervals from 1950 through 2010 for (a) Fayette and (b) Freestone counties.
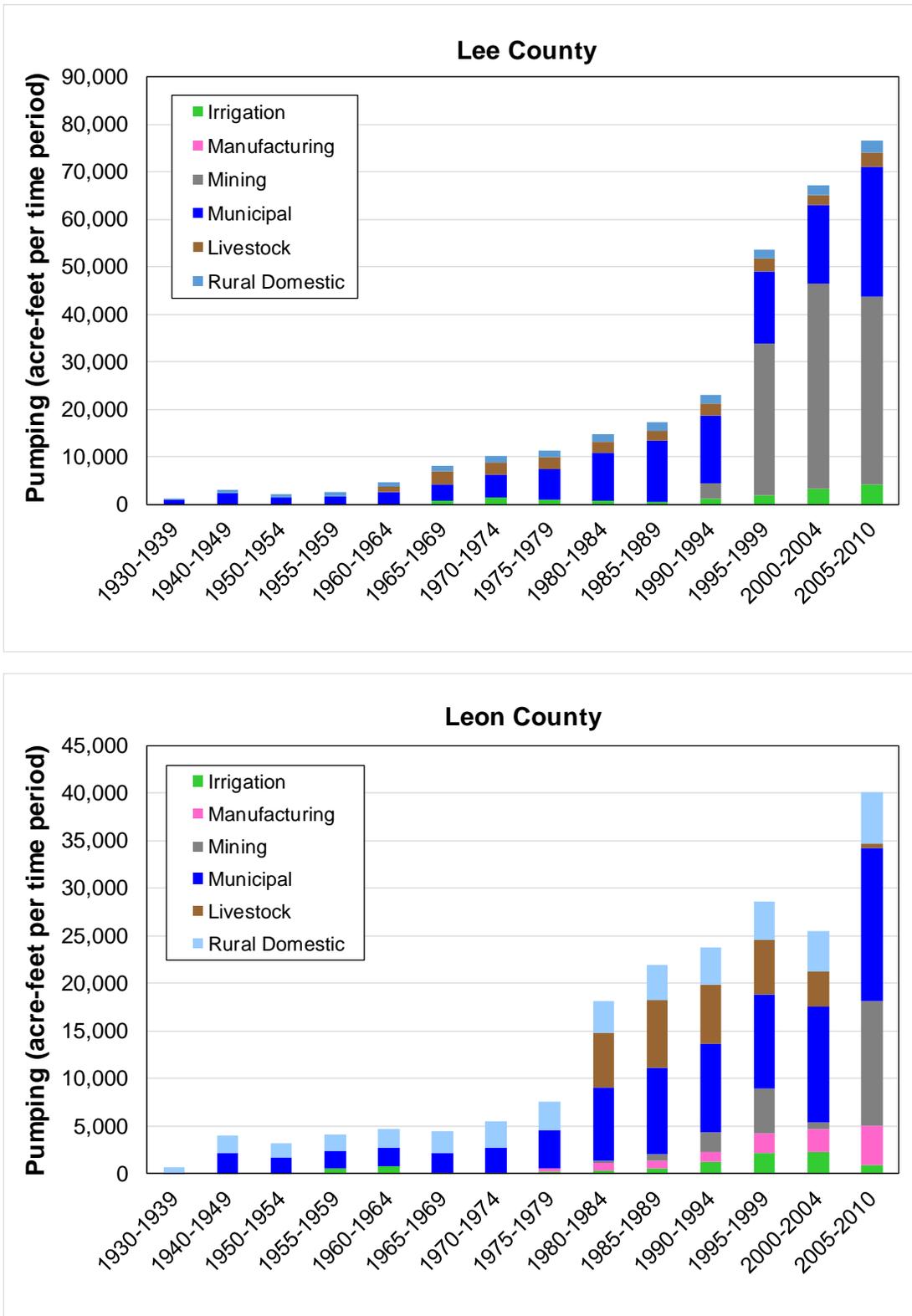
Figure 3.2.2.7d.   Bar chart of combined pumping from the Carrizo-Wilcox, Queen City, and Sparta
aquifers by type for 10-year intervals from 1930 through 1949 and 5-year intervals from
1950 through 2010 for (a) Lee and (b) Leon counties.
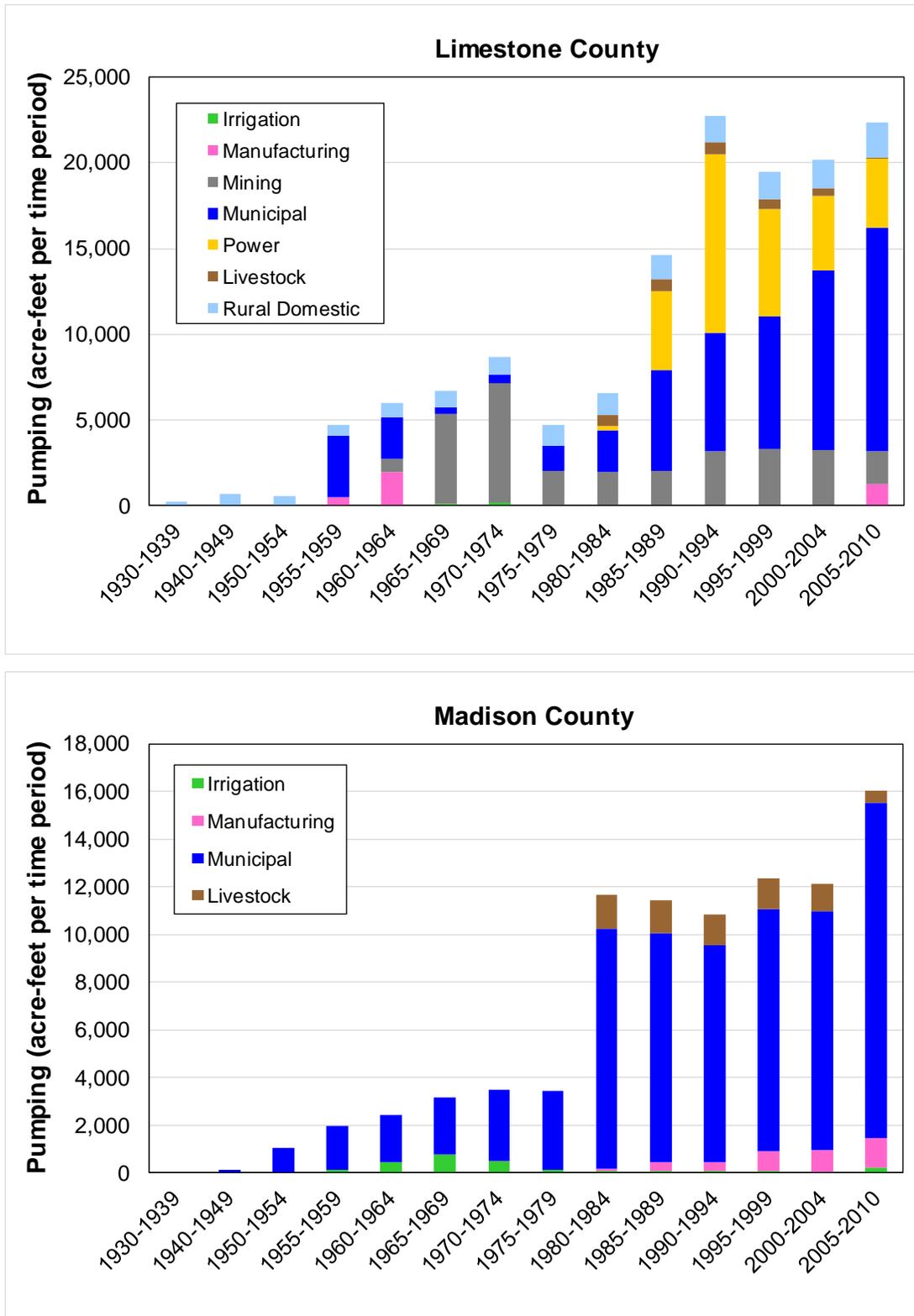
Figure 3.2.2.7e. Bar chart of combined pumping from the Carrizo-Wilcox, Queen City, and Sparta aquifers by type for 10-year intervals from 1930 through 1949 and 5-year intervals from 1950 through 2010 for (a) Limestone and (b) Madison counties.
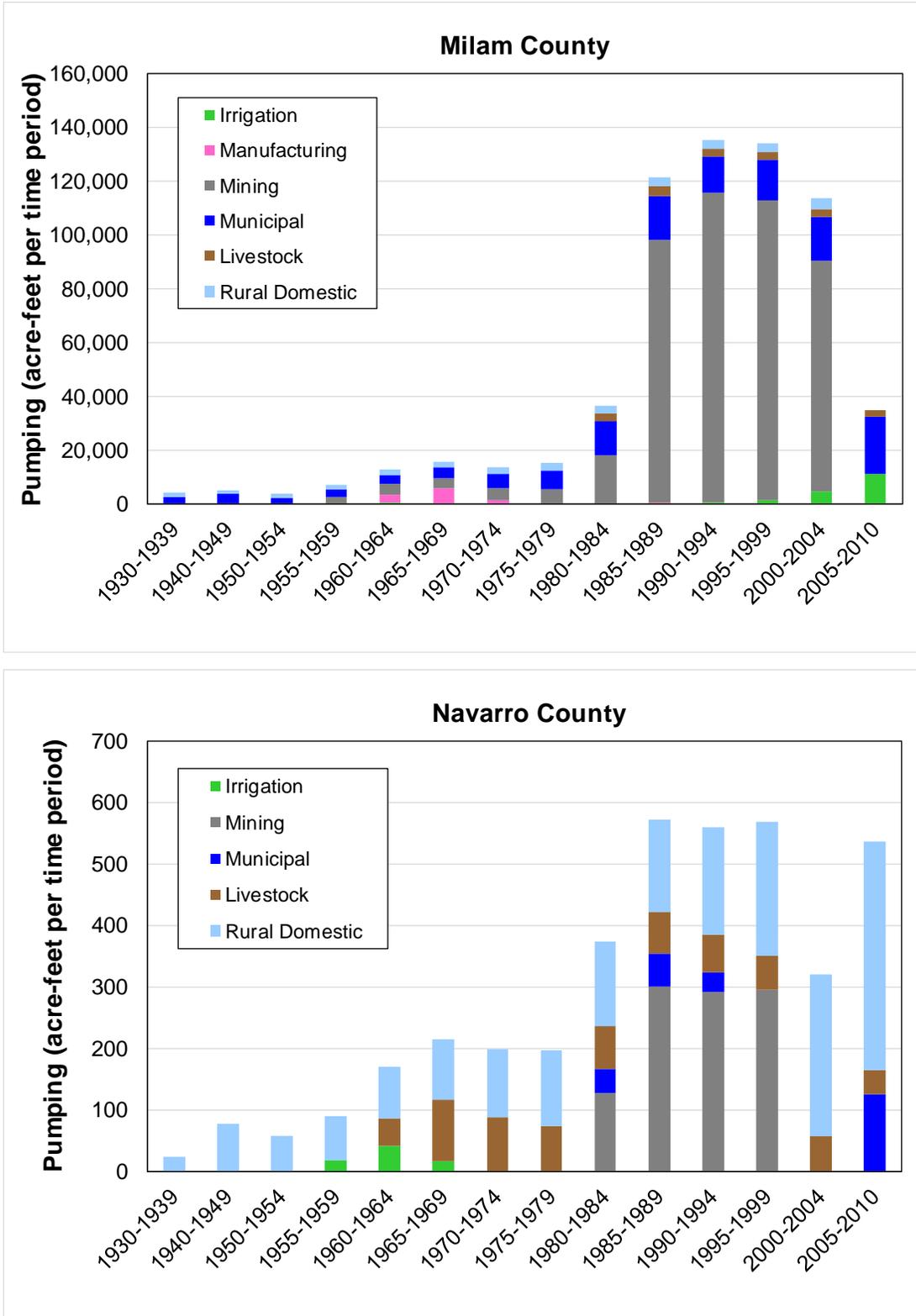
Figure 3.2.2.7f. **Bar chart of combined pumping from the Carrizo-Wilcox, Queen City, and Sparta aquifers by type for 10-year intervals from 1930 through 1949 and 5-year intervals from 1950 through 2010 for (a) Milam and (b) Navarro counties.**
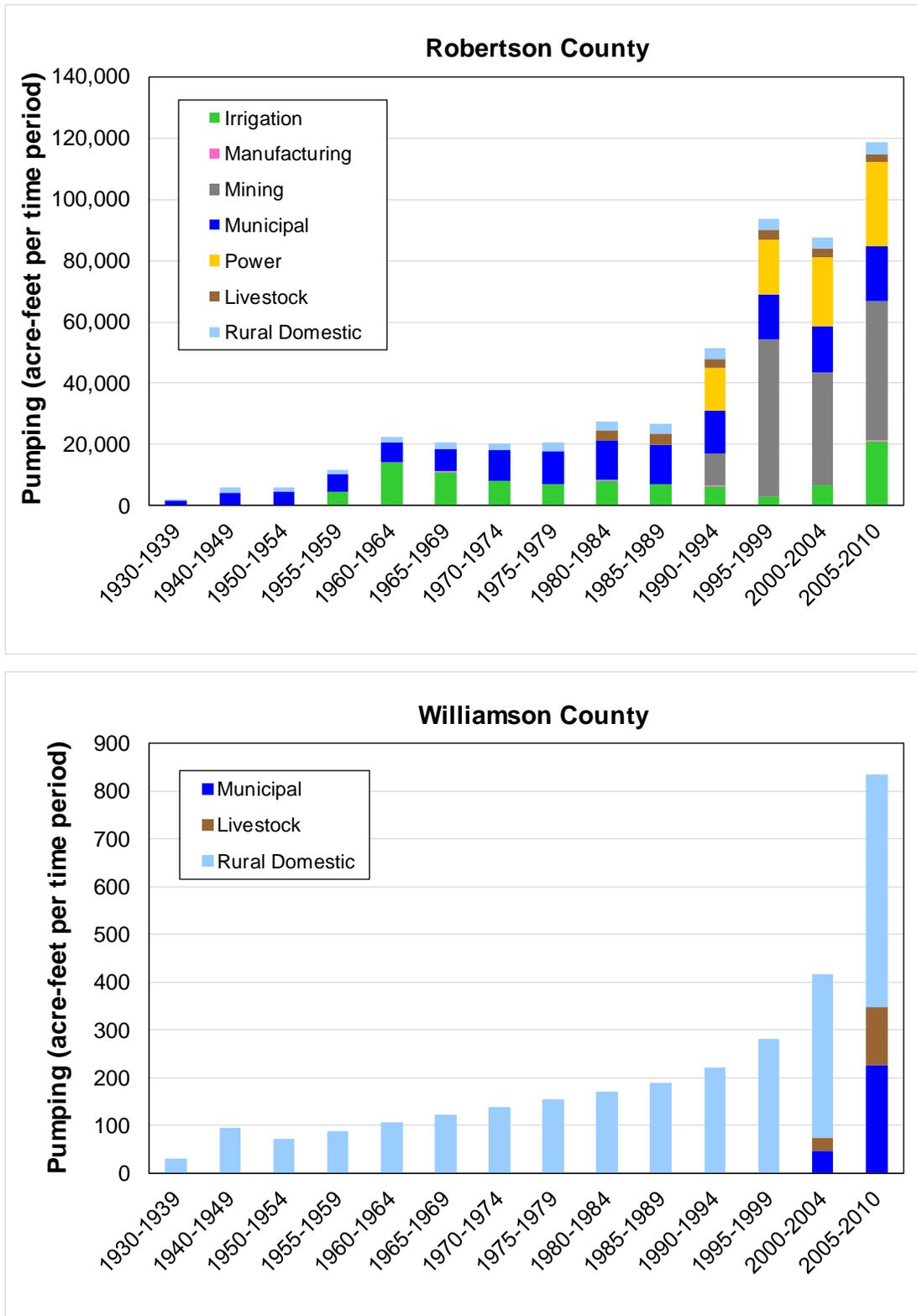
Figure 3.2.2.7g. **Bar chart of combined pumping from the Carrizo-Wilcox, Queen City, and Sparta aquifers by type for 10-year intervals from 1930 through 1949 and 5-year intervals from 1950 through 2010 for (a) Robertson and (b) Williamson counties.**
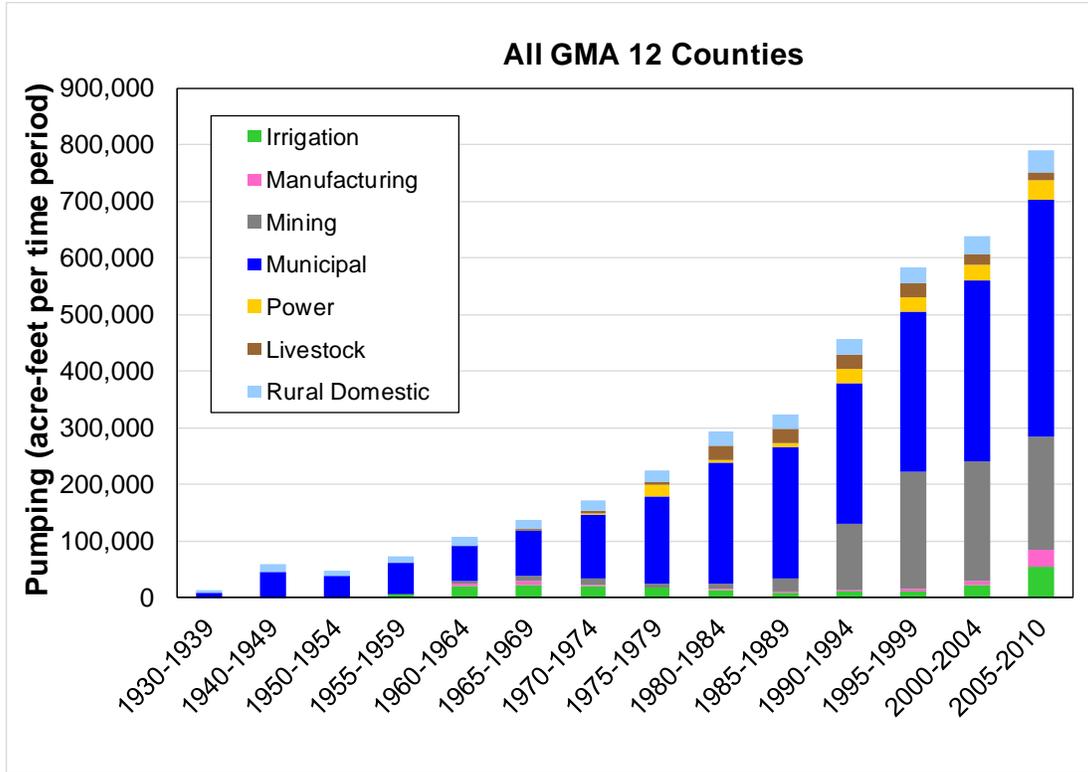
Figure 3.2.2.7h. **Bar chart of combined pumping from the Carrizo-Wilcox, Queen City, and Sparta aquifers by type for 10-year intervals from 1930 through 1949 and 5-year intervals from 1950 through 2010 for all Groundwater Management Area (GMA) 12 counties.**

3.2.2.8 Pumping Data Summary for the Alluvium

The conceptualization of pumping for the Brazos River Alluvium Aquifer was taken from Ewing and others (2016). Tables and plots of pumping for this aquifer can be found in Section 4.6.2 of that report.

Figure 3.2.2.8a shows a bar chart of total pumping from the Colorado River alluvium, as reported by the pumping source. Pumping is summed for 10-year intervals from 1930 through 1949 and 5-year intervals for 1950 through 2010. Table 3.2.2.8a provides the total pumping from the Colorado River alluvium, as reported by the pumping source, for the years 1980, 1985, 1990, 1995, 2000, 2005, and 2010. All pumping from the Colorado River alluvium occurs in Bastrop County and is used for municipal purposes.

Table 3.2.2.8a. **Summary of total pumping in acre-feet from the Colorado River alluvium for the years 1980, 1985, 1990, 1995, 2000, 2005, and 2010.**

County	1980	1985	1990	1995	2000	2005	2010
Bastrop	922	63	486	928	1,212	1,348	1,405
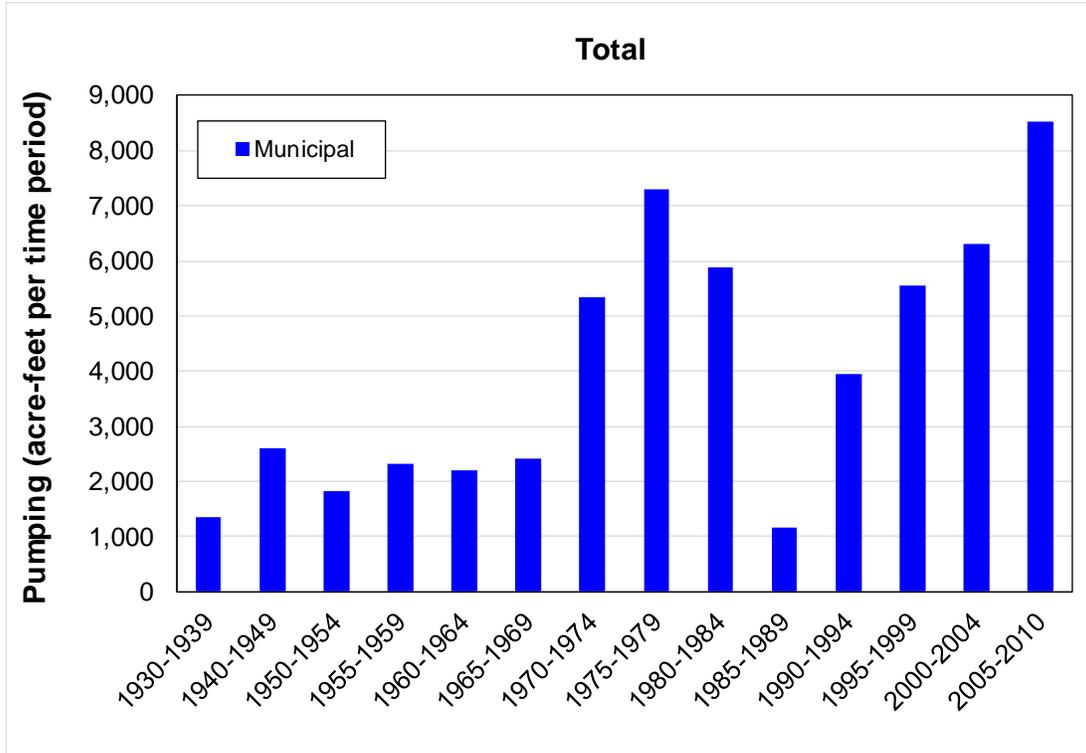
Figure 3.2.2.8a.   **Bar chart of total pumping from the Colorado River alluvium by type for 10-year intervals from 1930 through 1949 and 5-year intervals from 1950 through 2010.**

3.2.3 *Assignment of Wells to Model Grid*

The primary sources used to create the well dataset were the following databases maintained by the TWDB:

- The Groundwater database
- The BRACS database
- The Submitted Drillers Reports database

Additional sources were:

- The public water supply database maintained by the Texas Commission on Environmental Quality
- Well databases from the following groundwater conservation districts:
    - Brazos Valley Groundwater Conservation District
    - Evergreen Underground Water Conservation District
    - Fayette County Groundwater Conservation District
    - Gonzales County Underground Water Conservation District
    - Guadalupe County Groundwater Conservation District
    - Lost Pines Groundwater Conservation District
    - Mid-East Texas Groundwater Conservation District
    - Plum Creek Conservation District
    - Post Oak Savannah Groundwater Conservation District

- Information on lignite mine wells available in documents reviewed at the Texas Railroad Commission.
- Wells obtained from the lignite mine consultant (Harden and Associates, 2016a).

The wells from all of these sources were combined to create the initial well dataset, which includes all wells regardless of whether they were assigned pumping. All wells with water-level data were included in the dataset. Many of the groundwater conservation district databases include wells from the TWDB Groundwater database. Some wells are included in more than one of the TWDB databases. Duplicate wells were removed. With two exceptions, wells with no total depth or screened interval data were also removed from the well dataset because the model layer in which the well is completed could not be obtained and, consequently, the well could not be assigned to a model grid cell. The first exception was wells with assigned pumping from groundwater conservation districts. If no total depth or screen data were available for one of these wells, the well was assigned to the layer corresponding to the aquifer in which the well is completed as indicated by the groundwater conservation district. The second exception was dewatering and depressurization pumping wells associated with lignite mines. Total depth and completion data for the majority of these wells were not available. Based on documents at the Texas Railroad Commission, all dewatering pumping occurred from the Calvert Bluff Formation and all depressurization pumping occurred from the Simsboro Formation for lignite mines located in the model area. Using this information, the wells were assigned to the layer associated with the formation from which they pumped based on their pumping type.

For the remainder of the wells, which had screened data and/or total depth, they were assigned to model grid cells based on their spatial location and screened interval. For wells with total depth data only, a 50-foot screen located at the bottom of the well was assumed, which corresponds to about the 50th percentile of the available screened lengths (Figure 3.2.3a). The screen interval was compared to the model layers at the location of the well, and the layer in which the majority of the screen is located was assigned to the well. Some adjustments to the model layer determined with this method were made, especially to wells identified as completed in the layers representing the Weches and Reklaw formations. Once the model layer was finalized, a model grid node was assigned to each well.
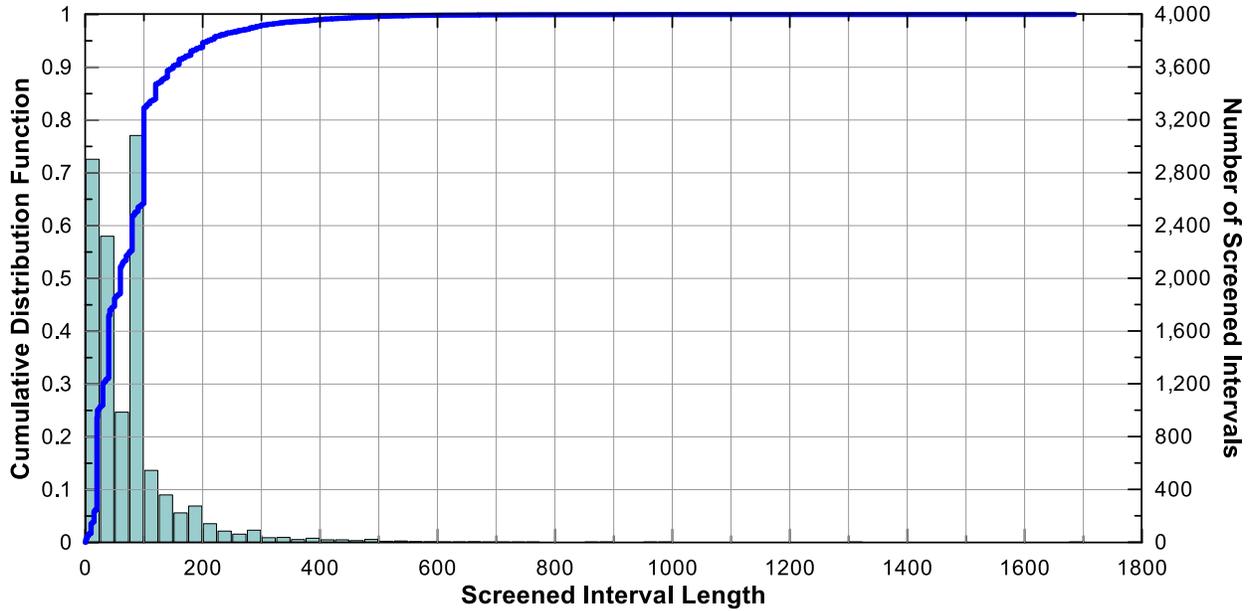
Figure 3.2.3a. **Cumulative distribution function and histogram of available screened lengths.**

3.2.4 Assignment of Pumping to Model Grid

3.2.4.1 Well-Specific Pumping

The well-specific pumping from the groundwater conservation districts and associated with lignite mining were assigned to the model grid based on the node in which the wells are completed.

For municipal, manufacturing, mining, and power pumping, the pumping was assigned to one of three model assignment categories:

1. Pumping for which wells associated with the pumping entity were identified based on the name of the pumping entity and the name of the well owner, referred to as entity-specific pumping assigned to a well.

2. Pumping for which wells associated with the pumping entity were not identified based on the name of the pumping entity and the name of the well owner, referred to as entity-specific pumping not assigned to a well.

3. For municipal, manufacturing, mining, and power water use types, the entity-specific pumping from the TWDB water use survey data was summed and subtracted from the total pumping as given by the TWDB historical groundwater pumping estimates for each county. In some cases, this resulted in pumping not associated with an entity, referred to as unspecified pumping. Wells for this unspecified pumping could not be determined because the name of the pumping entity was not reported.

The municipal, manufacturing, mining, and power pumping associated with model assignment category 1, entity specific pumping assigned to a well, was assigned to the nodes in which the wells for that entity are completed. For example, pumping for the city of Bastrop was assigned to

model nodes in which wells owned by the city of Bastrop are located. For municipal, manufacturing, mining, and power pumping associated with model assignment categories 2 and 3, entity-specific pumping not assigned to a well and unspecified pumping, respectively, the pumping could not be assigned in the model because wells in which to put the pumping could not be identified. In general, the vast majority of municipal, manufacturing, mining and power pumping in Groundwater Management Area 12 could be associated with a well(s) and assigned to the model (Figure 3.2.4a).

Except for groundwater conservation district data, all irrigation, livestock, and rural domestic pumping falls into model assignment category 3 (unspecified pumping) (Figure 3.2.4a). That is, the amount of pumping by each well owner is unknown. For irrigation and livestock uses, pumping was assigned by county to model nodes in which irrigation and livestock wells are located. The pumping for each year was equally distributed between wells. The distribution of pumping for rural domestic purposes is discussed in Section 3.2.4.2.

The spatial distribution of pumping was determined based on the location of wells and the drill date for the well. For wells with a drill date, no pumping was assigned to the model node in which the well is located until the year the well was drilled. The assumption was made that wells with no drill date are old wells, and pumping was assigned to the model node in which these wells are located for the first year of pumping for the entity that owns the well or the first year of irrigation or livestock pumping in the county.

The assignment of rural domestic pumping is discussed in Section 3.2.4.2. The well package for the groundwater availability model for the Brazos River Alluvium Aquifer (Ewing and Jigmond, 2016) was used to assign model pumping for that aquifer.
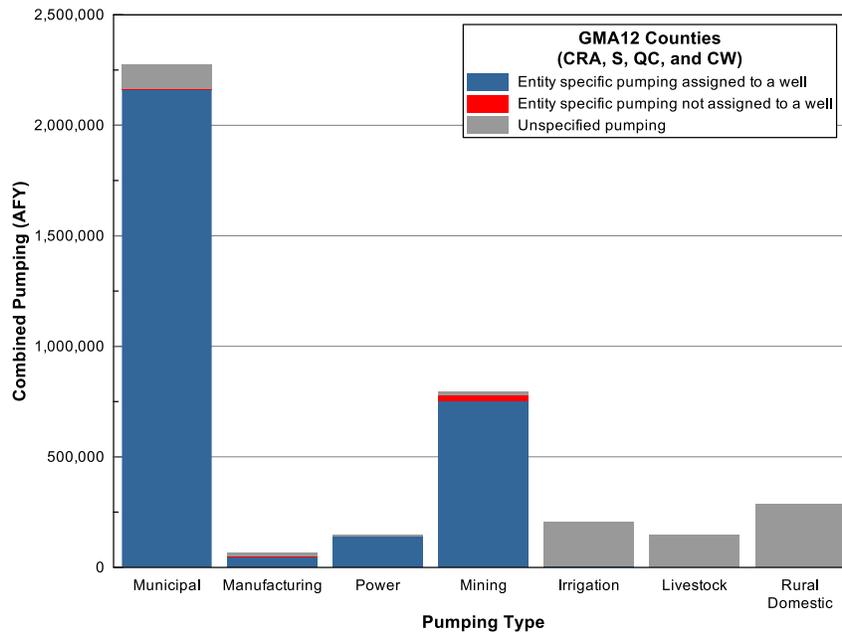
Figure 3.2.4a.   **Pumping magnitude summed from 1930 through 2010 for counties in Groundwater Management Area (GMA) 12 for which entity specific pumping could and could not be assigned to a well or wells and unspecified pumping by type.**

Note: CRA = Colorado River alluvium; CW = Carrizo Wilcox Aquifer; QC = Queen City Aquifer; S = Sparta Aquifer

3.2.4.2 Rural Domestic Pumping

Rural domestic pumping was developed based on rural population and estimates of per capita water use. Census block population data for 1990 and 2010 provided the foundational data used to estimate rural population. Across the outcrops of the modeled aquifers, rural domestic pumping was assumed to occur exclusively from the shallow aquifer zone. In the areas where the Sparta Aquifer subcrops beneath the Yegua-Jackson Aquifer, rural domestic pumping was assumed to occur in both the Yegua-Jackson Aquifer and the Sparta Aquifer, with the majority occurring in the former. The impact of all pumping in the Yegua-Jackson Aquifer and rural domestic pumping in the subcrop of the Sparta Aquifer on water levels was represented by general head boundary cells in the Sparta Aquifer.

The steps for developing rural domestic pumping consisted of:

- Extracting census blocks associated with non-urban areas in the outcrops from the 1990 and 2010 census block data using city boundaries and the assumption that any census block with a population density of 150 people per square mile or more is an urban area.
- Splitting and dissolving the non-urban census blocks by model node so that the rural population in each outcrop model node could be calculated.
- Linearly interpolating the rural population for each model node in the outcrop areas between zero in the year 1930 to that in 1990 and between the 1990 and 2010 rural populations.
- Calculating the rural domestic pumping for each year and model node as the rural population in that node times an assumed per capita water use of 110 gallons per person per day.

This process resulted in rural domestic pumping for each model node in the outcrop area for each year in the model simulation.

3.3 Recharge Estimates

3.3.1 Previous Studies of Recharge

As part of this study, we reviewed methods used by Dutton and others (2003) and Kelley and others (2004) to develop estimates for recharge rates. These methods include:

- Numerical modeling of infiltration rates
- Vertical distribution of environmental tracers in soil cores to estimate historical infiltration rates
- Stream gain-loss studies to estimate groundwater contribution to streamflow
- Simulation of groundwater-surface water interaction using Water Availability Models
- Base flow estimates based on hydrograph separation

Our approach to updating the estimated recharge is based on using hydrograph separation methods to estimate base flow. For this report, base flow represents the contribution of groundwater discharge to streamflow and is not directly influenced by runoff. Our approach for using base flow to estimate recharge is similar to Dutton and others (2003) in that average

recharge rates for a watershed are estimated by dividing a watershed's annual base flow by the area of the watershed. This approach has been used by previous researchers in Texas (Scanlon and others, 2012; Ewing and others, 2016; Kelley and others, 2004; Young and others, 2009).

3.3.2 Hydrograph Separation Methods

The hydrograph-separation method (sometimes called base flow separation) aims to distinguish streamflow derived from surface runoff from that derived from groundwater based solely on a stream hydrograph. A stream hydrograph is the time-series record of streamflow conditions. The hydrograph represents the aggregate of the different water sources that contribute to streamflow. The two main components that make up the streamflow hydrograph are:

1) Quickflow – flow in direct response to a rainfall event, including overland flow (runoff) and direct rainfall onto the stream surface (direct precipitation).

2) Base flow – the steady flow derived from groundwater discharge to the stream and lateral movement in the soil profile (interflow).

Many hydrograph-separation methods have been developed to estimate the base flow and runoff components of streamflow and, in recent years, have been implemented in a number of computer programs that facilitate the estimation process (Pettyjohn and Henning, 1979; Nathan and McMahon, 1990; Wahl and Wahl, 1995; Sloto and Crouse, 1996; Rutledge, 1998; Arnold and Allen, 1999; Eckhardt, 2005; Lim and others, 2005; Piggott and others, 2005). Although each method is based on formalized algorithms for identifying the base flow component of total streamflow, the algorithms are semi-empirical and not based on mathematical solutions to groundwater- or overland-flow equations. As a result, it is advantageous to use more than one hydrograph-separation method to analyze a streamflow record and then compare the results from the multiple methods. For this study, we investigated two hydrograph-separation techniques: the Base Flow Index Program (Institute of Hydrology, 1980a, b; Wahl and Wahl, 1995) and the Baseflow Program that was developed for use with Texas A&M's Soil and Water Assessment Tool (Arnold and others, 1995; Arnold and Allen, 1999).

3.3.2.1 Base Flow Index Program for Calculating Base Flow

The Base Flow Index Program (Institute of Hydrology, 1980a, b; Wahl and Wahl, 1995) uses a deterministic set of procedures to compute an annual base flow index for multiple years of data at one or more gage sites. The base flow index is the ratio of base flow to total flow volume for a given year and is defined by Equation 3-2.

$$BFI = \frac{V_b}{V_a} \qquad \text{(Equation 3-2)}$$

where:

BFI = base flow index
V_b = volume of water calculated as base flow
V_a = total volume of streamflow

The Base Flow Index Program algorithms are driven by two parameters, N and f. N represents the length of the intervals (measured in days) into which the period of record is divided. The

parameter *f* is used to compare each minimum to the adjacent minimum blocks and derive base flow ordinates (Gustard and others, 1992). The Base Flow Index Program uses default values of 5 and 0.9 for *N* and *f,* respectively. Wahl and Wahl (1995) suggest that the *N* value has the largest effect on the calculated base flow value and can be estimated by plotting base flow index versus *N* and locating the critical value where the slope of the line changes. Our application of the Base Flow Index Program used this procedure to find the critical value of *N*.

An example using this technique to find N was conducted for data from United States Geologic Survey river gage 08041500, whose location is shown in Figure 3.3.2.1a along with the location of all other United States Geologic Survey river gages in the vicinity of the model area. River gage 08041500 has a drainage area of approximately 860 square miles and is on Village Creek, a tributary to the Neches River. Figure 3.3.2.1b shows the mean annual base flow calculated over the period of record for this gage using the Base Flow Index Program versus the *N* parameter. The greatest change in the slope of this line occurs at an *N* value of 9. Therefore, this *N* value was selected when calculating base flow for this gage using the Base Flow Index Program. A similar evaluation was conducted to select the appropriate *N* value for all other river gages analyzed with the Base Flow Index Program.
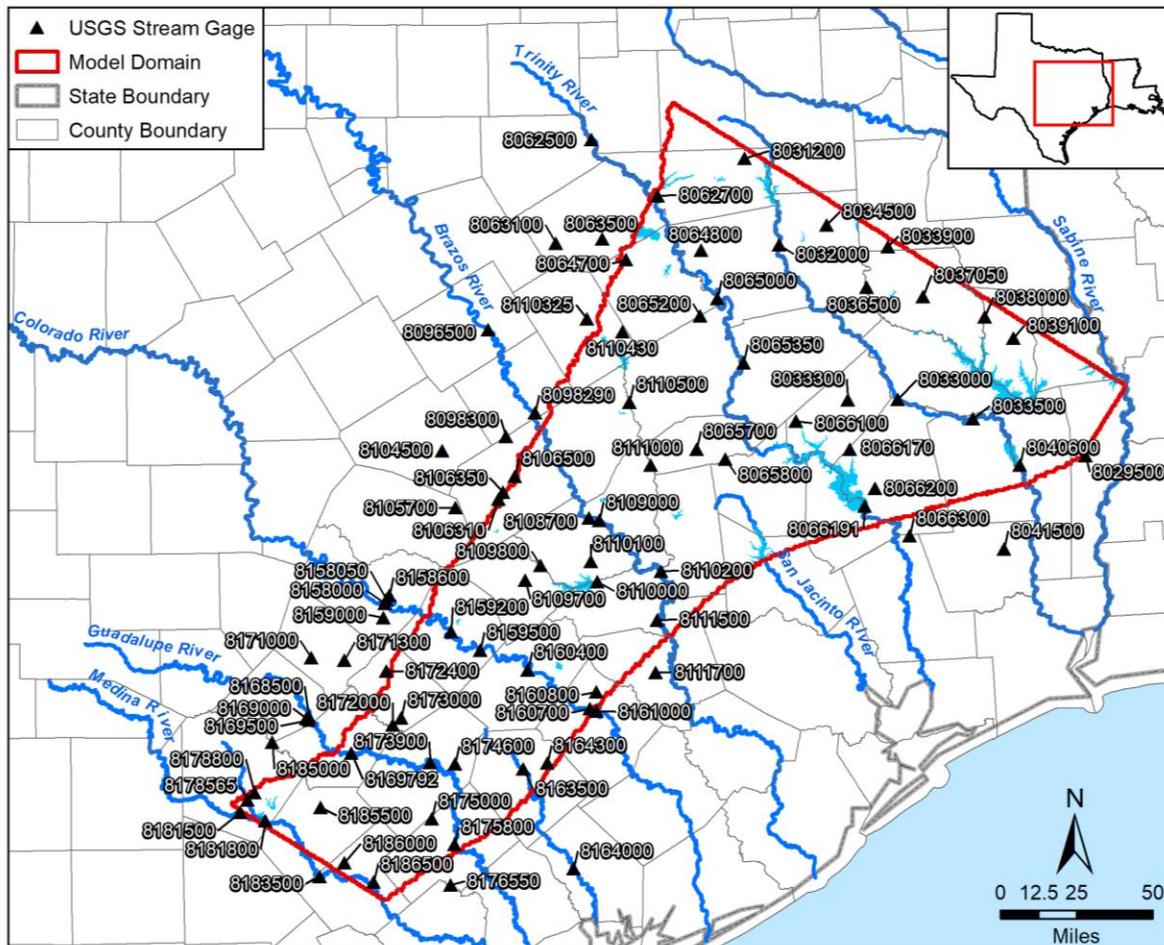
Figure 3.3.2.1a. Location of the 55 United States Geologic Survey (USGS) river gages considered for analysis using hydrograph separation to calculate base flow.
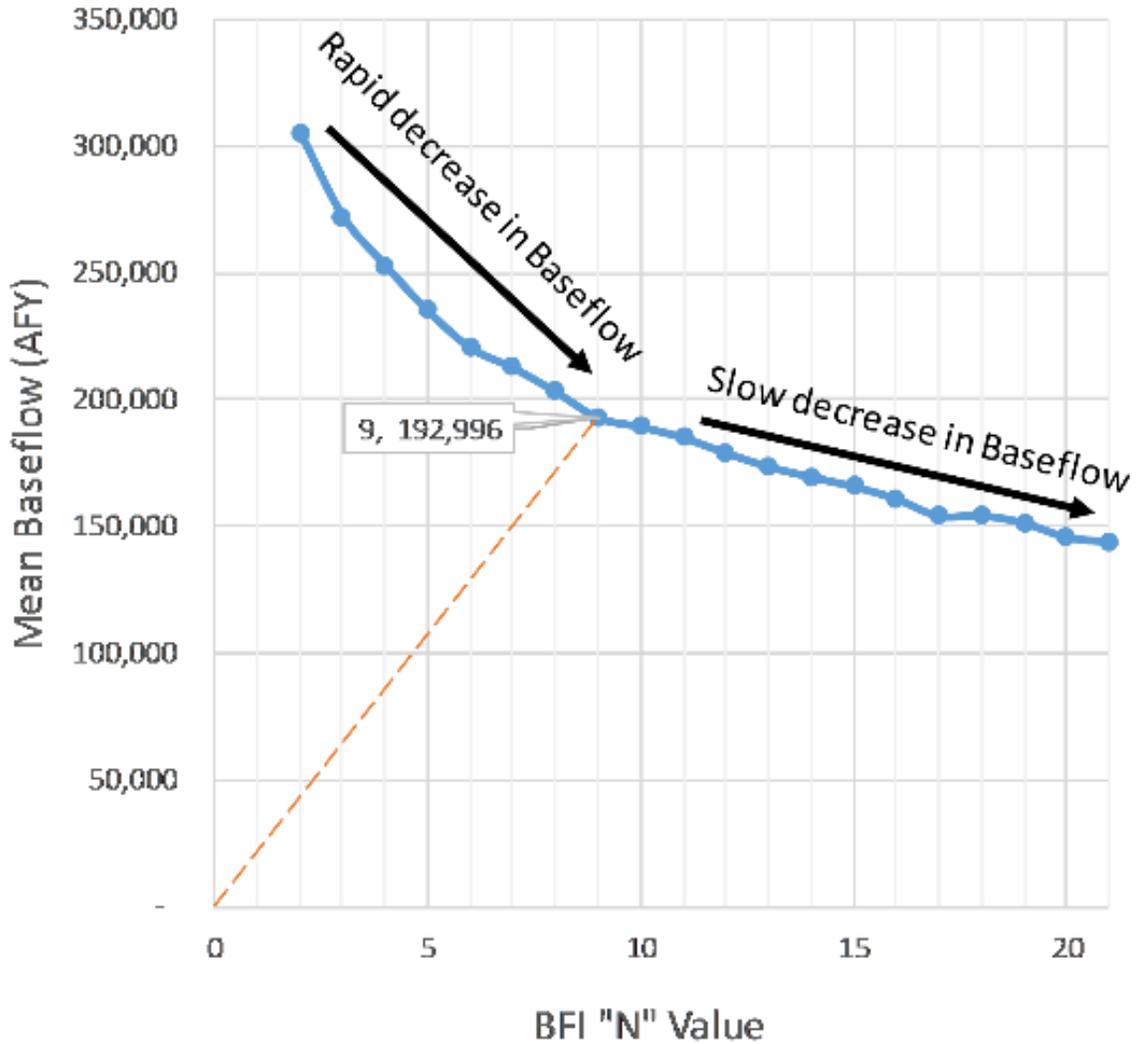
Figure 3.3.2.1b. **Mean base flow from the Base Flow Index Program (BFI) analysis for river gage 08041500 for different values of the *N* parameter, which shows that the greatest change in slope occurs for an *N* value of 9.**

Note: BFI = Base Flow Index, AFY = acre-feet per year

3.3.2.2 Baseflow Program for Calculating Base Flow

The Baseflow Program is based on techniques that were developed to perform signal analysis (Arnold and others, 1995). The Baseflow Program uses Equations 3-3 and 3-4 iteratively to calculate base flow from the total streamflow (Arnold and others, 1995).

$$q_t = \beta q_{t-1} + \frac{(1+\beta)}{2} * (Q_t - Q_{t-1}) \qquad \text{(Equation 3-3)}$$

$$b_t = Q_t - q_t \qquad \text{(Equation 3-4)}$$

where:

q_t =   filtered surface runoff at time step t

Q_t =   total streamflow at time t

β =   filter parameter equal to 0.925

b_t =   base flow at time t

The Baseflow Program applies the filter three times to the streamflow data. The first pass proceeds forward in time, the second pass is performed backwards in time, and the last pass is made in the forward direction again. Arnold and others (1995) suggest that each pass will, in general, produce less base flow. The instruction manual for the Baseflow Program (Arnold and others 2012) indicates that, for Soil and Water Assessment Tool modeling purposes, the base flow will usually lie somewhere between the first and second passes. For this study, the base flow values were calculated between the first and second pass.

3.3.3   *Recharge Calculation from Base Flow*

Hydrograph separation using the Base Flow Index and Baseflow programs on streamflow data was considered for the 55 United States Geological Survey gages shown in Figure 3.3.2.1a. For some watersheds, only one downstream gage was used to estimate recharge for a watershed. However, if a portion of the contributing area was outside the model boundary, the flow in a portion of the watershed was regulated, discharges made up a substantial portion of the base flow, or two watersheds overlapped, then upstream gage(s) were utilized to account for the upstream area(s).

The base flow calculated using hydrograph separation includes the contributions from springs and seeps. An underlying assumption for including flow at springs as part of the base flow is that the area contributing groundwater flow to the springs and seeps falls within the area of the watershed.

With base flow estimated for multiple years and gages, it was possible to calculate a long-term average recharge for each watershed. The base flow values determined from the Base Flow Index and Baseflow programs were filtered using several conditional criteria placed on the input data to the programs. If one of the four conditional criteria was not fully met, then the calculated base flows were not used to estimate recharge. The four conditional criteria were:

1. A minimum of 10 years of daily streamflow data for each gage.

2. The gage should be on a stream that is considered to be gaining and where 0 cubic feet per second flow is recorded for less than 25 percent of the days.

3. Low flows should not be dominated by discharges from anthropogenic sources and the National Pollutant Discharge Elimination System permitted return flows are less than 20 percent of mean base flow.

4. The contributing watershed area must be unregulated. If the contributing area's flow is affected by dam releases or return flows, then an upstream gage must be utilized to subtract the effects of that area.

A minimum of 10 years of data was adopted for this study because this amount of time is greater than most periods of severe drought or flooding and will result in a long-term average recharge

value that is not excessively skewed by extreme weather conditions. The second criterion ensures the validity of the base flow separation calculation. Chow and others (1988) suggest that, for a river with perennial flow (gaining), most of the basin yield usually comes from base flow, indicating that a large portion of the rainfall is infiltrated into the basin and reaches the stream as subsurface flow. However, if the gage is located on an intermittent stream, then most of the flow is generated from surface runoff and not applicable for this study.

The third and fourth criteria ensure that gains to the system are due to groundwater sources and not artificial ones. National Pollutant Discharge Elimination System permits were obtained for the study area using the Environmental Protection Agency's Enforcement and Compliance History Online website (Environmental Protection Agency, 2016). Estimates of the time periods where a stream was regulated (influenced by reservoir discharge) were taken from Slade and others (2002), who lists beginning and ending years of regulation for many active and discontinued streamflow gaging stations in Texas.

Out of the 55 river gages evaluated, 35 of the gages met the above criteria. The base flow values determined by the hydrograph separation for the river gages that met the above criteria were divided by the drainage area associated with the river gage to calculate recharge. Figures 3.3.3a and 3.3.3b show the long-term average recharge calculated from the Base Flow Index Program and Baseflow Program, respectively. Both sets of results show a trend of increasing recharge from the southwest to the northeast. For most of the watersheds, the recharge values from base flow estimated using the Baseflow Program were greater than those from base flow estimated using the Base Flow Index Program.

To develop a relationship between precipitation and recharge for each watershed, a regression was performed between the recharge and the natural logarithm of precipitation. Figure 3.3.3c illustrates the results of the regression for river gages 8111000 and 8065200. The regression was characterized using values for R-squared and p-value, which work together in a regression analysis to indicate whether the relationships in a model are statistically significant and the nature of the relationships. The R-squared values measure how close the data are to the fitted regression line. In general, the higher the R-squared, the better the model fits the data. The p-values for the coefficients indicate whether these relationships are statistically significant. In general, the lower the p-value, the more statistically significant the relationship.

Table 3.3.3a summarizes results from the regression analyses performed on the 35 river gages. Thirty-two out of the 35 river gages have a larger R-squared and a lower p-value for the Baseflow Program regressions. The average R-squared for the Baseflow Program regressions and the Base Flow Index Program regressions are 0.47 and 0.27, respectively. The average p-value for the Baseflow Program regressions and the Base Flow Index Program regressions are 0.0008 and 0.00001, respectively. Based on the comparison of the values for R-squared and p-value, the Baseflow Program regressions are statistically better models for estimating recharge than are the Base Flow Index Program regressions. As a result, the precipitation-recharge relationship based on the Baseflow Program regression was used to develop an approach for estimating annual recharge.

Table 3.3.3a. **Results of the regression between logarithm of annual precipitation and annual estimate recharge rates calculated using the Base Flow Index and Baseflow programs.**

River Gage[a]	Drainage Area (square miles)	Mean Precipitation (in /yr)	Results of Regression					
			Predicted Recharge (in/yr) for Mean Precipitation		R-squared		p-value	
			BFI	BFLOW	BFI	BFLOW	BFI	BFLOW
8029500	128	54.1	6.0	6.9	0.31	0.47	6.9E-06	4.4E-09
8031200	232	41.5	1.7	3.4	0.26	0.47	8.2E-03	1.0E-04
8033000	2,724	44.8	4.0	6.0	0.38	0.55	6.6E-06	4.9E-09
8033500	3,636	48.7	5.2	7.0	0.38	0.54	5.1E-06	7.0E-09
8033900	158	45.9	3.5	4.8	0.43	0.52	4.0E-04	4.4E-05
8037050	31	47.4	2.6	4.4	0.36	0.69	1.5E-03	3.2E-07
8038000	503	49.0	4.1	6.6	0.33	0.54	5.2E-05	1.1E-08
8039100	89	51.2	3.3	5.5	0.58	0.66	6.8E-06	4.1E-07
8041500	860	52.6	4.4	7.1	0.35	0.58	4.1E-08	6.7E-15
8062700	8,538	37.7	7.8	11.2	0.17	0.44	6.1E-03	8.1E-07
8063500	734	37.1	1.2	2.6	0.17	0.51	3.8E-02	1.9E-05
8064700	142	38.4	0.2	0.9	0.07	0.26	8.4E-02	7.1E-04
8064800	207	40.4	3.1	4.0	0.47	0.60	1.0E-04	3.0E-06
8065200	150	39.4	0.9	1.8	0.28	0.54	1.5E-04	4.1E-09
8065350	13,911	41.2	8.8	6.9	0.11	0.22	2.8E-02	1.1E-03
8066100	222	43.7	0.5	1.6	0.25	0.46	5.6E-02	5.6E-03
8066170	57	46.4	0.7	2.0	0.36	0.55	1.5E-05	7.9E-09
8066200	141	48.6	1.1	2.3	0.37	0.63	4.9E-06	2.3E-11
8066300	152	50.0	3.8	5.1	0.30	0.46	1.3E-04	4.0E-07
8108700	39,049	35.5	2.1	4.5	0.01	0.47	8.1E-01	3.2E-03
8109700	236	34.4	0.4	1.0	0.17	0.41	4.5E-03	1.1E-06
8109800	244	35.5	0.7	1.1	0.07	0.32	8.1E-02	4.0E-05
8110200	41,192	38.4	7.4	9.6	0.40	0.30	2.1E-02	2.9E-02
8110430	97	38.8	0.38	1.325	0.124	0.39	3.2E-02	5.2E-01
8111000	1,454	38.2	0.9	2.4	0.46	0.65	2.9E-06	5.2E-11
8111700	376	39.6	0.9	1.9	0.23	0.52	2.5E-03	2.8E-07
8160400	40,874	36.9	1.9	3.0	0.19	0.07	3.9E-01	4.8E-01
8160800	17	40.4	0.6	1.0	0.33	0.48	2.7E-05	8.4E-08
8164000	817	36.4	0.9	1.7	0.37	0.57	1.7E-08	1.9E-14
8164300	332	37.0	0.8	1.4	0.23	0.52	4.9E-04	7.6E-09
8172000	838	33.8	6.5	6.8	0.24	0.34	1.7E-04	4.7E-06

River Gage[a]	Drainage Area (square miles)	Mean Precipitation (in /yr)	Results of Regression					
			Predicted Recharge (in/yr) for Mean Precipitation		R-squared		p-value	
			BFI	BFLOW	BFI	BFLOW	BFI	BFLOW
8174600	460	34.9	0.2	0.8	0.11	0.57	1.1E-01	5.7E-06
8175800	4,934	33.9	6.6	3.8	0.07	0.01	5.8E-01	9.3E-01
8178800	189	31.7	0.9	0.9	0.15	0.25	2.1E-01	1.0E-01
8186000	827	30.5	0.5	1.1	0.01	0.72	9.8E-01	1.5E-01

[a] Bolded river gages used in development of recharge for implementation in the model (see Section 3.3.4)
Note: BFI = Base Flow Index Program, BFLOW = Baseflow Program; in/yr = inches per year
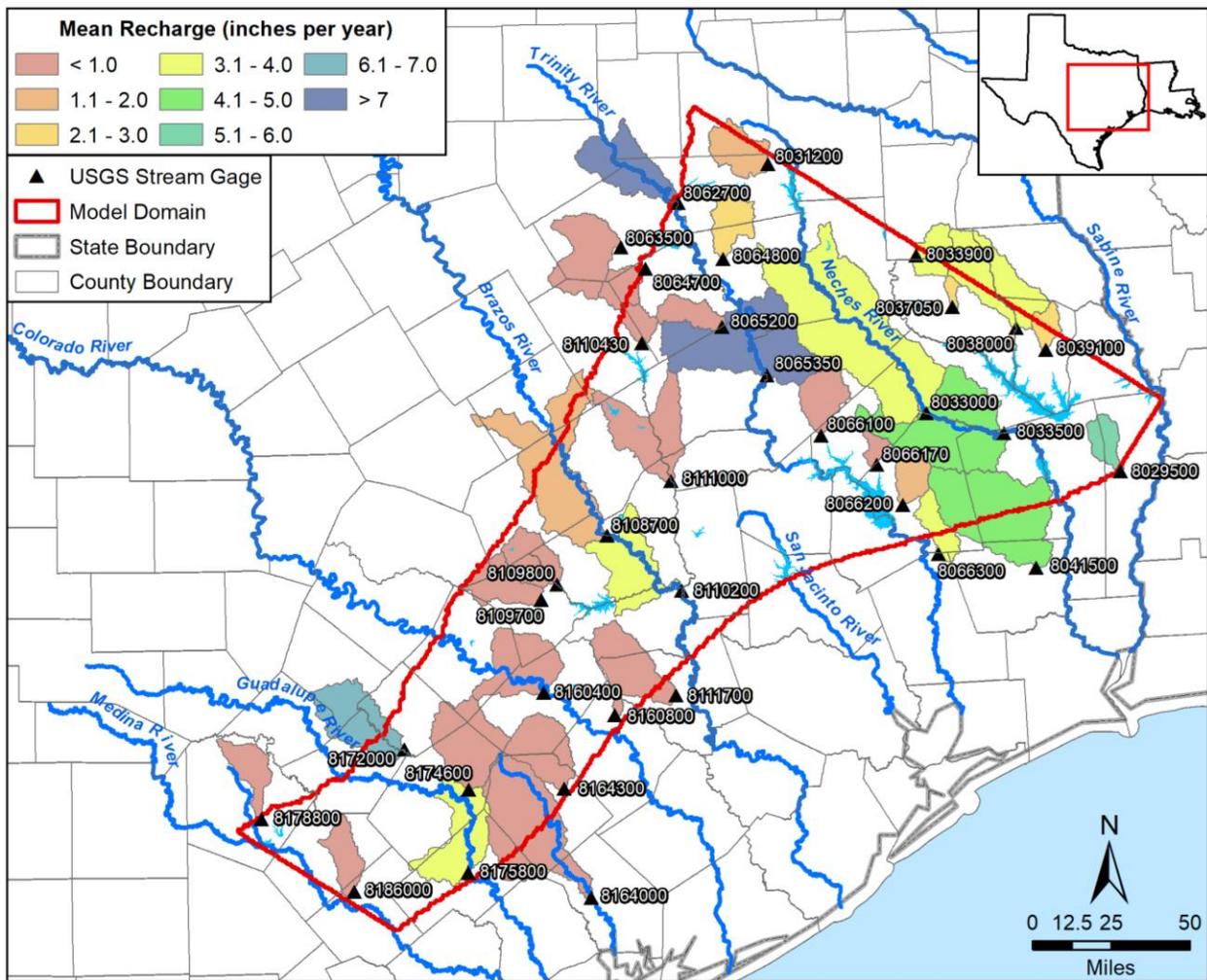
Figure 3.3.3a. **Long-term average annual recharge calculated from hydrograph separation using the Base Flow Index Program.**

Note: USGS = United States Geological Survey
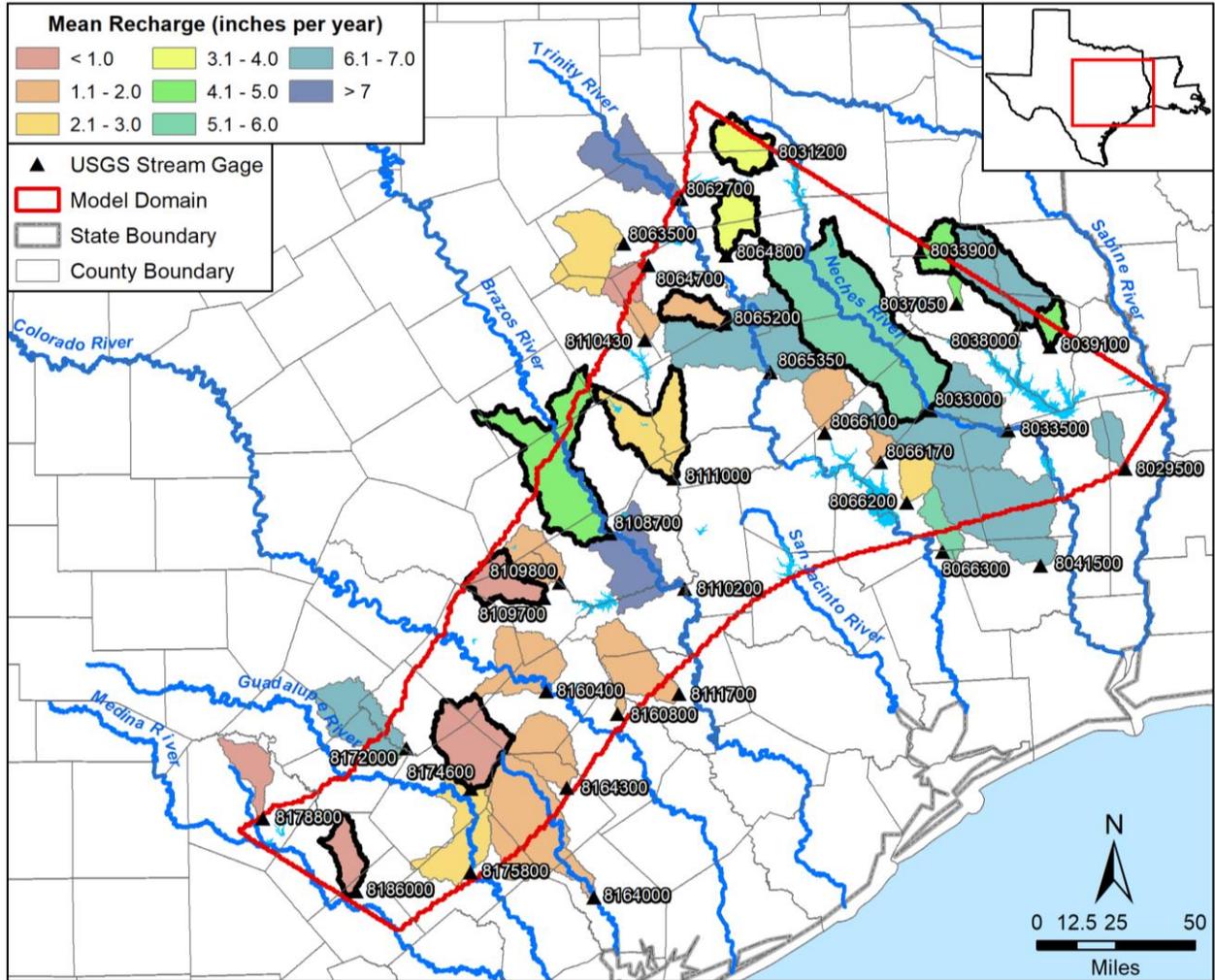
Figure 3.3.3b.   **Long-term average annual recharge calculated from hydrograph separation using the Baseflow Program. The twelve watersheds outlined in black are those listed in Table 3.3.4a.**

Note: USGS = United States Geological Survey
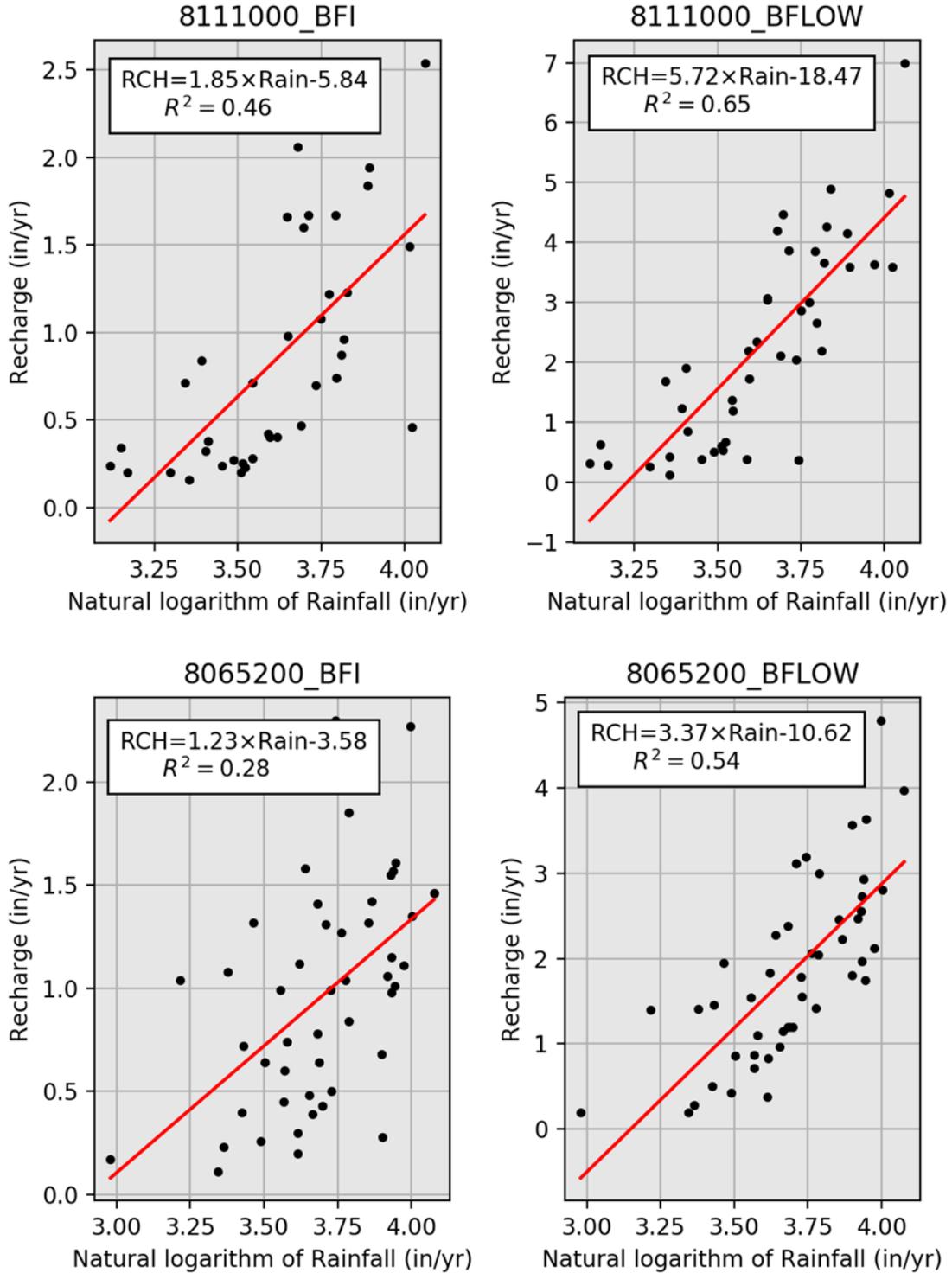
Figure 3.3.3c. Regression of recharge versus annual precipitation values produced by the application of the Base Flow Index Program and Baseflow Program hydrograph separation techniques for river gage 8111000 on the Navasota River in Brazos County and river gage 8065200 on the Upper Keechi Creek in Leon County.

Note: BFI = Base Flow Index Program; BFLOW = Baseflow Program; in/yr = inches per year; RCH = recharge; R^2 = R-squared

3.3.4   Development of Recharge Through Model Calibration

The method developed for implementing recharge in the model considered 12 of the river gages for which a hydrograph separation analysis was conducted using the Baseflow Program (Table 3.3.3a and Figure 3.3.3b). These 12 river gages were selected based on several criteria. One criterion was that the value of R-squared for the regression between recharge and precipitation (Table 3.3.3a) was greater than 0.4. Another criterion was that the majority of the watershed associated with the river gage lies within the outcrop area of the hydrogeologic units included in the model.

For developing the recharge used in the model, the recharge estimates obtained using the Baseflow Program hydrograph separation method for these 12 river gages were adjusted to account for differences in runoff and infiltration rates for different types of surface geology, bank storage, and bank flow associated with alluvium along rivers and flooding. Two adjustments were applied to account for bank flow: one related to the potential for bank storage in alluviums adjacent to streams, and the other related to precipitation, which impacts flooding. Each of these adjustments is described in the following subsections.

3.3.4.1   Adjustment for Surface Geology

The precipitation-recharge relationships captured in the regressions (Table 3.3.3a) do not account for differences in surface geology. Dutton and others (2003) and Kelley and others (2004) scaled recharge across outcrop areas based on hydraulic characteristics of the surface geology. Dutton and others (2003) scaled recharge based on a hydraulic conductivity estimate from soil maps, while Kelley and others (2004) scaled recharge based on the surface geology. A similar scaling, referred to here as the surface geology scaling factor, was implemented for the updated model to account for the impact of surface geology on the spatial distribution of recharge. For instance, recharge rates in sandy deposits associated with the Simsboro Formation should be higher than recharge rates in the clayey deposits associated with the Reklaw Formation. The surface geology scaling factor is applicable for both a single surface geology and an area across which a mixture of surface geologies occurs. Table 3.3.4.1a provides the surface geology scaling factors used by Kelley and others (2004) and those selected for this study for the nine hydrogeologic units found in the outcrop area of the model.

Table 3.3.4.1a.   Surface geology scaling factors used by Kelley and others (2004) and this study to adjust recharge base on the hydrogeologic units in the model outcrop area.

Hydrogeologic Unit	Surface Geology Scaling Factor	
	Kelley and others (2004)	This Study
Alluvium		1.0
Sparta Aquifer	0.8	0.6
Weches Formation	0.2	0.3
Queen City Aquifer	0.5	0.7
Reklaw Formation	0.2	0.3
Carrizo Aquifer	1.2	1.0
Calvert Bluff Formation	0.4	0.85
Simsboro Formation	1.2	1.0
Hooper Formation	0.3	0.75

The two sets of surface geology scaling factors in Table 3.3.4.1a are similar, with the highest scalar adjustment factors assigned to the sand-rich deposits, such as the Carrizo Aquifer and Simsboro Formation, and the lowest scalar adjustment factors assigned to the clay-rich deposits, such as the Reklaw and Weches formations. Among the differences in the two sets of surface geology scaling factors is the presence of river alluvium in this study and higher values for the Calvert Bluff and Hooper formations for this study than those used by Kelley and others (2004).

The surface geology scaling factors for the 12 river gages considered by this study, which have multiple hydrogeologic units in their associated watersheds, were developed using the surface geology scaling factors for the individual hydrogeologic units listed in Table 3.3.4.1a and the fraction of each hydrogeologic unit in the watershed (Table 3.3.4.1b). The hydrogeological units that comprise the outcrops of the 12 watersheds are provided in this table, along with the calculated surface geology scaling factor for the watershed. The higher the surface geology scaling factor, the greater the amount of recharge that will occur for a given amount of rainfall. The watershed associated with river gage 8038000 has a high value of 0.9 for its surface geology scaling factor because 83 percent of the watershed outcrop area is represented by hydrogeologic units with a surface geology scaling factor of 1.0.

Table 3.3.4.1b. **Hydrogeologic units and calculated surface geology scaling factor for the watersheds associated with the 12 river gages used to develop a relationship between precipitation and recharge for the model.**

Watershed River Gage	Fraction of Watershed Area Occupied by Hydrogeologic Unit										Surface Geology Scaling Factor[a]
	AL	SP	Wec	QC	Rek	Car	CB	SB	HP	Other	
8031200	0.09	0.00	0.00	0.40	0.13	0.07	0.26	0.05	0.00	0.00	0.75
8033000	0.17	0.15	0.06	0.31	0.09	0.00	0.00	0.00	0.00	0.22	0.63
8033900	0.09	0.03	0.05	0.11	0.20	0.34	0.09	0.09	0.00	0.00	0.77
8038000	0.15	0.00	0.03	0.03	0.09	0.34	0.03	0.34	0.00	0.00	0.90
8039100	0.13	0.43	0.27	0.00	0.10	0.07	0.01	0.00	0.00	0.00	0.57
8064800	0.08	0.00	0.00	0.73	0.17	0.02	0.00	0.00	0.00	0.00	0.66
8065200	0.13	0.00	0.00	0.11	0.19	0.11	0.47	0.00	0.00	0.00	0.77
8108700	0.29	0.05	0.01	0.07	0.06	0.02	0.07	0.05	0.15	0.23	0.72
8109700	0.10	0.15	0.08	0.03	0.02	0.04	0.28	0.15	0.14	0.00	0.78
8111000	0.16	0.16	0.03	0.24	0.18	0.06	0.14	0.02	0.00	0.01	0.69
8174600	0.10	0.06	0.04	0.15	0.21	0.04	0.00	0.00	0.00	0.40	0.57
8186000	0.22	0.05	0.06	0.29	0.13	0.05	0.00	0.00	0.00	0.19	0.66

[a] Surface geology scaling factor weighed by the area of each geologic unit comprising the watershed.
Note: AL = river alluvium; SP = Sparta Aquifer; Wec = Weches Formation; QC = Queen City Aquifer; Rek = Reklaw Formation; Car = Carrizo Aquifer; CB = Calvert Bluff Formation; SB = Simsboro Formation; HP = Hooper Formation; Other = Yegua Jackson Aquifer, Gulf Coast Aquifer, or Midway Group.

During model calibration, the sensitivity of the simulated recharge rates to the values of the surface geology scaling factors for the individual hydrogeologic units (that is, those in Table 3.3.4.1a) was investigated. This investigation led to the realization that reasonable values for recharge rates could only be obtained after provisions were made to account for bank storage and bank flow during model calibration. As a result, the surface geology scaling factors for the individual hydrogeologic units could not be determined through model calibration until the

calibration process included a methodology for accounting for bank storage and bank flow. The next section discusses the approach used to identify and separate bank flow effects as part of the model calibration process.

3.3.4.2 Adjustments for Bank Flow and Bank Storage

Groundwater flows that comprise base flow can be partitioned based on their source and place of origin. Groundwater originating from the groundwater basin that drains to a specific stream reach is referred to as basin storage. The primary source of basin storage is recharge from precipitation. Groundwater from basin storage that contributes to streamflow is referred to as basin flow. Groundwater that originates from stream water that infiltrates the river alluvium during periods of high stream water levels is referred to as bank storage. Groundwater from bank storage that leaves the alluvium and becomes streamflow is referred to bank flow.

Previous work using hydrograph separation methods to estimate recharge rates (Scanlon and others, 2012; Ewing and others, 2016; Kelley and others, 2004; Young and others, 2009) do not address the potential importance of bank flow. To help define bank flow and explain the need to account for bank flow in our hydrograph separation analyses, Figure 3.3.4.2a was created. This figure consists of six panels (A through E). Panel A represents average conditions for a hypothetical stream where the stream is gaining flow from groundwater because the water level in the aquifer is higher than the water level in the stream. Panels B and C show conditions during a precipitation event in which water levels in the stream become temporarily higher than the water level in the aquifer adjacent to the stream. For this condition, the stream becomes a losing stream as stream water flows from the stream into the aquifer. In addition, stream water enters the stream bank and becomes bank storage. After the flood event recedes, and the stream becomes a gaining stream again (panels D and E), the water held as bank storage flows back into the stream. When the stream begins to transition from a losing stream to a gaining stream, the majority of the groundwater that enters the stream is from bank flow. As the bank storage becomes depleted, the percent of groundwater entering the stream from bank flow decreases, and the amount that enters from basin flow increases. After bank flow has ceded, average stream conditions return (Panel E).

Accounting for bank-storage effects and bank flow can be important to surface water-groundwater interactions because it reduces the amount of base flow that originates as recharge from precipitation. Although the volume of bank storage at a certain time can be remarkably less than that of basin storage, the annual discharge from this source may equal or even exceed the share from basin storage due to frequent contribution and higher rate of discharge (Kunkle, 1962). Limited studies are available to quantify bank storage in Groundwater Management Area 12. However, a recent study performed by Rhodes and others (2017) indicates that bank flow can be appreciable. This study involved the analysis of water levels and water quality in the Brazos River and groundwater in Burleson County. Over a 4-month post-flood event period, Rhodes and others (2017) estimated that 96 percent of the groundwater that flowed to the Brazos River from the aquifer was from bank storage.

The approach to separate base flow values calculated for a river gage into bank flow and basin flow components involved applying two adjustments factors. One adjustment factor accounted

for the bank storage potential for river alluvium. This adjustment factor was based on the amount of alluvium in a watershed. The second adjustment factor accounted for the occurrence of high water or flooding conditions and was based on the amount of annual precipitation received by a watershed. The recharge predicted from base flow estimates through hydrograph separation analyses was reduced by up to 70 percent based on the combined effect of these two adjustment factors. Without these two adjustment factors, recharge rates higher than 10 inches per year were estimated based solely on the results from the hydrograph separation analyses for watersheds with high annual rainfalls.

The alluvium adjustment factor divides base flow into basin flow and bank flow based on the amount of river alluvium in a watershed. River alluvium is considered as an adjustment factor because the nature and extend of alluvium adjacent to a stream directly affects the potential for surface water-groundwater interaction. One rationale for considering alluvium as an adjustment factor is the fact that, across most of the model domain, the alluvium deposits identified by the *Geologic Atlas of Texas* maps (Barnes, 1970, 1979, 1981; Stoeser and others, 2007) are more permeable than the deposits they overlie. The potential importance of the alluvium to bank storage is provided by Dutton and others (2003):

> "Alluvium exchanges water between the Carrizo–Wilcox aquifer and the rivers. Groundwater in the bedrock formations can discharge into the alluvium, and water moves between the alluvial deposits and the surface-water channels. Alluvium can also store water that is recharged to the banks of rivers during flood flow; bank storage is released back to the rivers during low flow."

The alluvium adjustment factor was approximated as a linear function, where the percentage of base flow supplied by bank flow is 0 percent with no alluvium and increases to 40 percent where alluvium comprises 40 percent of the watershed.

The purpose of the second adjustment factor associated with bank storage and bank flow was to adjust the recharge rates based on precipitation. This adjustment factor, called the precipitation adjustment factor, depends solely on the amount of annual precipitation and its value equals the fraction of the base flow that originates from basin storage. Equations 3-5 and 3-6 were used to calculate the precipitation adjustment factor. For annual precipitation rates less than or equal to 35 inches per year, the precipitation adjustment factor was set to 1.0. For annual precipitation rates greater than 35 inches per year, the precipitation adjustment factor was assumed to decrease linearly to 0.4 for an annual precipitation of 75 inches per year.

$$If\ P \leq 35\ inches\ per\ year,\ PAF = 1.0 \qquad\qquad \text{(Equation 3-5)}$$

$$If\ P > 35\ inches\ per\ year,\ PAF = 1.0 - (P\text{-}35)\text{*}0.015 \qquad\qquad \text{(Equation 3-6)}$$

where:

PAF = precipitation adjustment factor
P = annual precipitation rate (inches per year)
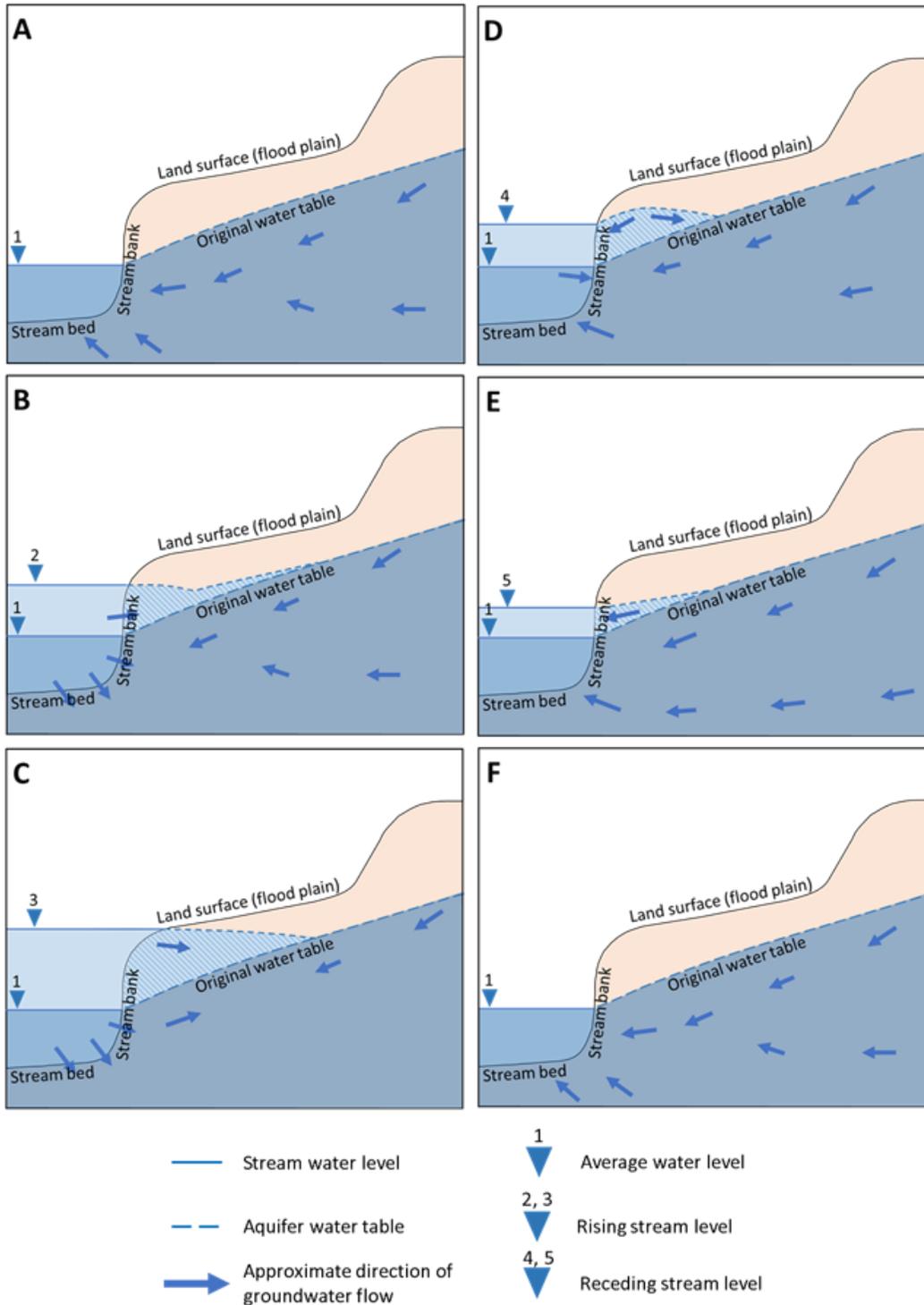
Figure 3.3.4.2a. Schematic showing groundwater flow toward a stream at sequential times. Water levels during average flow conditions at a gaining stream (A). Increase in stream elevation during a flooding event causes hydraulic gradient reversal at stream-aquifer interface. Streamflow enters aquifer and becomes bank storage in stream bank (B and C). Decrease in stream elevation after a flooding event. Bank storage flows back to the stream as bank flow as water level in the stream lowers over time (D and E). Water levels in stream and aquifer return to conditions that existed prior to flood event (F).

3.3.5 Approach for Calculation of Recharge Rates for the Updated Groundwater Availability Model

After developing the three adjustment factors, regressions were developed to estimate recharge as a function of precipitation for precipitation percentiles of 0.1, 0.2, 0.3, 0.4, 0.5, 0.6, 0.7, 0.8. and 0.9. The precipitation data used are time series raster data obtained from PRISM Climate Group (2012). The foundational recharge information used to develop these regressions were the regressions developed from the hydrograph separation analysis using the Baseflow Program conducted for the 12 river gages (Table 3.3.3a). For each precipitation percentile, the recharge associated with that precipitation was calculated from the regression developed for each of the 12 river gages.

So that these recharge estimates could be directly correlated, they were normalized to a surface geology scaling factor of 1.0 by dividing the recharge estimate from the regression by the surface geology scaling factor for the gage (Table 3.3.4.2b). This normalization was needed because the surface geology in the watersheds associated with these 12 gages are different. The recharge estimates calculated for the 12 gages were also adjusted for the amount of alluvium in each watershed using the alluvium adjustment factor.

The resultant recharge estimates, after being normalized for surface geology and adjusted for alluvium, was then plotted against the precipitation associated with that percentile for the 12 river gages, and a regression was fit through those data (Figure 3.3.5a). For example, the 0.1 percentile plot in Figure 3.3.5a shows 12 data points, one for each of the 12 river gages. Each data point reflects the 0.1 percentile of annual average precipitation in the watershed and the recharge for that precipitation value calculated using the regression fit for the gage provided in Table 3.3.3a normalized for surface geology and adjusted for alluvium. The regression fits for the different precipitation percentiles are tabulated in Table 3.3.5a. The values for R-squared and p-value for the regressions indicate that the regressions provide a good fit to the data.

Table 3.3.5a.   **Regressions developed for different precipitation percentiles for determining recharge.**

Precipitation Percentile	Regression for Calculating Recharge from Precipitation			
	Slope	Intercept	R-squared	p-value
0.1	0.177	-3.56	0.74	0.00032
0.2	0.219	-4.82	0.77	0.00020
0.3	0.251	-5.92	0.77	0.00017
0.4	0.284	-7.29	0.77	0.00016
0.5	0.310	-8.60	0.74	0.00031
0.6	0.340	-10.15	0.74	0.00035
0.7	0.348	-11.10	0.68	0.00098
0.8	0.396	-14.02	0.67	0.00112
0.9	0.386	-14.72	0.68	0.00093

The final process of assigning recharge to each grid block in the updated model for each year is summarized by the following four-steps:

1. Determined the annual precipitation for the grid cell and the year of interest using the historical time series precipitation raster data obtained from PRSIM Climate Group (2012). Determine the percentile for that annual precipitation relative to the average annual precipitation for the 81-year simulation period (1930 through 2010).

2. Apply the regression in Table 3.3.5a for the precipitation percentile and calculate a recharge rate. Note that the bank flow component of the recharge due to alluvium is already accounted for because it was incorporated into development of the regressions for each precipitation percentile.

3. Determine the precipitation adjustment factor using Equations 3-5 and 3-6. Multiply the recharge rate calculated in Step 2 by the precipitation adjustment factor.

4. Calculate the surface geology adjustment factor for the grid cell using the surface geology scaling factors for the individual geologic units in Table 3.3.4.1a and the percentage of each geologic unit assigned to the grid cell. Multiply the recharge rate determined in Step 3 by the surface geology adjustment factor.

To demonstrate its application, the four-step process was applied to the watersheds associated with the 12 river gages listed in Table 3.3.3a. After the recharge rates were calculated for each watershed, the watersheds were divided into three groups based on their spatial locations, and average recharge rates were calculated for each group and precipitation percentile (Table 3.3.5b). The recharges rates in Table 3.3.5b provide useful and informative trends for understanding the spatial and temporal variability in recharge. Across the entire model domain, the recharge rates vary temporally by at least a factor of two between the low and high precipitation years. Spatially, the rate of recharge increases from the south to the north. This trend occurs because both precipitation and the percentage of precipitation that becomes recharge increases from the south to the north. Annual recharge rates vary between 1 and 3 percent of the annual precipitation in the southern region of the model, 3 and 6 percent of the annual precipitation in the central region of the model, and 5 and 7 percent of the annual precipitation in the northern region of the model.

Table 3.3.5b. **Average recharge rates for watersheds grouped into the southern, central, and northern regions of the model domain determined using the regression in Table 3.3.5a and the percentile precipitation rates for each watershed.**

Precipitation Percentile	Two Watersheds in Southern Region[a]			Four Watersheds in Central Region[b]			Six Watersheds in Northern Region[c]		
	Average Precipitation (in/yr)	Recharge (in/yr)	Recharge divided by Precipitation	Average Precipitation (in/yr)	Recharge (in/yr)	Recharge divided by Precipitation	Average Precipitation (in/yr)	Recharge (in/yr)	Recharge divided by Precipitation
0.1	22.1	0.31	0.01	26.3	0.80	0.03	34.4	1.76	0.05
0.2	24.8	0.36	0.01	29.2	1.16	0.04	37.2	2.27	0.06
0.3	26.5	0.43	0.02	32.2	1.59	0.05	40.5	2.75	0.07
0.4	29.3	0.61	0.02	34.3	1.77	0.05	42.8	3.02	0.07
0.5	31.8	0.74	0.02	36.9	2.03	0.05	44.9	3.20	0.07
0.6	34.6	0.93	0.03	38.9	2.11	0.05	47.2	3.37	0.07
0.7	37.0	1.00	0.03	42.3	2.27	0.06	50.1	3.46	0.07
0.8	41.6	1.28	0.03	44.9	2.33	0.05	53.2	3.58	0.07
0.9	46.1	1.50	0.03	48.2	2.30	0.05	59.3	3.61	0.06

[a] Two watersheds associated with river gages 8174600 and 8186000
[b] Four watersheds associated with river gages 8186000, 8111000, 8108700, 8065200
[c] Six watersheds associated with river gages 8031200, 8064800, 8033000, 8033900, 8038000, 8039100
Note: in/yr = inches per year
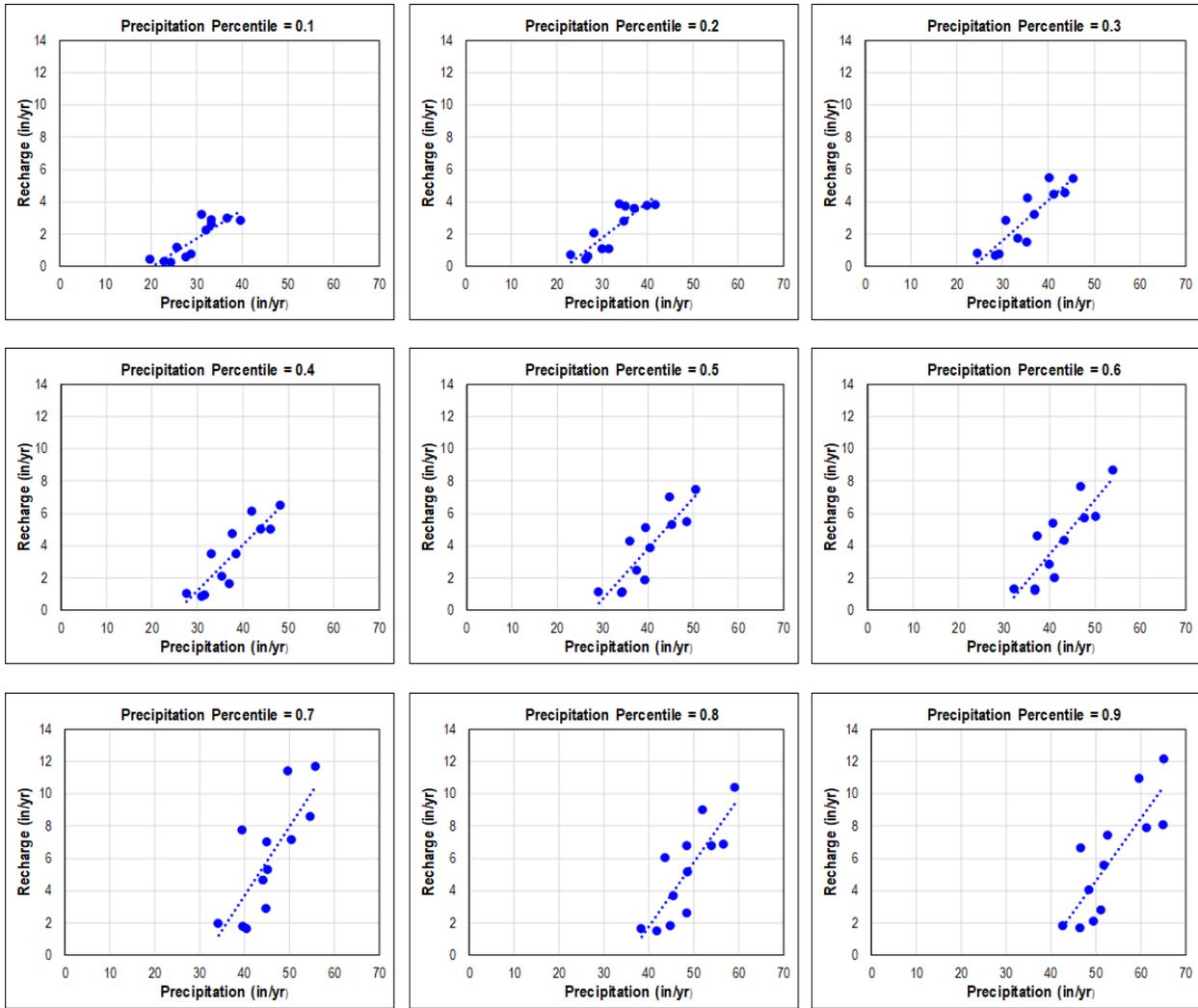
Figure 3.3.5a. **Recharge-precipitation data and regression fits developed for the different precipitation percentiles. The attributes associated with the regressions are provided in Table 3.3.5a.**

3.4   Surface Water and Groundwater Interaction

As illustrated in Figure 3.4a, groundwater moves along flow paths of varying lengths from areas of recharge to areas of discharge within a groundwater basin. Toth (1962, 1963) was among the first to conceptualize and demonstrate that large groundwater systems are comprised of groundwater flow paths of different spatial and time scales. Toth (1963) classified the different scales of groundwater flow paths as local, intermediate, and regional, which can be defined as:

- At the local scale, groundwater flow paths remain relatively shallow, recharge and discharge areas are adjacent to each other, and groundwater travel times are on the order of days or years.
- At the intermediate scale, groundwater flow paths can travel through multiple formations, recharge and discharge areas are separated by one or more topographic highs and lows, and groundwater travel times are on the order of decades or centuries.

- At the regional scale, groundwater flow paths can cross an entire basin, recharge areas are along groundwater divides, discharge areas lie at the bottom of major drainage basins, and groundwater travel times are on the order of millennia.

As a result of relatively large grid cells, which are typical 1 mile by 1 mile, and relatively thick model layers that are typically the thickness of an entire aquifer, groundwater availability models are constructed to better simulate regional-scale and intermediate-scale groundwater flow than shallower, local-scale groundwater flow. The potential problem with accurately representing surface water-groundwater interaction in the groundwater availability models is concisely explained by Mace and others (2007):

> "One of the difficulties in accurately representing surface water-groundwater interaction is the vertical resolution in the groundwater availability model. The interaction of a stream and an aquifer is an intimate affair that occurs locally on the order of feet to tens of feet. In many cases, the current groundwater availability models are too coarse, both laterally and vertically, to accurately represent surface water-groundwater interaction. The difference between a gaining stream and a losing stream can be the difference of a few feet of groundwater level change, especially for the aquifers along the Gulf Coast where there is not much topography."
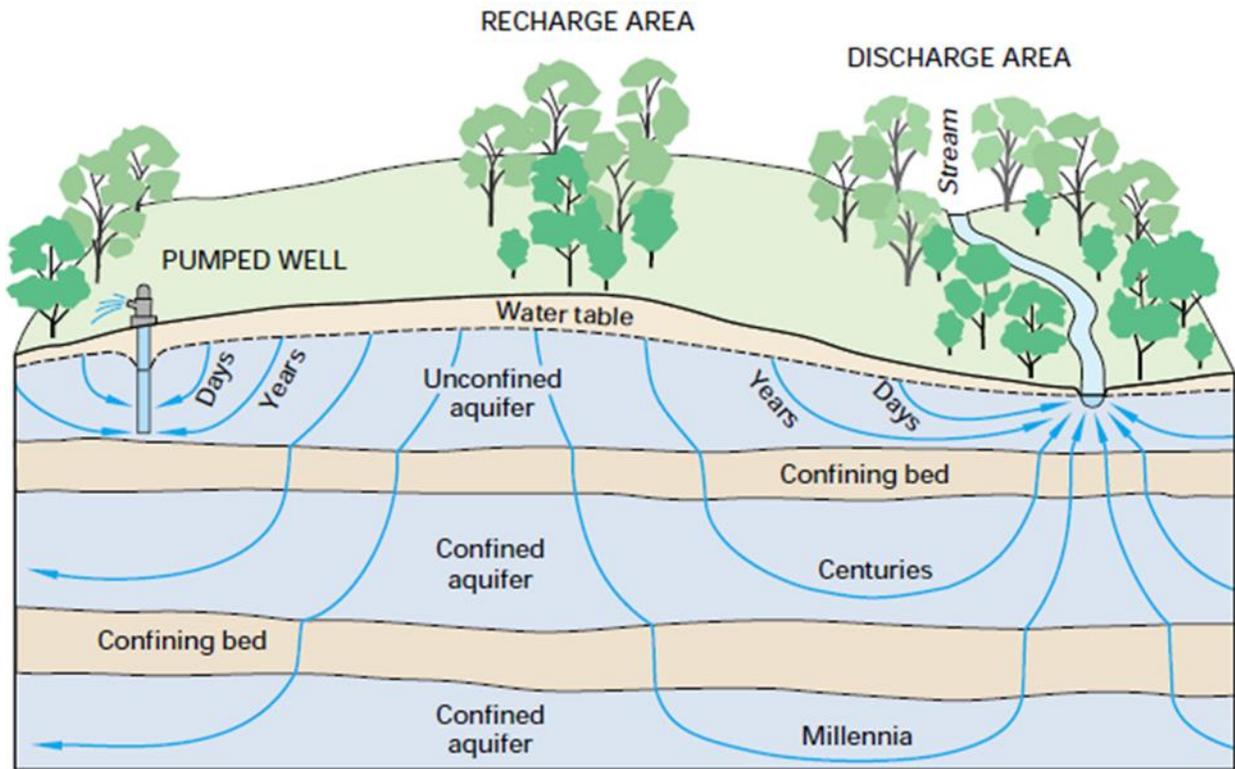
Figure 3.4a   **Schematic illustration of the different spatial and time scales of groundwater flow paths (Winter and others, 1999).**

3.4.1   Addition of Model Layers to Represent Shallow, Local-Scale Groundwater Flow

In their discussion of the difficulties with accurately representing surface water-groundwater interaction in groundwater availability models, Mace and others (2007) cite a modeling approach that appears promising for improving the ability of groundwater availability models to simulate surface water-groundwater interaction. The modeling approach was used to develop a regional groundwater model for the Lower Colorado River Basin in the Gulf Coast Aquifer (Budge and others, 2007) and it relied on creating a thin model layer near the surface. The approach of adding layers near the ground surface was used to improve this updated groundwater availability model's ability to simulate the interaction between surface water and groundwater.

The addition of model layers near land surface provides two potential benefits for improving the ability of the groundwater availability model to simulate groundwater flow. One of these benefits is the capability to better represent vertical hydraulic gradients near land surface and near rivers. The other benefit is an enhanced capability to more accurately locate well screens vertically in the model and to more likely avoid locating a pumping well in the same grid cell as a river cell.

In the updated groundwater availability model, the alluvium associated with the Colorado River and the Brazos River Alluvium Aquifer are represented by a model layer designed only to represent river alluvium. As a result, this model layer is active only in the vicinity of the Colorado and Brazos rivers. Beneath this model layer, the groundwater availability model includes another shallow model layer that extends across the entire outcrop area of the simulated hydrogeologic units. This shallow model layer provides an opportunity to model groundwater flow near the water table and in contact with surface water.

The addition of these two model layers to the groundwater availability model is illustrated by showing the model numerical grid along transects A-A′ and B-B′ (Figures 3.4.1a). Figure 3.4.1a shows an aerial view of the numerical grid along the Colorado River in Bastrop County. The refined 0.25-mile by 0.25-mile grid cells by the river are discussed in the next section. Figures 3.4.1b and 3.4.1c show the model layering beneath the Colorado River to a depth of about 400 feet for transects A-A′ and B-B′, respectively.
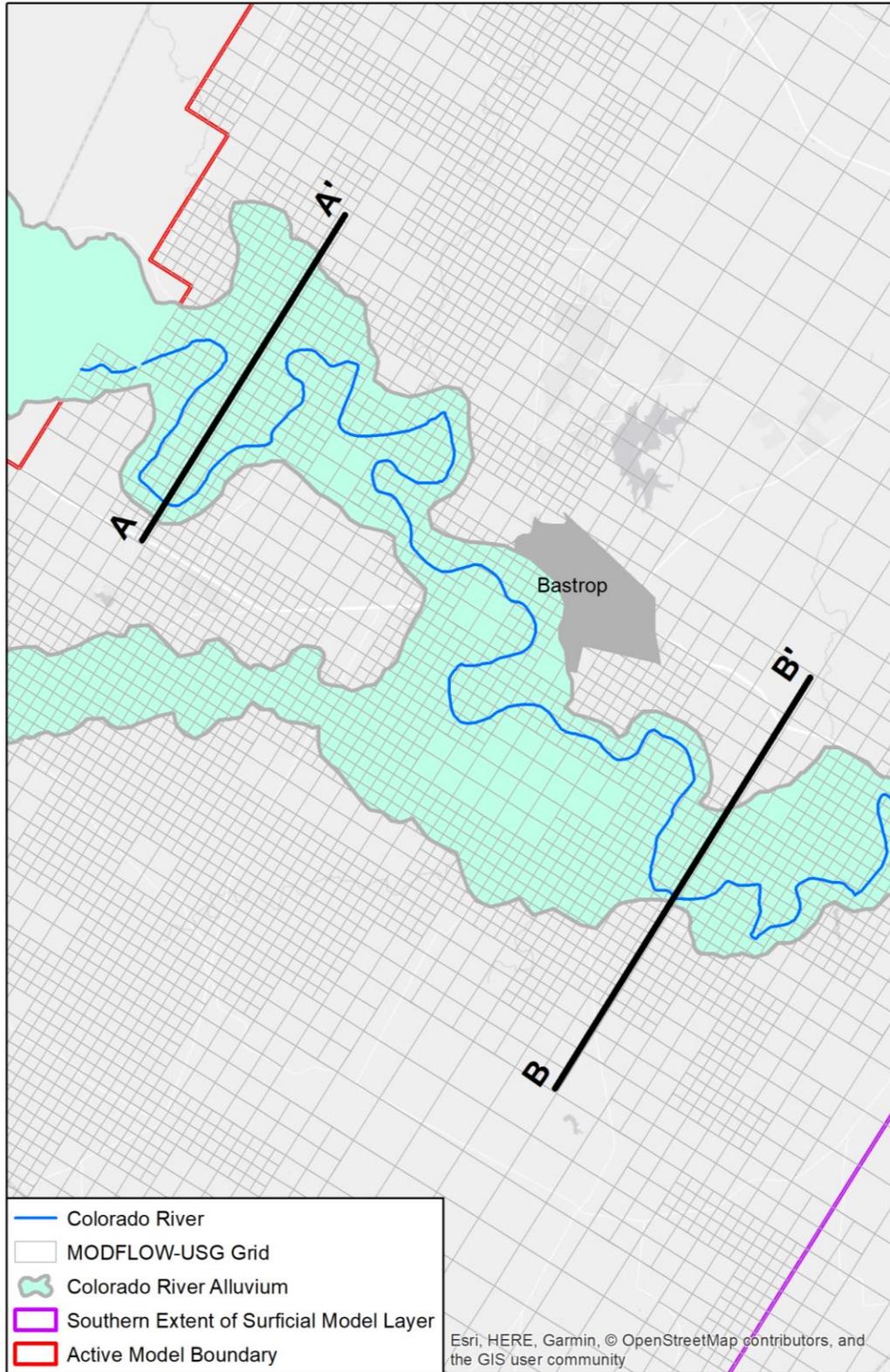
Figure 3.4.1a.   **Areal extent of the Colorado River alluvium mapped onto the numerical grid for the updated groundwater availability model for the central portion of the Carrizo-Wilcox, Queen City, and Sparta aquifers.**
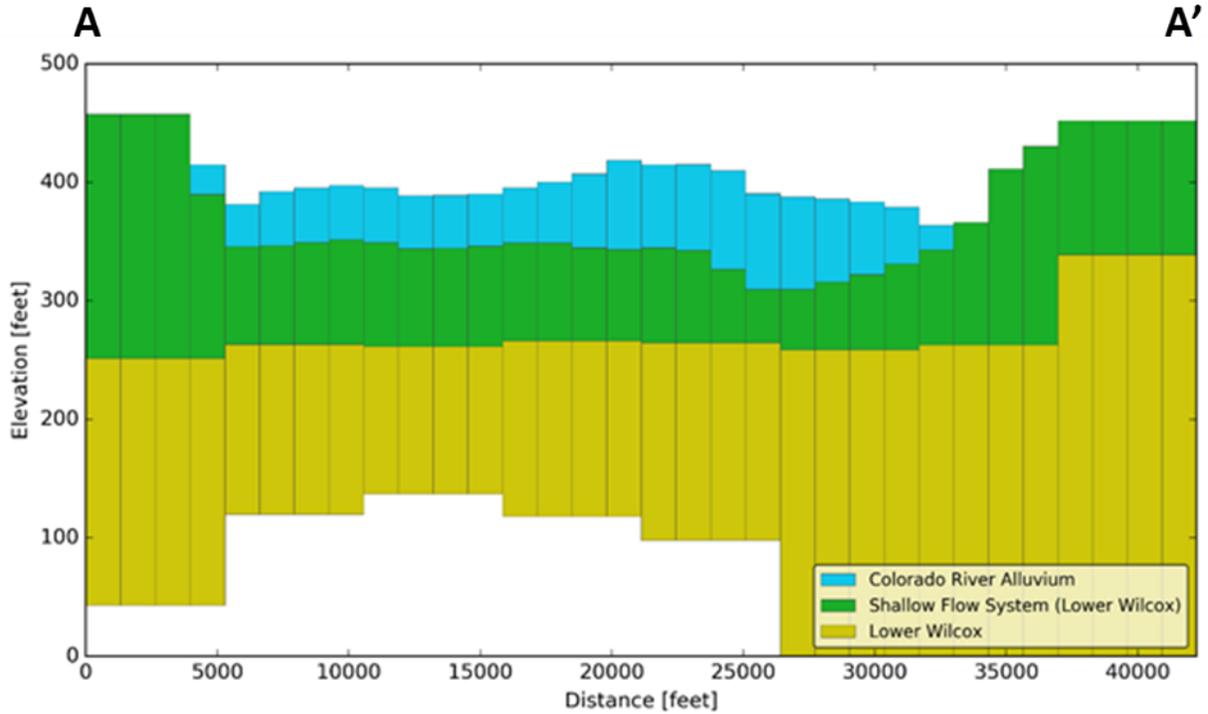
Figure 3.4.1b. Vertical cross-section for the updated model showing the model layers in the upper 400 feet along transect A-A′ shown in Figure 3.4.1a.
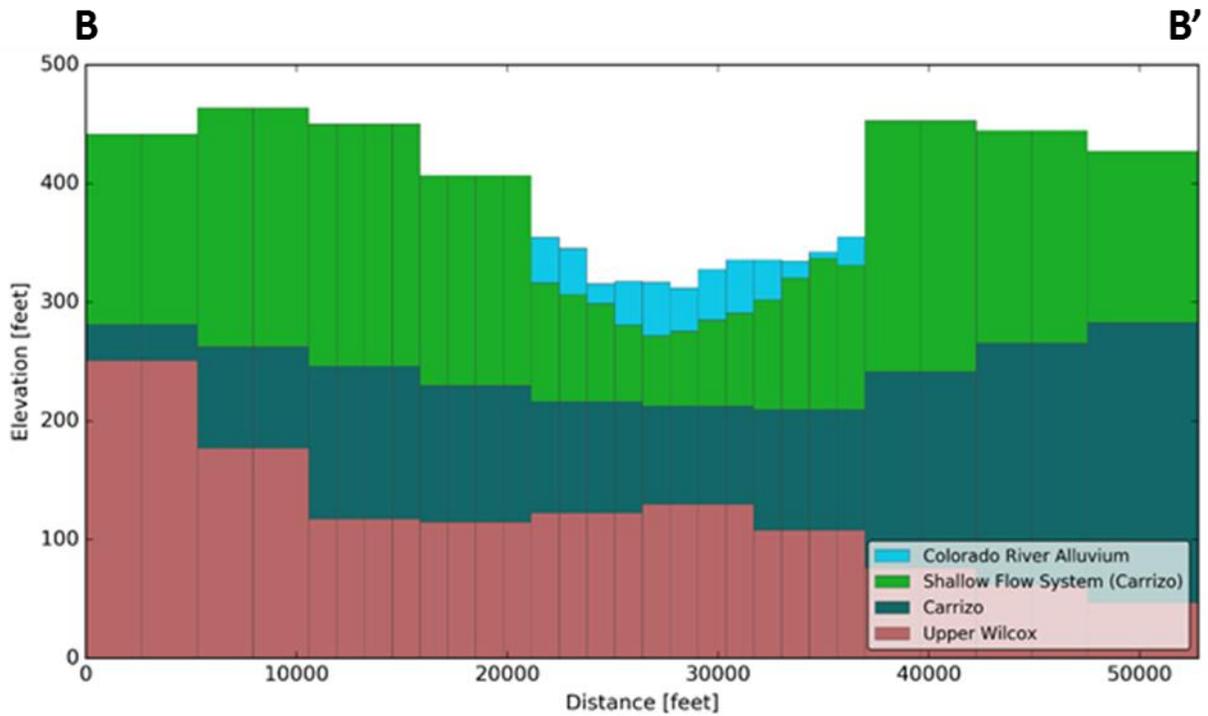
Figure 3.4.1c. Vertical cross-section for the updated model showing the model layers in the upper 400 feet along transect B-B′ shown in Figure 3.4.1a.

3.4.2   Addition of Grid Refinement in the Vicinity of the Colorado and Brazos Rivers

Mace and others (2007) state that groundwater availability models have difficulties with accurately representing surface water-groundwater interaction not only because they are too coarse vertically but also because they are too coarse laterally. In the updated model, the 1-mile by 1-mile numerical grids in the vicinity of the Colorado River and Brazos River were replaced with smaller grid cells. As shown in Figure 3.4.2a, in the vicinity of the Colorado River and its major tributaries, the grid cells in the updated model were reduced to 0.25 mile by 0.25 mile. As shown in Figure 3.4.2b, in the vicinity of the Brazos River and its major tributaries, the grid cells were reduced to 0.5 mile by 0.5 mile in the updated model. The refinement of the grid cells improves the capability of the model to represent the location of the pumping wells and the streams. In addition, the increased refinement provides for improved resolution for representing horizontal hydraulic gradients.
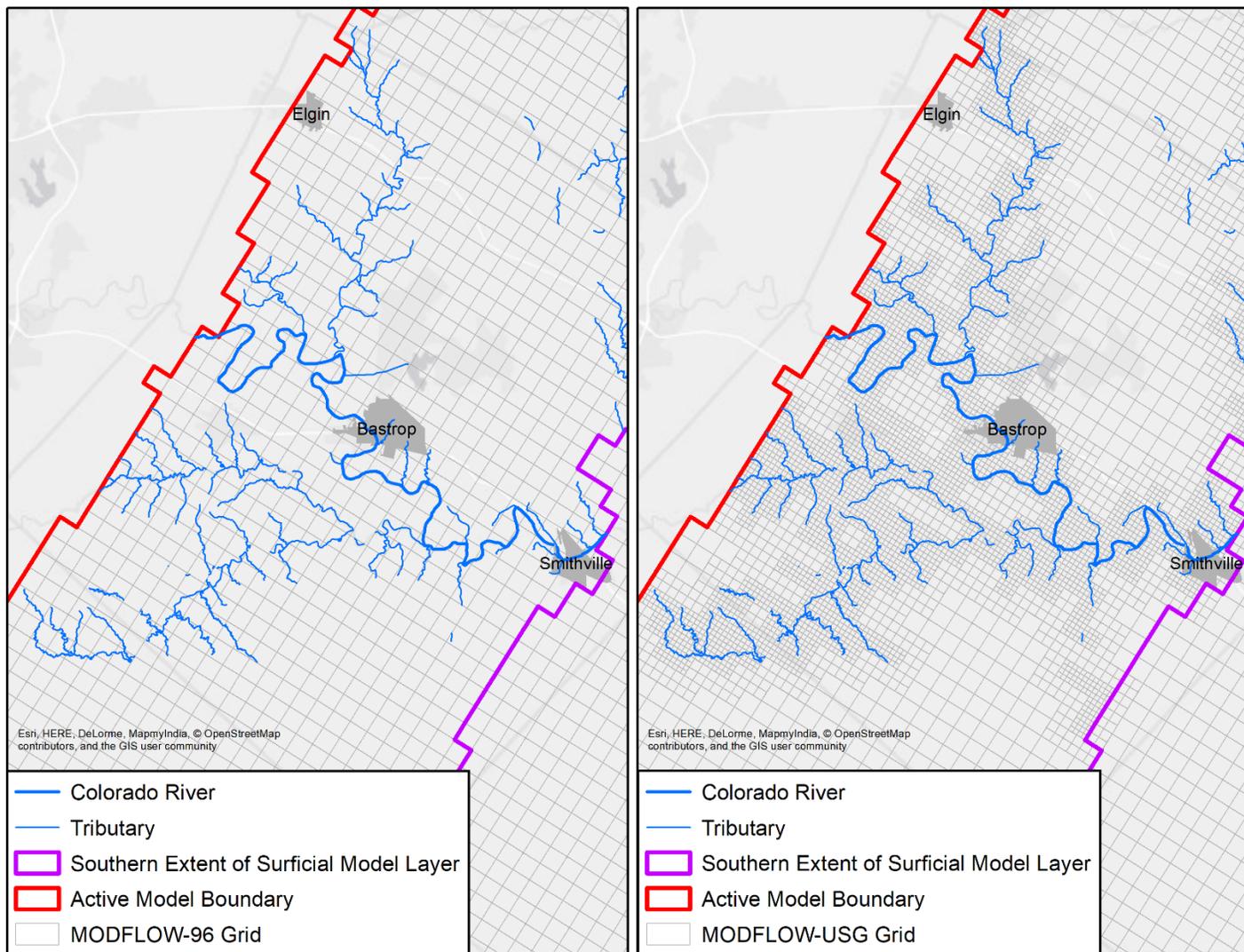
Figure 3.4.2a. Numerical grid showing the uniform 1-mile by 1-mile square grid cells in the 2004 groundwater availability model for the central portion of the Carrizo-Wilcox, Queen City, and Sparta aquifers (left) and the locally-refined grid with 0.25-mile by 0.25-mile square grid cells in the vicinity of the Colorado River and its major tributaries in the updated model (right).
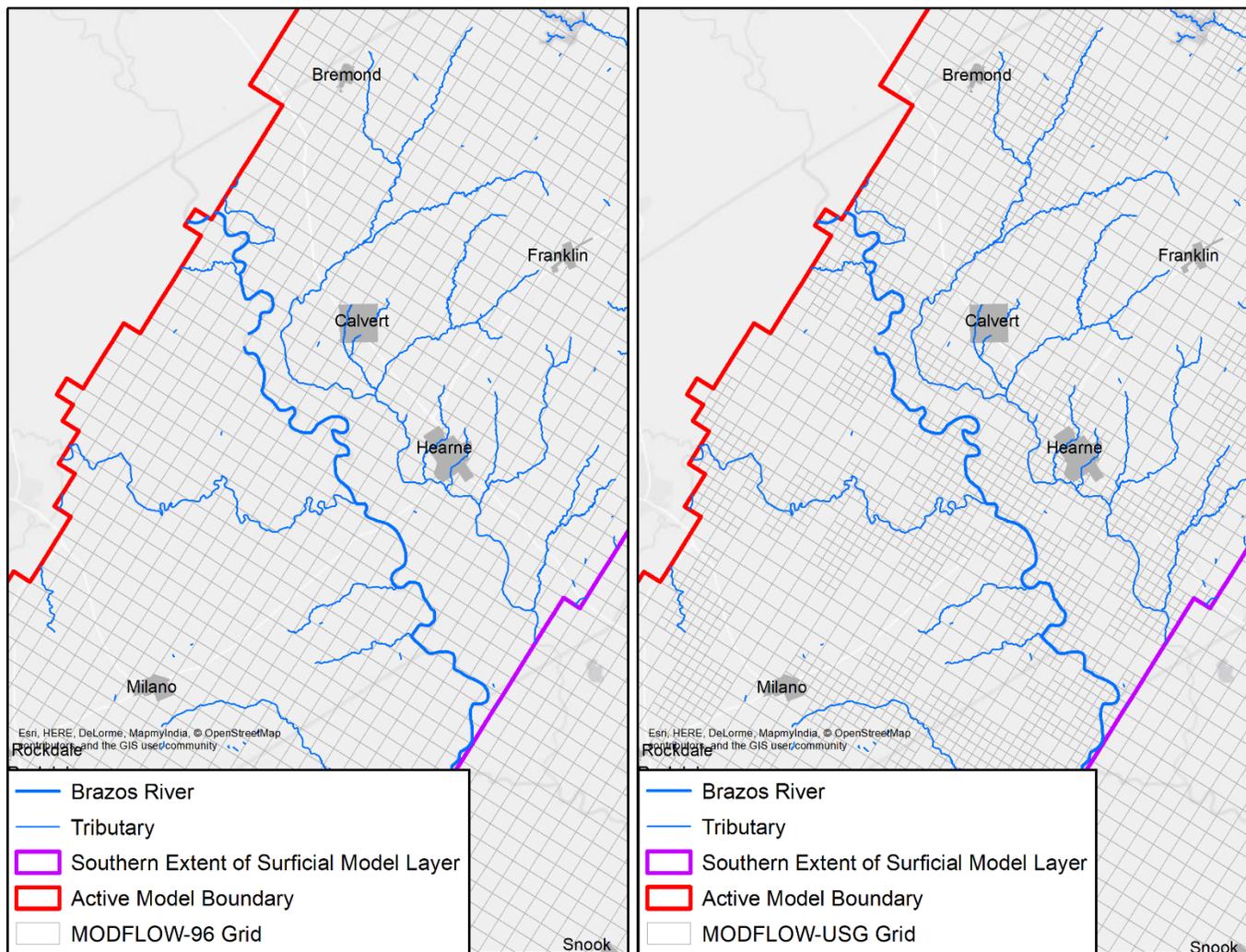
Figure 3.4.2b. **Numerical grid showing the uniform 1-mile by 1-mile square grid cells in the 2004 groundwater availability model for the central portion of the Carrizo-Wilcox, Queen City, and Sparta aquifers (left) and the locally-refined grid with 0.5-mile by 0.5-mile square grid cells in the vicinity of the Brazos River and its major tributaries in the updated model (right).**

3.5   Conceptual Model of Groundwater Flow

The conceptual model is a simplified representation of the hydrogeologic features that govern groundwater flow in the aquifers. These include the hydrostratigraphy, hydraulic properties, hydraulic boundaries, recharge and natural discharge, and anthropogenic stresses, such as pumping. The updated model is built on the conceptual model of the groundwater flow system for the Sparta, Queen City, and Carrizo-Wilcox aquifers that is presented by Kelley and others (2004). Figure 3.5a identifies the ten layers in the updated model and the major processes affecting groundwater flow within and across these layers.

The Colorado and Brazos rivers alluvium are represented by layer 1 in the model. Model layer 2 represents a shallow flow system that primarily includes the outcrops of the hydrogeologic units (Figure 3.5a). This model layer serves to promote lateral flow among the different aquifers and between groundwater and surface water. Model layers 3 through 10 represent the confined regions of the eight major hydrogeologic units that comprise the groundwater flow system. From youngest to oldest, these hydrogeological units are the: Sparta Aquifer, Weches Formation, Queen City Aquifer, Reklaw Formation, Carrizo Aquifer, and Wilcox Aquifer. The Wilcox Aquifer is comprised of the Calvert Bluff Formation, the Simsboro Formation, and the Hooper Formation. In the groundwater system, the Reklaw Formation represents a regional aquitard, and the Weches Formation consists of clayey deposits that often serve as a localized aquitard.

Groundwater flow within the aquifers is controlled by the topography, the structure, and the permeability variations within the different layers. Groundwater flow downdip into the confined portions of these aquifers is controlled by the high permeability sands relative to the lower permeability units. Three-dimensional flow is expected in the aquifers and primarily one-dimensional vertical flow is expected in the Weches and Reklaw formations. For these latter two formations, flow near ground surface would likely exit through evapotranspiration, surface-water runoff, or cross-formational flow to higher permeability units.

Recharge and evapotranspiration occurs on the outcrops of the hydrogeologic units. Recharge is a function of precipitation, geology, water level, soil moisture, and topography. Precipitation, evapotranspiration, water-table elevation, and soil moisture vary spatially and temporally, whereas soil type, geology, and topography vary spatially. In addition to natural phenomena, water levels are affected by pumpage and man-made surface-water reservoirs and lakes, which in turn affect recharge. Diffuse recharge occurs preferentially in topographically higher interstream areas within the outcrops. Focused recharge along streams can occur when the water table in the aquifer is below the stream-level elevation. If stream levels are lower than surrounding groundwater levels, groundwater discharges to the streams, resulting in gaining streams. In this case, water levels in the valley are typically close to land surface, and some of the shallow groundwater in this area can be lost to evapotranspiration.
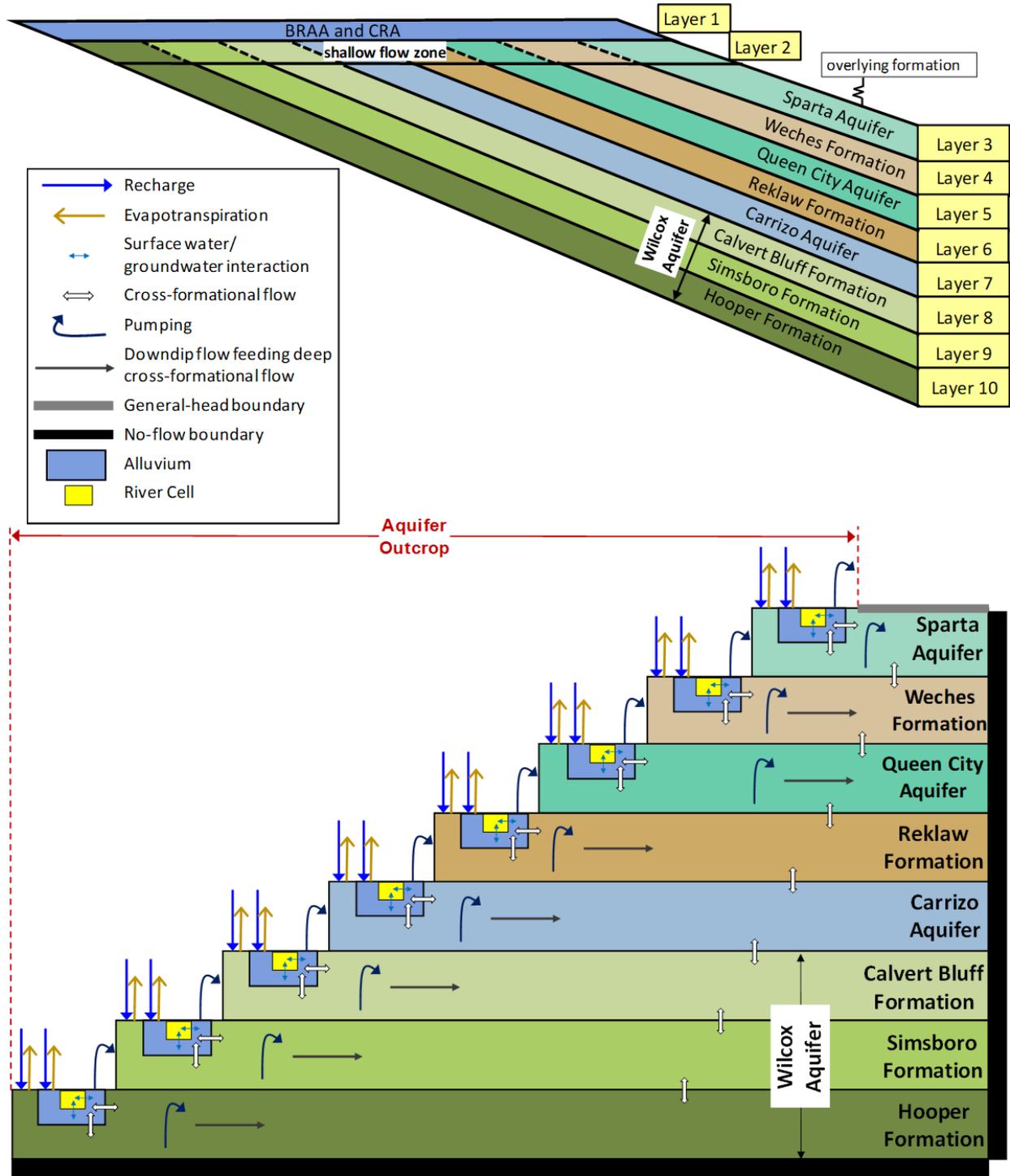
Figure 3.5a. Conceptual groundwater flow model for the updated groundwater availability model for the central portion of the Carrizo-Wilcox, Queen City, and Sparta aquifers.

This page is intentionally blank.

4 Model Overview and Packages

The code selected for the updated groundwater availability model for the central portion of the Carrizo-Wilcox, Queen City, and Sparta aquifers is MODFLOW-USG (Panday and others, 2013). MODFLOW-USG is a three-dimensional control volume finite difference groundwater flow code that is supported by boundary condition packages to handle recharge, evapotranspiration, streams, springs and reservoirs. MODFLOW-USG is an enhanced version of the MODFLOW family of codes developed and supported by the United States Geological Survey. Using MODFLOW-USG for the current effort has several benefits because MODFLOW: (1) incorporates the necessary physics of groundwater flow, (2) is the most widely accepted groundwater flow code in use today, (3) was written and is supported by the United States Geological Survey and is public domain, (4) is well documented (McDonald and Harbaugh, 1988; Harbaugh and McDonald, 1996; Harbaugh and others, 2000; Harbaugh, 2005; Niswonger and others, 2011; Panday and others, 2013), (5) has a large user group, and (6) allows for refinement in areas of interest in a computationally efficient manner. Additionally, there are numerous graphic user interfaces that can be used to develop MODFLOW-USG models and process model results.

The graphic user interface chosen in this case is Groundwater Vistas Version 6.84. The model grid was developed using Groundwater Vistas, with several packages being developed outside of the graphic user interface and then imported into Groundwater Vistas after calibration was complete. Thus, the workflow for model creation did not necessarily follow any workflow prescribed by the use of that graphic user interface.

A MODFLOW model consists of groupings of input text files (also called "packages") that describe various components of the groundwater flow system. The input packages and their corresponding filenames are shown in Table 4.0a. The output files written by MODFLOW contain water levels (HDS), drawdown (DDN), water budget information (CBB), and a listing of the characteristics of the run (LST) as shown in Table 4.0b. A description of the contents of the input packages (Table 4.0a) are provided in the subsections that follow.

Table 4.0a.   **Summary of model input files and filenames.**

File Type Abbreviation	File Type	Input File Name
BAS6	Basic Package	gma12.bas
DISU	Discretization File	gma12.dis
LPF	Layer Property Flow Package	gma12.lpf
WEL	Well Package	gma12.wel
DRN	Drain Package	gma12.drn
RCH	Recharge Package	gma12.rch
GHB	General-head Boundary Package	gma12.ghb
RIV	River Package	gma12.riv
EVT	Evapotranspiration Package	gma12.evt
HFB	Horizontal Flow Barrier	gma12.hfb
GNC	Ghost Node Correction Package	gma12.gnc
OC	Output Control Option	gma12.oc
SMS	Sparse Matrix Solver Package	gma12.sms

Table 4.0b.   **Summary of model output files and filenames.**

File Type	Output File Name
Binary flow file	gma12.cbb
Binary head file	gma12.hds
Binary drawdown file	gma12.ddn
List file	gma12.lst

4.1 Basic Package

The MODFLOW-USG Basic package (file type BAS6) is used to (1) specify which cells in each model layer are active or inactive and (2) specify the starting water levels in the layers for the simulation. The Basic package can also be used to specify constant head cells. The updated model was constructed to eliminate inactive areas and, thus, all cells are active. The extent of each model layer is presented in the next section. The updated model's construction also does not contain any constant head cells.

4.2 Discretization Package

The MODFLOW Unstructured Discretization (suffix DISU) package contains the model node dimensions, the nodal elevations of the model layers, the nodal connections, the connection areas and lengths between nodes, and a definition of the model stress periods.

4.2.1 Model Grid Specifications

The numerical grid for the updated groundwater availability model for the central portion of the Carrizo-Wilcox, Queen City, and Sparta aquifers was generated by refining the numerical grid developed by Kelley and others (2004) and by adding two model layers. As discussed in Section 3.4, the two additional model layers represent the Colorado and Brazos rivers alluvium in model layer 1 and a shallow groundwater flow system in model layer 2. Because the updated model was developed using MODFLOW-USG, the grid cells are no longer referred to by rows and columns but rather by unique node numbers. Because the numerical grid is unstructured, and each model layer represents different hydrogeologic units with different coverages, model layers contain a different number of nodes. Table 4.2.1a lists the number of nodes and hydrostratigraphic units associated with each model layer.

Table 4.2.1a.   **Number of nodes representing each model layer.**

Model Layer	Hydrogeologic Unit	Number of Nodes
1	Colorado River and Brazos River Alluviums	2,221
2	Shallow Flow System	19,089
3	Sparta Aquifer	16,185
4	Weches Formation	17,218
5	Queen City Aquifer	21,941

6	Reklaw Formation	23,315
7	Carrizo Aquifer	24,786
8	Calvert Bluff Formation	29,084
9	Simsboro Formation	30,954
10	Hooper Formation	34,123

The numerical grid for the model has the same numerical mesh consisting of 1-mile by 1-mile square grid cells as Kelly and others (2004), except in the vicinity of the Colorado and Brazos rivers, where the numerical mesh was refined using a quadtree mesh (see Figures 3.4.2a and 3.4.2b). The numerical grid is oriented 58 degrees west of north in the TWDB's designated coordinate system for groundwater availability models (Anaya, 2001). The lower left corner of the grid is positioned at groundwater availability model coordinates: 6175267.5649 easting, 18481980.9244 northing.

Figures 4.2.1a through 4.2.1j provide the top elevation of each of the 10 model layers. The top elevations for model layers 1 and 2 were adjusted from the values used by Kelly and others (2004) for two reasons: (1) if the 1-mile by 1-mile grid cell was refined by a quad tree mesh, a new ground elevation was assigned to each grid cell and (2) if the ground surface elevation was less than the average elevation calculated for the grid cell based on a United States Geological Survey 10-meter (32.8-foot) digital elevation model (United States Geological Survey, 2014), then the ground elevation was changed to the calculated ground elevation.

As shown in Figure 3.5a, model layer 2 represents a shallow flow system comprised of the updip regions of the hydrogeologic units that comprise model layers 3 through 10. Figure 4.2.1k shows the spatial distribution of the hydrogeologic units in layer 2. The properties and recharge assigned to grid cells in model layer 2 were based on the hydrogeologic unit assigned to the grid cell. The bottom surface of model layer 2 is also the top surface for the updip regions of model layers 3 through 10. The confined and downdip regions of these eight layers are based on grid cell elevations generated by Kelley and others (2004), except for the surface contact between the Calvert Bluff and Simsboro formations.

Adjustments were made to the surface contact between the Calvert Bluff and Simsboro formations at the locations marked by the letters A, B, and C in Figure 4.2.1i. At these locations, the Simsboro Formation was between 75 and 150 feet thick in the 2004 model. These small thicknesses were a result of Dutton and others' (2003) use of maps prepared by Ayers and Lewis (1985) that characterized the Simsboro Formation as channelized bands of thick sands in between which relatively thin sands exist. Prior to making changes to the top surface of the Simsboro Formation, the proposed changes and data supporting the changes were discussed with the groundwater consultants to the Brazos Valley Groundwater Conservation District (John Seifert, personal communication) and Lost Pines Groundwater Conservation District (Andy Donnelly, personal communication). These discussions led to agreement that the mapped Simsboro Formation thickness of less than 150 feet at those three locations should be changed to better reflect the regional Simsboro Formation thickness.

To help visualize the model layering, vertical cross-sections were created along the three transects shown in Figure 4.2.1l. Figure 4.2.1m shows a cross-section along Dip A-A′ that crosses through Bastrop, Fayette and Colorado counties. Figure 4.2.1n shows a cross-section along Dip B-B′ that crosses through Robertson, Brazos and Grimes counties. Figure 4.2.1o shows a cross-section along Strike C-C′ that crosses through Fayette, Lee, Burleson, Brazos, and Limestone counties. Only Dip A-A′ shows all ten model layers. Dips B-B′ and C-C′ show model layers 2 through 10.
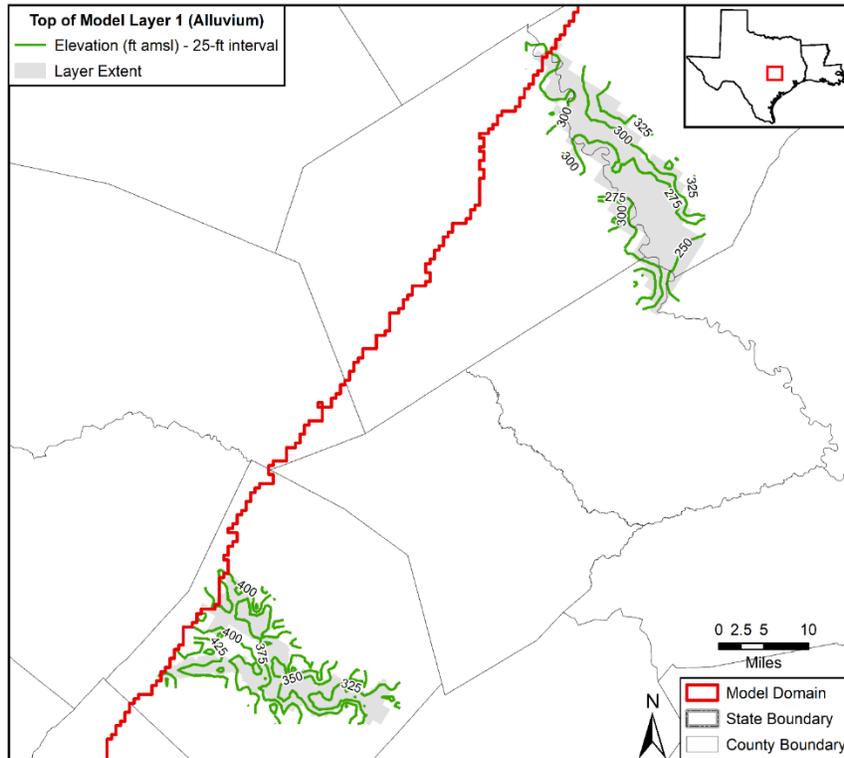
Figure 4.2.1a. **Elevation of the top of model layer 1 (alluvium) in feet (ft) above mean sea level (amsl).**
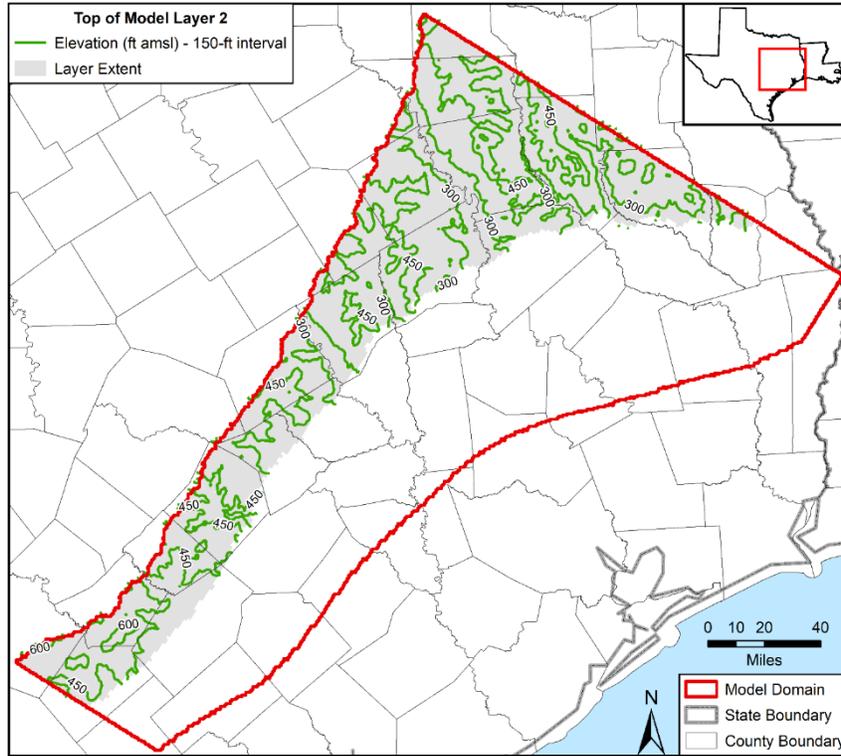
Figure 4.2.1b.   **Elevation of the top of model layer 2 in feet (ft) above mean sea level (amsl).**
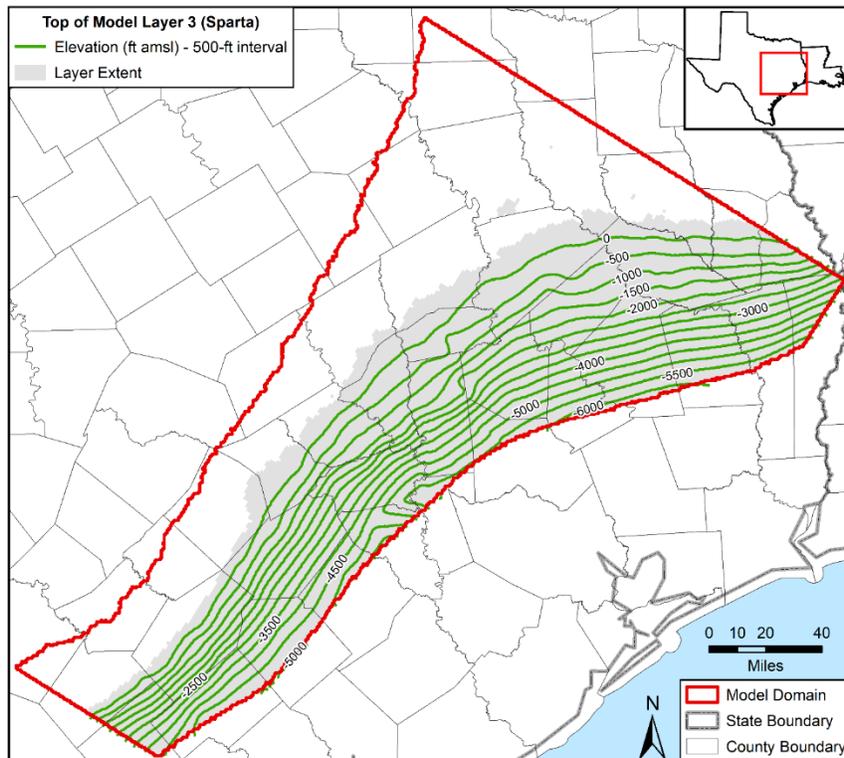
Figure 4.2.1c.   **Elevation of the top of model layer 3 in feet (ft) above mean sea level (amsl), which represents the downdip region of the Sparta Aquifer.**

Final Report: Groundwater Availability Model for the Central Portion
of the Carrizo-Wilcox, Queen City, and Sparta Aquifers
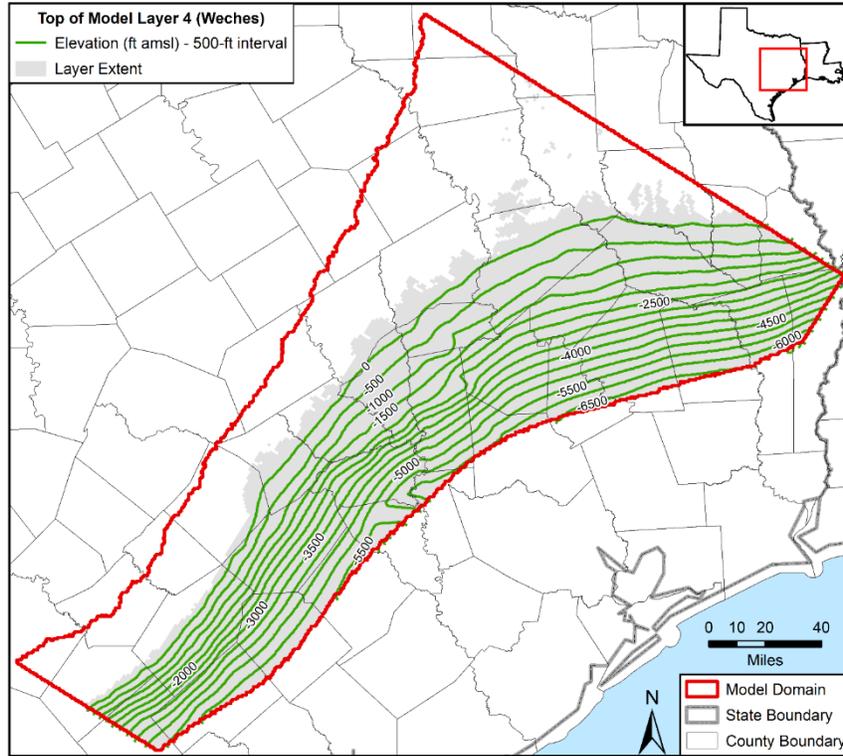
Figure 4.2.1d. **Elevation of the top of model layer 4 in feet (ft) above mean sea level (amsl), which represents the downdip region of the Weches Formation.**
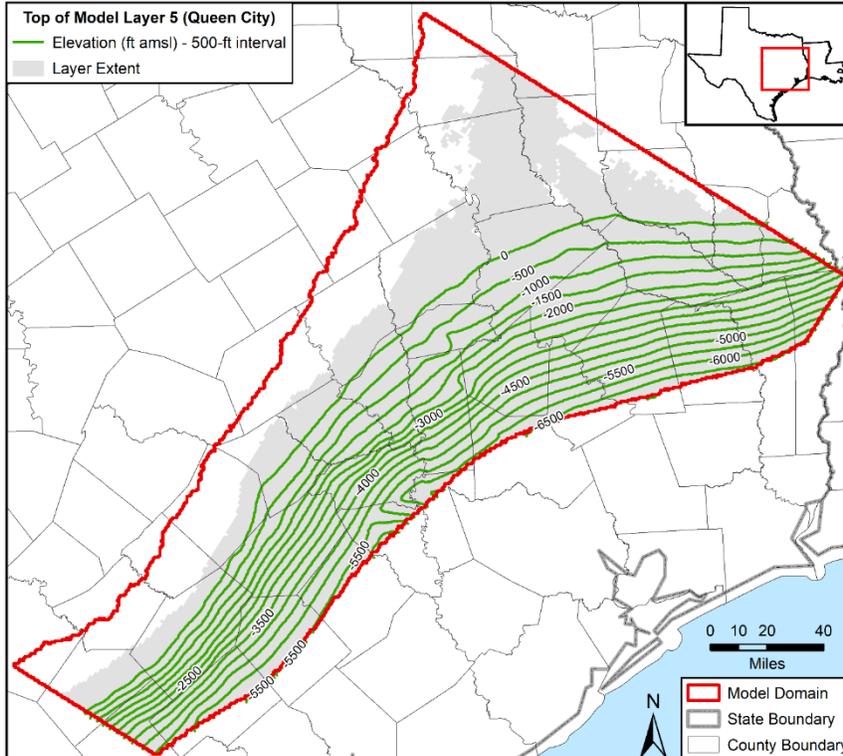
Figure 4.2.1e. **Elevation of the top of model layer 5 in feet (ft) above mean sea level (amsl), which represents the downdip region of the Queen City Aquifer.**
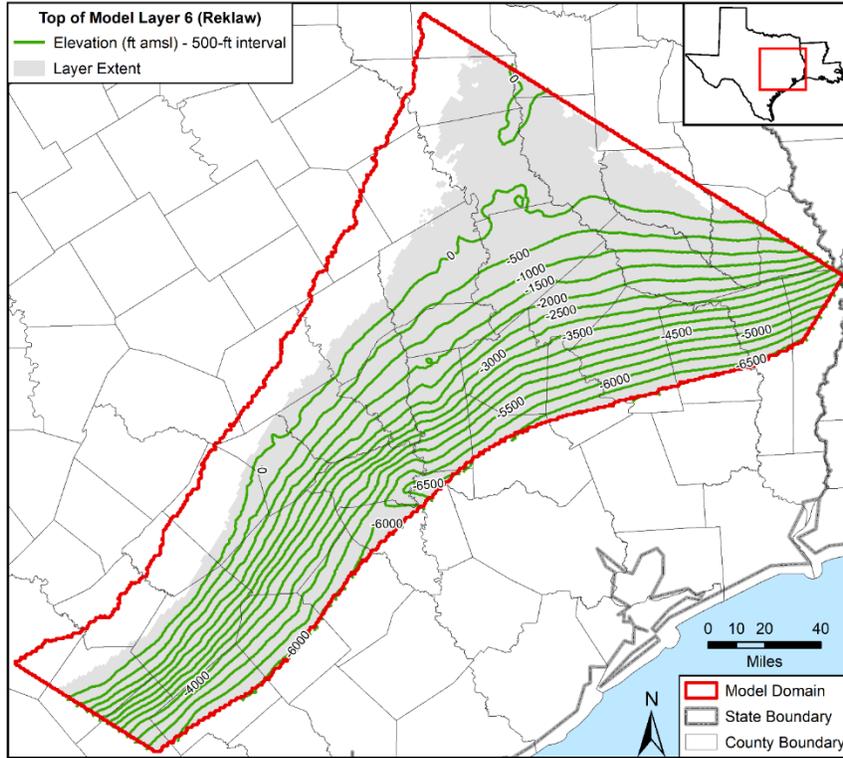
Figure 4.2.1f. Elevation of the top of model layer 6 in feet (ft) above mean sea level (amsl), which represents the downdip region of the Reklaw Formation.
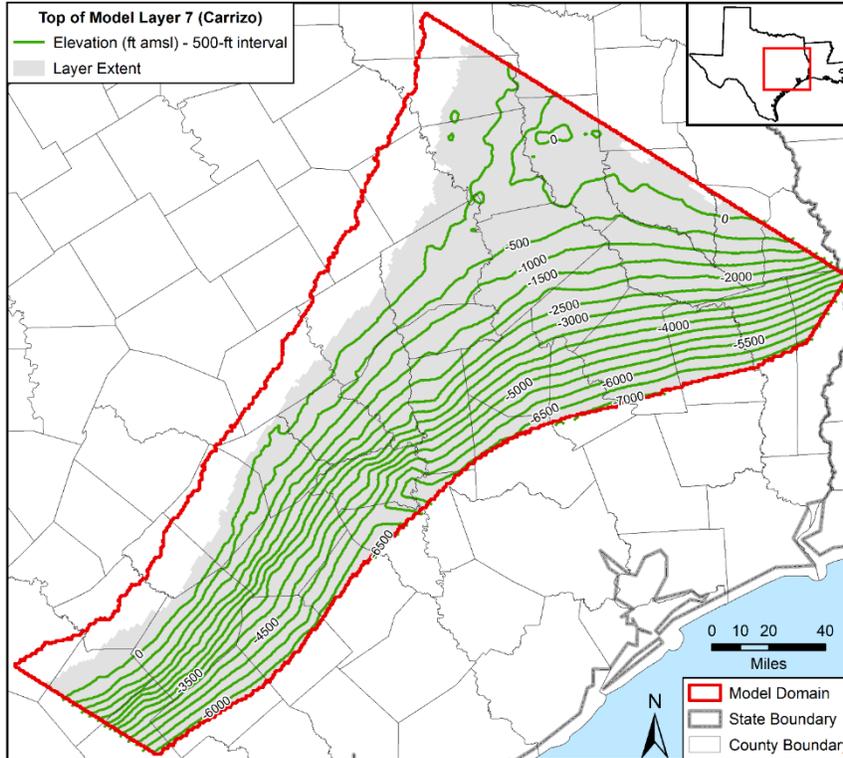
Figure 4.2.1g. Elevation of the top of model layer 7 in feet (ft) above mean sea level (amsl), which represents the downdip region of the Carrizo Aquifer.

Figure 4.2.1h. **Elevation of the top of model layer 8 in feet (ft) above mean sea level (amsl), which represents the downdip region of the Calvert Bluff Formation.**
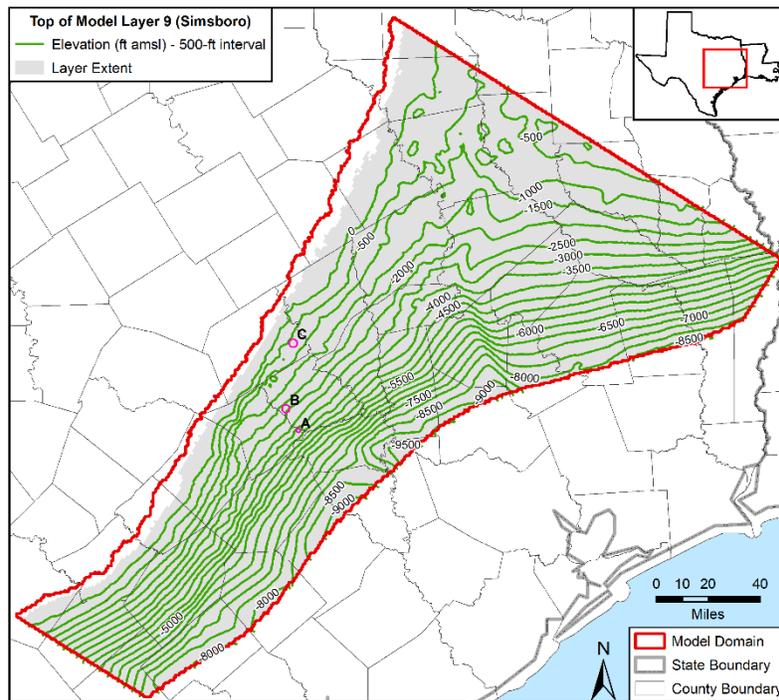
Figure 4.2.1i. **Elevation of the top of model layer 9 in feet (ft) above mean sea level (amsl), which represents the downdip region of the Simsboro Formation.**

Note: Red circles and letters indicate areas where the surface contact between the Calvert Bluff and Simsboro formations were adjusted in the updated model.
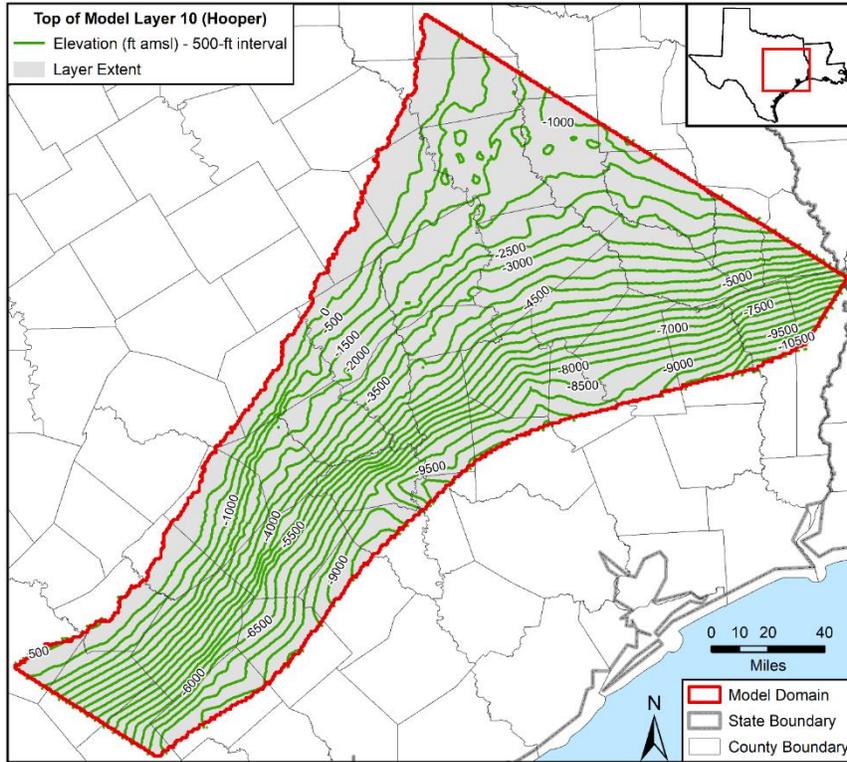
Figure 4.2.1j. **Elevation of the top of model layer 10 in feet (ft) above mean sea level (amsl), which represents the downdip region of the Hooper Formation**
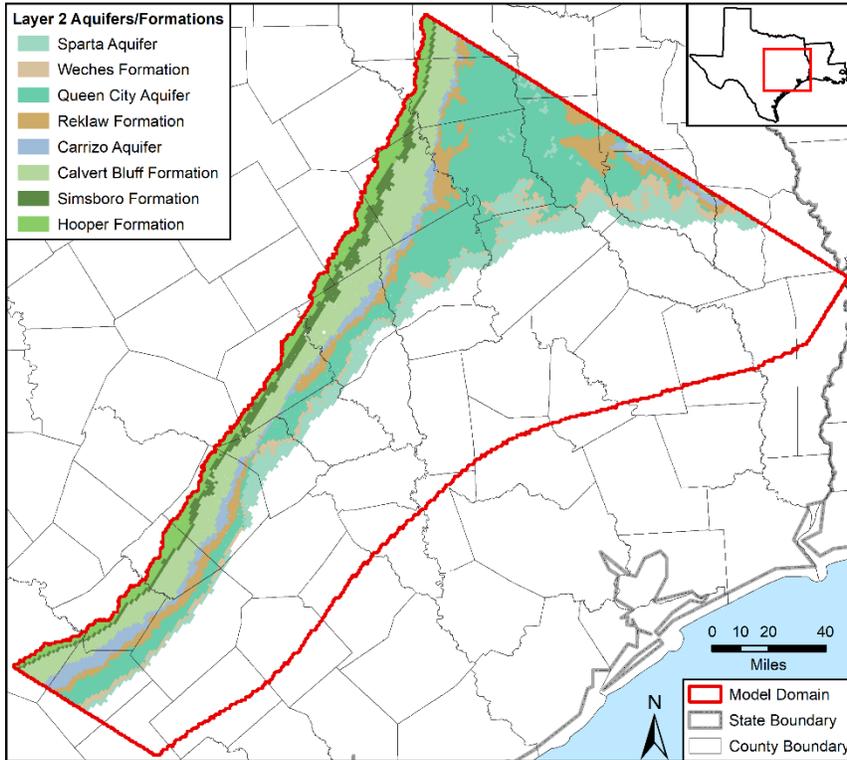
Figure 4.2.1k. **Spatial distribution of the hydrogeologic units that comprise model layer 2.**
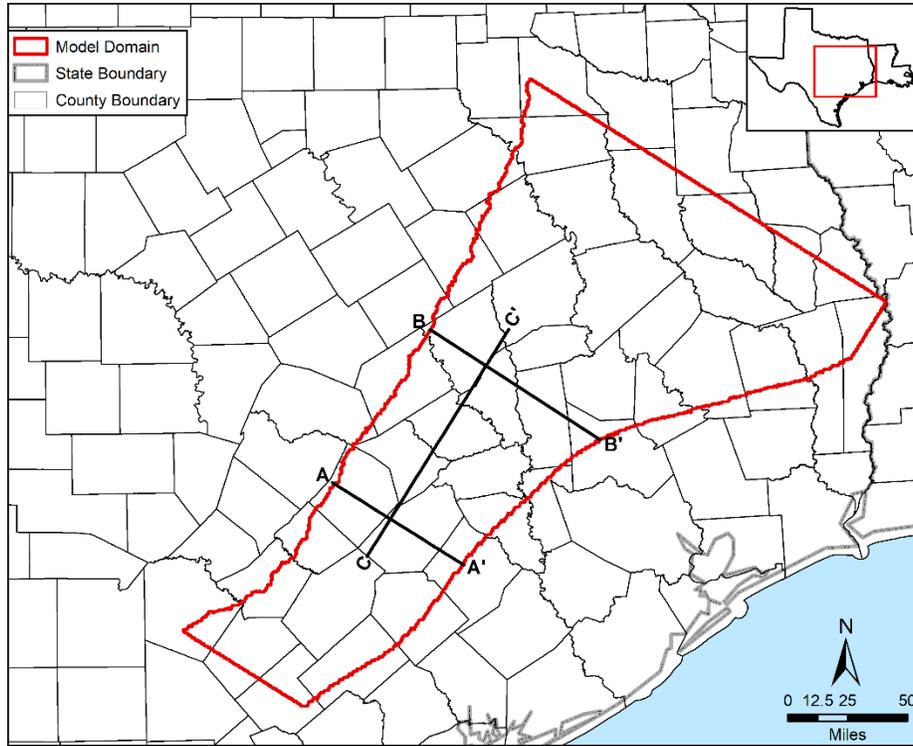
Figure 4.2.1l.   Locations of vertical cross-sections A-A′, B-B′, and C-C′ that show the model layers.
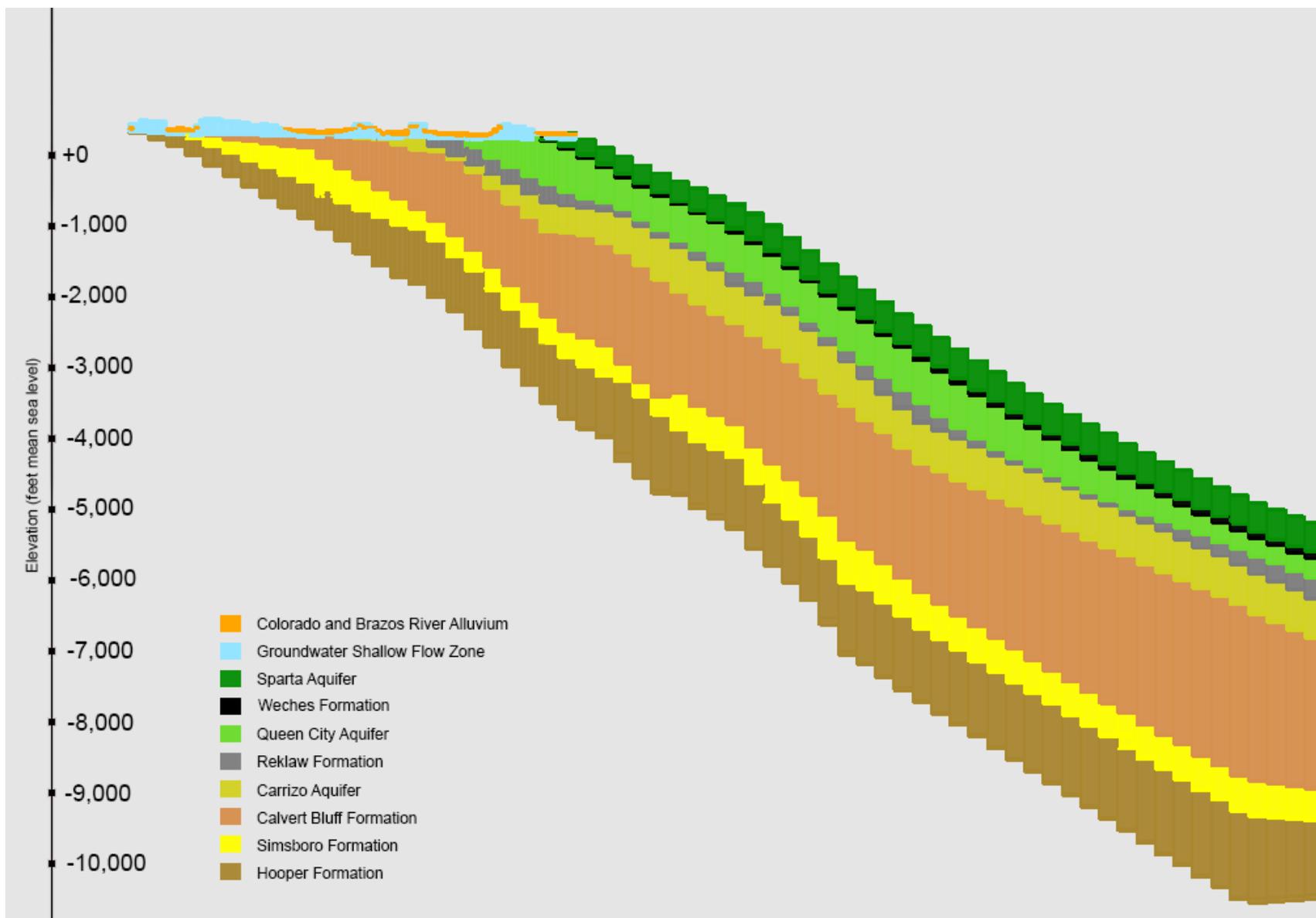
Figure 4.2.1m.   **Vertical cross-section showing the model layers along dip cross-section A-A′.**
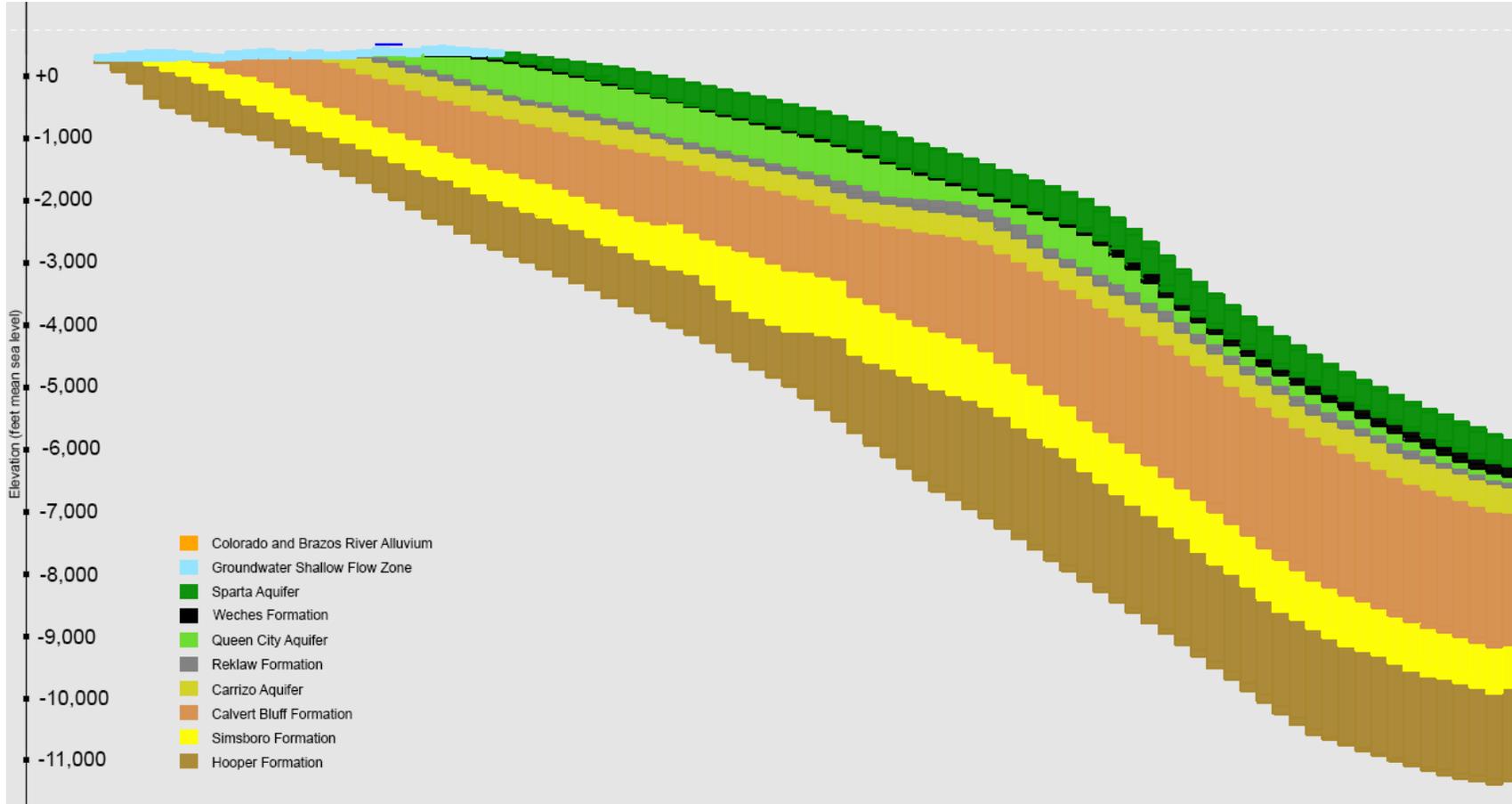
Figure 4.2.1n.   **Vertical cross-section showing the model layers along dip cross-section B-B′.**
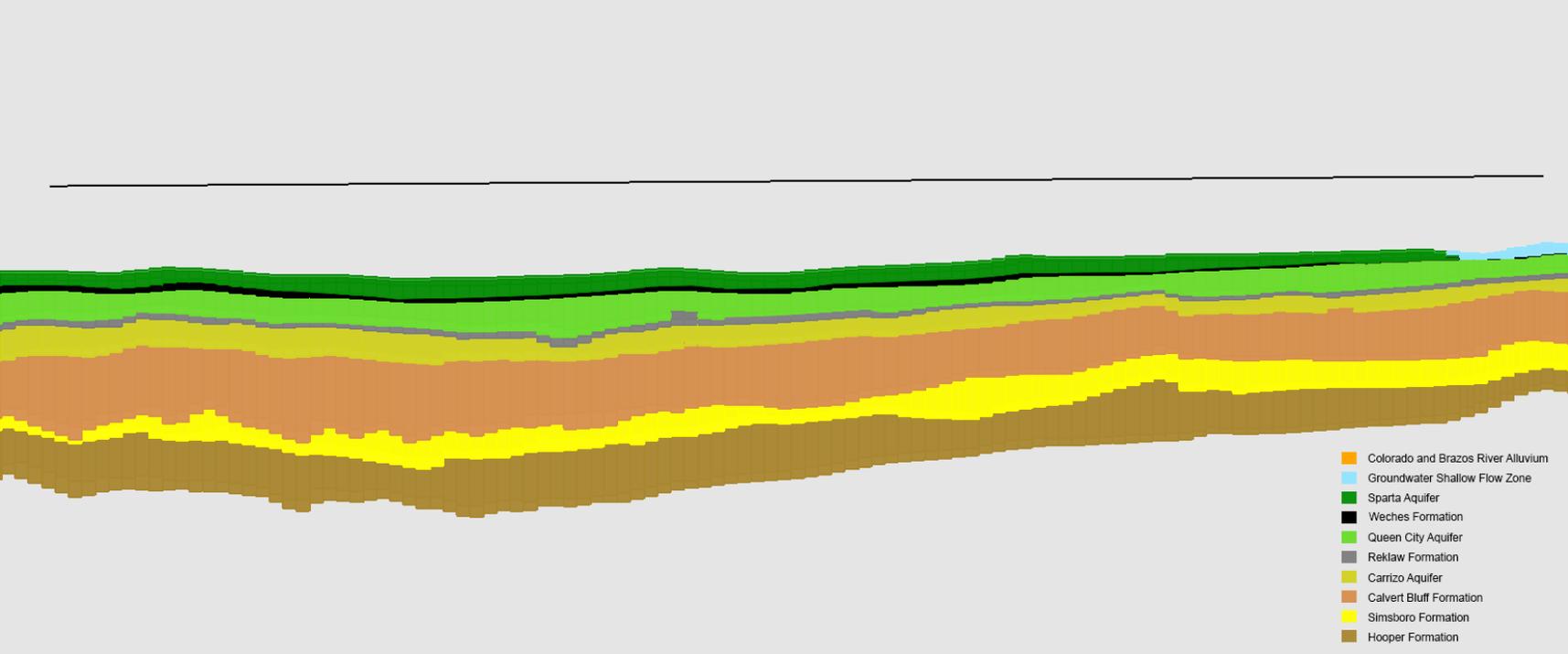
Figure 4.2.1o. **Vertical cross-section showing the model layers along strike cross-section C-C′.**

4.2.2 Stress Period Setup

The updated groundwater availability model for the central portion of the Carrizo-Wilcox, Queen City, and Sparta aquifers has 82 stress periods (Table 4.2.2a).

Table 4.2.2a.   **Table of stress period times and durations.**

Stress Period	Stress Period Length (Days)	Stress Period Begins	SS or TR	Stress Period	Stress Period Length (Days)	Stress Period Begins	SS or TR	Stress Period	Stress Period Length (Days)	Stress Period Begins	SS or TR
1	1	1929	SS	29	365.25	1/1/1957	TR	57	365.25	1/1/1985	TR
2	365.25	1/1/1930	TR	30	365.25	1/1/1958	TR	58	365.25	1/1/1986	TR
3	365.25	1/1/1931	TR	31	365.25	1/1/1959	TR	59	365.25	1/1/1987	TR
4	365.25	1/2/1932	TR	32	365.25	1/1/1960	TR	60	365.25	1/1/1988	TR
5	365.25	1/1/1933	TR	33	365.25	1/1/1961	TR	61	365.25	1/1/1989	TR
6	365.25	1/1/1934	TR	34	365.25	1/1/1962	TR	62	365.25	1/1/1990	TR
7	365.25	1/1/1935	TR	35	365.25	1/1/1963	TR	63	365.25	1/1/1991	TR
8	366.25	1/2/1936	TR	36	365.25	1/1/1964	TR	64	365.25	1/1/1992	TR
9	365.25	1/1/1937	TR	37	365.25	1/1/1965	TR	65	365.25	1/1/1993	TR
10	365.25	1/1/1938	TR	38	365.25	1/1/1966	TR	66	365.25	1/1/1994	TR
11	365.25	1/1/1939	TR	39	365.25	1/1/1967	TR	67	365.25	1/1/1995	TR
12	365.25	1/1/1940	TR	40	365.25	1/1/1968	TR	68	365.25	1/1/1996	TR
13	365.25	1/1/1941	TR	41	365.25	1/1/1969	TR	69	365.25	1/1/1997	TR
14	365.25	1/1/1942	TR	42	365.25	1/1/1970	TR	70	365.25	1/1/1998	TR
15	365.25	1/1/1943	TR	43	365.25	1/1/1971	TR	71	365.25	1/1/1999	TR
16	365.25	1/1/1944	TR	44	365.25	1/1/1972	TR	72	365.25	1/1/2000	TR
17	365.25	1/1/1945	TR	45	365.25	1/1/1973	TR	73	365.25	1/1/2001	TR
18	365.25	1/1/1946	TR	46	365.25	1/1/1974	TR	74	365.25	1/1/2002	TR
19	365.25	1/1/1947	TR	47	365.25	1/1/1975	TR	75	365.25	1/1/2003	TR
20	365.25	1/1/1948	TR	48	365.25	1/1/1976	TR	76	365.25	1/1/2004	TR
21	365.25	1/1/1949	TR	49	365.25	1/1/1977	TR	77	365.25	1/1/2005	TR
22	365.25	1/1/1950	TR	50	365.25	1/1/1978	TR	78	365.25	1/1/2006	TR
23	365.25	1/1/1951	TR	51	365.25	1/1/1979	TR	79	365.25	1/1/2007	TR
24	365.25	1/1/1952	TR	52	365.25	1/1/1980	TR	80	365.25	1/1/2008	TR
25	365.25	1/1/1953	TR	53	365.25	1/1/1981	TR	81	365.25	1/1/2009	TR
26	365.25	1/1/1954	TR	54	365.25	1/1/1982	TR	82	365.25	1/1/2010	TR
27	365.25	1/1/1955	TR	55	365.25	1/1/1983	TR				
28	365.25	1/1/1956	TR	56	365.25	1/1/1984	TR				

Note: SS = steady-state; TR = transient

4.3 Layer-Property Flow Package

The Layer-Property Flow (suffix LPF) package is used to specify hydraulic properties for MODFLOW-USG. These properties control how easily groundwater can flow through the aquifer and how it responds to pumping. These properties include hydraulic conductivity (both horizontal and vertical), specific yield, and storativity. This section provides the spatial distribution of hydraulic properties for each hydraulic property zone in the calibrated model, along with the field data and empirical relationships considered for these hydraulic properties during model calibration.

4.3.1 Hydraulic Property Zones

The model was calibrated using the ten hydrogeologic units listed in Table 4.2.1a. In layer 1, there are two hydraulic properties zones representing the alluvium of the Colorado and Brazos rivers, respectively. The remaining eight hydraulic conductivity zones represent two formations and eight aquifers. The two formations are the Weches and Reklaw formations. Based on the conceptual groundwater models presented by Dutton and others (2003) and Kelley and others (2004), these formations consist primarily of clayey marine deposits that can be represented as relatively homogenous units of low hydraulic conductivity. The eight aquifers represent formations dominated by progradational sandstones that contain spatially variable thick, laterally continuous, and permeable sands. The hydraulic conductivity of the aquifers is expected to be spatially variable, with the greatest sand thicknesses and permeable deposits occurring nearest the principal depositional zones.

The shallow aquifer system represented by model layer 2 is notably not a hydraulic property zone. Rather, this layer is comprised of a mosaic of hydraulic properties, consisting of eight hydraulic properties zones, which include zones 3 through 10 in Table 4.3.1a. The locations of these eight zones are consistent with the hydrogeologic unit extents shown in Figure 4.2.1k.

Table 4.3.1a.   Hydraulic property zones.

Hydraulic Property Zones		Model Layer(s)
Number	**Name**	
1	Colorado River Alluvium	1
2	Brazos River Alluvium	1
3	Sparta Aquifer	2 and 3
4	Weches Formation	2 and 4
5	Queen City Aquifer	2 and 5
6	Reklaw Formation	2 and 6
7	Carrizo Aquifer	2 and 7
8	Calvert Bluff Formation	2 and 8
9	Simsboro Formation	2 and 9
10	Hooper Formation	2 and 10

4.3.2 Hydraulic Property Values in the Calibrated Model

Figures 4.3.2a through 4.3.2i show the spatial distribution of horizontal hydraulic conductivity values in the calibrated model for the ten hydraulic properties zones. Figure 4.3.2j shows the spatial distribution of horizontal hydraulic conductivity values in the calibrated model for model layer 2, which represents the shallow groundwater flow system. In these figures, the horizontal hydraulic conductivity value of 75 feet per day is located in every grid cell that contains a river cell to represent permeable alluvium deposits.

Figures 4.3.2k through 4.3.2s show the spatial distribution of vertical hydraulic conductivity values in the calibrated model for the ten hydraulic properties zones. Figure 4.3.2t shows the spatial distribution of vertical hydraulic conductivity values in the calibrated model for model layer 2, which represents the shallow groundwater flow system.

For both the horizontal and vertical hydraulic conductivity values, there is a trend of decreasing values with depth. The function used to create the decrease in values with depth is explained in Section 4.3.3.1. Table 4.3.2a provides a statistical summary of the horizontal and vertical horizontal hydraulic conductivity values in the calibrated model for the ten hydraulic properties zones.

Table 4.3.2a. **Statistical summary of the horizontal, K_h, and vertical, K_v, hydraulic conductivity values in feet per day for the ten hydraulic property zones in the calibrated model.**

Property	Hydraulic Property Zone	Minimum	Maximum	Arithmetic Mean	Geometric Mean	Median
K_h	Colorado River Alluvium	75	75	75	75	75
	Brazos River Alluvium	27	1000	322	250	270
	Sparta Aquifer	0.21	8.9	1.7	1.1	0.9
	Weches Formation	0.01	2.0	0.4	0.2	0.1
	Queen City Aquifer	0.57	9.6	2.2	1.7	1.8
	Reklaw Formation	0.00	1.1	0.2	0.1	0.1
	Carrizo Aquifer	2.01	23.9	8.6	7.6	7.9
	Calvert Bluff Formation	0.03	6.7	1.4	0.5	1.0
	Simsboro Formation	0.89	45.7	8.4	6.2	6.5
	Hooper Formation	0.04	6.0	1.4	0.8	1.1
K_v	Colorado River Alluvium	0.75	0.75	0.75	0.75	0.75
	Brazos River Alluvium	2.7	100	32.2	15.1	27.1
	Sparta Aquifer	1.7E-04	4.5E-02	6.3E-03	2.7E-03	2.5E-03
	Weches Formation	2.0E-07	3.9E-03	1.9E-04	3.5E-05	2.5E-05
	Queen City Aquifer	2.5E-05	3.3E-02	4.4E-03	9.1E-04	1.0E-03
	Reklaw Formation	2.7E-07	2.1E-03	1.4E-04	1.6E-05	9.5E-06
	Carrizo Aquifer	5.5E-05	2.0E-02	3.7E-03	1.0E-03	2.0E-03
	Calvert Bluff Formation	3.5E-06	3.2E-02	2.1E-03	2.5E-04	3.8E-04
	Simsboro Formation	2.3E-05	1.2E-01	5.7E-03	5.4E-04	3.7E-04
	Hooper Formation	2.6E-06	2.8E-02	1.6E-03	1.1E-04	1.3E-04

Table 4.3.2b provides a statistical summary of the specific yield and specific storage properties
in the calibrated model for the ten hydraulic properties zones. All ten hydraulic properties zones
have a constant and uniform specific yield value, so no figures were generated show their spatial
distribution.

Table 4.3.2b. **Statistical summary of the specific yield, S_y, and specific storage, S_s, values for the ten
hydraulic property zones in the calibrated model.**

Property	Hydraulic Property Zone	Minimum	Maximum	Arithmetic Mean	Geometric Mean	Median
S_y (unitless)	Colorado River Alluvium	0.2	0.2	0.2	0.2	0.2
	Brazos River Alluvium	0.2	0.2	0.2	0.2	0.2
	Sparta Aquifer	0.1	0.1	0.1	0.1	0.1
	Weches Formation	0.087	0.087	0.087	0.087	0.087
	Queen City Aquifer	0.1	0.1	0.1	0.1	0.1
	Reklaw Formation	0.08	0.08	0.08	0.08	0.08
	Carrizo Aquifer	0.15	0.15	0.15	0.15	0.15
	Calvert Bluff Formation	0.1	0.1	0.1	0.1	0.1
	Simsboro Formation	0.15	0.15	0.15	0.15	0.15
	Hooper Formation	0.1	0.1	0.1	0.1	0.1
S_s (feet^{-1})	Colorado River Alluvium	6.4E-04	6.4E-04	6.4E-04	6.4E-04	6.4E-04
	Brazos River Alluvium	6.4E-04	6.4E-04	6.4E-04	6.4E-04	6.4E-04
	Sparta Aquifer	1.9E-07	4.6E-05	1.8E-06	6.6E-07	3.9E-07
	Weches Formation	1.9E-07	4.5E-04	1.3E-06	5.6E-07	3.6E-07
	Queen City Aquifer	1.9E-07	3.8E-05	2.2E-06	8.9E-07	6.2E-07
	Reklaw Formation	1.9E-07	1.5E-04	1.3E-06	6.3E-07	4.7E-07
	Carrizo Aquifer	1.4E-07	1.9E-05	6.0E-07	3.6E-07	2.8E-07
	Calvert Bluff Formation	1.7E-07	2.7E-05	1.6E-06	6.4E-07	4.5E-07
	Simsboro Formation	1.3E-07	1.5E-05	5.1E-07	2.9E-07	2.2E-07
	Hooper Formation	1.6E-07	2.3E-05	1.1E-06	4.6E-07	3.1E-07

Figures 4.3.2u through 4.3.2cc show the spatial distribution of specific storage values in the
calibrated model for the ten hydraulic properties zones. Figure 4.3.2u shows that a constant value
of 6.4E-04 feet^{-1} was assigned to the Colorado and Brazos rivers alluvium. The remaining
hydraulic property zones have very similar statistical summaries for their specific storage values.
This similarity occurs because the same function was used to generate the values for the different
hydraulic properties' zones. This function is discussed in Section 4.3.3.1.
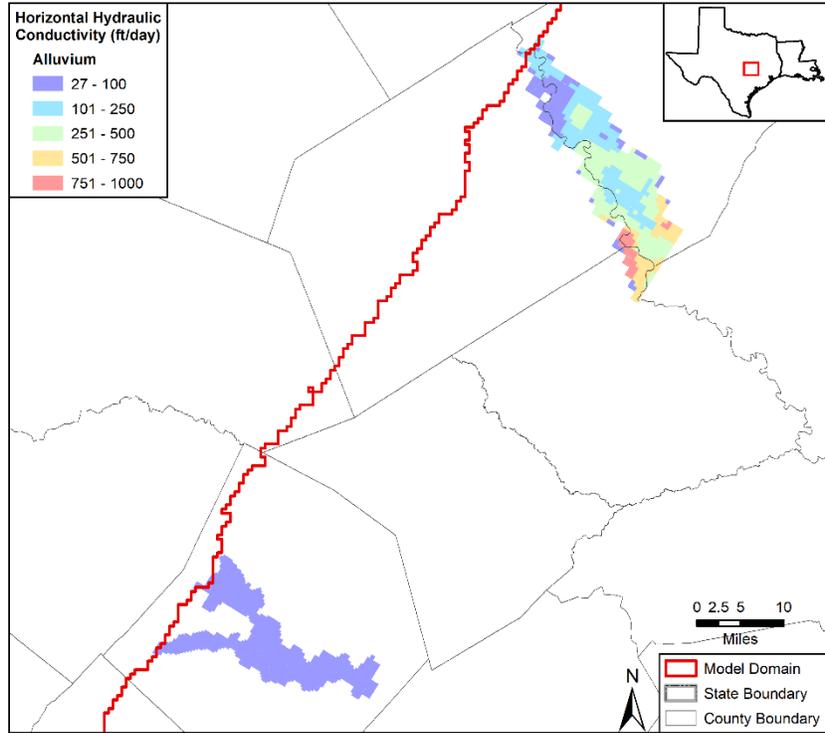
Figure 4.3.2a. Horizontal hydraulic conductivity values in the calibrated model in feet per day (ft/day) for the Colorado and Brazos rivers alluvium in model layer 1.
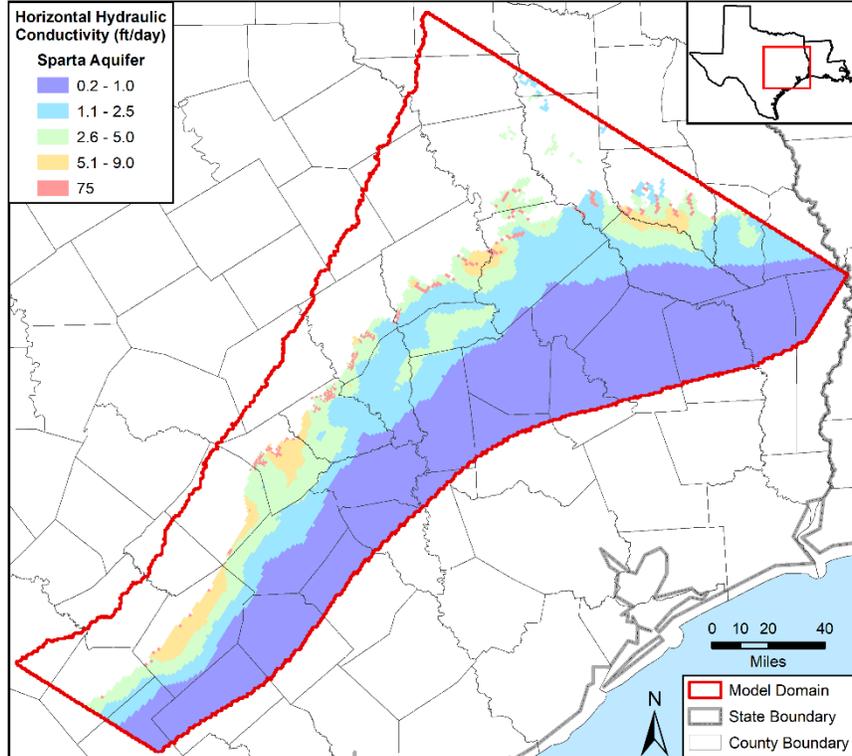
Figure 4.3.2b. Horizontal hydraulic conductivity values in the calibrated model in feet per day (ft/day) for the Sparta Aquifer in model layers 2 and 3.
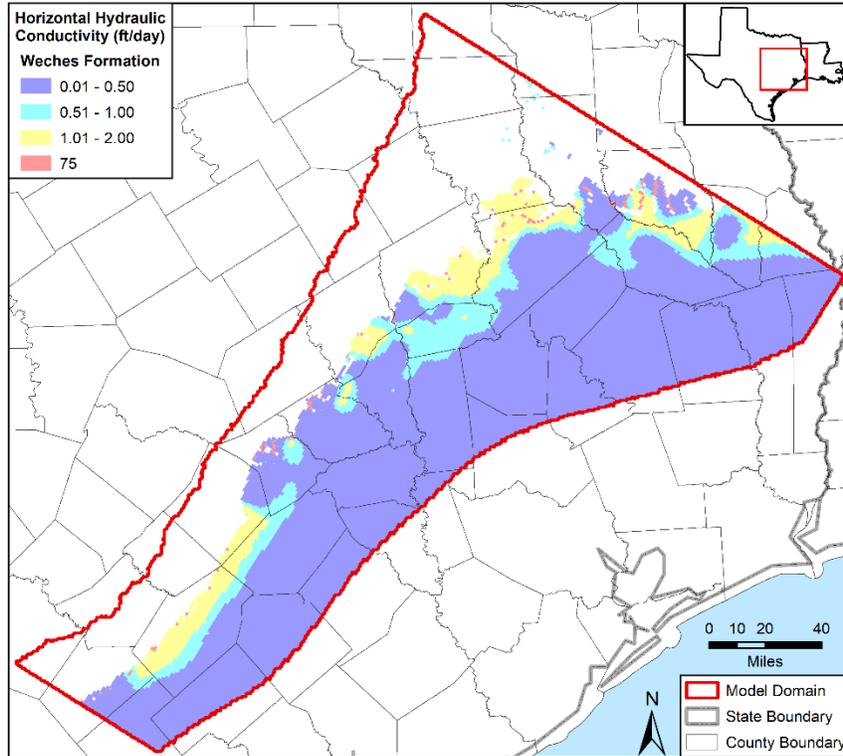
Figure 4.3.2c.   **Horizontal hydraulic conductivity values in the calibrated model in feet per day (ft/day) for the Weches Formation in model layers 2 and 4.**
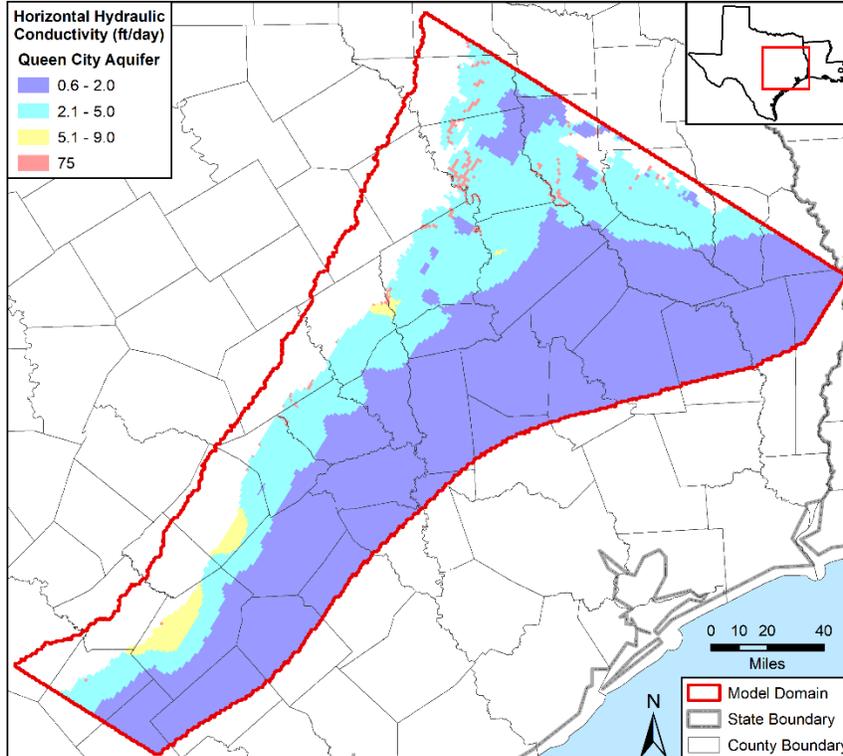
Figure 4.3.2d.   **Horizontal hydraulic conductivity values in the calibrated model in feet per day (ft/day) for the Queen City Aquifer in model layers 2 and 5.**
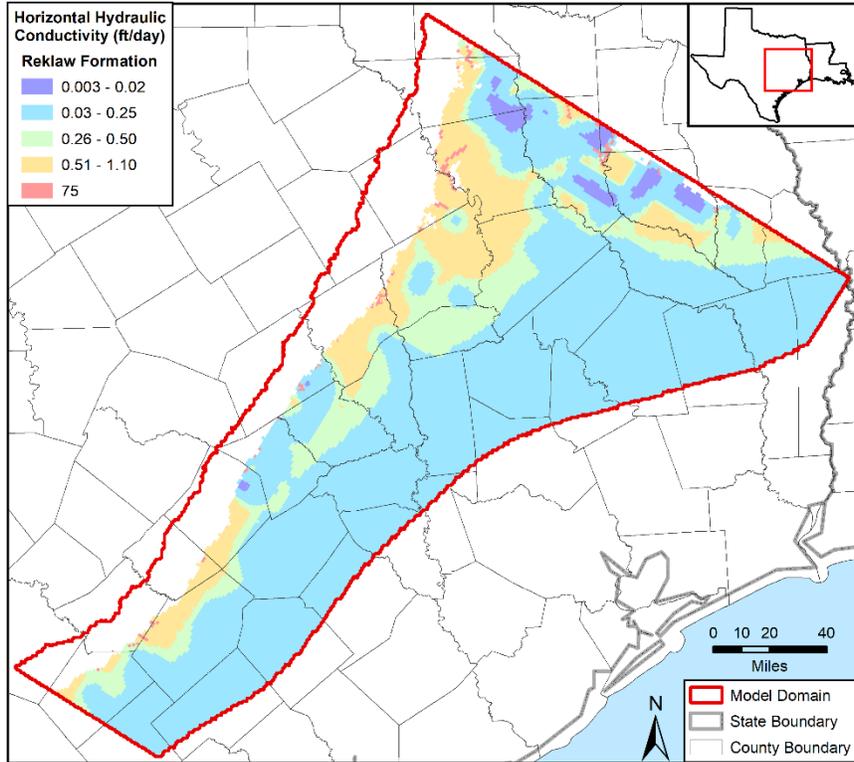
Figure 4.3.2e. **Horizontal hydraulic conductivity values in the calibrated model in feet per day (ft/day) for the Reklaw Formation in model layers 2 and 6.**
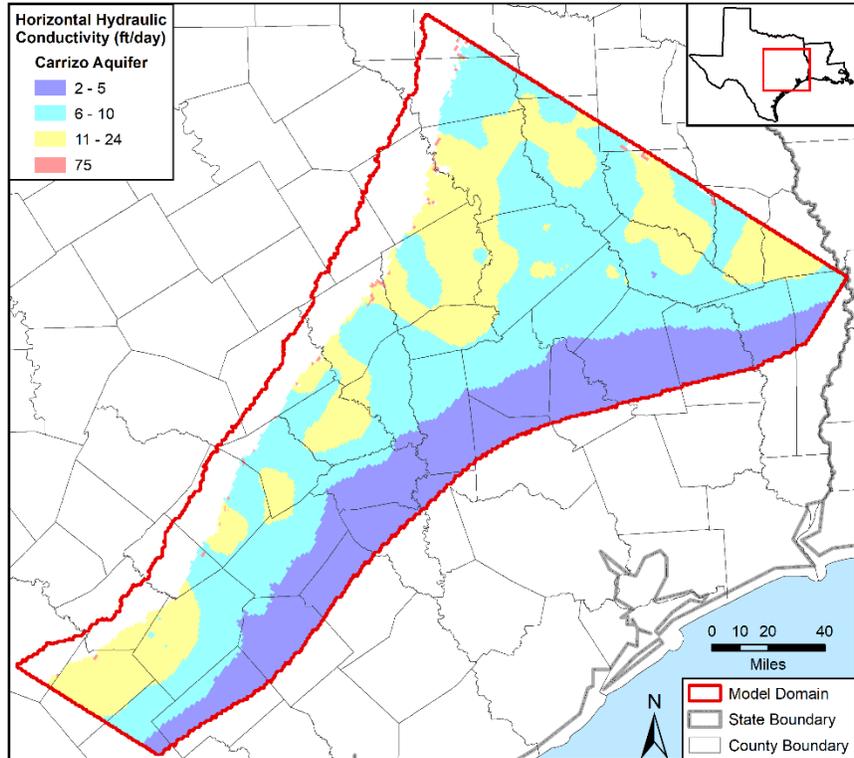
Figure 4.3.2f. **Horizontal hydraulic conductivity values in the calibrated model in feet per day (ft/day) for the Carrizo Aquifer in model layers 2 and 7.**
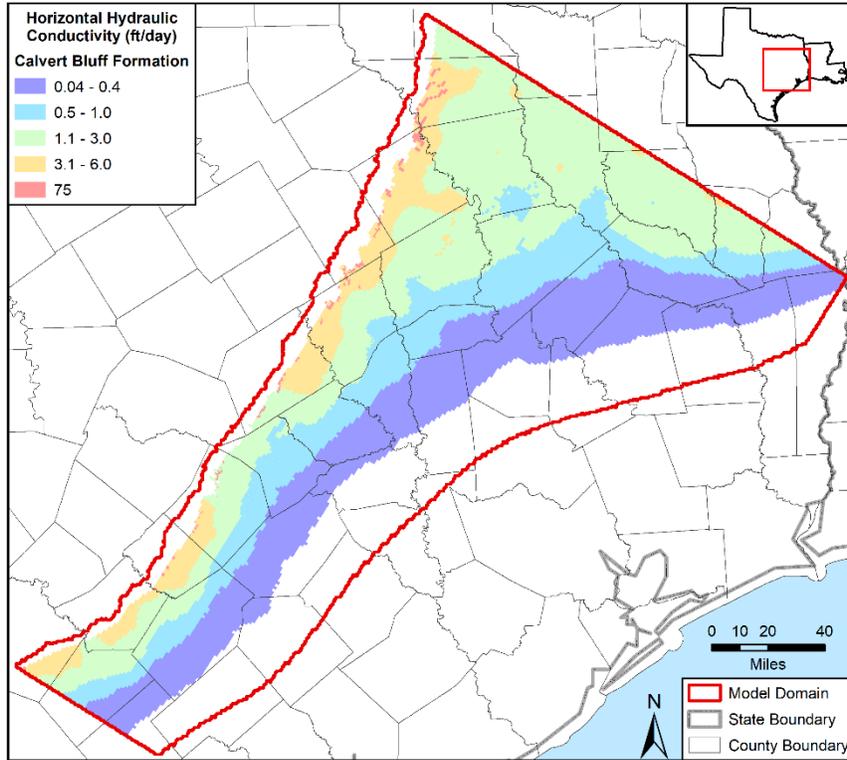
Figure 4.3.2g.   **Horizontal hydraulic conductivity values in the calibrated model in feet per day (ft/day) for the Calvert Bluff Formation in model layers 2 and 8.**
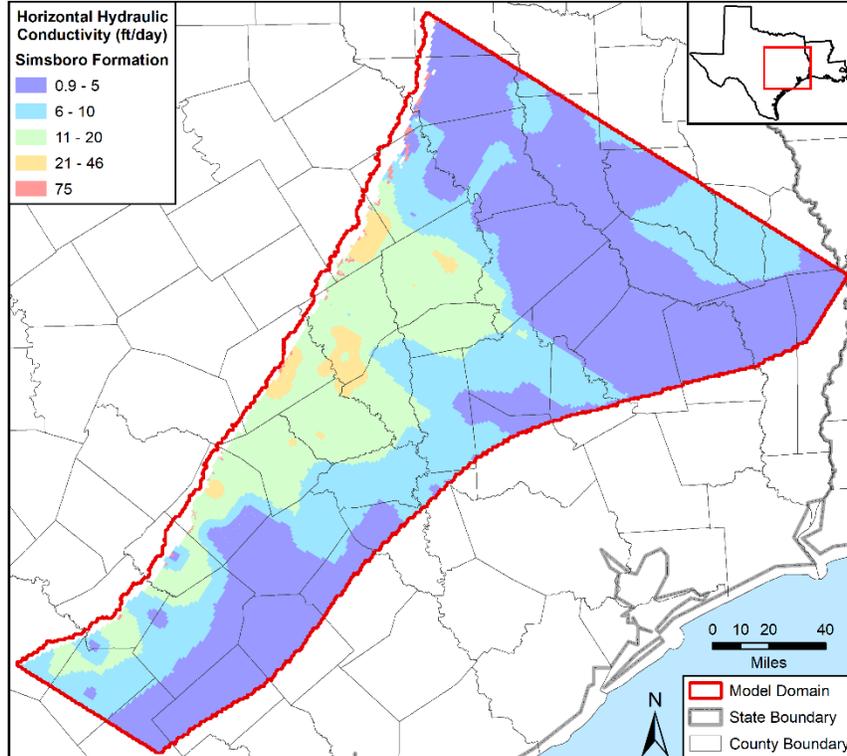
Figure 4.3.2h.   **Horizontal hydraulic conductivity values in the calibrated model in feet per day (ft/day) for the Simsboro Formation in model layers 2 and 9.**
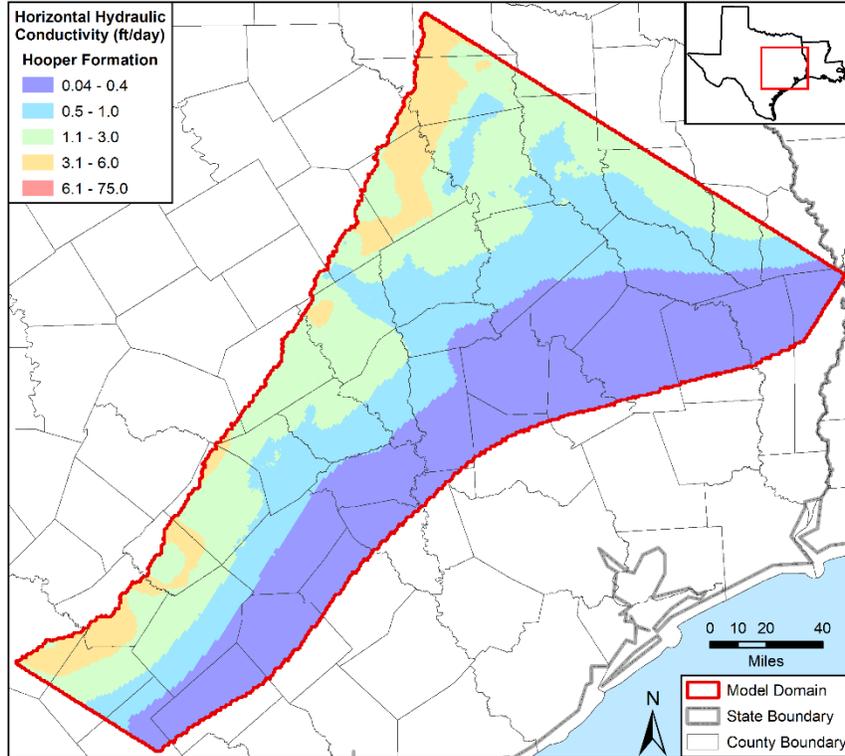
Figure 4.3.2i. **Horizontal hydraulic conductivity values in the calibrated model in feet per day (ft/day) for the Hooper Formation in model layers 2 and 10.**
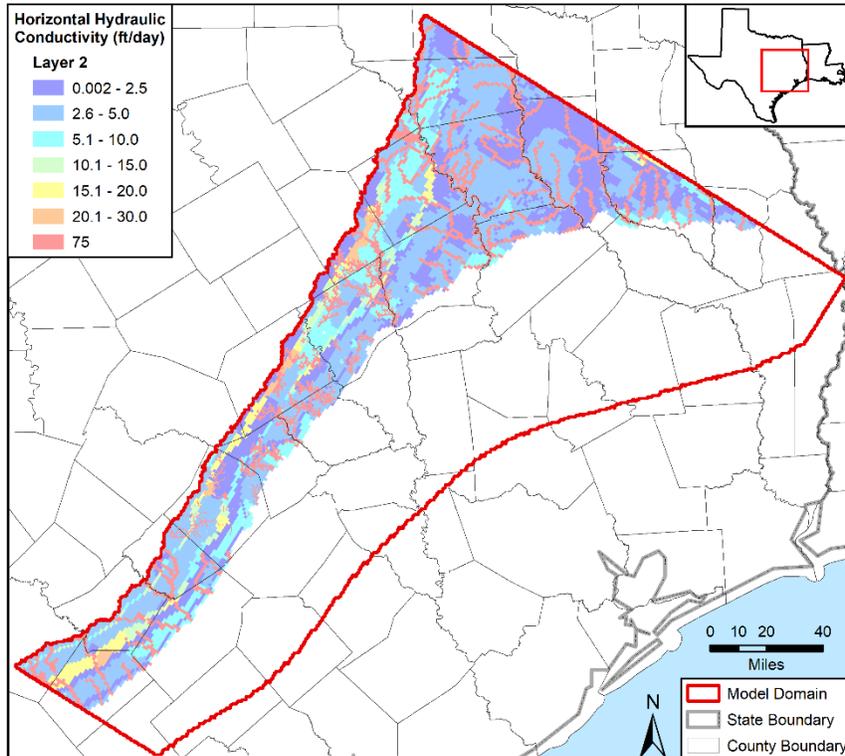
Figure 4.3.2j. **Horizontal hydraulic conductivity values in the calibrated model in feet per day (ft/day) for model layer 2, which represents the shallow groundwater flow system.**
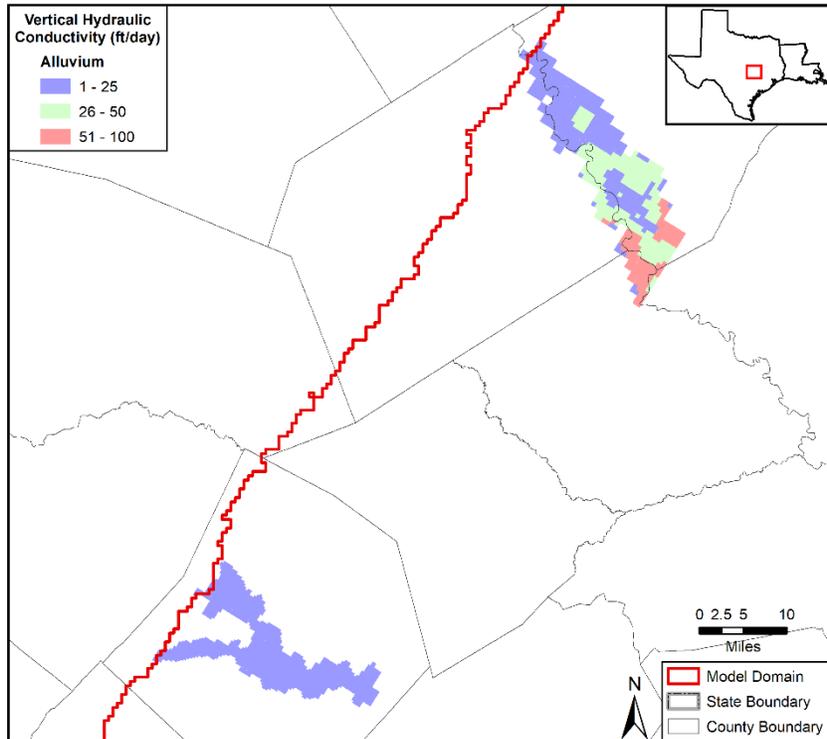
Figure 4.3.2k. **Vertical hydraulic conductivity values in the calibrated model in feet per day (ft/day) for the Colorado and Brazos rivers alluvium in model layer 1.**
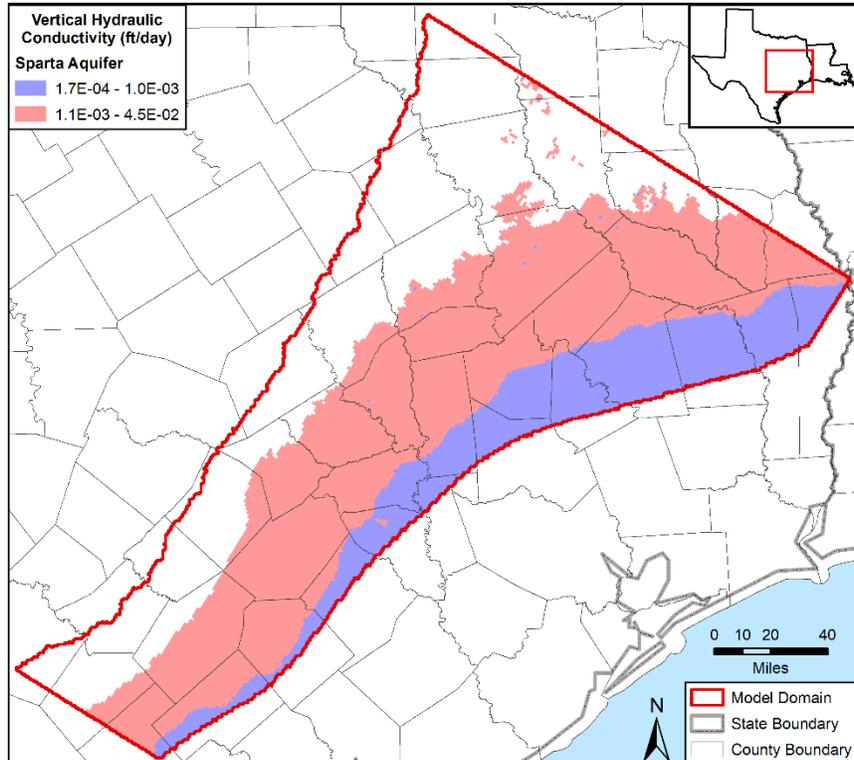
Figure 4.3.2l. **Vertical hydraulic conductivity values in the calibrated model in feet per day (ft/day) for the Sparta Aquifer in model layers 2 and 3.**
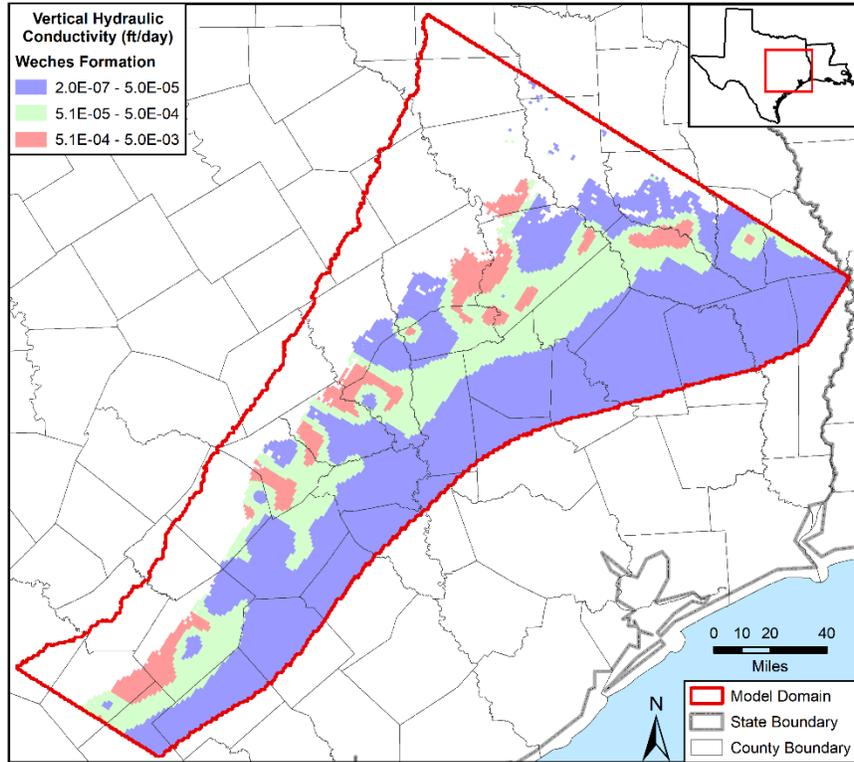
Figure 4.3.2m. **Vertical hydraulic conductivity values in the calibrated model in feet per day (ft/day) for the Weches Formation in model layers 2 and 4.**
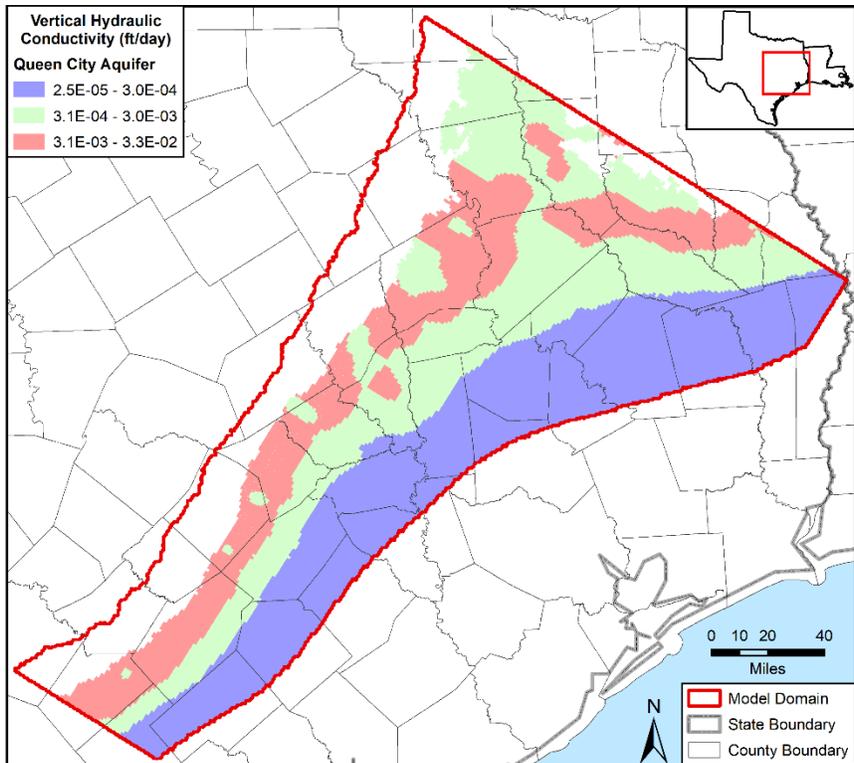
Figure 4.3.2n. **Vertical hydraulic conductivity values in the calibrated model in feet per day (ft/day) for the Queen City Aquifer in model layers 2 and 5.**
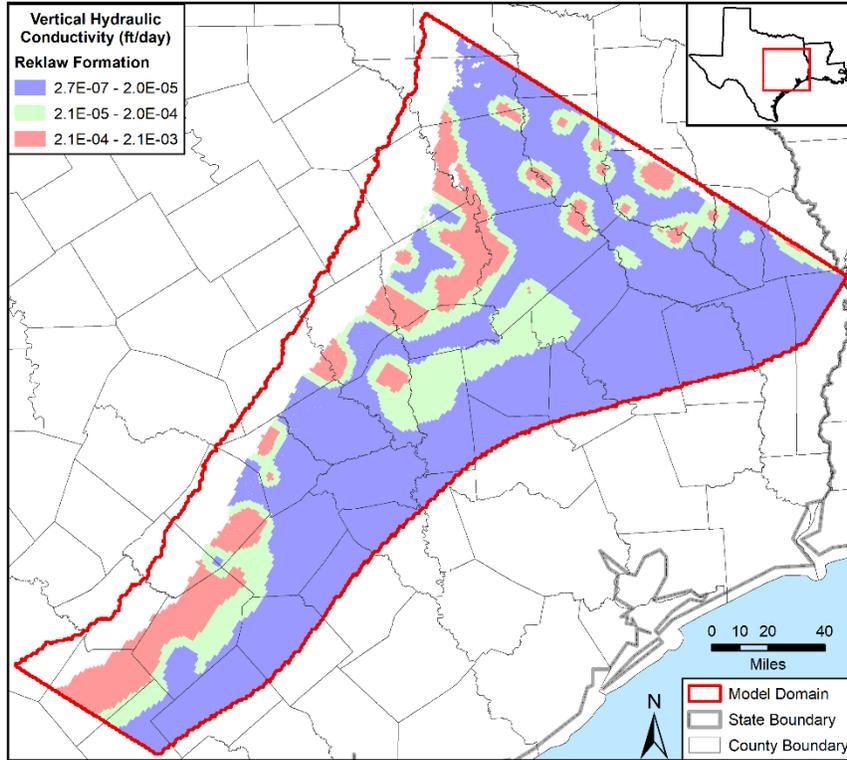
Figure 4.3.2o. Vertical hydraulic conductivity values in the calibrated model in feet per day (ft/day) for the Reklaw Formation in model layers 2 and 6.
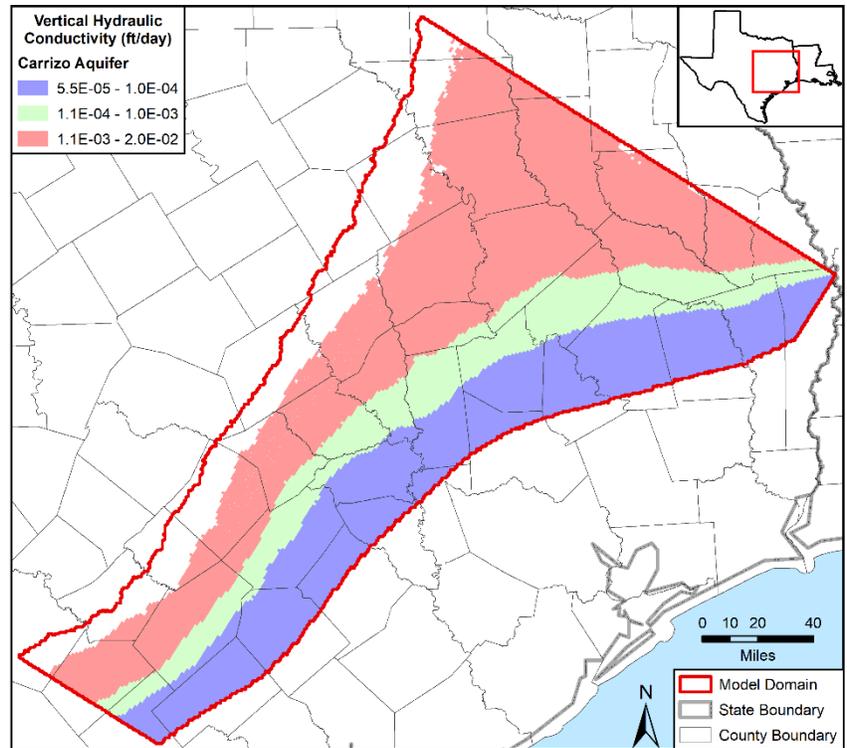
Figure 4.3.2p. Vertical hydraulic conductivity values in the calibrated model in feet per day (ft/day) for the Carrizo Aquifer in model layers 2 and 7.
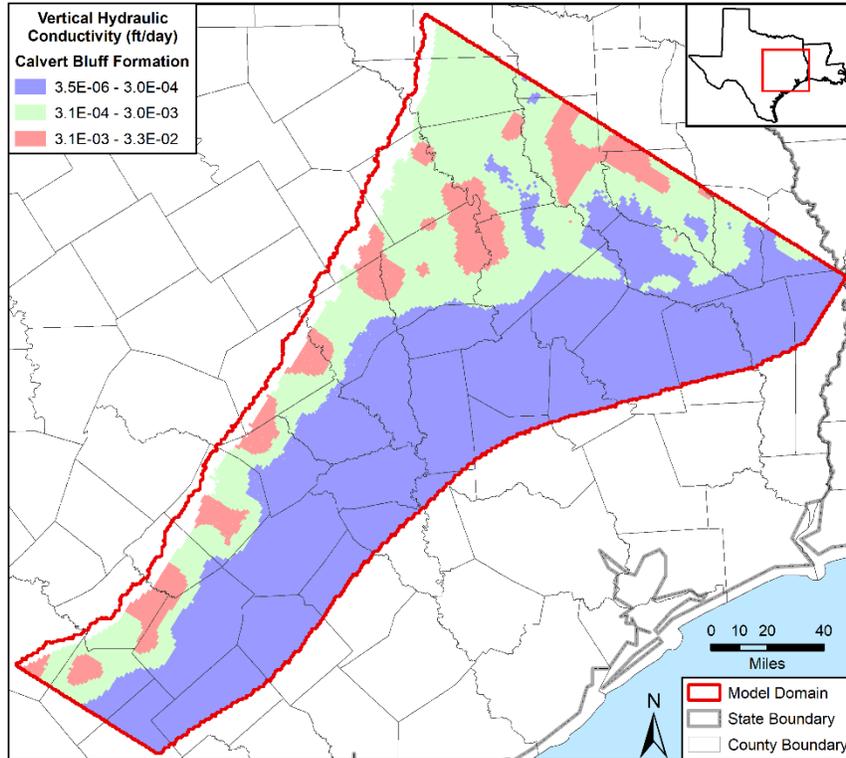
Figure 4.3.2q. Vertical hydraulic conductivity values in the calibrated model in feet per day (ft/day) for the Calvert Bluff Formation in model layers 2 and 8.
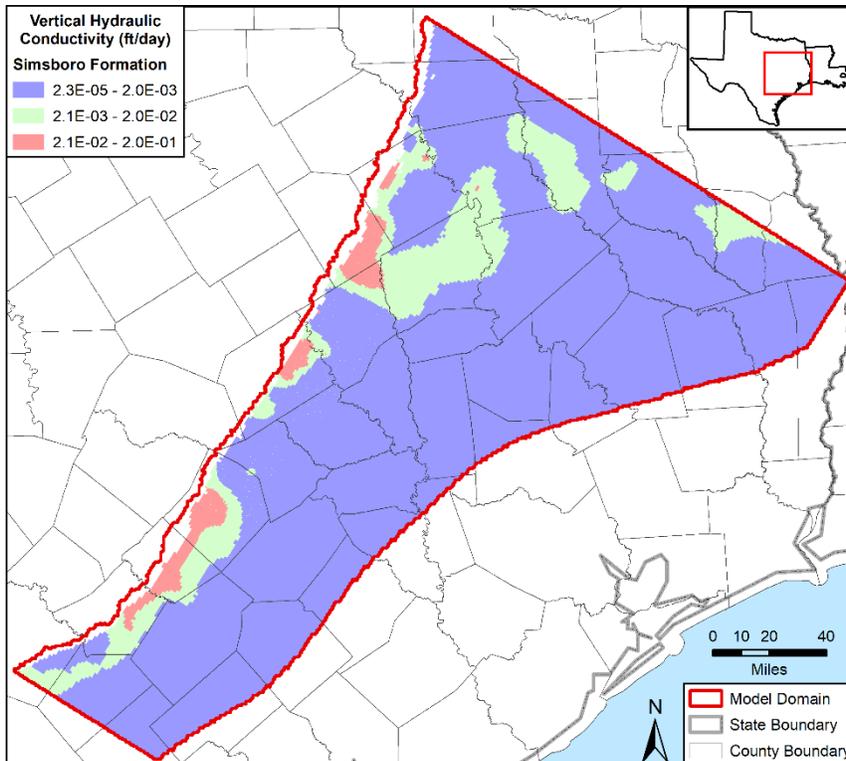
Figure 4.3.2r. Vertical hydraulic conductivity values in the calibrated model in feet per day (ft/day) for the Simsboro Formation in model layers 2 and 9.
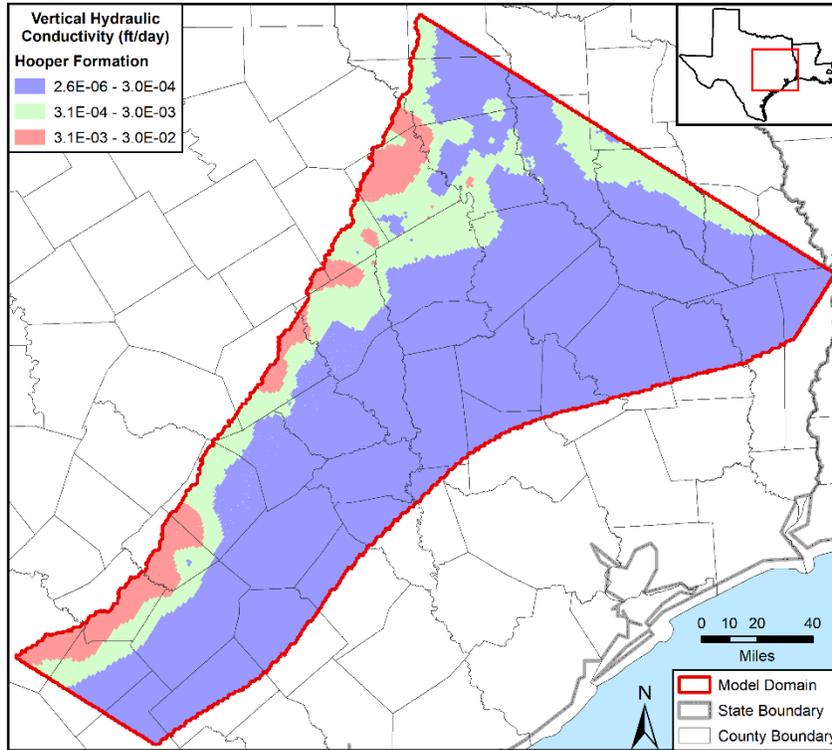
Figure 4.3.2s. **Vertical hydraulic conductivity values in the calibrated model in feet per day (ft/day) for the Hooper Formation in model layers 2 and 10.**
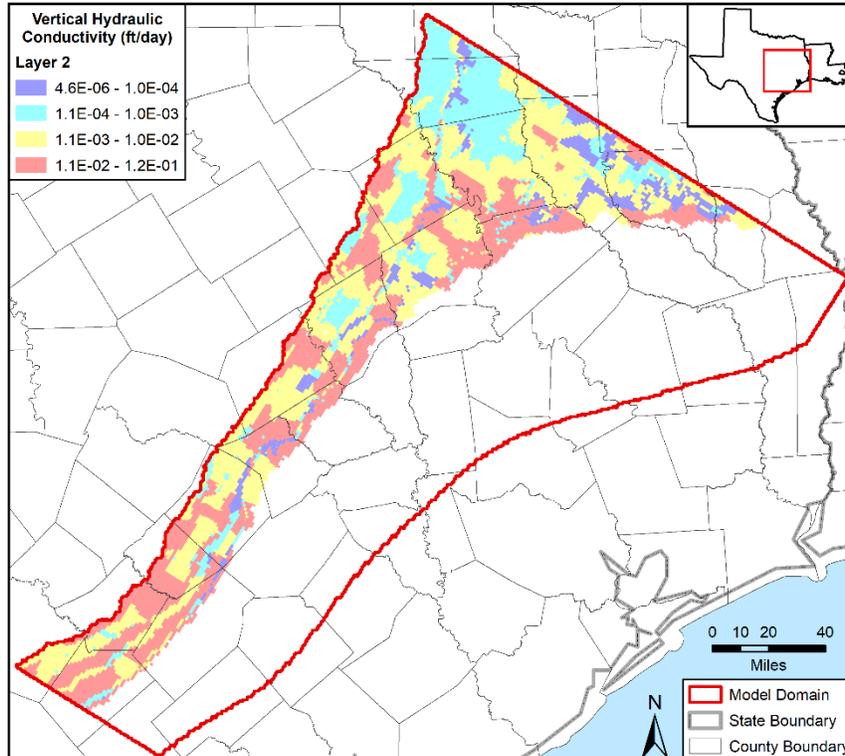
Figure 4.3.2t. **Vertical hydraulic conductivity values in the calibrated model in feet per day (ft/day) for model layer 2, which represents the shallow groundwater flow system.**
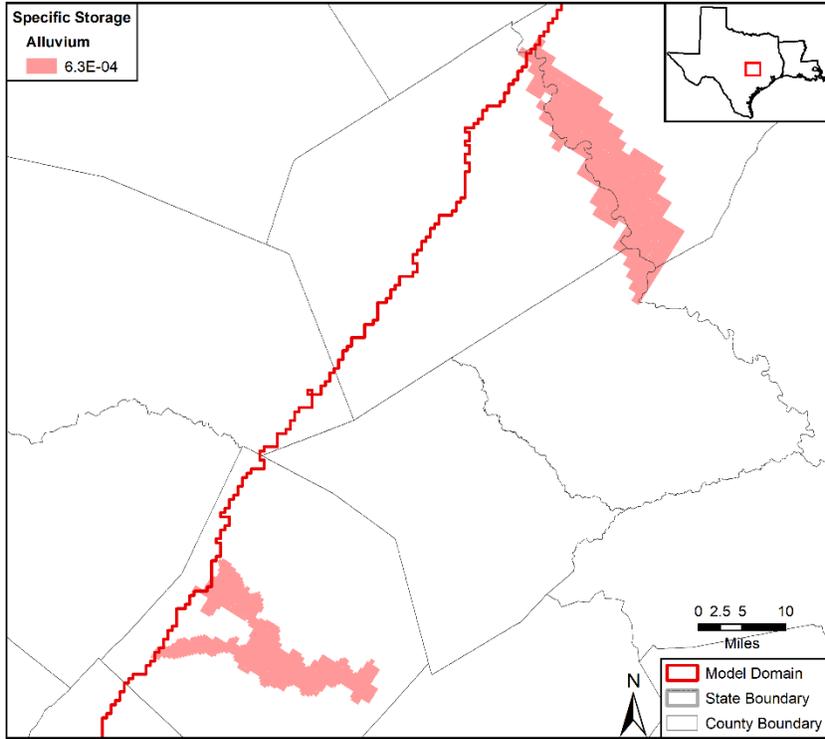
Figure 4.3.2u. Specific storage value in the calibrated model in feet^{-1} for the Colorado and Brazos rivers alluvium in model layer 1.
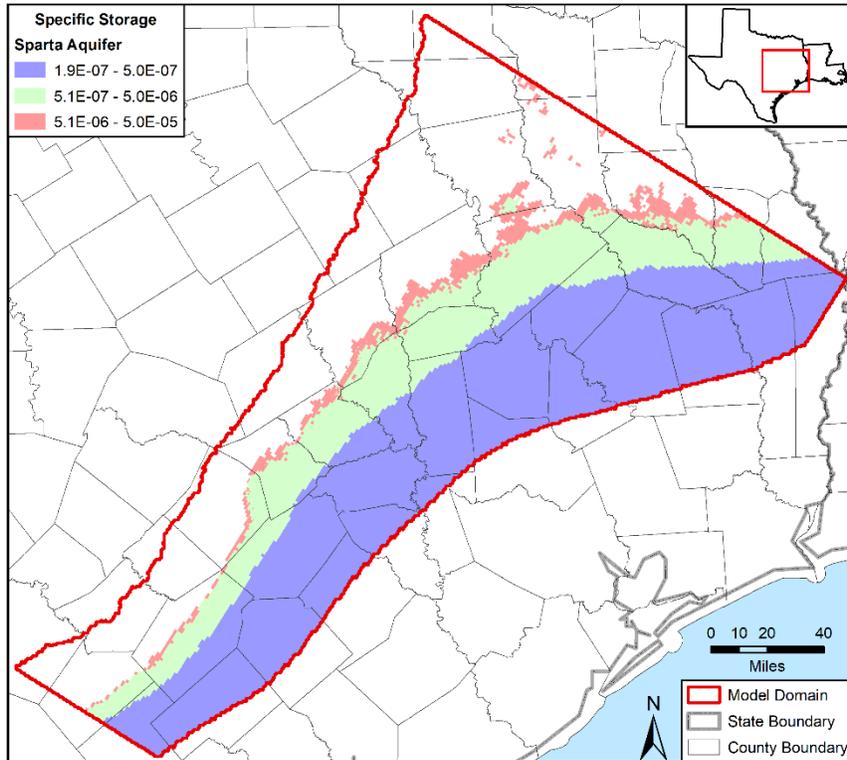
Figure 4.3.2v. Specific storage values in the calibrated model in feet^{-1} for the Sparta Aquifer in model layers 2 and 3.
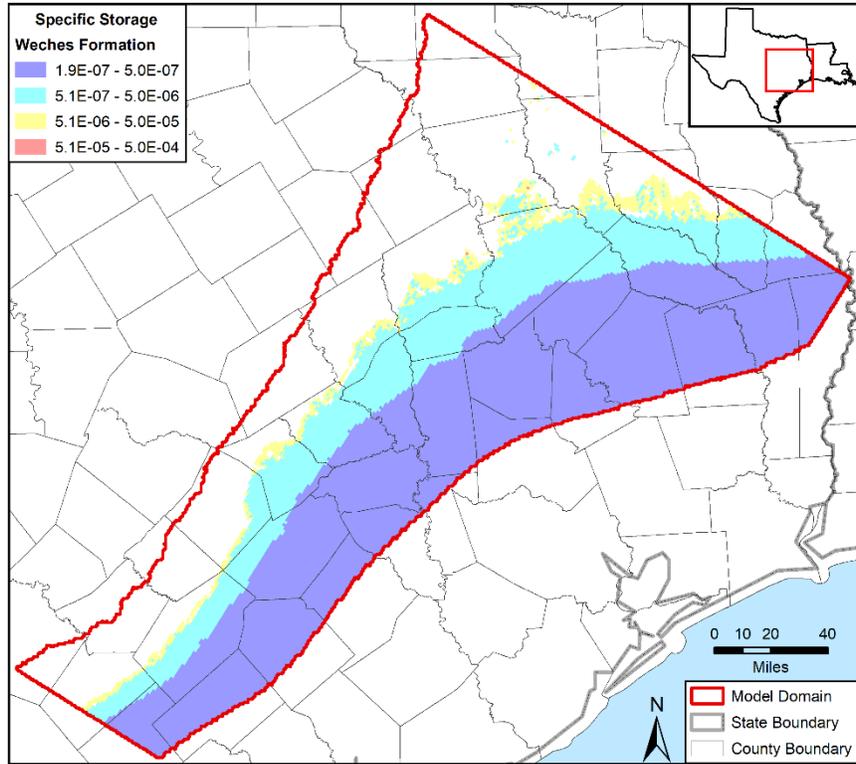
Figure 4.3.2w. **Specific storage values in the calibrated model in feet^{-1} for the Weches Formation in model layers 2 and 4.**
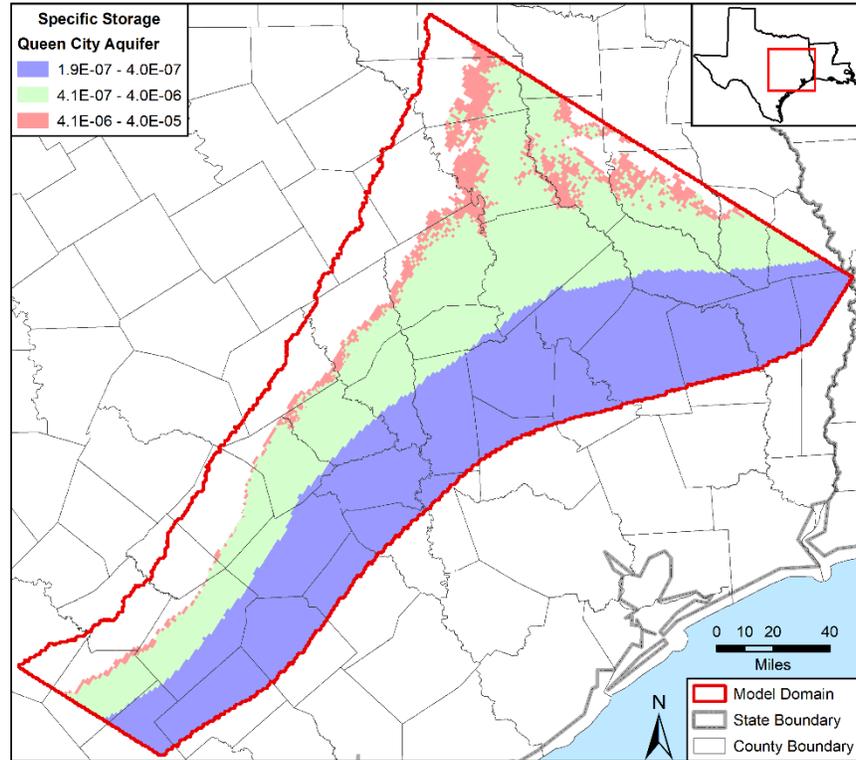
Figure 4.3.2x. **Specific storage values in the calibrated model in feet^{-1} for the Queen City Aquifer in model layers 2 and 5.**
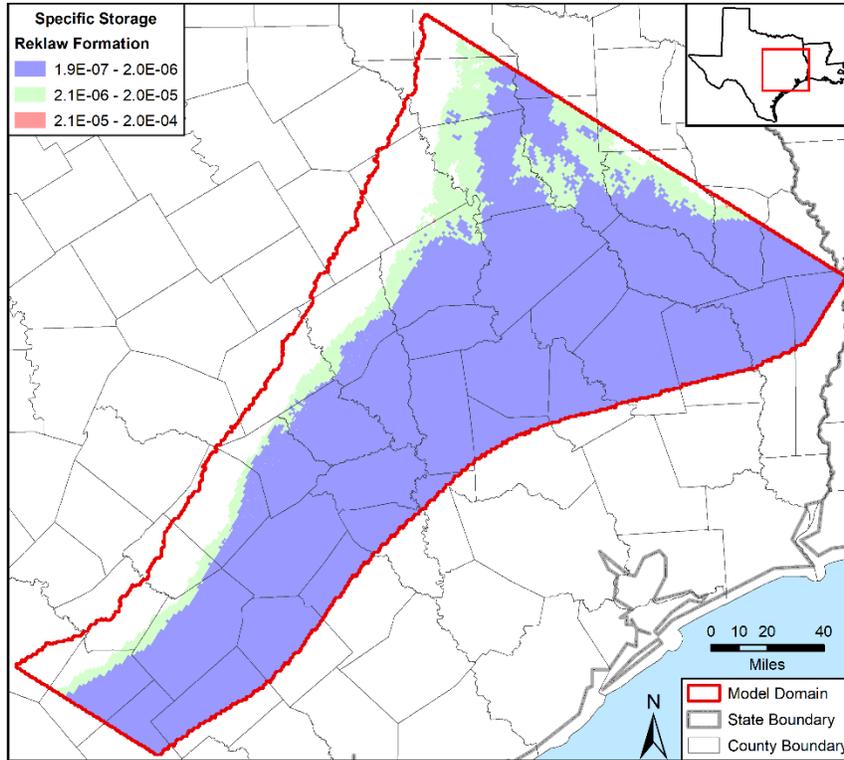
Figure 4.3.2y. **Specific storage values in the calibrated model in feet^{-1} for the Reklaw Formation in model layers 2 and 6.**
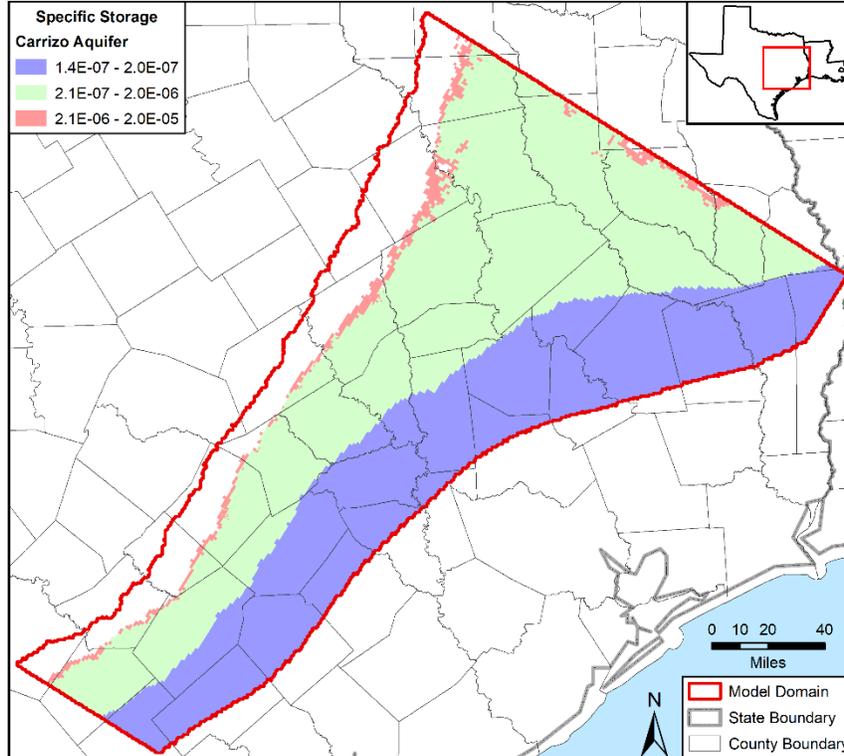
Figure 4.3.2z. **Specific storage values in the calibrated model in feet^{-1} for the Carrizo Aquifer in model layers 2 and 7.**
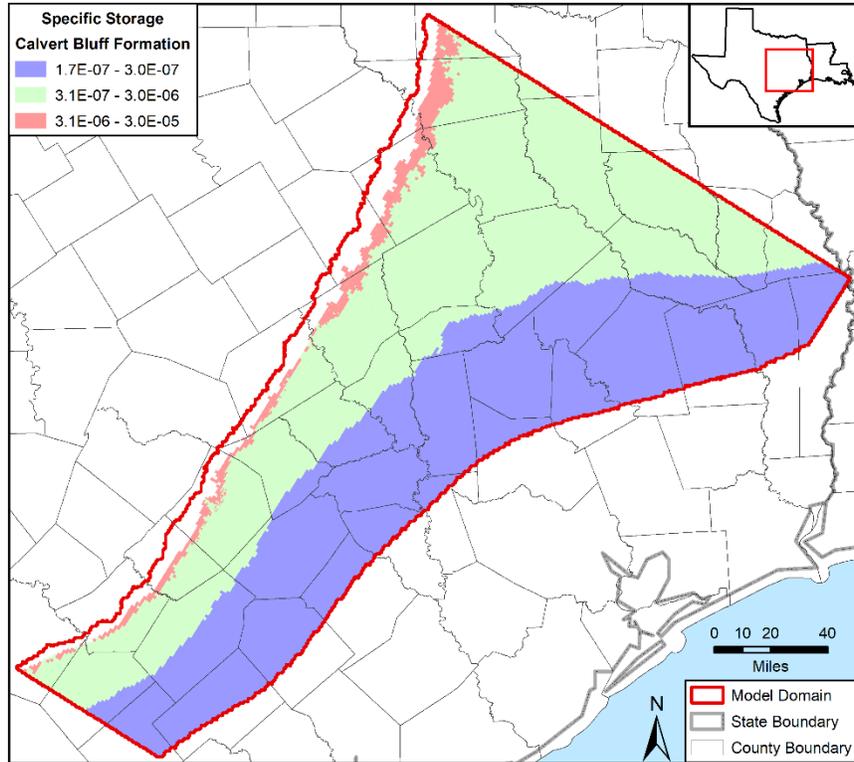
Figure 4.3.2aa. Specific storage values in the calibrated model in feet^{-1} for the Calvert Bluff Formation model layers 2 and 8.
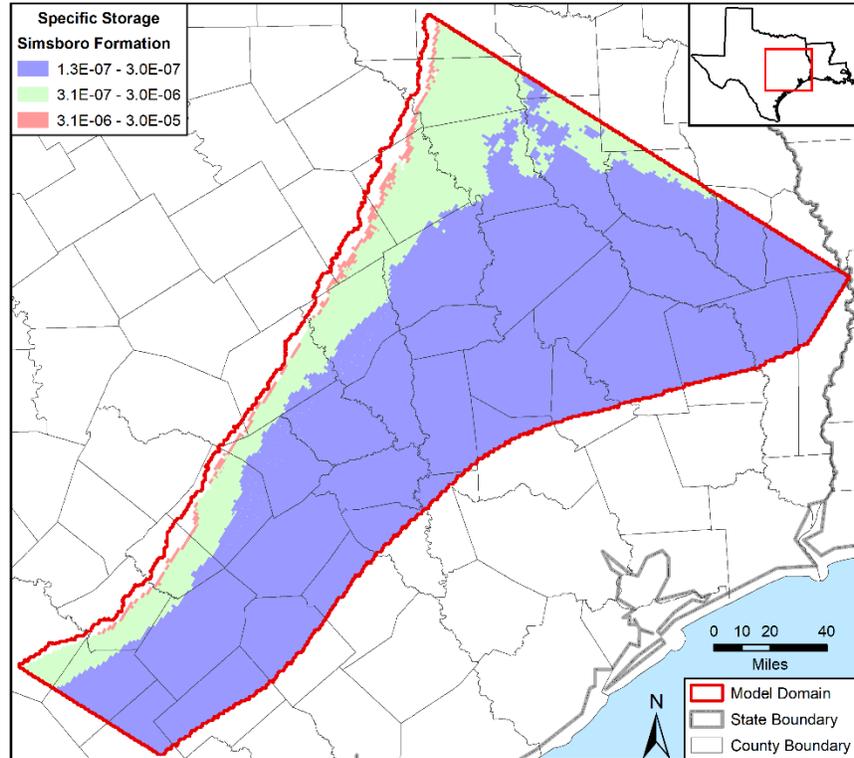
Figure 4.3.2bb. Specific storage values in the calibrated model in feet^{-1} for the Simsboro Formation in model layers 2 and 9.
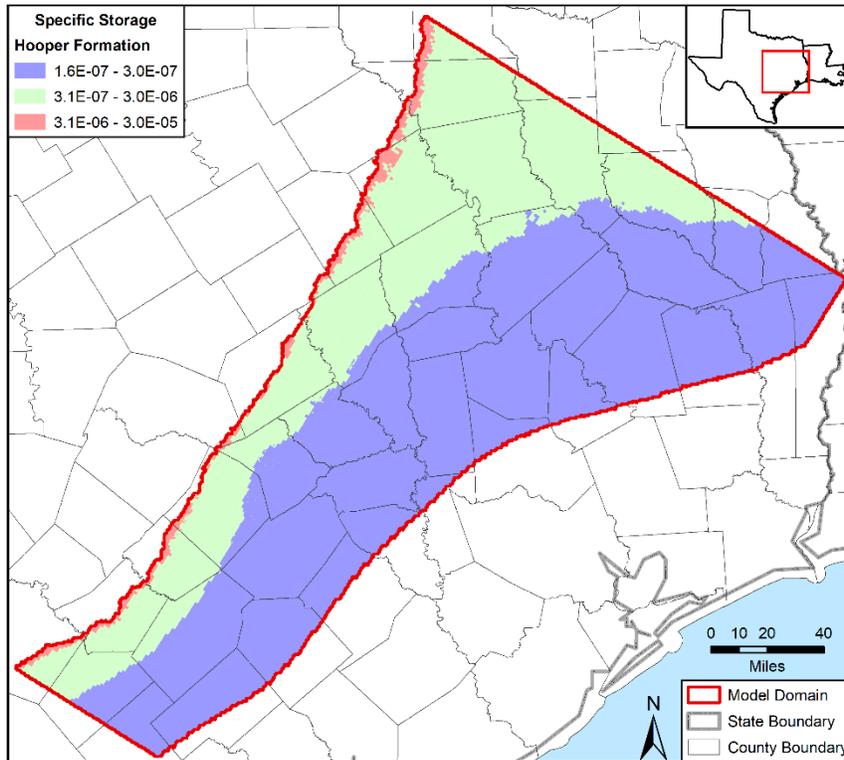
Figure 4.3.2cc. **Specific storage values in the calibrated model in feet^{-1} for the Hooper Formation in model layers 2 and 10.**
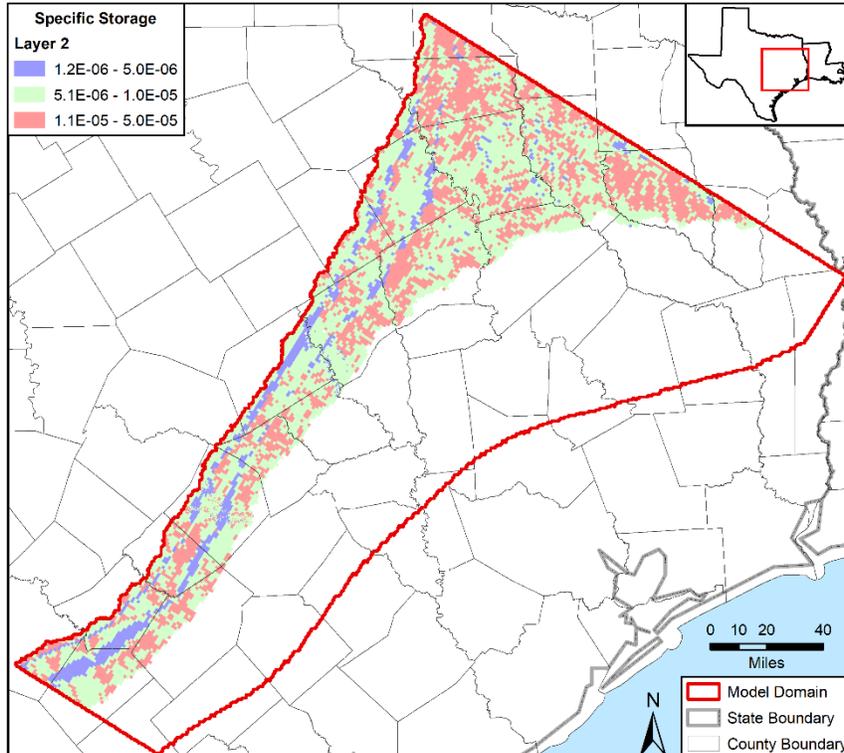
Figure 4.3.2dd. **Specific storage values in the calibrated model in feet^{-1} for model layer 2, which represents the shallow groundwater flow system.**

4.3.3 *Hydraulic Property Information and Data Used for Model Calibration*

Three sources of hydraulic property data were used for the model calibration. One source was the reports and datasets associated with the groundwater models developed for Texas aquifers in the Gulf Coast region. A second source was field and modeling studies that provided evidence that hydraulic conductivity and specific storage generally decrease with depth of burial. A third source was calculated hydraulic properties from field tests performed in wells.

4.3.3.1 Review of Groundwater Models

The most prominent groundwater availability models reviewed were the models for aquifers in Groundwater Management Area 12 (Dutton and others, 2003; Kelley and others, 2004; Ewing and Jigmond, 2016; Fogg and others, 1983). Other useful models included those developed for aquifers in Groundwater Management Area 11 (Fryar and others, 2003; Kelley and others, 2004; Fogg and others, 1983), for aquifers in Groundwater Management Area 13 (Kelley and others, 2004), and for the Gulf Coast Aquifer System (Ryder and Ardis, 1991; Williamson and others, 1990; Chowdhury and others, 2004; Young and others, 2009, 2016).

Among the useful information obtained from the model reviews was ranges and approaches for estimating vertical hydraulic conductivity. Vertical anisotropy (K_v/K_h), the ratio of vertical (K_v) to horizontal (K_h) hydraulic conductivity, expresses the degree to which vertical movement of groundwater may be restricted. Vertical anisotropy is related to the presence of sedimentary structures, bedding, and interbedded low-permeability layers. With regard to regional groundwater modeling, measurements for vertical hydraulic conductivity within large formations are not generally available. As a result, groundwater modeling generally provides the best means for estimation of vertical hydraulic conductivity at a regional scale (Anderson and Woessner, 1992).

Fogg and others (1983) performed a detailed sensitivity analysis to constrain the plausible ranges of horizontal to vertical hydraulic conductivity, K_h/K_v (hereafter referred to as the anisotropy ratio). Fogg and others (1983) concluded that a maximum reasonable anisotropy ratio for the Carrizo-Wilcox sequence was on the order of 10,000 to 1,000 based on reproducing the vertical head gradients within the Carrizo-Wilcox Aquifer. A similar scoping analysis was performed by Kelley and others (2004) for the Sparta and Queen City aquifers in Texas. Their analysis provided an estimated range of anisotropy ratios of 3,000 to 25,000 based on a hydraulic conductivity of 3×10^{-5} feet per day for clay. In their model of the Carrizo-Wilcox Aquifer, Dutton and others (2003) calculated geometric averages for the anisotropy ratio between 800 and 29,000. Based on these and other modeling results, an average anisotropy ratio less than 30,000 was used as a general constraint.

Ewing and Jigmond (2016) developed the groundwater availability model for the Brazos River Alluvium Aquifer. The hydraulic properties from their model were used to develop the spatial distribution of horizontal and vertical hydraulic conductivity values for the Brazos and Colorado rivers alluvium (Figures 4.3.2a and 4.3.2k, respectively).

4.3.3.2 Depth of Burial Effect on Hydrogeologic Unit Hydraulic Properties

Since the 1960s, researchers have presented evidence showing that permeability in a formation generally decreases with depth of burial. This reduction is associated with a porosity reduction with depth as a consequence of compaction and/or geochemical processes. Numerous studies in Texas (Magara, 1978; Neglia, 1979; Loucks and others, 1986; Prudic, 1991; Kuiper, 1994; Mace and Dutton, 1994; Williamson and Grubb, 2001) have presented evidence to support that permeability reduction with depth should be considered as part of regional groundwater models that simulate deep basin flow. Among the models in Texas that have accounted for a reduction in permeability with depth are Kelley and others (2004) and Young and others (2009, 2016). The most common form of the equation used to adjust permeability with depth is Equation 4-1. In Equation 4-1, the depth decay constant, λ, is a constant that is determined empirically using site specific data:

$$K_a = 10^{(-\lambda *D)}$$
<div align="right">Equation 4-1</div>

where:

K_a = reduction factor for permeability
Λ = depth-decay constant
D = depth (feet)

Equation 4-1 is the general relationship used by Prudic (1991) and Kelley and others (2004) to model permeability reduction with depth. As part of the model calibration process, Equation 4-1 was used to adjust both the horizontal and vertical permeability with depth for each hydraulic property zone, with the exception of the Colorado and Brazos alluvium zones. Table 4.3.3.2a lists the value for the depth decay constant used for each hydraulic property zone to develop the depth-decay relationships used in the calibrated model. Table 4.3.3.2b uses example values for the depth decay constant to show its impact on hydraulic conductivity.

Table 4.3.3.2a.   **Depth decay constants used to adjust hydraulic conductivity values for each hydraulic property zone.**

Hydraulic Property Zone	Depth-Decay Constant for Hydraulic Conductivity	
	Horizontal	Vertical
Sparta Aquifer	4.0E-04	2.93E-04
Weches Formation	4.0E-04	6.0E-04
Queen City Aquifer	4.0E-04	6.0E-04
Reklaw Formation	4.0E-04	6.0E-04
Carrizo Aquifer	1.6E-04	6.0E-04
Calvert Bluff Formation	4.0E-04	6.0E-04
Simsboro Formation	1.2E-04	6.0E-04
Hooper Formation	2.0E-04	6.0E-04

Table 4.3.3.2b.   Application of example depth decay constants.

Depth (feet)	Permeability Reduction Factor		
	$\lambda = 0.00012$	$\lambda = 0.0004$	$\lambda = 0.0006$
0	1.00	1.00	1.00
50	0.99	0.95	0.93
100	0.97	0.91	0.87
200	0.95	0.83	0.76
500	0.87	0.63	0.50
1000	0.76	0.40	0.25
2000	0.58	0.16	0.06
4000	0.33	0.03	0.004
6000	0.19	0.004	0.0003

A process that partly offsets the impacts of the depth-decay constant on permeability, which is caused primarily by the reduction in porosity, is the increase in the temperature of groundwater typically observed with depth because of the geothermal gradient. Because the updated model has depths that exceed several thousand feet, temperature effects on hydraulic conductivity were included in the updated model. A temperature adjustment was applied to adjust hydraulic conductivity to changes in the density and viscosity of water caused by an increase in temperature with depth (Freeze and Cherry, 1979):

$$K = k * \rho * g / \mu \qquad \text{(Equation 4-2)}$$

where

K	=	hydraulic conductivity of media (length per time)
k	=	intrinsic permeability of media (square length)
ρ	=	density of fluid (mass per cubic length)
g	=	gravitational constant (980.6 square centimeters per second)
μ	=	dynamic viscosity of fluid (mass per length times time)

In developing the hydraulic conductivity for the hydrogeologic units in the calibrated model, a thermal gradient of 17 degrees Fahrenheit per 1,000 feet was used. These conditions led to an increase in the hydraulic conductivity of approximately 125 and 230 percent at depths of 1,000 and 5,000 feet, respectively.

The increase in compressional forces with depth that causes porosity to reduce should also cause specific storage to decrease with depth. Shestakov (2002) postulated the relationship expressed by Equation 4-3 based on geomechanical considerations as:

$$S_s = A / [D + Zo] \qquad \text{(Equation 4-3)}$$

where

S_s = specific storage (length^{-1})
D = depth (length)
Zo = calibrated parameter
A = calibrated parameter

Shestakov (2002) showed that "A" in Equation 4-3 varied in the narrow range between 0.00020 to 0.00098 per foot for sandy rocks and between 0.0033 to 0.033 per foot for clayey rocks. Shestakov (2002) also shows that the variable "A" is also a function of the void space, such that, as the porosity becomes smaller, the specific storage value decreases, with all other factors remaining equal. This relationship is consistent with the Jacob Equation (Jacob, 1940) for calculating the specific storage from porosity and the compressibility of water and the rock matrix. The Shestakov model assumes a power-law relationship between porosity and depth, where the decrease is more pronounced at shallower depths than is allowed by a linear relationship between porosity and depth. The power-law relationship is consistent with the Magara (1978) observation that the rate of porosity decrease is fast at shallow depths and slows down with greater burial depth.

Previous application of the Shestakov model for estimating specific storage values include the Northern Trinity and Woodbine Aquifers Groundwater Availability Model (Kelley and others, 2014), the Yegua-Jackson Aquifer Groundwater Availability Model (Deeds and others, 2010), and the Gulf Coast Aquifer System (Young and others, 2009, 2016). These applications have involved a modified version of Equation 4-3 that allows accounting for mixed sands and clay layers and forces a minimal value of specific storage. Equation 4-4 was used to calculate specific storage values for the calibrated model.

$$S_s = Ss_{min} + \left\{ \frac{A1 * [\, SF + CM * (1 - SF)\,]}{A2 + D} \right\} \qquad \text{(Equation 4-4)}$$

where

S_s = specific storage (length^{-1})
Ss_{min} = set to 1.0 E-07 feet^{-1}
$A1$ = calibrated constant
SF = sand fraction
CM = clay multiplier, which is set to 10
$A2$ = a calibrated parameter that is set to 10
D = depth which is determined by the location of the grid cell (length)

For each formation, the sand fraction was set to a constant and the only adjustment made as part of the model calibration process was the value of A1. Table 4.3.3.2c lists the values for sand fraction and for the calibrated constant, A1, for each of the hydraulic property zones. Table 4.3.3.2d shows an application of Equation 4-4 for a range of the A1 and spontaneous potential values in Table 4.3.3.2c.

Table 4.3.3.2c. **Values used for sand fraction and the calibrated constant A1 for applying Equation 4-4 to generate specific storage values for each hydraulic property zone.**

Hydraulic Property Zone	Constants used in Equation 4-4 to Calculate Specific Storage Values	
	Sand Fraction	**A1**
Sparta Aquifer	0.5	0.0004
Weches Formation	0.3	0.0004
Queen City Aquifer	0.5	0.0004
Reklaw Formation	0.7	0.0004
Carrizo Aquifer	0.5	0.0002
Calvert Bluff Formation	0.5	0.0004
Simsboro Formation	0.7	0.0002
Hooper Formation	0.5	0.0004

Table 4.3.3.2d. **Values used for sand fraction (SF) and the calibrated parameter A1 for applying Equation 4-4 to generate specific storage values for each hydraulic property zone.**

Depth (feet)	Specific Storage (feet^{-1})	
	A1 = 0.0002	**A1 = 0.0004**
	SF = 0.7	**SF = 0.3**
0	4.22E-05	3.59E-04
50	7.11E-06	6.00E-05
100	3.93E-06	3.28E-05
200	2.11E-06	1.73E-05
500	9.31E-07	7.19E-06
1000	5.23E-07	3.71E-06
2000	3.13E-07	1.92E-06
4000	2.07E-07	1.02E-06
6000	1.72E-07	7.13E-07

4.3.3.3 Hydraulic Properties Determined from Field Tests

The model was calibrated by using pilot points to generate hydraulic conductivity values at the grid cell locations. Pilot points are fixed locations assigned to a hydraulic property zone where parameter values are used to generate a continuous two-dimensional parameter field that is used to assign parameter values at grid cell locations. During the model calibration, the parameter values at the pilot point locations were adjusted where needed to change the values assigned to grid cells to improve the model calibration. An important constraint on the parameter values at pilot point locations is the range of values that a modeler allows. Establishing a range for parameters at a pilot location allows the modeler to condition the development of model parameters to *a priori* information about the spatial variability associated with the parameter. The primary data used to set the upper and lower limits for hydraulic conductivity at each pilot

point location were hydraulic conductivity values determined from hydraulic tests and the values used by previously calibrated groundwater models.

The three principal sources of hydraulic conductivity values from fields studies were Mace and others (2000), the aquifer tests presented in Appendix B, and aquifer tests performed by the Vista Ridge project. Mace and others (2000) compiled and analyzed transmissivity, hydraulic conductivity, and storativity values from numerous sources for the entire Carrizo-Wilcox Aquifer in Texas. The datasets created by Mace and others (2000) were used by Dutton and others (2003) and Kelley and others (2004) to develop the hydraulic conductivity values for their models. Table 4.3.3.3a provides geometric means calculated by Dutton and others (2003) for the Hooper, Simsboro, and Calvert Bluff formations and the Carrizo Aquifer using the data from Mace and others (2000). Table 4.3.3.3b provides the geometric mean and median for hydraulic conductivity values for the Sparta and Queen City aquifers based on data from Mace and others (2000). These values were generated for this study by removing results for wells with a diameter less than 7.5 inches. Based on our analysis of the data generated by Mace and others (2000), the quality of the measured values decreases for wells with smaller diameters.

Table 4.3.3.3a. Geometric mean values for hydraulic conductivities based on values from Mace and others (2000) and calculated by Dutton and others (2003) for the central portion of the Carrizo-Wilcox Aquifer.

Metric	Hydraulic Property Zone			
	Hooper Formation	Simsboro Formation	Calvert Bluff Formation	Carrizo Aquifer
Geometric Mean (feet per day)	5.4	24.8	5.6	19.3

Table 4.3.3.3b. Geometric mean and median values for hydraulic conductivities based on values from Mace and others (2000) for wells with a diameter greater than or equal to 7.5 inches for the Queen City and Sparta aquifers.

Metric	Hydraulic Property Zone	
	Sparta Aquifer	Queen City Aquifer
Geometric Mean (feet per day)	5.4	2.8
Median (feet per day)	2.1	2.5
Count	5	65

The hydraulic conductivity values considered most reliable are those generated from the aquifer pumping tests contained in Appendix B and performed by the Vista Ridge project in Burleson County (Appendix E). For this analysis, the hydraulic conductivity values were determined by dividing the calculated transmissivity by the vertical length of the well screen. One criterion used to evaluate the reliability and representativeness of the calculated hydraulic conductivity values was the thickness of the formation tested. The greater the well screen coverage across the total thickness of the aquifer, the more representative the calculated hydraulic conductivity will be for the entire aquifer. Therefore, results for tests in wells with a screen length less than some

minimum value where not considered. Because the aquifers differ in their average thicknesses, the selected minimum screen length was different for the different aquifers. Aquifer tests that involved well screens above the minimum length were considered more reliable than those with shorter well screen lengths and were used in generating the values in Table 4.3.3.3c. The minimum well screen lengths for the Sparta, Queen City, and Carrizo aquifers and the Simsboro Formation used to produce the values in Table 4.3.3.3c were 160, 160, 260 and 360 feet, respectively. There are no values for the Queen City Aquifer in the table because none the of aquifer pumping tests involved a pumping well with a well screen length greater than 160 feet.

Table 4.3.3.3c. **Geometric means for hydraulic conductivity values from aquifer tests for the Sparta and Carrizo aquifers and the Simsboro Formation.**

Metric	Hydraulic Property Zone		
	Sparta Aquifer	Carrizo Aquifer	Simsboro Formation
Geometric Mean (feet per day)	5.8	14.7	21.3
Median (feet per day)	7.2	11.9	31.8
Count	6	8	22

4.4 Well Package

The MODFLOW Well (suffix WEL) package was used to simulate groundwater production. The Well package requires specification of a model cell location and a prescribed flow for each stress period.

A table of groundwater production for each of the hydrogeologic units by county and stress period is included in Appendix F. In Appendix F, the pumping rates for the alluvium include production from both the Colorado and Brazos rivers alluvium.

Figures showing the spatial distribution of annual pumping for the hydrogeologic units for each grid cell for the years 1950, 1970, 1990, and 2010 are provided in Appendix G.

4.4.1 *Treatment of Minimum Saturated Thickness by MODFLOW-USG*

One feature of MODFLOW-USG that is different from the previous version of MODFLOW used by Kelley and others (2004) is the ability for production in a cell to be automatically scaled back when the saturated thickness is one percent of the layer thickness. This simulates a decline in production that occurs in many cases when saturated thickness declines. As a result, a modeler using the updated groundwater availability model should, after a model simulation, check whether MODFLOW-USG automatically reduced any pumping. For the final model calibration run, the amount of pumping reduction was less than 0.01 percent for any stress period.

4.4.2 *Pumping Distribution for the Brazos River Alluvium Aquifer*

The pumping distribution for the Brazos River Alluvium Aquifer was generated from the MODFLOW-USG model files for the Brazos River Alluvium Aquifer groundwater availability

model (Ewing and Jigmond, 2016). Across the alluvium, the Brazos River Alluvium Aquifer groundwater availability model uses 0.125-mile by 0.125-mile square grid cells. These grid cells are smaller than the 0.5-mile by 0.5-mile square grid cells used by the updated model for the central portion of the Carrizo-Wilcox, Queen City, and Sparta aquifers. Because of the different grid cell sizes, the pumping from approximately 16 of the 0.125-mile by 0.125-mile square grid cells was used to determine the pumping in one of the 0.5-mile by 0.5-mile square grid cells.

4.4.3 Pumping Distribution for the Shallow Groundwater Flow System

Model layer 2 represents the shallow groundwater flow system. Across most of the model domain, the saturated thickness of this layer is relatively thin compared to the underlying hydrogeologic units. Only pumping for domestic and livestock uses was considered to occur in model layer 2, and this pumping was allowed only if the saturated thickness was greater than 60 feet. Any pumping that occurs in model layer 2 is represented in Appendices E and F as pumping for the hydrogeologic unit in which the pumping occurs.

4.5 Drain Package

The MODFLOW Drain (suffix DRN) package was used to simulate outflow from ephemeral streams, intermittent streams, and seeps. Figure 4.5a shows a map of streams based on a United States Geological Survey national hydrograph dataset. Figure 4.5b shows a map of the drain locations in the updated model, which were used to represent ephemeral streams. The initial locations of the drains were mapped directly from Kelley and others (2004). During model calibration, it was evident that additional drain locations would be required to prevent flooding conditions from existing in the outcrop areas. Flooding of a grid cell occurs when the simulated water table in the grid cell is higher than the land surface assigned to the grid cell. To prevent flooding from occurring in the outcrop areas, the area covered by drain cells was increased 25 percent relative to the area covered by drain cells in the groundwater availability model developed by Kelley and others (2004).

The number of grid cells in the model with drains is 7,013, which is too many entries to include as a table in an appendix. Appendix H describes the attributes of an electronic table in Excel that contains information on each drain cell, including the node number, the elevation head, and the drain conductance. The Excel file is included in the electronic delivery with this report.

The drain elevation generally corresponds to the ground surface elevation of the grid cell in which the drain is located minus 20 percent of the thickness of model layer 2. For the grid cells that are 1-mile by 1-mile square, the initial drain conductance was set to 20,000 square feet per day. During model calibration, the conductance values were raised or lowered to achieve a minimum conductance value sufficient to prevent flooding. For the 1-mile by 1-mile grid cells, the drain conductance values range between 100 and 57,000 square feet per day.
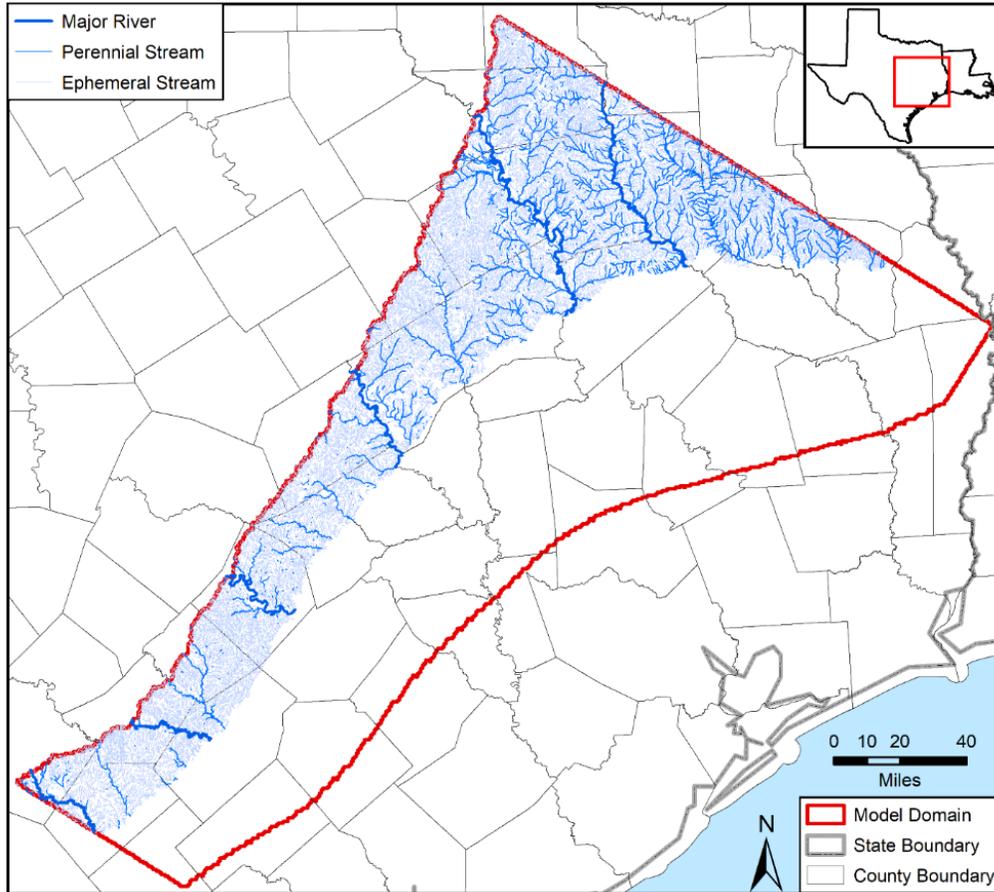
Figure 4.5a. **Locations of major rivers and perennial and ephemeral streams in the outcrop areas based on United States Geological Survey national hydrograph data.**
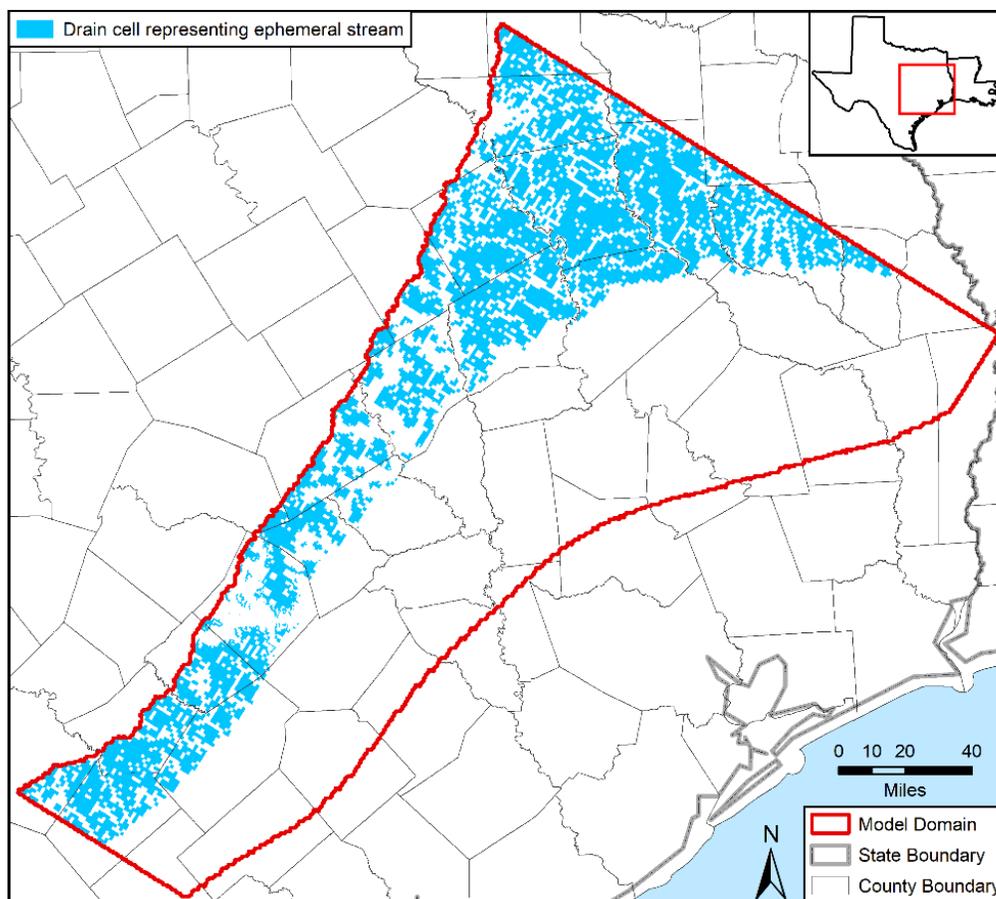
Figure 4.5b.   **Location of drain cells representing ephemeral streams in the model.**

4.6   Recharge Package

The MODFLOW Recharge (suffix RCH) package was used to simulate recharge to groundwater in the model. Section 3.3 describes the methodology used to generate annual recharge rates for each stress period. Tables 4.6a through 4.6d list annual recharge from 1930 to 1949, 1950 to 1969, 1970 to 1989, and 1990 to 2010, respectively, for the 28 counties in the model outcrop area. The average of the 81values for each county is also provided. The 81-year average listed for each county is the recharge rate used for the steady-state simulation.

Figure 4.6a shows the spatial distribution of recharge for the steady-state simulation. The steady-state recharge rates for the 28 counties in the outcrop area range from a low of 0.52 inches per year in Bexar County to a high of 2.9 inches per year in Angelina County. The general pattern of increasing recharge rates toward the northeast is attributed primarily to the general pattern of increasing annual precipitation from the southwest toward the northeast and decreasing evapotranspiration potential from the northeast to the southwest. The smaller scale spatial variability in the recharge rates is attributed to the variability in the infiltration capacity of the different surface geologies (see Figure 4.2.1k). The spatial distribution of recharge for the years 1950, 1970 1990, and 2010 are provided in Figures 4.6b, 4.6c, 4.6d, and 4.6e, respectively.

Table 4.6a.   **Annual recharge rates by county in the outcrop area in inches per year from 1930 to 1949.**

County	average	1930	1931	1932	1933	1934	1935	1936	1937	1938	1939	1940	1941	1942	1943	1944	1945	1946	1947	1948	1949
Anderson	2.36	2.45	2.33	3.28	2.13	2.35	3.07	1.69	2.33	1.66	1.85	3.13	1.69	2.28	1.41	3.12	3.02	3.04	2.14	1.05	1.76
Angelina	2.90	2.63	2.8	3.18	2.77	3.25	3.01	1.66	3.18	2.48	2.56	3.46	3.28	2.62	1.26	3.32	2.92	3.38	2.4	1.57	3
Bastrop	1.60	1.72	1.09	1.75	0.79	1.25	1.47	1.73	0.81	1.66	0.49	2.81	2.12	1.3	0.55	1.97	1.69	1.69	0.68	0.31	1.75
Bexar	0.52	0.4	0.99	0.67	0.33	0.74	1.17	0.62	0.5	0.42	0.3	0.56	0.54	2	0.37	0.85	0.61	2.24	0.31	0.36	1.33
Brazos	2.78	2.51	2.14	4.27	1.79	2.94	2.19	2.51	1.68	2.5	2.09	4.09	1.78	1.39	0.93	3.34	2.16	2.98	2.74	0.44	4.33
Burleson	1.64	1.39	1.15	2.37	0.89	1.69	1.39	1.36	0.95	1.34	0.98	2.51	1.37	0.54	0.36	1.94	1.44	1.49	1.4	0.25	2.63
Caldwell	1.37	1.43	0.55	1.37	0.49	0.78	1	1.35	0.6	1.33	0.38	1.32	1.37	1.36	0.39	1.79	1.99	1.49	0.55	0.35	0.77
Cherokee	2.47	2.48	2.73	3.33	2.67	2.74	3.37	1.59	2.39	1.96	2.17	3.15	2.5	2.54	1.4	3.28	3.25	3.36	2.54	1.32	1.91
Falls	2.00	2.25	1.17	2.94	0.93	1.07	2.08	1.81	1.88	1.38	1.25	1.73	0.73	1.78	0.93	2.1	2.95	1.71	1.06	0.56	0.97
Fayette	1.32	1.51	0.61	1.55	0.36	0.98	1.67	2.1	0.63	1.2	0.52	2.45	1.99	1.58	0.71	1.61	1.55	1.23	0.6	0.25	1.36
Freestone	2.54	2.86	2.01	3.71	1.49	1.84	2.96	1.86	2.55	1.89	1.53	2.85	0.93	2.84	1.39	2.73	3.42	2.08	2.29	1.08	1.73
Gonzales	0.91	0.64	0.28	1.01	0.42	0.67	1.36	1.38	0.39	0.76	0.27	0.96	1.32	1.07	0.28	0.76	0.98	1.67	0.42	0.36	0.55
Guadalupe	1.15	0.72	0.44	1.43	0.6	0.95	1.84	1.24	0.99	1.24	0.31	1.14	1.38	2.61	0.39	1.4	0.83	2.05	0.39	0.37	1.67
Henderson	2.46	2.59	1.88	3.11	1.82	1.75	2.65	1.91	2.15	1.76	1.94	2.22	2.01	3.09	2.16	2.79	3.77	3.67	2.31	1.19	1.82
Houston	2.29	2.2	2.51	2.87	2.13	2.5	3.24	1.46	2.37	1.55	2.01	3.09	2.2	2.15	1.11	2.83	2.09	2.41	2.12	0.93	1.77
Lee	1.46	1.26	0.95	1.87	0.63	1.35	1.32	1.35	0.85	1.21	0.47	2.66	1.48	0.71	0.31	1.69	1.23	1.1	0.84	0.21	2.25
Leon	2.19	2.39	2.03	3.03	1.55	2.04	2.76	1.42	2.39	1.67	1.7	2.51	0.93	2.48	1.15	2.78	2.49	2.24	1.99	0.94	2.22
Limestone	2.58	2.84	1.53	3.73	1.12	1.36	2.9	2.13	2.47	1.84	1.39	2.15	0.67	2.85	1.09	2.98	4.05	2.43	1.8	0.98	0.89
Milam	1.86	1.8	1.21	3.11	0.93	1.91	1.6	1.8	1.35	1.48	1.1	2.84	1.08	1.05	0.67	2.21	2.16	1.89	1.35	0.34	2.49
Nacogdoches	2.50	2.58	2.68	2.9	2.75	3.01	2.84	1.47	2.82	2.21	2.38	3.2	3.11	2.28	1.19	3.27	3.07	3.21	2.33	1.58	2.86
Navarro	2.40	2.74	1.55	3.26	1.22	1.35	2.24	2.25	2.13	1.94	1.6	2.37	1.75	3.28	2.17	2.32	3.65	2.92	2.07	1.09	0.97
Robertson	2.03	2.26	1.55	3.38	1.12	1.6	1.99	1.72	1.82	1.74	1.6	2.51	0.69	1.42	0.91	2.36	2.51	2.05	1.5	0.59	2.21
Rusk	2.33	2.52	2.76	3.25	2.84	2.62	3.28	1.34	2.57	2	2.22	2.79	2.77	2.45	1.2	3.29	3.29	3.23	2.45	1.51	2.32
San Augustine	2.86	2.85	2.91	2.87	3.02	3.35	2.89	2.06	3.15	2.84	2.83	3.25	3.34	2.35	1.37	3.38	3.32	3.38	2.73	1.91	3.56
Smith	2.49	2.5	2.3	3.19	2.52	1.94	3.3	1.61	2.08	1.77	2.21	2.57	1.8	2.95	2	3.61	3.89	3.62	2.71	1.23	2
Van Zandt	2.81	2.71	2.09	3.42	1.9	1.68	2.94	1.98	2.36	2.14	2.26	1.96	2.19	3.77	2.2	2.19	4.15	3.5	2.69	1.57	2.02
Williamson	1.57	1.54	1	2.1	0.78	1.63	1.55	1.63	1.09	1.31	0.43	2.93	1.27	1.37	0.41	1.54	1.37	1.47	0.62	0.26	1.91
Wilson	0.58	0.33	0.65	0.67	0.48	0.68	1.72	0.8	0.4	0.45	0.22	0.62	1.32	1.68	0.32	0.44	0.32	2.48	0.3	0.32	0.68

Table 4.6b.   **Annual recharge rates by county in the outcrop area in inches per year from 1950 to 1969.**

County	1950	1951	1952	1953	1954	1955	1956	1957	1958	1959	1960	1961	1962	1963	1964	1965	1966	1967	1968	1969
Anderson	1.92	1.22	2.14	1.85	1.03	1.55	0.85	3.61	2.46	3.27	2.5	2.88	2.06	0.47	1.17	2.87	2.68	1.52	2.92	2.97
Angelina	2.99	1.61	2.3	3.3	1.27	1.67	1.26	3.47	2.68	2.54	3.05	3.17	2.44	1	1.61	2.93	2.41	1.73	3.24	2.71
Bastrop	1.1	0.79	1.53	1.72	0.26	0.65	0.27	3.12	1.62	1.56	2.06	2.74	1.37	0.33	1.3	2.42	1.16	1.48	3.32	1.57
Bexar	0.31	0.39	0.5	0.36	0.25	0.32	0.24	1.81	2.31	0.49	0.61	0.48	0.38	0.3	0.46	0.73	0.42	0.78	0.86	1.03
Brazos	1.86	0.69	2.25	3.59	0.52	0.85	0.43	4.7	3.08	2.32	3.6	2.49	2.56	0.58	2	2.5	2.72	1.78	4.78	3.3
Burleson	1.11	0.38	1.14	1.9	0.26	0.49	0.27	2.81	1.83	1.15	2.2	2.02	1.63	0.29	1.06	1.73	1.77	1.17	3.04	1.71
Caldwell	0.67	0.57	2.07	1.36	0.24	0.64	0.26	2.44	1.05	1.03	1.67	2	0.7	0.32	0.81	2.29	0.96	0.61	2.71	1.1
Cherokee	2.44	1.58	2.1	2.69	1.06	1.66	0.92	3.45	2.56	2.76	2.86	3.04	2.57	0.71	1.34	2.71	2.55	1.66	3.2	3.04
Falls	0.45	0.5	1.62	1.82	0.32	1.42	0.32	3.47	1.4	2.48	2.01	1.26	0.8	0.32	0.97	2.81	1.95	1.04	2.13	2.06
Fayette	0.67	0.6	1.85	1.1	0.22	0.68	0.22	2.36	1.37	1.47	1.96	2.63	0.35	0.25	0.8	1.99	1.08	0.47	3.07	0.78
Freestone	1.37	0.94	2.34	1.82	0.55	1.26	0.8	3.87	2.3	3.66	1.46	3	1.58	0.32	1.11	3.86	3.22	2.02	2.75	2.88
Gonzales	0.29	0.26	1.4	0.62	0.18	0.44	0.18	1.88	0.79	0.49	1.21	1.01	0.5	0.21	0.34	1.44	0.49	0.88	1.76	0.75
Guadalupe	0.39	0.4	1.52	0.67	0.26	0.42	0.27	2.16	1.34	0.64	1.15	1.8	0.49	0.31	0.66	2.16	0.64	0.81	2.15	1.12
Henderson	2.53	1.62	2.5	1.54	1.76	2.01	0.97	3.82	2.81	3.67	2.14	2.07	2.71	0.66	1.03	1.77	3.17	2.57	2.81	3.01
Houston	1.57	1.06	1.92	2.21	0.89	1.43	0.71	3.37	2.24	2.38	2.82	2.69	1.82	0.76	1.17	2.91	2.35	1.22	3.02	2.49
Lee	1.15	0.34	0.96	1.46	0.24	0.5	0.26	2.73	1.81	0.82	1.89	2.43	1.57	0.27	0.89	1.69	1.49	1.38	2.69	1.29
Leon	1.08	1.08	1.83	1.95	0.55	1.42	0.7	3.3	2.07	2.49	2.15	2.67	1.01	0.32	1.18	2.98	2.34	1	2.3	2.32
Limestone	0.54	0.93	2.11	1.89	0.36	1.48	0.53	4.1	2.15	3.65	2.18	2.39	1.09	0.36	1.45	4.42	3.42	1.81	2.61	2.98
Milam	1.18	0.38	1.38	2.34	0.3	0.96	0.32	3.45	2.13	0.95	2.6	1.62	1.66	0.3	1.33	1.77	2.43	1.44	2.92	1.94
Nacogdoches	2.97	1.67	2.17	3.31	1.08	1.75	1.25	3.35	2.76	2.47	3.1	3.14	2.46	1.04	1.54	2.8	2.65	1.57	3.25	2.73
Navarro	1.83	1.03	2.28	0.91	0.88	1.61	1.07	3.91	2.1	3.4	0.93	2.14	2.59	0.36	0.8	2.36	3.1	2.67	2.22	2.51
Robertson	0.91	0.59	1.67	2.25	0.35	1.16	0.35	3.64	1.91	2.18	2.49	1.26	1.15	0.35	1.3	2.22	2.04	1.11	2.41	2.33
Rusk	2.66	1.56	2	2.75	1.3	1.87	1.06	3.4	2.7	2.29	3.28	3.17	2.52	0.59	1.06	2.81	2.88	1.67	3.34	3.02
San Augustine	3.19	2.08	2.65	3.51	1.19	2.11	1.27	3.38	3.2	2.8	3.2	3.44	2.6	1.64	1.83	2.61	2.71	1.72	3.31	2.63
Smith	2.59	1.7	2.29	2.36	1.48	1.88	0.84	3.69	2.98	3.37	2.68	2.55	2.42	0.61	0.83	1.65	2.95	1.73	3.14	3.12
Van Zandt	3.26	1.91	2.92	1.67	1.97	1.75	0.94	4.1	3.24	3.68	2.49	2.08	2.87	0.94	1.08	2	3.96	3.36	2.46	3.29
Williamson	1	0.39	1.19	1.55	0.25	0.75	0.28	3.07	2.22	0.9	1.79	2.21	1.86	0.29	1.03	1.85	1.62	1.58	2.43	1.23
Wilson	0.27	0.31	0.61	0.42	0.25	0.3	0.22	1.5	2.08	0.42	0.95	0.52	0.44	0.26	0.35	0.73	0.49	1.75	1.52	1.47

Table 4.6c. **Annual recharge rates by county in the outcrop area in inches per year from 1970 to 1989.**

County	1970	1971	1972	1973	1974	1975	1976	1977	1978	1979	1980	1981	1982	1983	1984	1985	1986	1987	1988	1989
Anderson	1.47	1.86	2.54	3.57	2.53	2.04	3.06	1.94	1.87	2.95	1.11	2.35	2.03	2.56	2.5	2.5	2.4	2.54	1.6	2.29
Angelina	1.64	1.79	2.87	3.48	3.31	2.47	2.21	1.52	1.65	3.24	1.43	2.57	3.61	2.85	3.01	3.1	2.87	2.39	1.18	3.23
Bastrop	1.73	0.53	1	2.69	2.28	2.81	2.97	0.89	1.85	1.1	0.53	2.52	1.21	2.13	0.94	1.64	1.99	2.47	0.35	1.13
Bexar	0.4	0.49	0.58	2.86	0.62	0.48	0.85	0.44	0.86	0.63	0.45	0.55	0.42	0.45	0.38	1.07	0.94	0.61	0.24	0.33
Brazos	3.06	1.63	1.17	4.41	2.97	2.28	2.5	1.25	2.09	3.91	1.74	2.66	2.91	3.91	2.77	1.68	2.79	2.23	0.44	1.87
Burleson	2.01	0.97	0.72	2.46	2	1.77	1.87	0.74	1.39	2.07	1.17	1.58	1.81	2.36	1.78	0.9	1.84	1.31	0.27	1.11
Caldwell	0.86	0.56	0.65	2.39	2.18	2.26	3.09	0.71	1.61	1.18	0.53	2.31	0.9	2.09	0.79	2.09	1.78	2.5	0.3	0.93
Cherokee	1.61	1.61	2.45	3.4	2.23	2.11	2.82	1.51	1.79	3	1.37	2.44	2.63	2.62	2.8	2.93	2.2	2.32	1.45	2.85
Falls	1.51	1.67	0.82	2.87	1.73	2.02	3.17	0.96	1.24	3.8	0.5	2.83	1.01	2.19	2.34	2.44	2.88	1.24	0.78	1.78
Fayette	1.19	0.93	0.96	2.36	1.57	1.93	2.77	1.02	1.84	1.84	0.34	2.94	1.22	1.54	1.02	0.79	1.98	2.03	0.24	1.25
Freestone	1.56	2.53	2.03	4.03	3.54	2.61	4.23	2.47	2.13	2.82	1.17	2.72	1.67	2.79	2.65	2.95	2.97	2.7	1.4	2.12
Gonzales	0.41	0.57	0.9	1.71	1.16	0.89	1.7	0.76	1.07	1.32	0.48	1.55	0.4	1.25	0.52	1	0.74	1.62	0.18	0.56
Guadalupe	0.53	0.54	0.98	2.08	1.51	0.85	2.19	0.49	1.3	1.16	0.78	1.22	0.42	1.28	0.42	1.76	1.06	1.89	0.27	0.45
Henderson	2.21	2	2.72	3.64	2.59	1.86	3.35	1.87	1.61	1.39	1.06	2.85	2.4	1.72	2.34	2.85	3.31	2.43	1.33	2
Houston	1.64	1.81	2.03	3.14	2.24	1.75	2.72	1.65	1.69	3.11	1.17	2.64	2.04	2.54	2.51	2.64	1.74	1.83	1.23	2.4
Lee	1.76	0.5	0.7	1.91	2.48	2.18	2.06	0.65	1.08	0.99	0.89	1.99	1.36	1.69	1.39	1.69	1.54	1.78	0.27	1.1
Leon	1.39	1.99	1.81	3.51	2.96	2.17	3.66	1.82	1.55	3.16	1.04	2.35	1.04	3.01	2.44	2.37	2.17	2.38	1.3	1.79
Limestone	1.65	2.45	1.91	4.41	2.76	2.92	4.43	1.9	1.74	3.56	0.79	3.37	1.31	2.79	2.58	3.19	3.28	2	1.07	1.8
Milam	2.27	1.38	1.15	2.27	1.89	2.08	2.26	0.63	1.46	2.75	1.26	2.31	1.67	2.18	1.55	1.14	2.01	1.69	0.39	1.16
Nacogdoches	1.72	1.7	2.77	3.25	3.01	2.74	2.02	1.58	1.84	3.21	1.55	2.47	3.42	2.75	2.66	3.07	2.75	2.48	1.23	3.27
Navarro	1.72	2.27	1.69	3.29	2.39	1.87	3.47	1.86	1.66	1.33	1.05	3.16	2.31	1.55	2.22	3	3.41	2.29	1.28	2.04
Robertson	2.31	1.55	1.22	3.4	1.99	2.11	2.5	0.96	1.53	3.74	0.94	2.38	1.71	2.5	1.93	2.11	2.61	1.62	0.94	1.75
Rusk	1.83	1.52	2.61	3.38	2.43	2.36	2.85	1.24	1.72	3.17	1.61	2.19	3.15	2.47	2.61	3.07	1.95	2.45	1.38	3.25
San Augustine	2.07	1.99	3.17	3.38	3.5	3.39	1.99	2.42	2.4	3.12	1.87	2.79	3.77	3.53	2.98	3.17	3.42	3.12	1.59	3.66
Smith	1.82	1.17	2.54	3.65	2.57	1.81	2.72	1.65	1.55	2.27	1.14	2.1	2.22	1.96	2.27	2.67	2.66	2.53	1.26	2.2
Van Zandt	2.87	2.8	2.48	3.92	2.78	1.43	3.75	2.16	1.74	1.79	1.37	2.99	2.79	1.78	2.31	3.25	3.48	2.89	1.59	2.17
Williamson	1.5	0.7	0.98	1.73	2.25	2.47	2.37	0.63	1.3	1.01	0.96	2.49	1.3	1.77	1.1	1.9	1.07	2.09	0.31	0.77
Wilson	0.36	0.35	0.54	2.37	0.63	0.46	0.98	0.47	1.07	1	0.53	0.45	0.41	0.5	0.29	0.76	0.45	0.69	0.19	0.33

Table 4.6d.   **Annual recharge rates by county in the outcrop area in inches per year from 1990 to 2010.**

County	1990	1991	1992	1993	1994	1995	1996	1997	1998	1999	2000	2001	2002	2003	2004	2005	2006	2007	2008	2009	2010
Anderson	3.87	3.61	2.59	2.96	2.83	1.93	1.48	2.89	2.36	1.57	3.27	3.11	2.5	2.14	2.6	0.65	2.1	3.04	2.06	2.71	1.28
Angelina	3.09	3.51	3.08	3.06	3.16	3.18	1.71	2.9	2.77	2.23	3.28	3.17	3.19	2.58	3.4	1.39	2.77	2.46	2.47	2.87	0.9
Bastrop	0.93	3.3	2.6	1.21	2.53	1.8	0.99	1.7	2.32	0.32	1.81	2.15	2.14	0.84	2.1	0.6	1.05	2.13	0.26	1.5	0.82
Bexar	0.92	0.87	1.88	1.06	0.67	0.38	0.29	0.62	1	0.31	0.6	0.86	2.2	0.5	1.3	0.3	0.34	2.82	0.25	0.47	0.93
Brazos	3.09	4.22	3.12	3.85	3	2.94	1.28	2.5	3.87	0.71	2.96	3.02	3.64	3.12	4.37	1.15	3.45	2.71	1.02	2.6	1.01
Burleson	1.62	2.67	2.04	1.99	1.79	2.05	0.71	0.97	2.1	0.3	1.92	1.79	2.28	1.82	2.8	0.78	1.88	1.89	0.37	1.57	0.62
Caldwell	1.34	3.22	2.31	1.79	2.04	1.2	0.84	1.76	2.56	0.3	1.72	2.17	2.54	0.49	2.84	0.43	0.75	2.01	0.25	1.44	0.53
Cherokee	3.64	3.43	2.78	3.05	2.73	2.27	1.51	3.08	2.49	1.93	3.1	3.33	2.59	2.34	2.94	0.96	2.38	2.88	2.39	2.71	1.06
Falls	3.29	3.8	1.8	2.1	2.57	2.18	0.9	3.08	2.35	0.68	2.87	1.61	1.97	2.09	3.08	0.6	2.16	3.53	1.3	2.75	1.39
Fayette	0.62	2.17	2.23	1.58	1.31	1.15	0.67	2.37	1.96	0.23	1.14	1.49	1.91	0.57	2.79	0.54	0.65	1.78	0.21	1.31	0.54
Freestone	3.73	3.47	2.6	3.08	2.17	2.27	1.28	3.13	3.08	1.58	3.68	2.85	2.58	1.91	3.27	0.64	1.97	3.71	1.9	2.75	1.44
Gonzales	0.46	1.78	1.99	1.47	1.22	0.73	0.49	0.92	1.81	0.22	1.11	1.14	1.69	0.31	1.96	0.28	0.32	1.51	0.19	1.3	0.48
Guadalupe	0.92	2.45	2.39	1.59	1.14	0.65	0.47	0.81	2.26	0.31	1.5	1.74	3.17	0.47	3.24	0.36	0.44	2.55	0.27	1.28	0.65
Henderson	3.93	3.07	2.08	2.16	3.43	2.15	1.79	2.94	3.01	1.62	3.58	2.72	2.28	1.83	2.15	0.54	1.41	3.82	2.79	3.81	1.49
Houston	2.67	3.37	2.94	3.14	2.52	2.19	1.18	2.52	2.12	1.8	2.91	3.12	2.65	2.14	2.95	0.89	2.53	2.39	1.94	2.05	1.11
Lee	0.68	3.06	2.05	0.98	2.08	1.91	0.44	0.7	1.37	0.28	1.87	1.81	2.27	1.23	2.49	0.83	1.4	1.96	0.26	1.46	0.74
Leon	2.45	3.07	2.85	3.2	1.45	1.95	0.79	2.55	2.07	1.43	2.81	2.82	2.47	1.93	2.54	0.63	2.34	2.51	1.57	1.81	0.98
Limestone	3.04	3.54	2.93	2.87	1.4	1.99	1.18	3.1	3.24	0.99	3.46	2.45	2.01	1.57	3.44	0.57	2.25	3.82	1.59	2.77	1.43
Milam	1.93	3.3	2.11	2.28	1.72	1.79	0.77	1.21	2.1	0.48	2.55	2.49	2.34	1.21	3.13	0.91	1.98	2.86	0.51	1.93	0.73
Nacogdoches	3.06	3.36	2.86	2.81	3	2.88	1.75	3.13	2.75	2.14	3.09	3.32	3.21	2.68	3.29	1.51	2.81	2.37	2.46	2.99	0.85
Navarro	3.58	2.87	2.42	2.4	2.9	2.31	1.66	3.21	3.41	1.11	3.65	2.33	2.23	1.47	2.69	0.48	1.3	4.04	2.18	3.54	1.63
Robertson	2.6	3.27	2.23	2.74	1.91	1.86	0.79	2.73	2.95	0.68	2.84	2.06	2.3	2	2.95	0.68	2.44	2.83	1.17	2.22	0.95
Rusk	3.62	3.51	2.57	3.06	2.56	2.42	1.61	3.17	2.7	2.15	3.12	3.39	2.84	2.44	3.11	1.14	2.38	2.68	2.57	3.02	0.99
San Augustine	3.09	3.39	3.17	3.04	3.26	3.19	1.88	3.31	3.24	2.47	3.25	3.34	3.29	3.13	3.39	1.89	3.49	2.57	2.8	3.52	1.12
Smith	3.88	3.16	2.42	2.43	2.74	1.42	1.58	2.87	2.8	2.01	3.58	3.23	2.39	2.48	2.07	0.66	1.86	3.68	3.16	3.63	1.38
Van Zandt	4.26	2.77	2.86	2.86	3.55	2.39	2.13	3.04	2.9	1.68	3.77	3.07	2.61	1.53	1.71	0.48	1.47	3.99	2.98	4.46	1.76
Williamson	0.61	3.3	2	0.65	1.85	1.87	0.5	1.09	1.39	0.34	2.34	2.3	2.17	0.72	2.62	0.84	1.42	2.6	0.3	1.6	0.92
Wilson	0.37	0.74	2.33	1.49	0.52	0.47	0.27	0.48	0.67	0.26	0.48	0.75	1.08	0.46	1.28	0.27	0.3	2.22	0.22	0.63	0.55
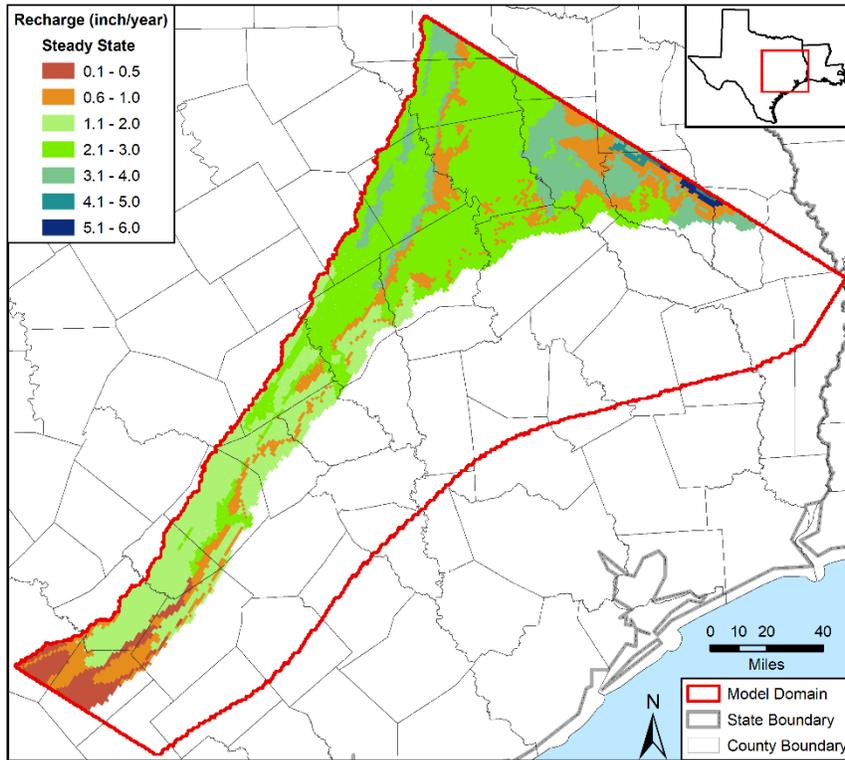
Figure 4.6a.   **Spatial distribution of recharge in inches per year for steady-state conditions.**
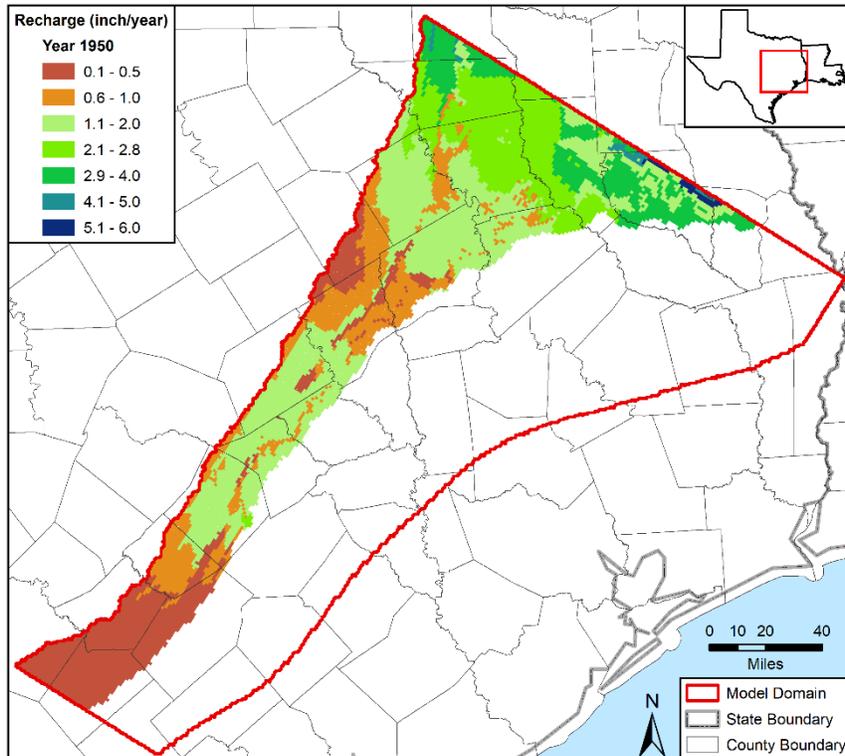
Figure 4.6b.   **Spatial distribution of recharge in inches per year for 1950.**
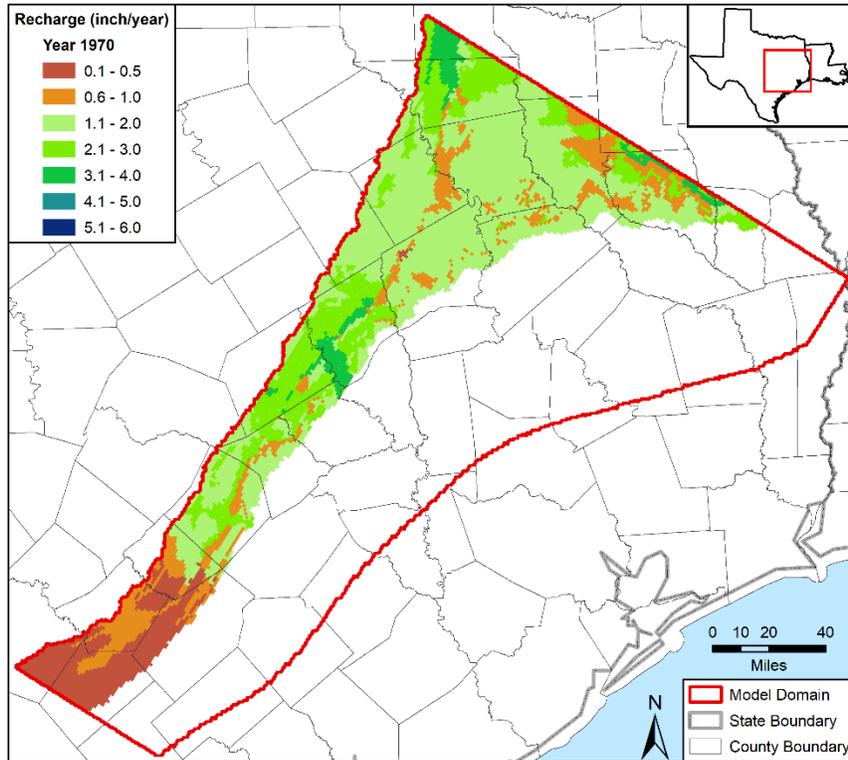
Figure 4.6c. **Spatial distribution of recharge in inches per year for 1970.**
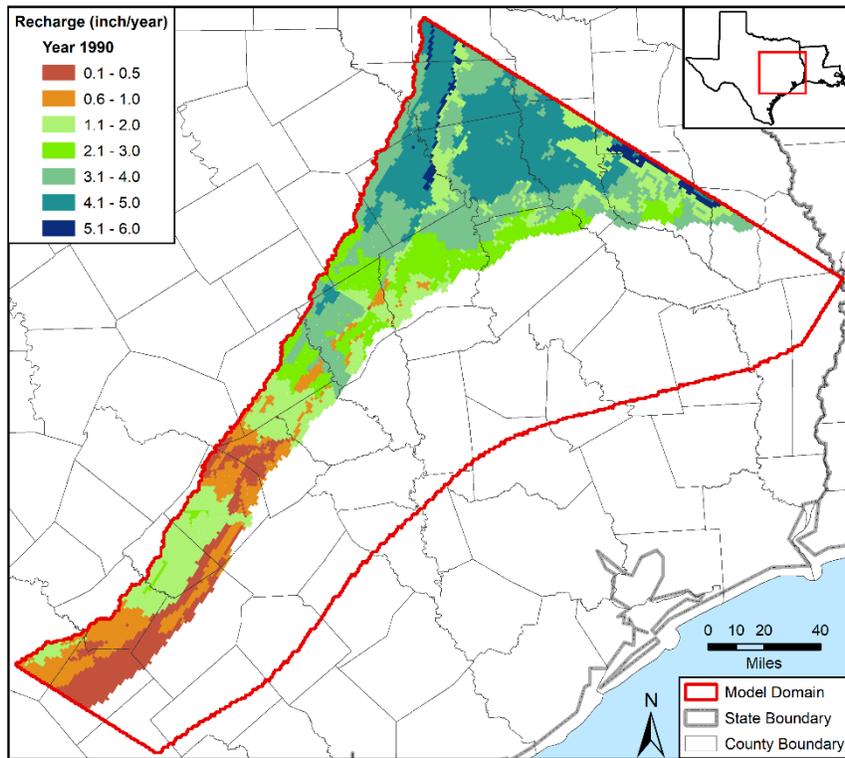
Figure 4.6d. **Spatial distribution of recharge in inches per year for 1990.**
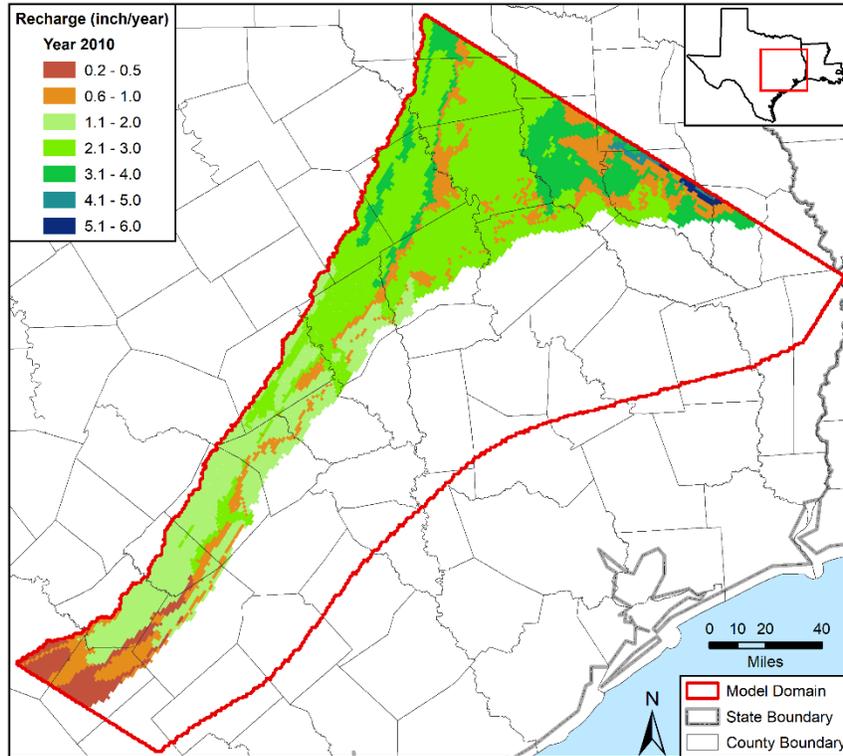
Figure 4.6e.   **Spatial distribution of recharge in inches per year for 2010.**

4.7   General-Head Boundary Package

The MODFLOW General-head Boundary (suffix GHB) package was used to simulate groundwater flow into and out of the model boundaries. The number of grid cells in the model with general head boundaries is 16,117, which is too many entries to include as a table in an appendix. Appendix I describes the attributes of an Excel table that contains information on each general-head boundary cell. The attributes include the hydraulic head elevation and the conductance for the general-head boundary. The Excel table is included in the electronic delivery with this report.

Figure 4.7a shows a footprint of the location of the grid cells that use the General-head Boundary package. Over 90 percent of the general-head boundary cells are in model layer 3, where they represent the groundwater exchange between the Sparta Aquifer and the overlying Cook Mountain Formation. The 15,026 grid cells that represent this vertical flow are within the yellow region in Figure 4.7a. The blue lines represent the locations where the general-head boundary cells enable lateral flow into or out of a hydrogeologic unit in the model domain with the same hydrogeologic unit outside of the model domain. The general-head boundary conductance values range between 0.1 and 100 square feet per day.
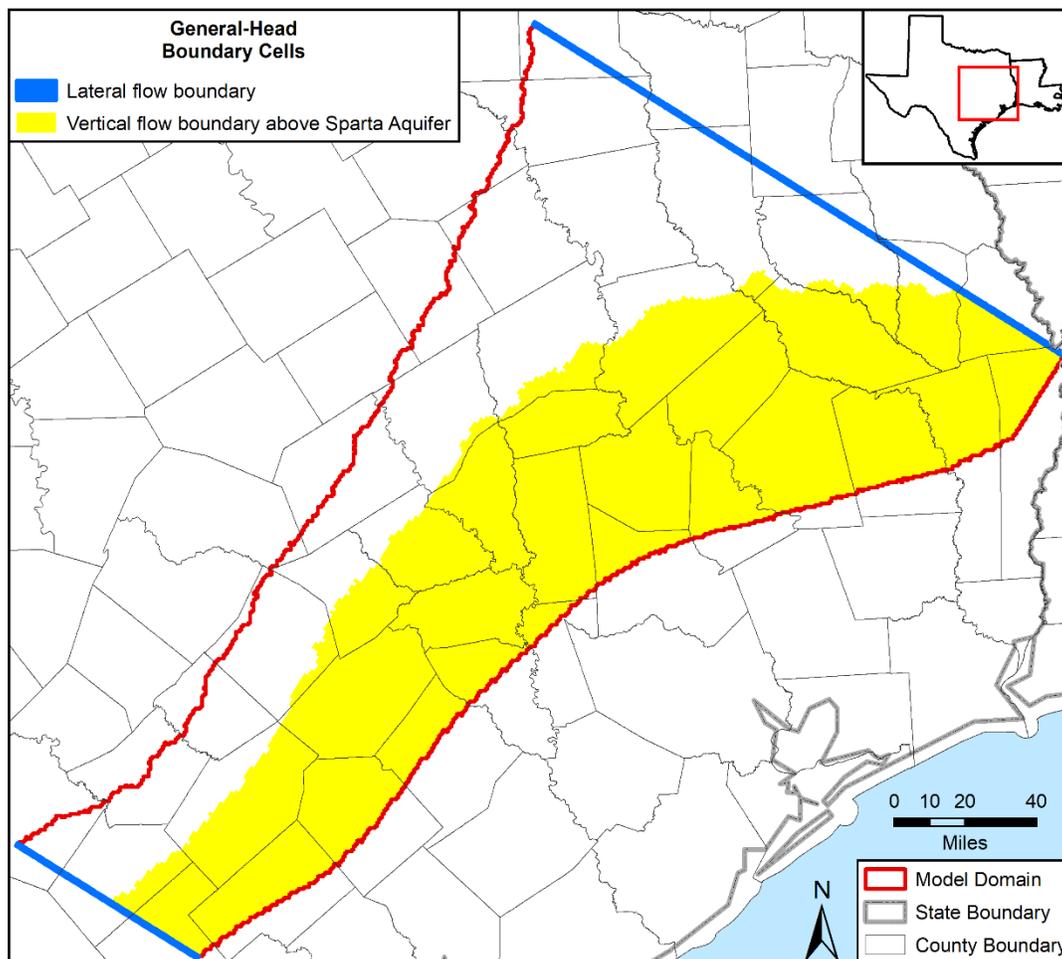
Figure 4.7a.   **Areal footprint showing the locations of general-head boundary cells.**

4.8 River Package

The MODFLOW River (suffix RIV) package was used to simulate groundwater exchange with major rivers and perennial streams. Figure 4.8a shows a map of the river cell locations. The number of river cells is 5,560, which is too many entries to include as a table in an appendix. Appendix J describes the attributes of an Excel table that contains information on each river cell. The attributes include the node number, the river bottom, river stage, and the river conductance. The Excel file that lists the river cells is included in the electronic delivery with this report.

The initial locations for the river cells were taken from the groundwater availability model developed by Kelley and others (2004). The locations of the river cells associated with the Brazos and Colorado rivers were changed to accommodate the refined numerical grid in the vicinity of those two rivers. The river cell locations were located on the refined grid using the United States Geological Survey national hydrograph dataset of rivers and streams that is mapped in Figure 4.5a. The river conductance values varied between 1,000 and 58,000 square feet per day.
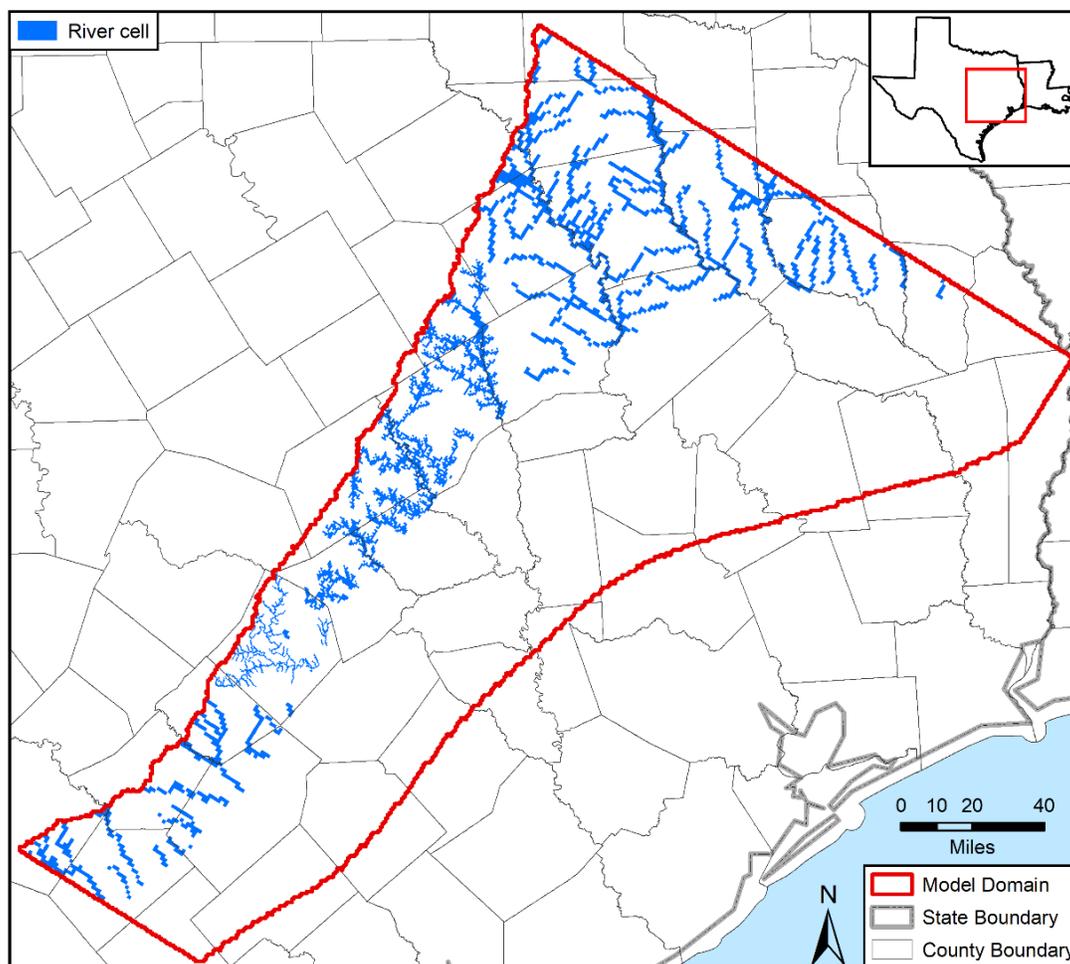
Figure 4.8a. **Locations of river cells.**

4.9 Evapotranspiration Package

The MODFLOW Evapotranspiration (suffix EVT) package was used to simulate groundwater evapotranspiration from the model. Note the distinction between overall evapotranspiration, which may occur either in the vadose or saturated zone, and groundwater evapotranspiration, the portion that occurs in the saturated zone. Groundwater evapotranspiration occurs primarily in riparian areas. To simulate evapotranspiration that may occur in riparian areas, evapotranspiration cells were added adjacent to cells representing perennial streams. The number of evapotranspiration cells is 10,524, which is too large to include as a table in an appendix. Appendix K describes the attributes of an Excel table that contains information on each evapotranspiration cell. The attributes include the node number, the elevation of the evapotranspiration surface, the maximum evapotranspiration rate, and the extinction depth. The Excel file that lists the evapotranspiration cells is included in the electronic delivery with this report.

The Evapotranspiration package, as implemented, required specification of the elevation of the evapotranspiration surface, the maximum evapotranspiration rate, and the extinction depth. If the

elevation of the water table exceeds the elevation of the evapotranspiration surface, evapotranspiration occurs at the maximum rate. As the water table drops below the elevation of the evapotranspiration surface, the rate decreases linearly until the extinction depth is reached, at which point the rate is zero.

The evapotranspiration surface was set to the average ground surface elevation in a model grid cell, which is coincident with the top of the uppermost model layer. The evapotranspiration rates in the model were based on the Soil Water Assessment Tool modeling performed by Kelley and others (2004). The Soil Water Assessment Tool was developed for the United States Department of Agriculture by the Blacklands Research Center in Temple, Texas (Neitsch and others, 2002). The Evapotranspiration package developed by Kelley and others (2004) was uploaded into the model and used, with only a few modifications. The evapotranspiration rates are depicted in Figure 4.9a. The extinction depth varies between 0.01 and 10 feet, which corresponds to the area-weighted average rooting depth for the various vegetation types in a given model cell. The extinction depths are depicted in Figure 4.9b.
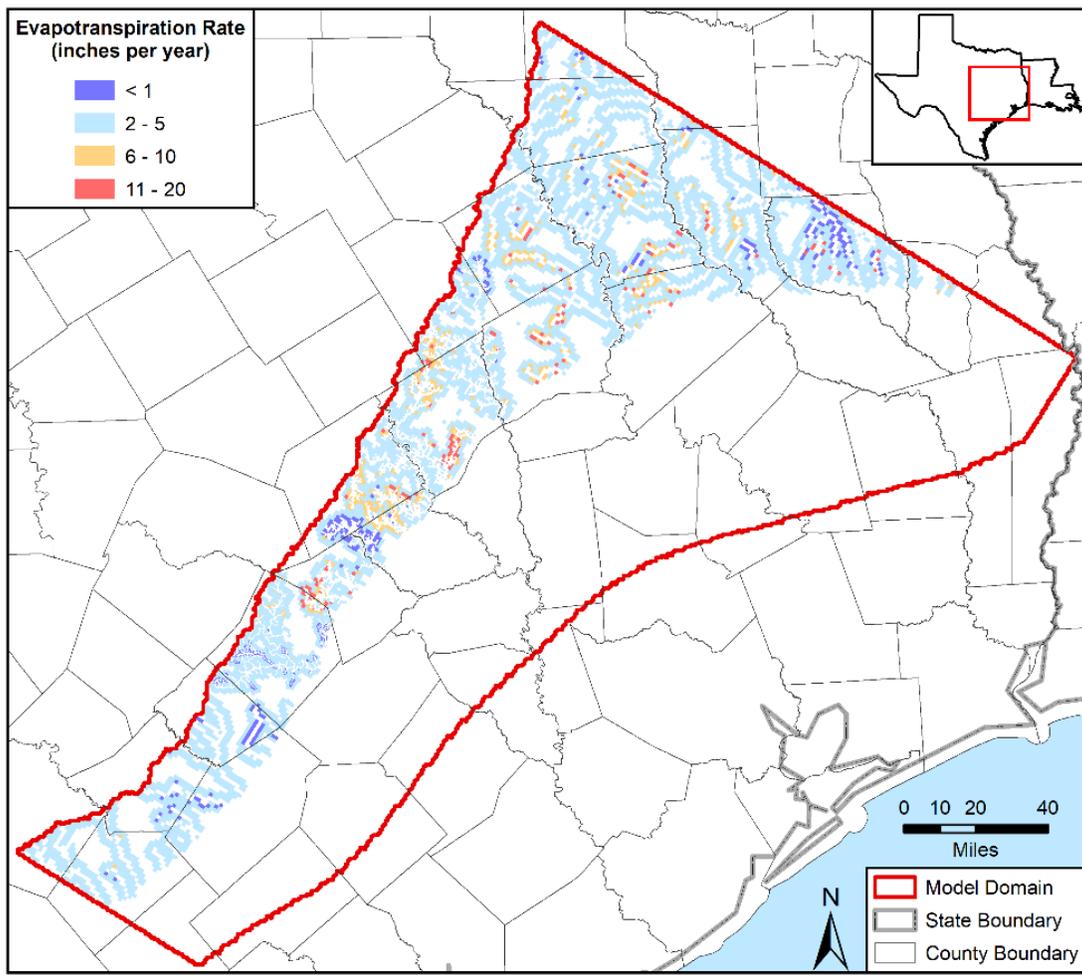
Figure 4.9a.   **Maximum evapotranspiration rate in inches per year for evapotranspiration cells.**
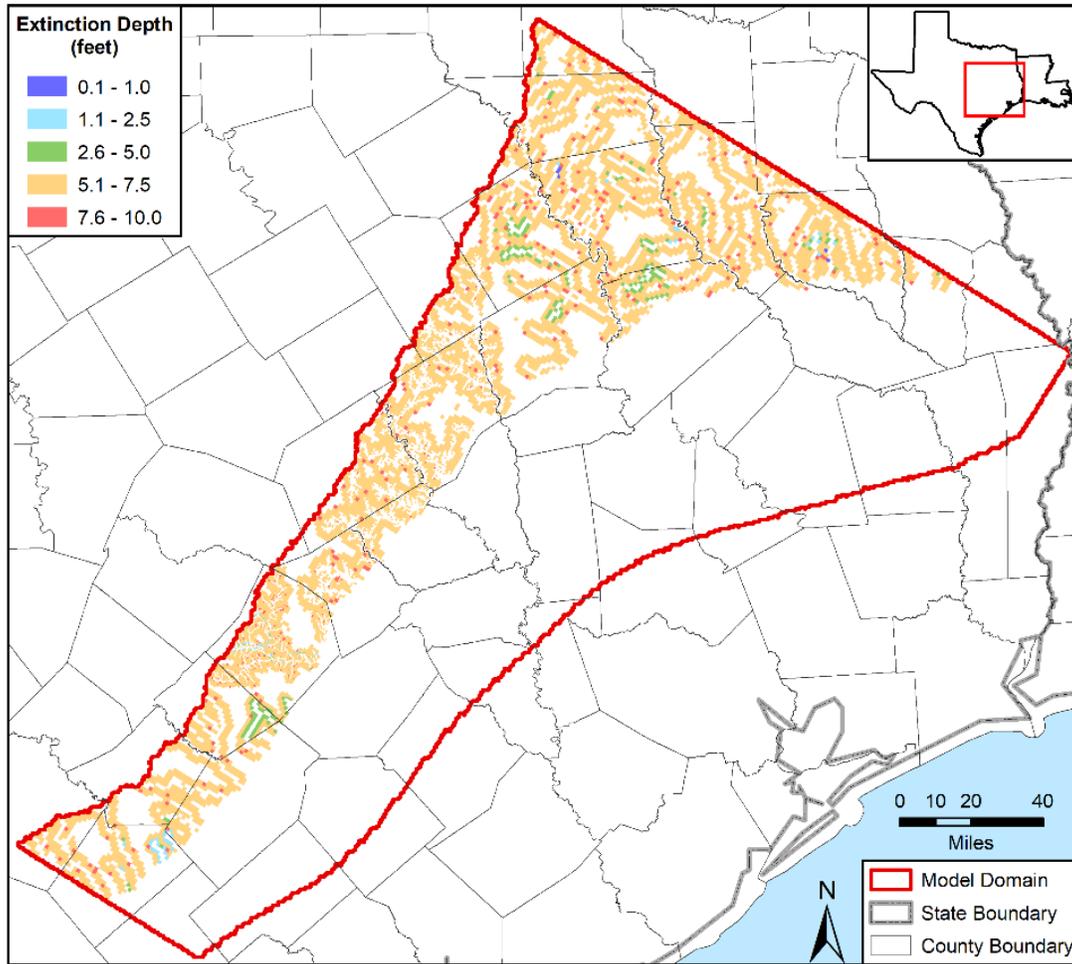
Figure 4.9b.　　　**Extinction depth in feet for evapotranspiration cells.**

4.10 Horizontal Flow Barrier Package

The MODFLOW Horizontal Flow Barrier (suffix HFB) package was used to simulate the impacts of faults on groundwater flow. The Horizontal Flow Barrier package provides the capability to place a groundwater flow barrier between two adjacent grid cells to impede groundwater flow. Hsieh and Freckleton (1993) describe the assumptions and algorithms used to model groundwater flow through the barrier. The Horizontal Flow Barrier package presumes that the width of the barrier is negligibly small in comparison with the horizontal dimensions of the cells in the grid and flow through the barrier is determined by a conductance. The conductance is defined as the horizontal flow barrier's hydraulic conductivity divided by the horizontal flow barrier's assumed width.

4.11 Ghost Node Correction Package

The refinement of the numerical grid was implemented using a specific option available in MODFLOW-USG called a quadtree grid. The quadtree grid provides the capability to partition the 1-mile by 1-mile grid cells into grid cells that are either 0.5 mile by 0.5 mile or 0.25 mile by

0.25 mile. In a quadtree grid, the line connecting two nodes is not always perpendicular to, and coincident with, the midpoint of the shared face. For these cases, the control volume finite difference formulation represents a lower order approximation than that for a regular grid. This can result in errors in simulated heads and flows. However, MODFLOW-USG includes an optional Ghost Node Correction (suffix GNC) package to correct these errors. A Ghost Node Correction package was developed specifically for the quadtree grid used in this model and included in the MODFLOW name file to take advantage of this correction to the control volume finite difference formulation.

4.12 Output Control File

The MODFLOW Output Control (suffix OC) package specifies when, during the simulation, water level and water budget information are saved to disk. The Output Control file was set up to save these results at the end of each stress period (that is, at the end of the pre-development period, and annually between 1930 and 2010).

4.13 Solver

The MODFLOW-USG Sparse Matrix Solver (suffix SMS) package was used to solve the matrix, which is comprised of a series of groundwater equations for the hydraulic head at each node. The Newton-Raphson linearization scheme was used for this simulation effort because it affords the most robust of solution schemes available in MODFLOW-USG and provides convergence to hard problems that arise with drying and rewetting of portions of the simulation domain. The formulation in MODFLOW-USG is the same as that of MODFLOW-NWT (Niswonger and others, 2011). The XMD linear matrix solver was selected from the two linear matrix solvers available. Nonlinear iterations using the Newton-Raphson linearization scheme were controlled using residual reduction and under-relaxation. In general, the solver parameter values suggested in the MODFLOW-USG manual were used.

The ORTHOMIN scheme of the XMD solver was selected to solve the asymmetric system of linear equations. Linear solver parameters that were significant to the simulation included the matrix ordering scheme (NORDER), the level of fill (ILEVEL), and number of orthogonal directions (NORTH). These parameters were varied depending on convergence behavior and ranged from the various ordering schemes available; ILEVEL = 1 to 29 and NORTH = 7 to 21. Final calibrated simulation values were: ILEVEL = 9; the RCM Ordering scheme (NORDER = 1), and NORTH = 21. The "drop tolerance" scheme was used with a drop-tolerance factor (DROPTOL) equal to 1.0×10^{-5}.

5 Model Calibration and Results

Once a model has been designed and constructed, it is usually calibrated to match observed characteristics of the aquifer. Typically, these calibration targets consist of observed water levels in wells but can also include discharge to surface water or other processes. The calibration process involves adjusting the hydraulic properties and flux boundaries of the model, within pre-defined constraints, in order that simulated output metrics better match observed metrics. This section describes that process of calibration and presents the simulated results in terms of heads and fluxes. In addition, the simulated water budgets, which account for all of the water flowing in and out of an aquifer, are presented.

5.1 Calibration Procedure

The model was calibrated by coupling PEST software (Doherty, 2018) with MODFLOW-USG. PEST is the name given to a suite of programs that collectively undertake calibration and uncertainty analysis for environmental and other numerical models. The motivation for its original development was to provide model calibration functionality in a model-independent manner, whereby it could interact with a model through the latter's own input and output files, thereby promulgating its use with any model without the need for re-compilation of either PEST or the model.

PEST was implemented using Python, an open source programming language. Many of the Python scripts used for the project were from a collection of Python-based open-source programs called SciPy (Jones and others, 2001), which includes NumPy (Oliphant, 2006), Pandas (McKinney, 2010), and Matplotlib (Hunter, 2007). A version of parallel PEST call BeoPEST (Schreüder, 2009) was used to facilitate model calibration on a computer cluster.

PEST and all of its utility software can be downloaded from: http://www.sspa.com/pest. PEST offers one of the most robust set of techniques and analyses to support groundwater modeling amongst model-independent parameter estimation packages that are publicly available. PEST's capabilities include:

- PEST and its ancillary software allow parameter estimation to be undertaken interchangeably using a number of different methods, these include both gradient-based methods and so-called global methods.
- PEST is able to undertake parameter estimation in both over-determined and undetermined calibration contexts. In the latter context, mathematical regularization can be implemented using Tikhonov and/or subspace methods.
- Model runs can be parallelized across PC networks or Linux clusters. Third party PEST developers have expanded these capabilities to include a variety of communications protocols between PEST and its model run supervisors.
- Source code for PEST and all of its utilities is freely available, as are compilation instructions.
- PEST is supported by a number of popular groundwater graphical user interfaces including Groundwater Vistas, GMS, Visual MODFLOW, and PMWIN. The level of

supported PEST functionality varies between these interfaces. At the time of this writing, the level of support is in the order just listed (with the first providing the most support).

Although PEST can be executed through several graphic user interface programs, these programs limit a modeler's availability to tailor a PEST application. For this reason, PEST was applied using a series of programs linked together through a batch file. A batch file allows programs to be tailored specifically for pre- and post-processing MODFLOW input and output files. The batch files used to apply PEST were geared to perform repeatedly the following six tasks: (1) read MODFLOW's input files; (2) run MODFLOW; (3) write MODFLOW's output files; (4) compare the simulated values with measured values for the calibration targets; (5) calculate the sensitivity of the model output to select model input parameters; and (6) use the model parameter sensitivities to determine how best to adjust model input parameters to improve the fit between the simulated and measured calibration targets.

During each PEST application, all of the MODFLOW files were created from scratch based solely on the inputs specified in the PEST input files. By using batch files, model input files were created seamlessly and run with relatively little opportunity for human error and with 100 percent reproducibility. One advantage of this approach was that it provided a platform from which quick modifications could be made to the model construction or to the calibration targets. In addition, the approach permits a third-party modeler familiar with PEST to quickly understand how to create and modify the model input files.

One factor that affects whether PEST can be applied successfully is whether there is adequate time and resources to run the model enough instances to generate all of the derivatives required for iteratively adjusting the model parameters. In some situations, such as the updated groundwater availability model, model calibration may require over 1,000 model simulations. During our model calibration, we ran most of the extensive transient model calibrations on computer clusters at the Texas Advanced Computer Center in Austin, Texas.

The modeling approach using PEST involved adjusting and constraining groundwater parameters using a combination of pilot points and equations. The key equations for defining or adjusting the aquifer properties used to construct a numerical simulator of the real aquifer system were discussed in Section 3. These equations involved "fitting" coefficients and variables that were adjusted by PEST during model calibration to define:

1. The value for specific storage properties for every grid cell in the entire groundwater system.

2. The effect of increased compressibility forces and reduced porosity with depth of burial on reducing the vertical and horizontal hydraulic conductivity values.

3. The impact of surface geology on recharge rates.

4. The partitioning of base flow into bank flow and basin flow based on considerations for the amount of river alluvium and the annual precipitation rate expressed as a percentile of the historical precipitation record.

For our model application, pilot points represent a set of scattered points used to create a spatially variable continuous field. Pilot points have mathematical properties that make them a superior parameterization device. The use of pilot points in groundwater model calibration was initiated by de Marsily and others (1984), Certes and de Marsily (1991), and Lavenue and Pickens (1992). PEST (Doherty, 2003) was the first groundwater code to use pilot points for model calibration in the context of highly parameterized models. Pilot points were used to adjust the conductance values of the general-head boundary, drain, and river cells, and to adjust horizontal and vertical hydraulic conductivity values. At each pilot point, an upper limit, a lower limit, and an initial value was assigned. Values were then assigned to model grid cells through spatial interpolation between these points. For our application, kriging was used to perform the interpolation. Other interpolation methods can be used, but kriging has the advantages that:

1. It is a smooth interpolator.

2. It respects parameter values at pilot points themselves.

3. Once interpolation factors have been generated, interpolation is computationally fast.

4. It can readily accommodate the presence of horizontal anisotropy.

The set of pilot points used to generate the conductance and hydraulic conductivity values were different. Figure 5.1a shows the pilot points used to generate the conductance values for general-head boundary, drain, and river cells. The upper values for the conductance were approximately 60,000, 30,000, and 1,000 square feet per day for the river cells, drain cells, and general-head boundary cells, respectively. After the application of PEST, further adjustments were made to drain cell conductance values above 30,000 square feet per day to prevent flooding. The highest density of pilot points was used to generate hydraulic conductivity values. These points were spaced approximately 7 miles apart and are shown in Figure 5.1b. The upper and lower limits for hydraulic conductivity varied among the different hydrologic property zones. As discussed in Section 3, the ranges of hydraulic conductivity values were based on spatial distributions in previous groundwater flow models and values calculated from aquifer pumping tests.

The hydraulic conductivity values from the aquifer pumping tests discussed in Section 3.1.4 were not treated as point values to be honored during the model calibration process. Rather they were grouped together into zones to help guide the upper and lower limits of hydraulic conductivity values assigned to pilot points. One of the reasons for not honoring the individual points was the uncertainty in the calculated hydraulic conductivity values. Sources of uncertainty included the potential impacts of geologic faults on the transmissivity values calculated from the observed aquifer drawdown responses and the assumptions used to calculate a hydraulic conductivity from the transmissivity values when the pumping well is not screened across the entire aquifer. For the 113 aquifer pumping tests interpreted, 50 percent of the pumping wells are screened across less than 35 percent of the aquifer. In our opinion, the well screen should fully penetrate an aquifer in order for a pumping test to provide an accurate estimate of the average hydraulic conductivity for the aquifer.

Hydraulic conductivities were estimated from the aquifer pumping tests by dividing the interpreted transmissivity values by the well screen length. Only values for pumping wells

screened across at least 70 percent of the aquifer thickness were considered. Even with this selection criteria, large variations were observed in hydraulic conductivity values for wells spaced close to each other. The concern regarding the impact of faults on the reliability of the calculated hydraulic conductivity can be demonstrated using the calculated hydraulic conductivity from four tests. The pumping wells for the four tests intersect more than 80 percent of the Simsboro Formation and are located within a circle with a radius of 1.5 miles in Lee County where faults exist. The calculated average hydraulic conductivity values for the Simsboro Aquifer from the four tests are 2.5 feet per day, 8.6 feet per day, 19.5 feet per day, and 25.3 feet per day. It is unlikely that this large range reflects actual variation in the aquifer transmissivity in this area. Rather, it is more likely caused by the impacts of faults on the transmissivity value calculated from the aquifer pumping tests.

In general, the model calibration was structured to minimize large spatial variations in hydraulic conductivity values in adjacent grid cells. The large variations observed in the hydraulic conductivity values for these nearby pumping tests was attributed more to the vertical variations of hydraulic conductivity in the aquifer and the impact of geologic faults than the spatial differences in the average hydraulic conductivity of the aquifer.

Because of our model calibration approach and the relatively few reliable measurements of hydraulic conductivity, the updated groundwater availability model does not reflect the spatial variability of hydraulic conductivity at the local scale. As a result, the updated model cannot provide accurate simulations of groundwater flow paths at the local scale using particle tracking.
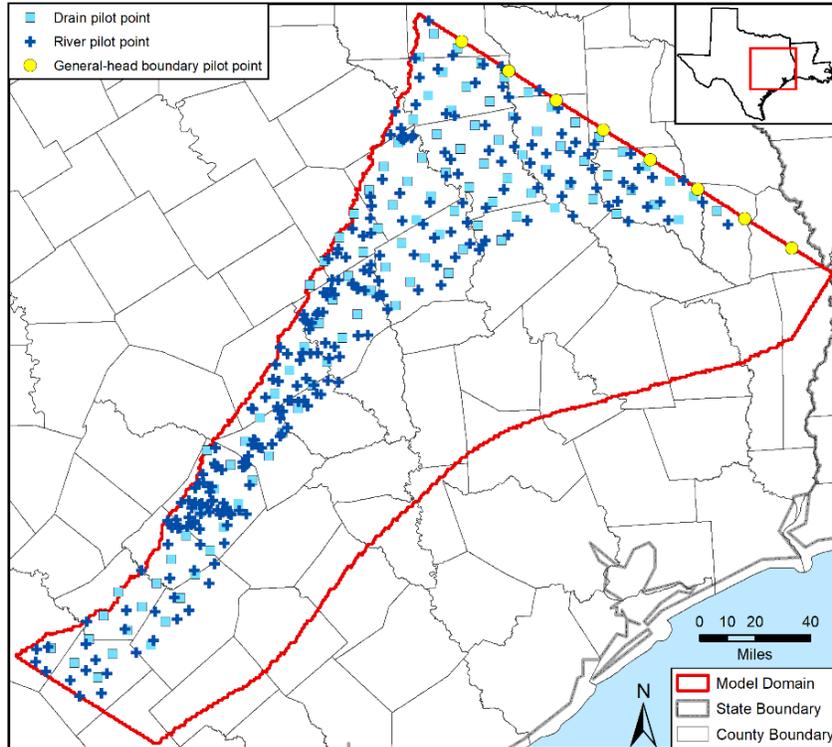
Figure 5.1a.   **Location of pilot points used for developing conductance values for general-head boundary, drain, and river cells.**
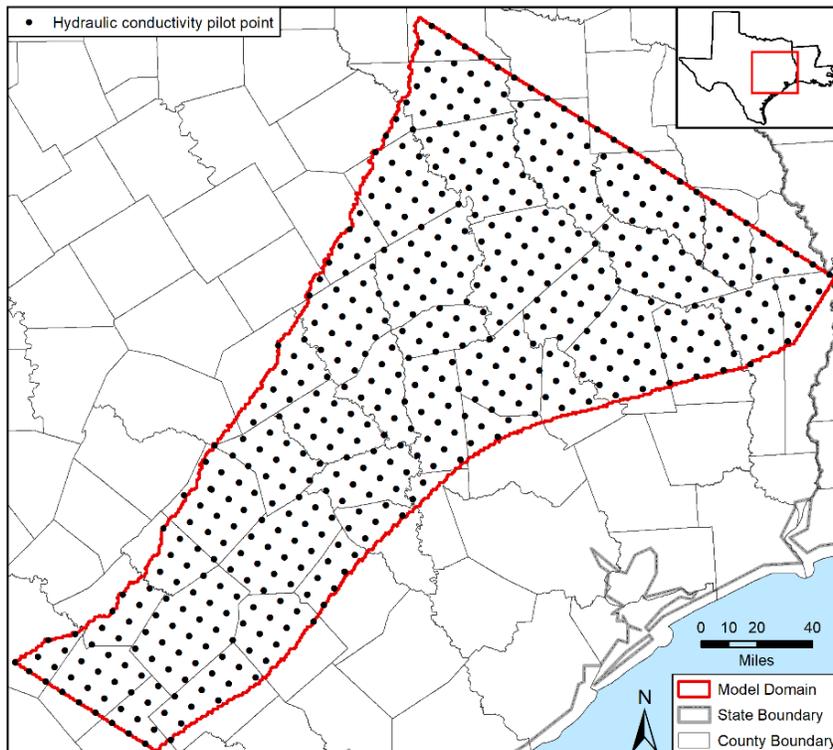
Figure 5.1b.   **Location of pilot points used for developing horizontal and vertical hydraulic conductivity values for model layers 2 through 10.**

5.2 Hydraulic Head Calibration Targets

The primary source for model calibration targets was observed hydraulic heads in wells. The hydraulic head data used to develop steady-state and transient calibration targets were obtained from the TWDB groundwater database. Only measurements identified in the TWDB groundwater database as publishable and having no remark indicating the measurement may be impacted by pumping were considered.

The steady-state model represents conditions prior to significant development of the aquifer system, which was considered to be prior to 1930. Selection of water-level measurements representative of predevelopment conditions is a challenge because early wells were installed for the purpose of pumping groundwater. The requirements that we used to select a hydraulic head as a steady-state target included (1) measured prior to 1950, (2) depth to water less than 50 feet, (3) maximum hydraulic head in a well if multiple measurements met the first two requirements, and (4) the elevation of the hydraulic head is consistent with other "steady-state" hydraulic heads within a radial distance of 1.5 miles. Steady-state targets were identified for all hydrogeologic units in the model. However, the first requirement eliminated head measurements in the Colorado River alluvium as steady-state targets.

The second requirement was implemented because pumping between 1930 and 1950 was significant in many counties (Section 3.2). For example, a total of between 10,000 and 25,000 acre-feet of pumping occurred in Anderson, Bastrop, Brazos, Henderson, and Nacogdoches counties, and over 100,000 acre-feet of pumping occurred in Angelina County prior to 1950. The assumption was made that water-level measurements with a depth to water greater than 50 feet were likely impacted by pumping and not representative of predevelopment conditions. The fourth requirement was implemented to further remove heads likely reflective of pumping conditions. If several wells within approximately 2 miles of each other had a steady-state head, and all but one of those heads was similar, the outlier head was not used as a steady-state target due to the likelihood that it reflected pumping conditions rather than predevelopment conditions.

Figure 5.2a shows the location of the 522 wells with a measured hydraulic head used as a target for steady-state conditions. Table 5.2a distributes these wells by groundwater management area and hydrogeologic unit. Figure 5.2b shows the location of 61 wells that were not considered for the steady-state calibration because their heads appeared to be notably different than heads associated with wells located within approximately 2 miles.

Table 5.2a.   Number of wells with hydraulic head targets for steady-state conditions.

Hydrogeologic Unit	Number of Wells			
	Total	**GMA 11**	**GMA 12**	**GMA 13**
Alluvium[a]	8	0	8	0
Sparta	61	40	20	1
Weches	15	11	4	0
Queen City	163	140	20	3

Hydrogeologic Unit	Number of Wells			
	Total	GMA 11	GMA 12	GMA 13
Reklaw	18	16	1	1
Carrizo	39	21	11	7
Calvert Bluff	144	36	81	27
Simsboro	17	2	13	2
Hooper	57	7	32	18
Total	522	273	190	59

[a] all in the Brazos River alluvium

The selection of wells for transient calibration targets considered the number of measurements in the well and the ability to assign the well to a model node with a reasonable degree of confidence. Only water-level data at wells with five or more measurements were included as transient calibration targets. Two complications are involved with the vertical assignment of well completion intervals to model nodes. The first is the variability in ground surface elevation across the predominately 1-mile by 1-mile model grid blocks, and the second is the lack of screened interval data for a many of the wells. Because of these two factors, care was taken in the final selection of wells for which water-level data were used as transient calibration targets. The entire transient record at a well was used to assess calibration, not just data since 1950. The considerations used to develop initial transient hydraulic head targets were: (1) at least five hydraulic head measurements in a well so a temporal trend could be detected if such a trend existed, (2) multiple hydraulic head values for a single year were averaged, and (3) hydraulic head values that did not fit the apparent trend of the data in a hydrograph and those that differed by more than 50 feet from heads at adjacent times were removed. The third requirement was implemented because heads that varied by more than 50 feet relative to immediately preceding or subsequent heads were considered anomalous, as 50-foot differences between measurements likely reflects an inaccurate measurement or a head impacted by the well being pumped prior to the measurement. Figure 5.2c shows several examples of head measurements not considered in development of the transient calibration targets based on this requirement.

During the early stages of the calibration process when regional trends in drawdown were being developed and before hydrographs of annual average water levels were created, water-level measurements with differences of greater than 50 feet in a year were observed for some wells in Angelina and Nacogdoches counties. These wells, a total of less than five, were omitted for consideration as transient calibration targets. To be consistent with the selection of wells between the steady-state and transient calibration, wells omitted from the steady-state calibration were also omitted from the transient calibration. Transient targets were identified for all hydrogeologic units in the model. However, the first requirement eliminated head measurements in the Colorado River alluvium as transient targets.

Figure 5.2d shows the locations of the 647 wells with measured hydraulic heads used as hydraulic head targets for transient conditions. Table 5.2b distributes these wells by groundwater management area and hydrogeologic unit.

Table 5.2b.   **Number of wells with hydraulic head targets for transient conditions.**

Hydrogeologic Unit	Number of Wells			
	Total	GMA 11	GMA 12	GMA 13
Alluvium[a]	50	0	50	0
Sparta	73	23	44	6
Weches	7	5	0	2
Queen City	79	28	32	19
Reklaw	28	7	7	14
Carrizo	197	67	29	101
Calvert Bluff	97	31	34	32
Simsboro	68	11	50	7
Hooper	47	10	21	16
Total	647[b]	182	267	197

[a] all in the Brazos River alluvium
[b] includes one Sparta Aquifer well in Washington County in Groundwater Management Area 14 that is not listed in the table
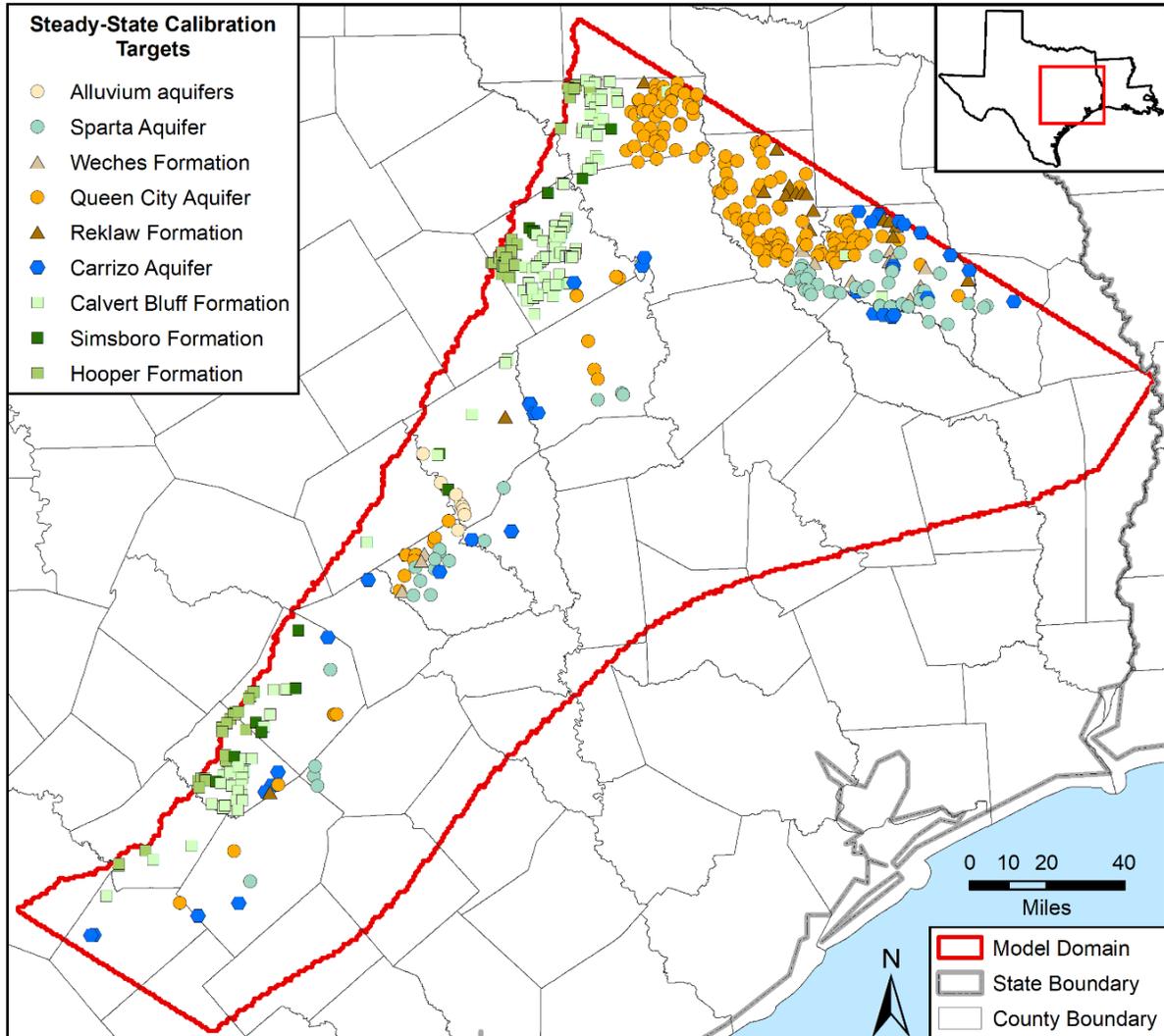
Figure 5.2a. **Spatial distribution of hydraulic heads targets for steady-state conditions.**
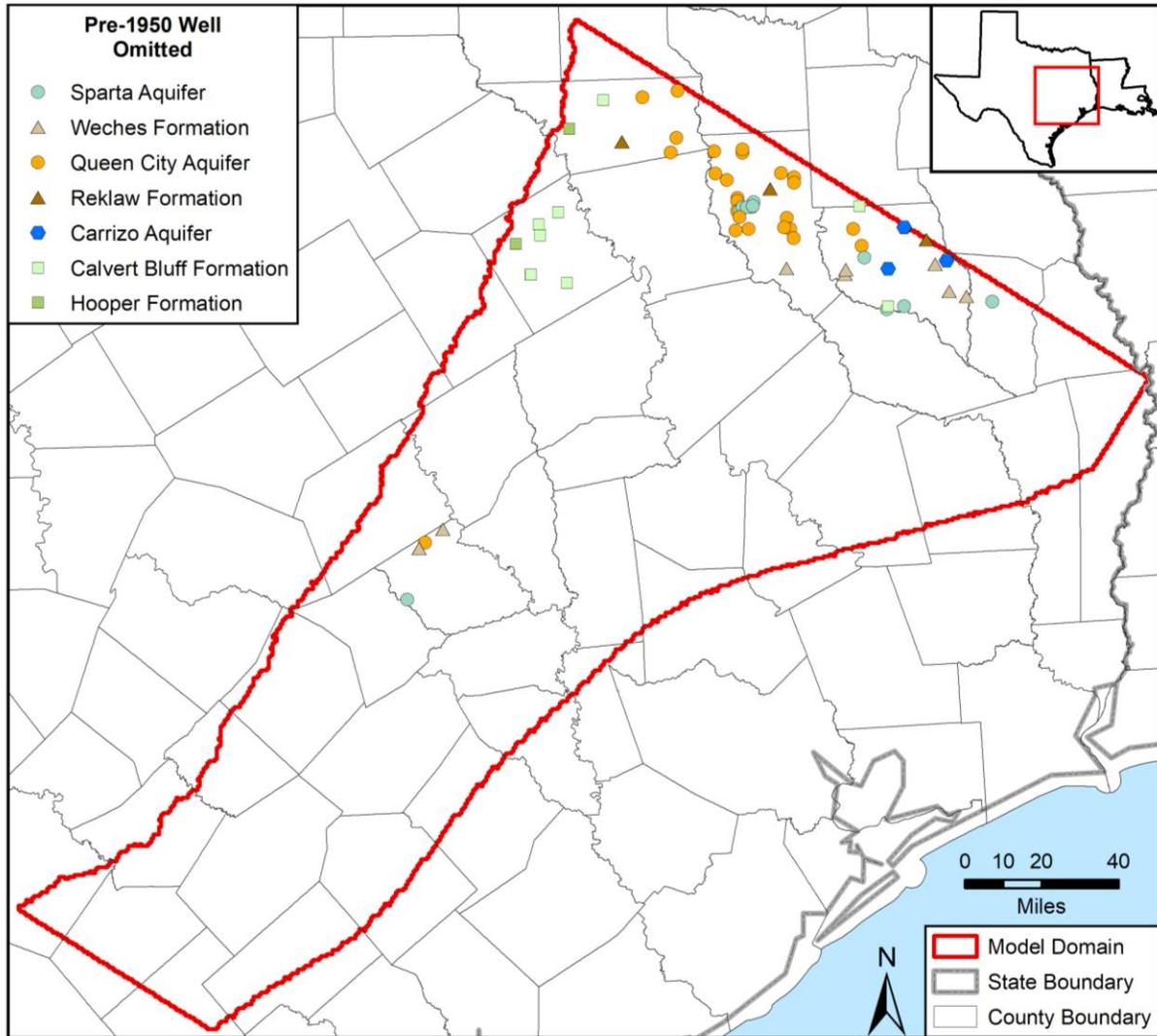
Figure 5.2b.   **Spatial distribution of wells with pre-1950 hydraulic heads that were not used as steady-state calibration targets because their head value was significantly different from the head value in nearby wells**
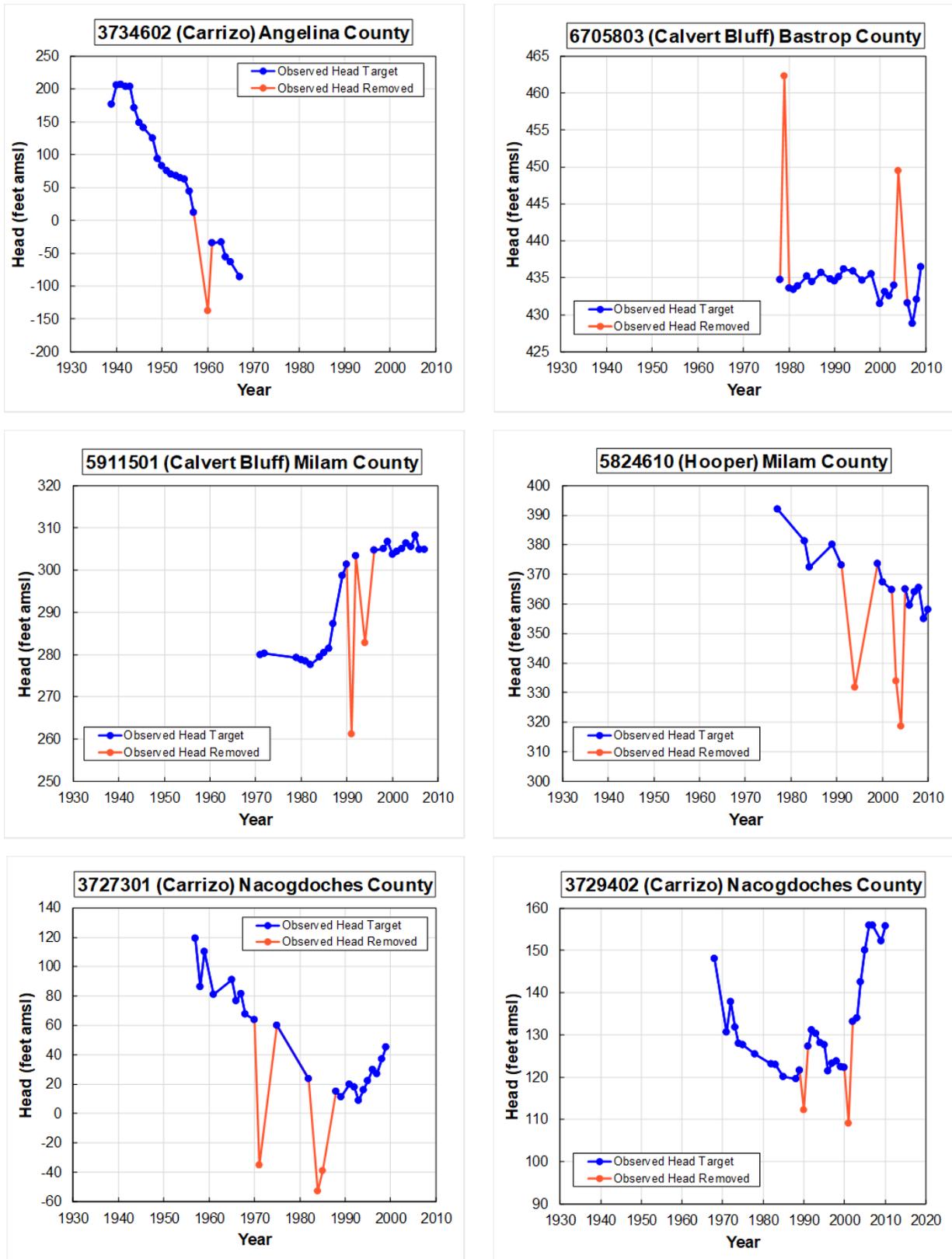
Figure 5.2c. Example of head measurements removed during development of transient calibration targets.
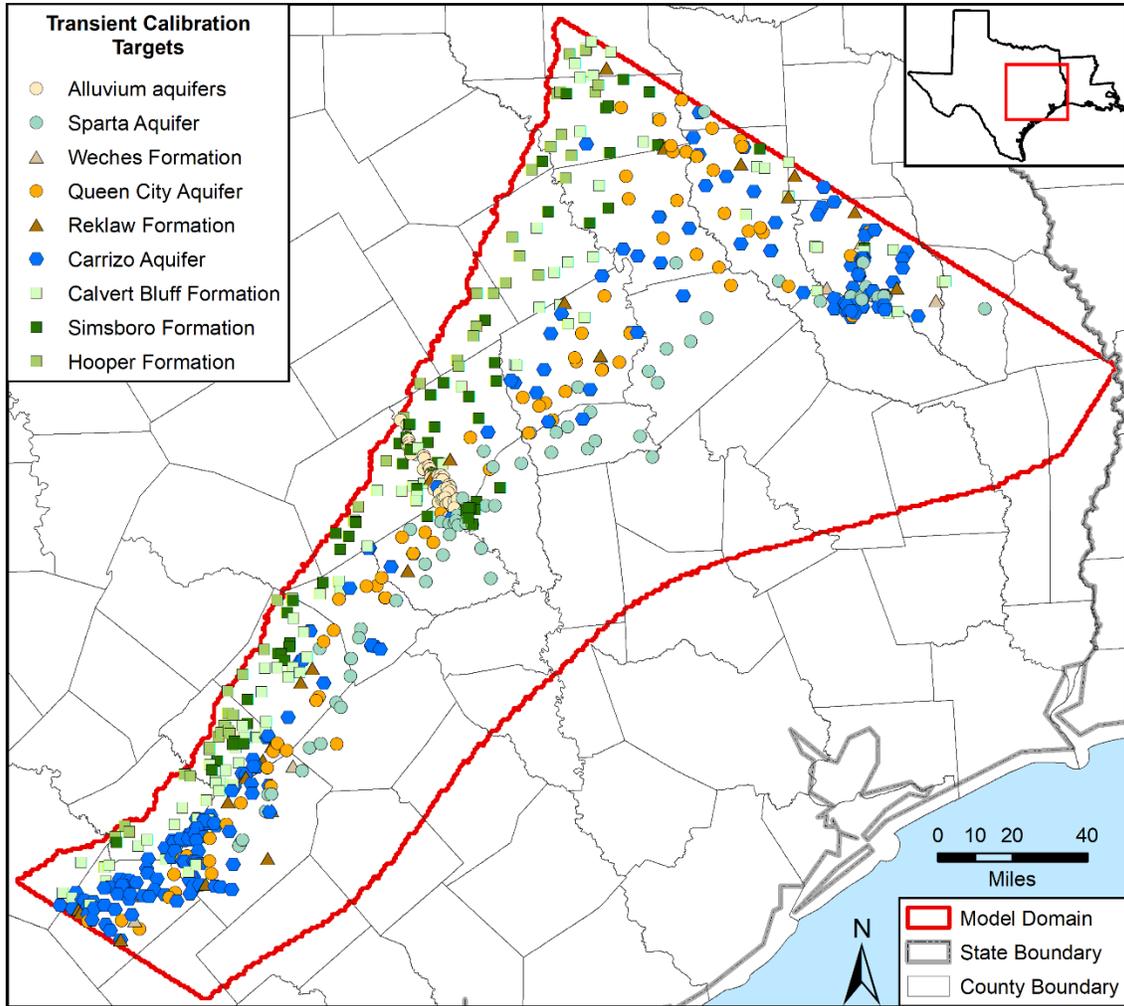
Figure 5.2d.   **Spatial distribution of hydraulic heads targets for transient conditions from 1930 to 2010.**

5.3 -Model Simulated Versus Measured Heads

This section describes the results of the model calibration to observed heads, both spatially and temporally. The calibration is discussed first in terms of summary statistics and scatter plots, followed by a discussion of trends in head residuals, both distribution about the mean and spatial distribution. Simulated head surfaces and simulated drawdowns are then presented, followed by hydrographs of simulated versus observed data.

5.3.1 Calibration Metrics for Hydraulic Head Targets

Conventional calibration metrics associated with simulating hydraulic heads are based on residuals (Anderson and Woessner, 1992). A residual, r, is defined as the difference between an observed and a simulated hydraulic head per Equation 5-1.

$$r = h_o\text{-}h_s \qquad \text{(Equation 5-1)}$$

where:

r = residual,
h_o = observed hydraulic head, and
h_s = simulated hydraulic head.

The root mean square error, which is traditionally the basic measure of calibration for hydraulic heads, is defined as the square root of the average square of the residuals and is expressed mathematically by Equation 5-2. Although the root mean square error is useful for describing model error on an average basis, it does not provide insight into spatial trends in the distribution of the residuals. Information about spatial trends is provided by the mean error and the mean absolute error. The mean error, which is described in Equation 5-3, is the average of the residuals. The absolute mean error, which is described in Equation 5-4, is the average of the absolute value of the mean error.

$$Root\ Mean\ Squared\ Error = \sqrt{\frac{1}{n}\sum_{t=1}^{n}(h_o - h_s)^2_t} \qquad \text{(Equation 5-2)}$$

$$Mean\ Error = \frac{1}{n}\sum_{t=1}^{n}(h_o - h_s)_t \qquad \text{(Equation 5-3)}$$

$$Absolute\ Mean\ Error = \frac{1}{n}\sum_{t=1}^{n}|h_o - h_s|_t \qquad \text{(Equation 5-4)}$$

where:

n = number of observations.

A typical calibration criterion for hydraulic heads is that the root mean square error and the mean absolute error are less than or equal to 10 percent of the observed hydraulic head range in the hydrogeologic unit being simulated. The mean absolute error is useful for describing model error

on an average basis but does not provide insight into spatial trends in the distribution of residuals. Examination of the distribution of residuals is necessary to determine if they are randomly distributed over the model grid and not spatially biased.

The goodness or acceptability of a set of residuals and their statistics is model- and site-dependent and based on the wide range of possible sources of error and uncertainty in a model simulation. For example, one should expect that hydraulic head residuals are affected by how accurately historical pumping is known. If historical pumping is well-characterized as a result of good pumping records, then the likely cause of poor matches between simulated and observed hydraulic heads is inappropriate modeling assumptions or inappropriate hydrogeologic unit properties. In such an instance, the model will likely not serve as a good predictor of future pumping impacts where it does a poor job of matching historical observed water levels. On the other hand, if historical pumping is poorly characterized due to a lack of pumping records, the inability of the model to simulate historical water levels accurately is not necessarily a valid indicator of the model's ability to provide good predictions of future pumping impacts. This is because the model's inability to match observed heads may be principally a result of incorrect pumping rather than a result of incorrect hydrogeologic unit properties.

5.3.2   *Statistics and Scatter Plots for Hydraulic Head Residuals for Steady-State Conditions*

Tables 5.3.2a and 5.3.3b present the calibration statistics for steady-state for the entire model and for Groundwater Management Area 12, respectively. Both tables include statistics for the shallow groundwater flow system. The residuals used to calculate these statistics for the shallow flow zone were also used to calculate the statistics for the respective hydrogeologic units represented in the shallow flow zone. About 80 percent of the hydraulic head calibration targets are associated with the shallow groundwater flow zone represented by model layer 2.

Table 5.3.2a.   **Calibration statistics for steady-state conditions for all hydraulic heads in the entire model domain.**

Hydrogeologic Unit	Count	Mean Error (feet)	Mean Absolute Error (feet)	Root Mean Square Error (feet)	Measured Range (feet)
Alluvium[a]	8	11	11.9	13.9	21
Sparta	61	-0.7	20.4	26.4	323
Weches	15	2.6	16.4	20.2	333
Queen City	163	-2.9	16	20.1	310
Reklaw	18	0.1	22	25.9	218
Carrizo	39	-8.3	23.9	31.1	285
Calvert Bluff	144	10.7	22.2	27.6	296
Simsboro	17	19.5	21.6	28.4	220
Hooper	57	-3.3	13.7	17.4	290
Shallow Groundwater Flow System	432	3.6	18	22.9	392
All	522[b]	1.9	18.9	24.3	400

[a] all in the Brazos River alluvium
[b] sum for hydrogeologic units

Table 5.3.2b.   **Calibration statistics for steady-state conditions for hydraulic heads in Groundwater Management Area 12.**

Hydrogeologic Unit	Count	Mean Error (feet)	Mean Absolute Error (feet)	Root Mean Square Error (feet)	Measured Range (feet)
Alluvium[a]	8	11	11.9	13.9	21
Sparta	20	-6.1	21.2	28	291
Weches	4	6.4	15.6	18.4	41
Queen City	20	3.9	17.4	20.4	155
Reklaw	1	-27.5	27.5	27.5	0
Carrizo	11	-3.6	19.1	23.4	211
Calvert Bluff	81	13.3	22.5	27.3	247
Simsboro	13	19.7	21.4	25.5	158
Hooper	32	-4.2	12.1	15.6	169
Shallow Groundwater Flow System	149	8.8	19	23.9	304
All	190[b]	6.3	19.3	24.1	348

[a] all in the Brazos River alluvium
[b] sum for hydrogeologic units

For both sets of calibration metrics (entire model domain and Groundwater Management Area 12), the mean absolute error and the root-mean square error are no more than 7 percent of the range in measured hydraulic heads considering all layers and hydrogeologic units. In addition, for those hydrogeologic units with more than 40 measurements, their mean absolute error and the root mean square error are no more than 10 percent of the range in the measured hydraulic heads for that unit. The tabulated results indicate that the steady-state model is adequately calibrated to provide a set of initial heads for transient simulations.

As discussed in Section 5.2, the pre-1950 hydraulic head for 61wells was not used as a steady-state calibration target because it was not considered representative of pre-development conditions. If these 61 wells had been included, the calibration statistics for the steady-state model would have been as shown in Table 5.3.2c.

Table 5.3.2c.   **Calibration statistics for the entire model domain calculated for the 522 steady-state calibration targets and the 61 hydraulic heads removed as being non-representative of pre-development conditions.**

Hydrogeologic Unit	Count	Mean Error (feet)	Mean Absolute Error (feet)	Root Mean Square Error (feet)	Measured Range (feet)
Alluvium[a]	8	11.0	11.9	13.9	21
Sparta	72	7.3	29.2	41.2	506
Weches	23	5.9	18.0	23.1	333
Queen City	188	1.7	19.7	28.6	423
Reklaw	21	-3.8	22.7	27.9	218

Final Report: Groundwater Availability Model for the Central Portion
of the Carrizo-Wilcox, Queen City, and Sparta Aquifers

Hydrogeologic Unit	Count	Mean Error (feet)	Mean Absolute Error (feet)	Root Mean Square Error (feet)	Measured Range (feet)
Carrizo	42	-7.2	23.0	30.2	285
Calvert Bluff	153	10.9	22.0	27.7	296
Simsboro	17	19.5	21.6	28.4	220
Hooper	59	-3.5	13.5	17.2	290
Shallow Groundwater Flow System	488	6.3	20.4	28.4	458
All	583[b]	4.2	21.1	29.1	520

[a] all in the Brazos River alluvium
[b] sum for hydrogeologic units

Figure 5.3.2a shows a scatter plot of simulated versus observed hydraulic heads for steady-state conditions for the entire model. Figures 5.3.2b and 5.3.2.c show scatter plots of simulated versus observed hydraulic heads for the individual hydrogeologic units that comprise the model. In Figure 5.3.2a, the points are well distributed about the 1:1 line, except for observed hydraulic head measurements that are less than 270 feet above mean sea level. For heads below that elevation, the model simulated hydraulic head tends to be about 50 feet higher than the observed value. The scatter plots for the different hydrogeologic units confirm a good match between simulated and observed hydraulic heads, except at the low end of the observed hydraulic head values. The reason attributed to this mismatch is the substantial drawdown that occurred in the Carrizo Aquifer in Angelina County prior to 1930. Figures 5.3.2d and 5.3.2e show the histograms of residuals, calculated based on interpolation of the nodal model results to the location of the well, for the scatter plots. Several of the histograms show distributions that are nearly bell-shaped and symmetrical, which suggests that the residuals are randomly distributed. Perhaps the most non-symmetrical distribution is that for the Carrizo Aquifer residuals, which are skewed toward large negative numbers, likely due to early drawdown in the aquifer caused by pre-1930 pumping.
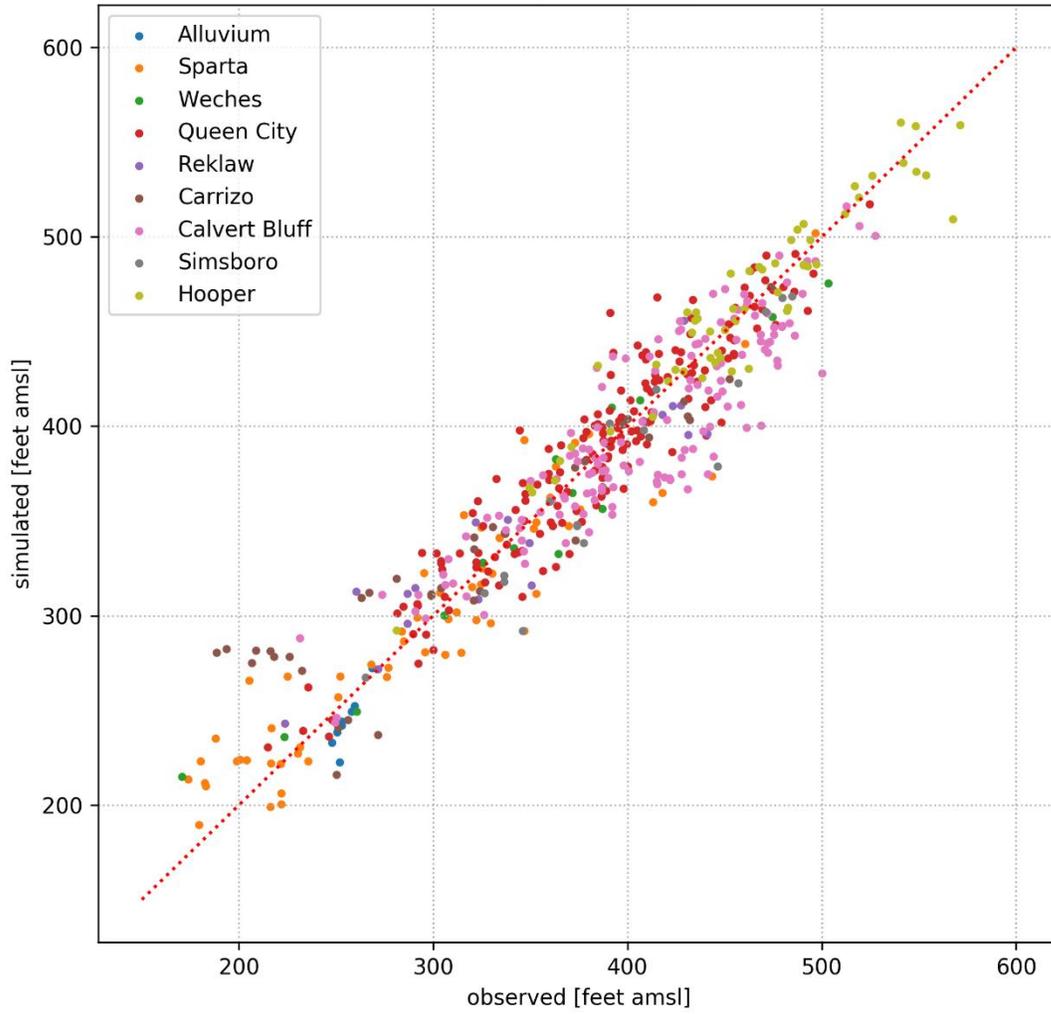
Figure 5.3.2a. **Scatter plot of simulated versus observed hydraulic heads for 522 calibration targets across the entire model for the steady-state period.**
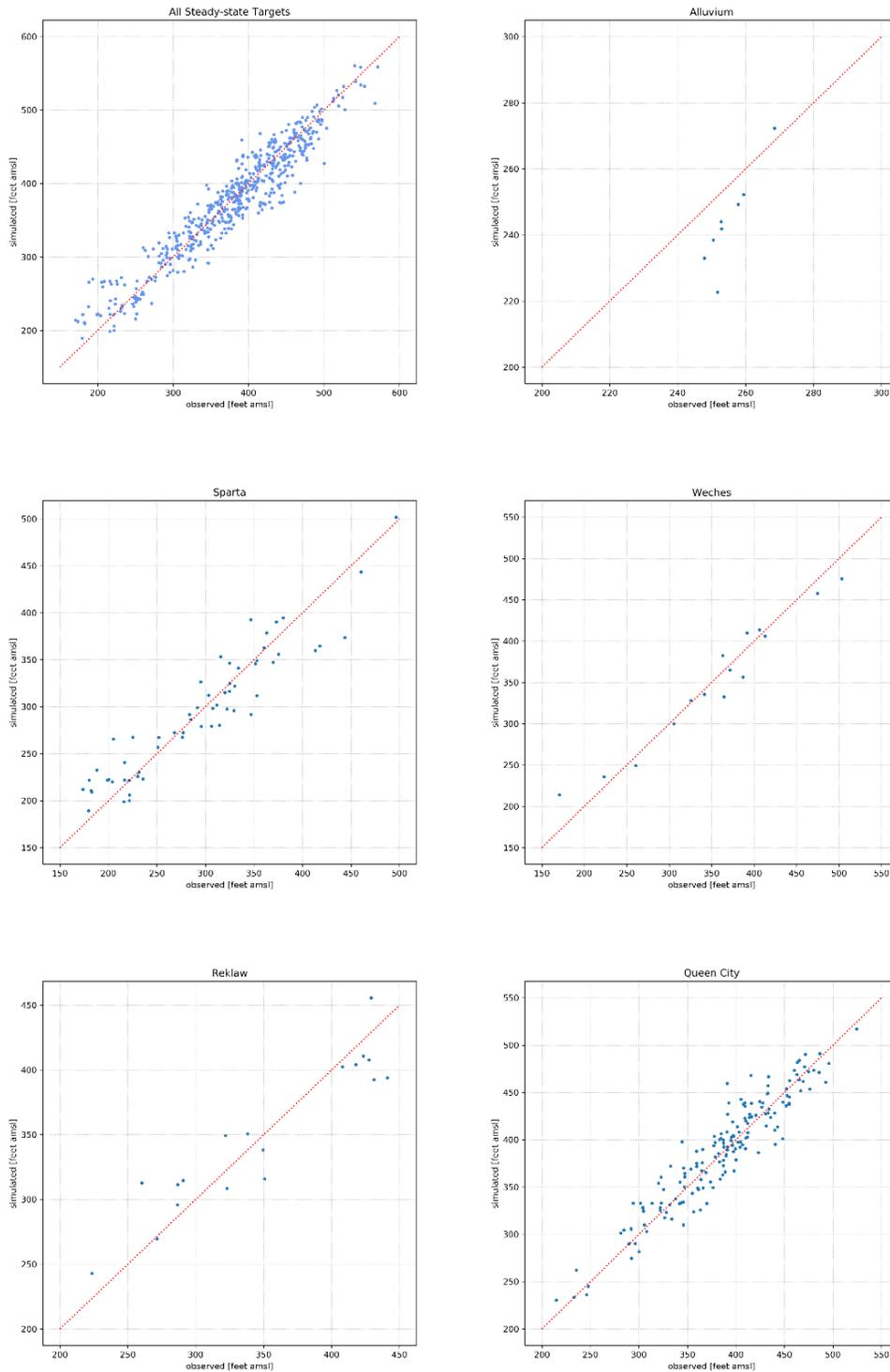
Figure 5.3.2b. Scatter plots of simulated versus observed hydraulic heads for calibration targets in the entire model domain, the Brazos River alluvium, the Sparta Aquifer, the Weches Formation, the Queen City Aquifer, and the Reklaw Formation across the entire model domain for the steady-state period.
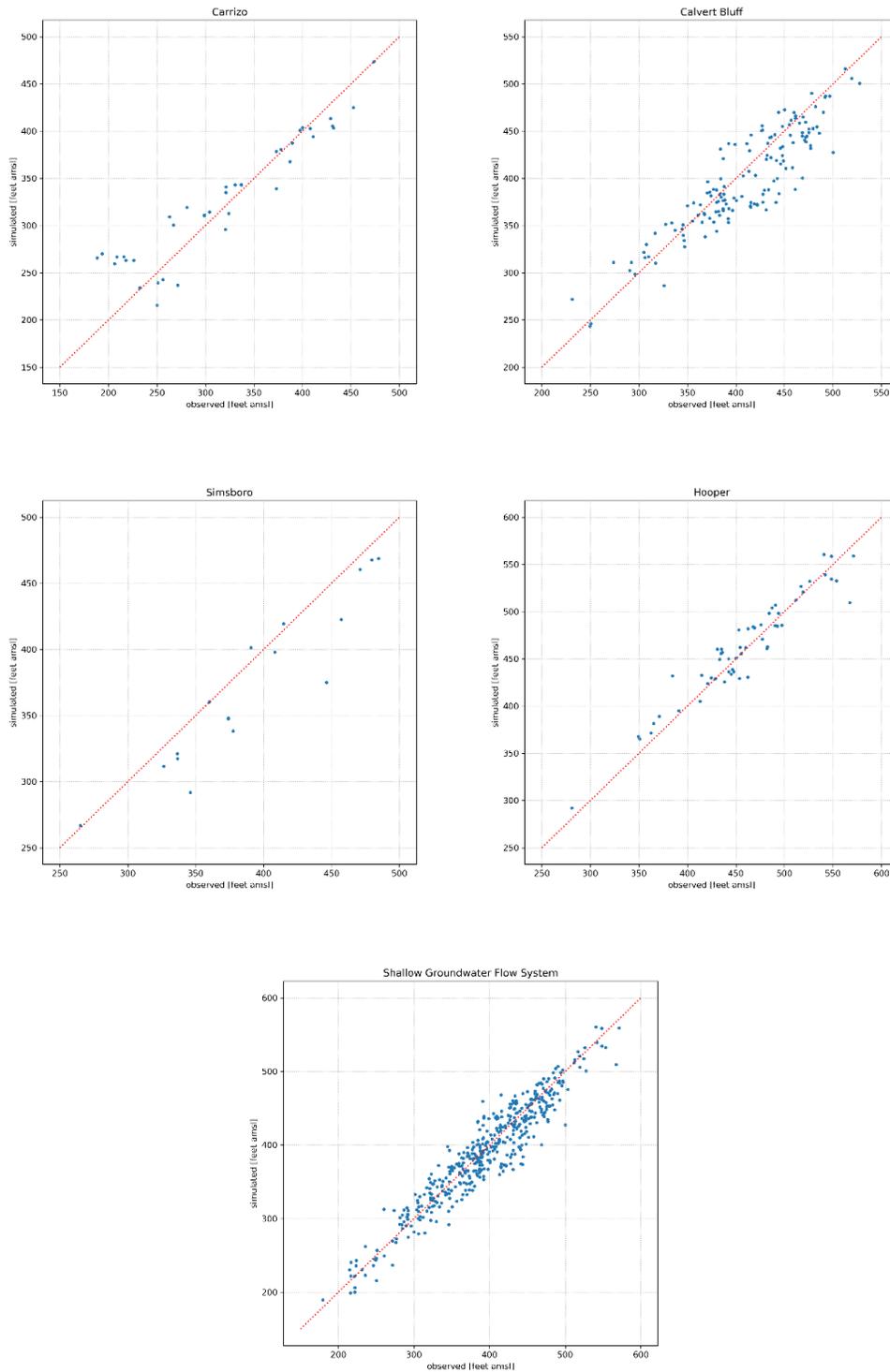
Figure 5.3.2c. Scatter plots of simulated versus observed hydraulic heads for calibration targets in the Carrizo Aquifer, the Calvert Bluff Formation, the Simsboro Formation, the Hooper Formation, and the shallow groundwater flow system across the entire model domain for the steady-state period.
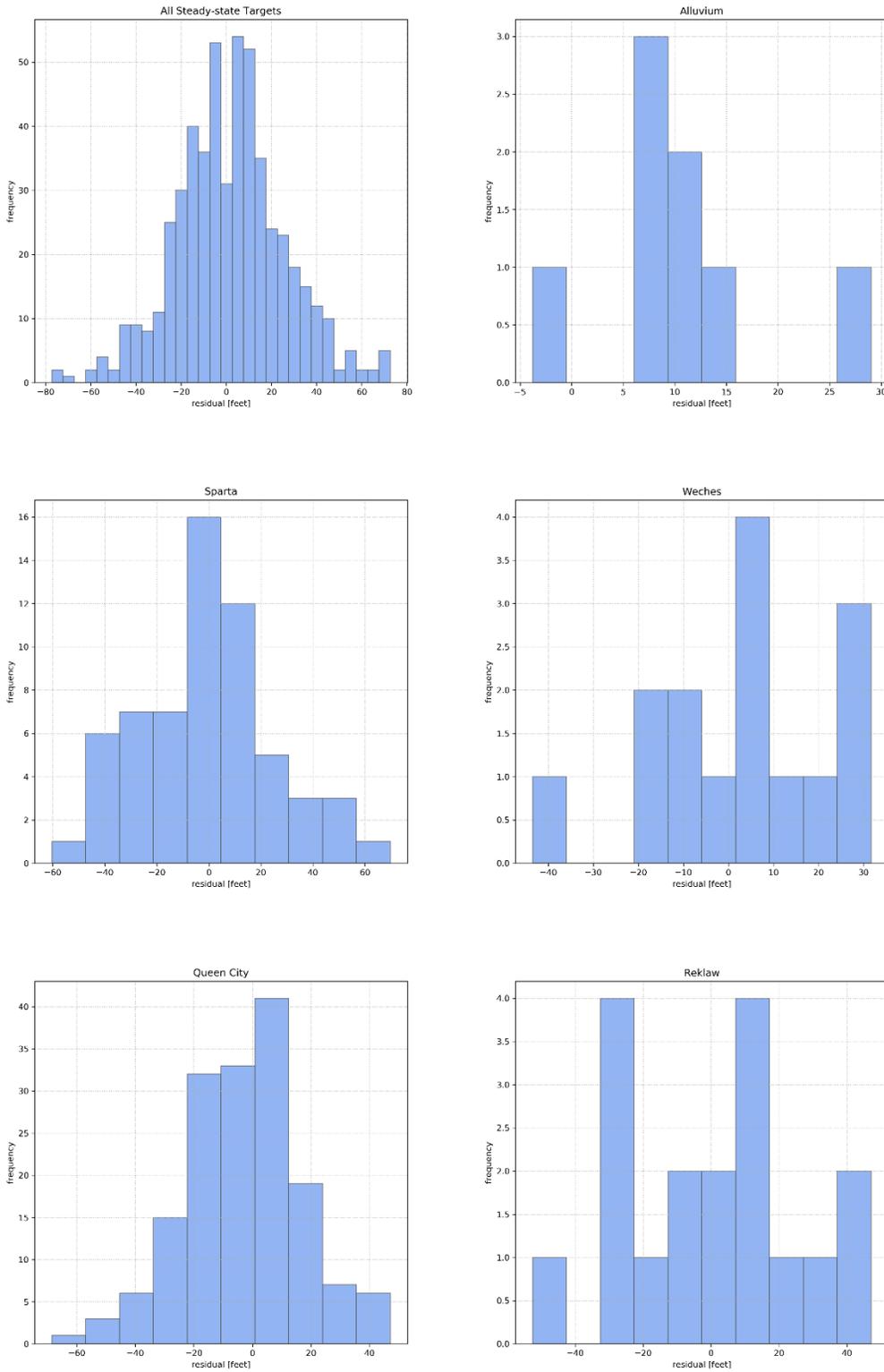
Figure 5.3.2d.   **Histograms of the hydraulic head residuals for the entire model domain, the Brazos River alluvium, the Sparta Aquifer, the Weches Formation, the Queen City Aquifer, and the Reklaw Formation the across the entire model domain for the steady-state period.**
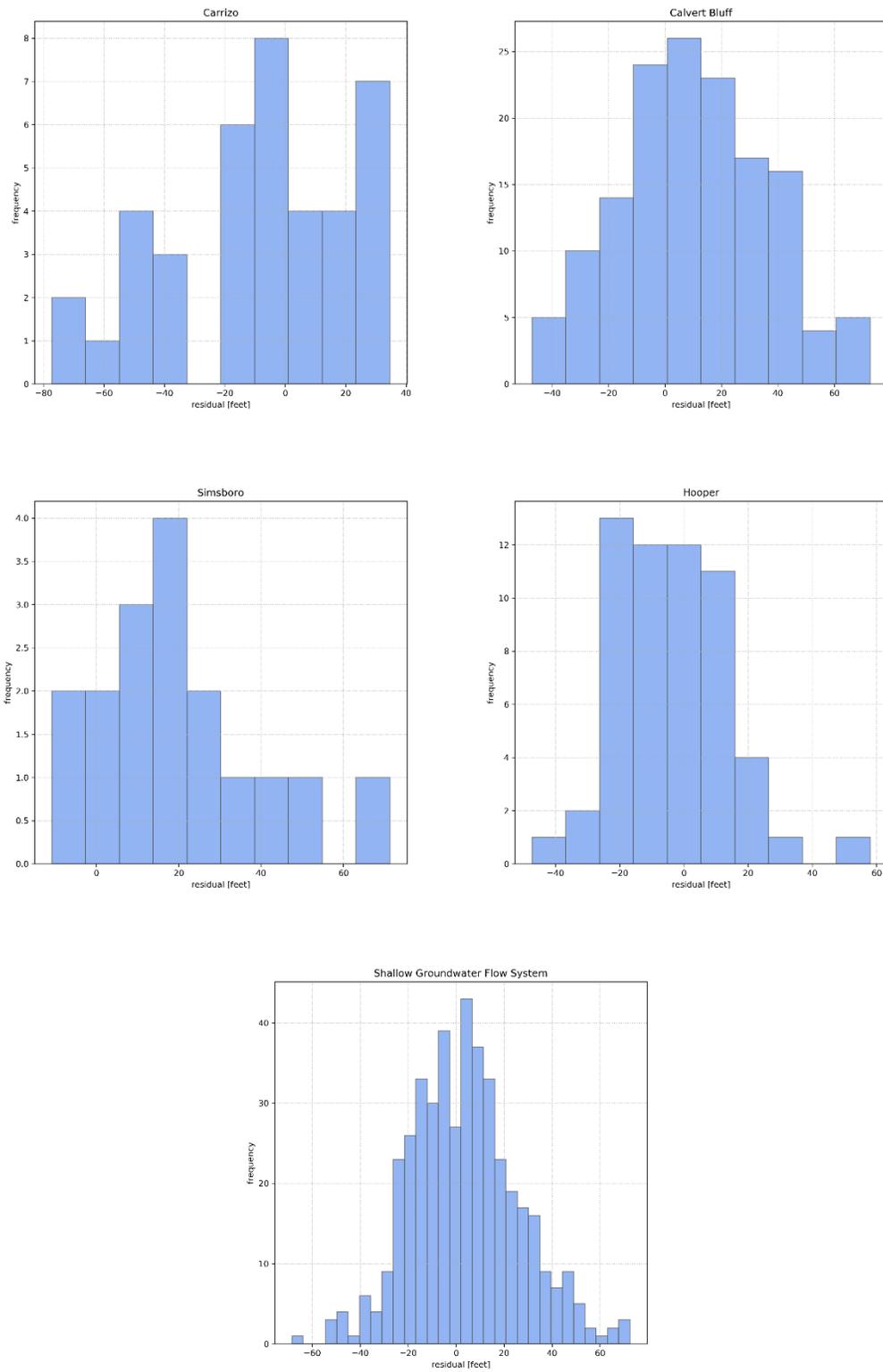
Figure 5.3.2e. **Histograms of the hydraulic head residuals for the Carrizo Aquifer, the Calvert Bluff Formation, the Simsboro Aquifer, the Hooper Aquifer, and the shallow groundwater flow system the across the entire model domain for the steady-state period.**

5.3.3 *Statistics and Scatter Plots for Hydraulic Head Residuals for Transient Conditions*

For the transient calibration, there is a wide range in the number of water-level measurements associated with each well, with many wells having more than 30 measured water levels. To account for biases associated with having an unequal number of residuals per well location, the calibration statistics were calculated using two weighting schemes. One scheme weighted all wells equally by considering a single hydraulic head value for each well, with that head value equal to the average hydraulic head at the well. The other scheme weighted all observed hydraulic head values for all wells equally. The calibration statistics for the first weighting scheme (equal by well) for the entire model domain and Groundwater Management Area 12 are given in Tables 5.3.3a and 5.3.3b, respectively. The calibration statistics for the second weighting scheme (equal by observed head) for the entire model domain and Groundwater Management Area 12 are shown in Tables 5.3.3c and 5.3.3d, respectively.

Table 5.3.3a. **Calibration statistics for transient conditions based on the equal-by-well weighting scheme for the entire model domain.**

Hydrogeologic Unit	Count[a]	Mean Error (feet)	Mean Absolute Error (feet)	Root Mean Square Error (feet)	Measured Range (feet)
Alluvium[b]	50	-1.1	3.5	4.4	66
Sparta	74	-2.7	14	19.2	393
Weches	7	2.3	12.9	20.1	217
Queen City	79	-6.4	14.5	22.7	344
Reklaw	28	-6.4	9.5	13.8	317
Carrizo	197	-3	14.8	22.4	618
Calvert Bluff	97	0.3	14.5	20.7	504
Simsboro	68	-11.3	19.8	25.5	501
Hooper	47	-11.8	19.4	26.2	291
Shallow Groundwater Flow System	106	2.4	14.9	20.7	367
All	647[c]	-4.3	14.4	21.3	743

[a] number of wells with hydraulic head targets
[b] all in the Brazos River alluvium
[c] sum for hydrogeologic units

Table 5.3.3b. **Calibration statistics for transient conditions based on the equal-by-well weighting scheme for Groundwater Management Area 12.**

Hydrogeologic Unit	Count[a]	Mean Error (feet)	Mean Absolute Error (feet)	Root Mean Square Error (feet)	Measured Range (feet)
Alluvium[b]	50	-1.1	3.5	4.4	66
Sparta	44	-4.4	14.5	19.8	389
Queen City	32	-2.3	12.1	19.6	317
Reklaw	7	-5.4	6.8	8.3	112
Carrizo	29	-7.4	10.1	15.2	279
Calvert Bluff	34	-7.8	15.1	22.5	179
Simsboro	50	-7.9	17.3	21.2	382
Hooper	21	-6.6	15.2	20	245
Shallow Groundwater Flow System	33	3.1	12.7	17.2	304
All	267[c]	-5.2	12.1	17.9	421

[a] number of wells with hydraulic head targets
[b] all in the Brazos River alluvium
[c] sum for hydrogeologic units

Table 5.3.3c. **Calibration statistics for transient conditions based on the equal-by-observed-head weighting scheme for the entire model domain.**

Hydrogeologic Unit	Count[a]	Mean Error (feet)	Mean Absolute Error (feet)	Root Mean Square Error (feet)	Measured Range (feet)
Alluvium[b]	802	-1.4	4.5	5.7	81
Sparta	1,167	-1.5	13.1	17.9	446
Weches	105	-0.6	8.1	12.8	226
Queen City	1,493	-4.2	14	22.2	414
Reklaw	505	-5.7	10.3	15.5	423
Carrizo	3,392	-4.6	17.7	28.3	727
Calvert Bluff	1,759	-2	12.5	17.4	579
Simsboro	1,132	-9.7	19	25	609
Hooper	1,023	-10.1	17.6	24	307
Shallow Groundwater Flow System	1,881	2.2	12.7	17.3	372
All	11378[c]	-4.6	14.7	22.6	845

[a] number of hydraulic head targets
[b] all in the Brazos River alluvium
[c] sum for hydrogeologic units

Table 5.3.3d. **Calibration statistics for transient conditions based on the equal-by-observed-head weighting scheme for Groundwater Management Area 12.**

Hydrogeologic Unit	Count[a]	Mean Error (feet)	Mean Absolute Error (feet)	Root Mean Square Error (feet)	Measured Range (feet)
Alluvium[b]	802	-1.4	4.5	5.7	81
Sparta	773	-3.7	12.8	17.3	441
Queen City	601	-0.5	11.7	17.9	322
Reklaw	150	-3.9	7.2	9.1	122
Carrizo	538	-7.7	11.8	17.9	292
Calvert Bluff	594	-6.2	14.4	19.8	191
Simsboro	806	-6.3	17.1	21.3	425
Hooper	503	-8	14.8	20.9	261
Shallow Groundwater Flow System	609	2.7	11.2	14.8	309
All	4,767[c]	-4.6	12.1	17.4	473

[a] number of hydraulic head targets
[b] all in the Brazos River alluvium
[c] sum for hydrogeologic units

For the 647 wells in the entire model domain, the statistical analysis produced a mean error, mean absolute error, and root mean square error of -4.3 feet, 14.4 feet, and 21.3 feet, respectively (Table 5.3.3a). For the 267 wells in Groundwater Management Area 12, the statistical analysis produced a mean error, mean absolute error, and root mean square error of -5.2 feet, 12.1 feet, and 17.9 feet, respectively (Table 5.3.3b). Based on the statistics using the average hydraulic head at each well, the model has a better match to historical water levels in Groundwater Management Area 12 than for the entire model domain.

For the 11,378 measured water levels at the 647 wells in the entire model domain, the statistical analysis produced a mean error, mean absolute error, and root mean square error of -4.6 feet, 14.7 feet, and 22.6 feet, respectively (Table 5.3.3c). For the 4,767 measured water levels at the 267 wells in Groundwater Management Area 12, the statistical analysis produced a mean error, mean absolute error, and root mean square error of –4.6 feet, 12.1 feet, and 17.4 feet, respectively (Table 5.3.3d). Based on the statistics for all measured hydraulic heads, the model

has a better match to historical water levels in Groundwater Management Area 12 than for the entire model domain.

A potentially useful statistical metric for evaluating model calibration is the magnitude of the root-mean square error relative to the range of the measurements. A guideline for evaluating the calibration fit is about 10 percent. For example, if the range of measured water levels is 100 feet, a goal for model calibration is a root-mean square error of 10 feet or less.

For both weighting schemes, the root-mean square error is consistently less than 5 percent of the observed range in water levels considering all of the hydrogeologic units in the model collectively for both the entire model domain and Groundwater Management Area 12. For both weighting schemes, the root-mean square error is consistently less than 10 percent of the observed range in water levels for each hydrogeologic unit individually for the entire model domain and for all but the Calvert Bluff Formation in Groundwater Management Area 12. The root-mean square error is 12.6 percent and 10.4 percent of the range in the Calvert Bluff Formation in Groundwater Management Area 12 using the equal-by-well and equal-by-observed-head weighting schemes, respectively.

The percentages slightly greater than 10 percent for the Calvert Bluff Formation in Groundwater Management Area 12 are not considered to represent a problem for three reasons. One reason is that the percentages are very close to the 10 percent guideline. The second is that the primary reason for the variance is not because of a high-root mean square error but rather because of a low value for the range in measured head values. The addition of just one observed head value for the Calvert Bluff Formation that differs more than 10 feet from any of the observed head values would have increased the range from 191 to 201 feet and reduced the percentage from 10.4 percent to 8.8 percent. The third reason is that some pumping in the Calvert Bluff Formation in Groundwater Management Area 12 was likely missed or miscategorized as pumping from the Simsboro Formation in the groundwater model. In Groundwater Management Area 12, the presumption exists that the Simsboro Formation (or middle Wilcox Group) is more prolific than the other formations comprising the Wilcox Aquifer, a presumption not made in Groundwater Management Areas 11 and 13. A comparison of observed and simulated hydraulic head data (see Section 5.3.6 and Appendix H) for several Calvert Bluff Formation wells in Groundwater Management Area 12 support this notion. For two such wells (well 3946902 in Leon County and well 5910907 in Milam County), the hydrographs of observed versus simulated hydraulic heads show simulated hydraulic heads within 5 feet of measured heads in 1970 at well 3946902 and in 1985 at well 5910907 followed by observed heads declining at a faster rate than simulated heads.

The calibration statistics for both the entire model domain and Groundwater Management Area 12 indicate that the model is well calibrated with respect to the hydraulic head residuals. To help identify potential biases in the residuals, cross plots of simulated versus observed hydraulic heads were generated as well as histograms that show the distribution of the residuals.

Figures 5.3.3a through 5.3.3f show scatter plots of the simulated versus observed calibration targets and residual histograms for all calibration targets at each well averaged. That is, one calibration target for each well equal to the average of all calibration targets for the well. Scatter plots for the hydrogeologic units for the entire model domain and Groundwater Management Area 12 are shown in Figures 5.3.3a and 5.3.3b, respectively. Both figures show points that are located near and randomly distributed about the 1:1 line. There are no notable biases evident in

these scatter plots. Figures 5.3.3c and 5.3.3d provide scatter plots for all hydrogeologic units combined and for each hydrogeologic unit individually for the entire model domain. Figures 5.3.3e and 5.3.3f provide histograms that show the distribution of residuals, calculated based on interpolation of the nodal model results to the location of the well, that comprise each of these scatter plots. The histograms for both values in the entire model domain and values in the shallow groundwater flow system exhibit a narrow bell-shaped distribution, which suggests a good and unbiased model calibration. For the transient case, approximately 12 percent of the total number of hydraulic head measurements are from the shallow groundwater flow system.

Figures 5.3.3g through 5.3.3l show scatter plots of the simulated versus observed hydraulic heads for all calibration targets in all wells and residual histograms for all calibration targets. Figures 5.3.3g and 5.3.3h show scatter plots for the hydrogeologic units for the entire model domain and Groundwater Management Area 12, respectively. Both figures show points that are located near and randomly distributed about the 1:1 line. There are no notable biases evident in the scatter plots. Figures 5.3.3i and 5.3.3j provide scatter plots for all hydrogeologic units combined and for each hydrogeologic unit individually for the entire model domain. Figures 5.3.3k and 5.3.3l provide histograms that show the distribution of residuals.
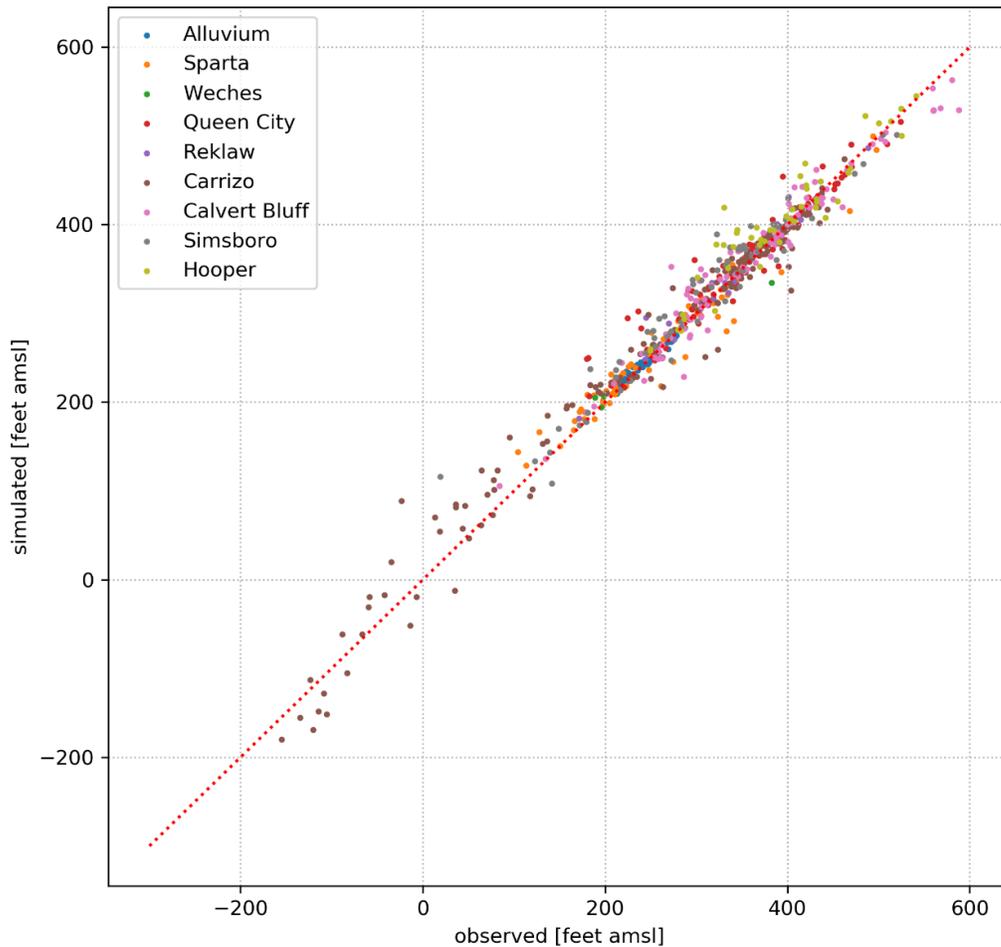
Figure 5.3.3a. Scatter plot of the average simulated versus average observed hydraulic heads at each of the 467 wells in the entire model domain with calibration targets for the transient period 1930 to 2010.
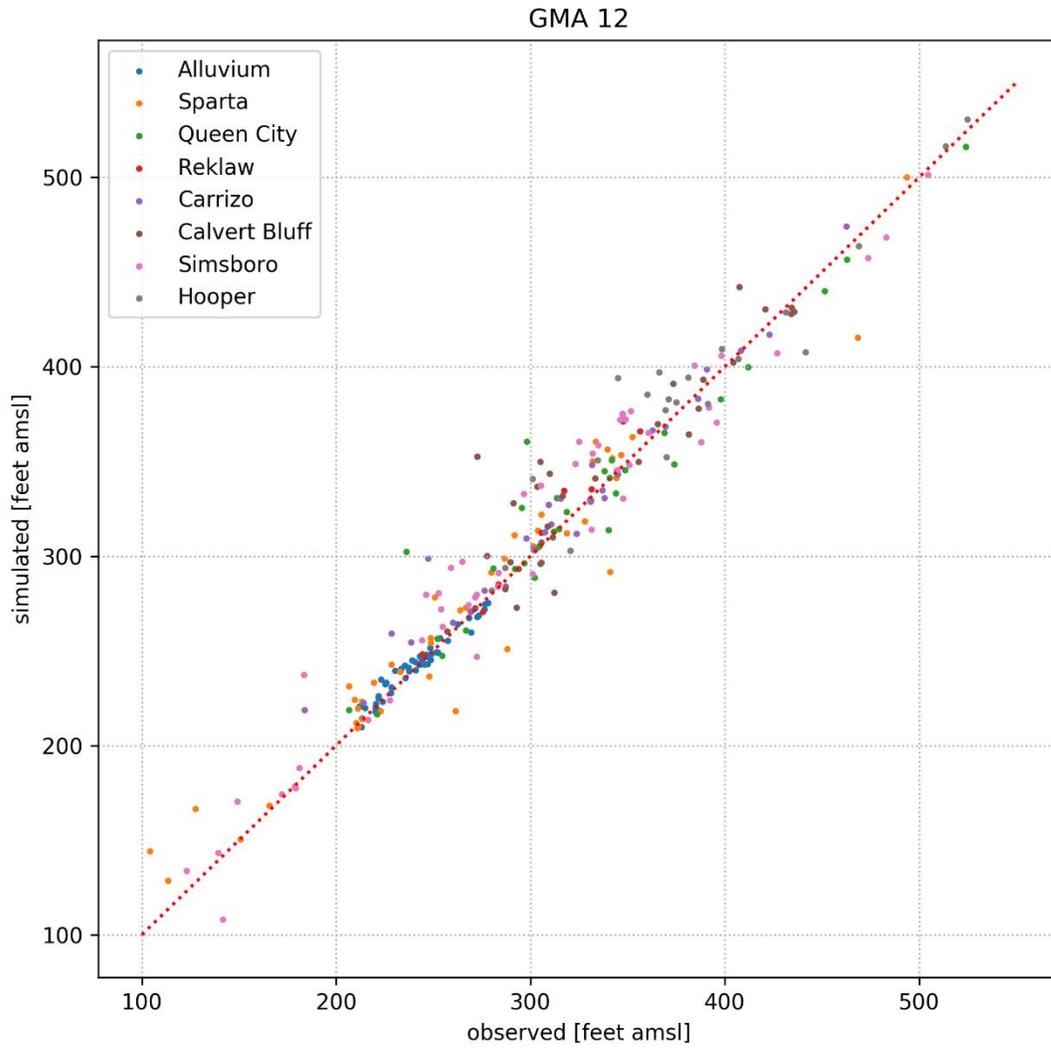
Figure 5.3.3b. **Scatter plot of the average simulated versus average observed hydraulic heads at each of the 267 wells in Groundwater Management Area 12 with calibration targets for the transient period 1930 to 2010.**
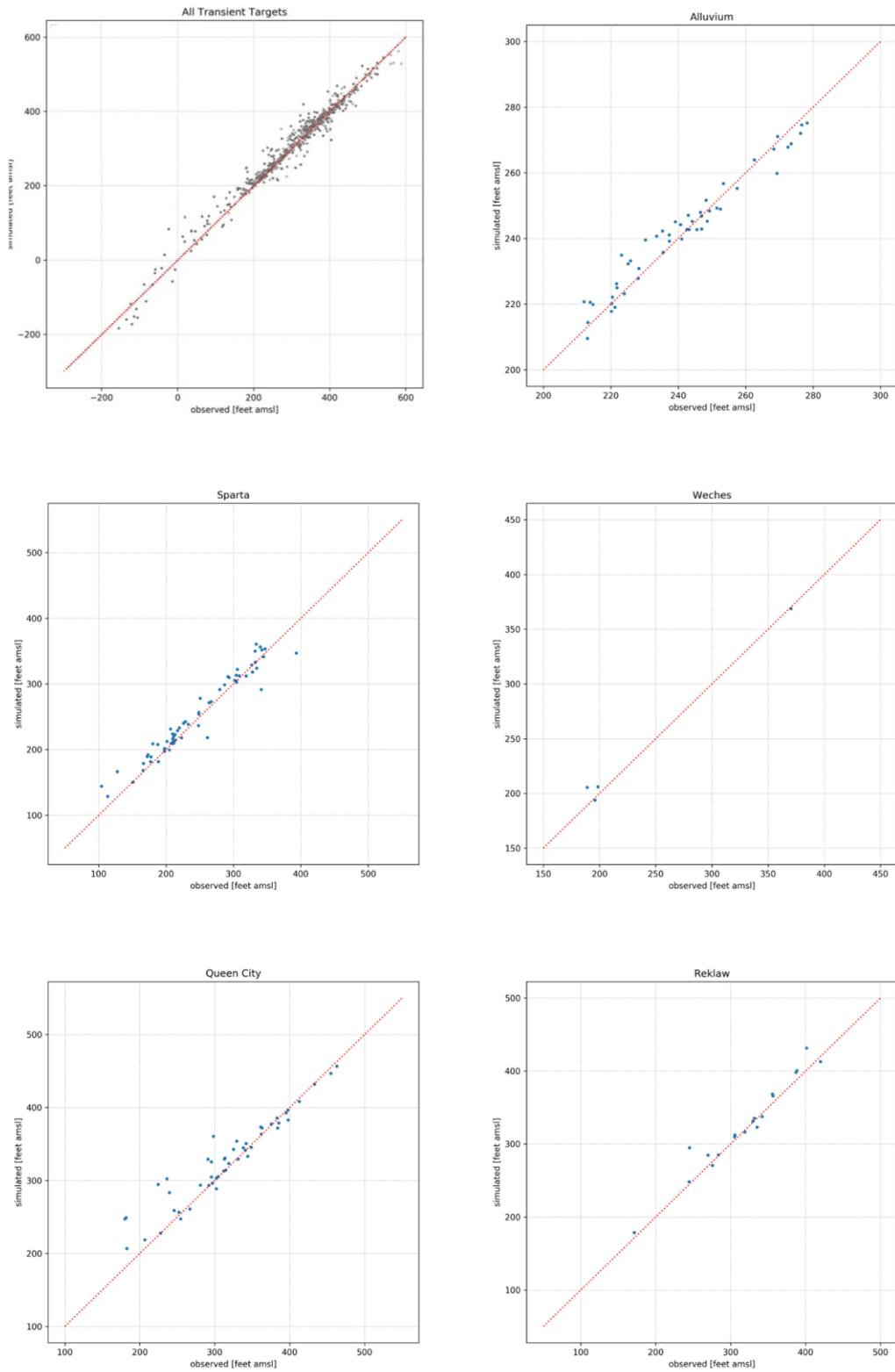
Figure 5.3.3c. Scatter plots of the average simulated versus average observed hydraulic heads at wells with calibration targets in the entire model domain, the Brazos River alluvium, the Sparta Aquifer, the Weches Formation, the Queen City Aquifer, and the Reklaw Formation for the transient period 1930 to 2010.
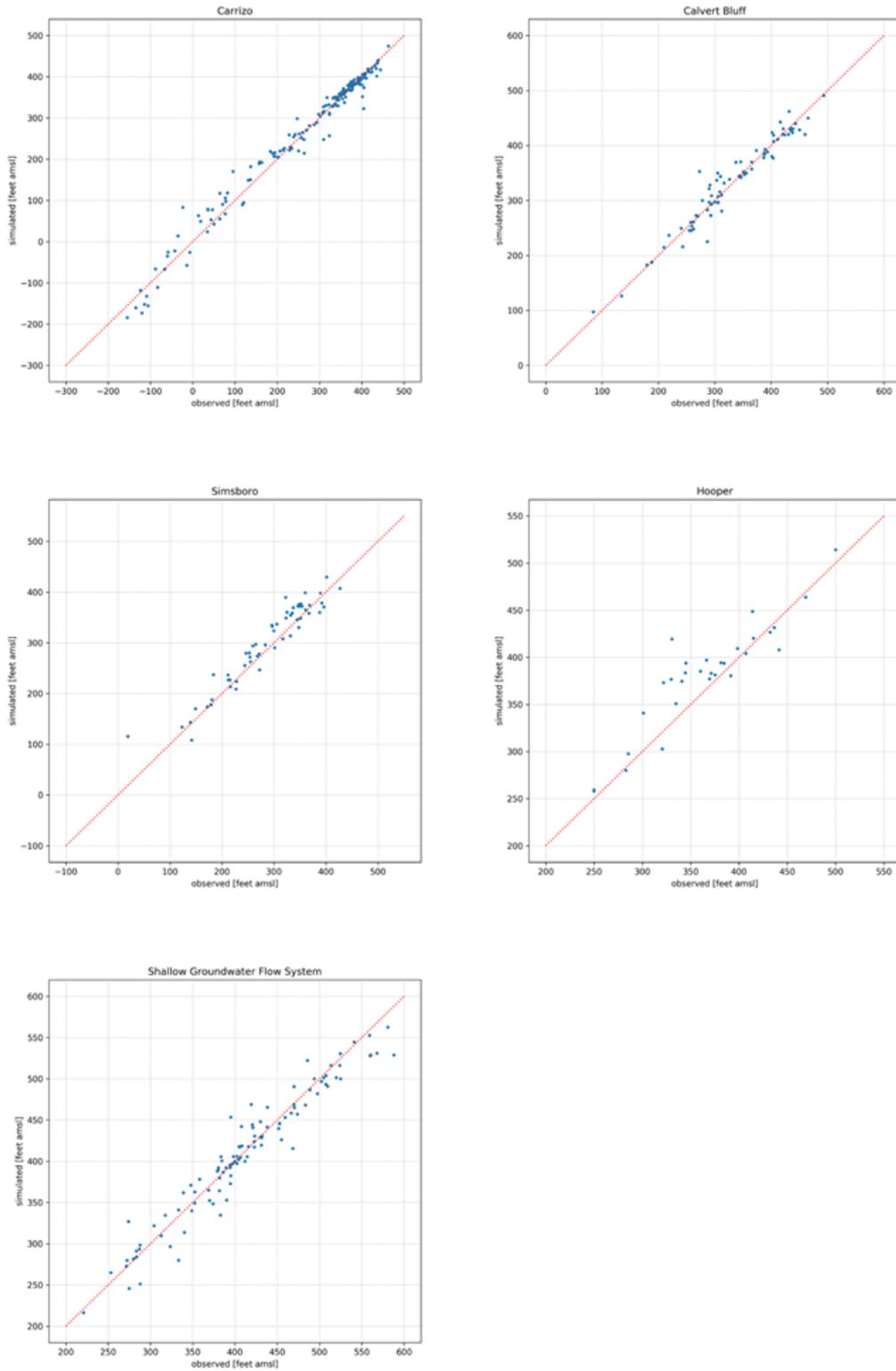
Figure 5.3.3d. Scatter plots of the average simulated versus average observed hydraulic heads at wells with calibration targets in the Carrizo Aquifer, the Calvert Bluff Formation, the Simsboro Formation, the Hooper Formation and the shallow groundwater flow system for the transient period 1930 to 2010.
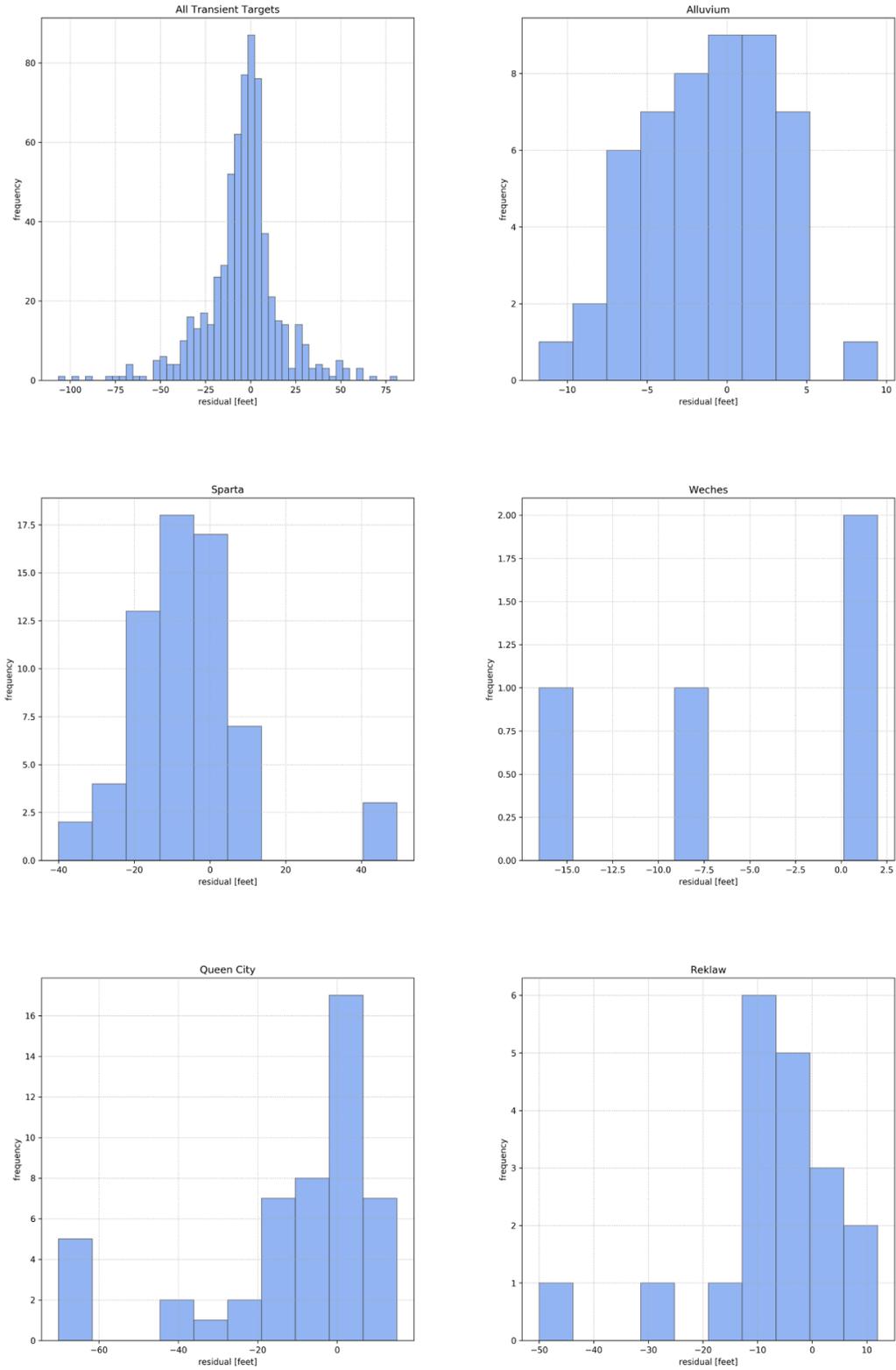
Figure 5.3.3e.   **Histograms of the average hydraulic head residuals for wells in the entire model domain, the Brazos River alluvium, the Sparta Aquifer, the Weches Formation, the Queen City Aquifer, and the Reklaw Formation for the transient period 1930 to 2010.**
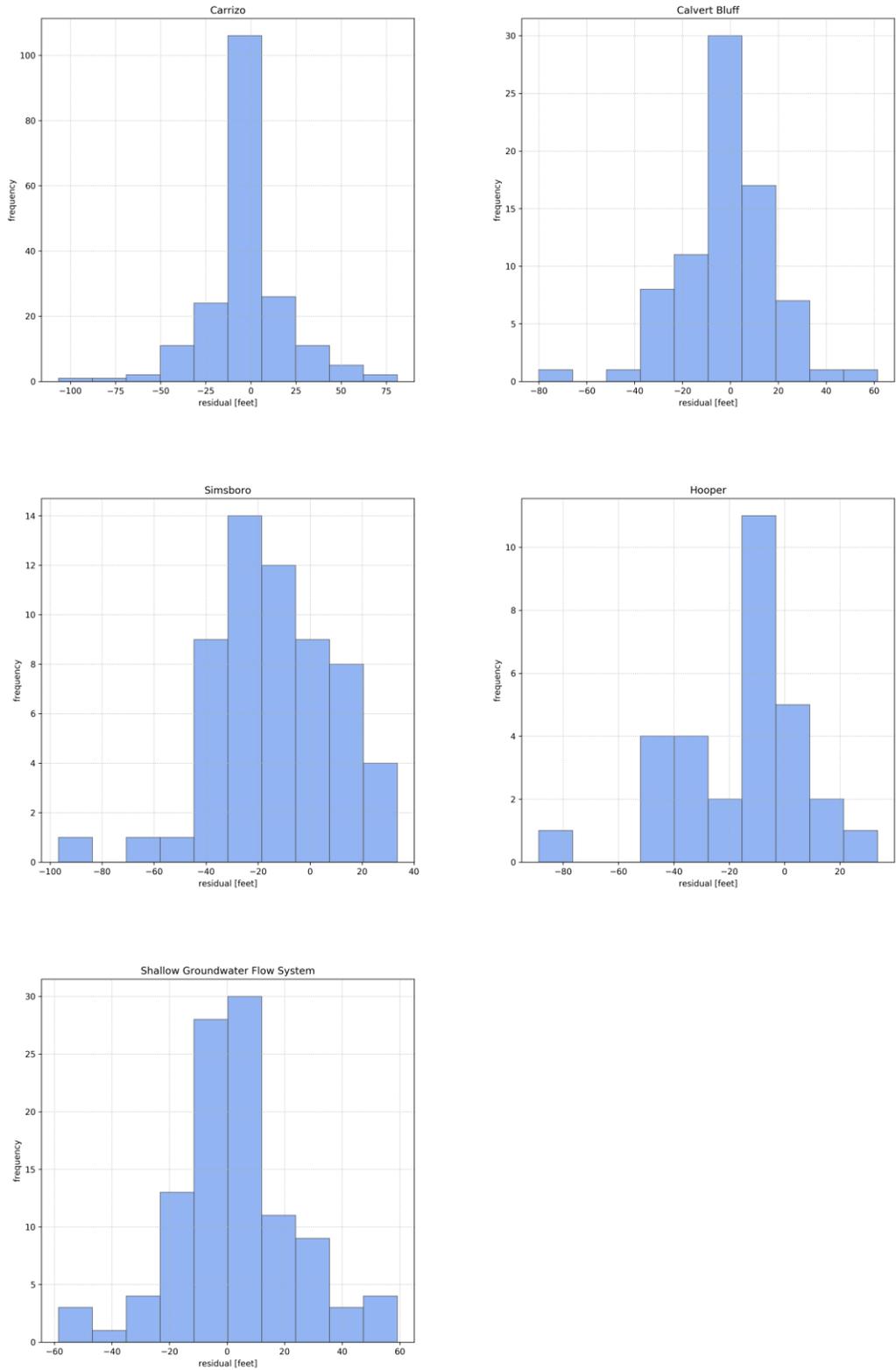
Figure 5.3.3f. **Histograms of the average hydraulic head residuals for wells in the Carrizo Aquifer, the Calvert Bluff Formation, the Simsboro Aquifer, the Hooper Aquifer, and the shallow groundwater flow system for the transient period 1930 to 2010.**

All Transient Targets
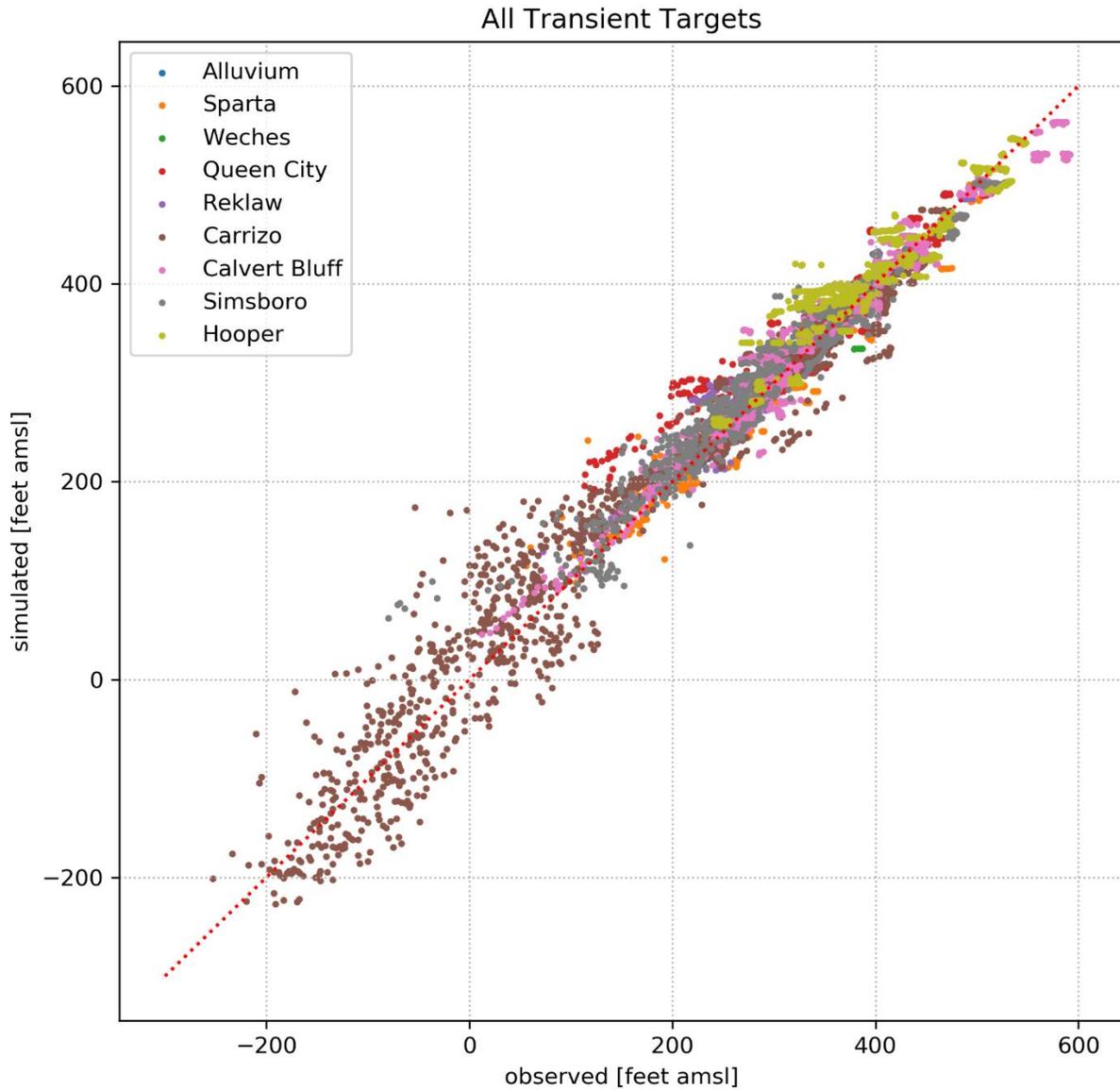
Figure 5.3.3g.   **Scatter plot of simulated versus observed hydraulic heads for the 11,378 water levels used as calibration targets across the entire model for the transient period 1930 to 2010.**
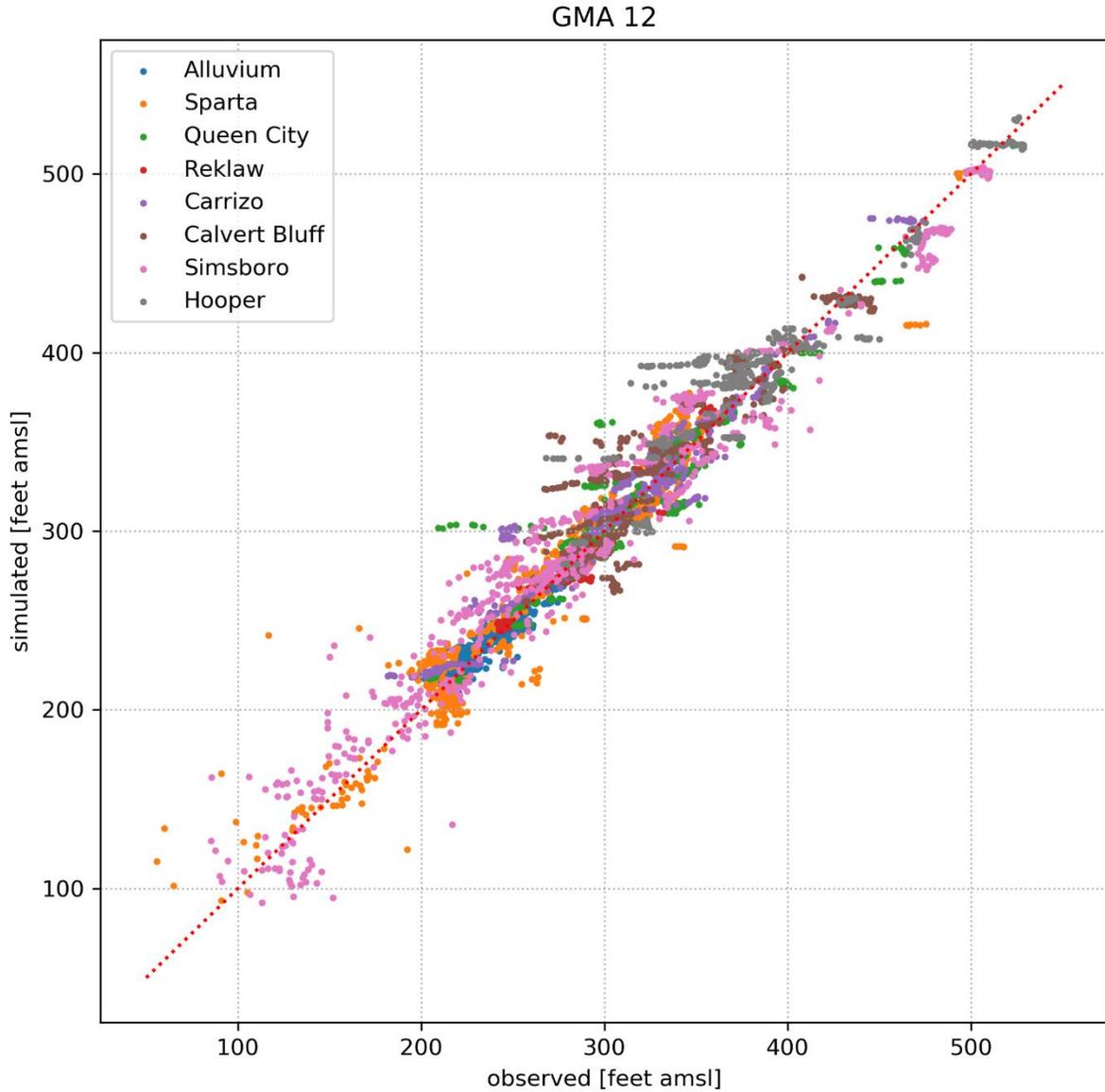
Figure 5.3.3h. **Scatter plot of simulated versus observed hydraulic heads for the 4,767 water levels used as calibration targets in Groundwater Management Area 12 for the transient period 1930 to 2010.**
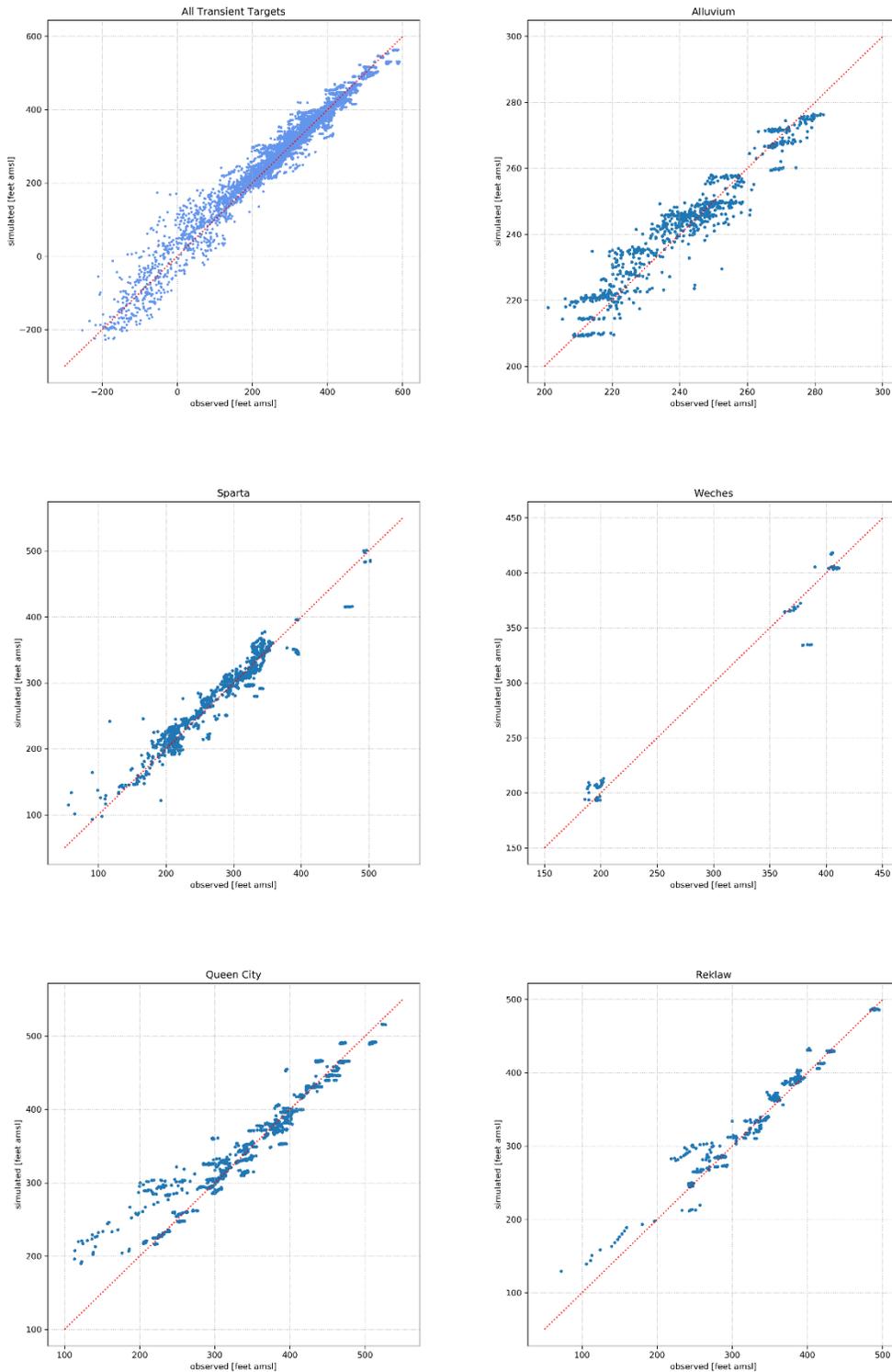
Figure 5.3.3i. **Scatter plots of simulated versus observed hydraulic heads for all calibration targets in all wells in the entire model domain, the Brazos River alluvium, the Sparta Aquifer, the Weches Formation, the Queen City Aquifer, and the Reklaw Formation for the transient period 1930 to 2010.**
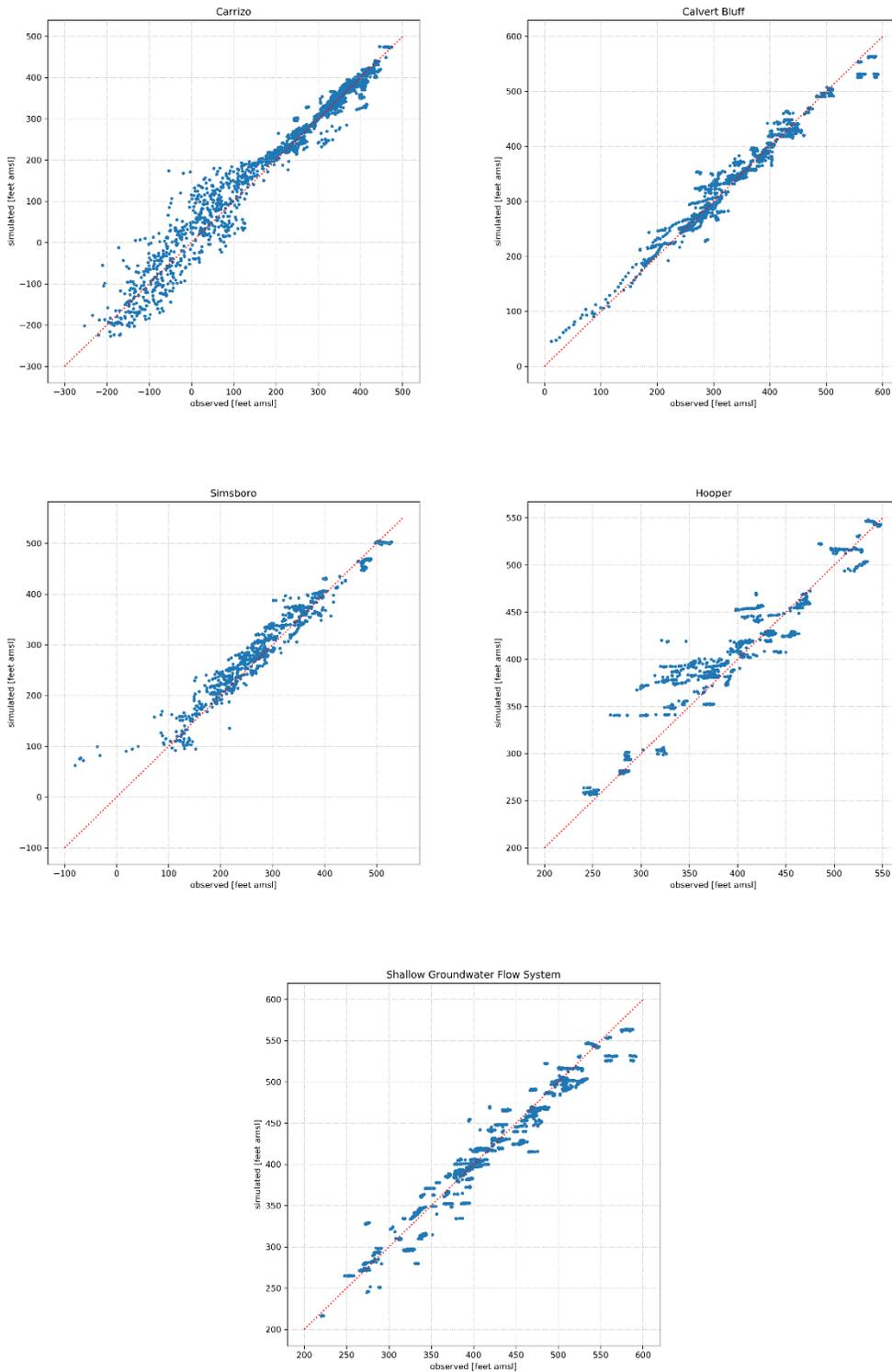
Figure 5.3.3j.   **Scatter plots of simulated versus observed hydraulic heads for all calibration targets in all wells in the Carrizo Aquifer, the Calvert Bluff Formation, the Simsboro Formation, the Hooper Formation and the shallow groundwater flow system for the transient period 1930 to 2010.**
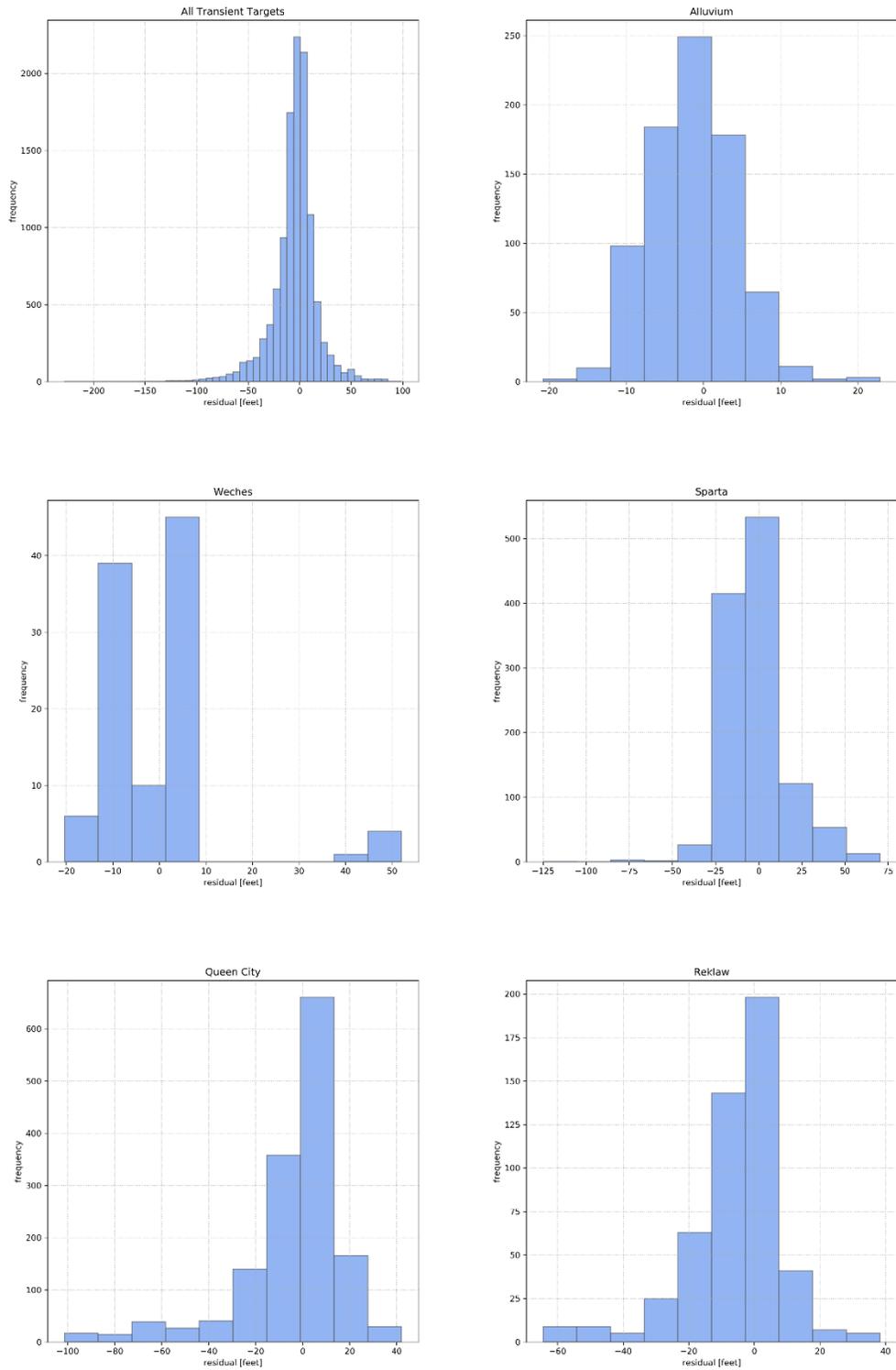
Figure 5.3.3k. **Histograms of the hydraulic head residuals for all calibration targets in all wells in the entire model domain, the Brazos River alluvium, the Sparta Aquifer, the Weches Formation, the Queen City Aquifer, and the Reklaw Formation for the transient period 1930 to 2010.**

Figure 5.3.3l. **Histograms of the hydraulic head residuals for all calibration targets in all wells in the Carrizo Aquifer, the Calvert Bluff Formation, the Simsboro Aquifer, the Hooper Aquifer, and the shallow groundwater flow system for the transient period 1930 to 2010.**

5.3.4   Contours of Simulated Hydraulic Head

In this section, contours of simulated hydraulic heads for the nine hydrogeologic units are presented for steady-state conditions and the years 1950, 1970, 1990, and 2010. On each plot, the calculated residuals are posted. For the contour plots at select years during the transient period, the residuals are the average for a three-year period centered on the year of the contours. Appendix L provides histograms of the residuals by hydrogeologic units for these four select years. The series of contour plots provide information regarding the evolution of groundwater flow directions and the spatial distribution of residuals for each hydrological unit.

Figures 5.3.4a through 5.3.4e show contours generated from simulated hydraulic heads in the Colorado and Brazos rivers alluvium for steady-state conditions and the years 1950, 1970, 1990, and 2010, respectively. When interpreted jointly with other hydraulic head contours in this section, the contours indicate that groundwater flow in the alluvium is consistently toward a river with an eastern slant toward the Gulf Coast. Evidence of gaining stream conditions are indicated by bends in the water table contours in the alluvium that point in the upstream direction (Winter and others, 1999). In the Colorado River alluvium, contours at both 350 and 300 feet above mean sea level have bends that point upstream. These bends indicate converging flow to a line source that is the Colorado River. In the Brazos River alluvium, the contour at 250 feet above mean sea level bends upstream. The groundwater flow directions that can be inferred from the contours are consistent with the conceptual flow system presented by Ewing and others (2016) A comparison of the hydraulic head contours over time does not provide evidence that the general flow direction has changed from 1930 to 2010. The hydraulic head residuals for 1970 and 1990 provide good coverage across the Brazos River alluvium and do not indicate systematic bias or anomalies in the simulated hydraulic heads. As previously noted, there are no steady-state or transient hydraulic head targets in the Colorado River alluvium.
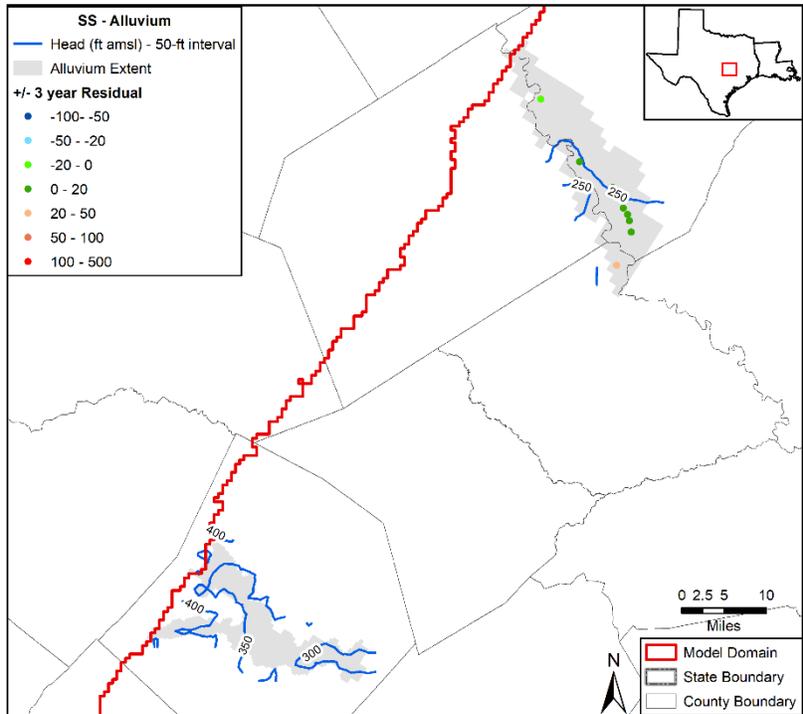
Figure 5.3.4a. Contours in feet (ft) above mean sea level (amsl) developed from simulated hydraulic heads for steady-state conditions in the Colorado and Brazos rivers alluvium with residuals for the Brazos River alluvium posted.
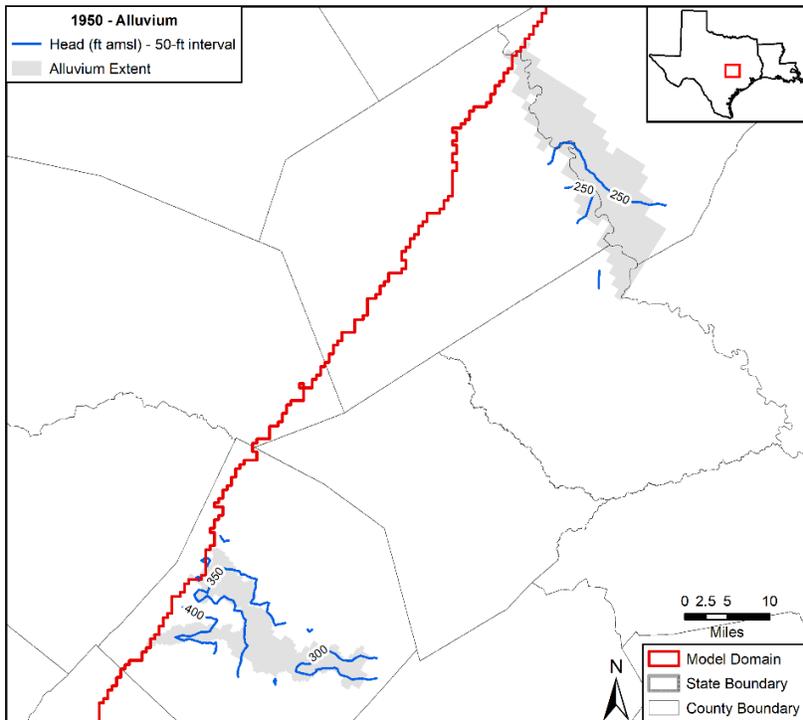
Figure 5.3.4b. Contours in feet (ft) above mean sea level (amsl) developed from simulated hydraulic heads for 1950 in the Colorado and Brazos rivers alluvium. No calibration targets available for this time.
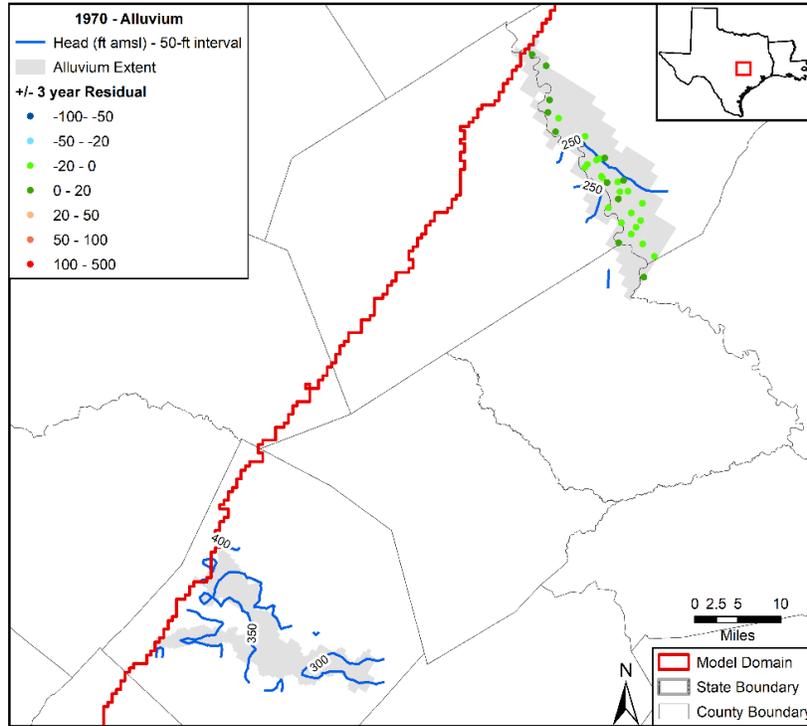
Figure 5.3.4c. Contours in feet (ft) above mean sea level (amsl) developed from simulated hydraulic heads for 1970 in the Colorado and Brazos rivers alluvium with residuals for the Brazos River alluvium posted.
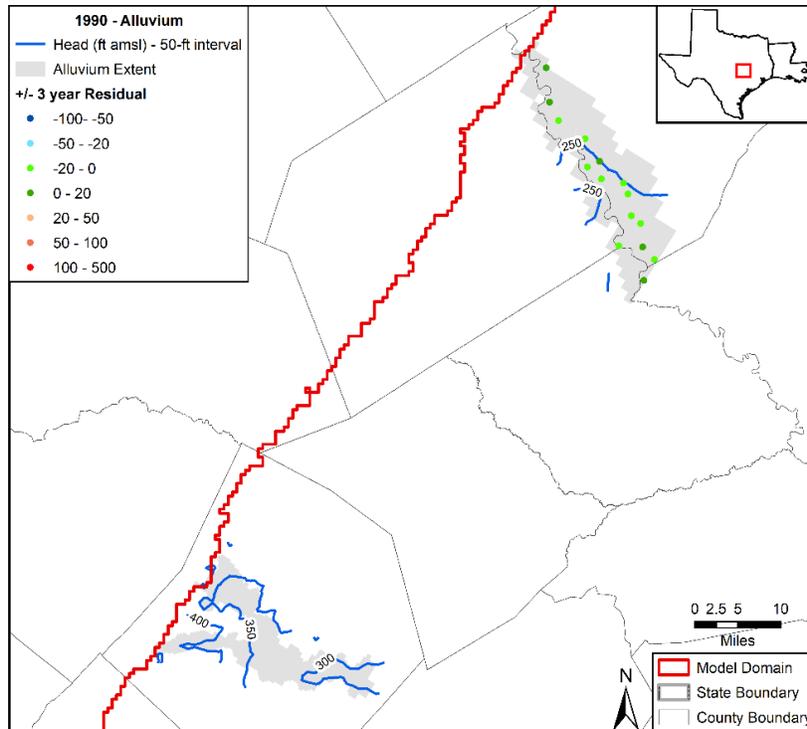
Figure 5.3.4d. Contours in feet (ft) above mean sea level (amsl) developed from simulated hydraulic heads for 1990 in the Colorado and Brazos rivers alluvium with residuals for the Brazos River alluvium posted.
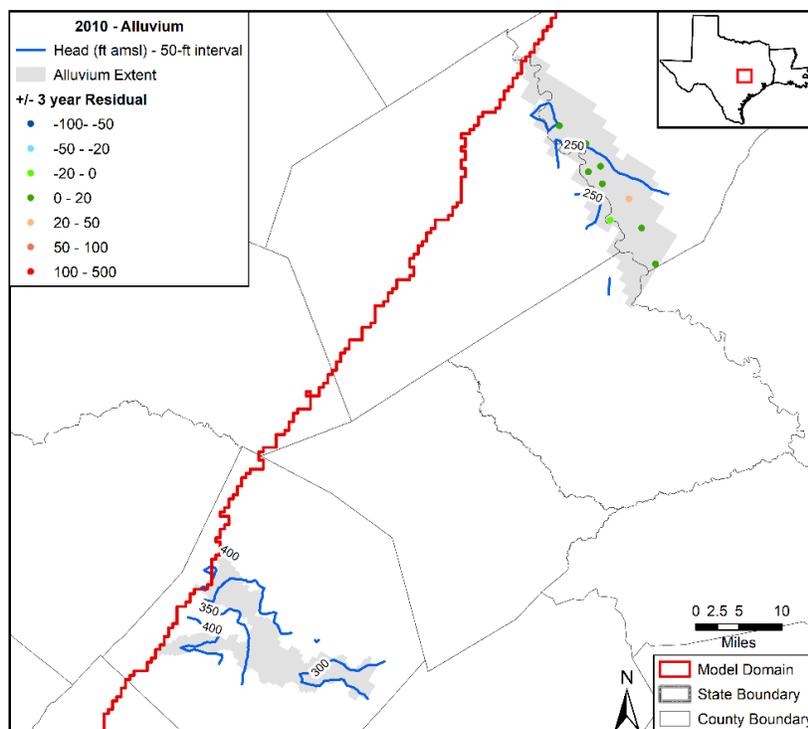
Figure 5.3.4e. Contours in feet (ft) above mean sea level (amsl) developed from simulated hydraulic heads for 2010 in the Colorado and Brazos rivers alluvium with residuals for the Brazos River alluvium posted.

Figures 5.3.4f through 5.3.4j show contours generated from simulated hydraulic heads in the Sparta Aquifer for steady-state conditions and the years 1950, 1970, 1990, and 2010. The general direction of regional groundwater flow remains similar for all five time periods. The regional and downdip flow is toward the Gulf Coast. In the updip portion of the Sparta Aquifer, groundwater flow is compartmentalized into localized flow systems that originate near topographic highs and are characterized by semi-radial flow toward low-lying areas. Near the Sparta Aquifer outcrop, the effect of major rivers on the shape of the contours is evident. The contours appear to represent boundaries that divide shallow groundwater basins because the rivers, which exist in local topographic lows, act as sinks for groundwater flow. Overall, the flow system for the Sparta Aquifer inferred from the hydraulic head contours is consistent with the conceptual model discussed by Kelley and others (2004). Our analysis of the plotted hydraulic head residuals does not suggest any systematic bias or anomalies in the simulated hydraulic heads. In general, the residuals are lowest in the southern and central portions of the model. In Cherokee and Angelina counties in the northern region of the model the residuals become larger and more variable. The principal reason attributed to this concentration of variability in the residual values in these two counties are the use of a 1-mile by 1-mile grid where topography is hilly.
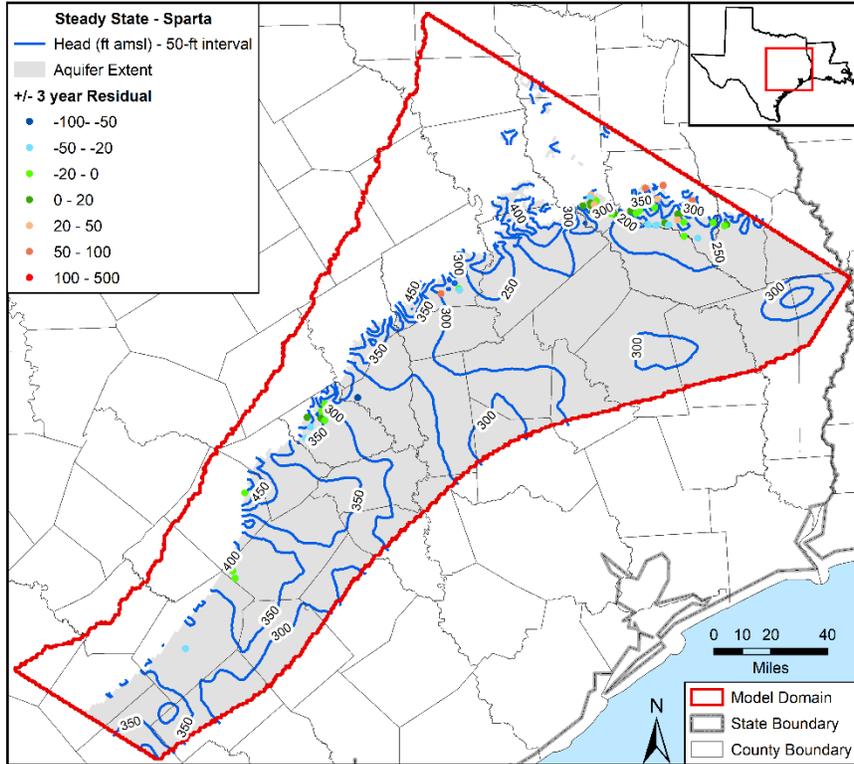
Figure 5.3.4f. Contours in feet (ft) above mean sea level (amsl) developed from simulated hydraulic heads for steady-state conditions in the Sparta Aquifer with residuals posted.
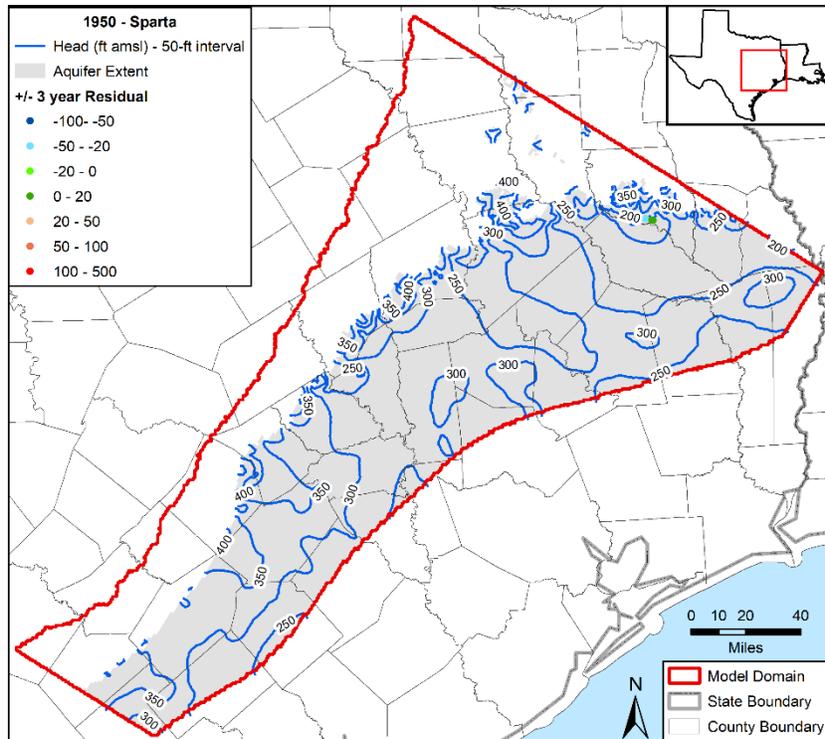
Figure 5.3.4g. Contours in feet (ft) above mean sea level (amsl) developed from simulated hydraulic heads for 1950 in the Sparta Aquifer with residuals posted.
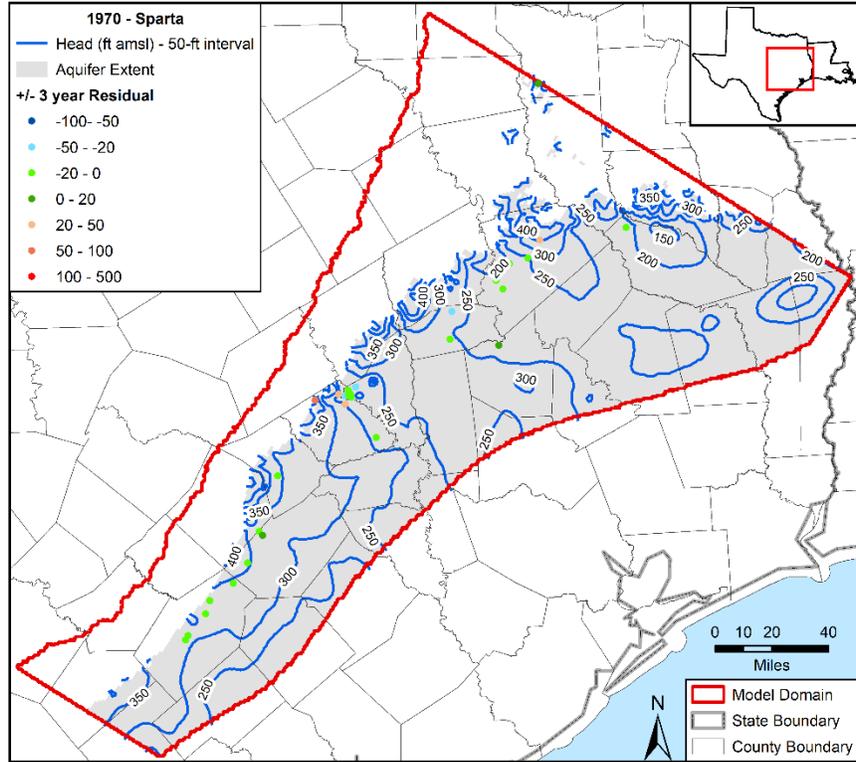
Figure 5.3.4h. Contours in feet (ft) above mean sea level (amsl) developed from simulated hydraulic heads for 1970 in the Sparta Aquifer with residuals posted.
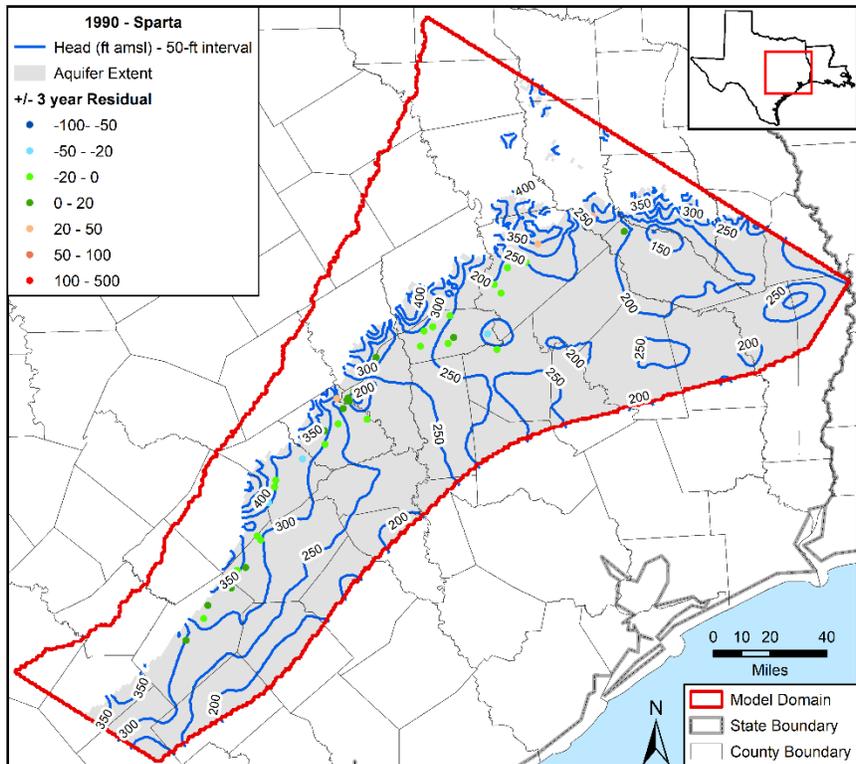
Figure 5.3.4i. Contours in feet (ft) above mean sea level (amsl) developed from simulated hydraulic heads for 1990 in the Sparta Aquifer with residuals posted.
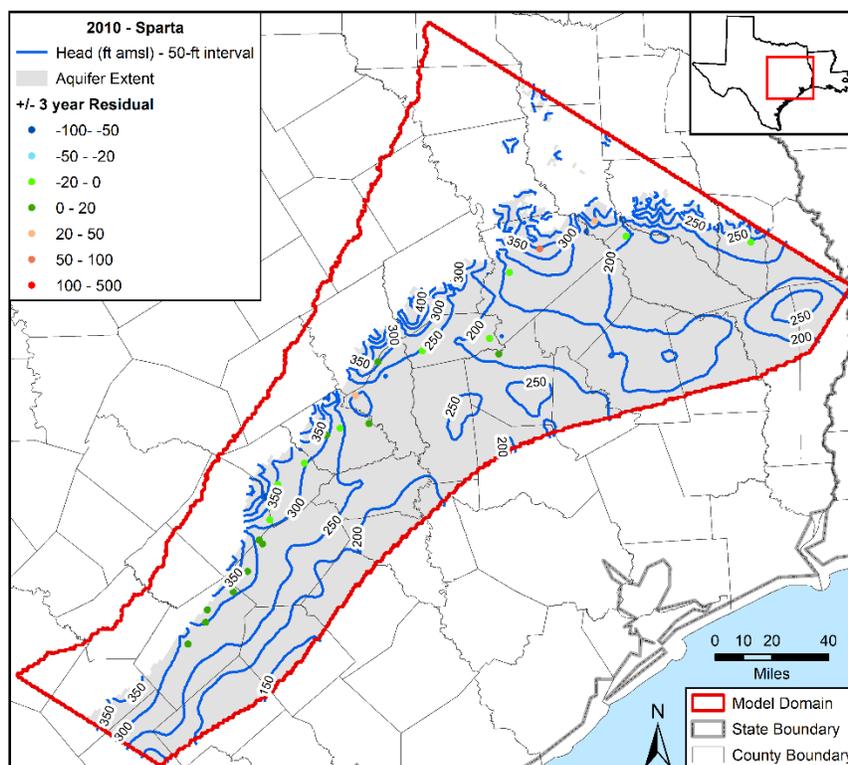
Figure 5.3.4j. **Contours in feet (ft) above mean sea level (amsl) developed from simulated hydraulic heads for 2010 in the Sparta Aquifer with residuals posted.**

Figures 5.3.4k through 5.3.4o show contours generated from simulated hydraulic heads in the Weches Formation for steady-state conditions and the years 1950, 1970, 1990, and 2010 in the transient period. The groundwater flow directions inferred from the contours are very similar to those discussed for the Sparta Aquifer. In the downdip portion of the formation, regional groundwater flow is toward the Gulf Coast. In the updip portion of the formation, groundwater flow is compartmentalized into localized flow systems that originate near topographic highs and are characterized by semi-radial flow toward low-lying areas. The inferred groundwater flow directions are consistent with the conceptual model of the system. Based on hydrogeologic considerations, the flow directions in the Weches Formation should be reflective of the groundwater flow systems in the Sparta and Queen City aquifers, which it separates, for two reasons. First, because of its relatively low transmissivity, the Weches Formation will exert a minimal amount of control on regional groundwater flow directions. Second, because there is very limited groundwater pumping in the Weches Formation, there are few hydraulic boundaries sufficient to affect groundwater flow across a large area. There are relatively few hydraulic head residuals shown on the figures because there are few wells in the Weches Formation. In the southern and central portions of the Weches Formation, there are four or less residuals shown on the figures. In the northern portion of the formation, there are 11 or less hydraulic head residuals shown on the figures. A review of these residuals does not indicate any systematic bias or anomalies in the simulated hydraulic heads.
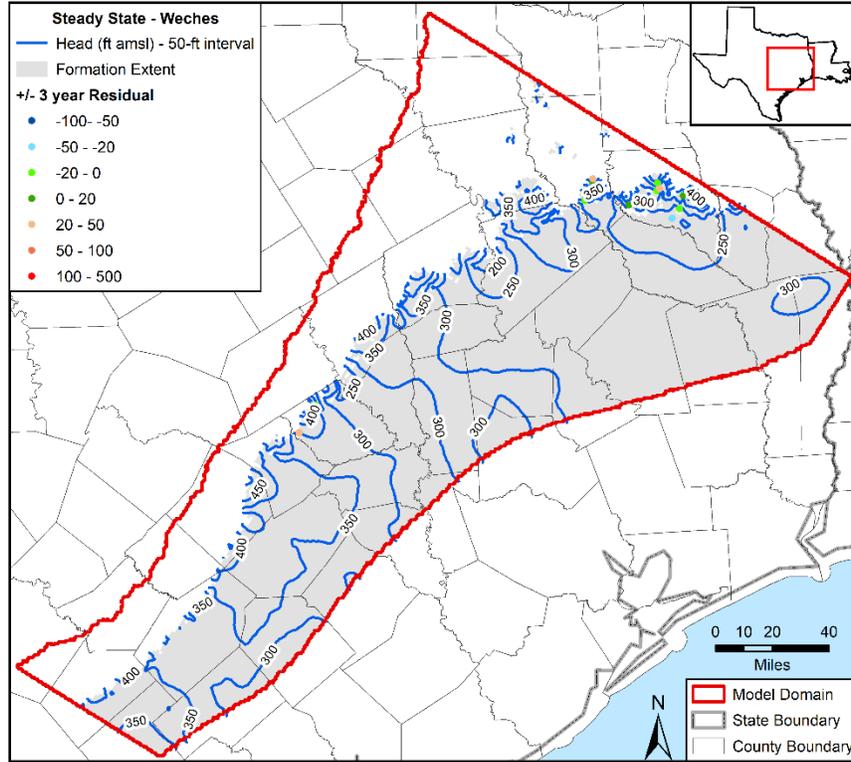
Figure 5.3.4k. Contours in feet (ft) above mean sea level (amsl) developed from simulated hydraulic heads for steady-state conditions in the Weches Formation with residuals posted.
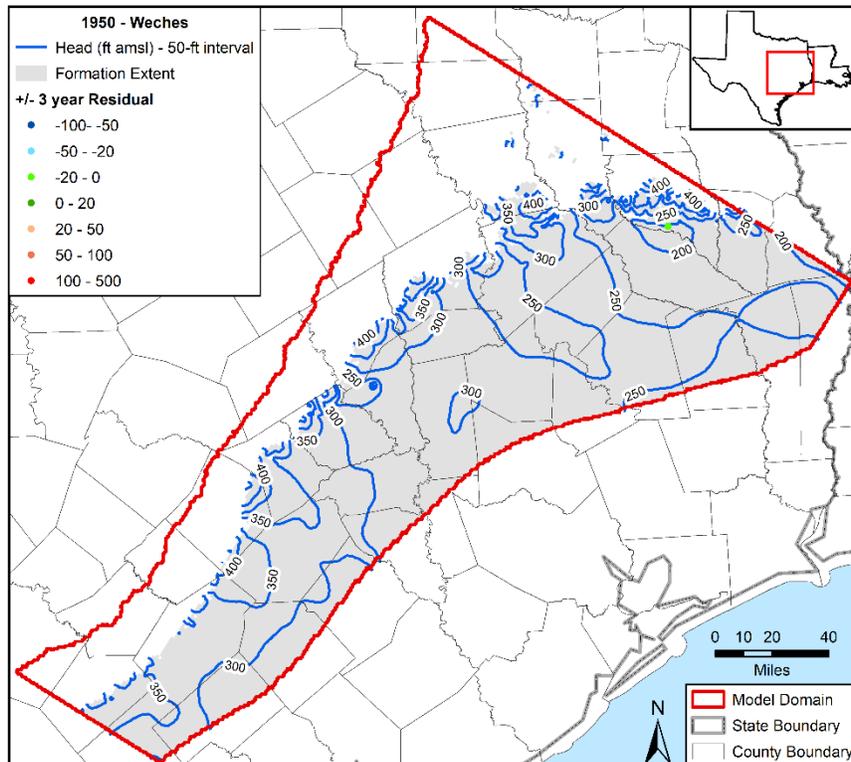
Figure 5.3.4l. Contours in feet (ft) above mean sea level (amsl) developed from simulated hydraulic heads for 1950 in the Weches Formation with residuals posted.
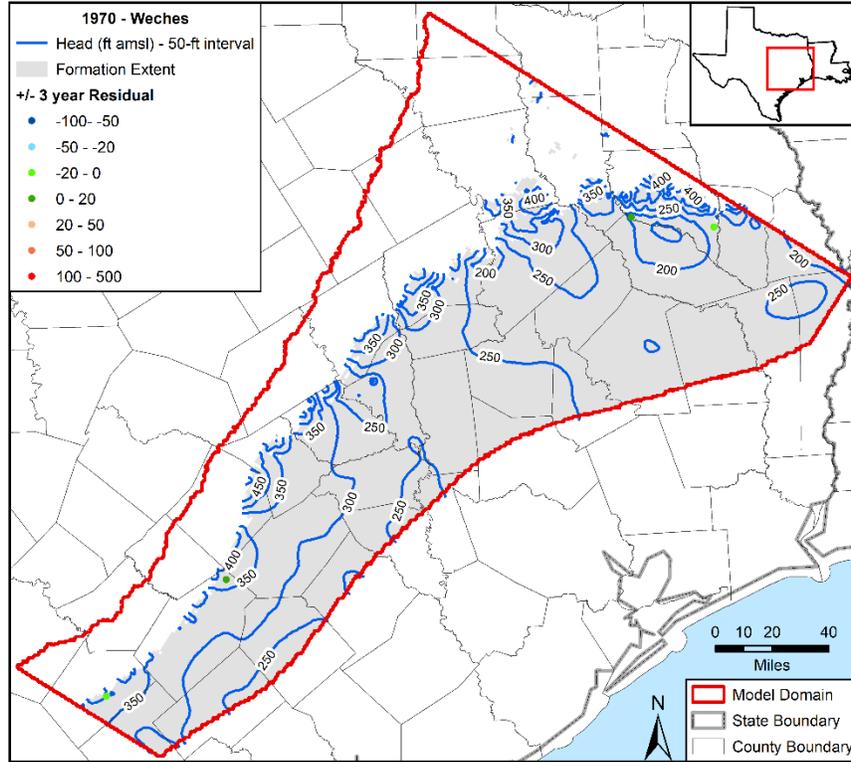
Figure 5.3.4m. Contours in feet (ft) above mean sea level (amsl) developed from simulated hydraulic heads for 1970 in the Weches Formation with residuals posted.
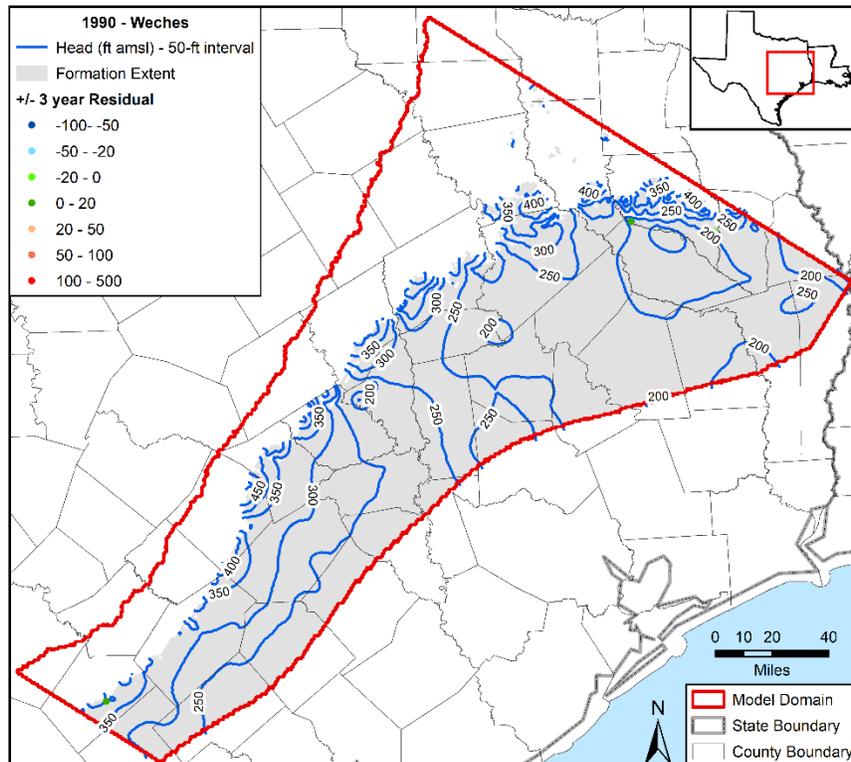
Figure 5.3.4n. Contours in feet (ft) above mean sea level (amsl) developed from simulated hydraulic heads for 1990 in the Weches Formation with residuals posted.
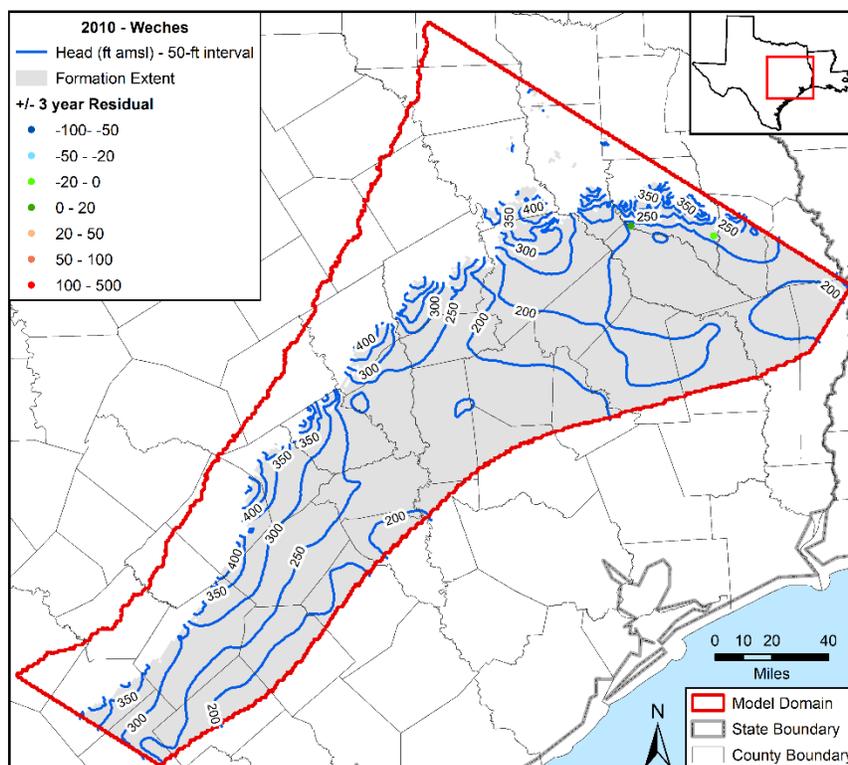
Figure 5.3.4o.   **Contours in feet (ft) above mean sea level (amsl) developed from simulated hydraulic
heads for 2010 in the Weches Formation with residuals posted.**

Figures 5.3.4p through 5.3.4t show contours generated from simulated hydraulic heads in the
Queen City Aquifer for steady-state conditions and the years 1950, 1970, 1990, and 2010 in the
transient period. The flow directions can be fairly easily inferred from the contours, except in the
northeast region of the model. In the southern region of the model, the flow directions and
patterns are similar to those observed for the Sparta Aquifer. The regional flow in the confined
and downdip portions of the aquifer transitions from towards the coast and the southeast in the
south to flow towards the coast and the northeast in the north. Over time, the regional flow
direction in the confined, downdip regions of the aquifer in the southern and central portions of
the model changes and develops a stronger northeast component. In the shallow and unconfined
updip regions of the aquifer, groundwater flow paths are consistent with flow from topographic
highs to topographic lows at scales of 10 to 20 miles in the south but at much smaller scales of a
few miles in the north. The influence of rivers, particularly the Trinity River, on flow in the
outcrop is evident. Across the large outcrop area in the north, large elevation changes in the
topography exhibit a strong control on groundwater flow and cause the contours to be tightly
spaced and convoluted. The validity of the tortuosity of the hydraulic head contours is supported
by the values and pattern in the hydraulic residuals shown for steady-state conditions and the
year 1970. From both regional- and local-scale assessments, the groundwater flow directions
inferred from the hydraulic contours agree with the conceptual model provided by Kelley and
others (2004).
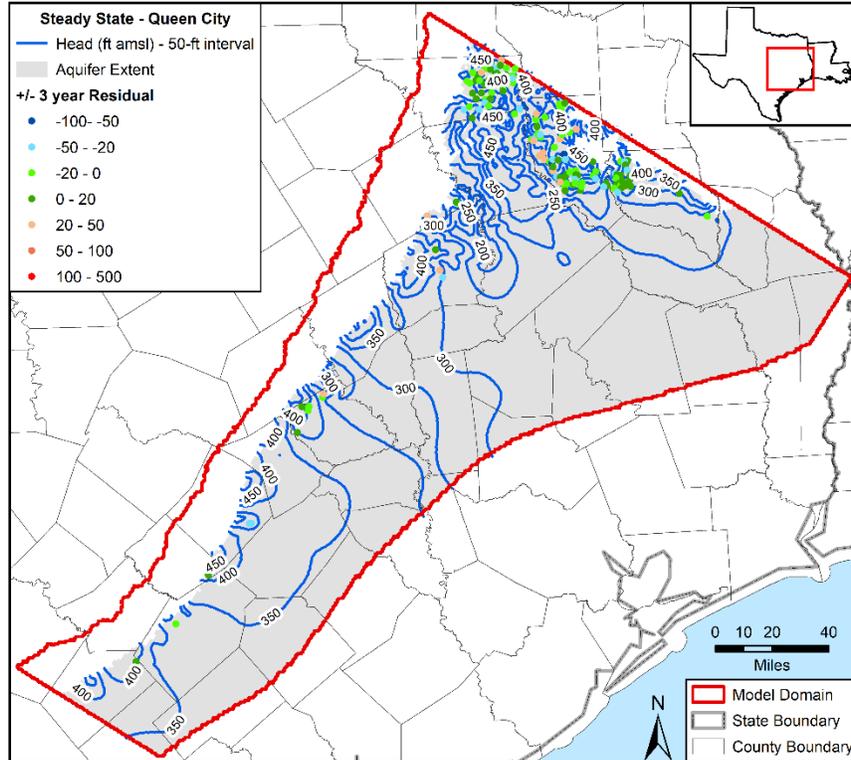
Figure 5.3.4p. Contours in feet (ft) above mean sea level (amsl) developed from simulated hydraulic heads for steady-state conditions in the Queen City Aquifer with residuals posted.
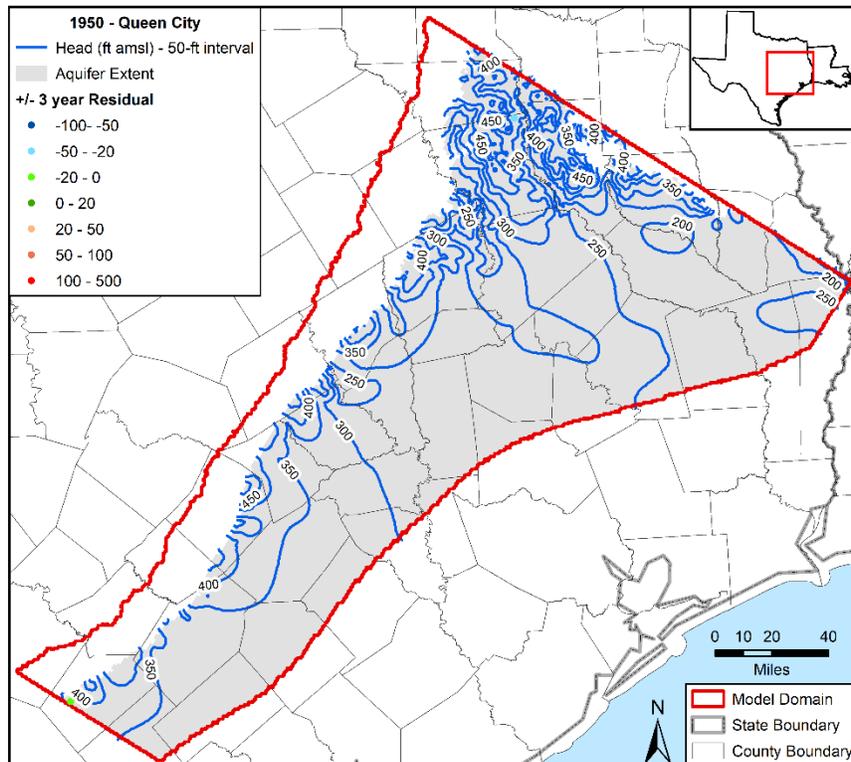
Figure 5.3.4q. Contours in feet (ft) above mean sea level (amsl) developed from simulated hydraulic heads for 1950 in the Queen City Aquifer with residuals posted.
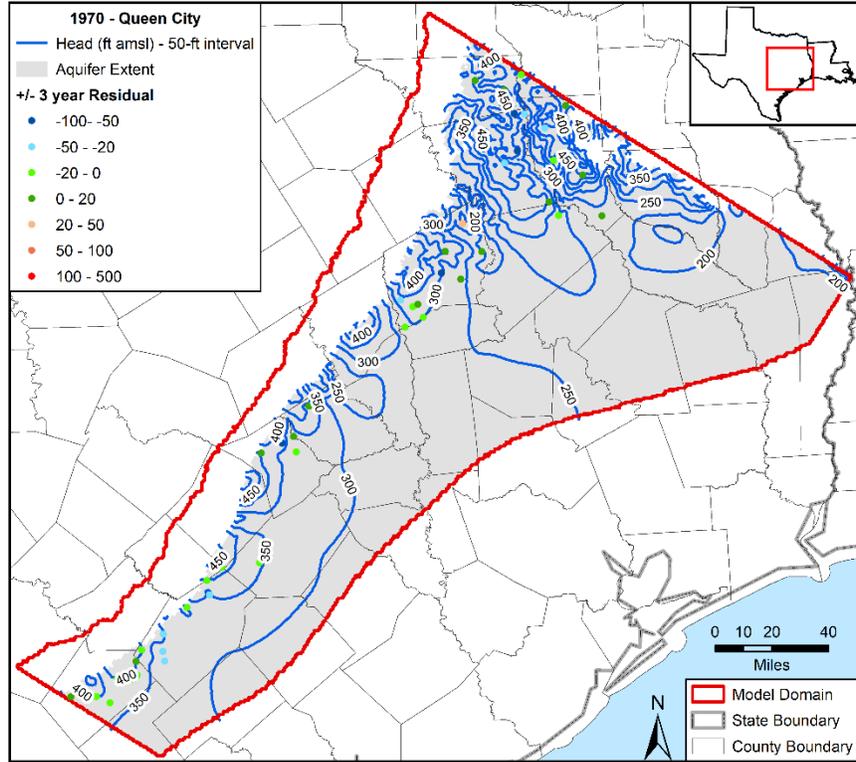
Figure 5.3.4r.   **Contours in feet (ft) above mean sea level (amsl) developed from simulated hydraulic heads for 1970 in the Queen City Aquifer with residuals posted.**
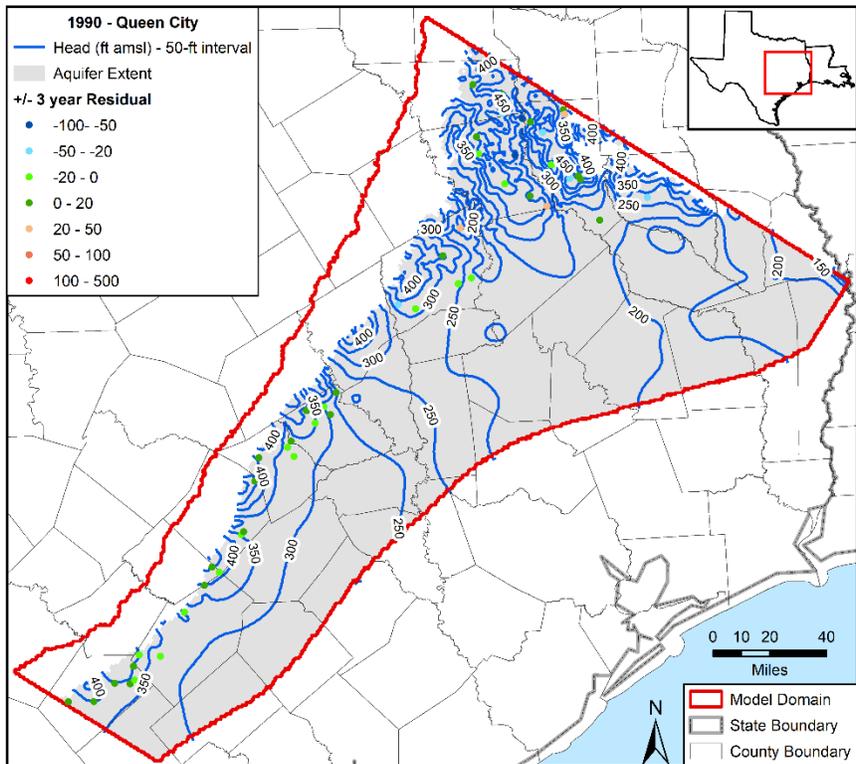
Figure 5.3.4s.   **Contours in feet (ft) above mean sea level (amsl) developed from simulated hydraulic heads for 1990 in the Queen City Aquifer with residuals posted.**

Figure 5.3.4t.   **Contours in feet (ft) above mean sea level (amsl) developed from simulated hydraulic heads for 2010 in the Queen City Aquifer with residuals posted.**

Figures 5.3.4u through 5.3.4y show contours generated from simulated hydraulic heads in the Reklaw Formation for steady-state conditions and the years 1950, 1970, 1990, and 2010 in the transient period. Based on hydrogeologic considerations, the flow directions in the Reklaw Formation should be reflective of the flow systems in the Queen City and Carrizo aquifers, which it separates, for two reasons. First, because of its relatively low transmissivity, the Reklaw Formation will have a minimal amount of influence on regional groundwater flow directions. Second, because of the limited groundwater pumping in the Reklaw Formation, there are too few areas of large discharges to collectively affect regional groundwater flow. A comparative analysis of the contours among the hydrogeologic units shows that there are strong similarities between the Reklaw Formation and the Carrizo Aquifer. This observation is consistent with our conceptual model that would predict that the contours in the Reklaw Formation would be similar to those in the Carrizo Aquifer, which is considerably more permeable and transmissive than the Queen City Aquifer.
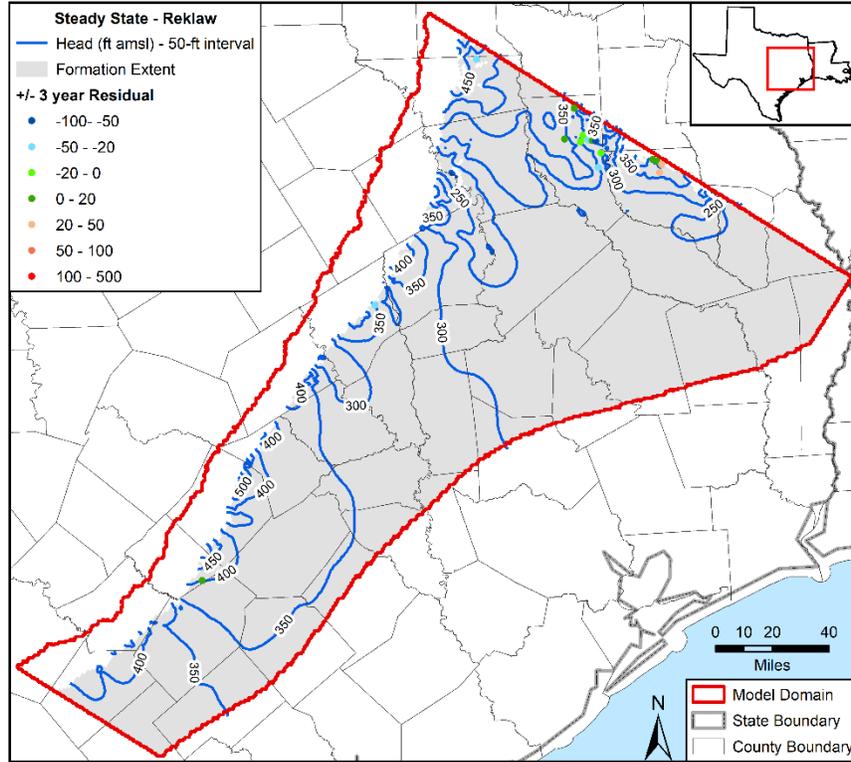
Figure 5.3.4u. Contours in feet (ft) above mean sea level (amsl) developed from simulated hydraulic heads for steady-state conditions in the Reklaw Formation with residuals posted.
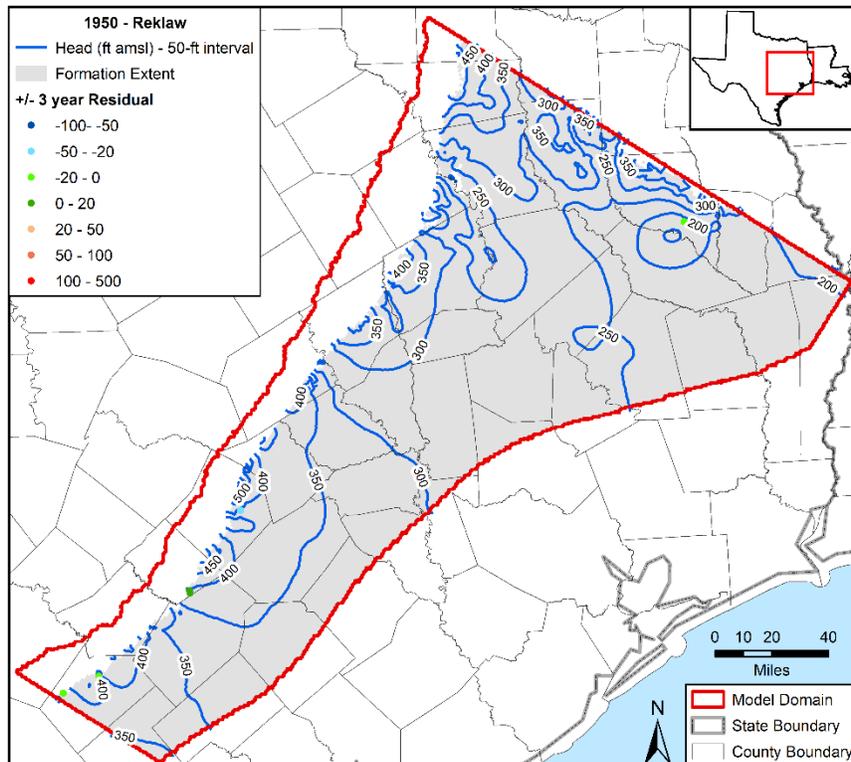
Figure 5.3.4v. Contours in feet (ft) above mean sea level (amsl) developed from simulated hydraulic heads for 1950 in the Reklaw Formation with residuals posted.

Final Report: Groundwater Availability Model for the Central Portion
of the Carrizo-Wilcox, Queen City, and Sparta Aquifers
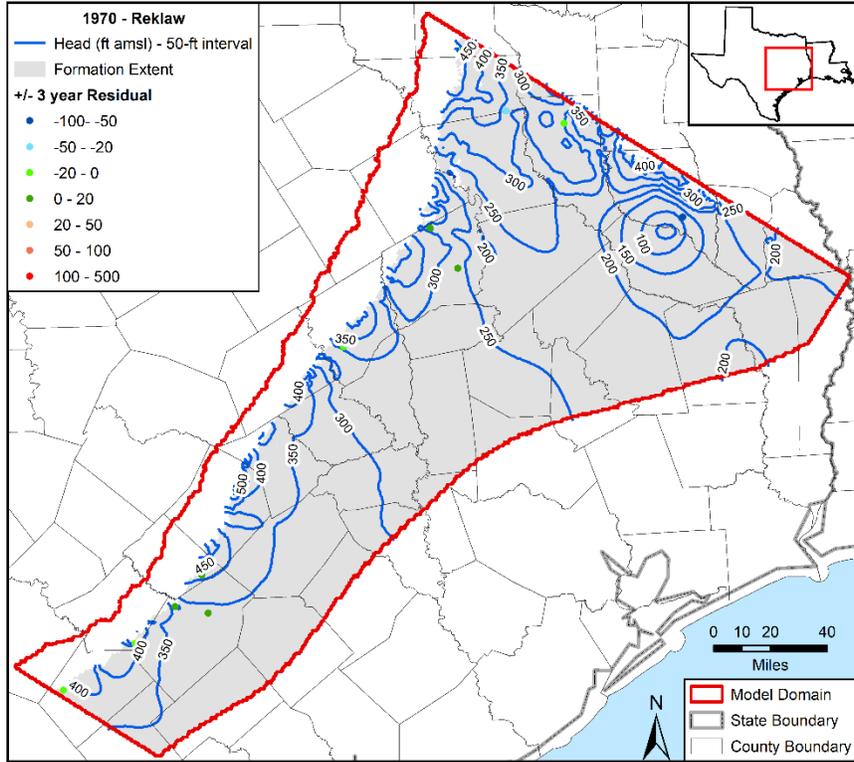
Figure 5.3.4w. Contours in feet (ft) above mean sea level (amsl) developed from simulated hydraulic heads for 1970 in the Reklaw Formation with residuals posted.
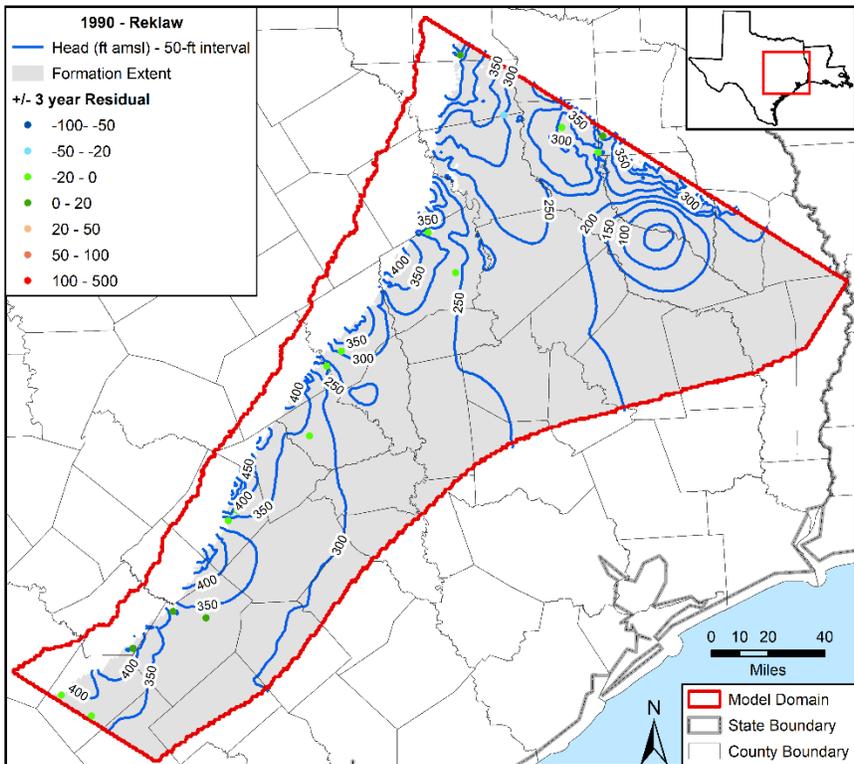
Figure 5.3.4x. Contours in feet (ft) above mean sea level (amsl) developed from simulated hydraulic heads for 1990 in the Reklaw Formation with residuals posted.
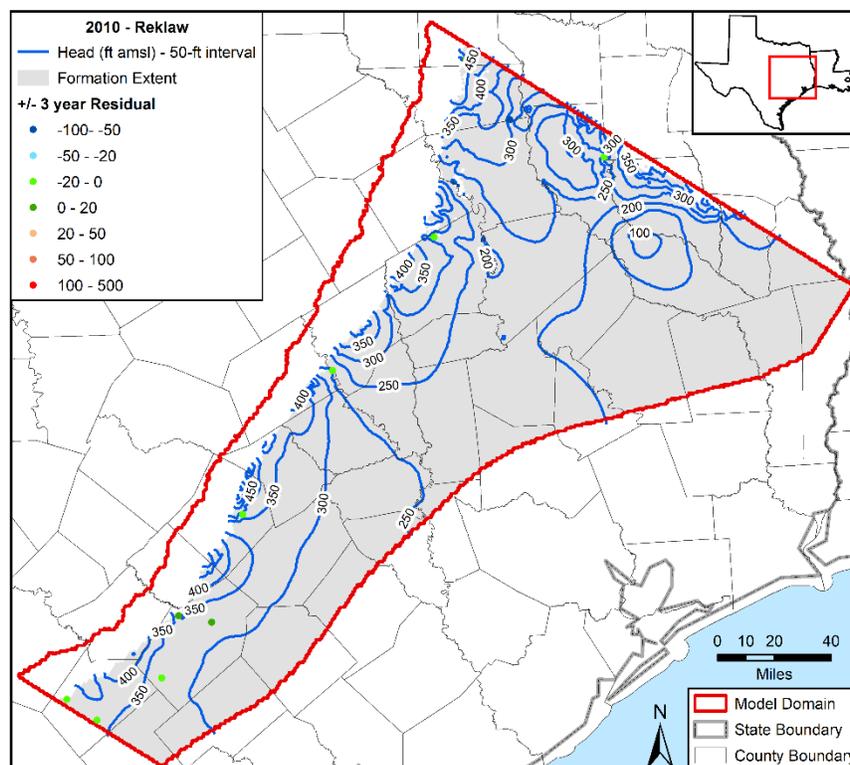
Figure 5.3.4y.   **Contours in feet (ft) above mean sea level (amsl) developed from simulated hydraulic heads for 2010 in the Reklaw Formation with residuals posted.**

Figures 5.3.4z through 5.3.4dd show contours generated from simulated hydraulic heads in the Carrizo Aquifer for steady-state conditions and the years 1950, 1970, 1990, and 2010 in the transient period. A salient feature of these figures is the development of a major cone of depression in the downdip and confined section of the aquifer in Angelina and Nacogdoches counties. The deepening and expansion of this drawdown area occurs quickly from 1930 to 1970 and then slows. At the center of the depression, the hydraulic head values decline almost 700 feet over the 80-year simulation period. Among the interesting aspects of the model are the residuals and hydraulic heads for steady-state conditions.

For the updated model, the steady-state conditions represent predevelopment conditions. Our records of historical pumping (Section 3.2) indicate that significant pumping did not begin in Angelina and Nacogdoches counties until the early 1930s. However, there are two indicators in Figure 5.3.4z that suggest that substantial pumping occurred prior to 1930. Both of these indicators involve hydraulic head residuals from the Carrizo Aquifer. One group of residuals are along the model boundary in Nacogdoches County. The small absolute values of the green-colored residuals suggest that the simulated hydraulic head contours reflect real-world groundwater conditions and that the cone of depression created by the general-head boundaries along the northeastern boundary of the model domain (see Figure 4.7a) likely represents a real cone of depression. The location of pumping that caused the reduced hydraulic heads is marked by blue-colored residuals along the Angelina/Nacogdoches counties border, which show that the model over-predicts hydraulic heads between 50 and 100 feet in this area. The suspected location

of the pumping is confirmed by the cone of depression that exists at that location in 1950 and later years.

As a result of the significant Carrizo Aquifer pumping that occurs throughout the entire simulation period, groundwater flow in the confined regions of the aquifer has a pronounced direction toward the center of the cone of depression in Angelina County. The model indicates that this pumping in Angelina County has decreased the hydraulic heads and impacted the direction of groundwater flow in the confined region of the Carrizo Aquifer across Groundwater Management Area 12.

In the updip portion of the Carrizo Aquifer, groundwater flow is compartmentalized into localized flow systems that originate near topographic highs and are characterized by semi-radial flow toward low-lying areas. This observation is consistent with the conceptual model discussed by Kelley and others (2004) and Dutton and others (2003). The simulated hydraulic head contours in the shallow and unconfined regions of the Carrizo Aquifer do not show any appreciable change over time. In the southern portion of the model and in Leon County, the numerous green-colored residuals confirm that the simulated hydraulic head values in the Carrizo Aquifer match the observed values relatively well.
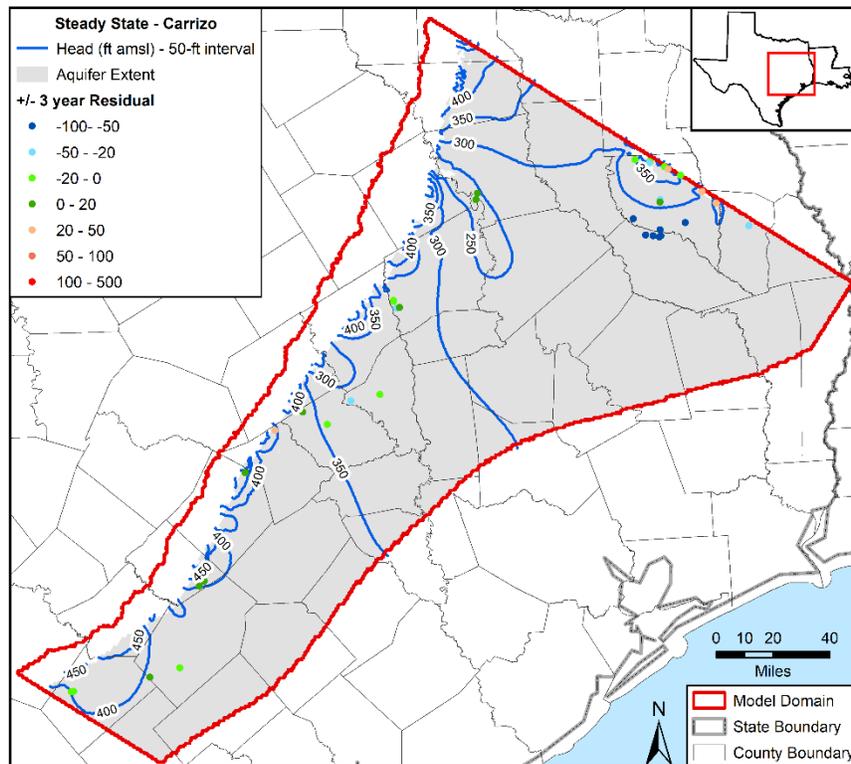
Figure 5.3.4z. Contours in feet (ft) above mean sea level (amsl) developed from simulated hydraulic heads for steady-state conditions in the Carrizo Aquifer with residuals posted.
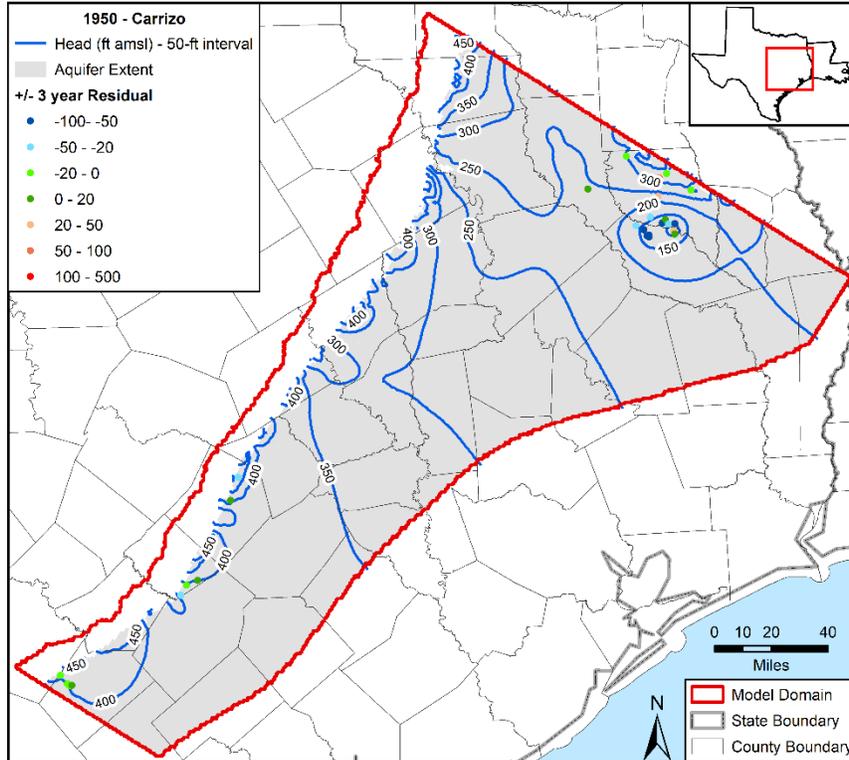
Figure 5.3.4aa. Contours in feet (ft) above mean sea level (amsl) developed from simulated hydraulic heads for 1950 in the Carrizo Aquifer with residuals posted.
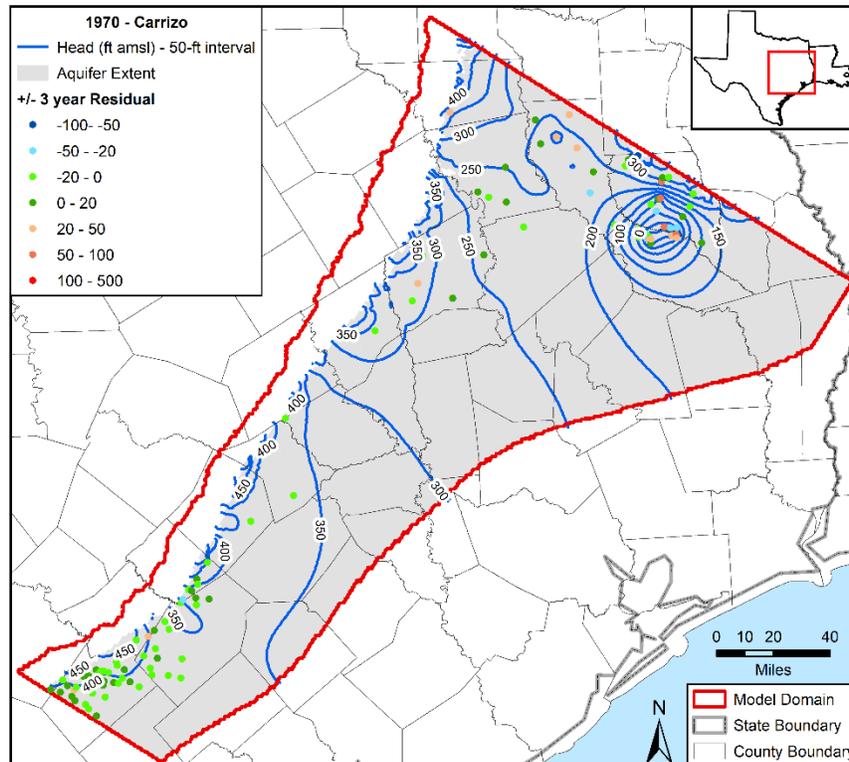
Figure 5.3.4bb. Contours in feet (ft) above mean sea level (amsl) developed from simulated hydraulic heads for 1970 in the Carrizo Aquifer with residuals posted.
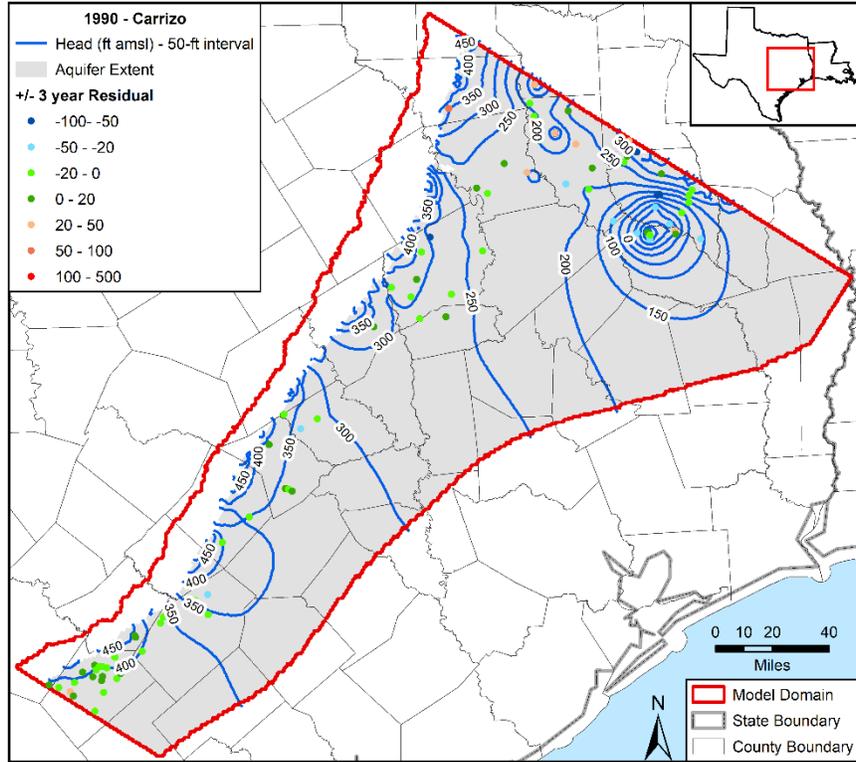
Figure 5.3.4cc. Contours in feet (ft) above mean sea level (amsl) developed from simulated hydraulic heads for 1990 in the Carrizo Aquifer with residuals posted.
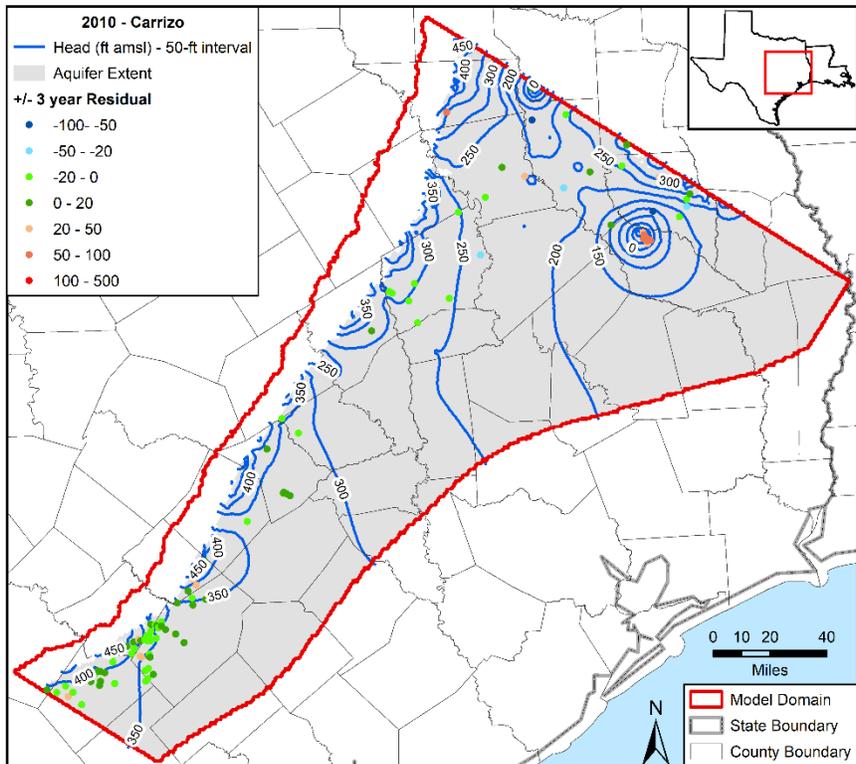
Figure 5.3.4dd. Contours in feet (ft) above mean sea level (amsl) developed from simulated hydraulic heads for 2010 in the Carrizo Aquifer with residuals posted.

Figures 5.3.4ee through 5.3.4ii show contours generated from simulated hydraulic heads in the Calvert Bluff Formation for steady-state conditions and the years 1950, 1970, 1990, and 2010 in the transient period. A prominent feature of the figures during the transient period is the similarity in the pattern of the hydraulic head contours in the confined region with the hydraulic head contours in the Carrizo Aquifer. By 1950, a cone of depression in the Calvert Bluff Formation in Angelina County is well established. Based on the similarity in the two sets of contours, the regional flow direction in the confined Calvert Bluff Formation is largely influenced by the groundwater flow field in the Carrizo Aquifer. In 1990, the contours in the confined portion of the Calvert Bluff Formation in the vicinity of Brazos County began to alter from the pattern in the Carrizo Aquifer until a notable cone of depression develops in 2010. This cone of depression is caused by pumping in the Simsboro Formation in the cities of Bryan and College Station. In the far downdip region of the Calvert Bluff Formation, groundwater flow is to the northeast and parallel to the model boundary. This is consistent with the conceptualization of approximating the Wilcox Fault Zone (see Figure 2.4a) as a no-flow boundary condition.

The hydraulic head contours indicate that a topographic-driven shallow groundwater flow zone is well established in the Calvert Bluff Formation. The Calvert Bluff Formation outcrop is about 8 to 15 miles wide, and, across most of that area, groundwater flow is compartmentalized into localized flow systems that originate near topographic highs and are characterized by semi-radial flow toward low-lying areas. The hydraulic head contours suggest that both the Brazos and Trinity rivers act as major sinks for the groundwater basin.
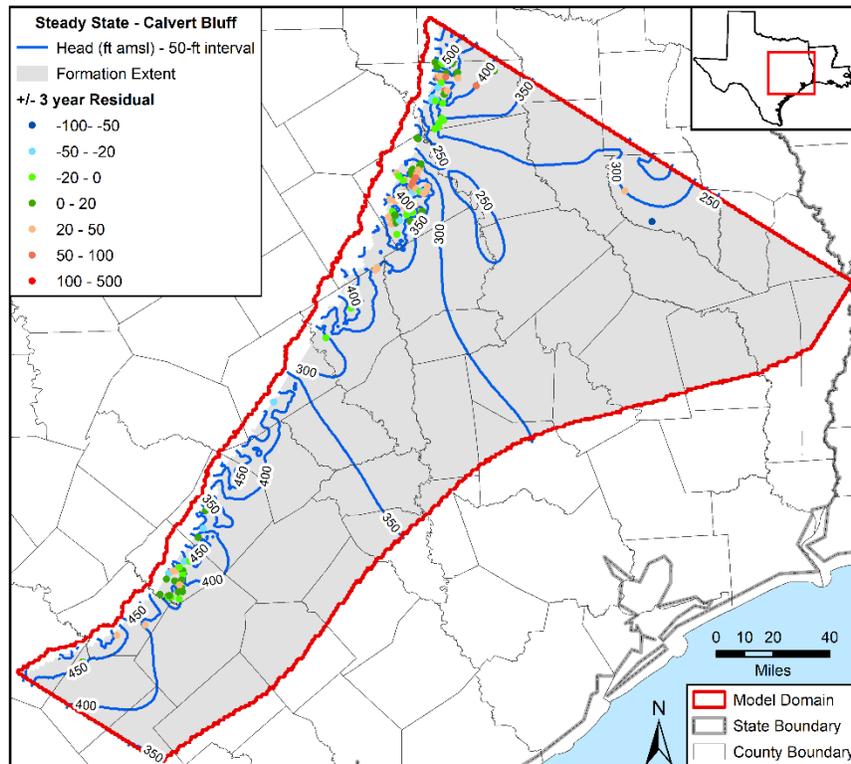
Figure 5.3.4ee.   **Contours in feet (ft) above mean sea level (amsl) developed from simulated hydraulic heads for steady-state conditions in the Calvert Bluff Formation with residuals posted.**
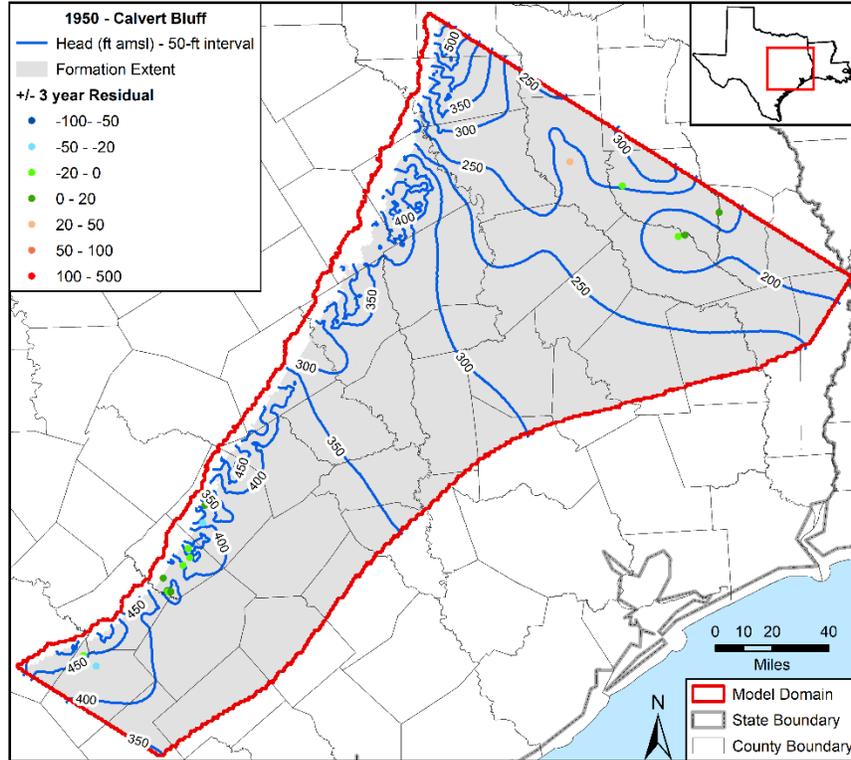
Figure 5.3.4ff. Contours in feet (ft) above mean sea level (amsl) developed from simulated hydraulic heads for 1950 in the Calvert Bluff Formation with residuals posted.
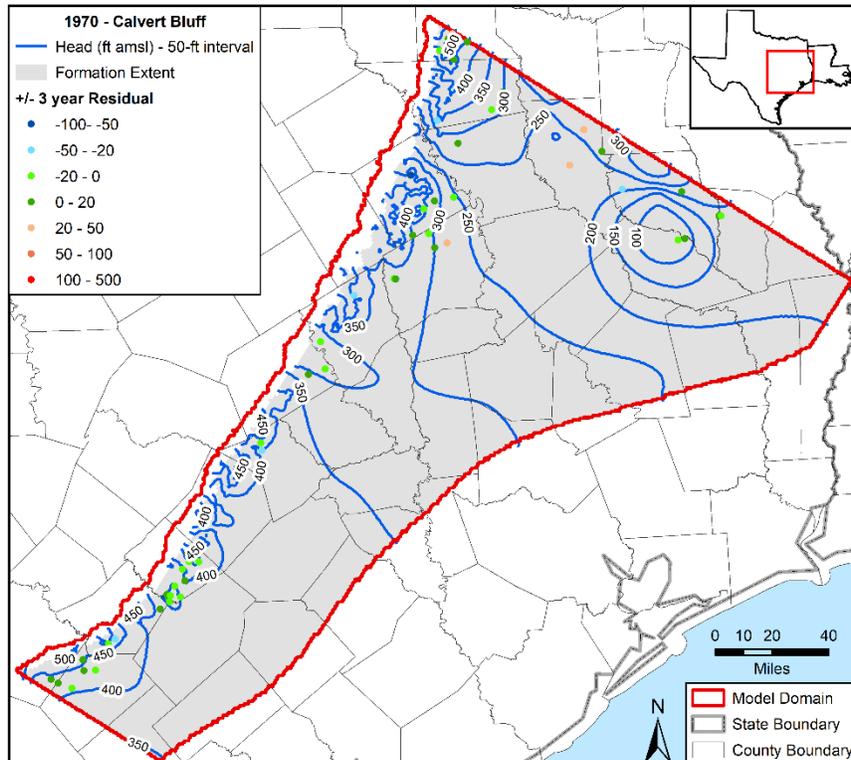
Figure 5.3.4gg. Contours in feet (ft) above mean sea level (amsl) developed from simulated hydraulic heads for 1970 in the Calvert Bluff Formation with residuals posted.
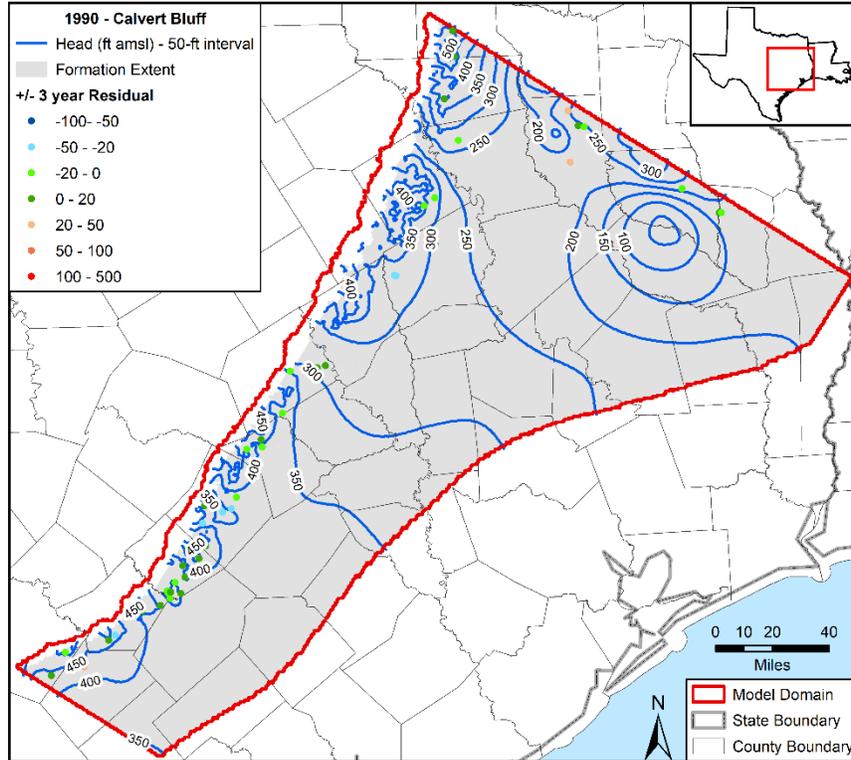
Figure 5.3.4hh. Contours in feet (ft) above mean sea level (amsl) developed from simulated hydraulic heads for 1990 in the Calvert Bluff Formation with residuals posted.
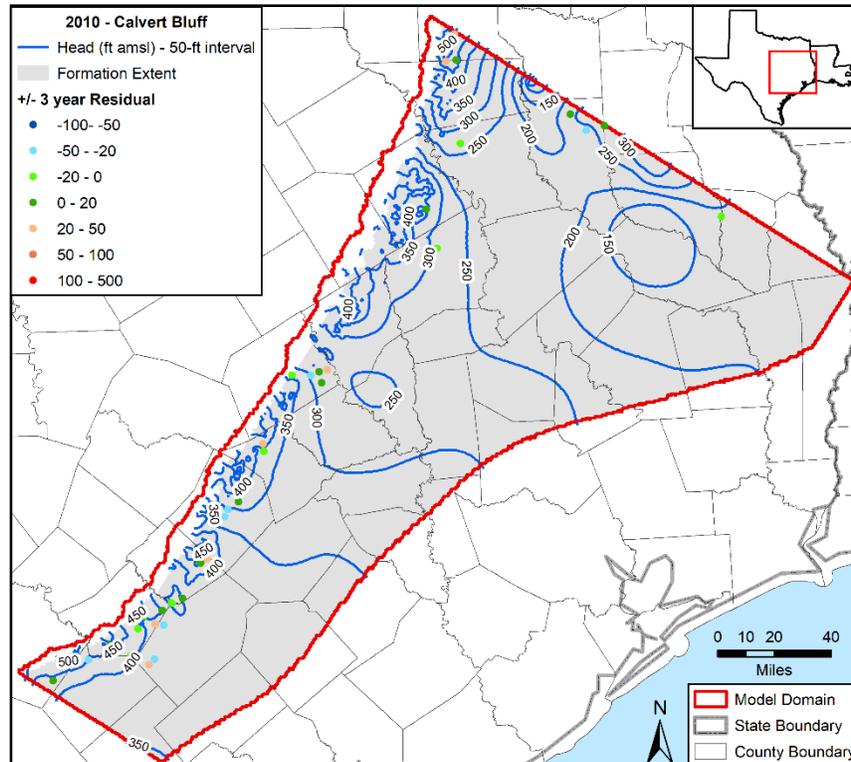
**Figure 5.3.4ii.** Contours in feet (ft) above mean sea level (amsl) developed from simulated hydraulic heads for 2010 in the Calvert Bluff Formation with residuals posted.

Figures 5.3.4jj through 5.3.4nn show contours generated from simulated hydraulic heads in the Simsboro Formation for steady-state conditions and the years 1950, 1970, 1990, and 2010 in the transient period. A prominent feature is the cone of depression centered on the city of Bryan in Brazos County that is well established in 2010. The effect of the pumping in Bryan on regional flow is evident in 1970 and continues to expand through 2010. The green-colored residuals at the center of the cone of depression indicate that the model has adequately represented the decreased hydraulic heads caused by this pumping and the groundwater flow directions around the well field. For most of the simulation period, regional flow of groundwater in the confined portion of the Simsboro Formation has a strong northeast directional component. In the southern region of the model, this northeastward flow component becomes stronger while, in the northern region of the model, it lessens with continued pumping at the City of Bryan. In the far downdip region of the Simsboro Formation, groundwater flow is to the northeast and parallel to the model boundary. This is consistent with the conceptualization of approximating the Wilcox Fault Zone (see Figure 2.4a) as a no-flow boundary condition. In the updip extent of the Simsboro Formation, groundwater flow is compartmentalized into localized flow systems that originate near topographic highs and are characterized by semi-radial flow toward low-lying areas. The presence of these local systems is supported by the hydraulic head contours and the green colored and light-blue colored residuals. The hydraulic head contours suggest that the Colorado, Brazos, and Trinity rivers act as major sinks for groundwater flow from the Simsboro Formation.
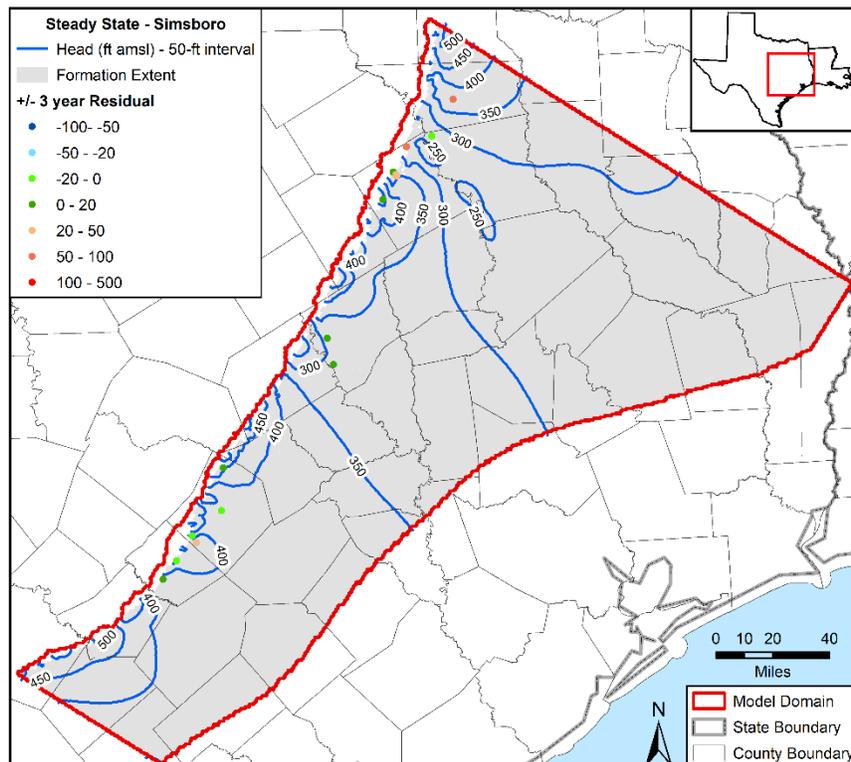
Figure 5.3.4jj.   **Contours in feet (ft) above mean sea level (amsl) developed from simulated hydraulic heads for steady-state conditions in the Simsboro Formation with residuals posted.**
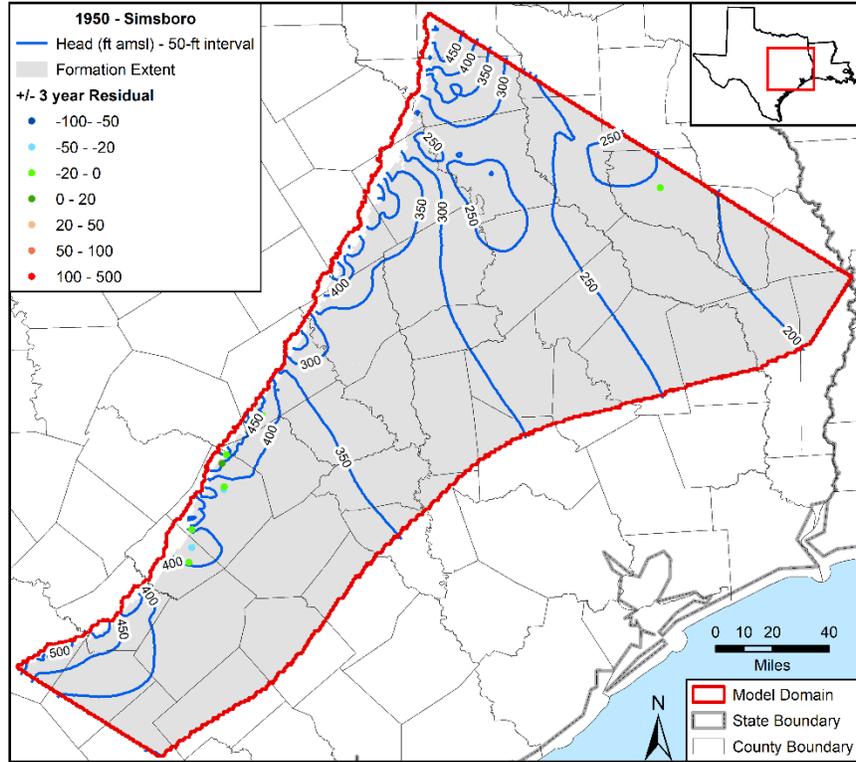
Figure 5.3.4kk. Contours in feet (ft) above mean sea level (amsl) developed from simulated hydraulic heads for 1950 in the Simsboro Formation with residuals posted.
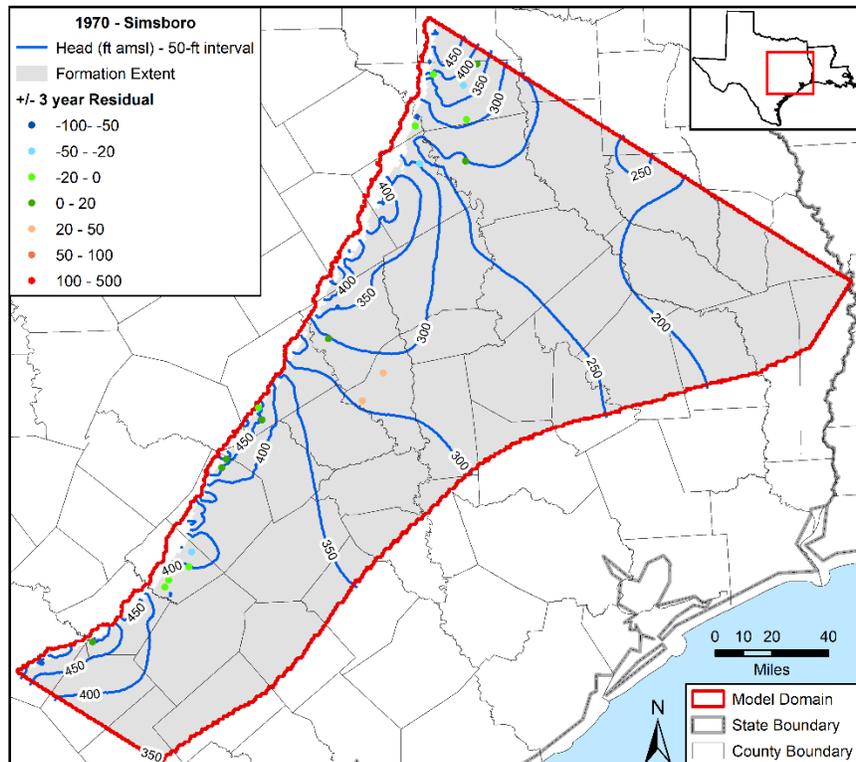

Figure 5.3.4ll. Contours in feet (ft) above mean sea level (amsl) developed from simulated hydraulic heads for 1970 in the Simsboro Formation with residuals posted.
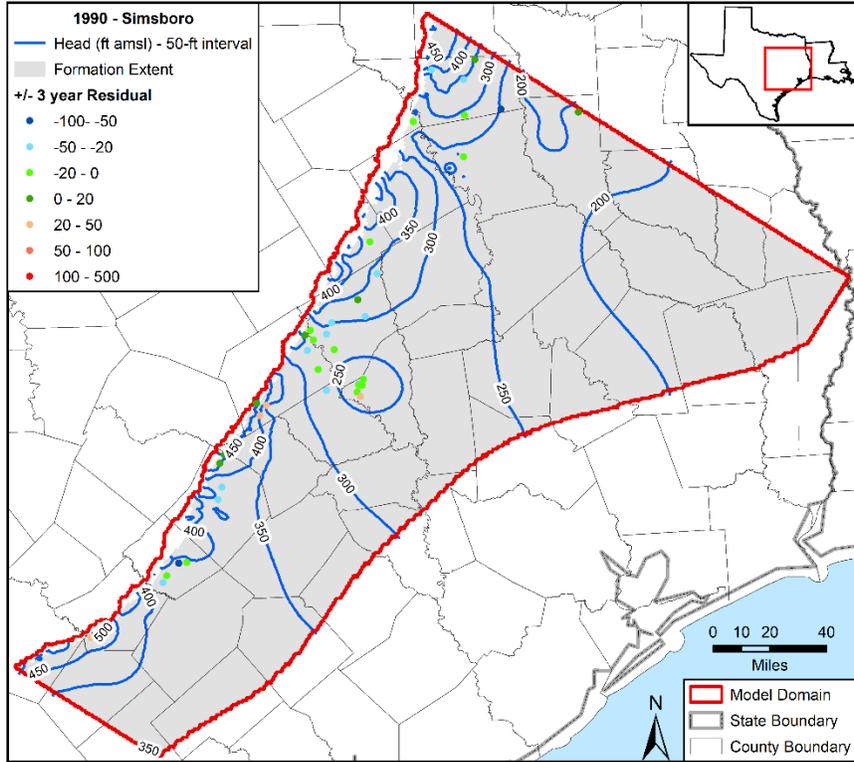
Figure 5.3.4mm. Contours in feet (ft) above mean sea level (amsl) developed from simulated hydraulic heads for 1990 in the Simsboro Formation with residuals posted.
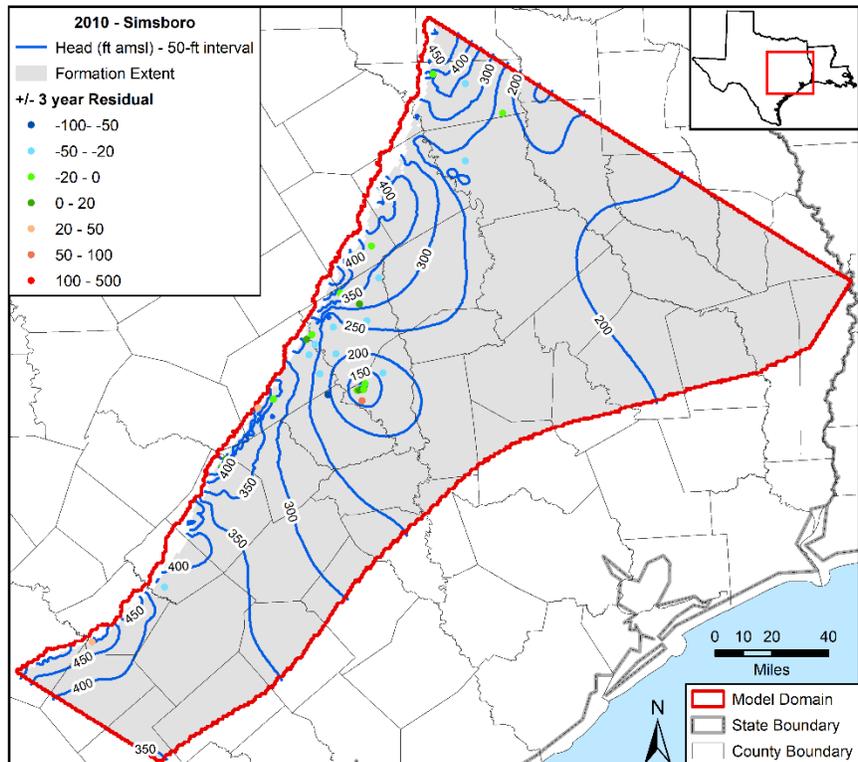
Figure 5.3.4nn. Contours in feet (ft) above mean sea level (amsl) developed from simulated hydraulic heads for 2010 in the Simsboro Formation with residuals posted.

Figures 5.3.4oo through 5.3.4ss show contours generated from simulated hydraulic heads in the Hooper Formation for steady-state conditions and the years 1950, 1970, 1990, and 2010 in the transient period. Groundwater flow in the downdip region is characterized by a predominate northeast directional component that indicates that groundwater is flowing parallel along the downdip boundary of the model. This flow direction is consistent with the conceptualization of approximating the Wilcox Fault Zone (see Figure 2.4a) as a no-flow boundary condition. Changes in the location of contour lines with time in Robertson and Brazos counties is evidence that pumping from Simsboro Formation wells near the city of Bryan is impacting hydraulic heads in the Hooper Formation. However, the effect on the flow pattern is less than that in the Calvert Bluff Formation. Like all of the other aquifers, the hydraulic head contours in the updip regions of the Hooper Formation suggest that groundwater flow is compartmentalized into localized flow systems that originate near topographic highs and are characterized by semi-radial flow toward low-lying areas. Across much of the Hooper Formation outcrop, the contours are accompanied by green-colored residuals, which indicate that the simulated hydraulic heads provide a reasonable match to observed measurements. The hydraulic head contours suggest that the Colorado, Brazos, and Trinity rivers act as major sinks for groundwater flow from the Hooper Formation. With regard to inferred regional flow directions in the downdip and updip regions of the aquifer, the simulated flow directions are consistent with the conceptual flow model discussed by Dutton and others (2003) and Kelley and others (2004).
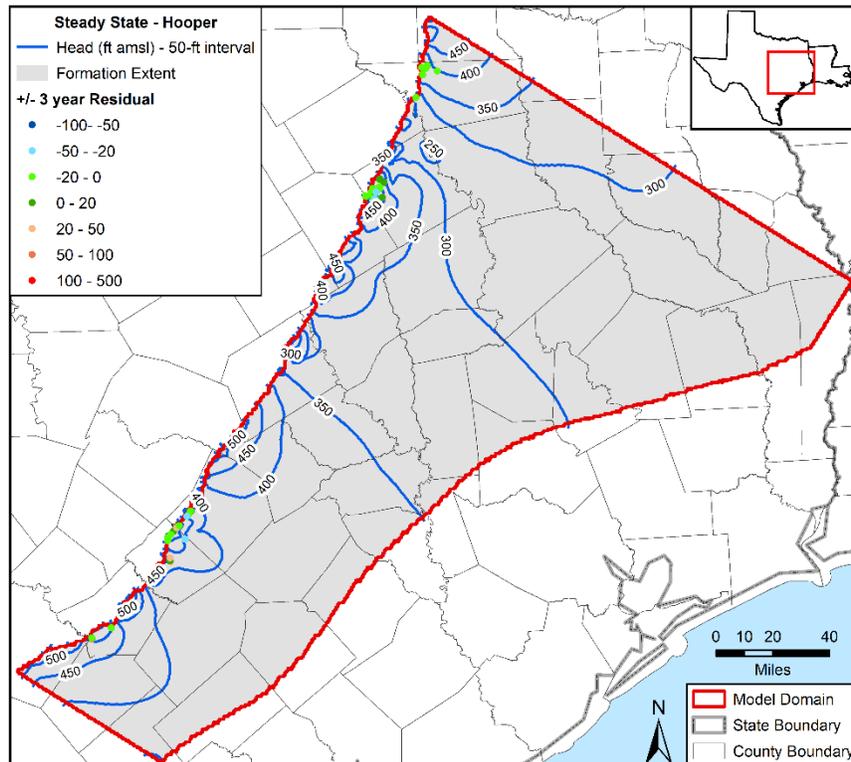

Figure 5.3.4oo. Contours in feet (ft) above mean sea level (amsl) developed from simulated hydraulic heads for steady-state conditions in the Hooper Formation with residuals posted.
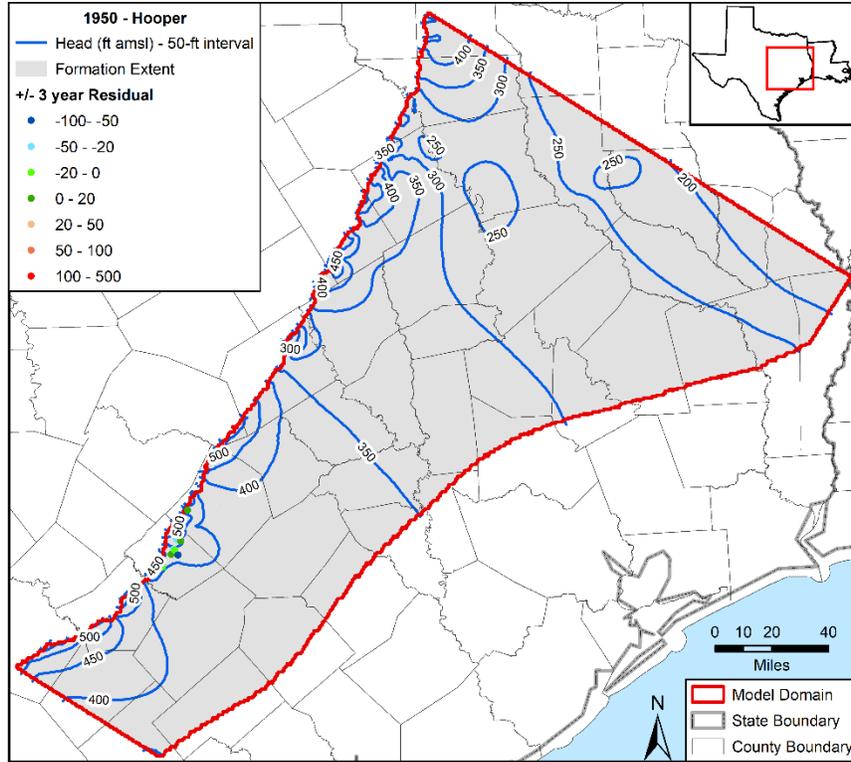
Figure 5.3.4pp.   Contours in feet (ft) above mean sea level (amsl) developed from simulated hydraulic heads for 1950 in the Hooper Formation with residuals posted.
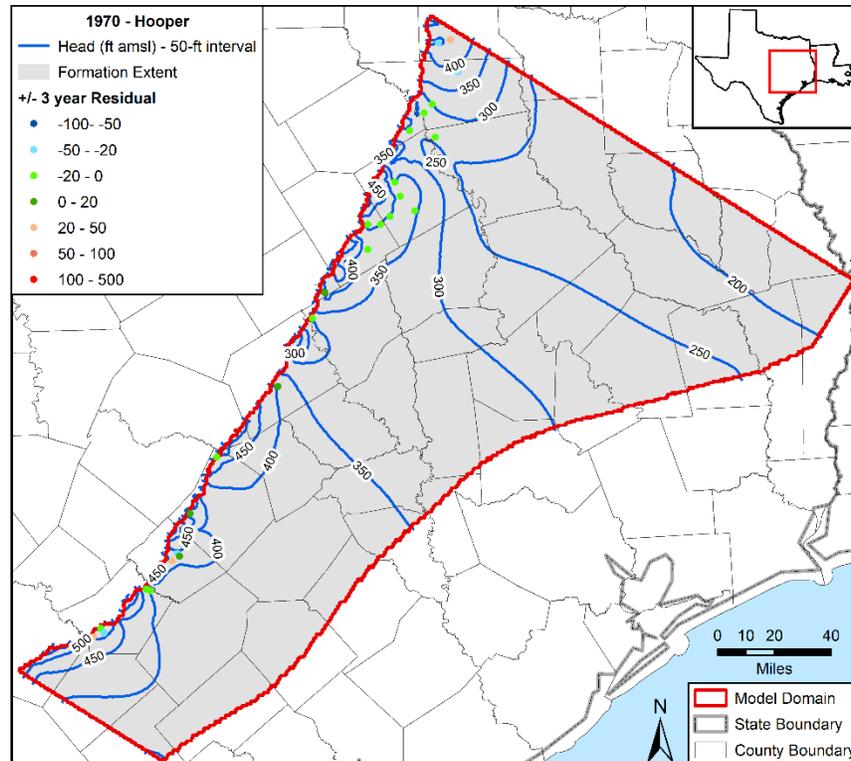
Figure 5.3.4qq.   Contours in feet (ft) above mean sea level (amsl) developed from simulated hydraulic heads for 1970 in the Hooper Formation with residuals posted.
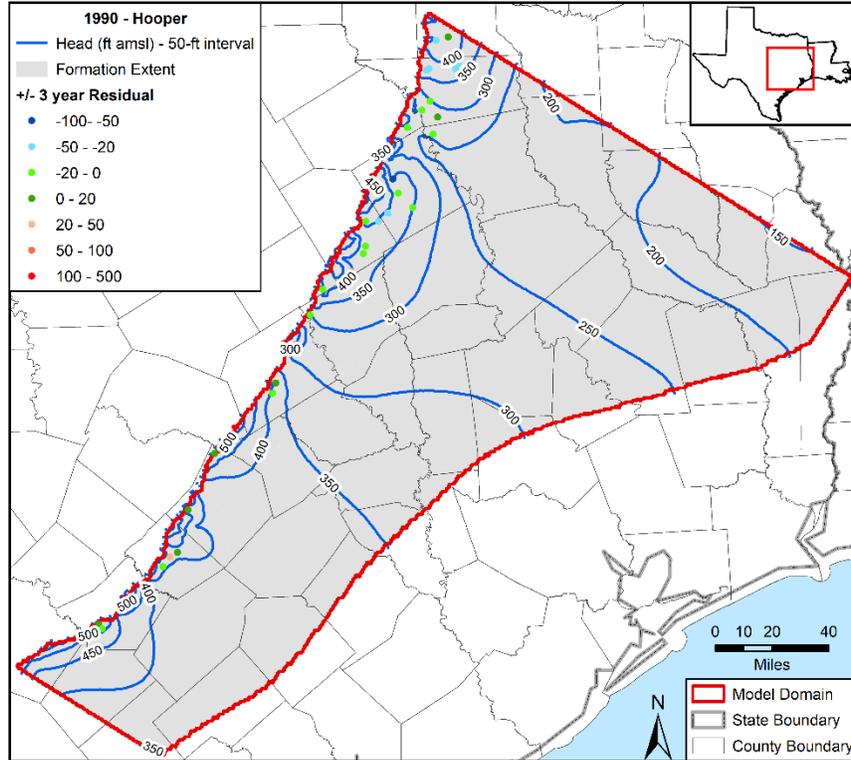
Figure 5.3.4rr. Contours in feet (ft) above mean sea level (amsl) developed from simulated hydraulic heads for 1990 in the Hooper Formation with residuals posted.
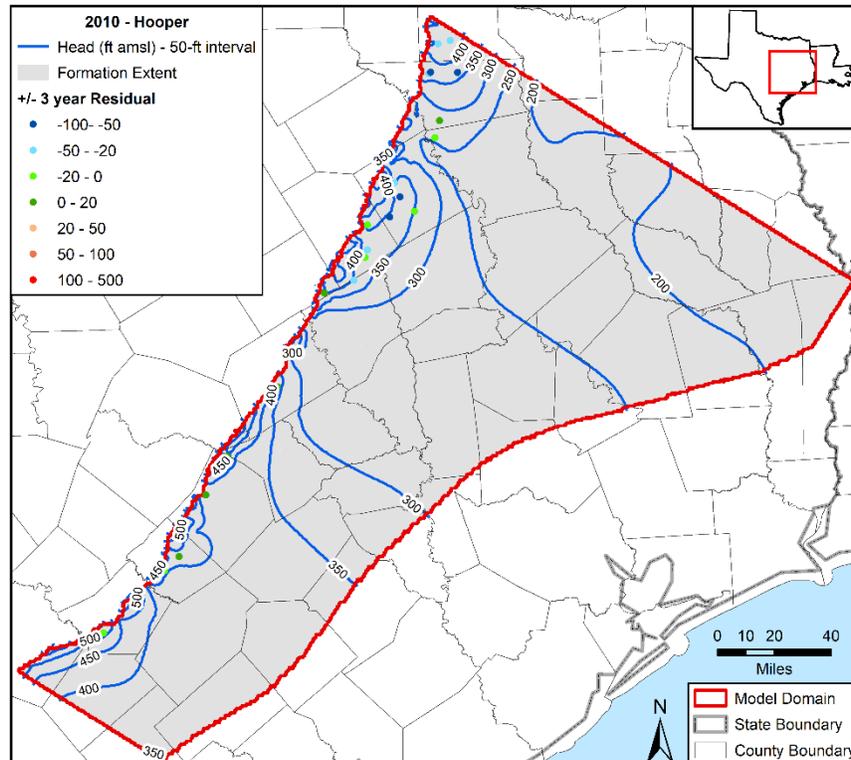

Figure 5.3.4ss. Contours in feet (ft) above mean sea level (amsl) developed from simulated hydraulic heads for 2010 in the Hooper Formation with residuals posted.

5.3.5 *Simulated Drawdowns*

Figures 5.3.5a through 5.3.5i show the simulated change in hydraulic head from the start of the transient period in 1930 to the end of the transient period in 2010 plotted as drawdown. The drawdown was calculated at each grid cell as the predicted hydraulic head in 2010 minus the predicted steady-state hydraulic head. The figures show drawdown contours for each of the nine hydrogeologic units.

Figure 5.3.5a shows contours of the simulated drawdown for the Colorado and Brazos rivers alluvium. The maximum simulated drawdown is less than 20 feet in the Colorado River alluvium and less than 30 feet in the Brazos River alluvium. Across both alluviums, most of the area has a drawdown of less than 10 feet. The area with the highest drawdown is in southern Robertson County, where significant pumping in the Brazos River alluvium has occurred since 2004.

Figures 5.3.5b, 5.3.5c, and 5.3.5d show contours of the simulated drawdown for the Sparta Aquifer, Weches Formation, and Queen City Aquifer, respectively. The drawdown patterns for these three hydrogeologic units are similar. Across the confined regions, the drawdown typically ranges between 50 and 125 feet, with drawdowns greater than 100 feet occurring in the southern portion of the model. In the outcrops, the drawdown values are typically less than 25 feet. The general trend is lower drawdowns updip and larger drawdowns downdip.

Figures 5.3.5e and 5.3.5f show contours of the simulated drawdown for the Reklaw Formation and the Carrizo Aquifer, respectively. These two hydrogeologic units have similar patterns in their drawdown contours. The prominent features in both units are cones of depression in the northern part of the model caused by pumping in the Carrizo Aquifer. In the Carrizo Aquifer, the greatest drawdowns occur in northwest Angelina County where the cone of depression, as defined by the 150-foot contour, encompasses an area of about 729 square miles and has a maximum drawdown of 450 feet. A second, smaller cone of depression exists at the corner of Cherokee and Smith counties. This cone of depression encompasses drawdowns greater than 150 feet across about 225 square miles and has a maximum drawdown of 410 feet. The shapes of these cones of depression are evident in the drawdown contours for the Reklaw Formation, but these magnitudes are less than those in the Carrizo Aquifer. The maximum drawdown in the Reklaw Formation for the cones of depression in Angelina County and near the Smith/Cherokee counties boundary is 235 and 195 feet, respectively. In the southern and central regions of the model, the drawdowns are much lower, between 25 and 75 feet, for most of the region, with lower values occurring near the outcrops and higher values occurring downdip.

Figures 5.3.5g, 5.3.5h, and 5.3.5i show contours of the simulated drawdown for the Calvert Bluff, Simsboro, and Hooper formations, respectively. In Groundwater Management Area 12, the most salient feature in these figures is the drawdowns associated with a cone of depression centered in Brazos County caused by pumping in the Simsboro Formation in the cities of Bryan and College Station. In the Simsboro Formation, this cone of depression encompasses drawdowns greater than 150 feet across 380 square miles and has a maximum drawdown of 250 feet. A potentially important feature about the pumping in Brazos County is that the cone of influence is skewed to the downdip side. In the Simsboro Formation outcrop, the drawdown values are typically less than 25 feet. In the Simsboro Formation, the highest drawdown values

occur in the central region of the model as a result of the pumping in the cities of Bryan and College Station.

The impact of the pumping in the Simsboro Formation in Brazos County is evident in the drawdown contours for the Calvert Bluff and Hooper formations. At the same location where the maximum drawdown occurs in the Simsboro Formation, the drawdown in the Calvert Bluff and Hooper formations is about 75 feet. Across the Hooper Formation, the drawdown generally increases in the confined regions toward the northeast. Values are the lowest in the southern region of the model, where drawdowns are typically less than 25 feet, and highest in the northern region, where drawdowns are typically between 50 and 100 feet. This spatial trend is similar for the Calvert Bluff Formation. Values are generally the lowest in the southern region of the model, where drawdowns are typically less than 40 feet, and highest in the northern region, where drawdowns are typically between than 75 and 100 feet. However, the Carrizo Aquifer pumping in Angelina County and near the Smith/Cherokee counties boundary has also resulted in cones of depression with maximum drawdowns of 175 and 335 feet, respectively, in the Calvert Bluff Formation.
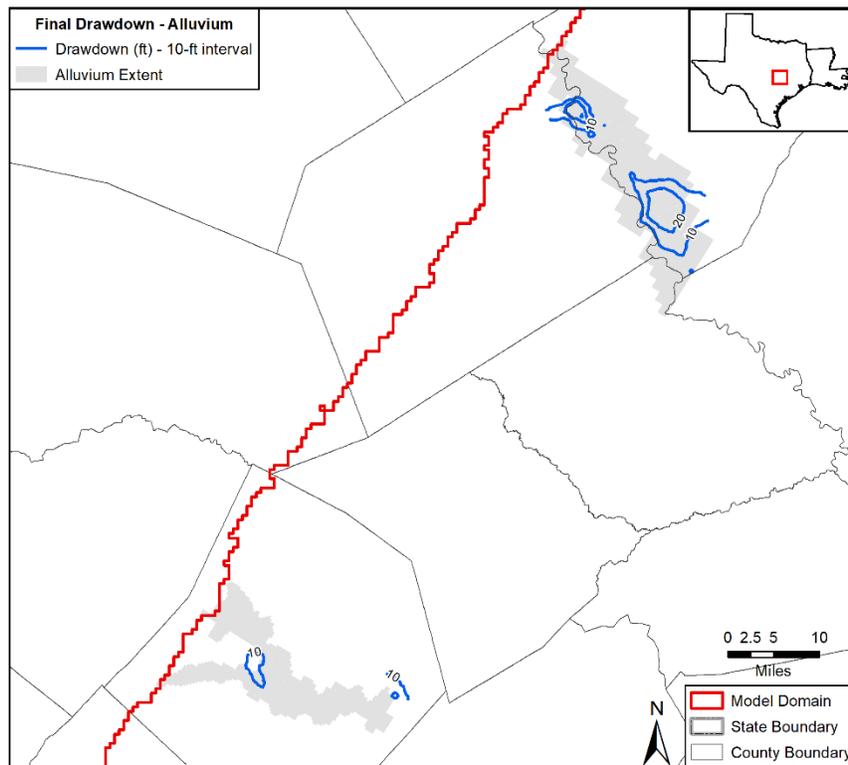
Figure 5.3.5a.   **Contours of the change in hydraulic head (drawdown) in the Colorado River alluvium and the Brazos River alluvium from 1930 to 2010.**
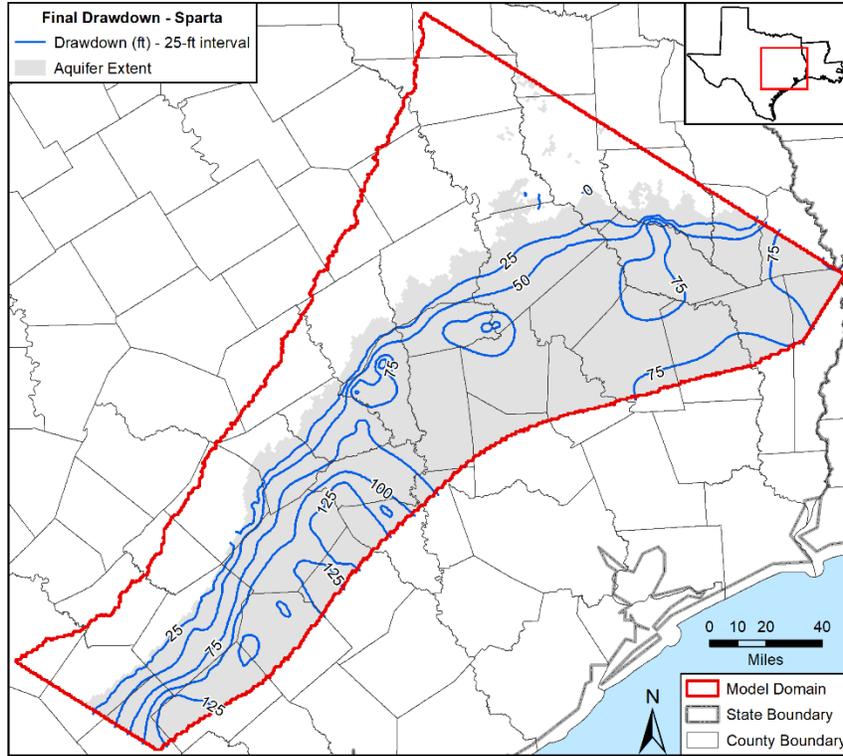
Figure 5.3.5b.   **Contours of the change in hydraulic head (drawdown) in the Sparta Aquifer from 1930 to 2010.**
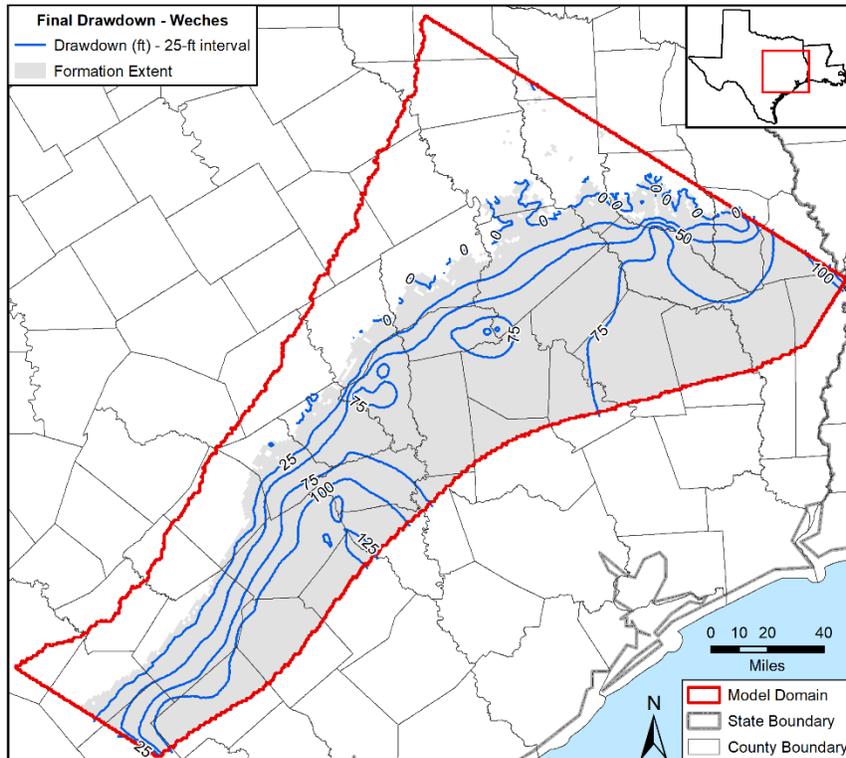
Figure 5.3.5c.   **Contours of the change in hydraulic head (drawdown) in the Weches Formation from 1930 to 2010.**
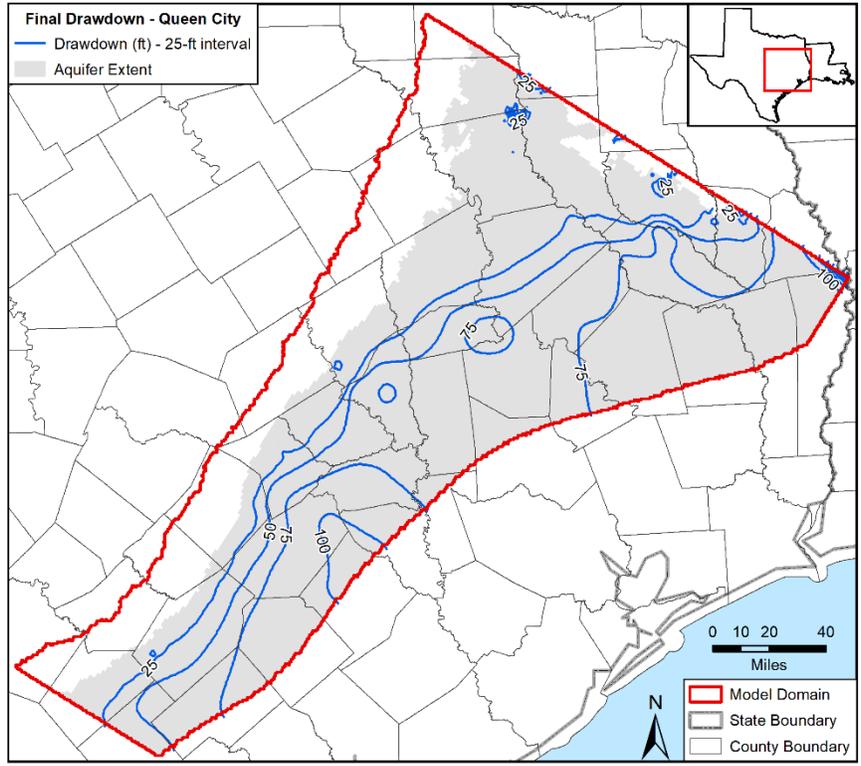
Figure 5.3.5d. **Contours of the change in hydraulic head (drawdown) in the Queen City Aquifer from 1930 to 2010.**
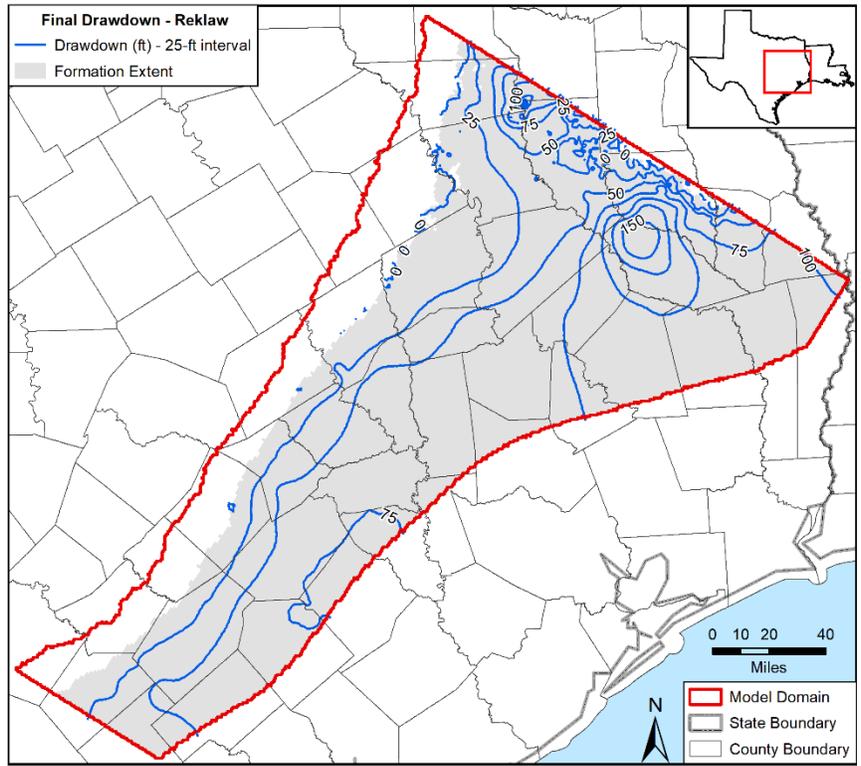
Figure 5.3.5e. **Contours of the change in hydraulic head (drawdown) in the Reklaw Formation from 1930 to 2010.**
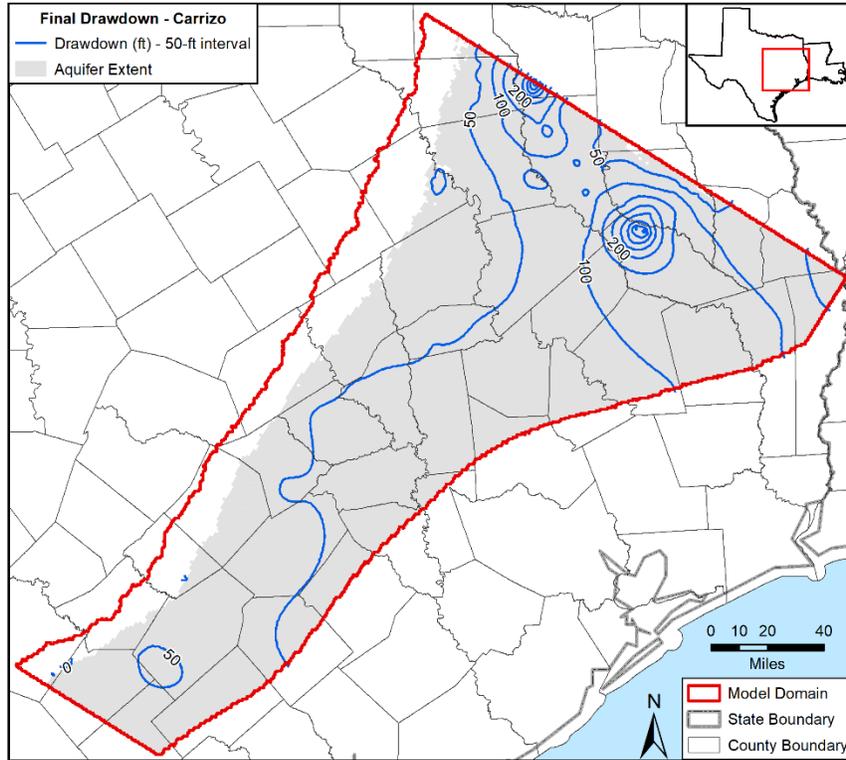
Figure 5.3.5f. **Contours of the change in hydraulic head (drawdown) in the Carrizo Aquifer from 1930 to 2010.**
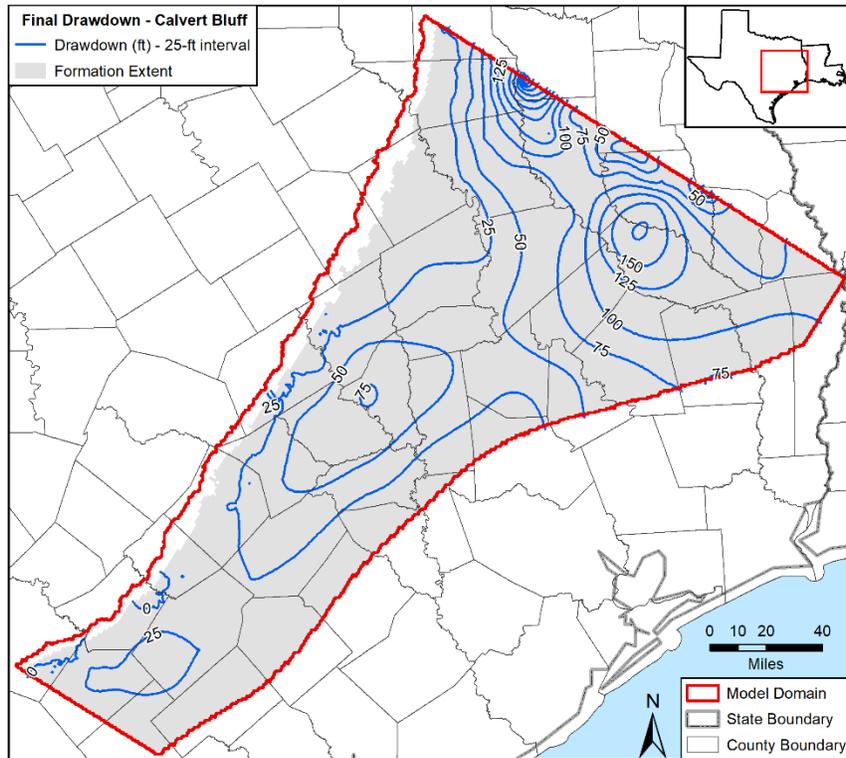
Figure 5.3.5g. **Contours of the change in hydraulic head (drawdown) in the Calvert Bluff Formation from 1930 to 2010.**
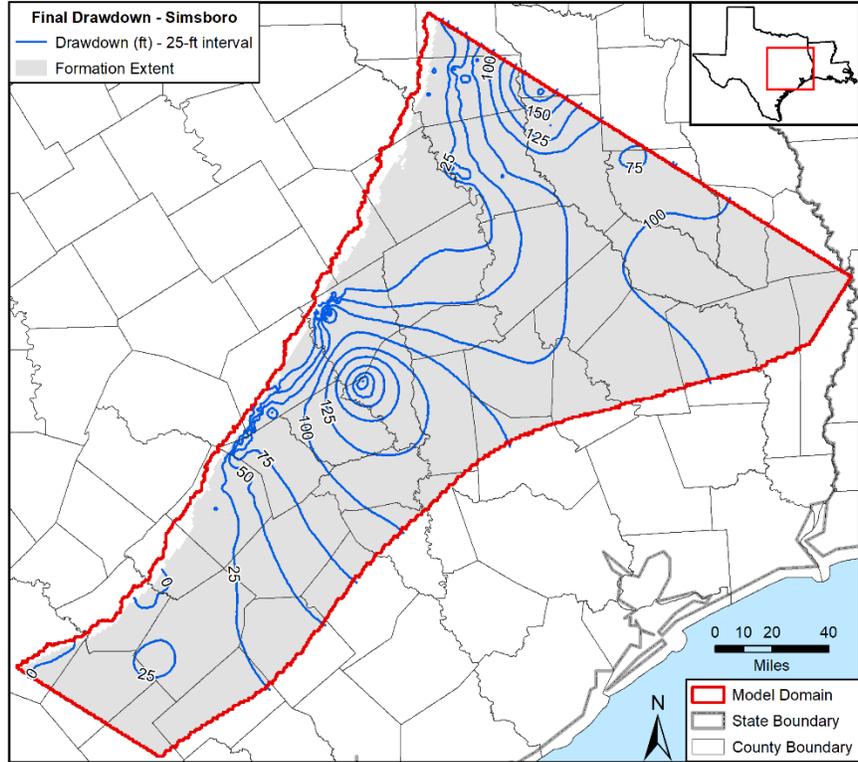
Figure 5.3.5h. Contours of the change in hydraulic head (drawdown) in the Simsboro Formation from 1930 to 2010.
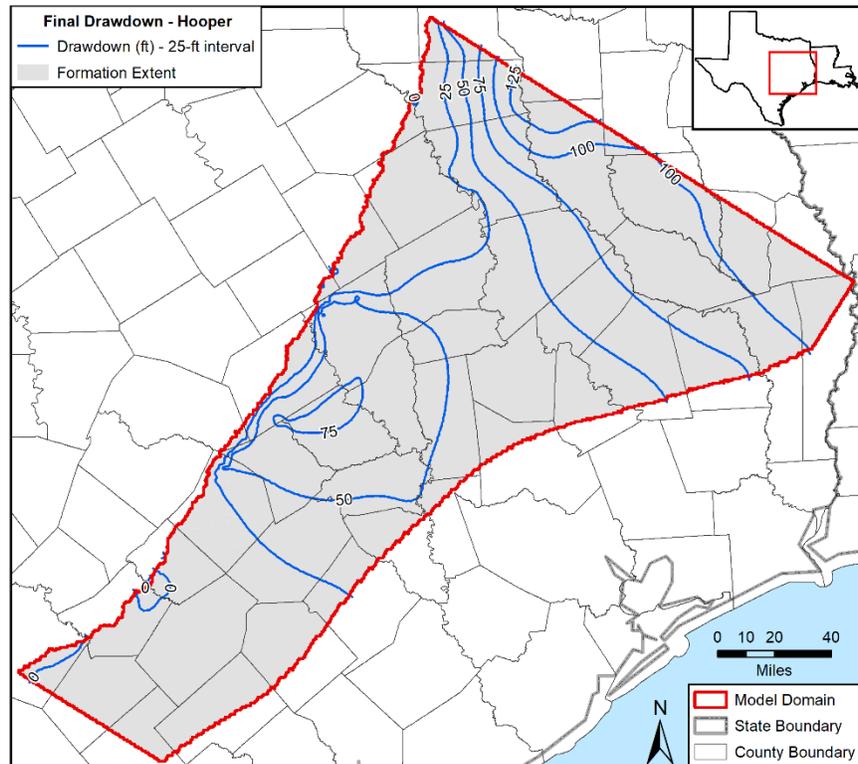
Figure 5.3.5i. Contours of the change in hydraulic head (drawdown) in the Hooper Formation from 1930 to 2010.

5.3.6   Simulated Hydrographs

Figures 5.3.6a through 5.3.6j show hydrographs for 80 wells. The wells are identified by their seven-digit state well number and grouped according to groundwater conservation district and/or groundwater management area. Each figure shows three sets of hydraulic head data for the well: measured hydraulic head values (blue lines), hydraulic heads simulated by the model for the middle of the grid cell or node containing the well (dotted red line), and hydraulic heads interpolated from the nodal values onto the location of the well (solid red line). Appendix M provides hydrographs for all 647 wells used for the transient calibration.

Figures 5.3.6a and 5.3.6b show 16 hydrographs at wells in Milam and Burleson counties, which are managed by the Post Oak Savannah Groundwater Conservation District. The locations of the wells provide good coverage with respect to geography and the different hydrogeologic units. All of the hydrographs show a favorable comparison between observed and simulated values.

Figures 5.3.6c and 5.3.6d show 16 hydrographs at wells in Robertson and Brazos counties, which are managed by the Brazos Valley Groundwater Conservation District. These wells were selected to provide good coverage across Robertson County and in the vicinity of where the Simsboro Formation is being pumped in northern Brazos County. The Simsboro Formation hydrographs in Brazos County show that the model does a very good job reproducing the 150 feet of drawdown at five locations. In Robertson County, the model's match to drawdown in the Simsboro Formation is not quite as good but, nonetheless, provides a reasonable and acceptable match to the historical drawdown, given that all of the pumping may not be properly accounted for in the Wilcox Aquifer. For hydrographs in Robertson County where drawdown values are small, the model does a very good job of matching the measured values.

Figures 5.3.6e and 5.3.6f show 16 hydrographs at wells in Lee and Bastrop counties, which are managed by the Lost Pines Groundwater Conservation District. The locations of the wells provide good coverage with respect to geography and the different hydrogeologic units. Except for two wells, the hydrographs show relatively constant hydraulic head elevations. For the majority of these hydrographs, the model does a very good job of matching the measured hydraulic head elevations. The two wells with measured drawdowns greater than 25 feet are in the Carrizo Aquifer. For these two wells, the model provides a favorable match to the measured hydraulic heads.

Figures 5.3.6g and 5.3.6hf show 16 hydrographs at wells in Leon, Madison, and Freestone counties, which are managed by the Mid-East Groundwater Conservation District. These wells provide good geographic coverage across Madison and Leon counties and the southern portion of Freestone County. For the nine wells that have less than 25 feet of measured drawdown, the model provides reasonably good matches. Vertical offsets of more than 20 feet occur at two wells. For the seven wells that have more than 25 feet of measured change in hydraulic head, the model provides good matches, except for well 3843101, which is in the Carrizo Aquifer. A possible reason for the lack of a simulated drawdown response is that the model may not have pumping adequately represented in the Carrizo Aquifer near that well.

Figure 5.3.6i shows eight hydrographs at wells in Fayette County, which is managed by the Fayette County Groundwater Conservation District, and in three counties in Groundwater

Management Area 13. The wells are located in the Sparta and Carrizo aquifers and the Calvert Bluff Formation. Three of the eight hydrographs have measured drawdowns that are greater than 25 feet. For all the wells, the model provides good matches to the measured hydraulic heads.

Figure 5.3.6j shows eight hydrographs at wells in Groundwater Management Area 11. Four of the wells have measurement drawdowns between 125 and 400 feet. The model does a reasonably good job of capturing the time and the magnitude of the aquifer drawdown responses. At the other four wells, the measured drawdowns are less than 25 feet. At those wells, the model does a good job of simulating the measured water levels.
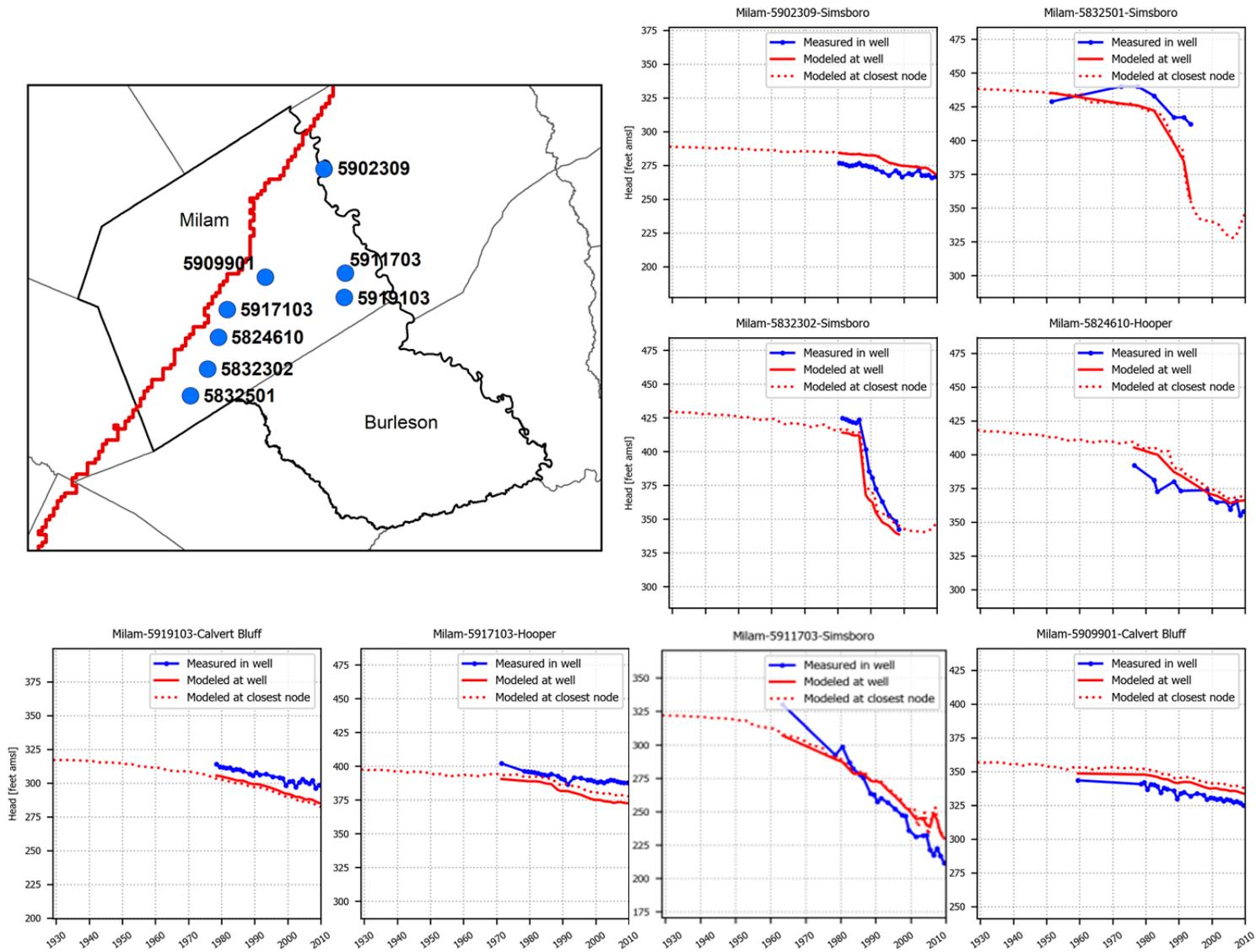
Figure 5.3.6a. Hydrographs showing simulated and measured hydraulic heads (in feet above mean sea level) in the Post Oak Savannah Groundwater Conservation District at eight wells with state well numbers 5902309, 5832501, 5832302, 5824610, 5911703, 5917103, 5911402, and 5909901.
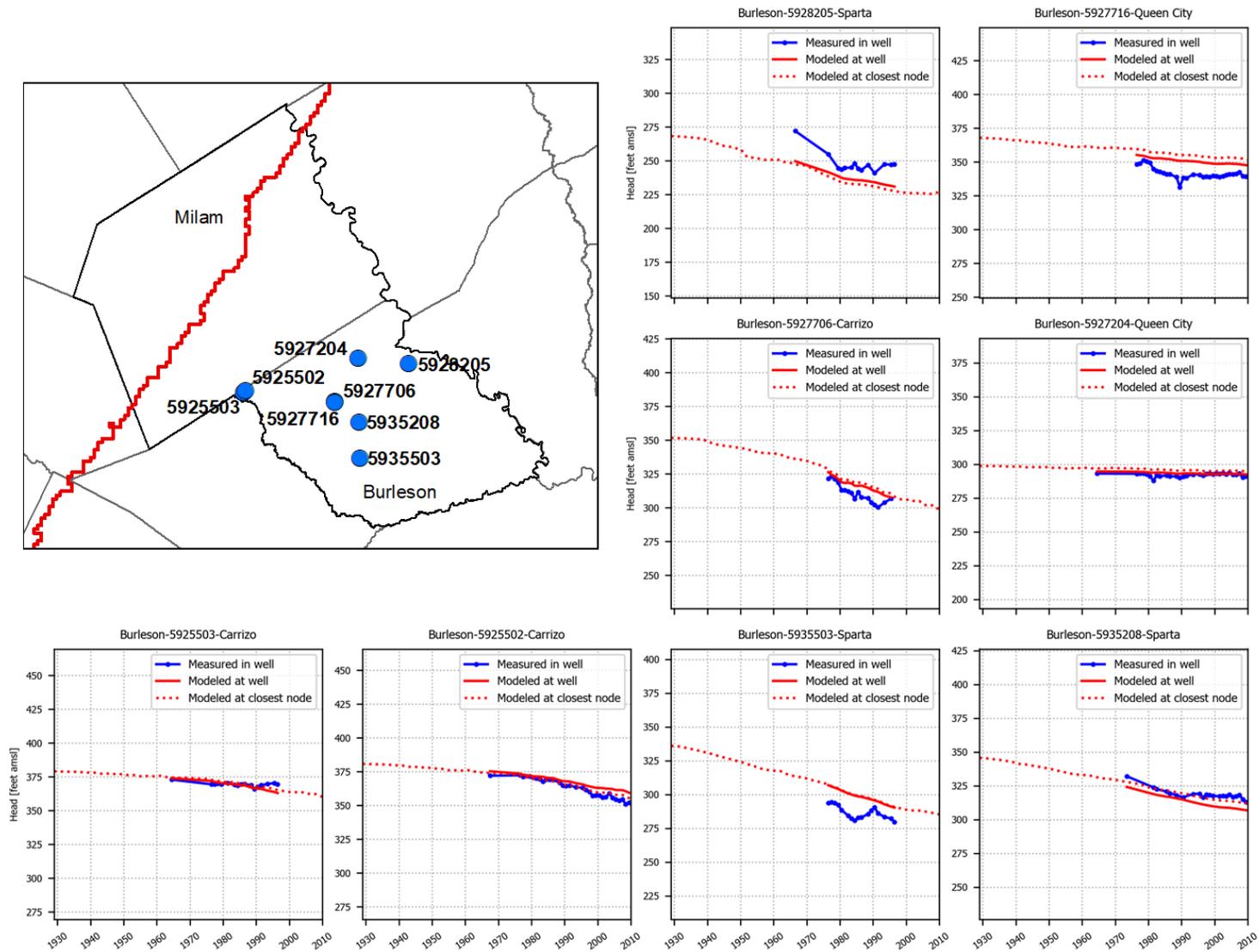
Figure 5.3.6b. Hydrographs showing simulated and measured hydraulic heads (in feet above mean sea level) in the Post Oak Savannah Groundwater Conservation District at eight wells with state well numbers 5928205, 5927716, 5927706, 5927204, 5925503, 5925502, 5935503, 5935208.
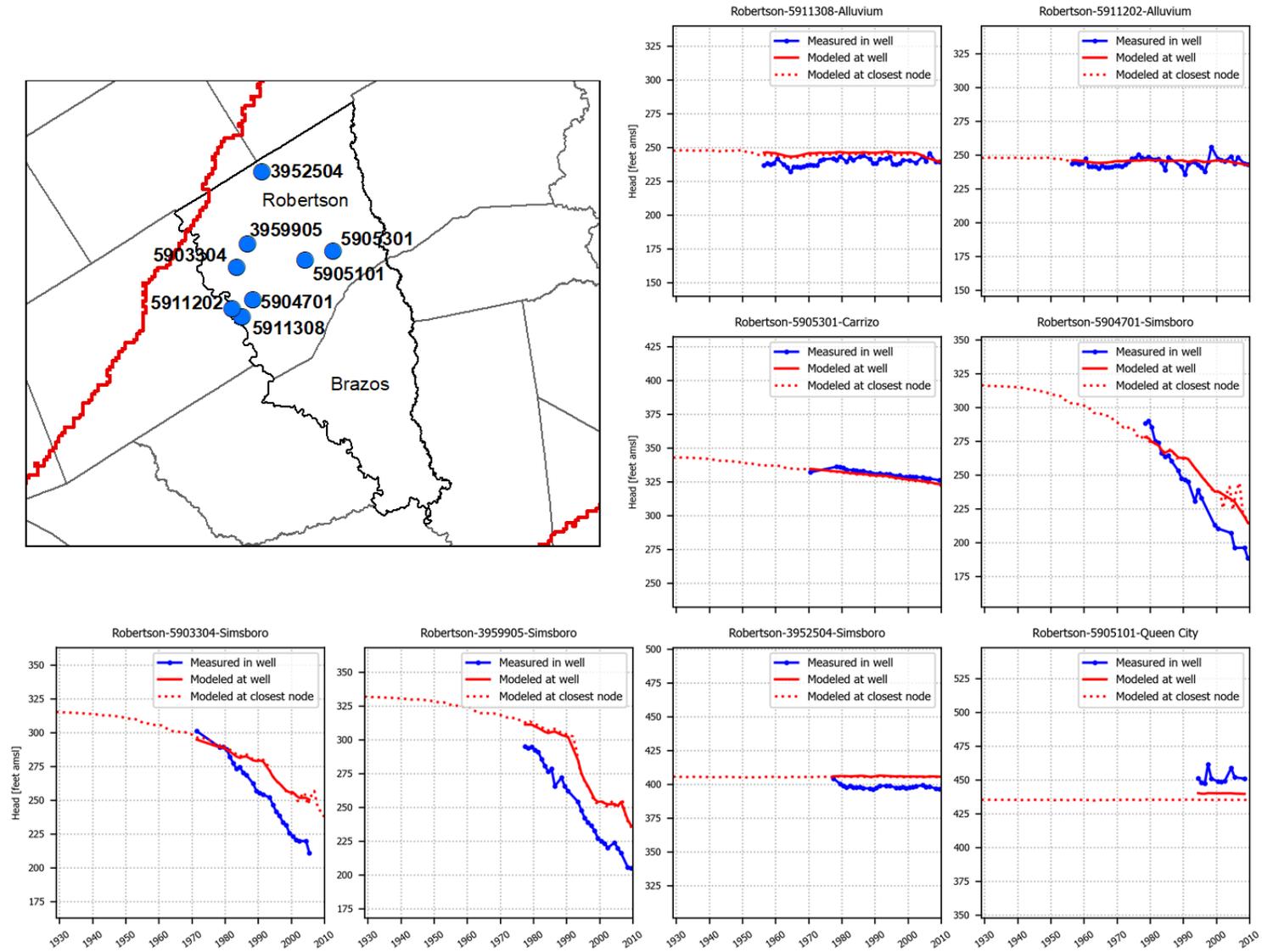
Figure 5.3.6c. Hydrographs showing simulated and measured hydraulic heads (in feet above mean sea level) in the Brazos Valley Groundwater Conservation District at eight wells with state well numbers 5911308, 5911202, 05905301, 05904701, 05903304, 03959905, 03952504, 03952504, 05905101.
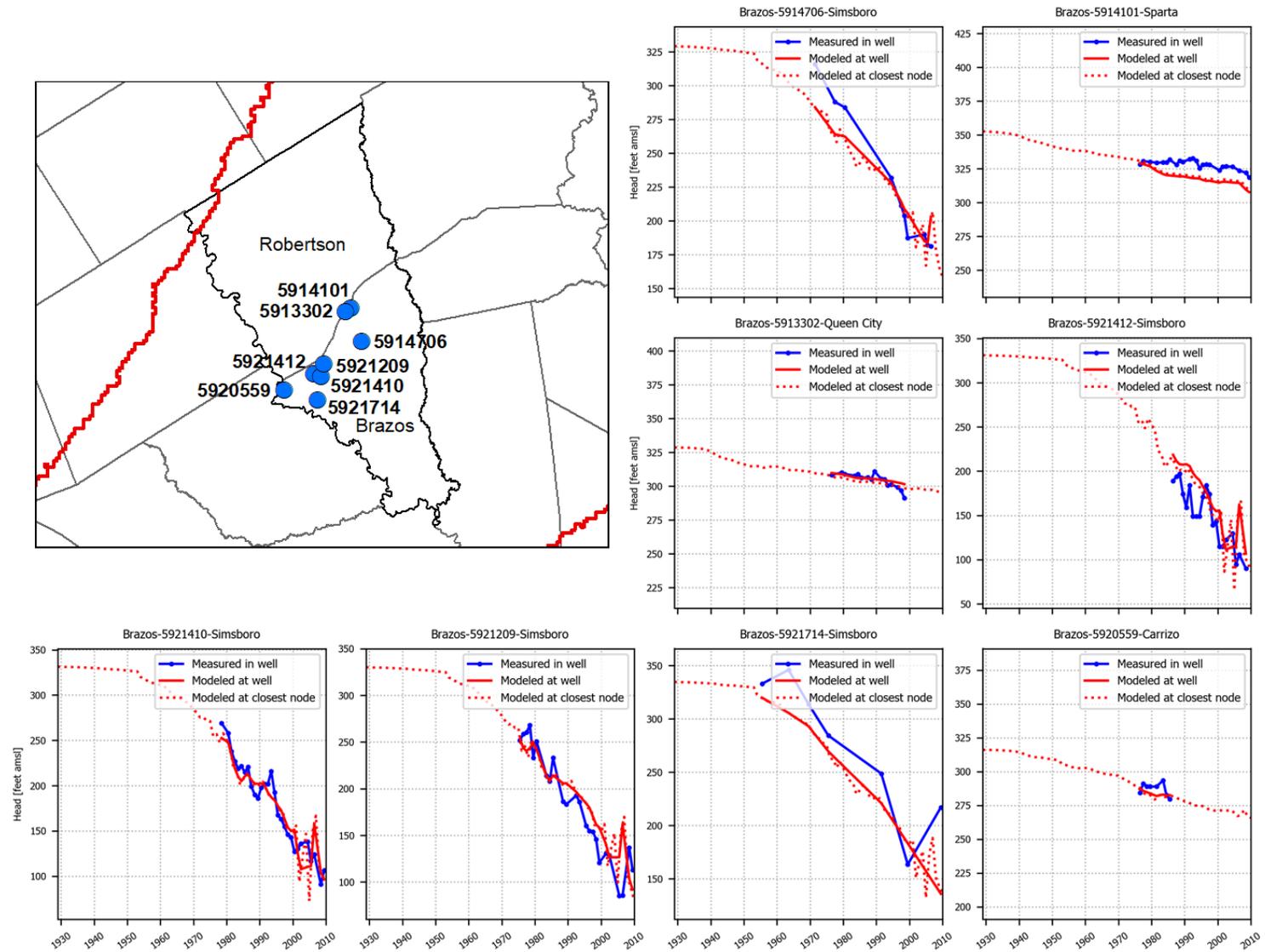
Figure 5.3.6d. **Hydrographs showing simulated and measured hydraulic heads (in feet above mean sea level) in the Brazos Valley Groundwater Conservation District at eight wells with state well numbers 5914706, 5914101, 5913302, 5921412, 5921410, 5921209, 5921714, and 5920559.**
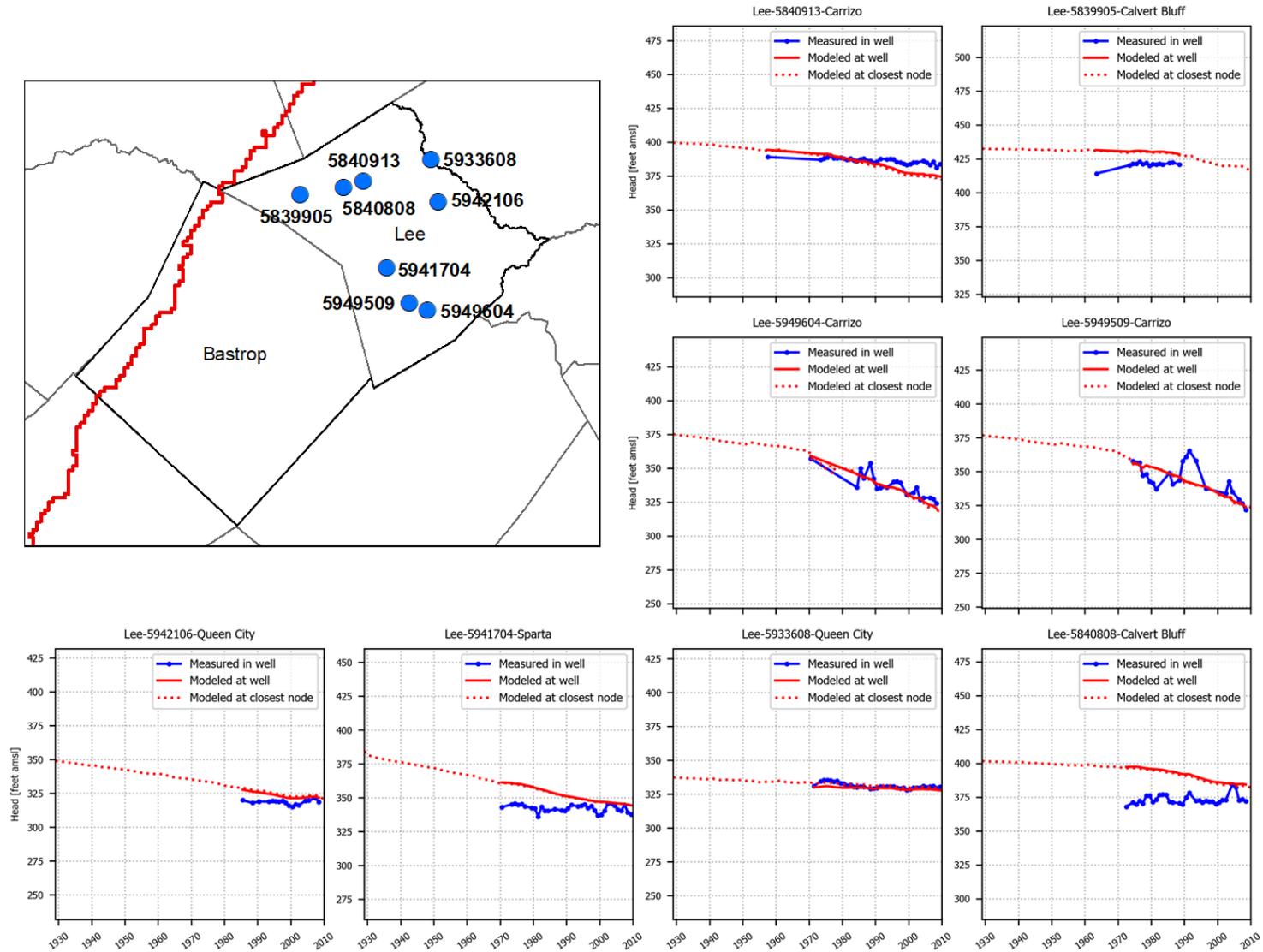
Figure 5.3.6e. Hydrographs showing simulated and measured hydraulic heads (in feet above mean sea level) in the Lost Pines Groundwater Conservation District at eight wells with state well numbers 5840913, 5839905, 5949604, 5949509, 5942106, 5941704, 5933608, and 5840808.
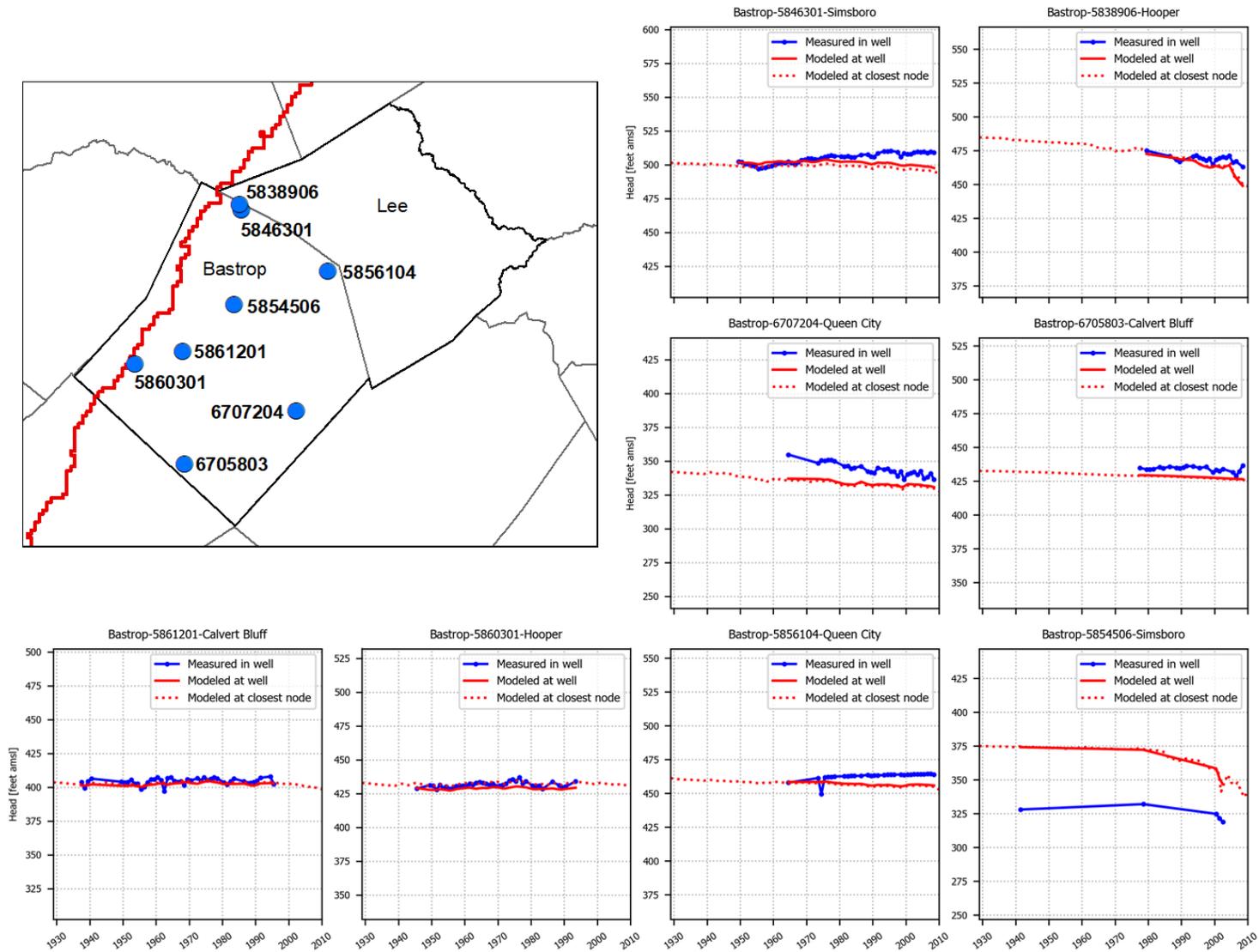
Figure 5.3.6f. Hydrographs showing simulated and measured hydraulic heads (in feet above mean sea level) in the Lost Pines Groundwater Conservation District at eight wells with state well numbers 5846301, 5838906, 6707204, 6705803, 5861201, 5860301, 5856104, and 5854506.
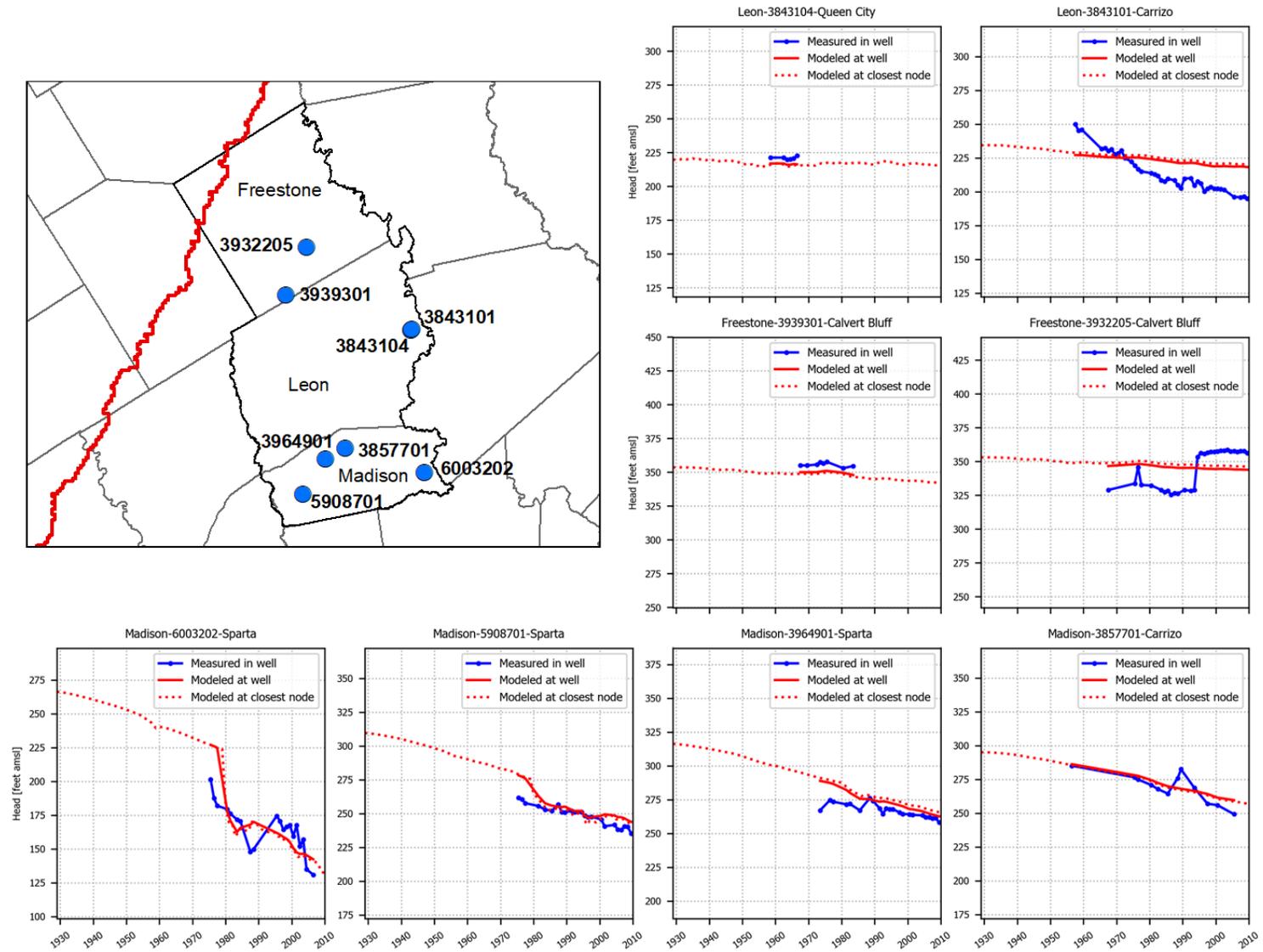
Figure 5.3.6g. **Hydrographs showing simulated and measured hydraulic heads (in feet above mean sea level) in the Mid-East Texas Groundwater Conservation District at eight wells with state well numbers 3843104, 3843101, 3939301, 3932205, 6003202, 5908701, 3964901, and 3857701.**
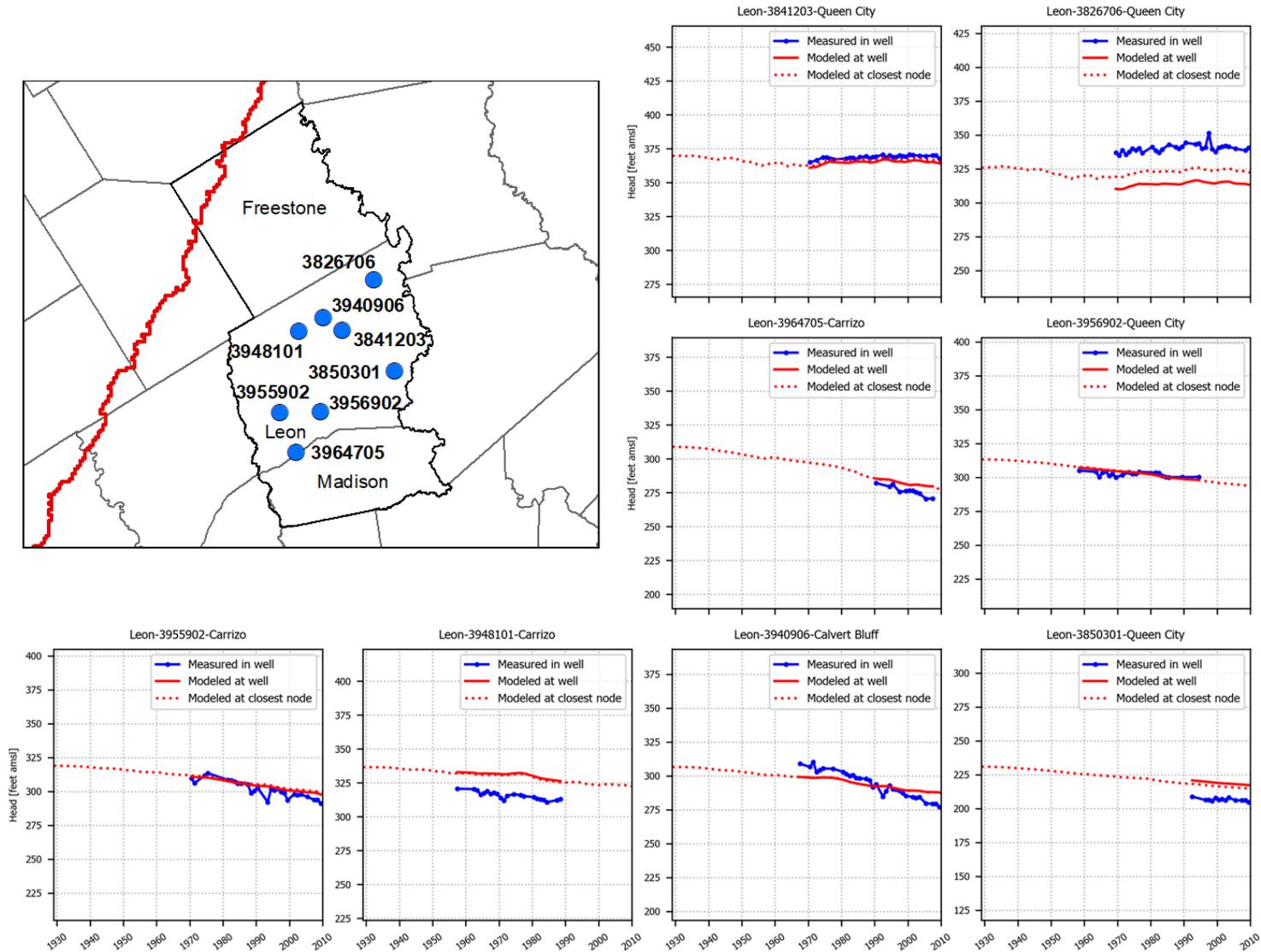
Figure 5.3.6h. Hydrographs showing simulated and measured hydraulic heads (in feet above mean sea level) in the Mid-East Texas Groundwater Conservation District at eight wells with state well numbers 3841203, 3826706, 3964705, 3956902, 3955902, 3948101, 3940906, and 3850301.
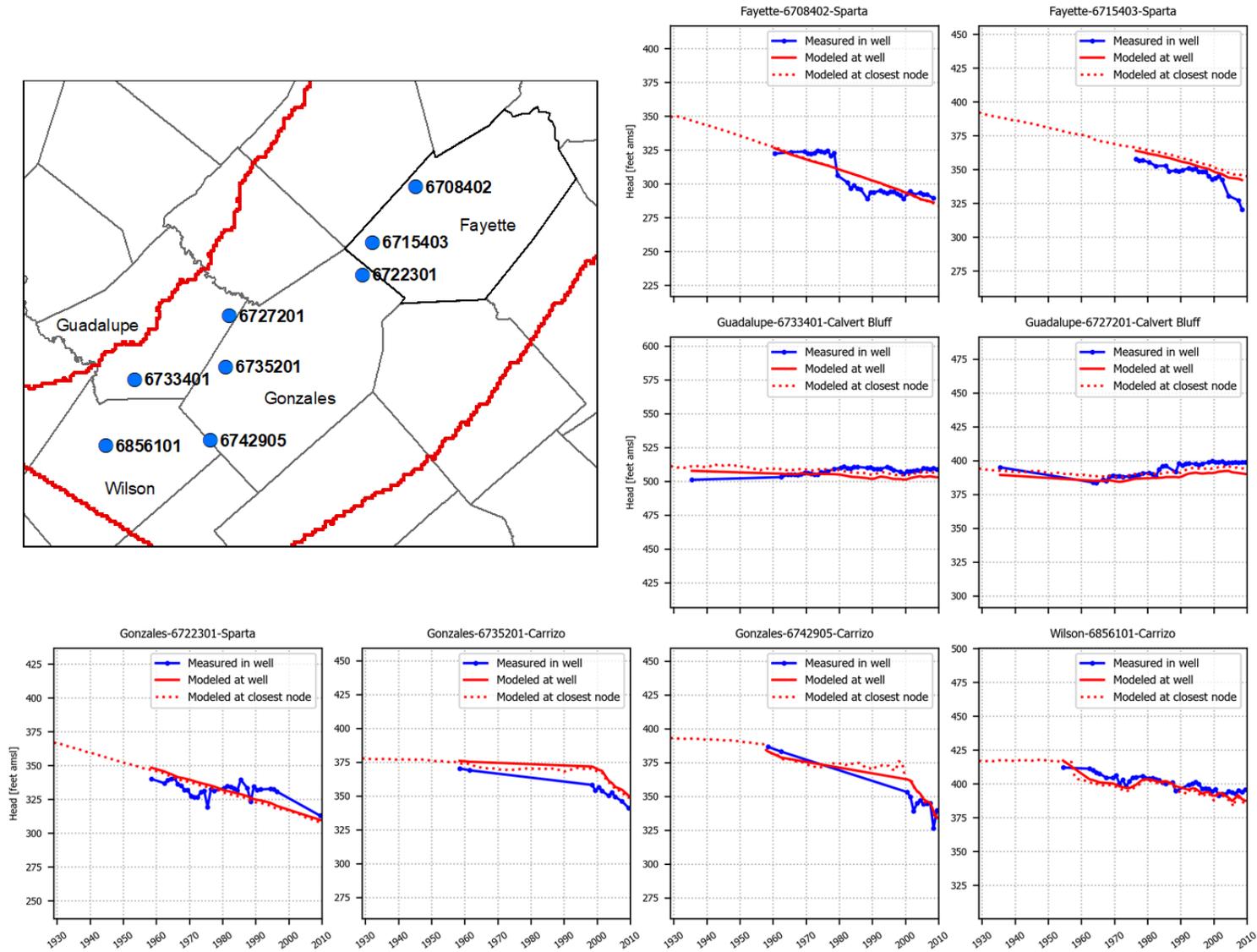
Figure 5.3.6i. Hydrographs showing simulated and measured hydraulic heads (in feet above mean sea level) in the Fayette County Groundwater Conservation District and Groundwater Management Area 13 at eight wells with state well numbers 6708402, 6715403, 6733401, 6727201, 6722301, 6735201, 6742905, and 6856101.
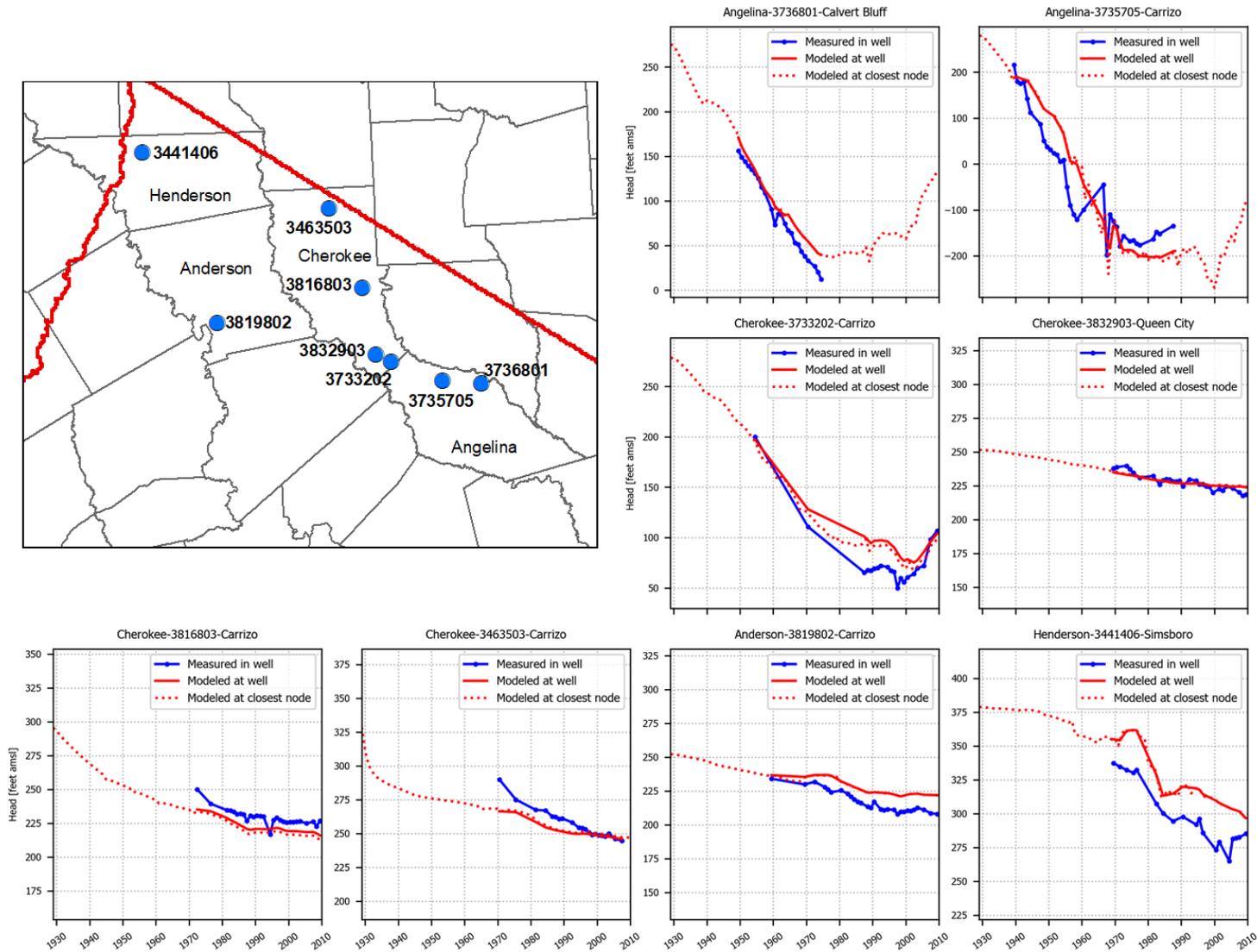
Figure 5.3.6j. Hydrographs showing simulated and measured hydraulic heads (in feet above mean sea level) in Groundwater Management Area 11 at eight wells with state well numbers 3736801, 3935705, 3733202, 3832903, 3816803, 3463503, 3819802, and 3441406.

5.4   Model Simulated Surface Water-Groundwater Interaction

In this section, the simulated surface water-groundwater interaction for the steady-state and transient stress periods are discussed. Figure 5.4a shows the location of the 12 river gages used to develop algorithms to generate recharge across the model domain based on annual precipitation rates and surface geology (Section 3.3.4). Each river gage is associated with a drainage area that was delineated based on the topographic gradients. For five of the 12 gages, more than 90 percent of the drainage area is in the outcrop of the model. These five drainage areas, outlined in green on Figure 5.4a, were used to compare the model simulated base flow to the base flow determined from the Baseflow Program and Base Flow Index Program analyses and simulated by the groundwater availability model developed by Kelley and others (2004). Model base flow values were generated by summing the fluxes associated with the drain and river cells in the drainage area of the river gages. This calculation was performed across the same group of grid cells for this updated model and for the groundwater availability model developed by Kelley and others (2004). To facilitate the comparison of base flows among different-sized drainage basins, the base flow values were divided by the area of their watershed to generate an equivalent recharge rate.

In Section 3.3.4.2, groundwater that comprises base flow was partitioned based on its source and place of origin. Groundwater that drains to a specific stream reach originating from the groundwater basin was considered basin flow. Groundwater originating from stream water that infiltrates the river alluvium during periods of high stream water levels is considered bank flow. To calculate a recharge rate from base flow, base flow needs to be partitioned into basin flow and bank flow. To include this in the comparison of model results to base flow estimates from gage data, the base flow numbers from the Baseflow Program analysis adjusted to account for bank flow using the method discussed in Section 3.3.4.2 are also shown.
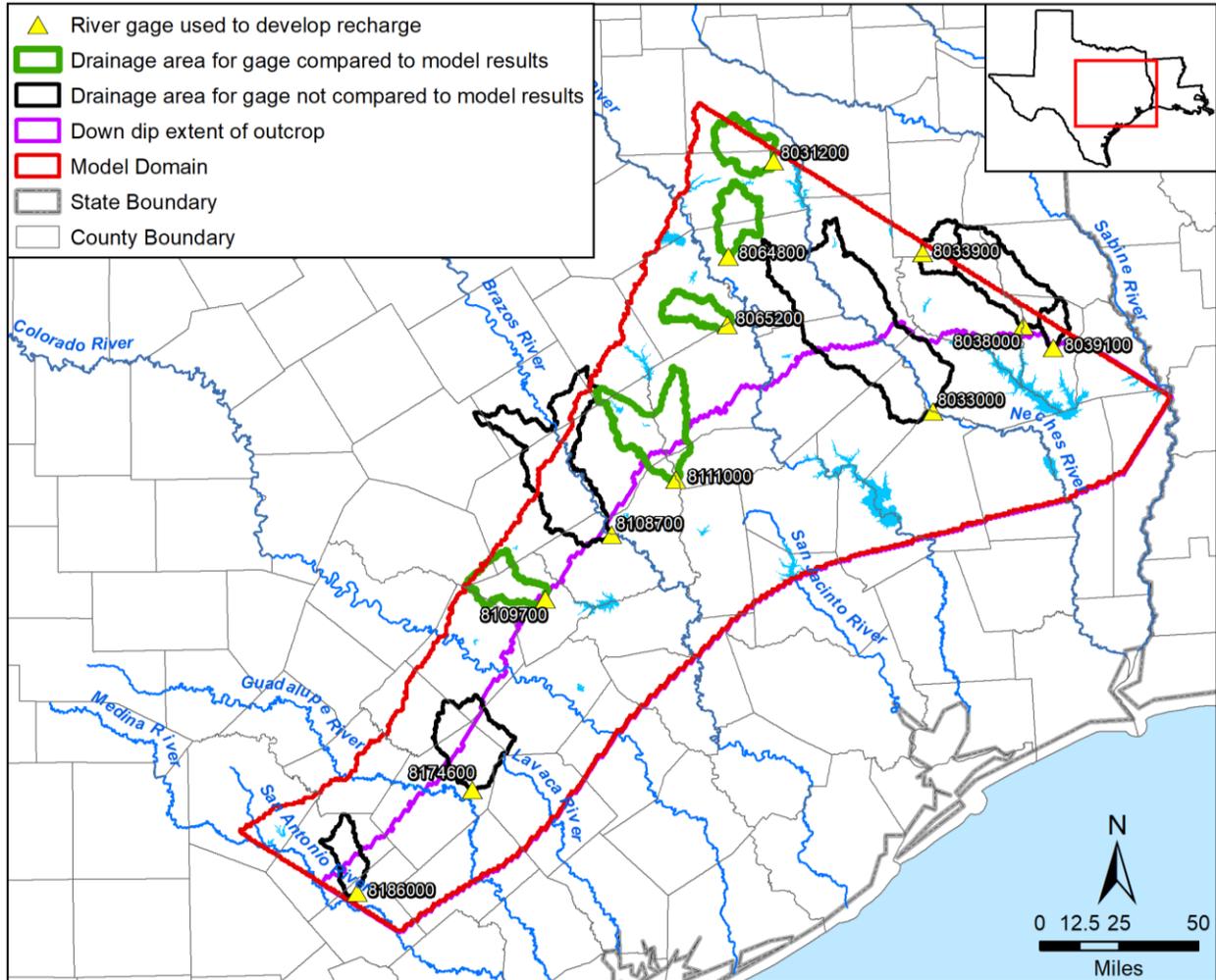
Figure 5.4a. Location of five out of 12 river gages used to develop regression between recharge rate and annual precipitation that have watersheds with more than 90 percent of their area in the outcrop of the model domain.

5.4.1 Surface Water-Groundwater Interaction for Steady-State Conditions

Table 5.4.1a provides the measured and modeled base flow values for the five watersheds outlined in green in Figure 5.4a. The five watersheds cover the central and northern regions of the model. The adjustments to the base flow values from the Baseflow Program analysis suggest that, on average, about 25 percent of the base flow is comprised of bank flow. The recharge rates for the five watersheds based on the adjusted Baseflow Program values range from 0.85 to 3.04 inches per year and average 1.88 inches per year. The model recharge rates for the five watersheds range from 1.38 to 2.12 inches per year and average 1.81 inches per year. Based on this limited data, it appears that the modeling approach over-predicts low base flow values and under-predicts high base flow values.

Table 5.4.1a   **Measured and modeled base flow values for steady-state conditions**

River Gage	Recharge Rate for Watershed (inches per year)		
	Average BFLOW Value	Average BFLOW Value (Adjusted)	Modeled by this Study
8031200	3.19	2.54	2.12
8064800	3.73	3.04	1.97
8065200	1.81	1.35	1.87
8109700	1.00	0.86	1.386
8111000	2.26	1.62	1.701
Average	2.40	1.88	1.81

Note: BFLOW = Baseflow Program

5.4.2   Surface Water-Groundwater Interaction for the Transient Conditions

Figures 5.4.2a and 5.4.2b show base flow values expressed as recharge for the five river gages during the transient period. For each gage, there are five different base flow values representing:

- BFLOW – base flow values calculated using the Baseflow Program as discussed in Section 3.3.3

- BFLOW(adj) –base flow values from the Baseflow Program analysis adjusted for bank flow based on the approach discussed in Section 3.3.4.2

- BFI – base flow values calculated using the Base Flow Index Program as discussed in Section 3.3.3

- This study's Model – Base flow values calculated from the calibrated transient model discussed in this report

- 2004 Model – Base flow value calculated from the groundwater availability model developed by Kelley and others (2004)

From our analysis in Section 3.3.4.2, the most appropriate representation of base flow is that originating from basin flow, which is most represented by the adjusted Baseflow Program values. The figures show that the model developed by this study provides a significantly better job at predicting the base flow values than does the model by Kelley and others (2004). Table 5.4.2a provides the averages of the yearly measurements for each plot. The average Baseflow Program values for the steady-state and transient model are identical because the estimated recharge values from data available only during the transient period were averaged to estimate a recharge value for use in the steady-state model.

Table 5.4.2a   **Measured and modeled base flows for transient conditions.**

River Gage	Recharge Rate for Watershed (inches per year)				
	Average BFI Value	Average BFLOW Value	Average BFLOW Value (Adjusted)	Modeled by this Study	2004 Model
8031200	1.64	3.19	2.54	2.12	<0.01
8064800	2.97	3.73	3.04	1.97	<0.01
8065200	0.96	1.81	1.36	1.87	<0.01
8109700	0.40	1.00	0.85	1.386	<0.01
8111000	0.71	2.26	1.62	1.701	<0.01
Average	1.34	2.40	1.88	1.81	<0.01

Note: BFI = Base Flow Index Program; BFLOW = Baseflow Program

Besides hydrographs at river gages, comparison of model results to results from gain-loss studies can be used to check the accuracy of the model simulation of surface-water groundwater interaction. Gain-loss studies considered for this study include the low-flow studies performed in the Colorado River by Saunders (2005, 2006, 2009). However, considerable work to the model would be needed to generate model output comparable to results from gain-loss studies. That level of work, which includes generating monthly time steps, was beyond the scope of this project and was not performed.
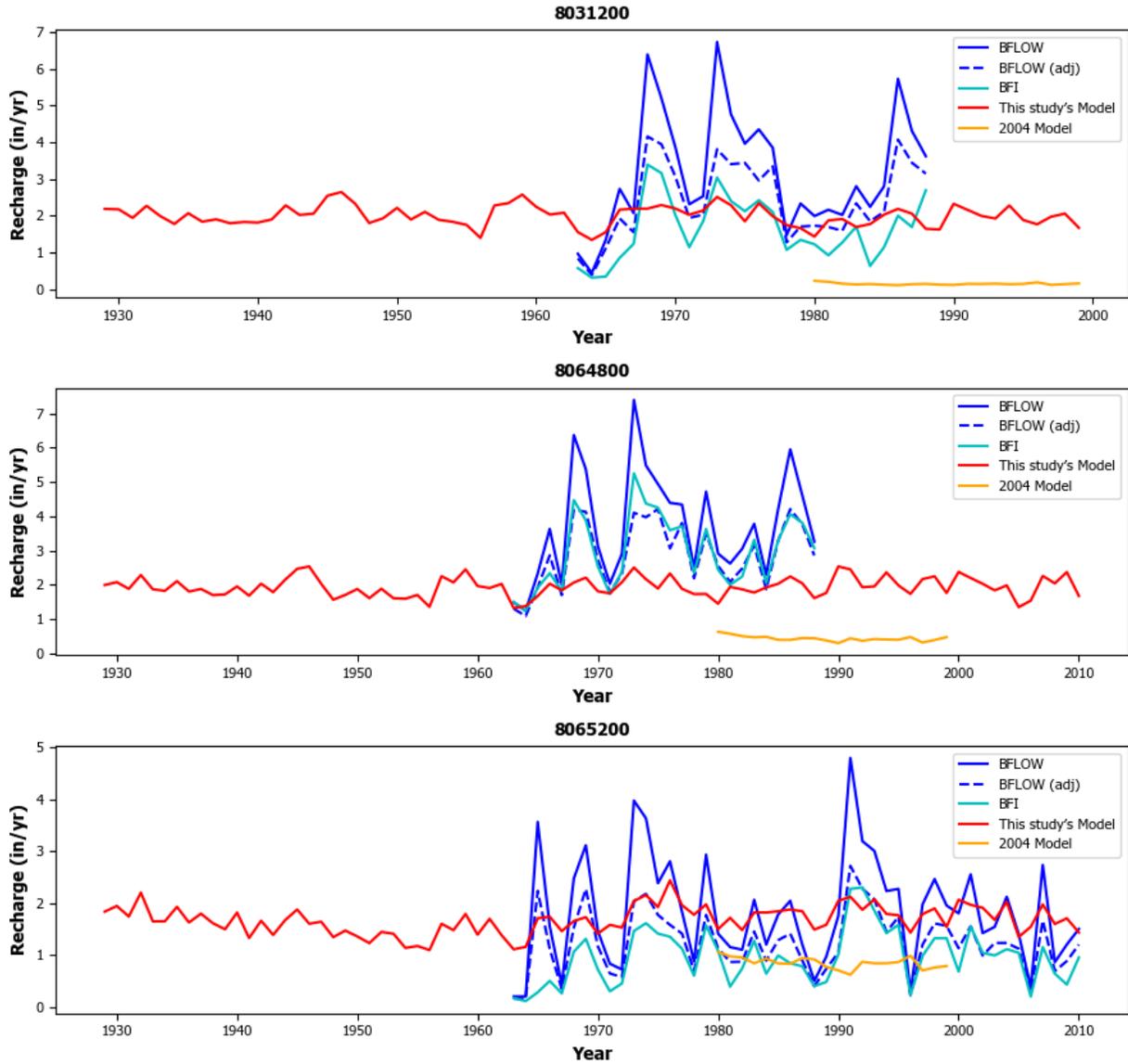
Figure 5.4.2a   Comparison of recharge rates (in inches per year) calculated from base flow for river gages 8031200, 8064800, and 8065200 based on the Baseflow Program analysis and adjusted Baseflow Program values, the Base Flow Index Program analysis, and calculated from this study's model and the 2004 groundwater availability model by Kelley and others (2004). The model values equal the model calculated discharge to rivers/streams.
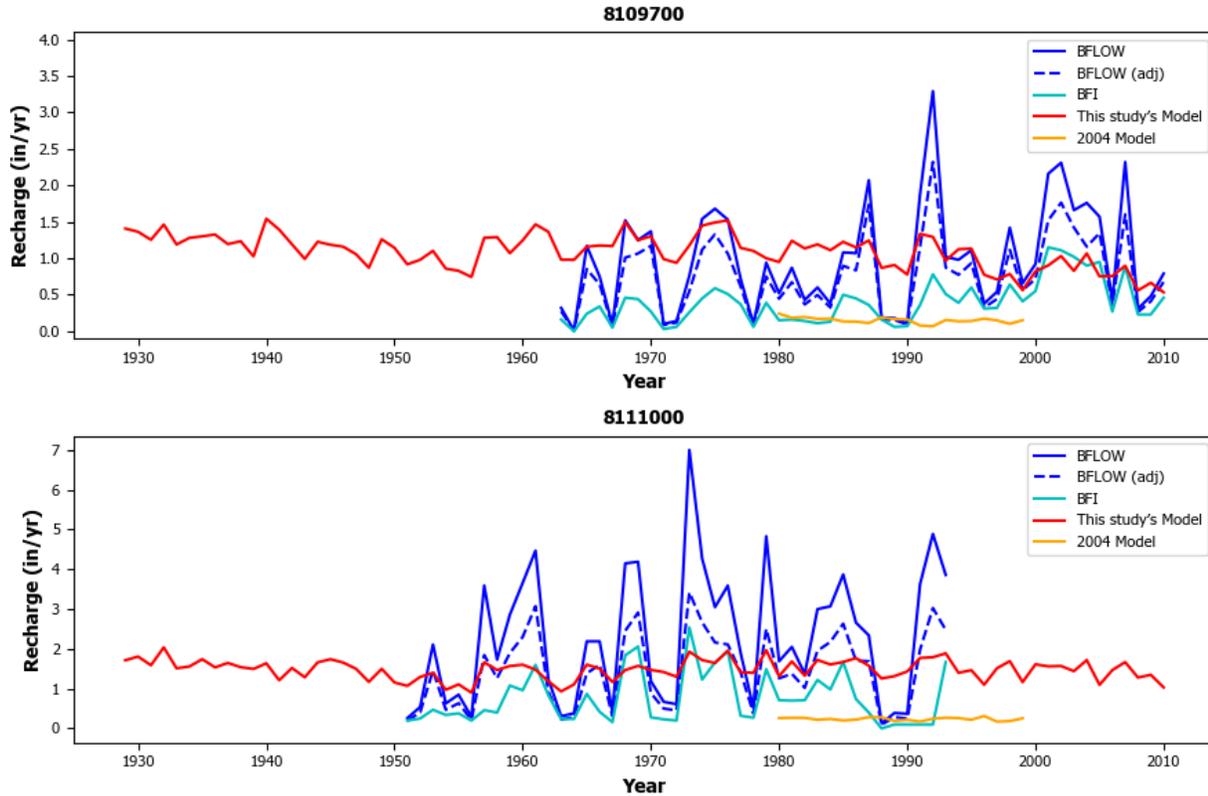
Figure 5.4.2b. Comparison of recharge rates (in inches per year) calculated from base flow for river gages 8109700 and 8111000 based on the Baseflow Program analysis and adjusted Baseflow Program values, the Base Flow Index Program analysis, and calculated from this study's model and the 2004 groundwater availability model by Kelley and others (2004). The model values equal the model calculated discharge to rivers/streams.

5.5 Model Simulated Water Budget

In this section, the simulated water budgets for the steady-state and transient stress periods are discussed. Water budgets are provided with respect to both model layers and hydrogeologic units and with respect to both the entire model domain and Groundwater Management Area 12.

5.5.1 Steady-State Water Budgets

Table 5.5.1a provides the steady-state water budget for the entire model domain by layer. Recharge is the only source of inflow, and the primary outflow is through rivers. The average recharge rate across the entire model is 2 inches per year. Approximately 68 percent of the groundwater discharge is to the major rivers, with discharge to streams, seeps, and spring flow making up approximately 30 percent. Approximately 1 percent of the groundwater discharge exits through the general-head boundary conditions, and another 1 percent exits as evapotranspiration.

Table 5.5.1a.   Steady-state water budget in acre-feet per year for the entire model domain by model layer.

Model Layer	Recharge	River-Groundwater Exchange	Streams/Seeps/ Spring Flow	Lateral Flow	Vertical Flow	ET	General Head Boundary
1	35,283	-88,635	-983	0	54,564	-228	0
2	1,164,758	-719,725	-362,894	0	-68,428	-13,675	0
3	0	0	0	0	-2,900	0	2,900
4	0	0	0	0	491	0	-491
5	0	0	0	0	2,230	0	-2,234
6	0	0	0	0	491	0	-491
7	0	0	0	0	2,294	0	-2,294
8	0	0	0	0	3,093	0	-3,093
9	0	0	0	0	4,137	0	-4,137
10	0	0	0	0	4,027	0	-4,027
Total	1,200,042	-808,360	-363,877	0	0	-13,903	-13,868

Note: ET = evapotranspiration

For model layer 1, which includes only the Colorado and Brazos rivers alluvium, 99 percent of the outflow is comprised of discharge to the rivers. The source for the alluvium groundwater flow to the rivers is recharge (39 percent) and cross-formational flow from the underlying formations (61 percent). The average recharge rate across the alluvium is 2.2 inches per year.

In model layers 3 through 10, the flow associated with the general-boundary conditions includes an exchange of lateral flow across northeastern and southwestern model boundaries in Groundwater Management Areas 11 and 13, respectively. In model layer 3, the flow associated with the general-boundary conditions also includes vertical groundwater flow between the Sparta Aquifer and overlying Cook Mountain Formation.

Table 5.5.1b provides the steady-state water budget for Groundwater Management Area 12 by model layer. The distribution among water budget components is similar to the distribution for the entire model domain, except for the general-head boundaries. In Groundwater Management Area 12, general-head boundaries only exist on the Sparta Aquifer and they represent vertical flow between the Sparta Aquifer and the overlying Cook Mountain Formation. The lateral flow component in this water budget represents flow across the Groundwater Management Area 12 boundary.

Table 5.5.1b. **Steady-state water budget in acre-feet per year for Groundwater Management Area 12 by model layer.**

Model Layer	Recharge	River-Groundwater Exchange	Streams/Seeps/ Spring Flow	Lateral Flow	Vertical Flow	ET	General Head Boundary
1	35,189	-88,635	-983	88	54,571	-228	0
2	491,603	-315,066	-115,797	2,003	-57,812	-4,931	0
3	0	0	0	324	-607	0	284
4	0	0	0	36	-36	0	0
5	0	0	0	-406	406	0	0
6	0	0	0	85	-84	0	0
7	0	0	0	-1,661	1,661	0	0
8	0	0	0	-865	865	0	0
9	0	0	0	-1,597	1,597	0	0
10	0	0	0	560	-559	0	0
Total	526,793	-403,701	-116,780	-1,433	0	-5,160	284

Note: ET = evapotranspiration

Tables 5.5.1c and 5.5.1d provide the steady-state water budgets by hydrogeologic unit for the entire model domain and Groundwater Management Area 12, respectively. The total fluxes for these two water budgets are the same as those by layer in Tables 5.5.1a and 5.5.1b. The primary difference between the two sets is that the water budget components in model layer 2 have been partitioned into their respective hydrogeologic units.

Table 5.5.1c **Steady-state water budget in acre-feet per year for the entire model domain by hydrogeologic unit.**

Hydro-geologic Unit	Recharge	River-Groundwater Exchange	Streams/Seeps/ Spring Flow	Lateral Flow	Vertical Flow	ET	General Head Boundary
Alluvium	35,283	-88,635	-983	0	54,563	-228	0
Sparta	167,356	-104,816	-41,305	0	-22,018	-2,117	2,900
Weches	16,443	-24,274	-5,726	0	14,538	-491	-491
Queen City	458,759	-258,321	-180,856	0	-9,950	-7,406	-2,234
Reklaw	30,014	-33,400	-12,017	0	16,461	-567	-491
Carrizo	94,130	-47,051	-16,219	0	-28,414	-155	-2,294
Calvert Bluff	235,006	-168,859	-63,644	0	1,672	-1,084	-3,093
Simsboro	70,669	-47,905	-8,888	0	-9,680	-60	-4,137
Hooper	92,369	-35,127	-34,241	0	-17,172	-1,796	-4,027
Total	1,200,029	-808,387	-363,879	0	0	-13,904	-13,868

Note: ET = evapotranspiration

Table 5.5.1d.   Steady-state water budget in acre-feet per year for the Groundwater Management Area 12 by hydrogeologic unit.

Hydro-geologic Unit	Recharge	River-Groundwater Exchange	Streams/Seeps/Spring Flow	Lateral Flow	Vertical Flow	ET	General Head Boundary
Alluvium	35,189	-88,635	-983	88	54,570	-228	0
Sparta	51,151	-38,537	-7,887	697	-5,398	-311	284
Weches	4,951	-6,231	-1,209	28	2,621	-160	0
Queen City	110,791	-73,710	-30,719	1,003	-4,943	-2,419	0
Reklaw	10,095	-7,736	-2,985	146	701	-221	0
Carrizo	41,488	-18,193	-8,723	-1,486	-12,995	-91	0
Calvert Bluff	152,489	-108,796	-34,487	421	-9,162	-465	0
Simsboro	58,690	-42,093	-4,573	-1,241	-10,782	0	0
Hooper	61,944	-19,764	-25,214	-510	-15,190	-1,266	0
Total	526,788	-403,694	-116,781	-855	-578	-5,160	284

Note: ET = evapotranspiration

Tabulated steady-state water budgets by county and layer can be found in Appendix N and by county and hydrogeologic unit can be found in Appendix O. Water budgets by layer and hydrogeologic unit for the groundwater conservation districts in the model domain are provided in Appendices P and Q, respectively.

5.5.2   Transient Water Budgets

Figures 5.5.2a through 5.5.2c show the transient water budget by model layer from 1930 to 2010 for the entire model domain. The figures show the same water budget components associated with the steady-state water budgets, but with the added components of pumping and storage. In model layer 1, the groundwater flow to the major rivers exhibits a decrease over time. This trend is most evident after 1998. After 2002, the decline in the groundwater flow to the Colorado and Brazos rivers is strongly correlated with the increase in pumping from 20,000 to 70,000 acre-feet per year.

For model layers 1 and 2, recharge has a large temporal variability reflecting the temporal variability in precipitation, which was used to generate the recharge values. In model layers 1 and 2, the storage budgets are inversely correlated with the recharge budgets. During periods with high recharge rates, the aquifer water level rises, and groundwater fills void spaces and, therefore, exits the groundwater flow system. During periods with low recharge rates, the aquifer water level declines, and water drains from the void spaces and becomes part of the groundwater flow system. In model layer 2, the water budget component that exhibits the least amount of fluctuations is vertical flow. Vertical flow from the shallow groundwater flow zone can be viewed as deep recharge. Over time, the vertical flow from layer 2 to the underlying layers is gradually increasing. This gradual increase is a result of pumping in the deeper layers.

In model layers 3 through 10, annual pumping rates are the driver that most affects the water budget. Groundwater removed by pumping is balanced by water removed by storage and

groundwater flow into the model layer. Model layers 2 and 3 have the least amount of change in their water budget over time because these two model layers have the least amount of pumping.

A comparison of Figure 5.5.2a to Table 5.5.1a shows that the general-head boundaries take out more flow during the transient conditions than during the steady-state conditions for model layer 3, which is the Sparta Aquifer. Moreover, during the transient period, groundwater flow to the general- head boundaries increases with time. The majority of this flow represents cross-formational flow from the Sparta Aquifer to the overlying Yegua-Jackson Aquifer.

Figures 5.5.2d through 5.5.2f show the transient water budget by layer from 1930 to 2010 for Groundwater Management Area 12. The general observations discussed with regard to the water budgets for the entire model are valid for Groundwater Management Area 12.

Figures 5.5.2g through 5.5.2i show the transient water budget by hydrogeologic units from 1930 to 2010 for the entire model. Figures 5.5.2j through 5.1.2l show the transient water budget by hydrogeologic units from 1930 to 2010 for Groundwater Management Area 12.

Transient water budgets by county and layer can be found in Appendix R and by county and hydrogeologic unit can be found in Appendix S. Water budgets by layer and hydrogeologic unit for the groundwater conservation districts in the model domain are provided in Appendices T and U, respectively.

Final Report: Groundwater Availability Model for the Central Portion
of the Carrizo-Wilcox, Queen City, and Sparta Aquifers
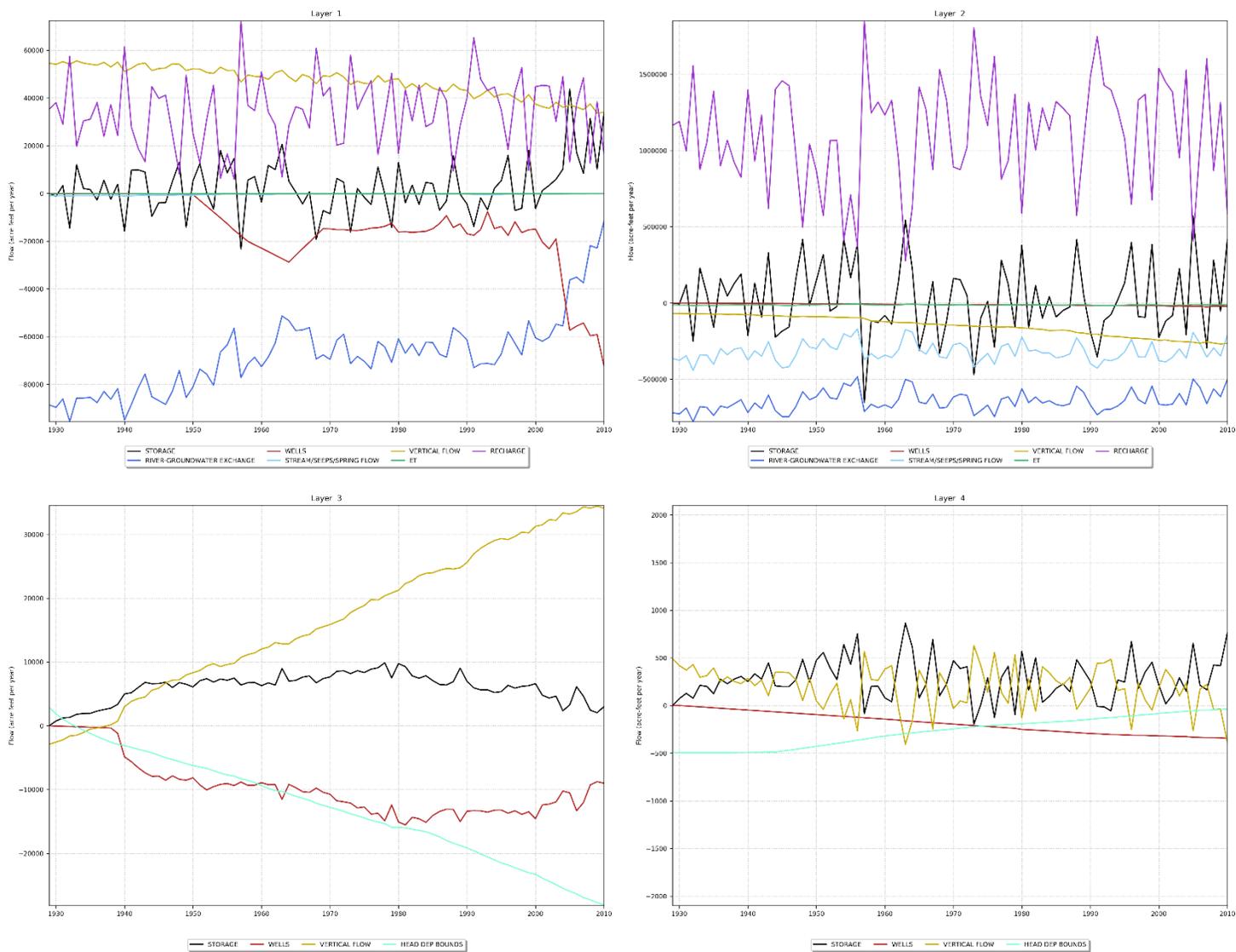
Figure 5.5.2a. Transient water budget for the entire model domain for model layers 1, 2, 3 and 4.
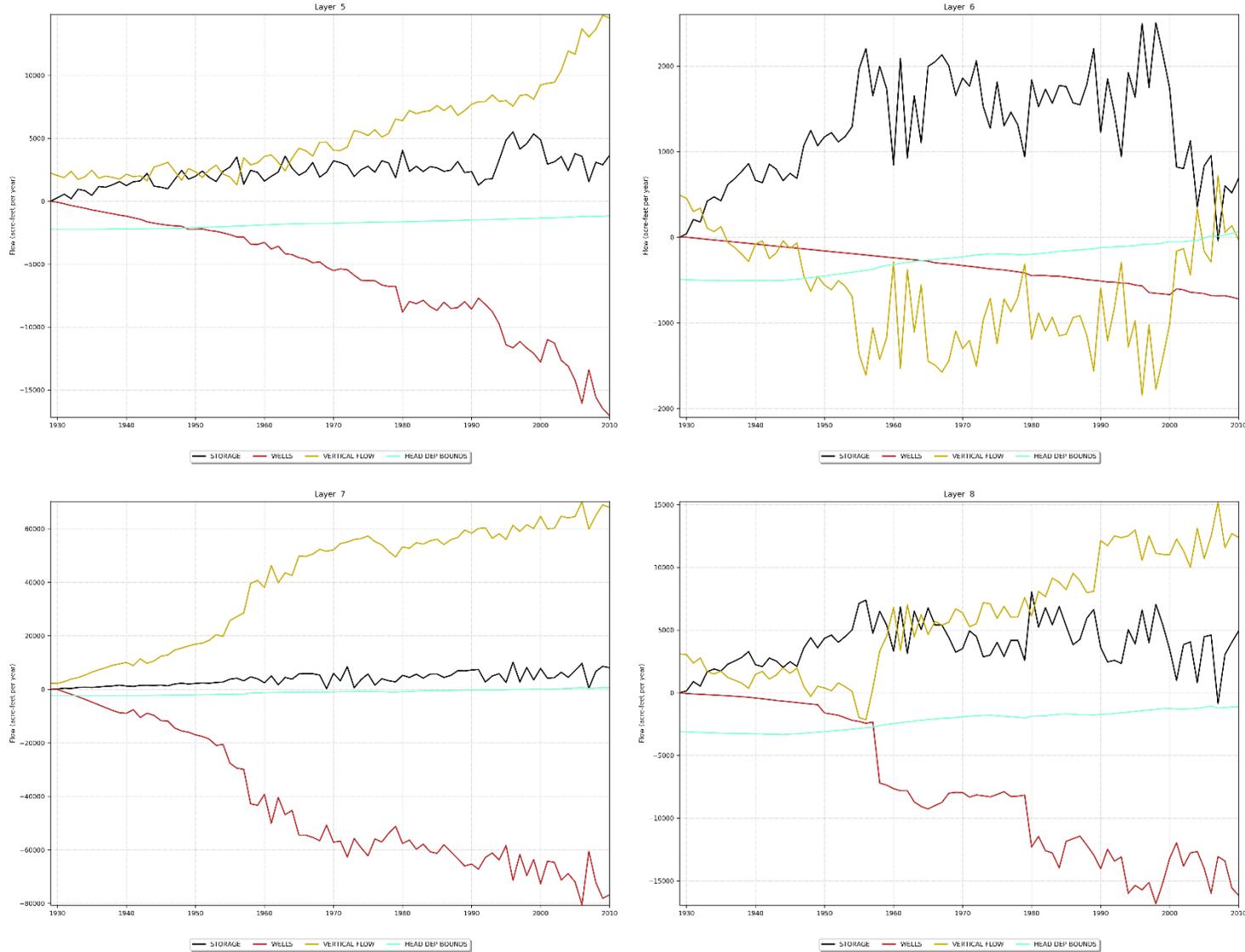
Figure 5.5.2b. **Transient water budget for the entire model domain for model layers 5, 6, 7, and 8.**

Final Report: Groundwater Availability Model for the Central Portion
of the Carrizo-Wilcox, Queen City, and Sparta Aquifers
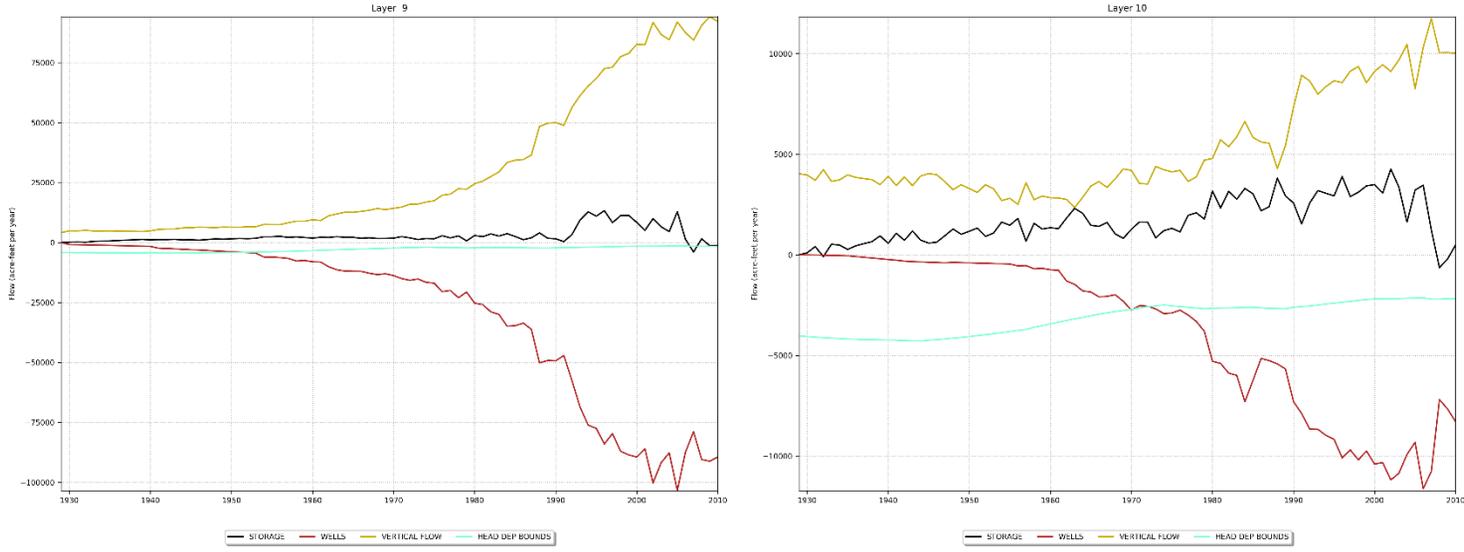
Figure 5.5.2c.   **Transient water budget for entire the model domain for model layers 9 and 10.**
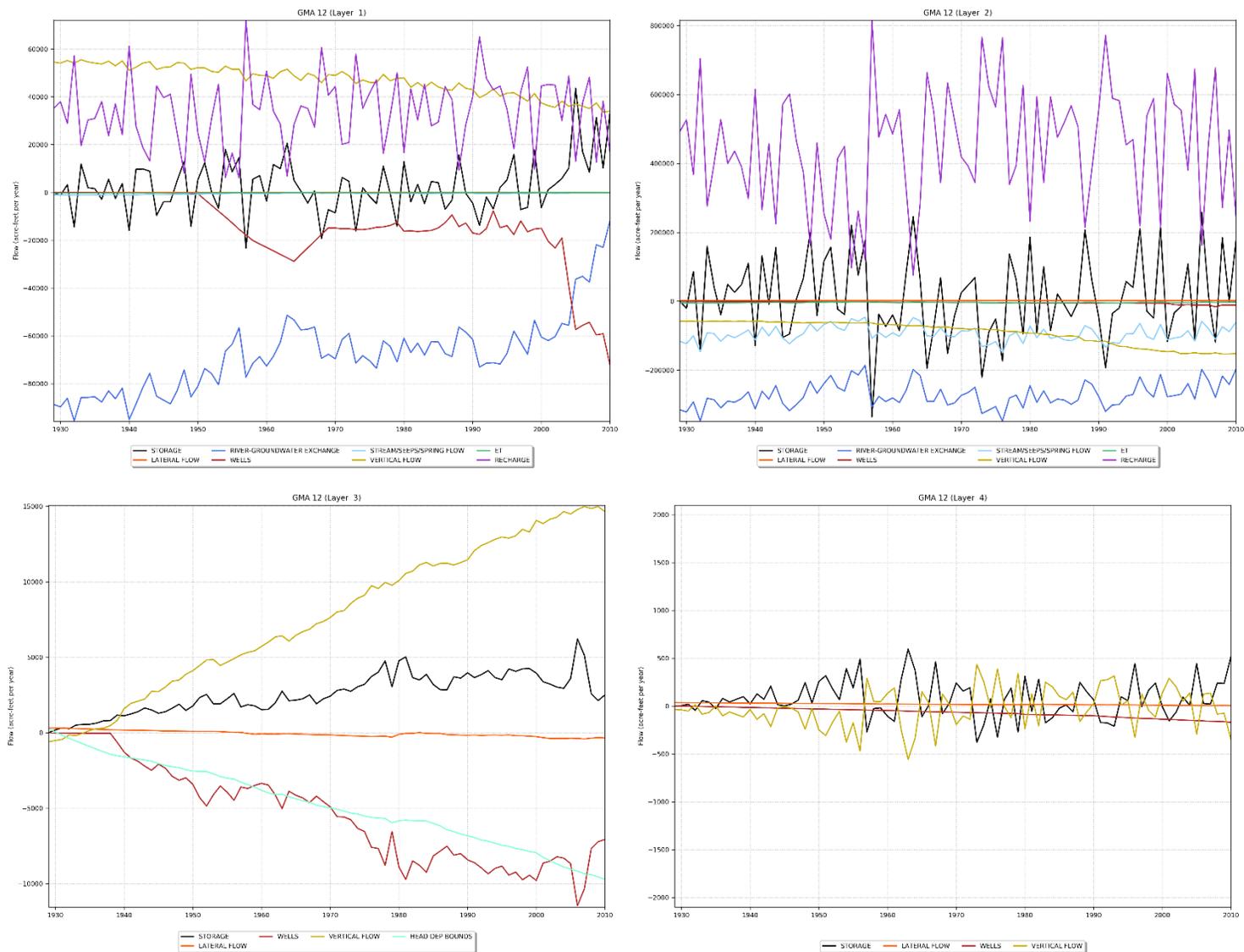
Figure 5.5.2d. **Transient water budget for Groundwater Management Area 12 for model layers 1, 2, 3, and 4.**
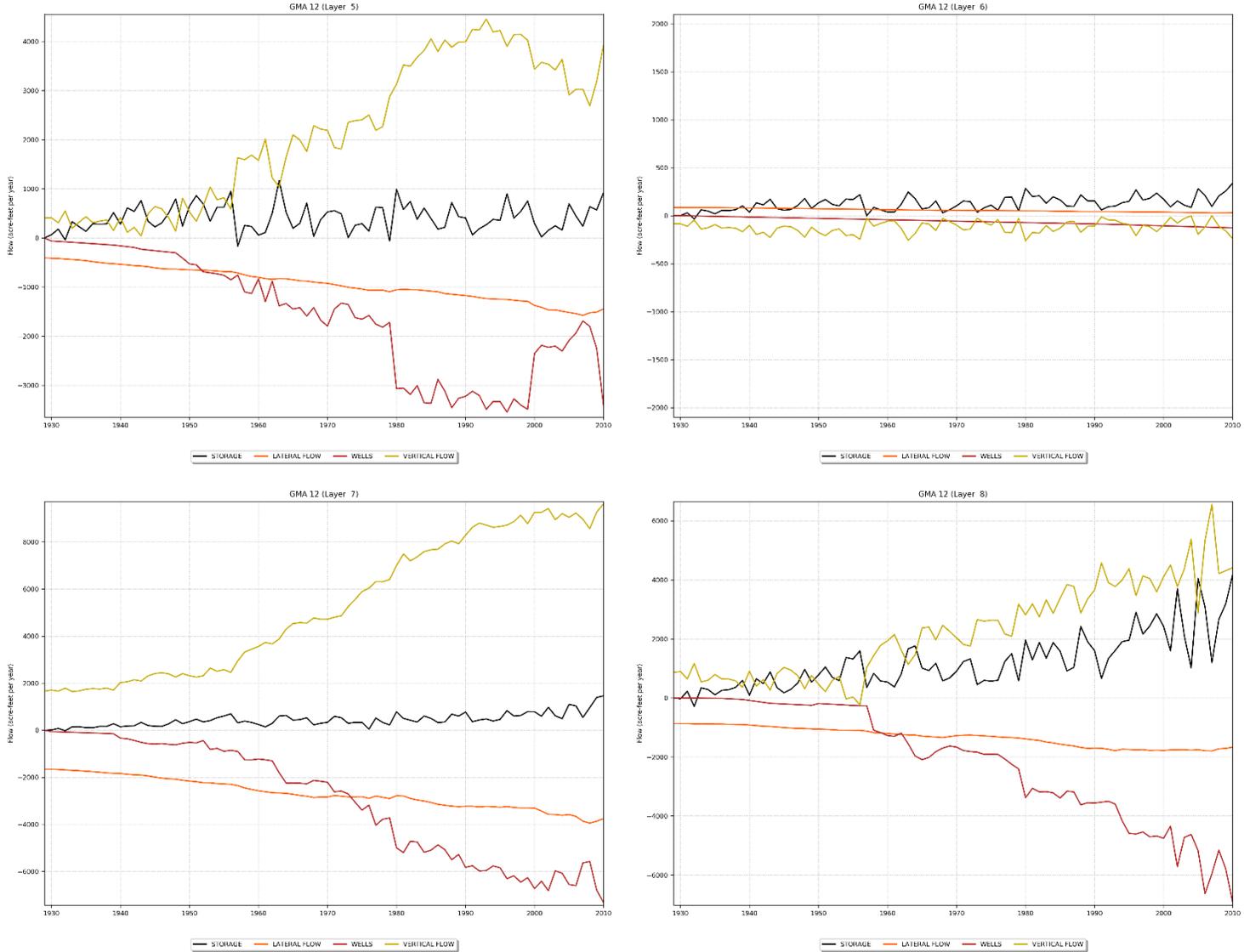
Figure 5.5.2e.   **Transient water budget for Groundwater Management Area 12 for model layers 5, 6, 7, and 8.**
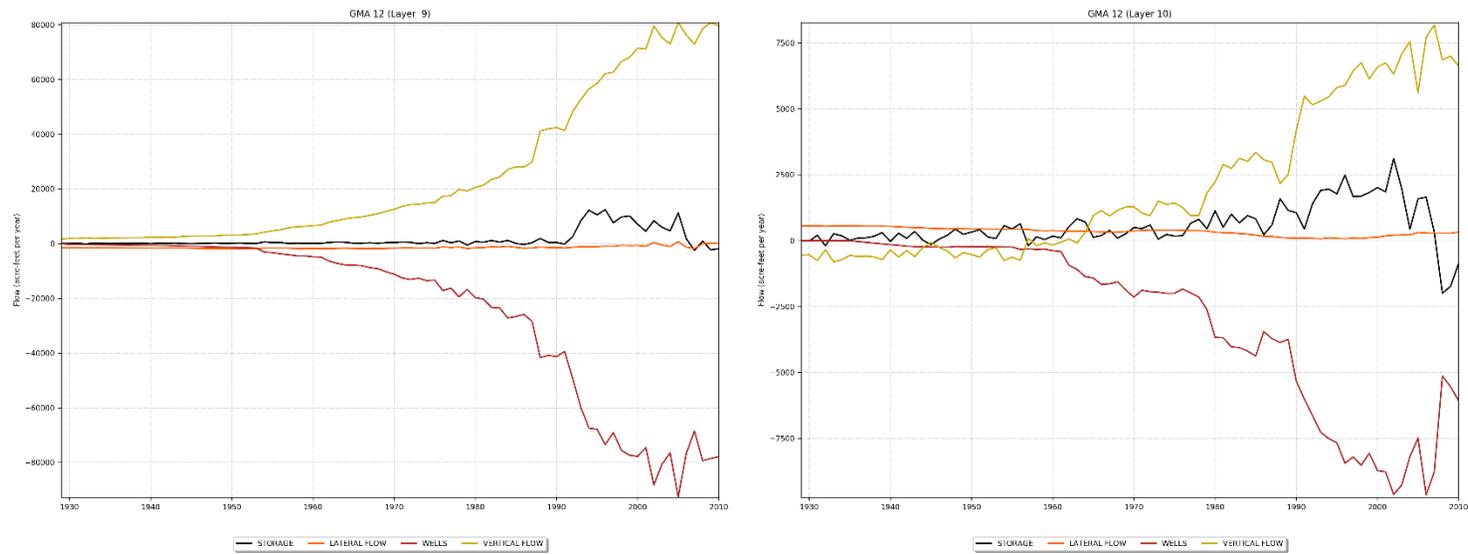
Figure 5.5.2f. **Transient water budget for Groundwater Management Area 12 for model layers 9 and 10.**
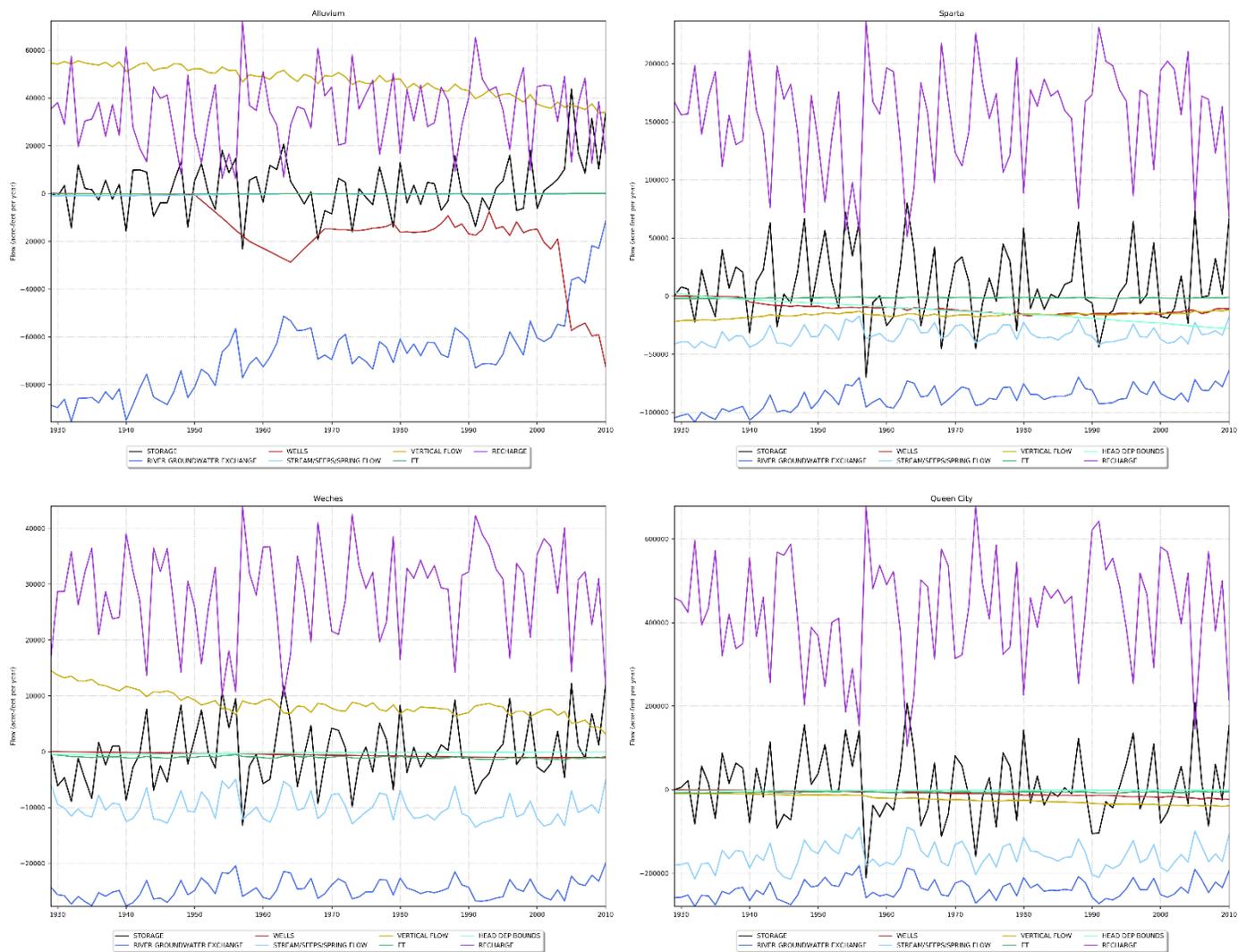
Figure 5.5.2g.   **Transient water budget for the entire model domain for the Colorado and Brazos rivers alluvium, Sparta Aquifer, Weches Formation, and Queen City Aquifer.**
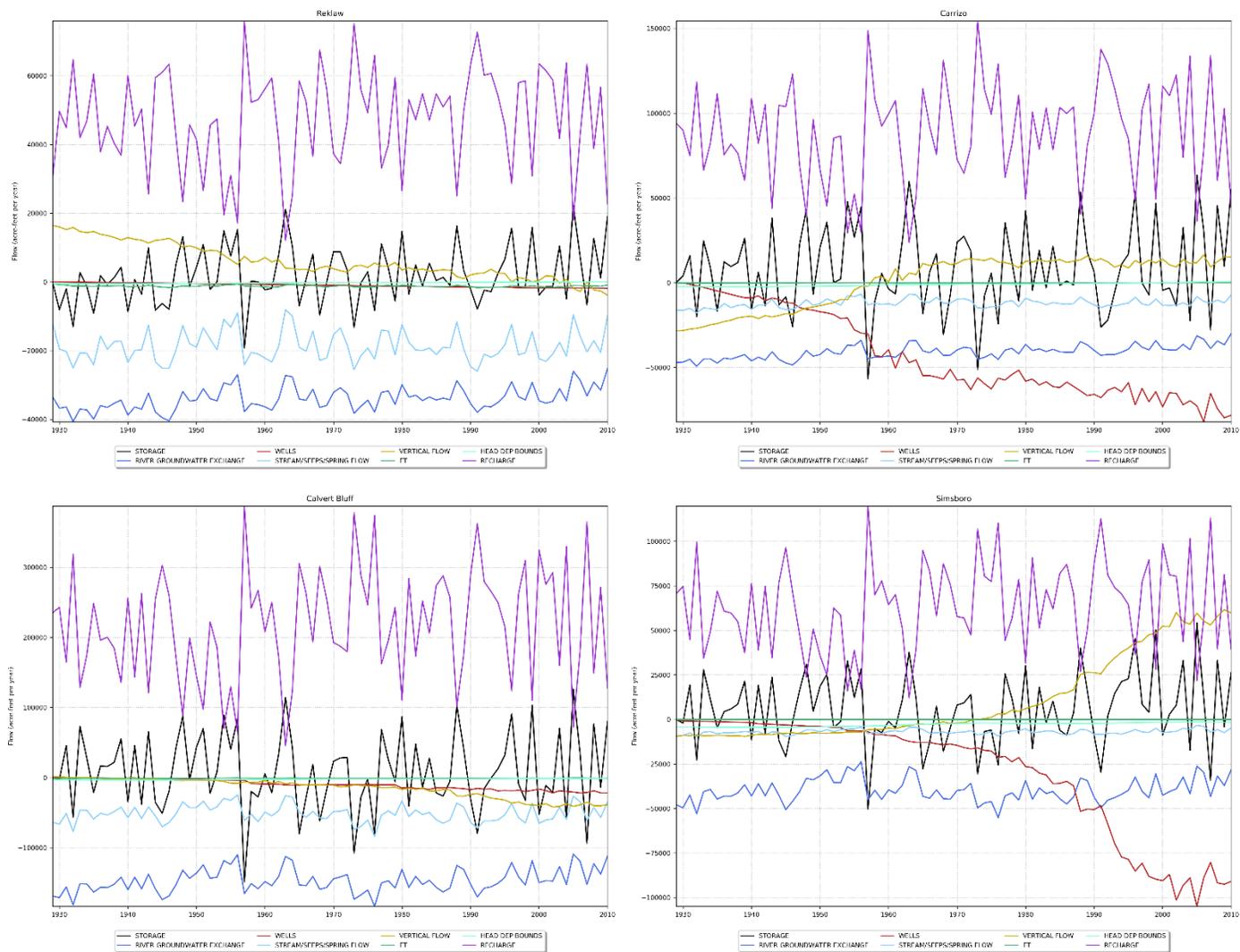
Figure 5.5.2h.   **Transient water budget for the entire model domain for the Reklaw Formation, Carrizo Aquifer, and Calvert Bluff and Simsboro formations.**
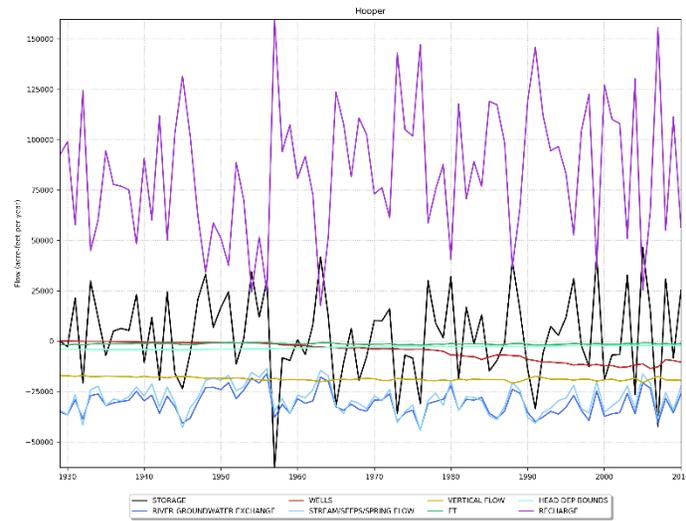
Figure 5.5.2i.   **Transient water budget for the entire model domain for the Hooper Formation.**
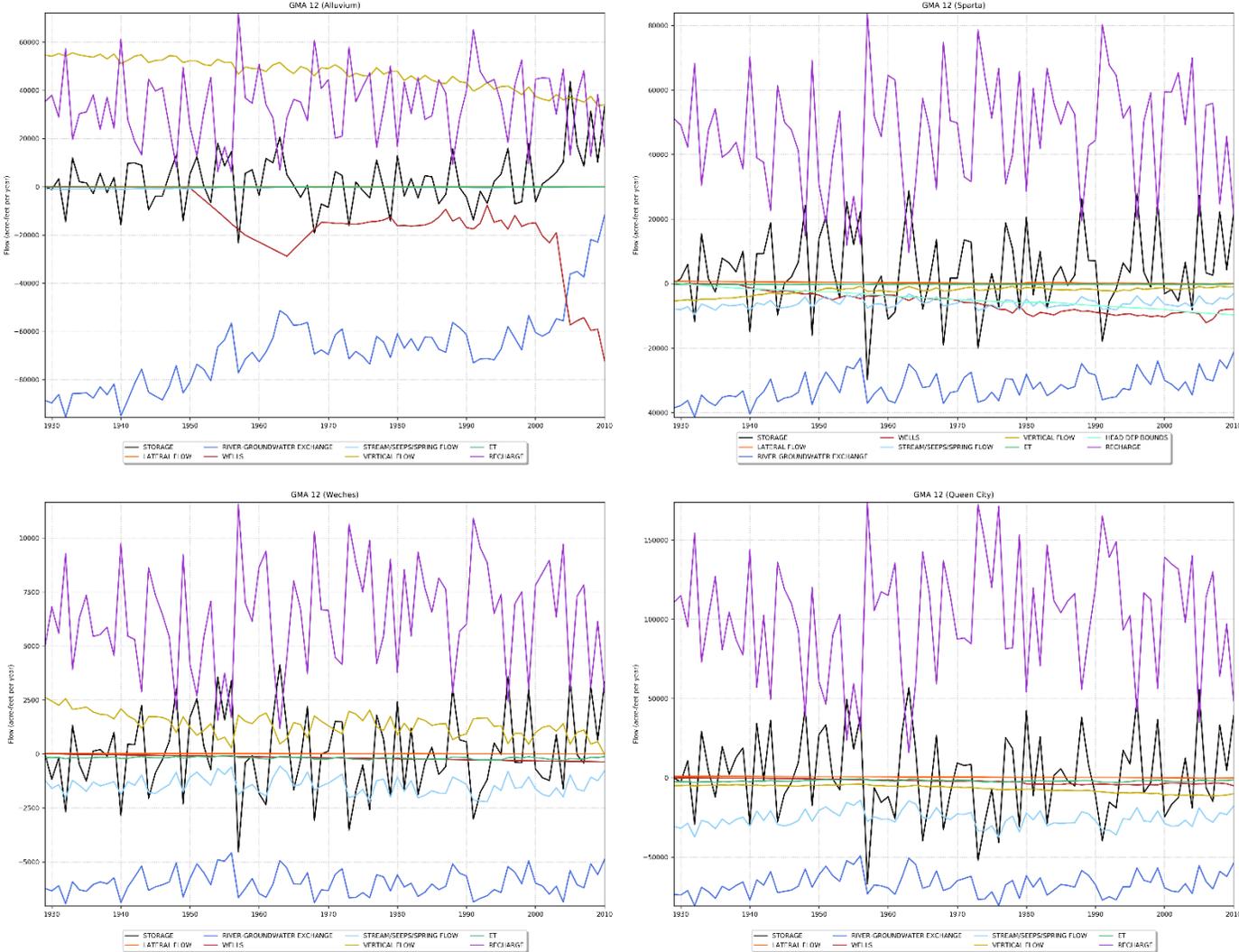
Figure 5.5.2j. **Transient water budget for Groundwater Management Area 12 for the Colorado and Brazos rivers alluvium, Sparta Aquifer, Weches Formation, and Queen City Aquifer.**
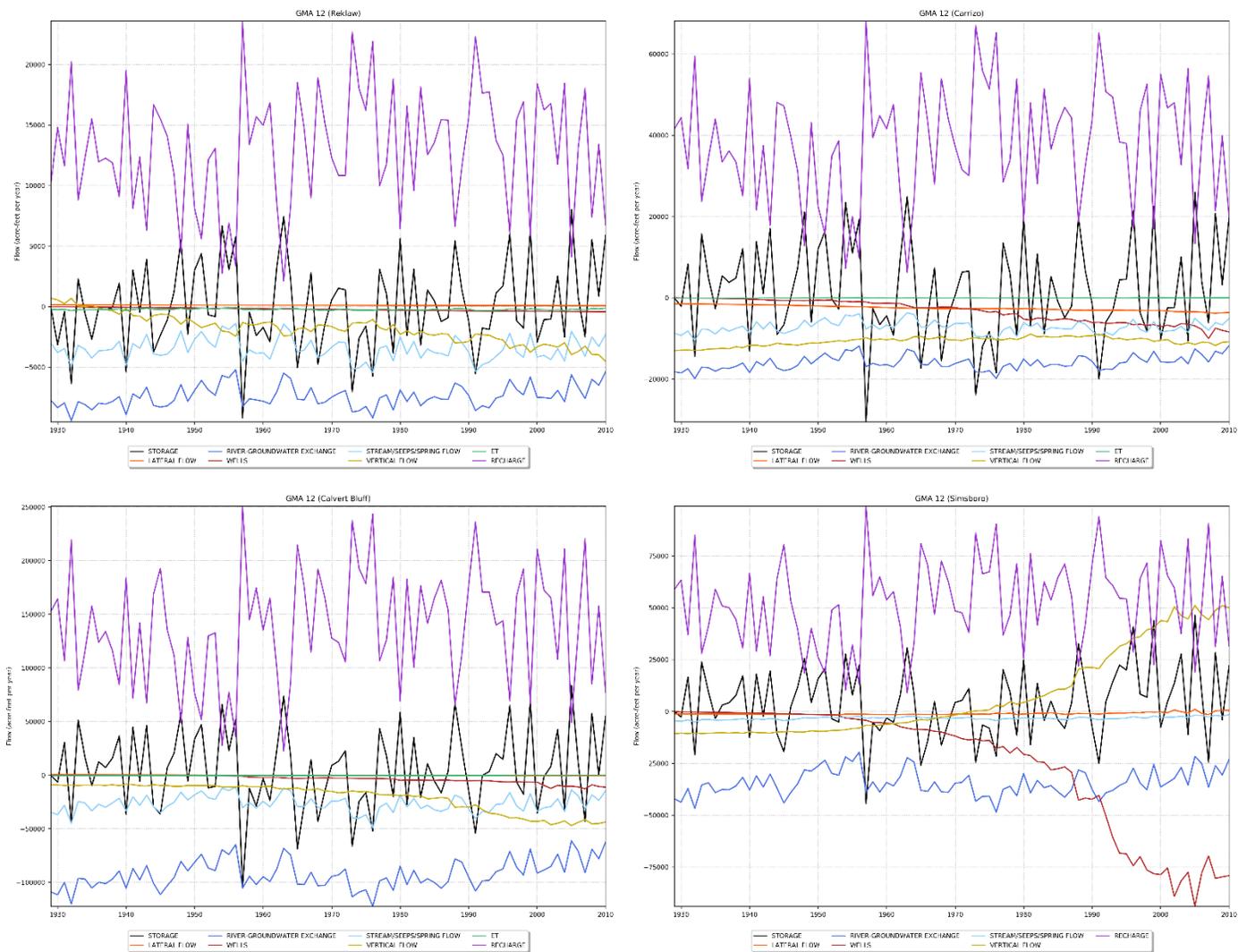
Figure 5.5.2k. **Transient water budget for Groundwater Management Area 12 for the Reklaw Formation, Carrizo Aquifer, and Calvert Bluff and Simsboro formations.**
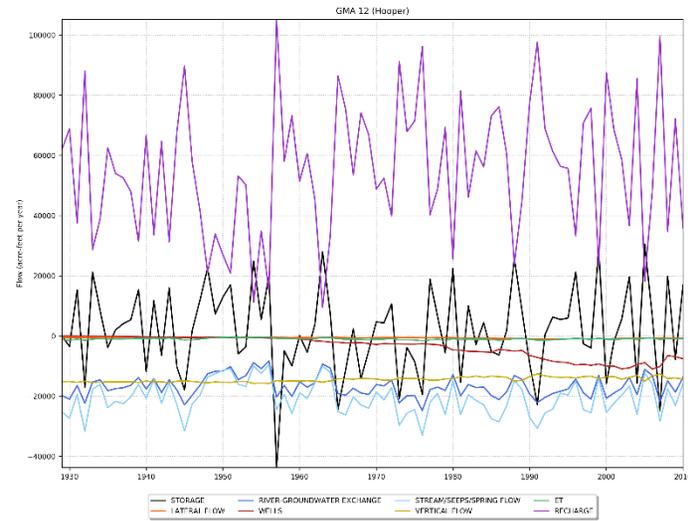
Figure 5.5.2l. **Transient water budget for Groundwater Management Area 12 for the Hooper Formation.**

6   Sensitivity Analysis

A sensitivity analysis was performed on the calibrated model to determine the impact of changes in calibrated parameters on the predictions of the calibrated model. A sensitivity analysis provides a means of formally describing the impact of varying specific parameters or groups of parameters on model outputs. In this sensitivity analysis, input parameters were systematically increased and decreased from their calibrated values while select model results were recorded. Informally, this is referred to as a standard "one-off" sensitivity analysis. This means that hydraulic parameters or stresses were adjusted from their calibrated "base case" values one at a time while all other hydraulic parameters remained unperturbed.

Section 6.1 describes the sensitivity analysis procedure. Section 6.2 contains a discussion of the results of the steady-state and transient sensitivity analyses, primarily presented using spider plots and summary tables. In addition, the sensitivity of transient simulated hydrograph responses to several parameters is shown at the end of the section.

6.1   Sensitivity Analysis Procedure

Four simulations were completed for each parameter sensitivity, where the input parameters were varied either according to:

$$\text{(new parameter)} = \text{(old parameter)} * \text{factor} \qquad \text{(Equation 6-1)}$$

or

$$\text{(new parameter)} = \text{(old parameter)} * 10^{(\text{factor - 1})} \qquad \text{(Equation 6-2)}$$

and the factors were 0.5, 0.9, 1.1, and 1.5. Parameters such as recharge rate and specific storage were varied linearly using Equation 6-1. For parameters such as hydraulic conductivity, which are typically thought of as log-varying, Equation 6-2 was used. For the output variable, the mean difference between the calibrated simulated hydraulic head and the sensitivity simulated hydraulic head was calculated as:

$$MD = \frac{1}{n} \sum_{i=1}^{n} \left(h_{sens,i} - h_{cal,i} \right) \qquad \text{(Equation 6-3)}$$

where:

MD = mean difference
$h_{sens,i}$ = sensitivity simulation hydraulic head at active grid cell i
$h_{cal,i}$ = calibrated simulation hydraulic head at active grid cell i
n = number of active grid cells, or the number of target locations

Similarly, the mean difference in fluxes was calculated for flux boundaries as:

$$MD = \frac{1}{n} \sum_{i=1}^{n} \left(q_{sens,i} - q_{cal,i} \right) \qquad \text{(Equation 6-4)}$$

where:

MD	=	mean difference
$q_{sens,i}$	=	sensitivity simulation flow at active grid cell i
$q_{cal,i}$	=	calibrated simulation flow at active grid cell i
n	=	number of cells for flow boundary

For the steady-state sensitivity analysis, the 24 model parameters listed in Table 6.1a were evaluated. Because modifying each parameter involved performing four model simulations, a total of 96 simulations were performed for the steady-state sensitivity analysis. For each input parameter listed in Table 6.1a, the sensitivities were assessed for the average hydraulic head in each hydrogeologic unit, fluxes to hydraulic boundaries, the number of flooded grid cells, and the model calibration statistics.

Table 6.1a.   **List of 24 model parameters varied for the steady-state sensitivity analysis.**

Number	Parameter	Type Multiplication Factor
1	Horizontal hydraulic conductivity of Colorado River and Brazos River Alluvium	log-varying
2	Vertical hydraulic conductivity of Colorado River and Brazos River Alluvium	log-varying
3	Horizontal hydraulic conductivity of Sparta	log-varying
4	Vertical hydraulic conductivity of Sparta	log-varying
5	Horizontal hydraulic conductivity of Weches	log-varying
6	Vertical hydraulic conductivity of Weches	log-varying
7	Horizontal hydraulic conductivity of Queen City	log-varying
8	Vertical hydraulic conductivity of Queen City	log-varying
9	Horizontal hydraulic conductivity of Reklaw	log-varying
10	Vertical hydraulic conductivity of Reklaw	log-varying
11	Horizontal hydraulic conductivity of Carrizo	log-varying
12	Vertical hydraulic conductivity of Carrizo	log-varying
13	Horizontal hydraulic conductivity of Calvert Bluff	log-varying
14	Vertical hydraulic conductivity of Calvert Bluff	log-varying
15	Horizontal hydraulic conductivity of Simsboro	log-varying
16	Vertical hydraulic conductivity of Simsboro	log-varying
17	Horizontal hydraulic conductivity of Hooper	log-varying
18	Vertical hydraulic conductivity of Hooper	log-varying
19	Drain Conductance	linear varying
20	River Conductance	linear varying
21	General-head boundary conductance for Layer 3 (Sparta-Cook Mountain)	linear varying
22	Maximum evapotranspiration rate	linear varying
23	Evapotranspiration extinction (rooting) depth	linear varying
24	Recharge rate	linear varying

In addition to the steady-state sensitivity analysis, a sensitivity analysis was performed on the transient model using the 20 model parameters listed in Table 6.1b. Because modifying each parameter involved performing four model simulations, a total of 80 simulations were performed for the transient sensitivity analysis. For each input parameter listed below, the sensitivities of drawdown from 1930 to 2010 in the Sparta, Queen City, and Carrizo aquifers and the Simsboro Formation; fluxes to hydraulic boundaries; and model calibration statistics were assessed.

Table 6.1b.   **List of 20 model parameters used for the transient sensitivity analysis.**

Number	Parameter	Type Multiplication Factor
1	Horizontal hydraulic conductivity of Sparta	log-varying
2	Vertical hydraulic conductivity of Sparta	log-varying
3	Horizontal hydraulic conductivity of Queen City	log-varying
4	Vertical hydraulic conductivity of Queen City	log-varying
5	Horizontal hydraulic conductivity of Carrizo	log-varying
6	Vertical hydraulic conductivity of Carrizo	log-varying
7	Horizontal hydraulic conductivity of Simsboro	log-varying
8	Vertical hydraulic conductivity of Simsboro	log-varying
9	Specific storage of Sparta	linear varying
10	Specific yield of Sparta	linear varying
11	Specific storage of Queen City	linear varying
12	Specific yield Queen City	linear varying
13	Specific storage of Carrizo	linear varying
14	Specific yield Carrizo	linear varying
15	Specific storage of Simsboro	linear varying
16	Specific yield Simsboro	linear varying
17	Recharge rate	linear varying
18	Drain conductance	linear varying
19	River conductance	linear varying
20	Pumping rate	linear varying

6.2 Sensitivity Analysis Results

Results of the steady-state and transient sensitivity analyses are presented in the following subsections.

6.2.1 *Steady-State Sensitivities*

Output metrics for the steady-state sensitivity analysis were average hydraulic head for the nine hydrogeologic units; total flux in the general-head, drain, and river hydraulic boundary cells; and the total number of flooded cells in the model. The model calibration statistics were also assessed. Twenty-four sets of results, one for each of the 24 parameters varied in the sensitivity analysis, are shown in Figures 6.2.1a through 6.2.1x. Each of these figures contains the following four plots:

- Top left plot – sensitivity of average hydraulic head in the nine hydrogeologic units model-wide.

- Top right plot – sensitivity of total flux in the hydraulic boundaries (general-head boundary cells, drain cells, and river cells) model-wide. Included on this figure are the base case total fluxes for these hydraulic boundary types.
- Bottom left plot – sensitivity of the total number of flooded cells model-wide.
- Bottom right plot – the model-wide calibration statistics.

These figures show the details of how each metric responses to each change in parameter value.

To distill the results into a meaningful understanding of the sensitivity of the steady-state model, a systematic methodology was developed to assess the sensitivity to the 24 input parameters modified. For each metric, a ranking was developed to represent the impact on that metric as a result of the change in the parameter value. The rankings are provided in Tables 6.2.1a and 6.2.1b. A ranking of 1 indicates little impact and is associated with a small change relative to the base case value; a ranking of 6 indicates a large impact and is associated with a large change relative to the base case value. A change in the average hydraulic head of greater than 3.5 feet from the base case value, and an increase in the number of flooded cells in the model of greater than 100 were considered large impacts (Table 6.2.1a). For the hydraulic boundary fluxes, a greater than 10 percent change relative to the base case value was considered a large impact (Table 6.2.1b).

Table 6.2.1a.   **Ranking for assessing impact to average hydraulic head and number of flooded cells.**

Ranking	Change in Average Hydraulic Head from Base Case Value (feet)	Number of Additional Flooded Cells
1	0 to 0.5	6
2	0.5 to 1	12
3	1 to 1.5	25
4	1.5 to 2.25	50
5	2.25 to 3.5	100
6	> 3.5	>100

Table 6.2.1b.   **Ranking for assessing impact to hydraulic boundary fluxes.**

Ranking	Change in Hydraulic Boundary Flux Relative to Base Case Value (acre-feet per year)		
	General-Head Boundary	**Drain Boundary**	**River Boundary**
1	9	3,000	4,000
2	19	6,000	8,000
3	38	10,000	16,000
4	75	15,000	35,000
5	150[a]	40,000[a]	80,000[a]
6	>150	>40,000	>80,000

[a] represents about a 10 percent change relative to the base case value

The results from the sensitivity analysis were summarized based on the rankings presented above to determine the parameters to which the steady-state model is most sensitive. The ranking summary for change in average hydraulic head across the model by hydrogeologic unit for the

24 parameters considered by the sensitivity analysis is provided in Table 6.2.1c. Also included in this table is the average of the rankings for each parameter. Based on these averages, the five parameters having the greatest impact on hydraulic head in the steady-state model, in order of importance, are: the recharge rate, the horizontal hydraulic conductivity of the Queen City Aquifer, the vertical hydraulic conductivity of the Reklaw Formation, the horizontal hydraulic conductivity of the Sparta Aquifer, and the horizontal hydraulic conductivity of the Simsboro Formation. The model has little sensitivity, based on the hydraulic head metric to 13 out of the 24 parameters as determined by ranking averages of 1.5 or less in Table 6.2.1c. These include all of the conductance values for the hydraulic boundary cells and the evapotranspiration parameters.

The ranking summary for how the 24 parameters impact change in hydraulic boundary fluxes is provided in Table 6.2.1d. This table also includes the average value for how each parameter impacts the change in the fluxes to drain cells, river cells, and the general head boundary cells. Based on the average for these three fluxes, the three parameters having the greatest impact on hydraulic boundary fluxes are: the recharge rate, the horizontal hydraulic conductivity of the Queen City Aquifer, and the horizontal hydraulic conductivity of the Sparta Aquifer. Four parameters are tied for the fourth greatest impact on the hydraulic boundary fluxes: the vertical hydraulic conductivity of the Queen City Aquifer, the horizontal hydraulic conductivity of the Carrizo Aquifer, the horizontal hydraulic conductivity of the Calvert Bluff Formation, and the horizontal hydraulic conductivity of the Simsboro Formation.

Table 6.2.1d also includes the ranking for the number of additional flooded cells for each of the 24 parameters. Based on these rankings, the four parameters having the greatest impact on the number of flooded cells in the steady-state model are: recharge rate, the horizontal hydraulic conductivity of the Queen City Aquifer, the drain conductance, and the river conductance. Three parameters are tied for the fifth greatest impact on the hydraulic boundary fluxes: the horizontal hydraulic conductivity of the Calvert Bluff Formation, the horizontal hydraulic conductivity of the Hooper Formation, and the maximum rate for evapotranspiration.

Table 6.2.1c. **Summary for change in average hydraulic head across the model by hydrogeologic unit for the 24 parameters considered by the steady-state sensitivity analysis.**

Number	Parameter	Ranking for Change in Average Hydraulic Head									Average of Rankings
		Alluvium	Sparta	Weches	Queen City	Reklaw	Carrizo	Calvert Bluff	Simsboro	Hooper	
1	Kx of Alluvium	4	1	1	1	1	1	1	1	1	1.33
2	Kv of Alluvium	1	1	1	1	1	1	1	1	1	1.00
3	Kx of Sparta	1	6	6	5	4	3	2	2	1	3.33
4	Kv of Sparta	1	1	1	1	1	1	1	1	1	1.00
5	Kx of Weches	1	1	2	1	1	1	1	1	1	1.11
6	Kv of Weches	1	1	1	2	1	1	1	1	1	1.11
7	Kx of Queen City	1	3	5	6	5	5	4	4	3	4.00
8	Kv of Queen City	1	2	2	4	5	4	2	2	2	2.67
9	Kx of Reklaw	1	1	1	1	4	1	1	1	1	1.33
10	Kv of Reklaw	1	1	1	2	4	6	5	5	5	3.33
11	Kx of Carrizo	1	1	2	2	3	3	2	2	2	2.00
12	Kv of Carrizo	1	1	1	1	1	4	3	3	2	1.89
13	Kx of Calvert Bluff	1	1	1	1	1	1	3	3	4	1.78
14	Kv of Calvert Bluff	1	1	1	1	1	1	5	5	5	2.33
15	Kx of Simsboro	1	1	2	2	5	5	5	5	3	3.22
16	Kv of Simsboro	1	1	1	1	1	1	2	2	2	1.33
17	Kx of Hooper	1	1	1	1	1	2	3	3	6	2.11
18	Kv of Hooper	1	1	1	1	1	1	1	1	5	1.44
19	Drain Conductance	1	1	1	1	1	1	1	1	1	1.00
20	River Conductance	2	1	1	1	1	1	1	1	1	1.11
21	GHB Conductance for Layer 3	1	1	1	1	1	1	1	1	1	1.00
22	ET Evaporation Rate	1	1	1	1	1	1	1	1	1	1.00
23	ET Extinction Depth	1	1	1	1	1	1	1	1	1	1.00
24	Recharge Rate	4	5	6	6	6	6	6	6	6	5.67

Note: Kx = horizontal hydraulic conductivity; Kv = vertical hydraulic conductivity; GHB = general-head boundary; ET = evapotranspiration

Table 6.2.1d. **Summary for change in total hydraulic boundary fluxes and additional number of flooded cells for the 24 parameters considered by the steady-state sensitivity analysis.**

| Number | Parameter | Ranking for Change in Hydraulic Boundary Flux | | | Average of Flux Rankings | Ranking for Flooded Cells |
		General-Head Boundary Cells	Drain Cells	River Cells		
1	Kx of Alluvium	5	1	1	2.3	2
2	Kv of Alluvium	1	1	1	1.0	1
3	Kx of Sparta	6	5	4	5.0	3
4	Kv of Sparta	6	1	1	2.7	1
5	Kx of Weches	6	2	2	3.3	2
6	Kv of Weches	6	1	1	2.7	1
7	Kx of Queen City	6	6	5	5.7	5
8	Kv of Queen City	6	4	3	4.3	2
9	Kx of Reklaw	5	2	2	3.0	2
10	Kv of Reklaw	6	3	3	4.0	1
11	Kx of Carrizo	6	4	3	4.3	1
12	Kv of Carrizo	6	2	1	3.0	1
13	Kx of Calvert Bluff	4	5	4	4.3	4
14	Kv of Calvert Bluff	5	4	3	4.0	1
15	Kx of Simsboro	6	4	3	4.3	3
16	Kv of Simsboro	4	2	1	2.3	1
17	Kx of Hooper	5	4	3	4.0	4
18	Kv of Hooper	1	1	1	1.0	1
19	Drain Conductance	5	3	2	3.3	5
20	River Conductance	6	3	3	4.0	5
21	GHB Conductance for Layer 3	6	1	1	2.7	1
22	ET Evaporation Rate	3	1	1	1.7	4
23	ET Extinction Depth	1	1	1	1.0	1
24	Recharge Rate	6	6	6	6.0	6

Note: Kx = horizontal hydraulic conductivity; Kv = vertical hydraulic conductivity; GHB = general-head boundary; ET = evapotranspiration

Rankings were also developed for changes in calibration statistics to assess the sensitivity of the steady-state model (Table 6.2.1e). A change in the mean error greater than 1 foot relative to the base case value and changes in the mean absolute error and the root mean square error of greater than 15 percent relative to the base case value were considered a large impact.

Table 6.2.1e. **Ranking for assessing impact to calibration statistics.**

Ranking	Change Relative to Base Case Value (feet)		
	Mean Error	**Mean Absolute Error**	**Root Mean Square Error**
1	0 to 0.06	0 to 0.19	0 to 0.25
2	0.06 to 0.16	0.19 to 0.38	0.25 to 0.5
3	0.16 to 0.25	0.38 to 0.75	0.5 to 1
4	0.25 to 0.5	0.75 to 1.5	1 to 2
5	0.5 to 1	1.5 to 3	2 to 4
6	> 1	> 3	> 4

Note: > = greater than

The ranking summary for model calibration statistics and the average of the rankings for the 24 parameters considered by the sensitivity analysis are provided in Table 6.2.1f. Based on these averages, the five parameters having the greatest impact on the calibration statistics for the steady-state model, in order of importance, are: the recharge rate, the horizontal hydraulic conductivity of the Calvert Bluff Formation, the horizontal hydraulic conductivity of the Queen City Aquifer, the vertical hydraulic conductivity of the Calvert Bluff Formation, and the horizontal hydraulic conductivity of the Carrizo Aquifer The model has some sensitivity, based on the calibration statistics metric, to most of the parameters considered in the analysis. The impact of change in each of the 24 parameters on the calibration statistics can also be quickly assessed using this table.

Table 6.2.1f. **Summary for change in calibration statistics for the 24 parameters considered by the steady-state sensitivity analysis.**

Number	Parameter	Ranking for Calibration Statistics			Average of Calibration Statistics Rankings
		Mean Error	Mean Absolute Error	Root Mean Square Error	
1	Kx of Alluvium	2	1	1	1.33
2	Kv of Alluvium	1	1	1	1.00
3	Kx of Sparta	6	2	2	3.33
4	Kv of Sparta	3	1	1	1.67
5	Kx of Weches	3	1	1	1.67
6	Kv of Weches	2	1	1	1.33
7	Kx of Queen City	6	4	4	4.67
8	Kv of Queen City	5	1	2	2.67
9	Kx of Reklaw	3	1	1	1.67
10	Kv of Reklaw	4	1	1	2.00
11	Kx of Carrizo	5	4	4	4.33
12	Kv of Carrizo	2	1	1	1.33
13	Kx of Calvert Bluff	6	5	5	5.33
14	Kv of Calvert Bluff	6	4	3	4.33
15	Kx of Simsboro	5	3	3	3.67
16	Kv of Simsboro	3	1	1	1.67
17	Kx of Hooper	6	3	3	4.00
18	Kv of Hooper	2	1	1	1.33
19	Drain Conductance	3	1	1	1.67
20	River Conductance	4	1	1	2.00
21	GHB Conductance for Layer 3	1	1	1	1.00
22	ET Evaporation Rate	2	1	1	1.33
23	ET Extinction Depth	1	1	1	1.00
24	Recharge Rate	6	6	6	6.00

Note: Kx = horizontal hydraulic conductivity; Kv = vertical hydraulic conductivity; GHB = general-head boundary; ET = evapotranspiration
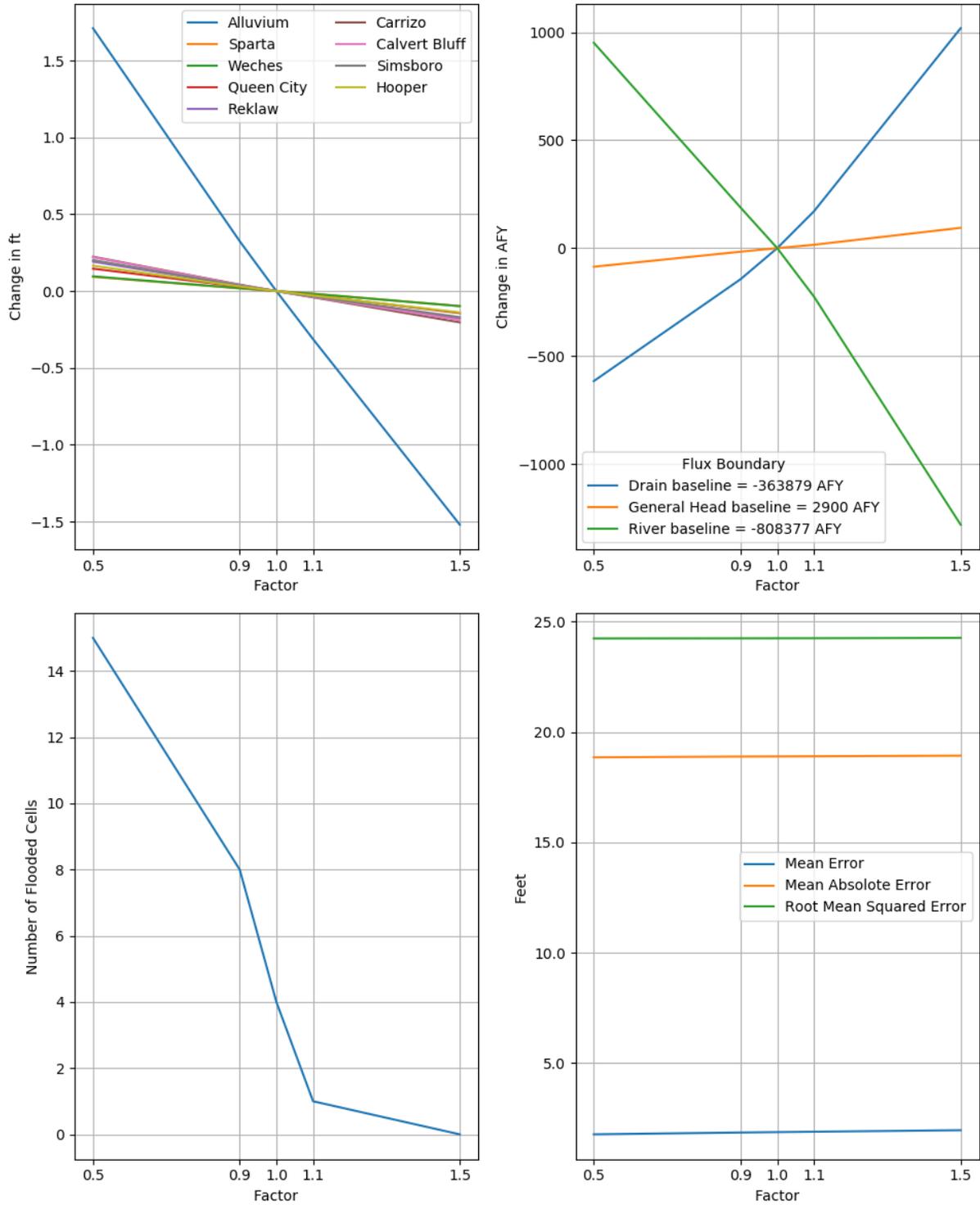
Figure 6.2.1a. Sensitivity of averaged hydraulic head in hydrogeologic units (top left), hydraulic boundary fluxes (top right), additional flooded grid cells (bottom left), and calibration statistics (bottom right) to the horizontal hydraulic conductivity of the Colorado River and Brazos rivers alluvium for the steady-state model.

Note: ft = feet; AFY = acre-feet per year
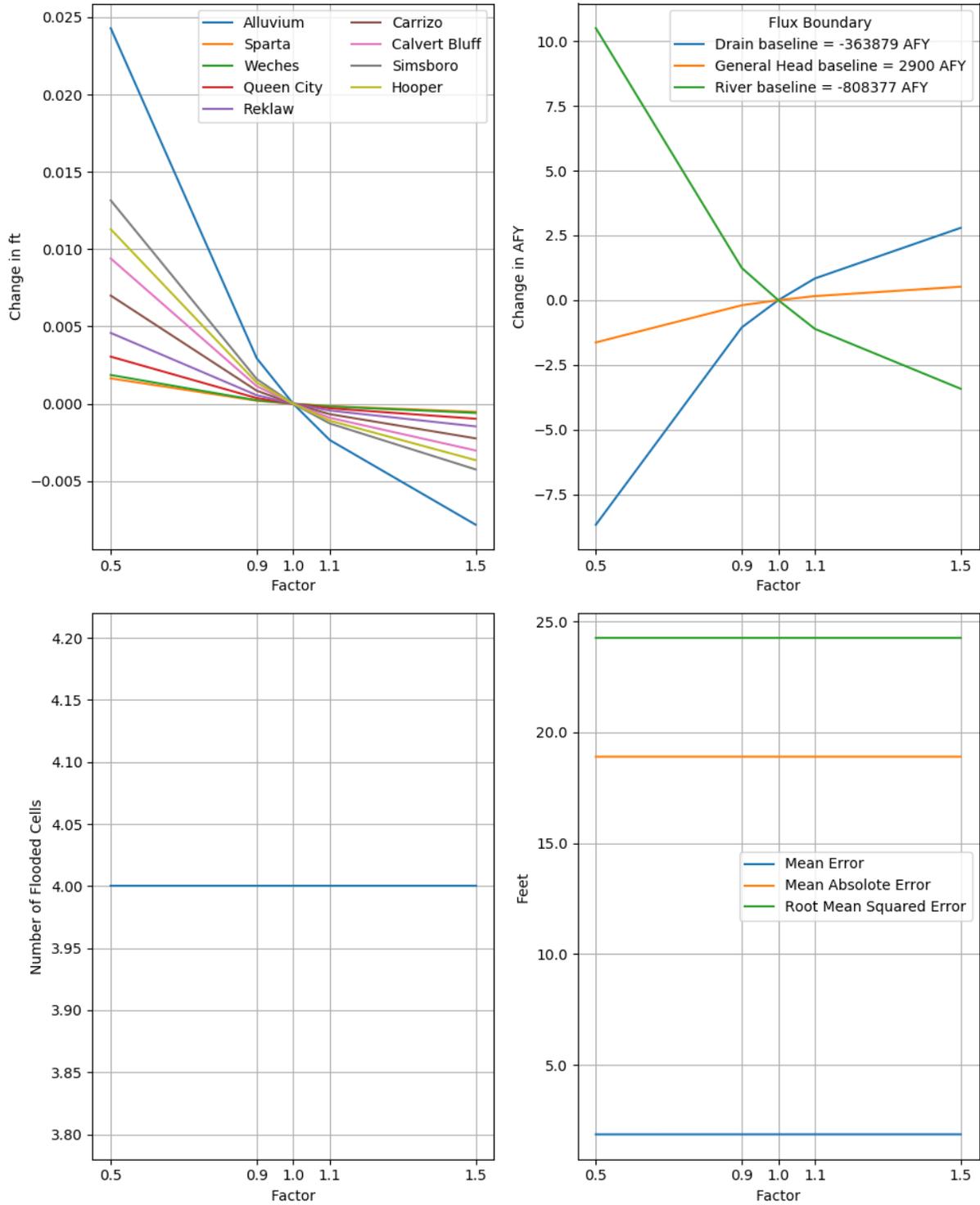
Figure 6.2.1b. Sensitivity of averaged hydraulic head in hydrogeologic units (top left), hydraulic boundary fluxes (top right), additional flooded grid cells (bottom left), and calibration statistics (bottom right) to the vertical hydraulic conductivity of the Colorado River and Brazos rivers alluvium for the steady-state model.

Note: ft = feet; AFY = acre-feet per year
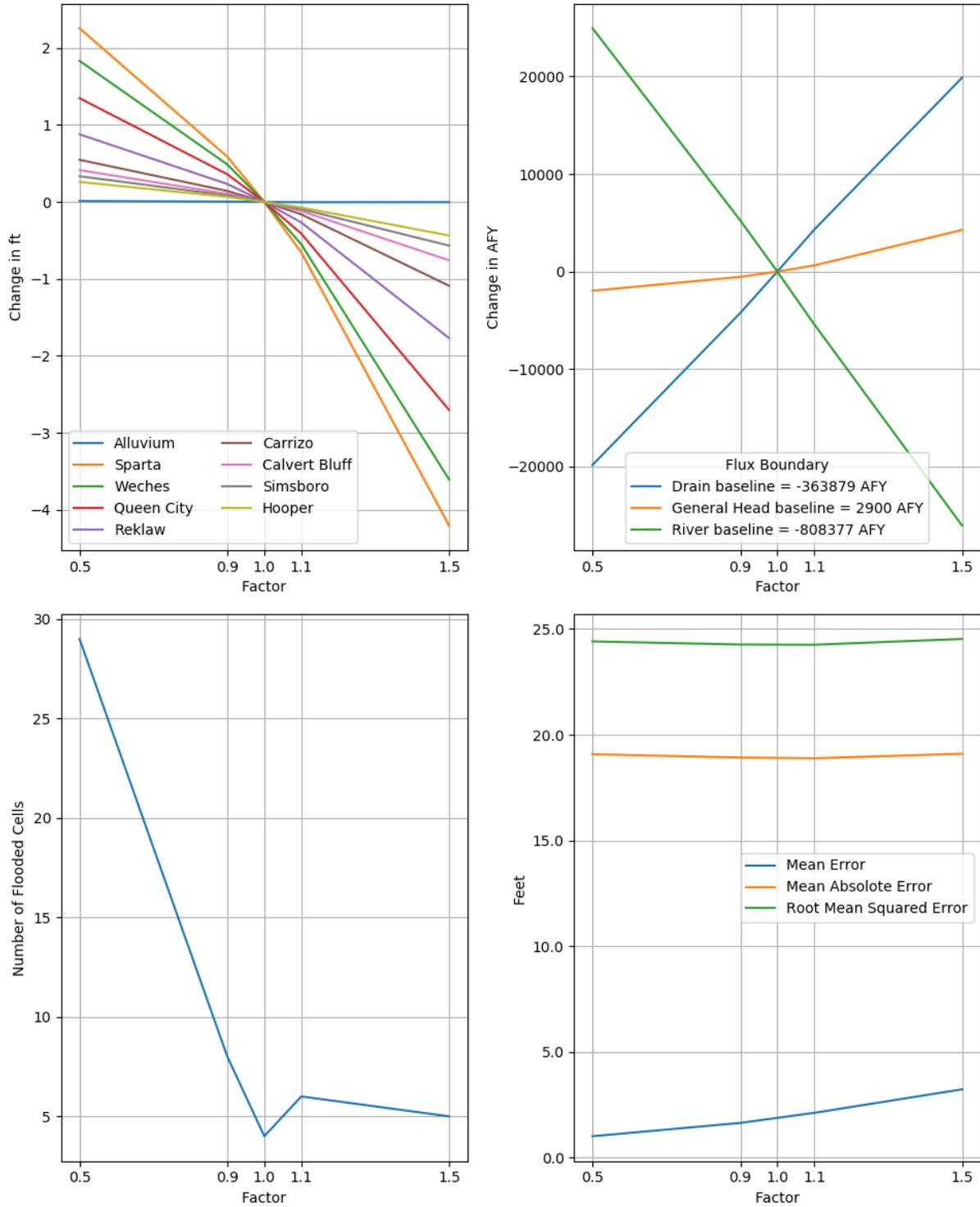
Figure 6.2.1c.   **Sensitivity of averaged hydraulic head in hydrogeologic units (top left), hydraulic boundary fluxes (top right), additional flooded grid cells (bottom left), and calibration statistics (bottom right) to the horizontal hydraulic conductivity of the Sparta Aquifer for the steady-state model.**

Note: ft = feet; AFY = acre-feet per year
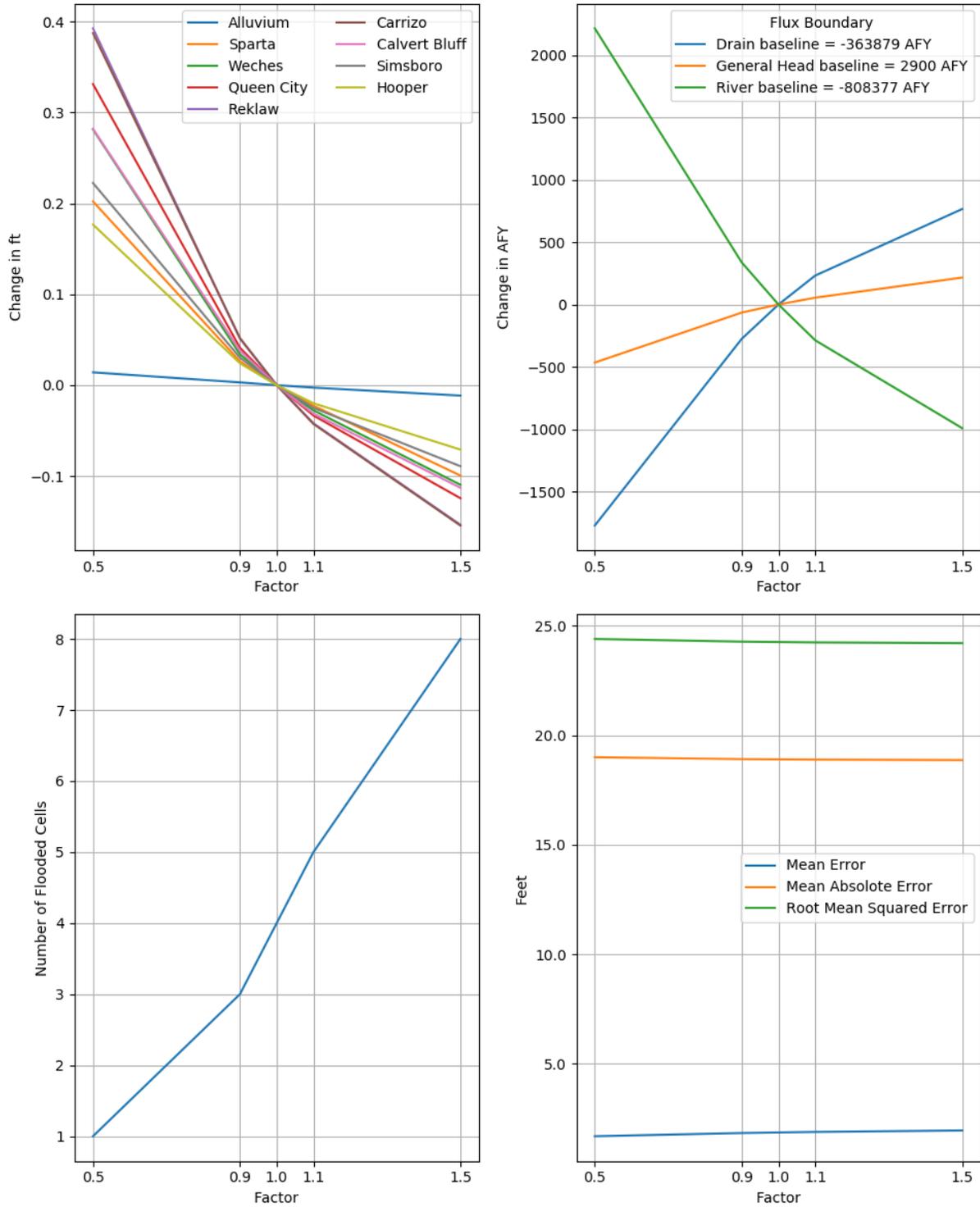
Figure 6.2.1d. **Sensitivity of averaged hydraulic head in hydrogeologic units (top left), hydraulic boundary fluxes (top right), additional flooded grid cells (bottom left), and calibration statistics (bottom right) to the vertical hydraulic conductivity of the Sparta Aquifer for the steady-state model.**

Note: ft = feet; AFY = acre-feet per year
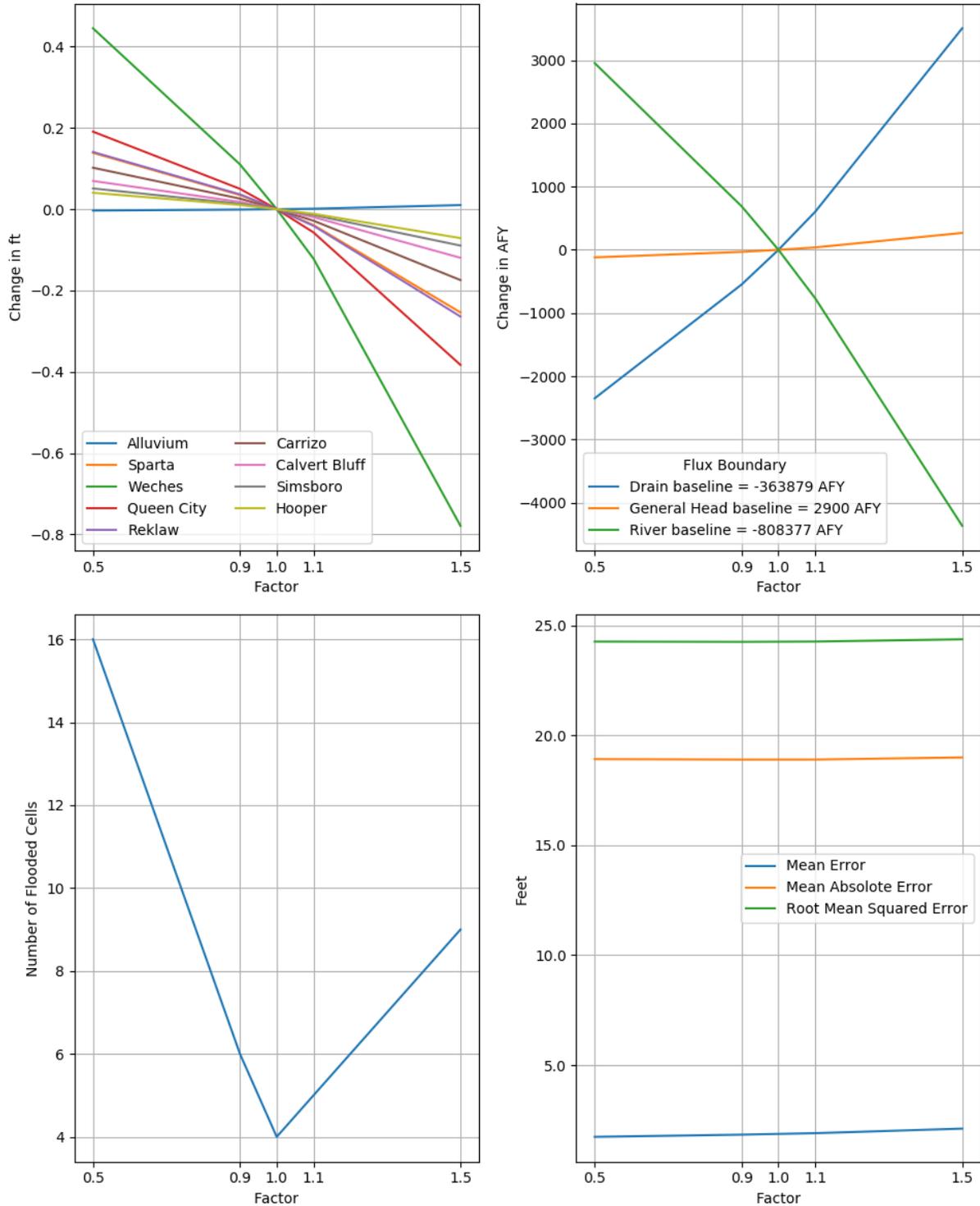
Figure 6.2.1e. **Sensitivity of averaged hydraulic head in hydrogeologic units (top left), hydraulic boundary fluxes (top right), additional flooded grid cells (bottom left), and calibration statistics (bottom right) to the horizontal hydraulic conductivity of the Weches Formation for the steady-state model.**

Note: ft = feet; AFY = acre-feet per year
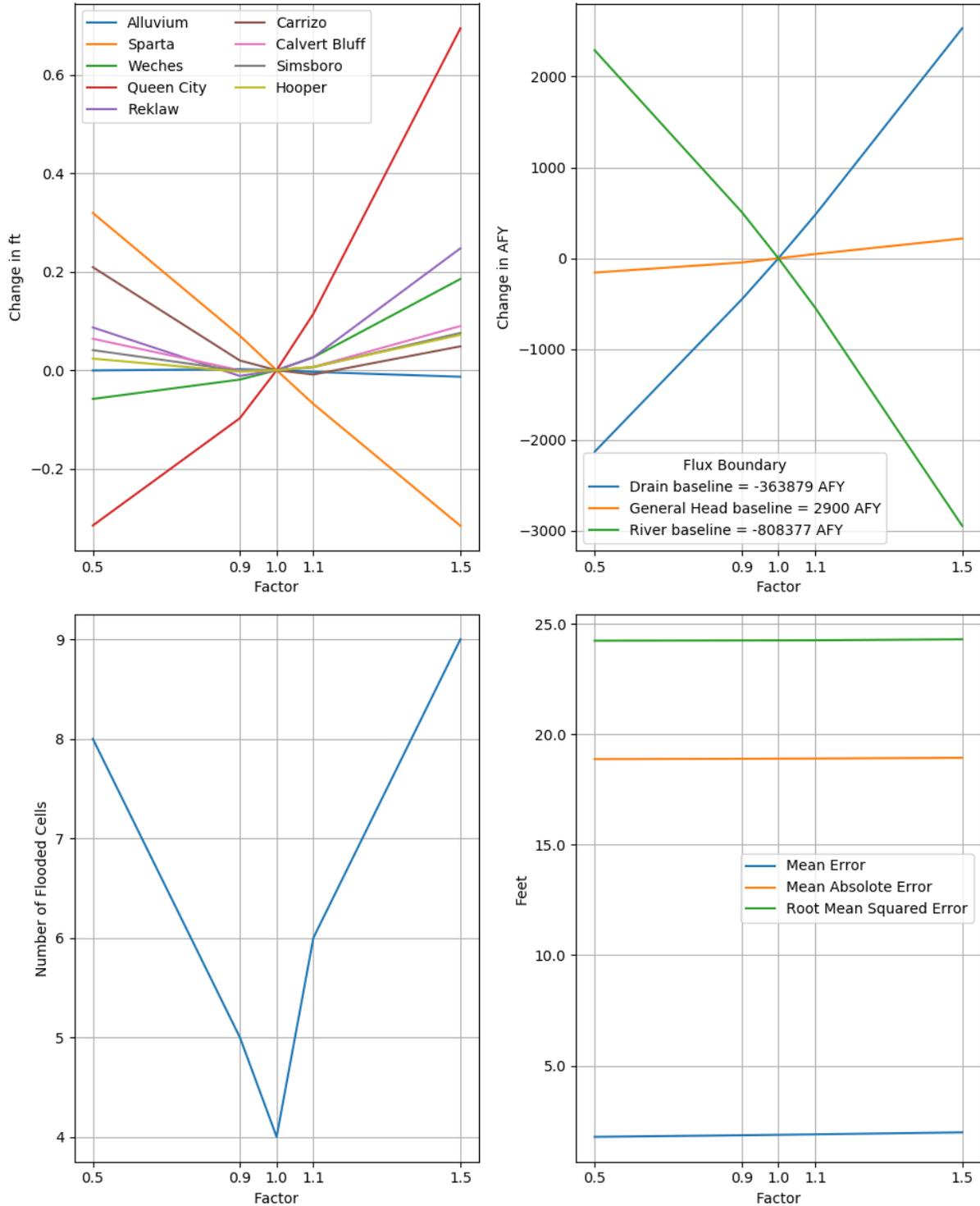
Figure 6.2.1f.   **Sensitivity of averaged hydraulic head in hydrogeologic units (top left), hydraulic boundary fluxes (top right), additional flooded grid cells (bottom left), and calibration statistics (bottom right) to the vertical hydraulic conductivity of the Weches Formation for the steady-state model.**

Note: ft = feet; AFY = acre-feet per year
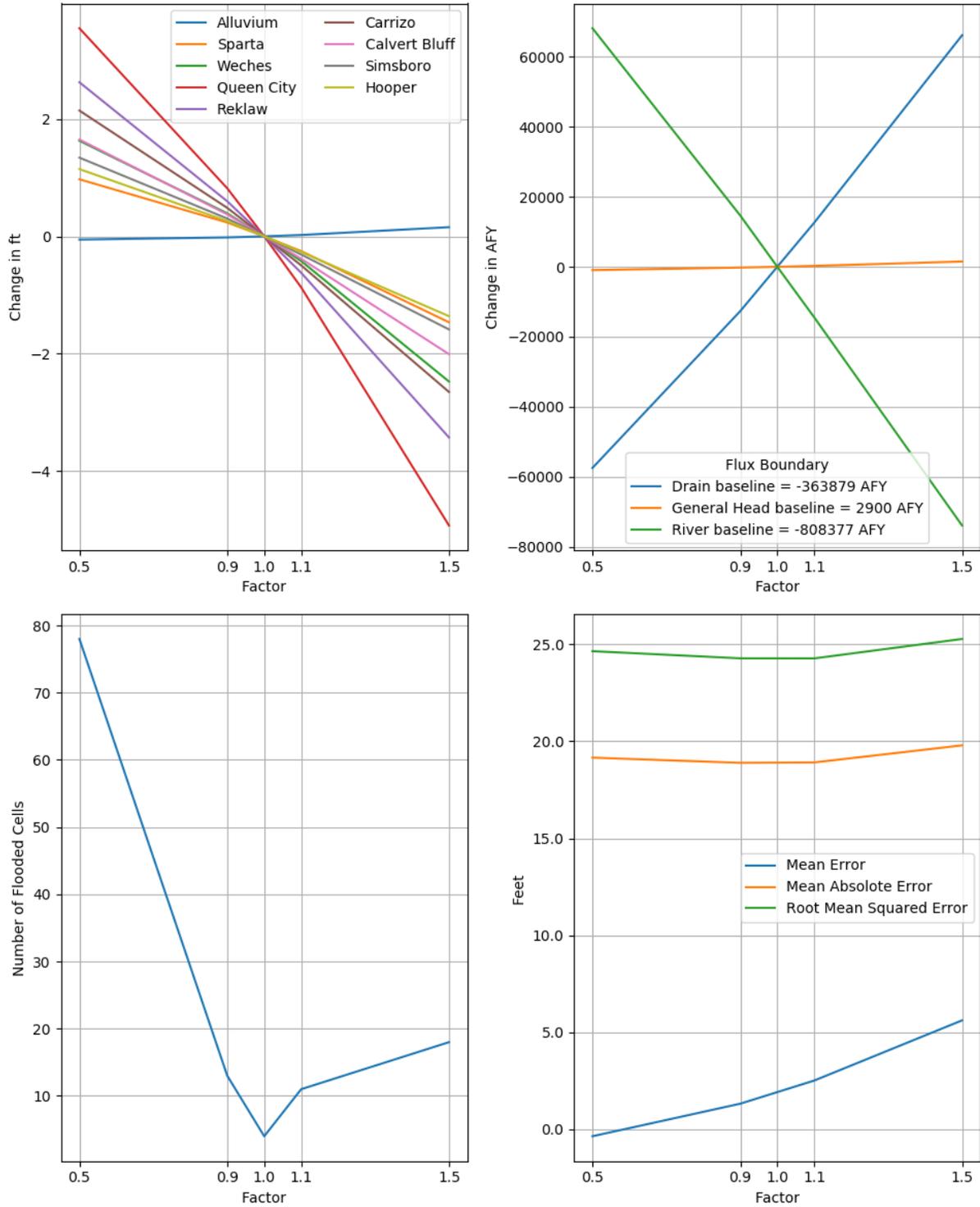
Figure 6.2.1g.   **Sensitivity of averaged hydraulic head in hydrogeologic units (top left), hydraulic boundary fluxes (top right), additional flooded grid cells (bottom left), and calibration statistics (bottom right) to the horizontal hydraulic conductivity of the Queen City Aquifer for the steady-state model.**

Note: ft = feet; AFY = acre-feet per year
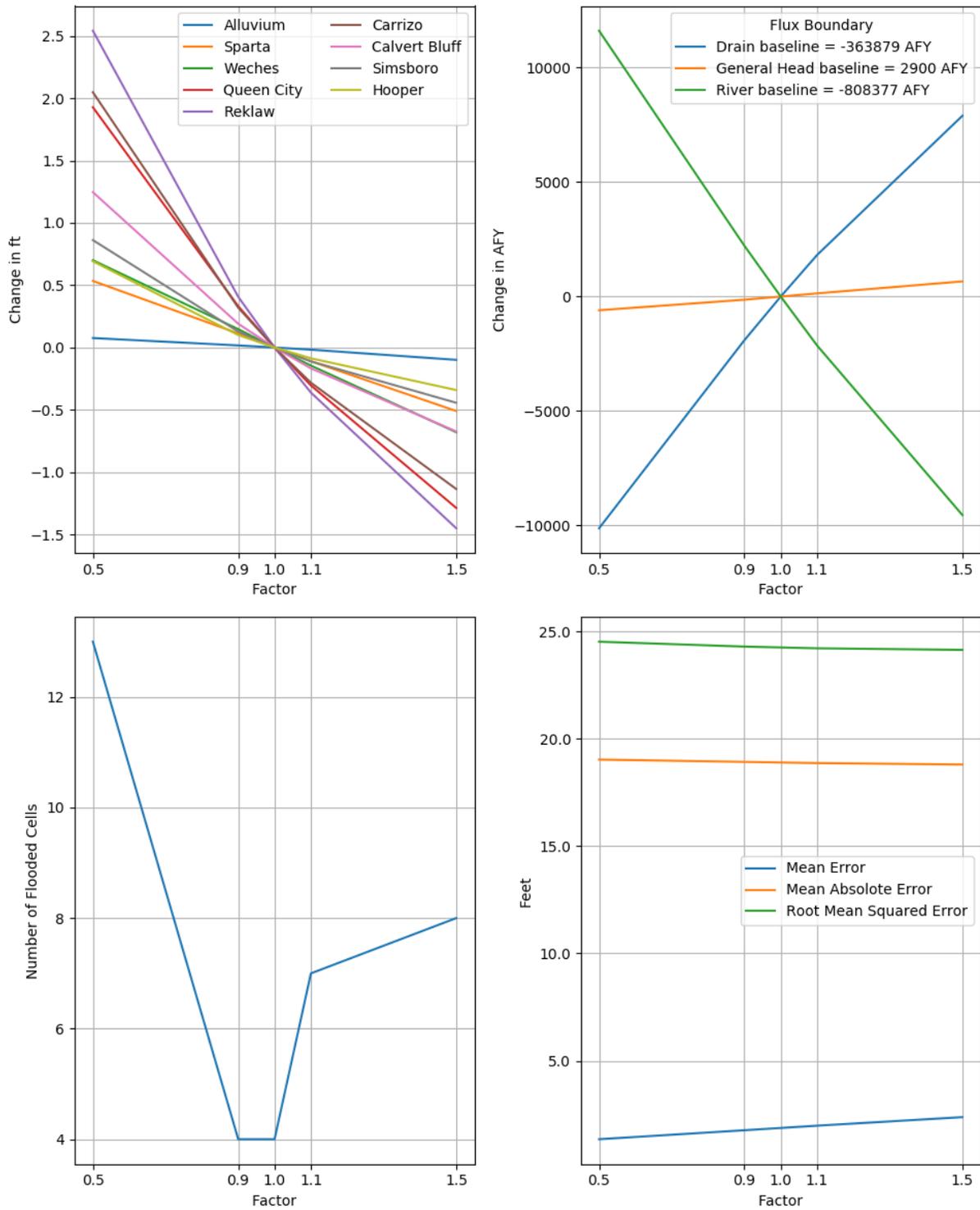
Figure 6.2.1h. Sensitivity of averaged hydraulic head in hydrogeologic units (top left), hydraulic boundary fluxes (top right), additional flooded grid cells (bottom left), and calibration statistics (bottom right) to the vertical hydraulic conductivity of the Queen City Aquifer for the steady-state model.

Note: ft = feet; AFY = acre-feet per year
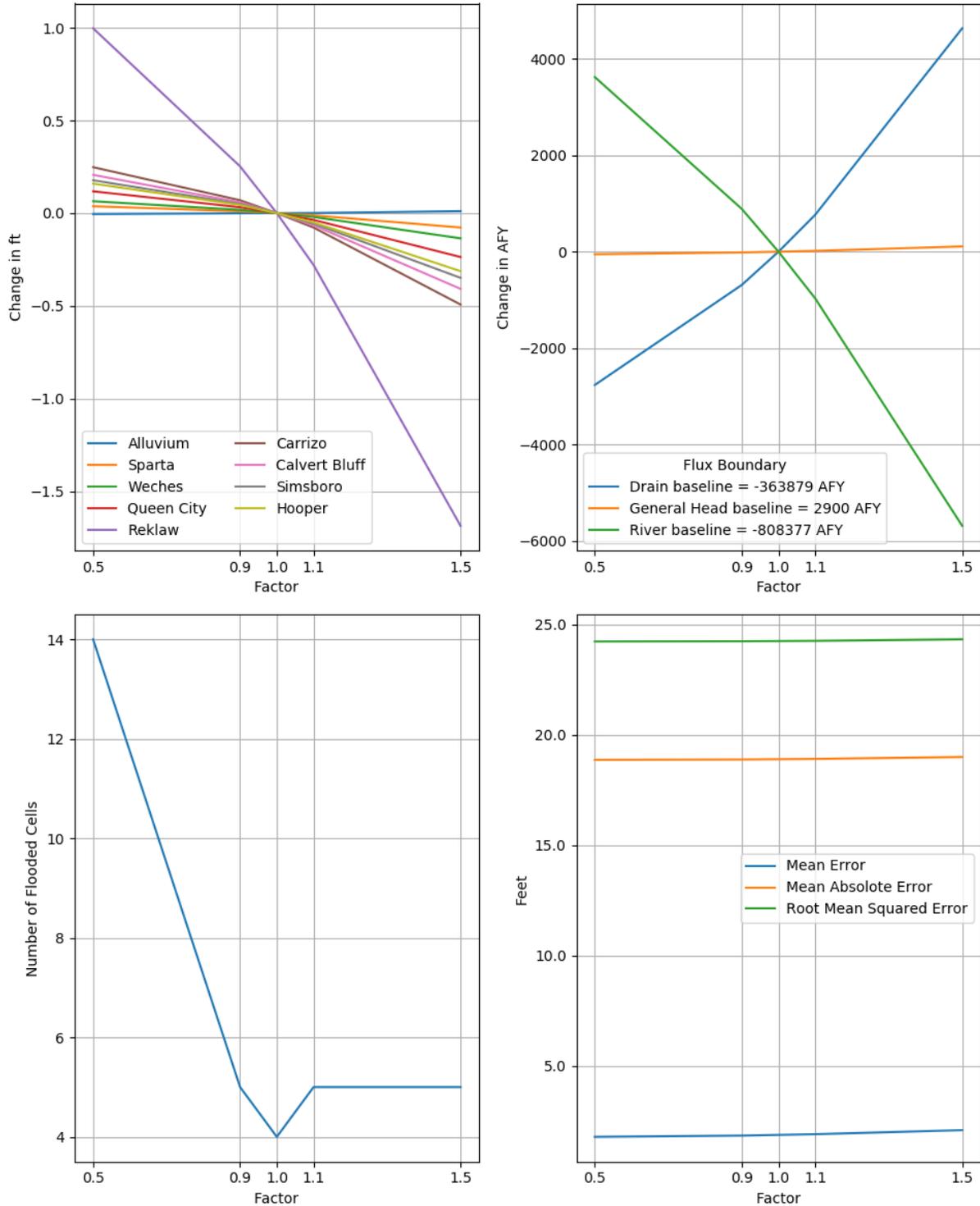
Figure 6.2.1i. **Sensitivity of averaged hydraulic head in hydrogeologic units (top left), hydraulic boundary fluxes (top right), additional flooded grid cells (bottom left), and calibration statistics (bottom right) to the horizontal hydraulic conductivity of the Reklaw Formation for the steady-state model.**

Note: ft = feet; AFY = acre-feet per year
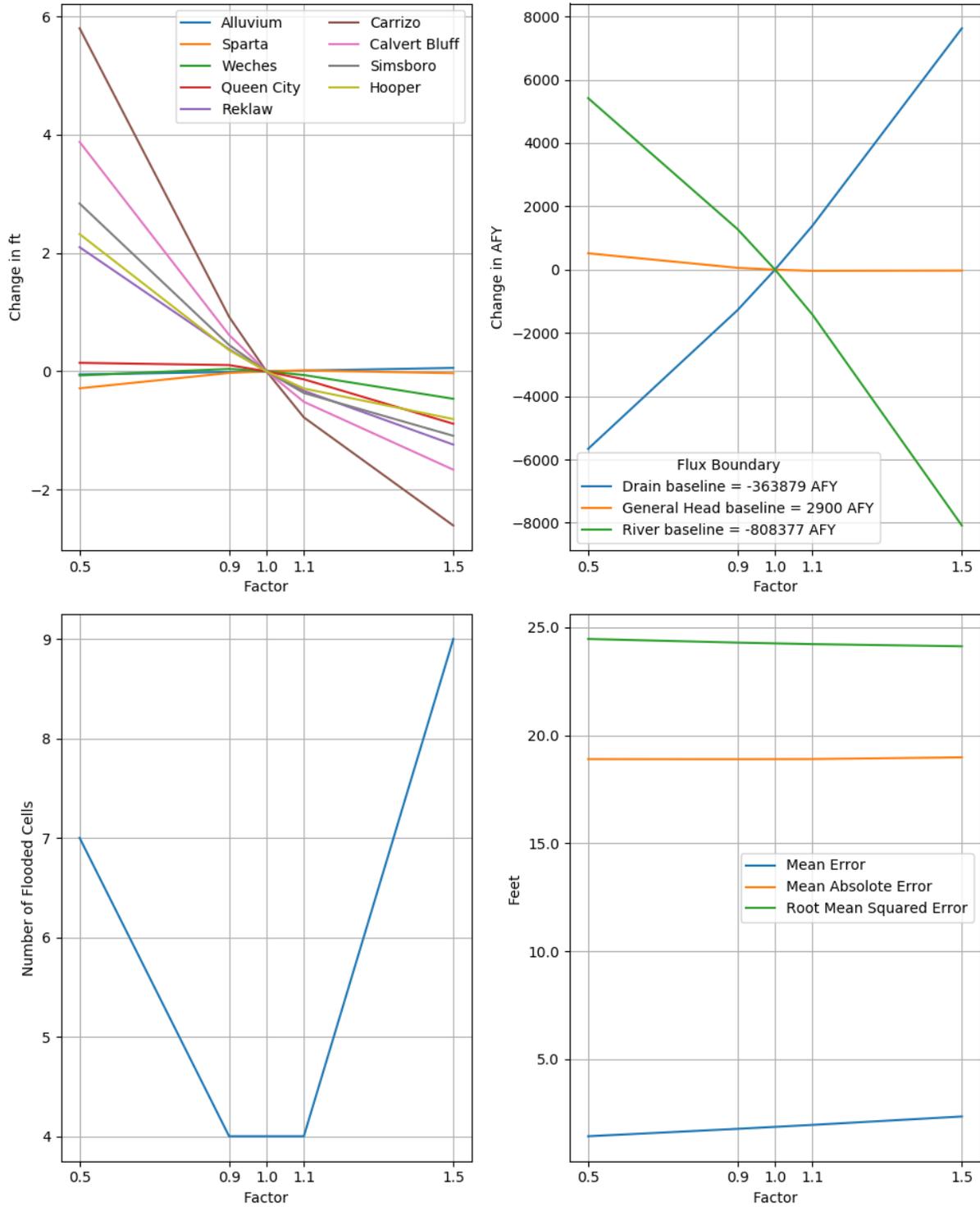
Figure 6.2.1j. **Sensitivity of averaged hydraulic head in hydrogeologic units (top left), hydraulic boundary fluxes (top right), additional flooded grid cells (bottom left), and calibration statistics (bottom right) to the vertical hydraulic conductivity of the Reklaw Formation for the steady-state model.**

Note: ft = feet; AFY = acre-feet per year
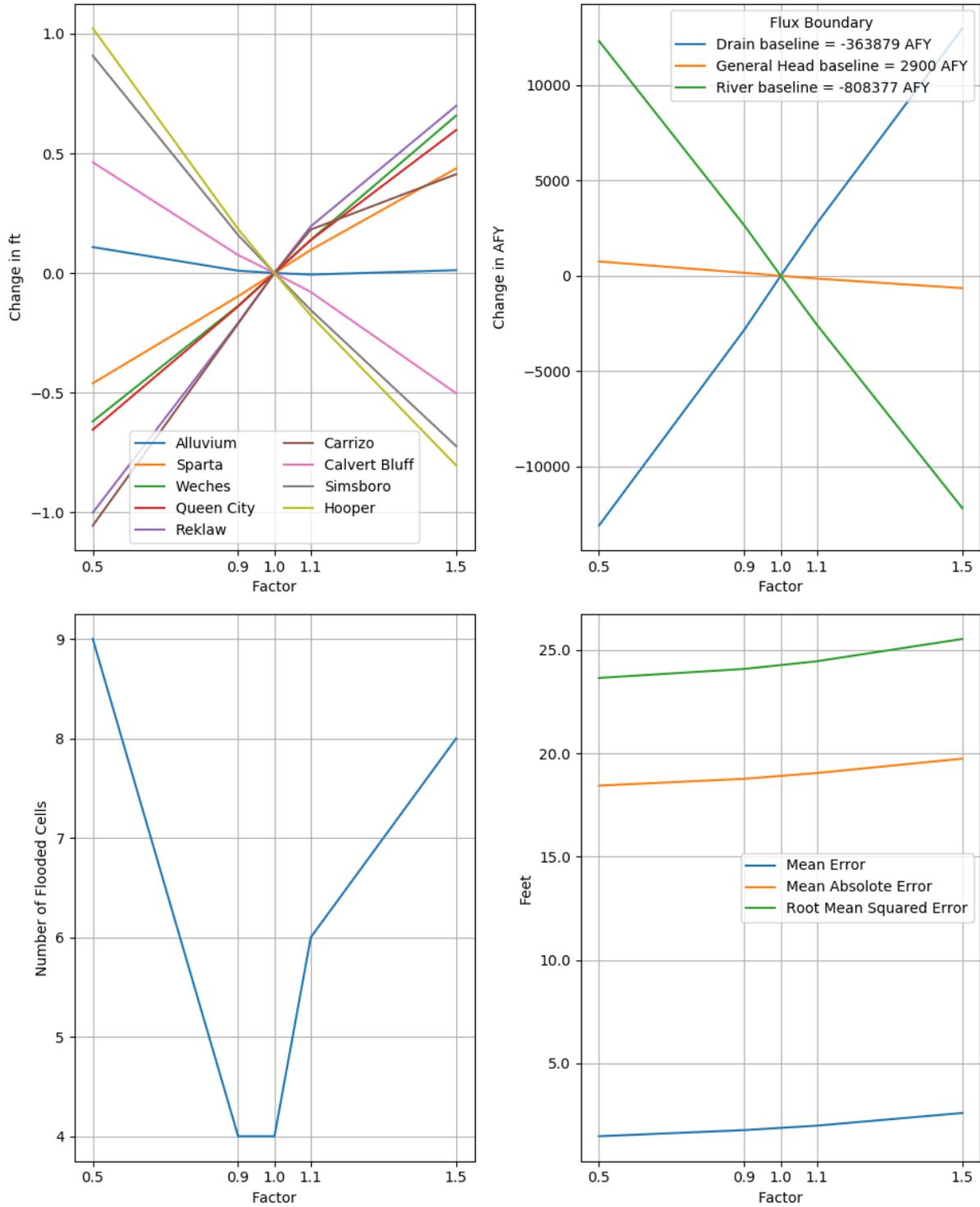
Figure 6.2.1k. **Sensitivity of averaged hydraulic head in hydrogeologic units (top left), hydraulic boundary fluxes (top right), additional flooded grid cells (bottom left), and calibration statistics (bottom right) to the horizontal hydraulic conductivity of the Carrizo Aquifer for the steady-state model.**

Note: ft = feet; AFY = acre-feet per year

Figure 6.2.1l. **Sensitivity of averaged hydraulic head in hydrogeologic units (top left), hydraulic boundary fluxes (top right), additional flooded grid cells (bottom left), and calibration statistics (bottom right) to the vertical hydraulic conductivity of the Carrizo Aquifer for the steady-state model.**

Note: ft = feet; AFY = acre-feet per year

Figure 6.2.1m. **Sensitivity of averaged hydraulic head in hydrogeologic units (top left), hydraulic boundary fluxes (top right), additional flooded grid cells (bottom left), and calibration statistics (bottom right) to the horizontal hydraulic conductivity of the Calvert Bluff Formation for the steady-state model.**

Note: ft = feet; AFY = acre-feet per year
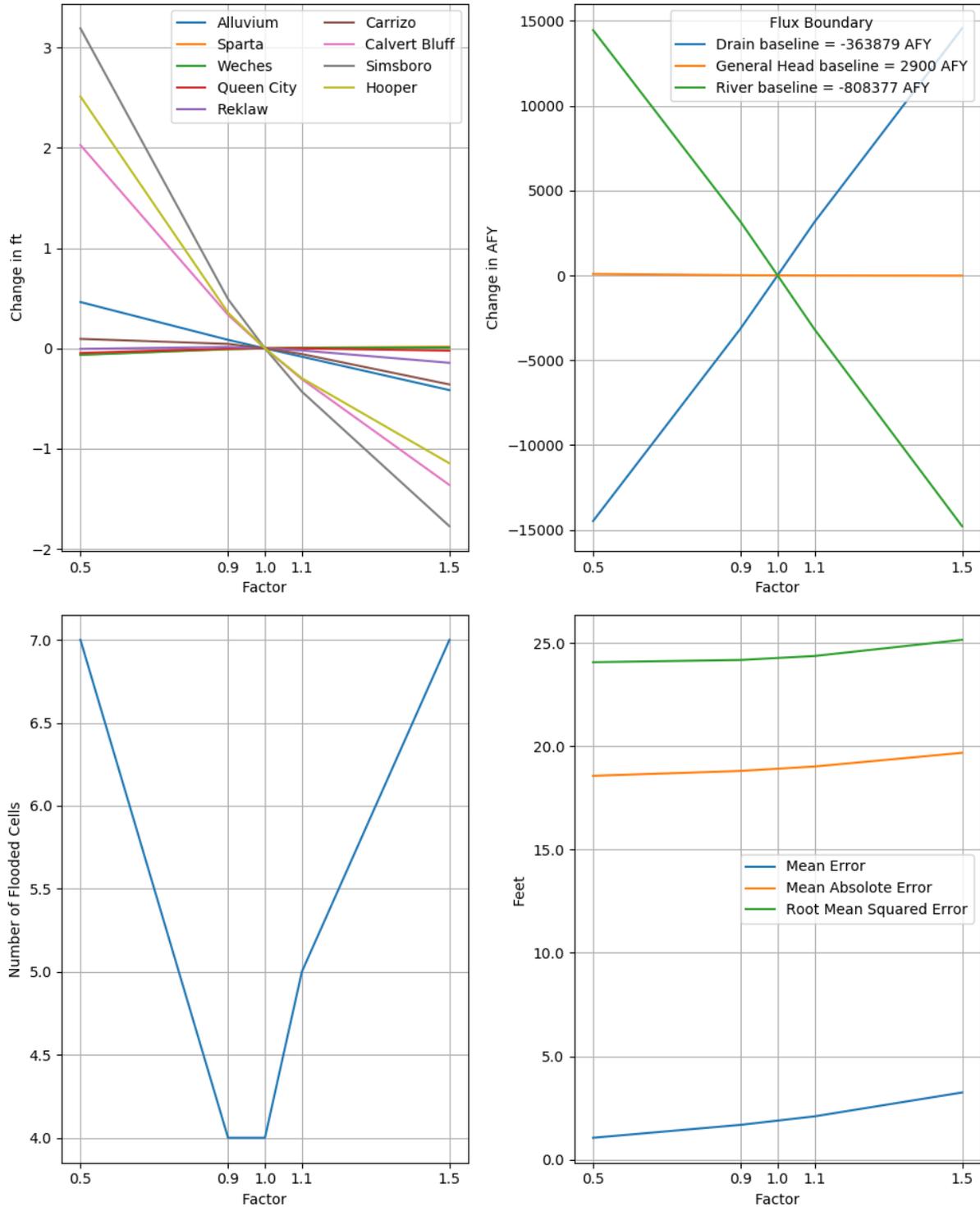
Figure 6.2.1n. **Sensitivity of averaged hydraulic head in hydrogeologic units (top left), hydraulic boundary fluxes (top right), additional flooded grid cells (bottom left), and calibration statistics (bottom right) to the vertical hydraulic conductivity of the Calvert Bluff Formation for the steady-state model.**

Note: ft = feet; AFY = acre-feet per year

Figure 6.2.1o. **Sensitivity of averaged hydraulic head in hydrogeologic units (top left), hydraulic boundary fluxes (top right), additional flooded grid cells (bottom left), and calibration statistics (bottom right) to the horizontal hydraulic conductivity of the Simsboro Formation for the steady-state model.**

Note: ft = feet; AFY = acre-feet per year

Figure 6.2.1p. Sensitivity of averaged hydraulic head in hydrogeologic units (top left), hydraulic boundary fluxes (top right), additional flooded grid cells (bottom left), and calibration statistics (bottom right) to the vertical hydraulic conductivity of the Simsboro Formation for the steady-state model.

Note: ft = feet; AFY = acre-feet per year
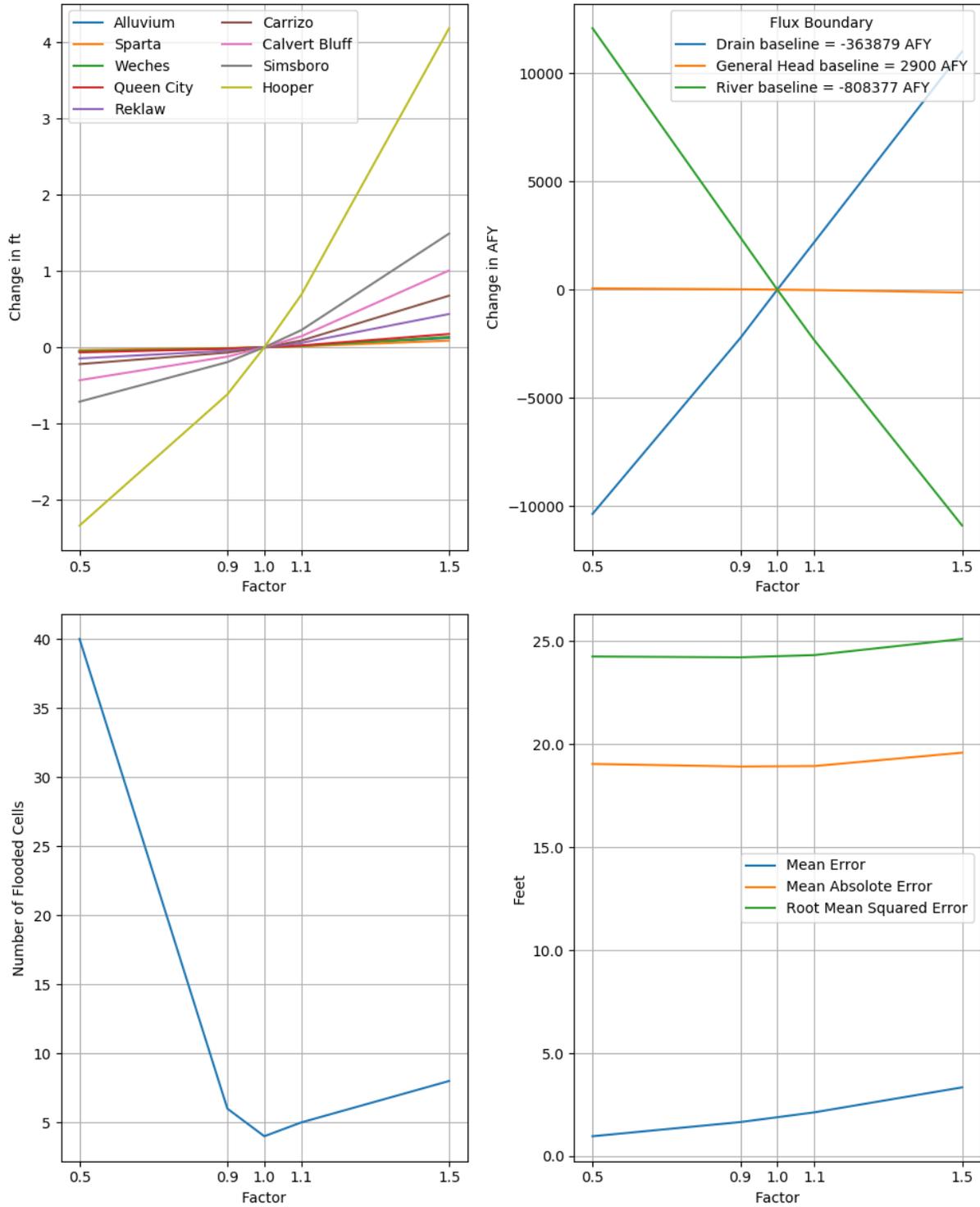
Figure 6.2.1q. Sensitivity of averaged hydraulic head in hydrogeologic units (top left), hydraulic boundary fluxes (top right), additional flooded grid cells (bottom left), and calibration statistics (bottom right) to the horizontal hydraulic conductivity of the Hooper Formation for the steady-state model.

Note: ft = feet; AFY = acre-feet per year
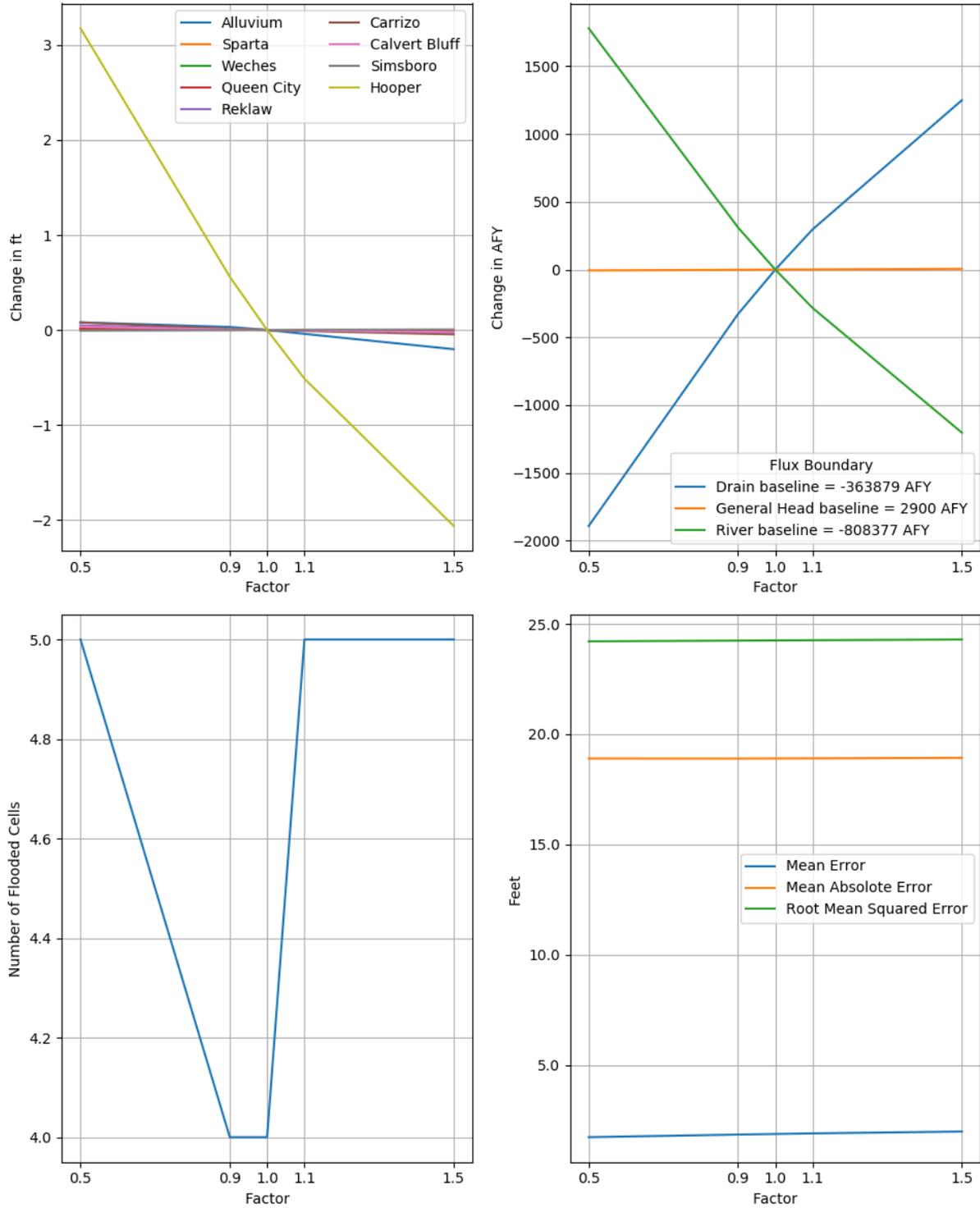
Figure 6.2.1r.   **Sensitivity of averaged hydraulic head in hydrogeologic units (top left), hydraulic boundary fluxes (top right), additional flooded grid cells (bottom left), and calibration statistics (bottom right) to the vertical hydraulic conductivity of the Hooper Formation for the steady-state model.**

Note: ft = feet; AFY = acre-feet per year
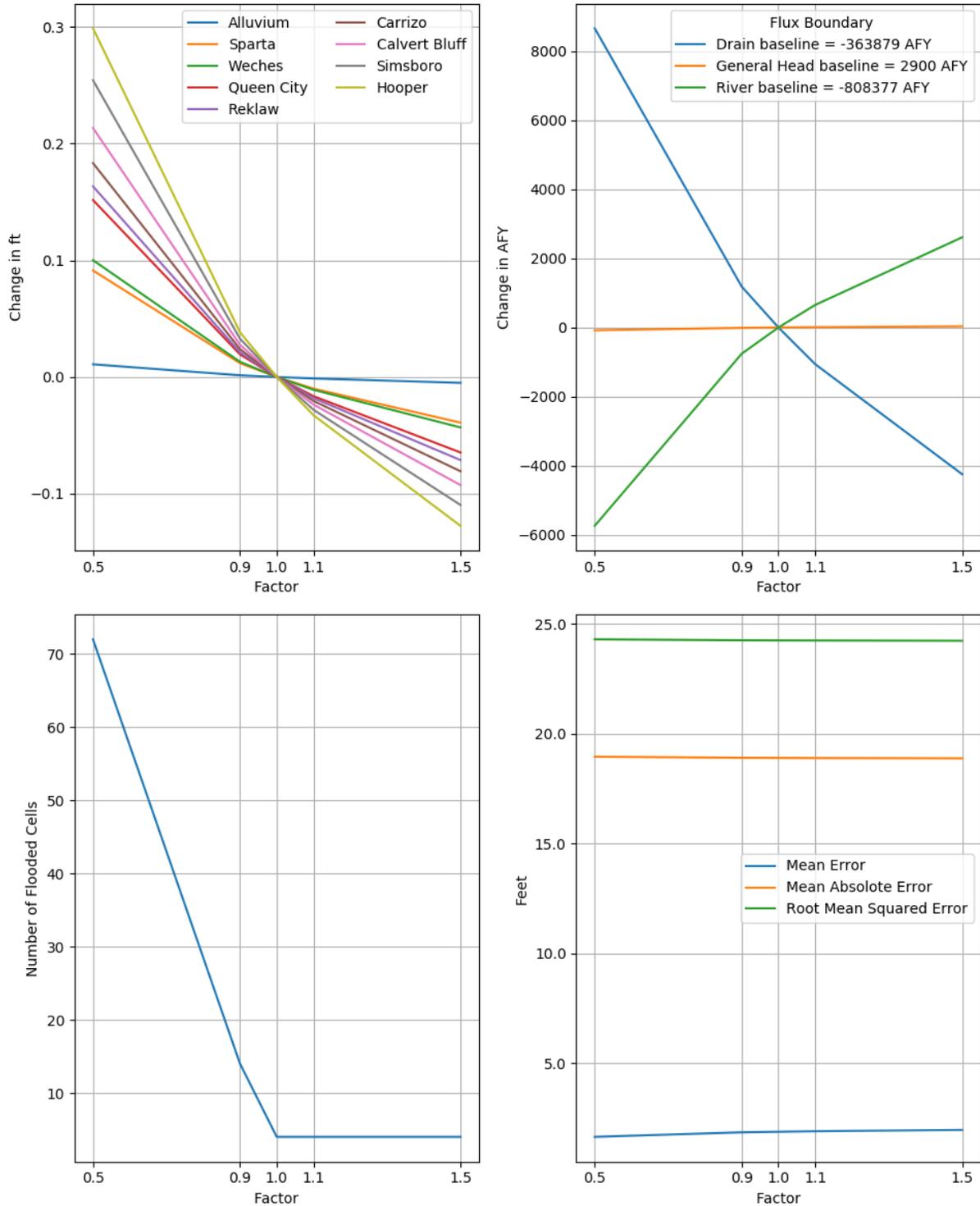
Figure 6.2.1s. Sensitivity of averaged hydraulic head in hydrogeologic units (top left), hydraulic boundary fluxes (top right), additional flooded grid cells (bottom left), and calibration statistics (bottom right) to the conductance of drain cells for the steady-state model.

Note: ft = feet; AFY = acre-feet per year
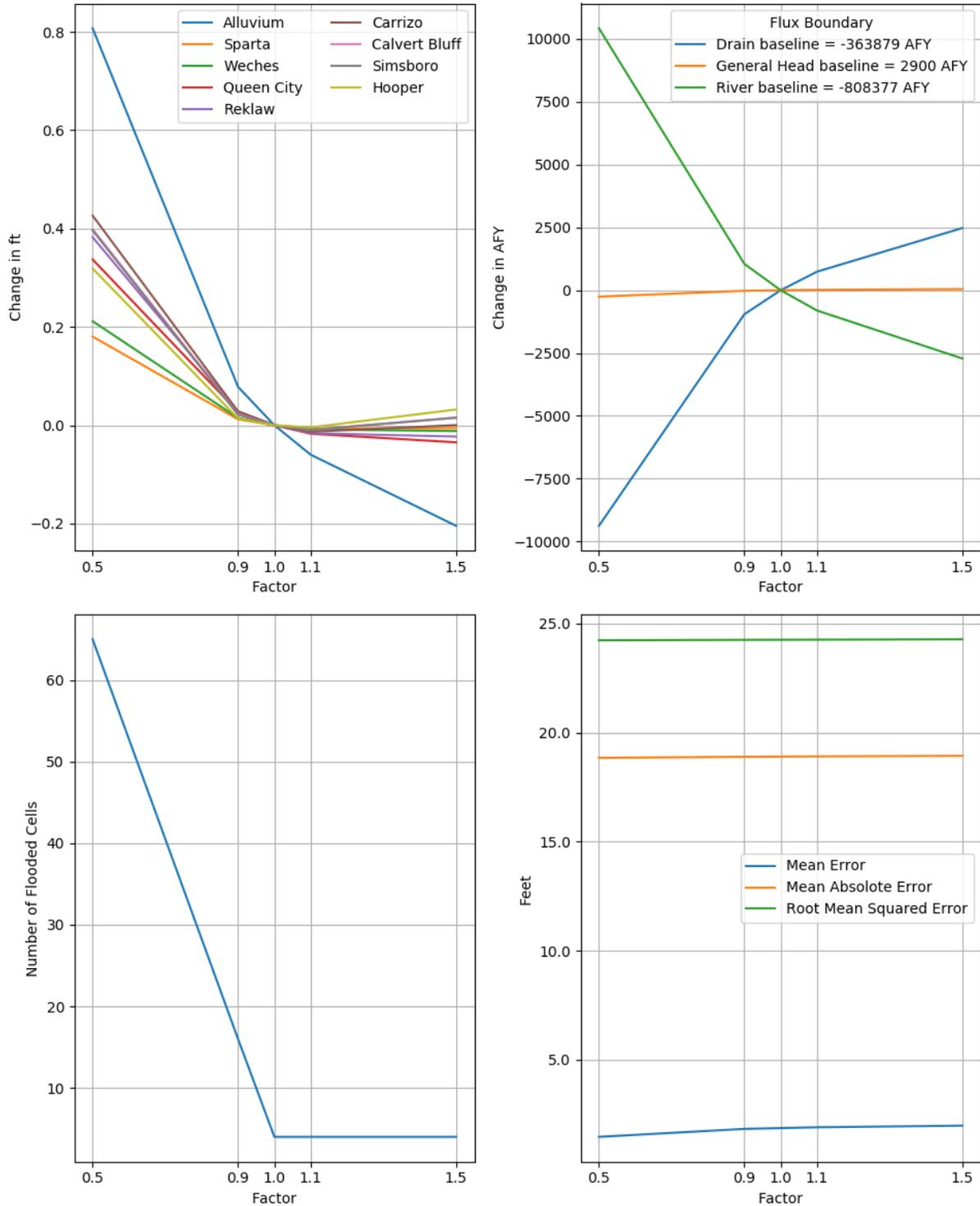
Figure 6.2.1t.   **Sensitivity of averaged hydraulic head in hydrogeologic units (top left), hydraulic boundary fluxes (top right), additional flooded grid cells (bottom left), and calibration statistics (bottom right) to the conductance of river cells for the steady-state model.**

Note: ft = feet; AFY = acre-feet per year
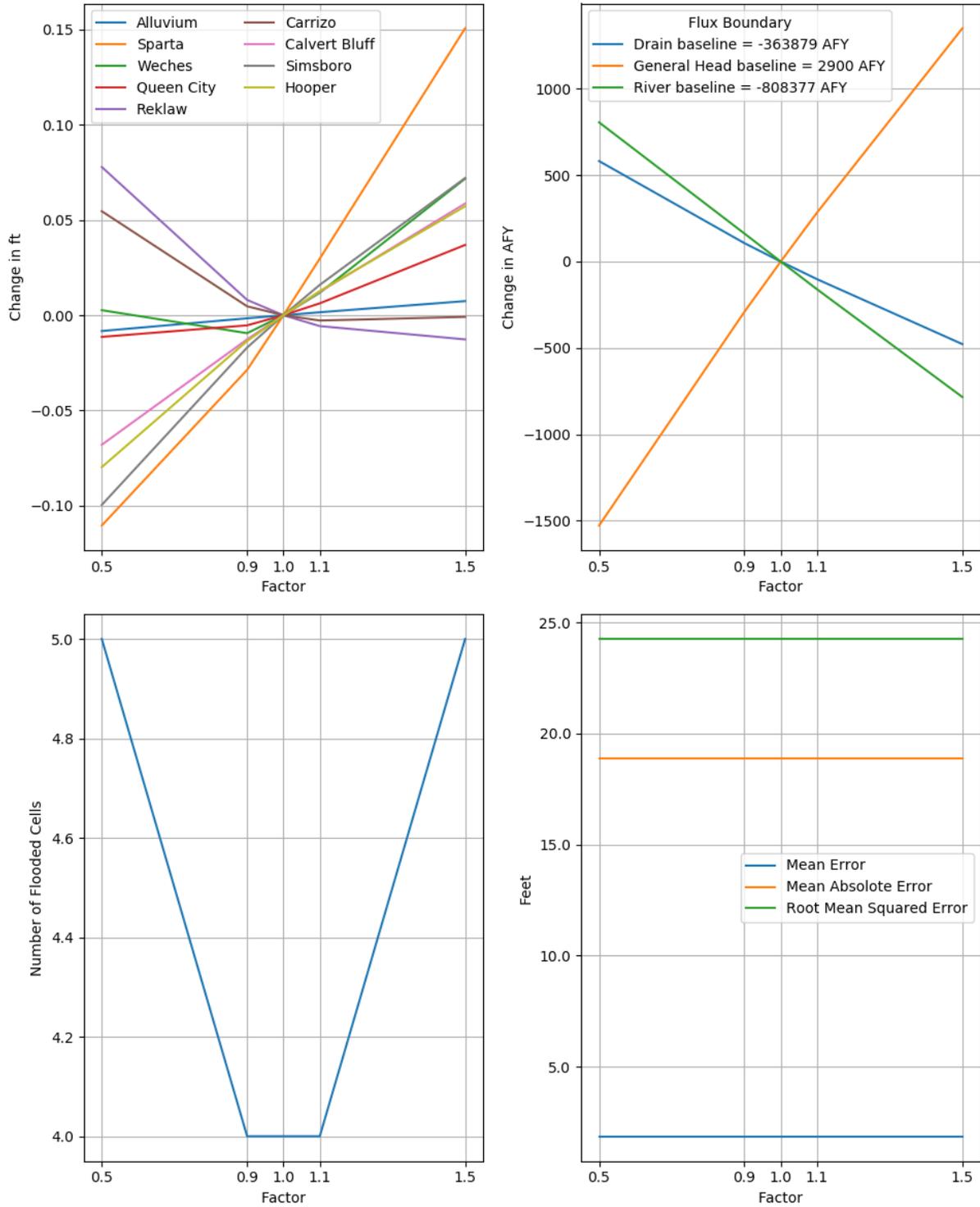
Figure 6.2.1u. **Sensitivity of averaged hydraulic head in hydrogeologic units (top left), hydraulic boundary fluxes (top right), additional flooded grid cells (bottom left), and calibration statistics (bottom right) to the conductance of general-head boundary cells for the steady-state model.**

Note: ft = feet; AFY = acre-feet per year
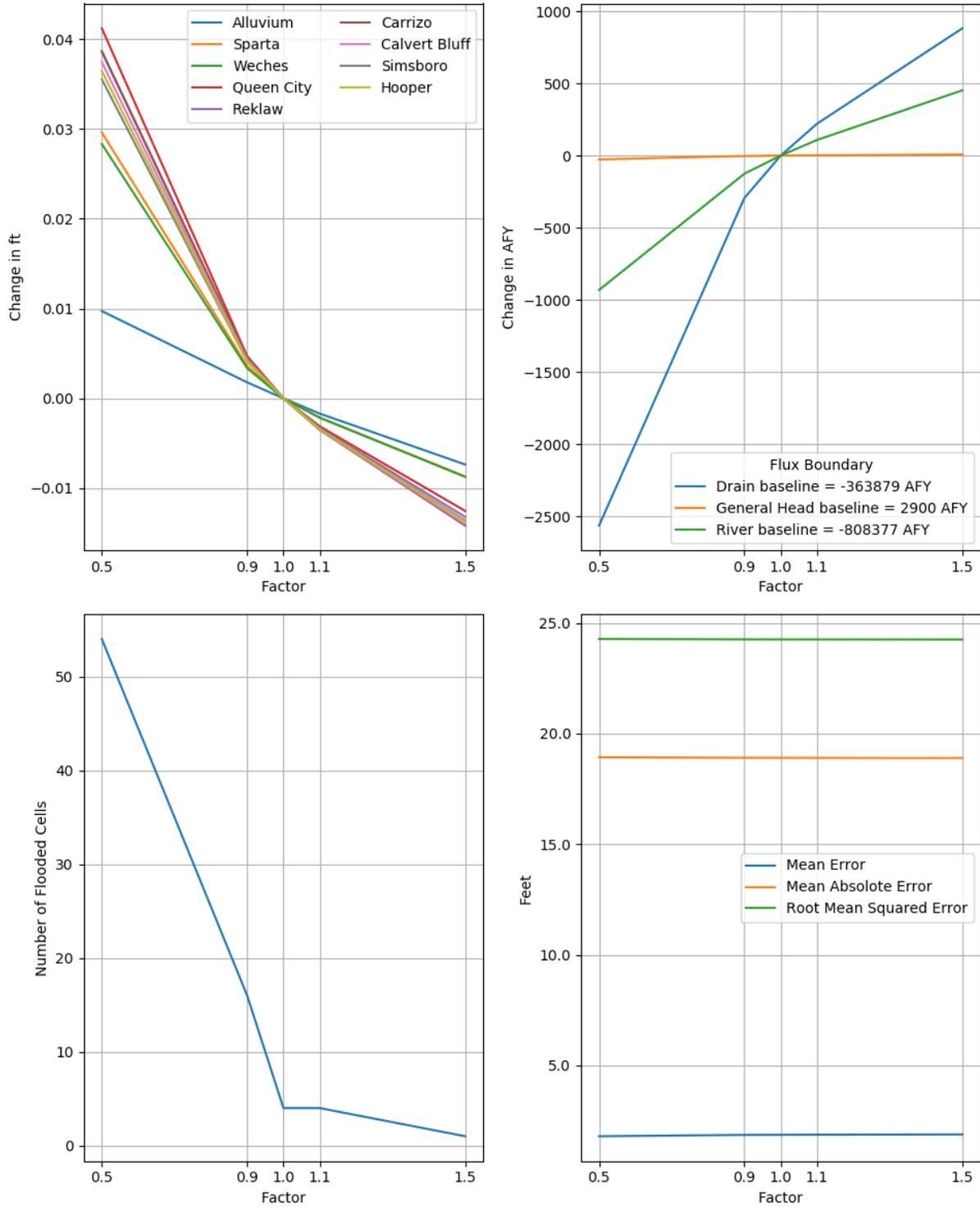
Figure 6.2.1v. Sensitivity of averaged hydraulic head in hydrogeologic units (top left), hydraulic boundary fluxes (top right), additional flooded grid cells (bottom left), and calibration statistics (bottom right) to the evapotranspiration rate of evapotranspiration cells for the steady-state model.

Note: ft = feet; AFY = acre-feet per year
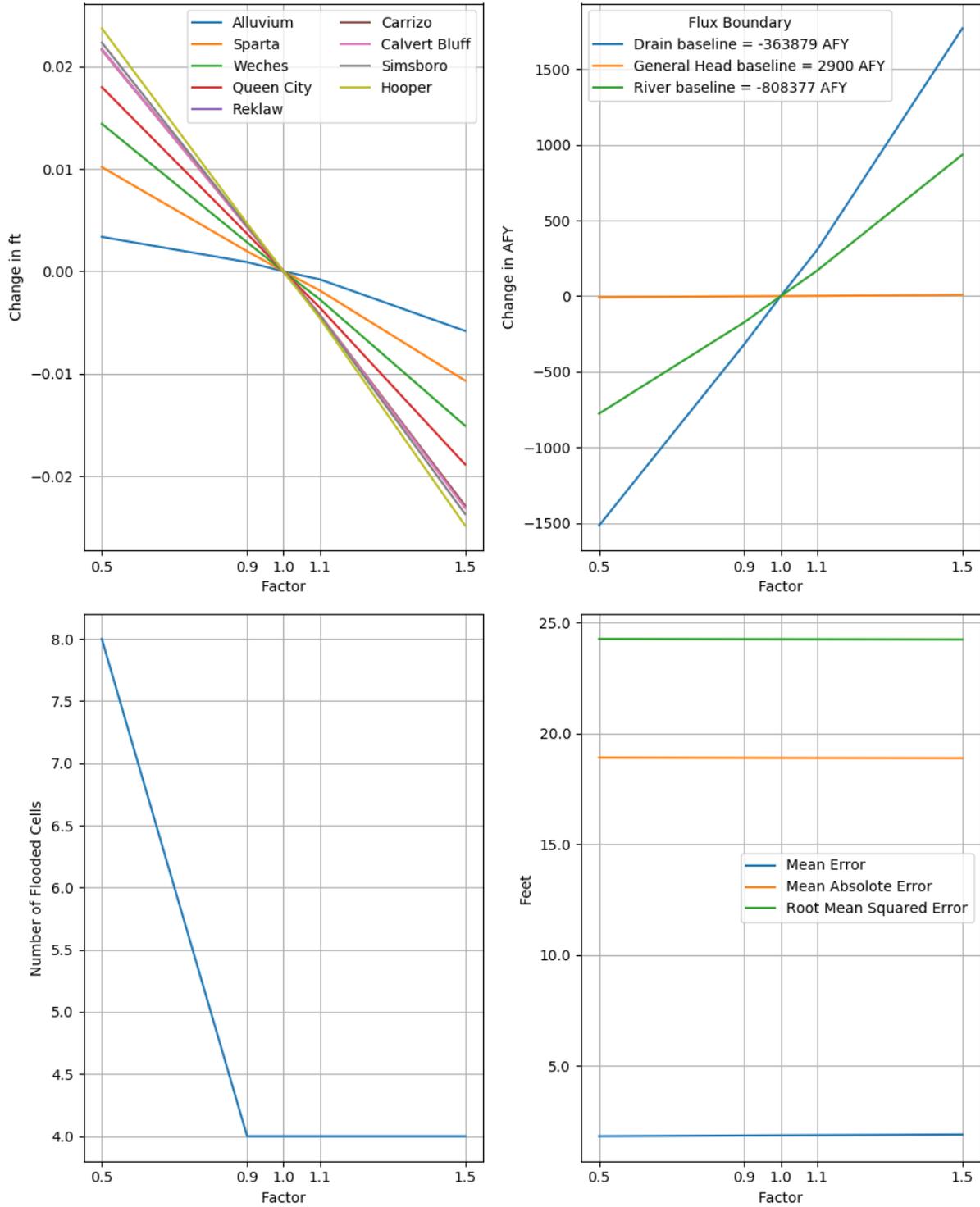
Figure 6.2.1w. **Sensitivity of averaged hydraulic head in hydrogeologic units (top left), hydraulic boundary fluxes (top right), additional flooded grid cells (bottom left), and calibration statistics (bottom right) to the extinction depth of evapotranspiration cells for the steady-state model.**

Note: ft = feet; AFY = acre-feet per year
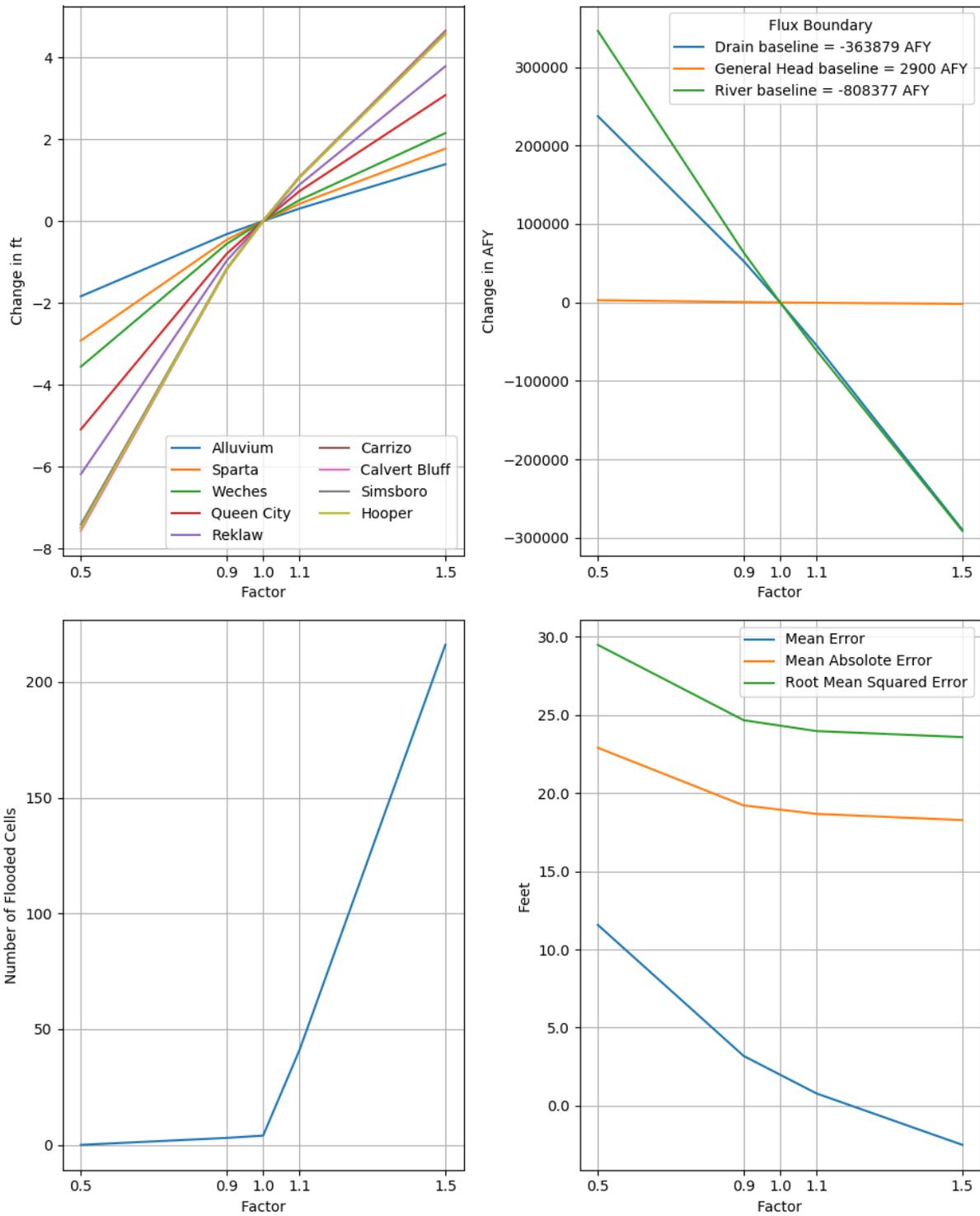
Figure 6.2.1x. **Sensitivity of averaged hydraulic head in hydrogeologic units (top left), hydraulic boundary fluxes (top right), additional flooded grid cells (bottom left), and calibration statistics (bottom right) to the recharge rate for the steady-state model.**

Note: ft = feet; AFY = acre-feet per year

6.2.2 Transient Sensitivities

Output metrics for the transient sensitivity analysis were drawdown from steady-state conditions to 2010 for the Sparta, Queen City, and Carrizo aquifers and the Simsboro Formation; total flux in the drain and river hydraulic boundary cells; and model calibration statistics. Twenty sets of results, one for each of the 20 parameters varied in the sensitivity analysis (Table 6.1b), are shown in Figures 6.2.2a through 6.2.2t. Each of these figures contains the following three plots:

- Top plot – sensitivity of 2010 drawdown from steady-state conditions to 2010 for the Sparta, Queen City, and Carrizo aquifers and the Simsboro Formation model-wide.
- Middle plot – sensitivity of total flux for the drain and river cells model-wide.
- Bottom plot – the model-wide calibration statistics.

These figures show the details of how each metric responses to each change in parameter value.

The methodology used to assess the sensitivity of the transient model parameter changes was the same as that used for assessing sensitivity of the steady-state model. The rankings for 2010 drawdown are provided in Table 6.2.2a. The ranges used for this ranking are the same as those used for the average hydraulic head change in the assessment of the steady-state model (Table 6.2.1a). The rankings used for the drain and river boundary fluxes were the same as those used for the steady-state sensitivity analysis (Table 6.2.1b), as were the rankings for the model calibration statistics (Table 6.2.1e).

Table 6.2.2a.   Ranking for assessing impact to 2010 drawdown.

Ranking	Change in 2010 Drawdown from Base Case Value (feet)
1	0 to 0.5
2	0.5 to 1
3	1 to 1.5
4	1.5 to 2.25
5	2.25 to 3.5
6	> 3.5

Note: > = greater than

The ranking summary for change in 2010 drawdown in the Sparta, Queen City, and Carrizo aquifers and the Simsboro Formation across the model for the 20 parameters considered by the transient sensitivity analysis is provided in Table 6.2.2b. Also included in this table is the average of the rankings for each parameter. Based on these averages, the five parameters having the greatest impact on 2010 drawdowns in the transient model, in order of importance, are: the pumping rate, horizontal hydraulic conductivity of the Carrizo Aquifer, horizontal hydraulic conductivity of the Queen City Aquifer, the horizontal hydraulic conductivity of the Sparta Aquifer, and the horizontal hydraulic conductivity of the Simsboro Formation. Based on this metric, the model has little sensitivity to changes in the storage parameters and drain and river cell conductance values, with the exception of the specific storage of the Simsboro Formation

and the specific yield of the Queen City Aquifer. In addition, 2010 drawdowns are relatively insensitive to recharge for the transient model. The impact of change in each of the 20 parameters on the 2010 drawdowns in Sparta, Queen City, and Carrizo aquifers and the Simsboro Formation the can be quickly assessed using Table 6.2.2b.

Table 6.2.2b. **Summary for change in 2010 drawdown across the model in the Sparta, Queen City, and Carrizo aquifers and the Simsboro Formation for the 20 parameters considered by the transient sensitivity analysis.**

Number	Parameter	Ranking for Change in 2010 Drawdown				Average of Rankings
		Sparta	Queen City	Carrizo	Simsboro	
1	Kx of Sparta	6	6	4	2	4.5
2	Kv of Sparta	2	1	1	1	1.3
3	Kx of Queen City	6	6	5	2	4.8
4	Kv of Queen City	3	2	1	2	2.0
5	Kx of Carrizo	3	5	6	6	5.0
6	Kv of Carrizo	1	2	3	2	2.0
7	Kx of Simsboro	1	2	5	6	3.5
8	Kv of Simsboro	1	1	2	6	2.5
9	Ss of Sparta	3	2	1	1	1.8
10	Sy of Sparta	1	1	1	1	1.0
11	Ss of Queen City	2	3	2	1	2.0
12	Sy of Queen City	1	1	1	1	1.0
13	Ss of Carrizo	1	1	2	1	1.3
14	Sy of Carrizo	1	1	2	1	1.3
15	Ss of Simsboro	1	1	3	6	2.8
16	Sy of Simsboro	1	1	1	1	1.0
17	Recharge rate	1	1	1	1	1.0
18	Drain conductance	1	1	1	1	1.0
19	River conductance	1	1	1	1	1.0
20	Pumping Rate	6	6	6	6	6.0

Note: Kx = horizontal hydraulic conductivity; Kv = vertical hydraulic conductivity; Ss = specific storage; Sy = specific yield

One of the interesting findings of the sensitivity analysis is that the 2010 drawdown in the Sparta Aquifer is more sensitive to the vertical hydraulic conductivity of the Queen City Aquifer than is the 2010 drawdown in the Queen City Aquifer. This result is attributed to the fact that groundwater flow through the Queen City Aquifer is much greater than groundwater flow through the Sparta Aquifer. Because the Sparta Aquifer has lower groundwater flow than the Queen City Aquifer, the water levels in the Sparta Aquifer are more susceptible to changes in the vertical flux through the Weches Formation than is the Queen City Aquifer.

The ranking summary for the change in drain and river boundary fluxes and the average of the rankings for the 20 parameters considered by the transient sensitivity analysis are provided in Table 6.2.2c. Based on these averages, the five parameters having the greatest impact on drain and river boundary fluxes in the transient model, in order of importance, are: the recharge rate, the horizontal hydraulic conductivity of the Queen City Aquifer, the horizontal hydraulic conductivity of the Sparta Aquifer, the horizontal hydraulic conductivity of the Carrizo Aquifer

and the pumping rate. The model has little sensitivity, based on the drain and river flux metric, to the specific storage and specific yield parameters, and the vertical hydraulic conductivity of all but the Queen City Aquifer. The impact of change in each of the 20 parameters on the total flux for the drain and river boundaries can also be quickly assessed using Table 6.2.2c.

Table 6.2.2c.   **Summary for change in drain and river boundary fluxes for the 20 parameters considered by the transient sensitivity analysis.**

| Number | Parameter | Ranking for Change in Hydraulic Boundary Flux | | Average of Rankings |
		Drain Cells	River Cells	
1	Kx of Sparta	6	4	5.0
2	Kv of Sparta	1	1	1.0
3	Kx of Queen City	6	5	5.5
4	Kv of Queen City	3	3	3.0
5	Kx of Carrizo	4	3	3.5
6	Kv of Carrizo	1	1	1.0
7	Kx of Simsboro	3	2	2.5
8	Kv of Simsboro	2	1	1.5
9	Ss of Sparta	1	1	1.0
10	Sy of Sparta	1	1	1.0
11	Ss of Queen City	1	1	1.0
12	Sy Queen City	1	1	1.0
13	Ss of Carrizo	1	1	1.0
14	Sy of Carrizo	1	1	1.0
15	Ss of Simsboro	1	1	1.0
16	Sy of Simsboro	1	1	1.0
17	Recharge rate	6	6	6.0
18	Drain conductance	3	2	2.5
19	River conductance	3	2	2.5
20	Pumping Rate	3	4	3.5

Note: Kx = horizontal hydraulic conductivity; Kv = vertical hydraulic conductivity; Ss = specific storage; Sy = specific yield

The ranking summary for model calibration statistics and the average of the rankings for the 20 parameters considered by the transient sensitivity analysis are provided in Table 6.2.2d. Based on these averages, the five parameters having the greatest impact on the calibration statistics for the transient model, in order of importance, are: the pumping rate and the horizontal hydraulic conductivity of the Carrizo Aquifer, the horizontal hydraulic conductivity of the Simsboro Formation, the recharge rate, and the horizontal hydraulic conductivity of the Queen City Aquifer. The model has little sensitivity, based on the model calibration statistics metric, to the specific storage and specific yield parameters; conductance values for the drain and river cells; and the vertical hydraulic conductivity of the Sparta and Carrizo aquifers. The impact of change in each of the 20 parameters on the calibration statistics can also be quickly assessed using Table 6.2.2d.

Table 6.2.2d. **Summary for change in model calibration statistics for the 20 parameters considered by the transient sensitivity analysis.**

Number	Parameter	Ranking for Change in Model Calibration Statistics			Average of Rankings
		Mean Error	Mean Absolute Error	Root Mean Square Error	
1	Kx of Sparta	1	3	3	2.3
2	Kv of Sparta	1	1	1	1.0
3	Kx of Queen City	6	4	4	4.7
4	Kv of Queen City	1	2	3	2.0
5	Kx of Carrizo	6	6	6	6.0
6	Kv of Carrizo	1	1	1	1.0
7	Kx of Simsboro	6	5	6	5.7
8	Kv of Simsboro	6	3	3	4.0
9	Ss of Sparta	1	1	1	1.0
10	Sy of Sparta	1	1	1	1.0
11	Ss of Queen City	1	1	1	1.0
12	Sy Queen City	1	1	1	1.0
13	Ss of Carrizo	1	1	1	1.0
14	Sy Carrizo	1	1	1	1.0
15	Ss of Simsboro	1	1	1	1.0
16	Sy Simsboro	1	1	1	1.0
17	Recharge rate	6	5	4	5.0
18	Drain conductance	1	1	1	1.0
19	River conductance	1	1	1	1.0
20	Pumping Rate	6	6	6	6.0

Note: Kx = horizontal hydraulic conductivity; Kv = vertical hydraulic conductivity; Ss = specific storage; Sy = specific yield

Hydrograph plots for 12 wells each showing measured values, model base case values, and sensitivity values for the four factors were created for the Sparta, Queen City, and Carrizo aquifers and the Simsboro Formation (Figures 6.2.2u through 6.2.2x, respectively). The parameter changed was the horizontal and vertical hydraulic conductivity of the hydrogeologic unit. For example, the figures for the Sparta Aquifer show plots of the model sensitivity to the horizontal hydraulic conductivity of the Sparta Aquifer on the left and the model sensitivity to the vertical hydraulic conductivity for the Sparta Aquifer on the right. For each plot, the observed data are shown in blue, the base case (or calibrated) model results are shown in red, and the results from the sensitivity analysis are shown by orange lines. The labels in the figure legend for the sensitivity results are Factor -2, Factor -1, Factor 1, and Factor 2, which correspond to log-variations in the parameter of 0.5, 0.9, 1.1, and 1.5, respectively.
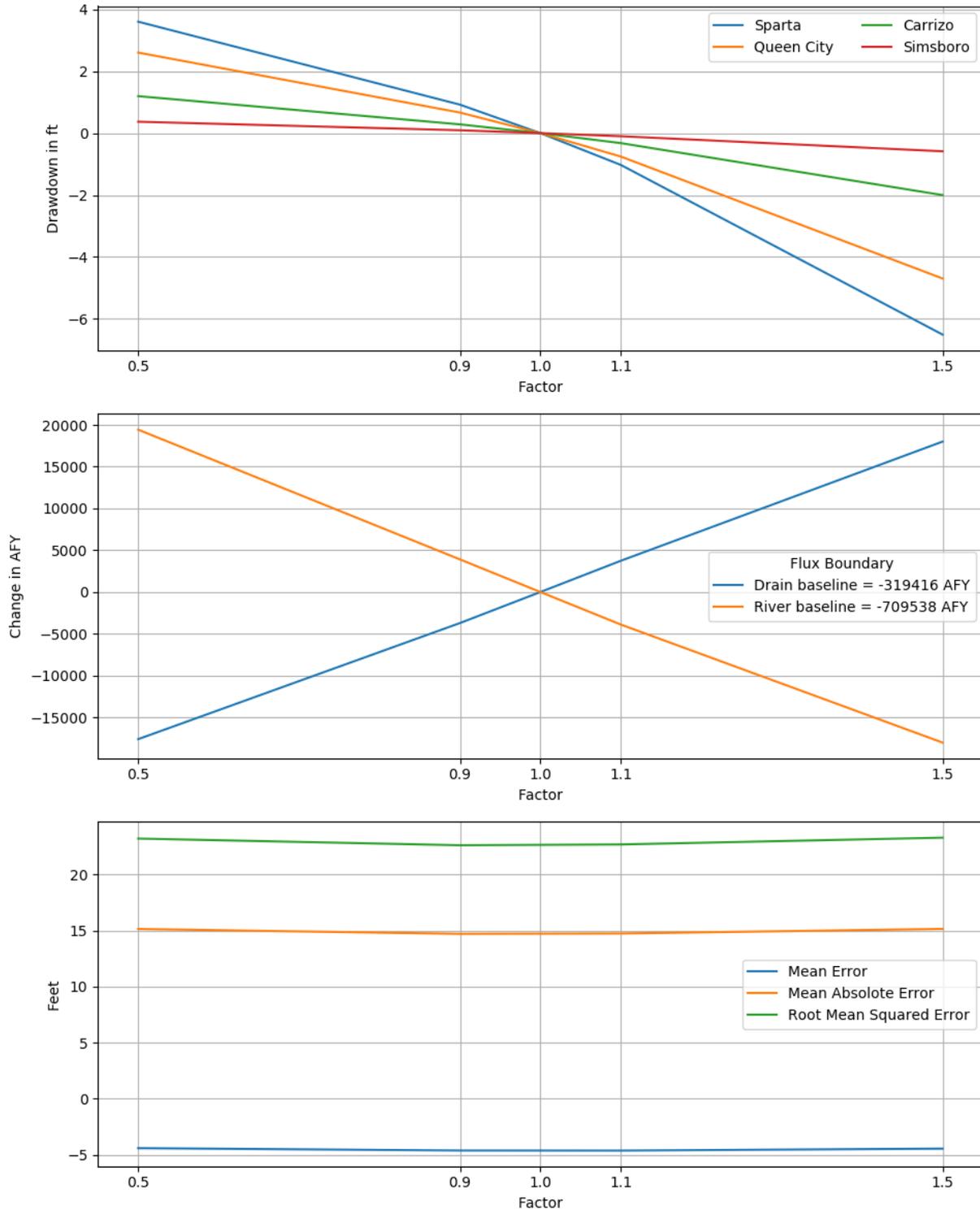
Figure 6.2.2a. Sensitivities of 2010 drawdown in hydrogeologic units (top), hydraulic boundary fluxes (center), and calibration statistics (bottom) to the horizontal hydraulic conductivity of the Sparta Aquifer for the transient model.

Note: ft = feet; AFY = acre-feet per year
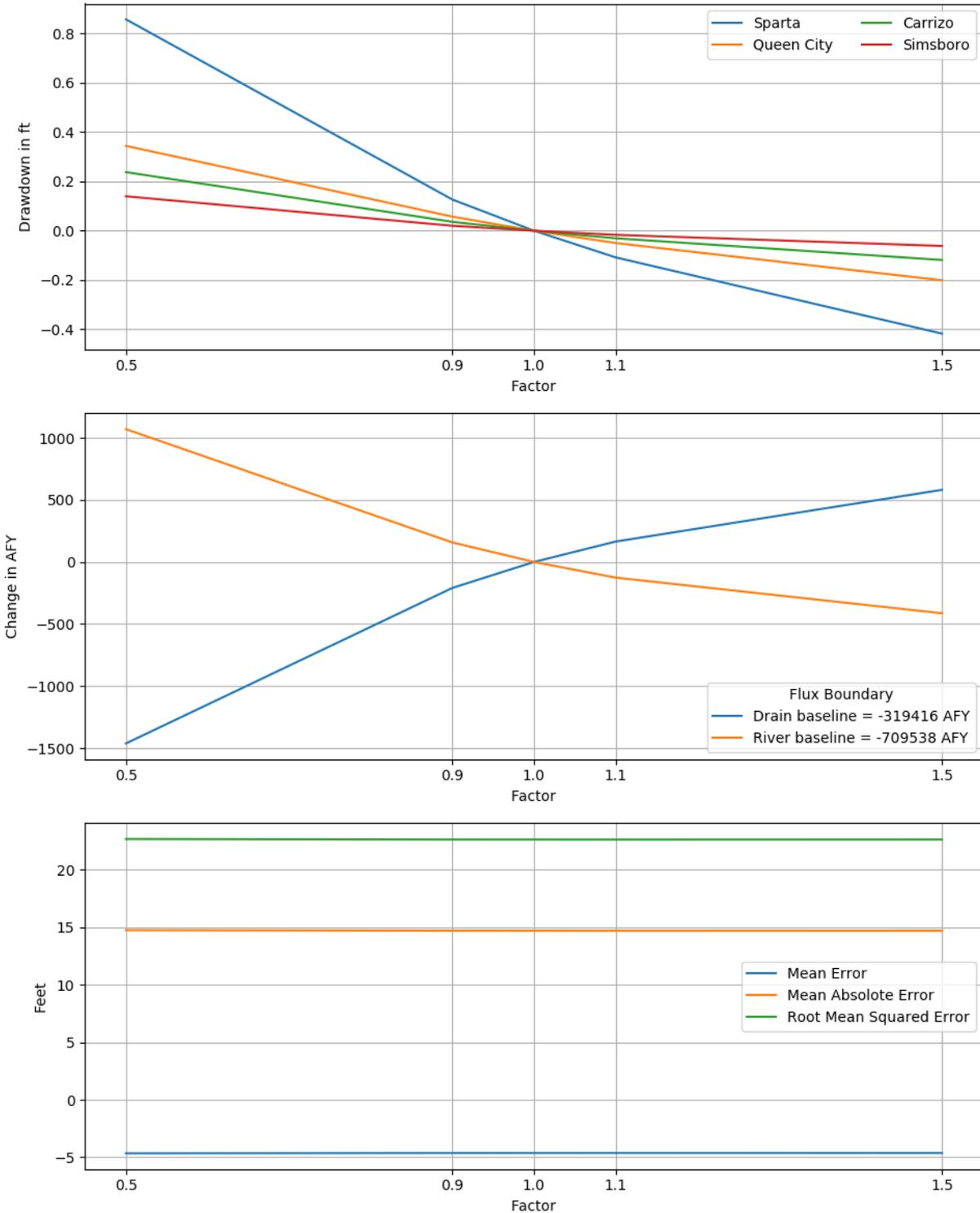
Figure 6.2.2b. Sensitivities of 2010 drawdown in hydrogeologic units (top), hydraulic boundary fluxes (center), and calibration statistics (bottom) to the vertical hydraulic conductivity of the Sparta Aquifer for the transient model.

Note: ft = feet; AFY = acre-feet per year
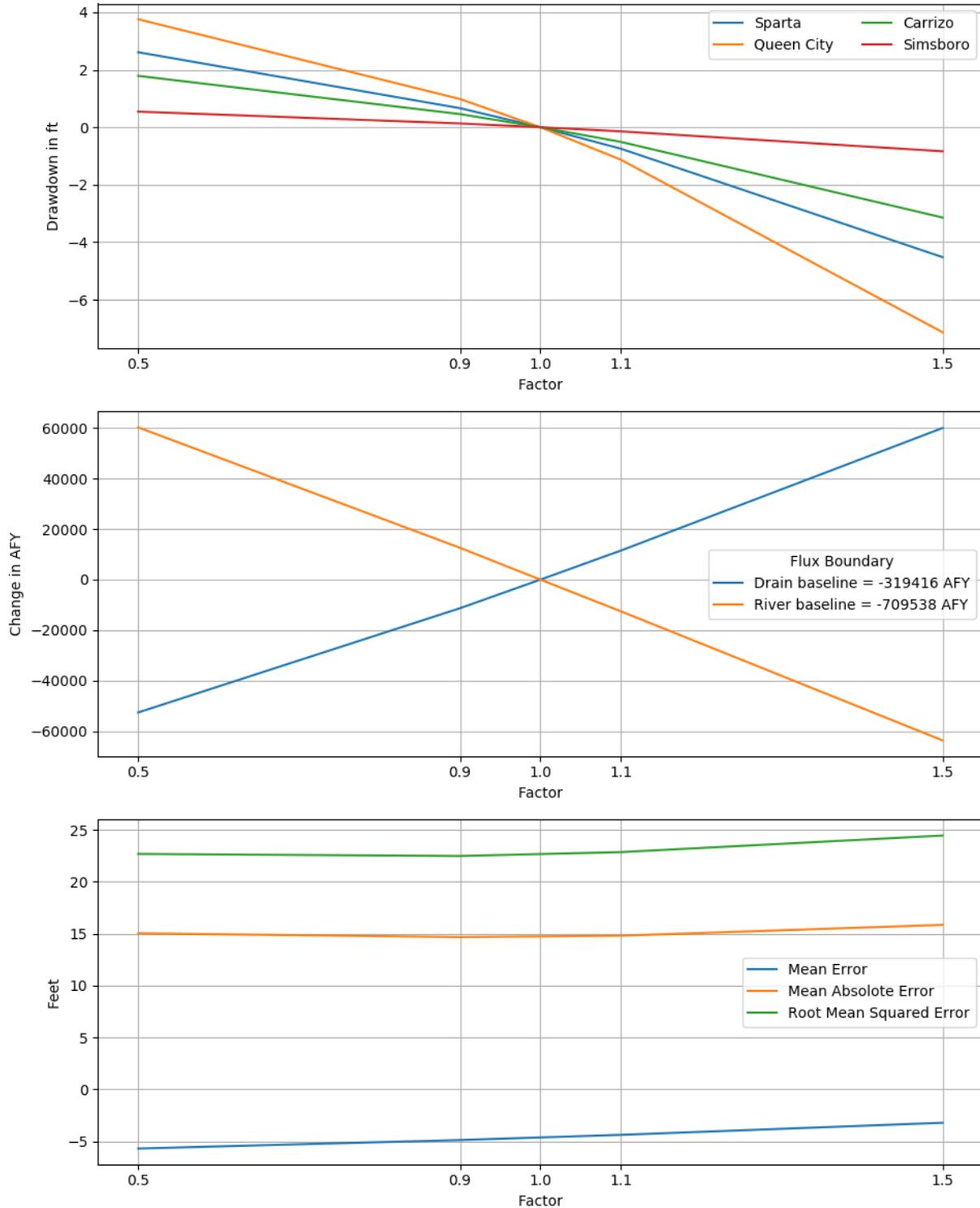
Figure 6.2.2c.   Sensitivities of 2010 drawdown in hydrogeologic units (top), hydraulic boundary fluxes (center), and calibration statistics (bottom) to the horizontal hydraulic conductivity of the Queen City Aquifer for the transient model.

Note: ft = feet; AFY = acre-feet per year
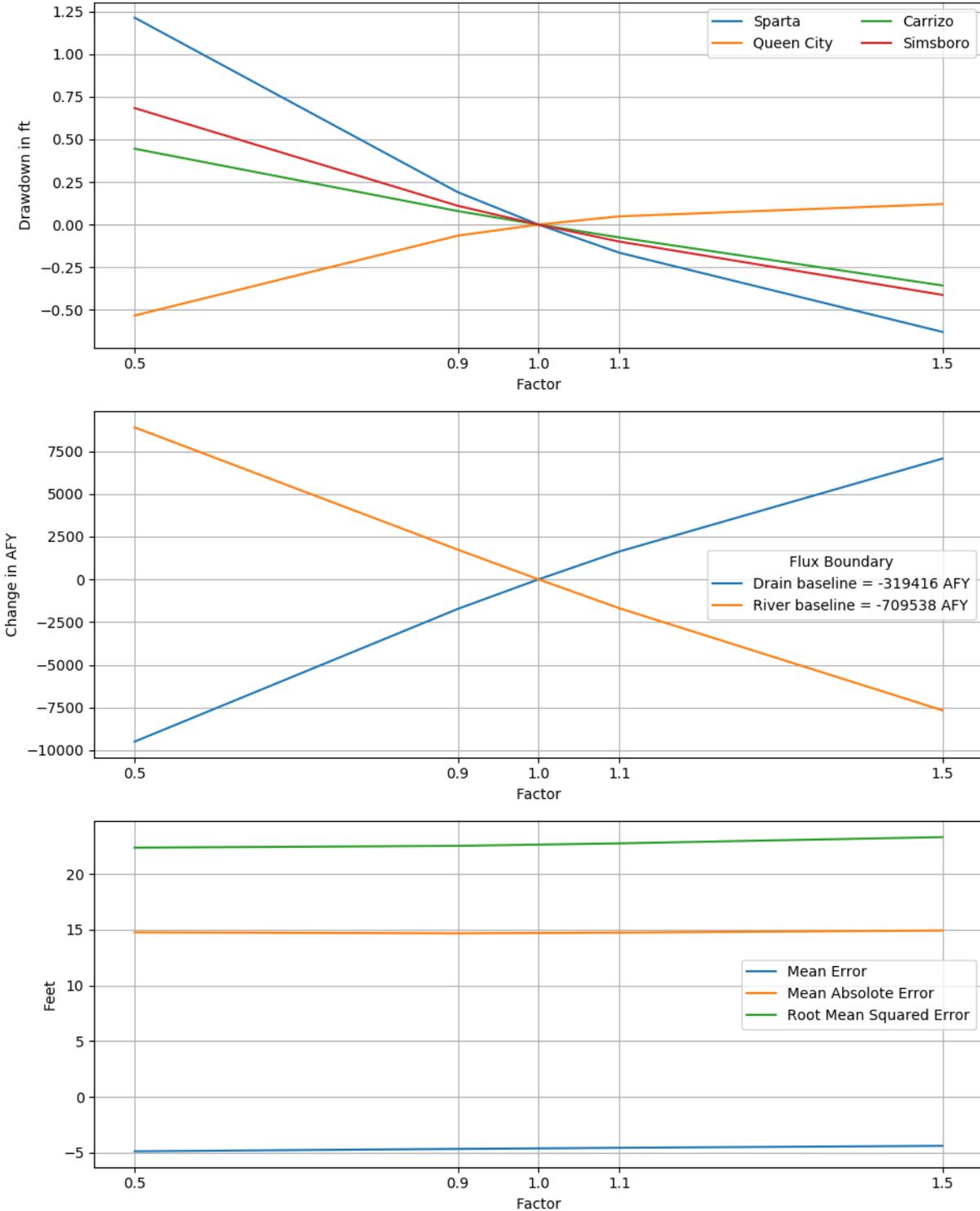
Figure 6.2.2d. **Sensitivities of averaged drawdown in hydrogeologic units (top), hydraulic boundary fluxes (center), and calibration statistics (bottom) to the vertical hydraulic conductivity of the Queen City Aquifer for the transient model.**

Note: ft = feet; AFY = acre-feet per year
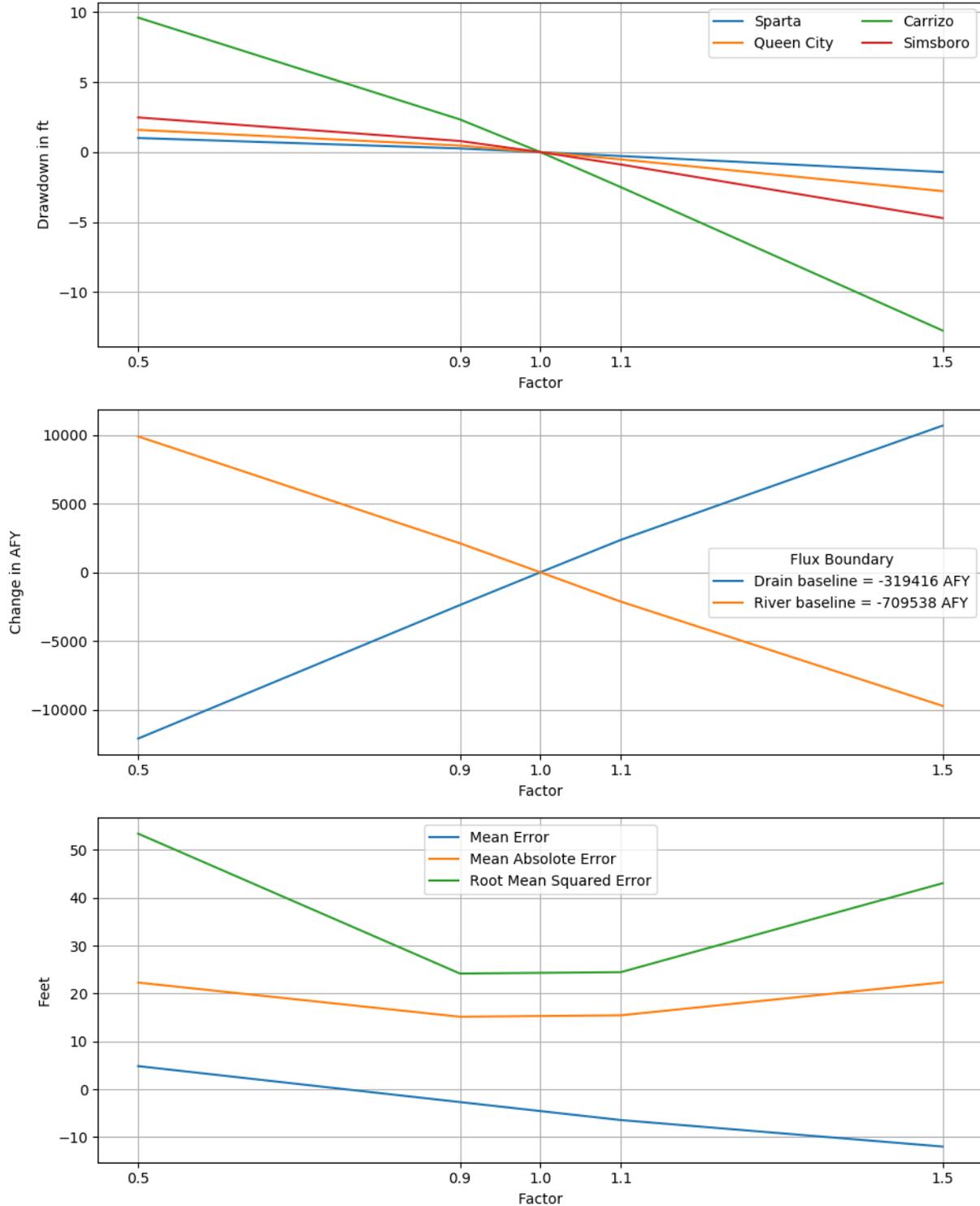
Figure 6.2.2e. **Sensitivities of 2010 drawdown in hydrogeologic units (top), hydraulic boundary fluxes (center), and calibration statistics (bottom) to the horizontal hydraulic conductivity of the Carrizo Aquifer for the transient model.**

Note: ft = feet; AFY = acre-feet per year
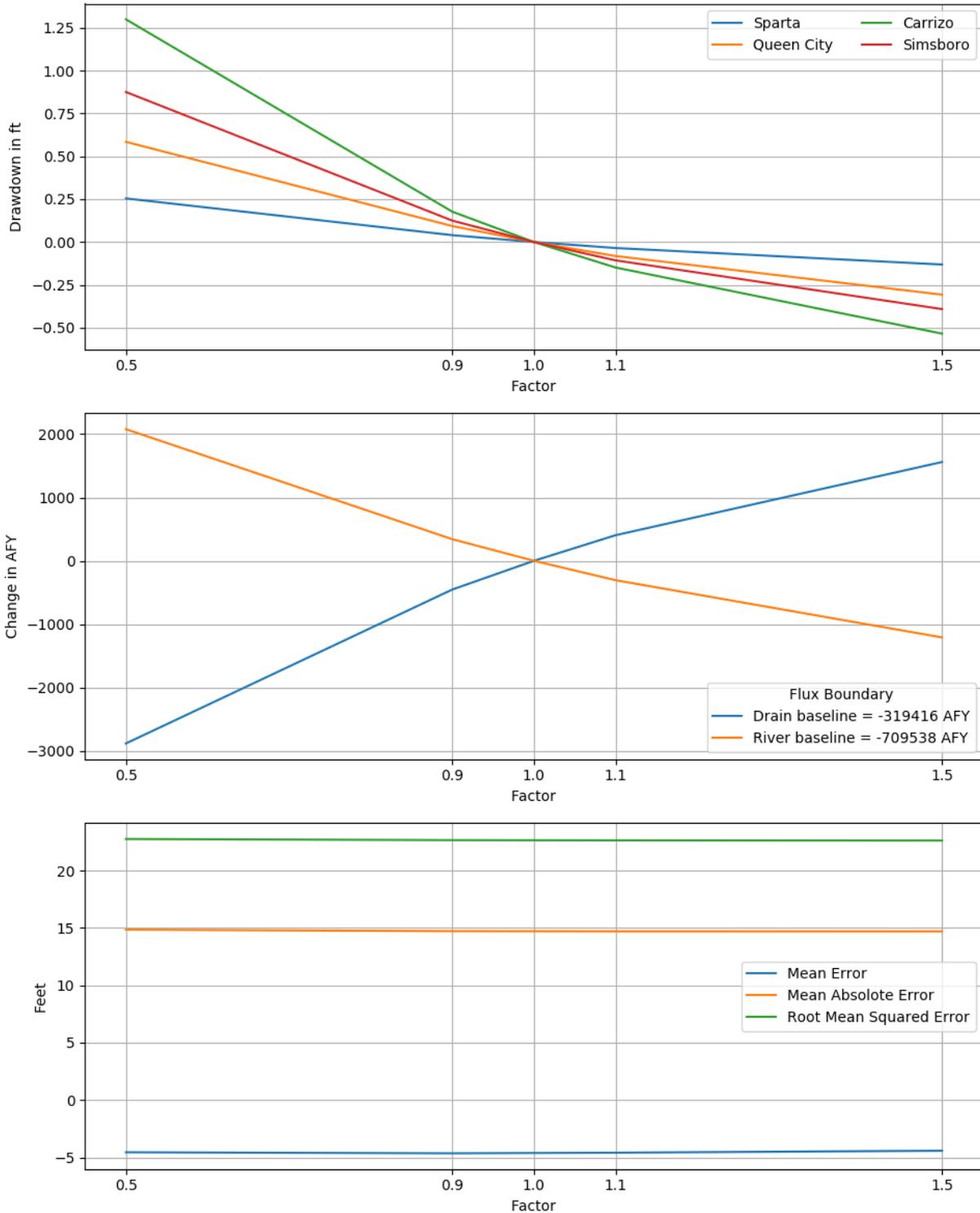
Figure 6.2.2f.　Sensitivities of 2010 drawdown in hydrogeologic units (top), hydraulic boundary fluxes (center), and calibration statistics (bottom) to the vertical hydraulic conductivity of the Carrizo Aquifer for the transient model.

Note: ft = feet; AFY = acre-feet per year
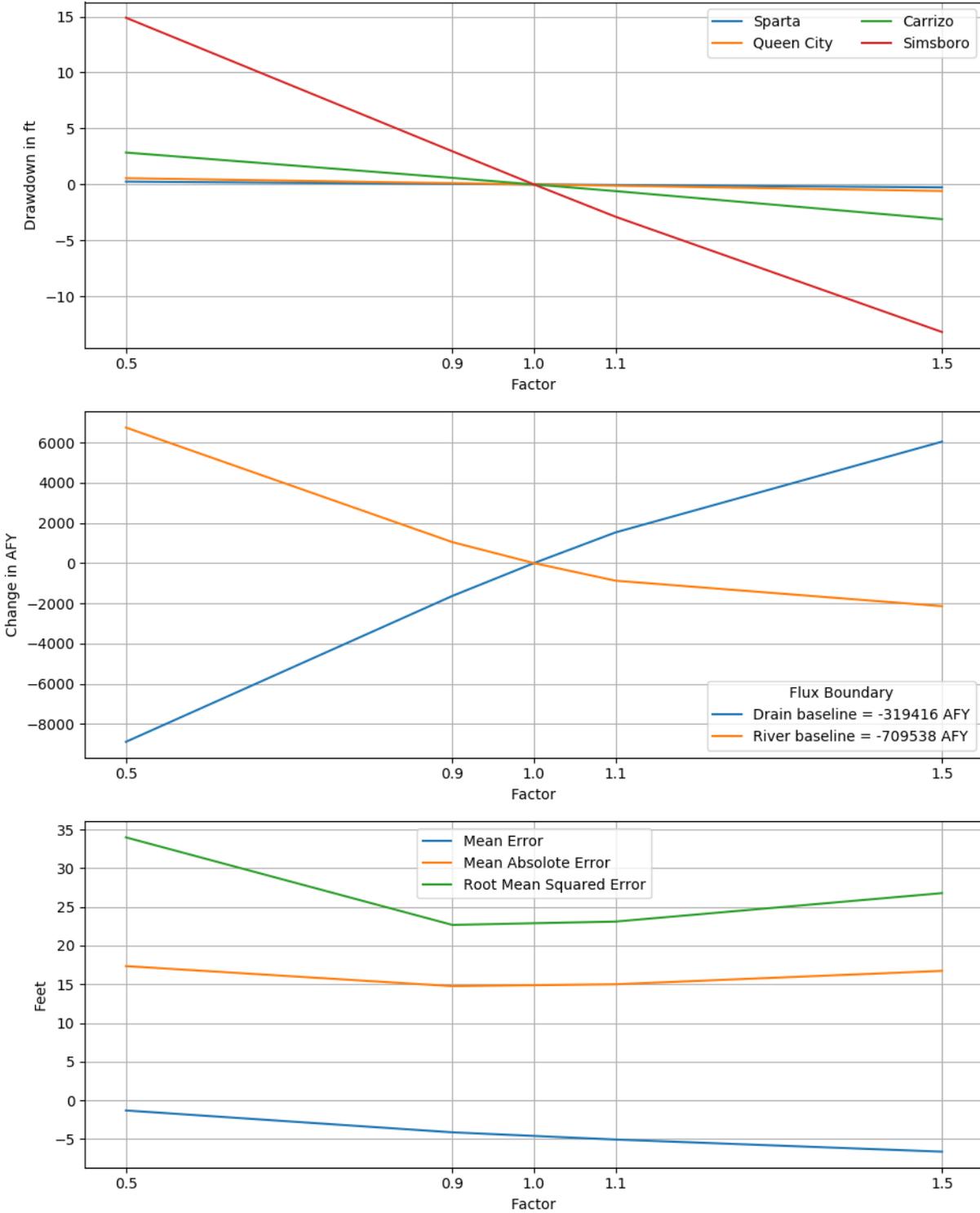
Figure 6.2.2g. Sensitivities of 2010 drawdown in hydrogeologic units (top), hydraulic boundary fluxes (center), and calibration statistics (bottom) to the horizontal hydraulic conductivity of the Simsboro Formation for the transient model.

Note: ft = feet; AFY = acre-feet per year
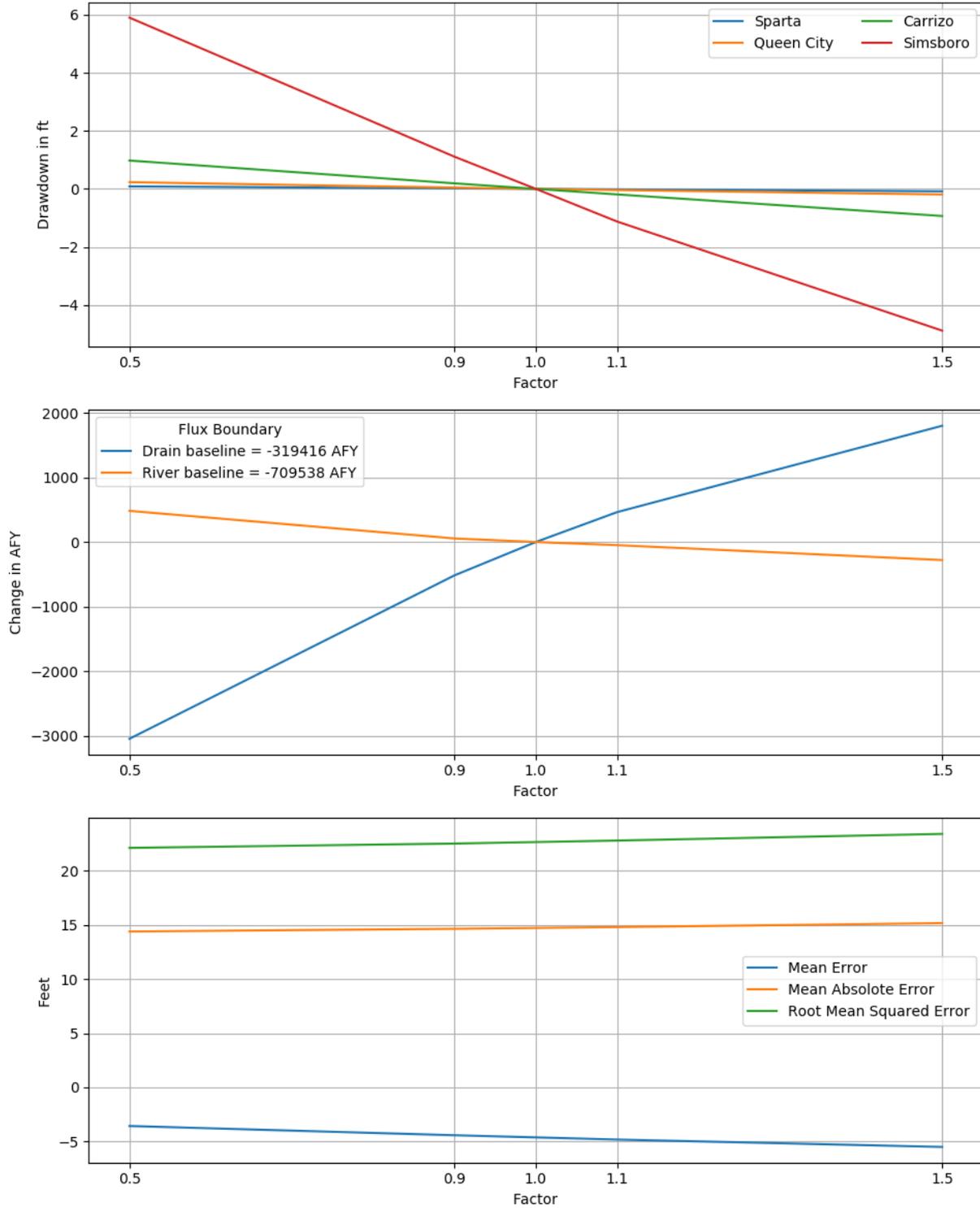
Figure 6.2.2h. **Sensitivities of 2010 drawdown in hydrogeologic units (top), hydraulic boundary fluxes (center), and calibration statistics (bottom) to the vertical hydraulic conductivity of the Simsboro Formation for the transient model.**

Note: ft = feet; AFY = acre-feet per year
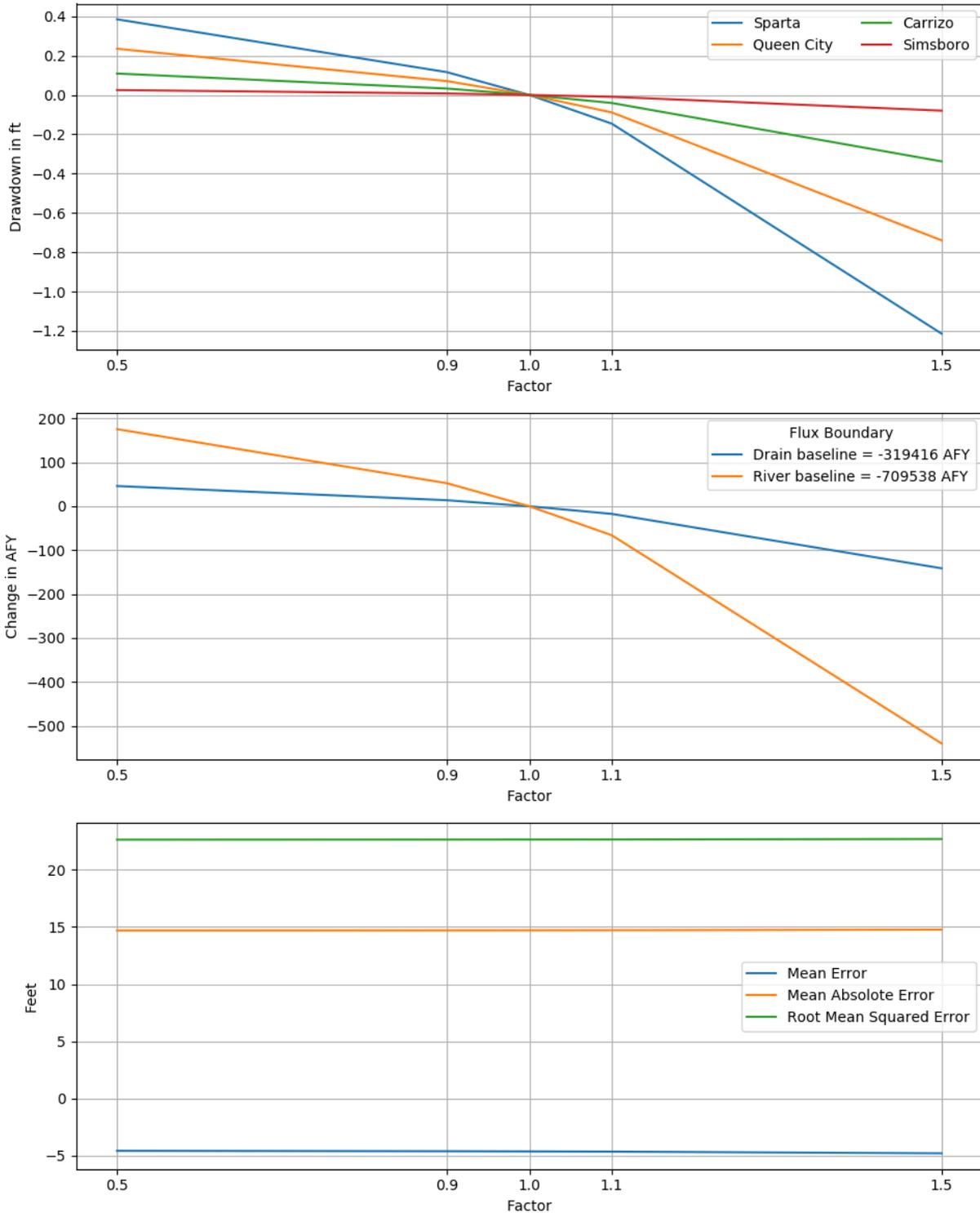
Figure 6.2.2i.   **Sensitivities of 2010 drawdown in hydrogeologic units (top), hydraulic boundary fluxes (center), and calibration statistics (bottom) to the specific storage of the Sparta Aquifer for the transient model.**

Note: ft = feet; AFY = acre-feet per year
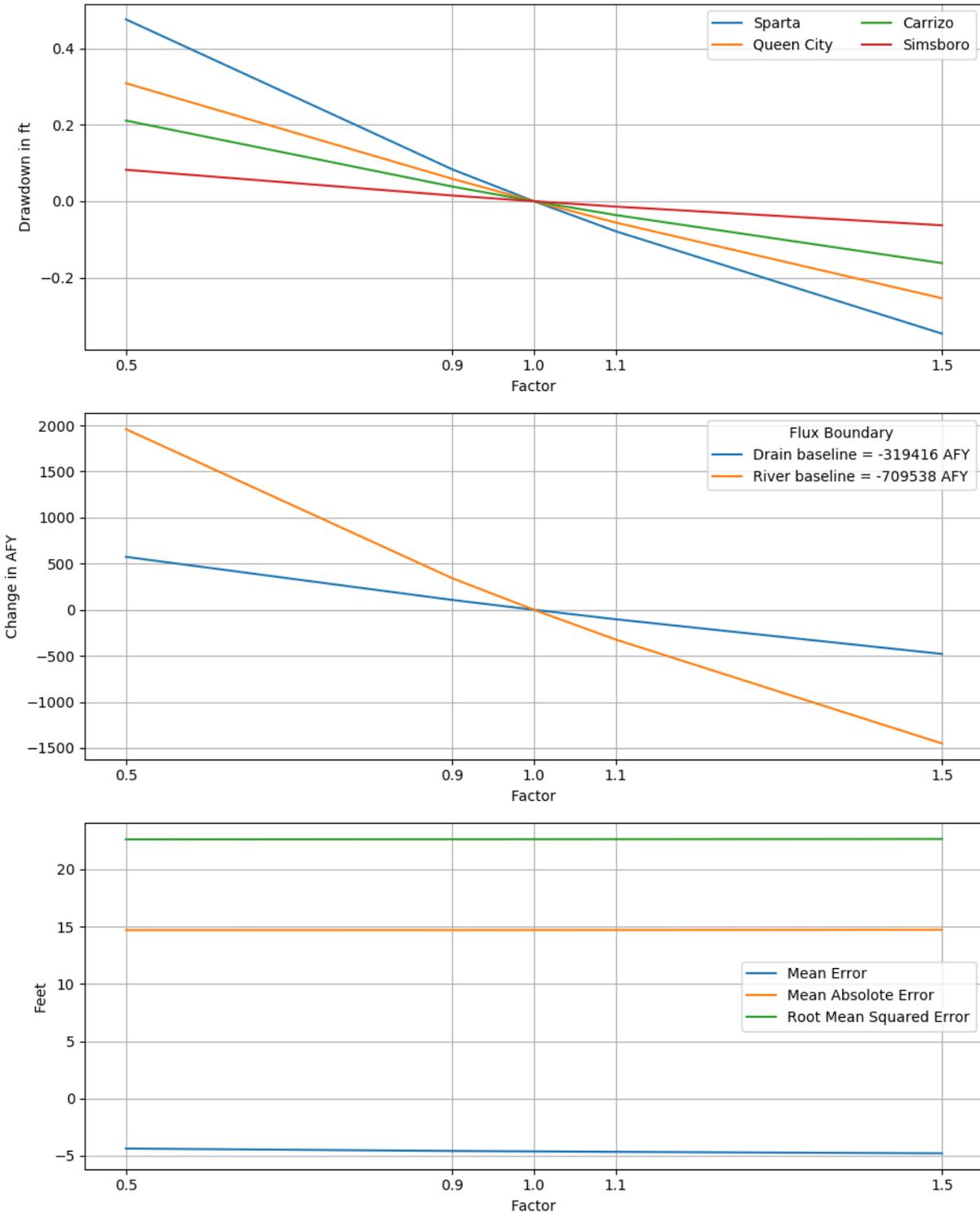
Figure 6.2.2j. **Sensitivities of 2010 drawdown in hydrogeologic units (top), hydraulic boundary fluxes (center), and calibration statistics (bottom) to the specific yield of the Sparta Aquifer for the transient model.**

Note: ft = feet; AFY = acre-feet per year
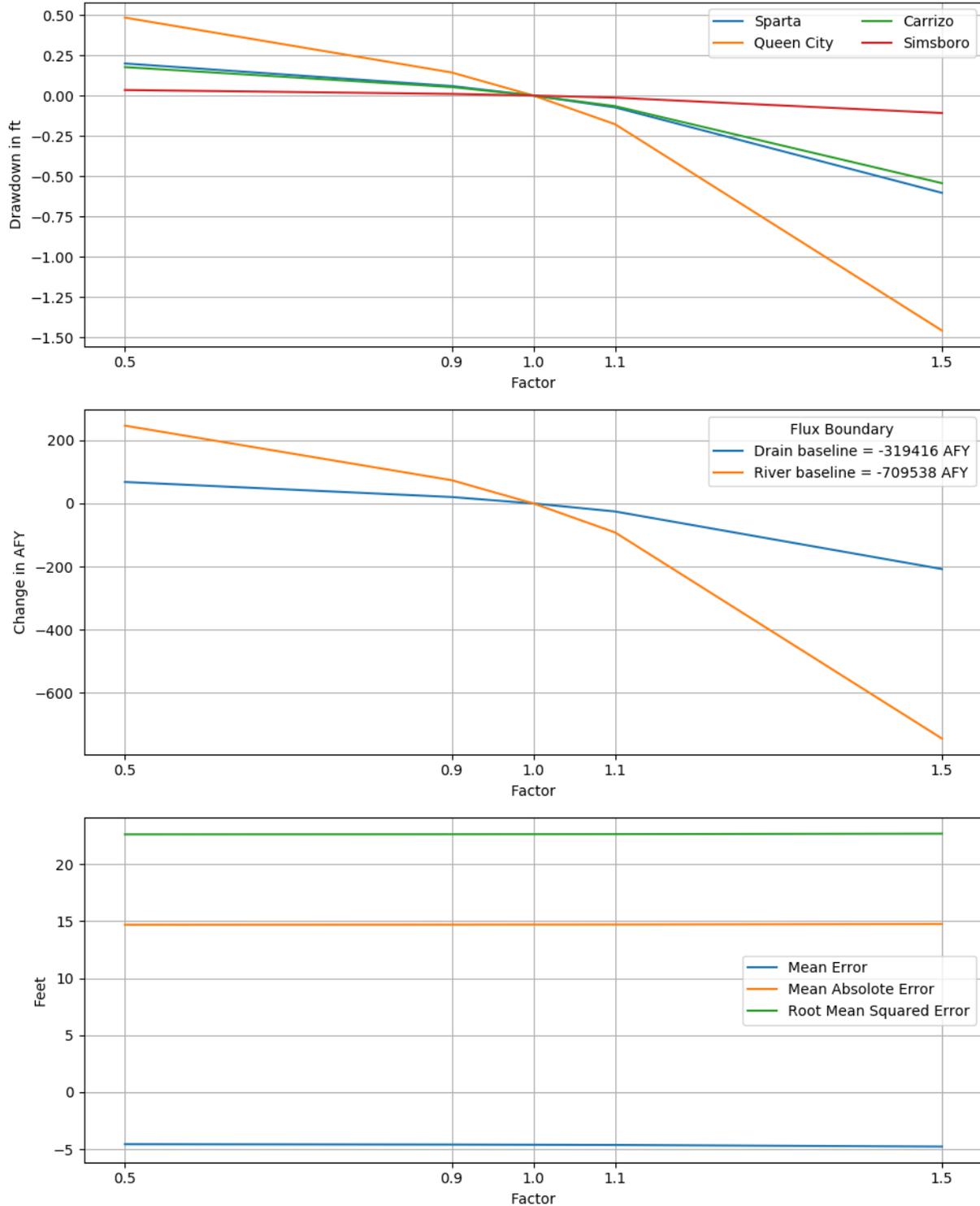
Figure 6.2.2k. Sensitivities of 2010 drawdown in hydrogeologic units (top), hydraulic boundary fluxes (center), and calibration statistics (bottom) to the specific storage of the Queen City Aquifer for the transient model.

Note: ft = feet; AFY = acre-feet per year
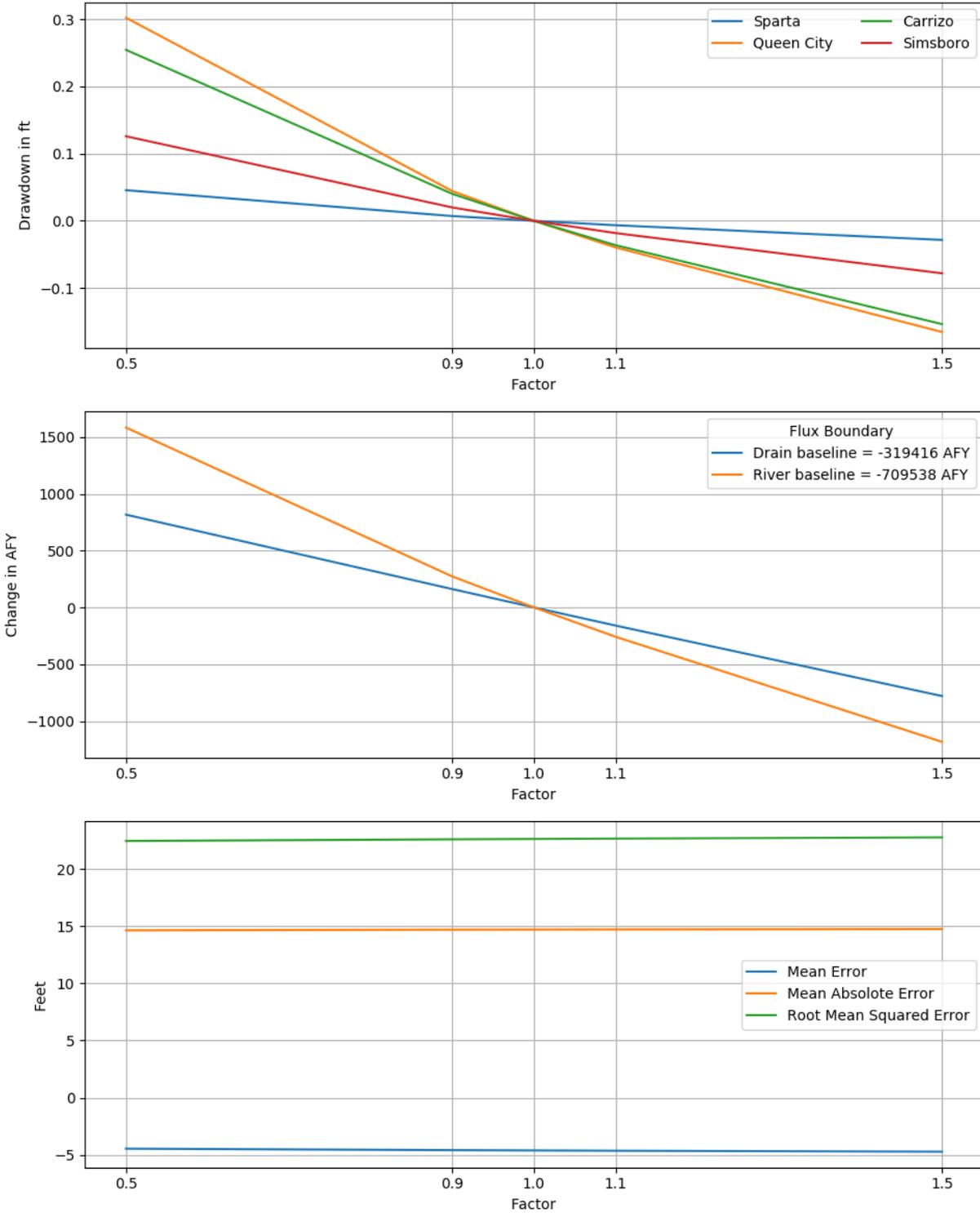
Figure 6.2.2l. **Sensitivities of 2010 drawdown in hydrogeologic units (top), hydraulic boundary fluxes (center), and calibration statistics (bottom) to the specific yield of the Queen City Aquifer for the transient model.**

Note: ft = feet; AFY = acre-feet per year
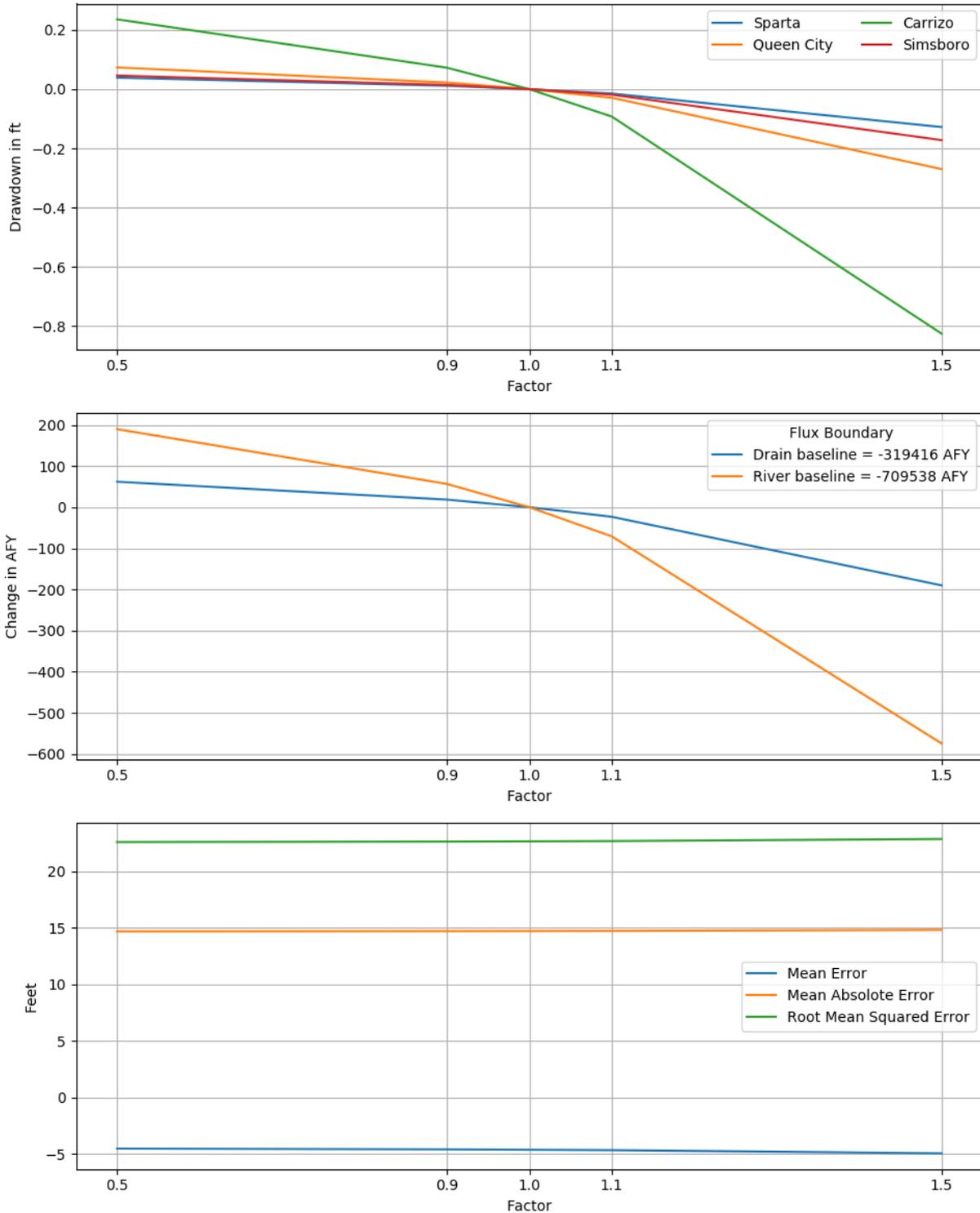
Figure 6.2.2m.   **Sensitivities of 2010 drawdown in hydrogeologic units (top), hydraulic boundary fluxes (center), and calibration statistics (bottom) to the specific storage of the Carrizo Aquifer for the transient model.**

Note: ft = feet; AFY = acre-feet per year
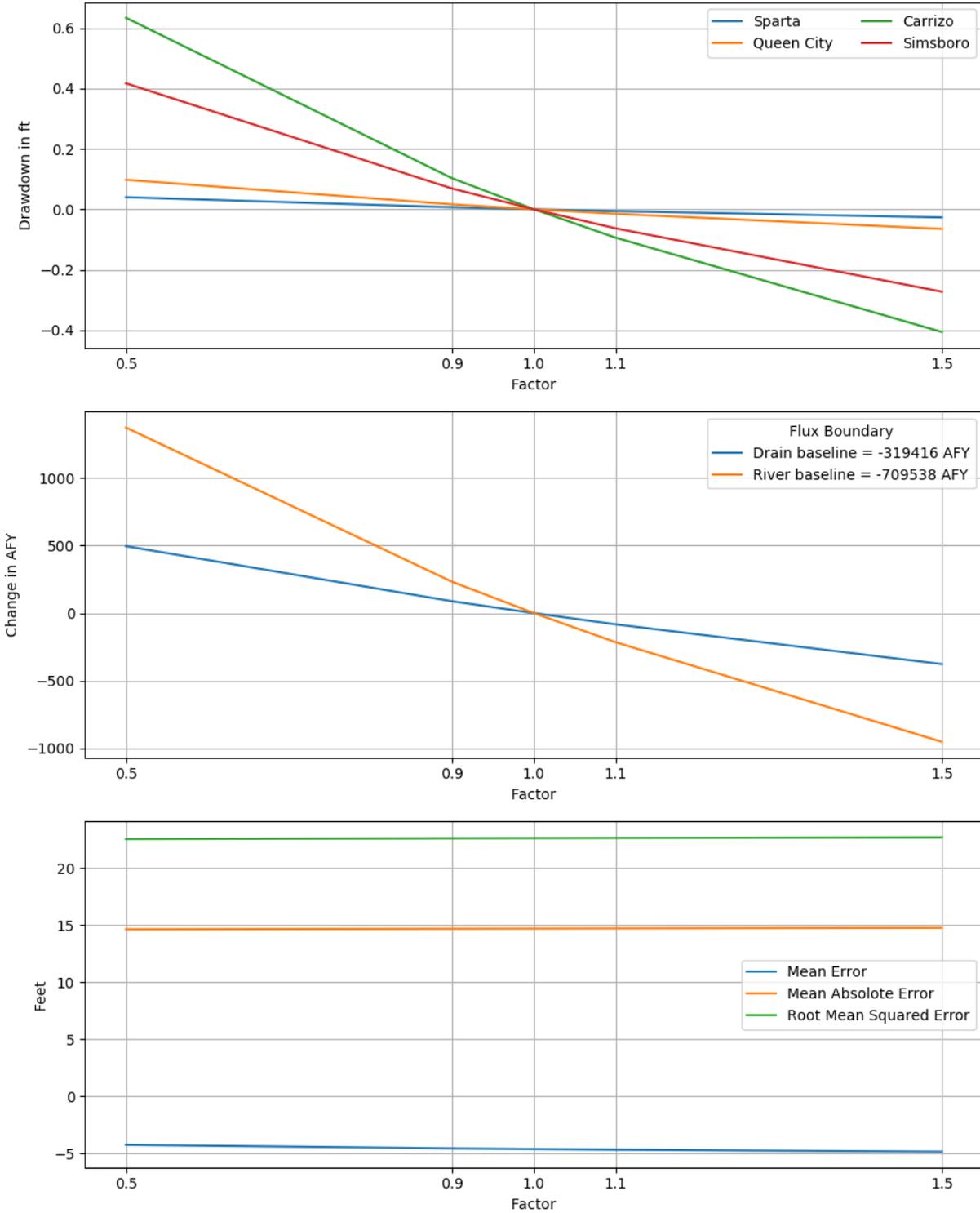
Figure 6.2.2n. **Sensitivities of 2010 drawdown in hydrogeologic units (top), hydraulic boundary fluxes (center), and calibration statistics (bottom) to the specific yield of the Carrizo Aquifer for the transient model.**

Note: ft = feet; AFY = acre-feet per year
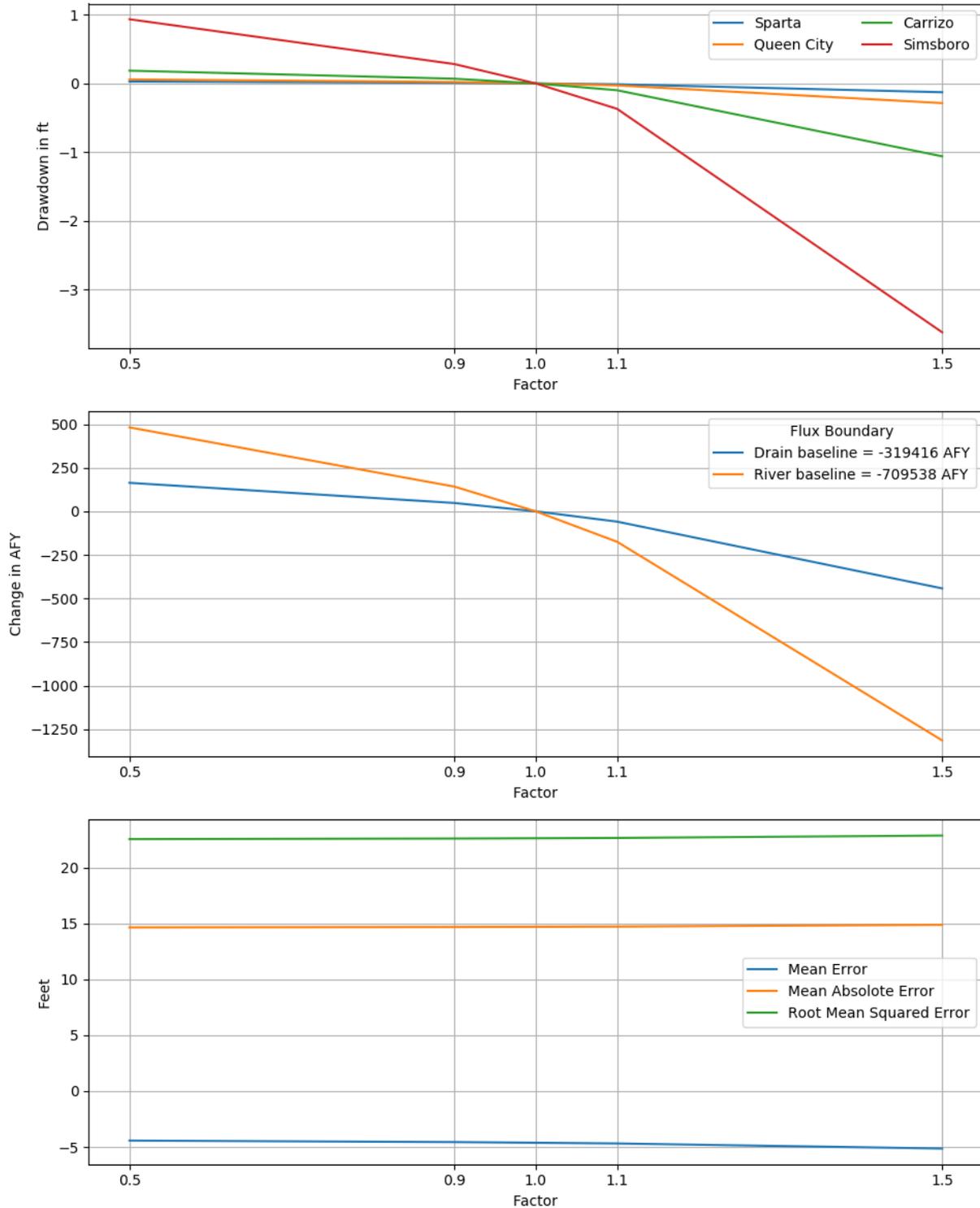
Figure 6.2.2o.   **Sensitivities of 2010 drawdown in hydrogeologic units (top), hydraulic boundary fluxes
(center), and calibration statistics (bottom) to the specific storage of the Simsboro
Formation for the transient model.**

Note: ft = feet; AFY = acre-feet per year
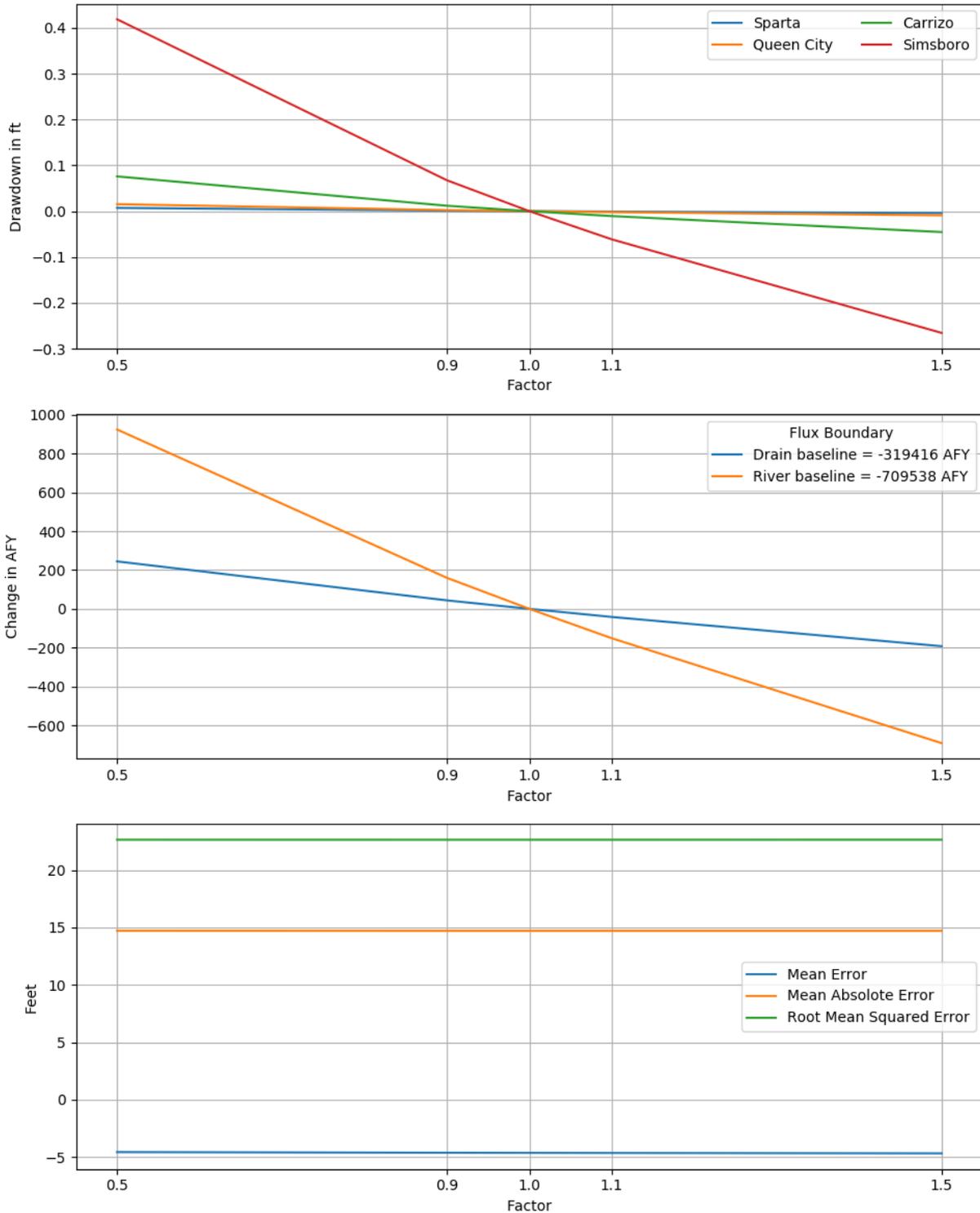
Figure 6.2.2p. **Sensitivities of 2010 drawdown in hydrogeologic units (top), hydraulic boundary fluxes (center), and calibration statistics (bottom) to the specific yield of the Simsboro Formation for the transient model.**

Note: ft = feet; AFY = acre-feet per year
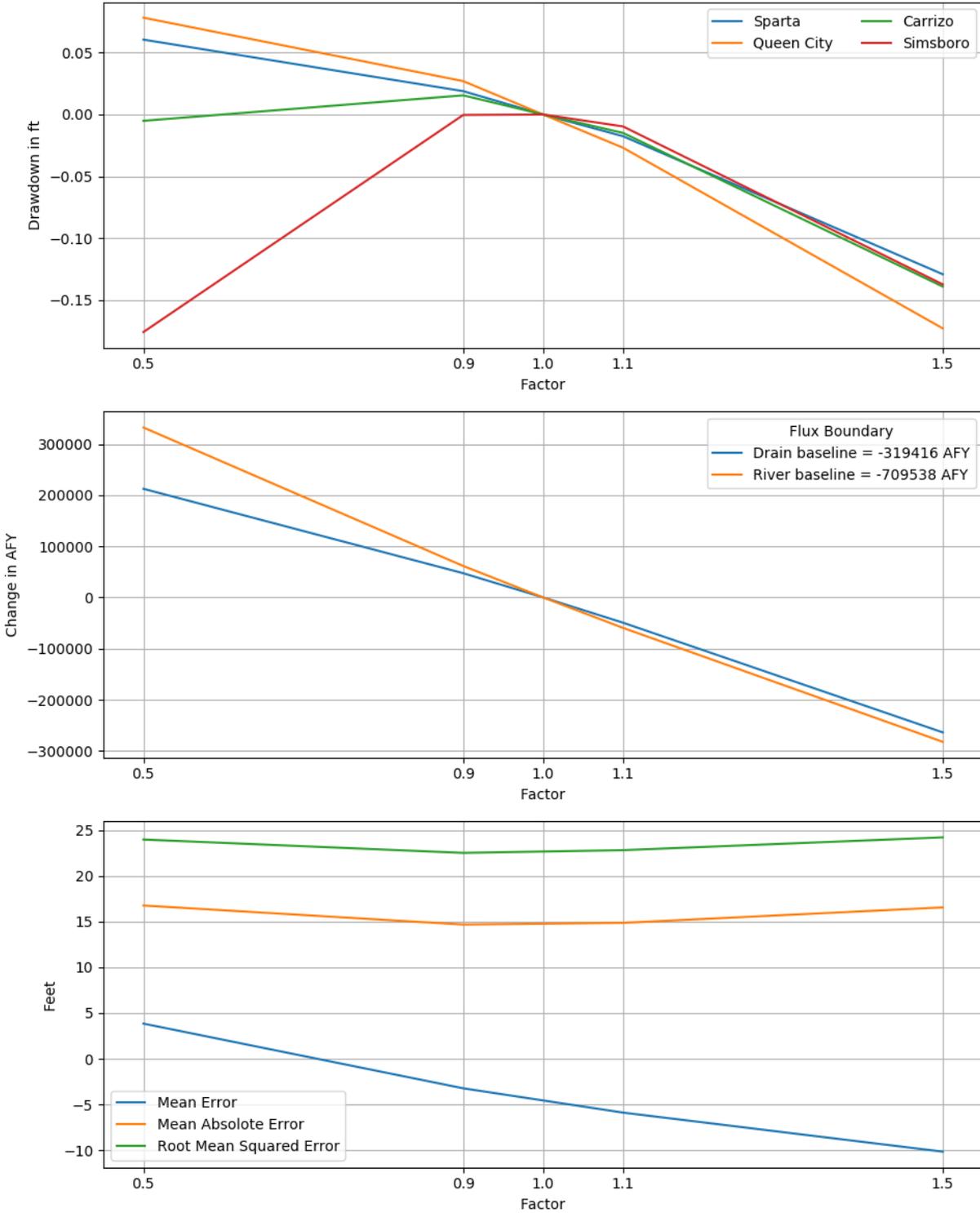
Figure 6.2.2q. **Sensitivities of 2010 drawdown in hydrogeologic units (top), hydraulic boundary fluxes (center), and calibration statistics (bottom) to the recharge rate for the transient model.**

Note: ft = feet; AFY = acre-feet per year
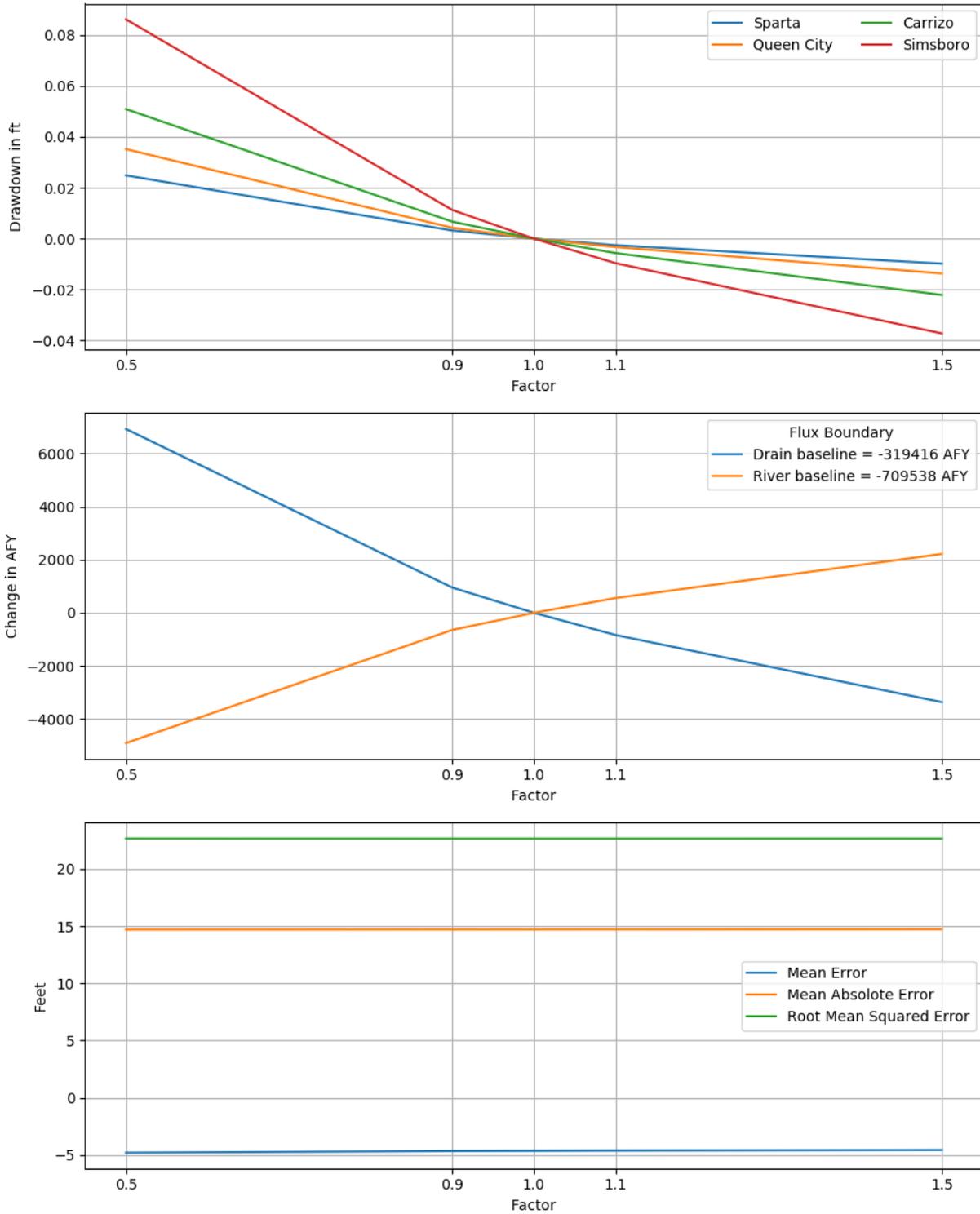
Figure 6.2.2r. **Sensitivities of 2010 drawdown in hydrogeologic units (top), hydraulic boundary fluxes (center), and calibration statistics (bottom) to the conductance of drain cells for the transient model.**

Note: ft = feet; AFY = acre-feet per year
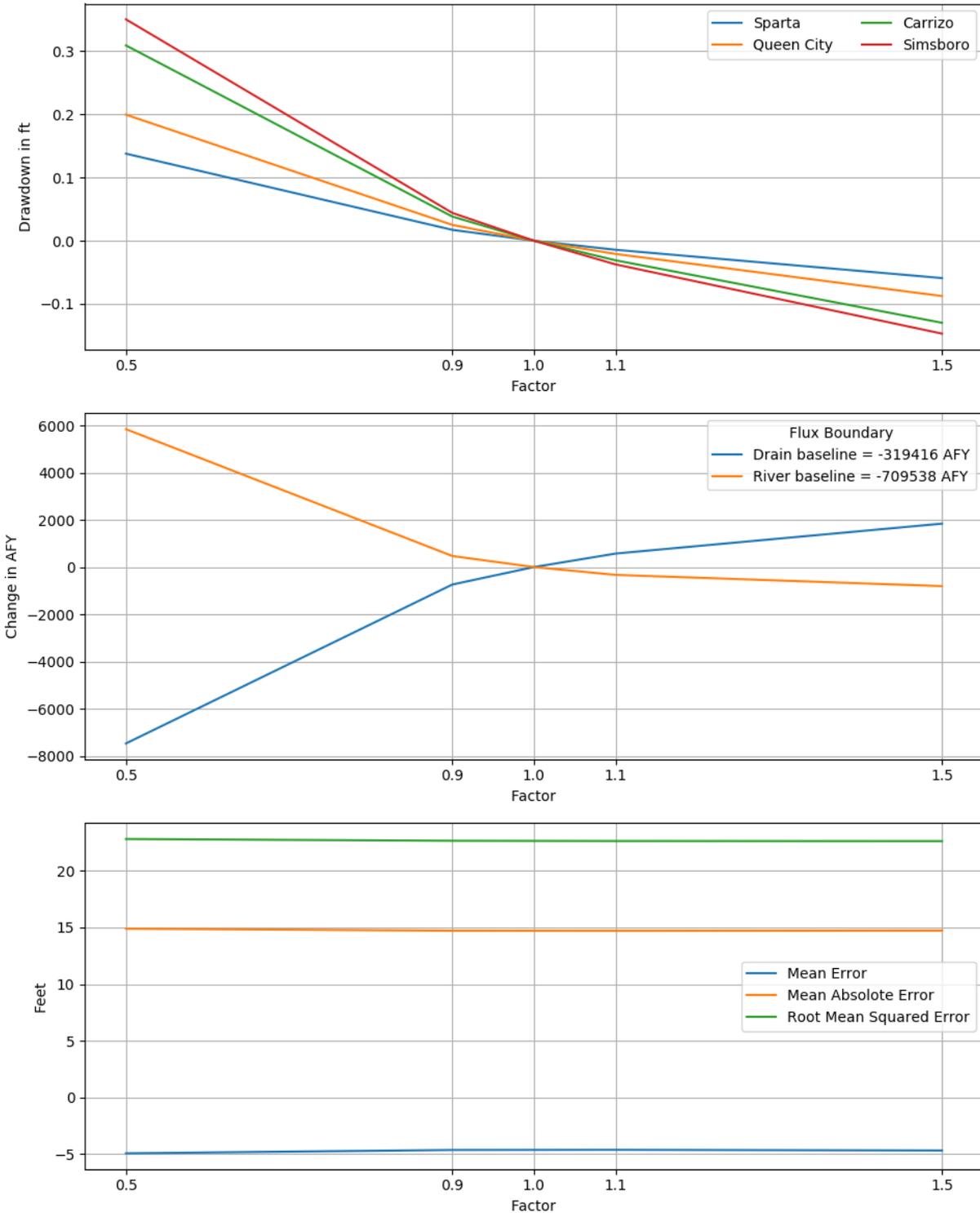
Figure 6.2.2s.   **Sensitivities of 2010 drawdown in hydrogeologic units (top), hydraulic boundary fluxes (center), and calibration statistics (bottom) to the conductance of river cells for the transient model.**

Note: ft = feet; AFY = acre-feet per year
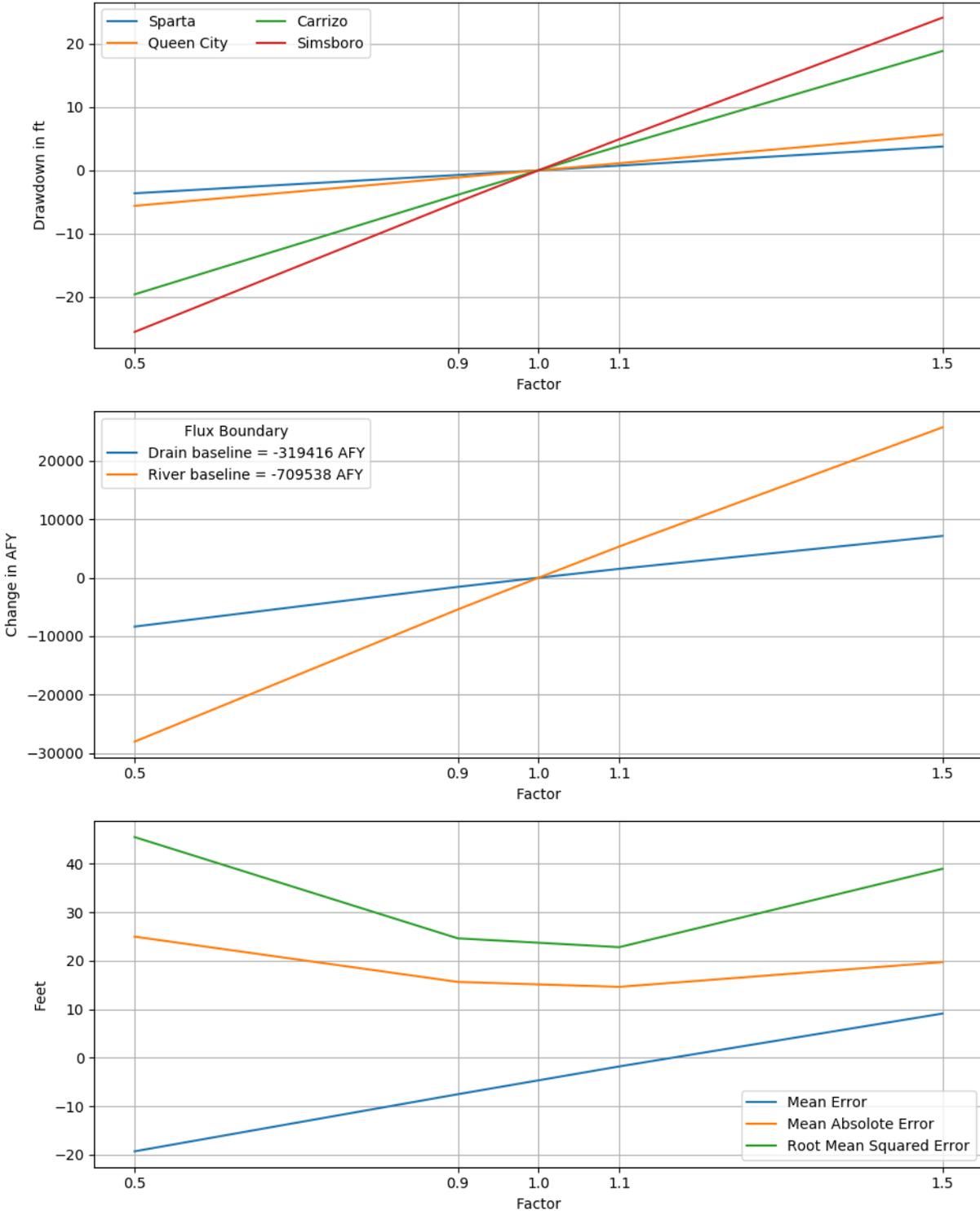
Figure 6.2.2t. Sensitivities of 2010 drawdown in hydrogeologic units (top), hydraulic boundary fluxes (center), and calibration statistics (bottom) to the pumping rate for the transient model.

Note: ft = feet; AFY = acre-feet per year
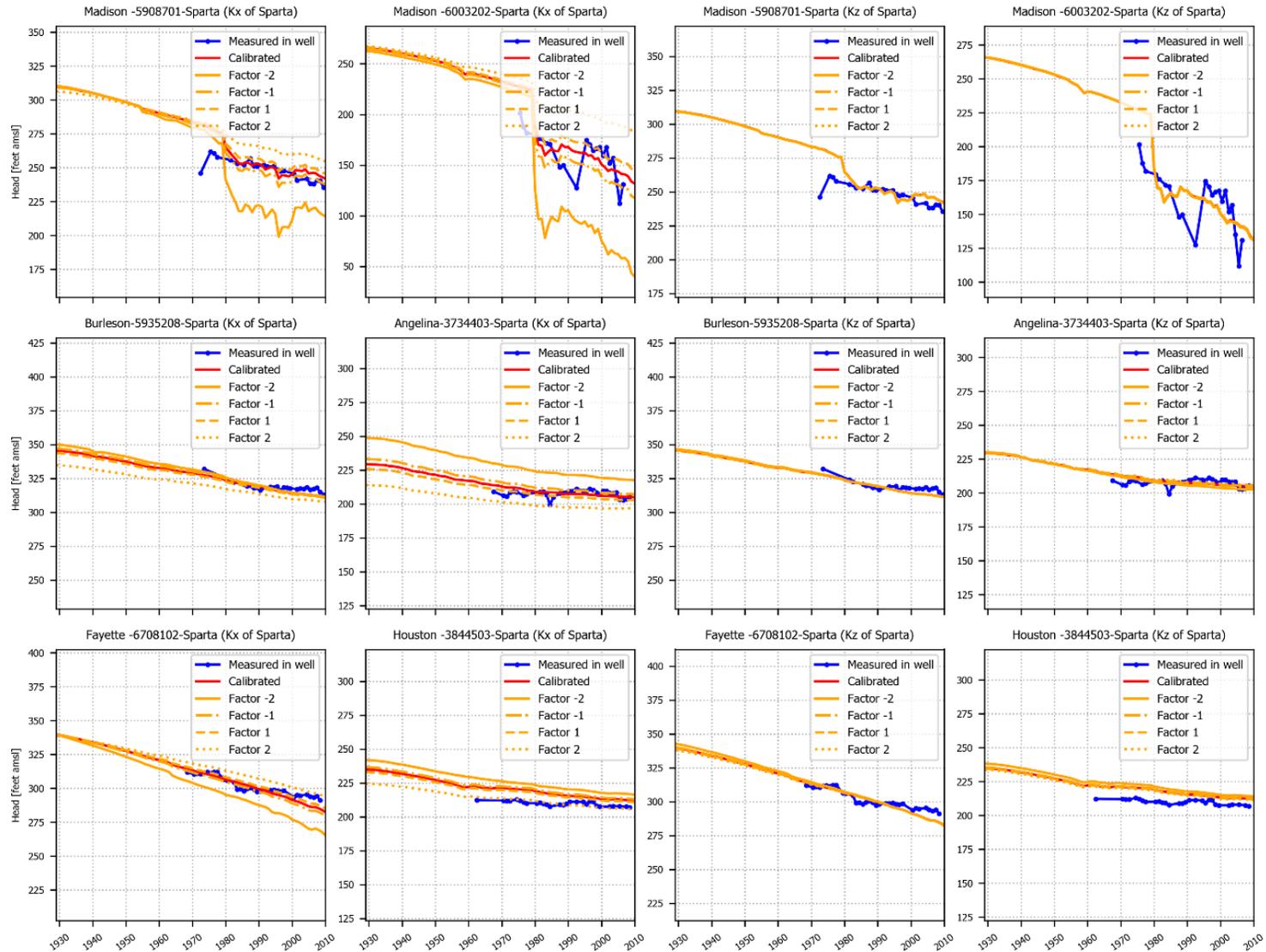
Figure 6.2.2u. Hydrographs showing sensitivity of heads (in feet above mean sea level) to changes in the horizontal and vertical hydraulic conductivity of the Sparta Aquifer for select wells completed in the Sparta Aquifer.

Note: Kx = horizontal hydraulic conductivity; Kz = vertical hydraulic conductivity
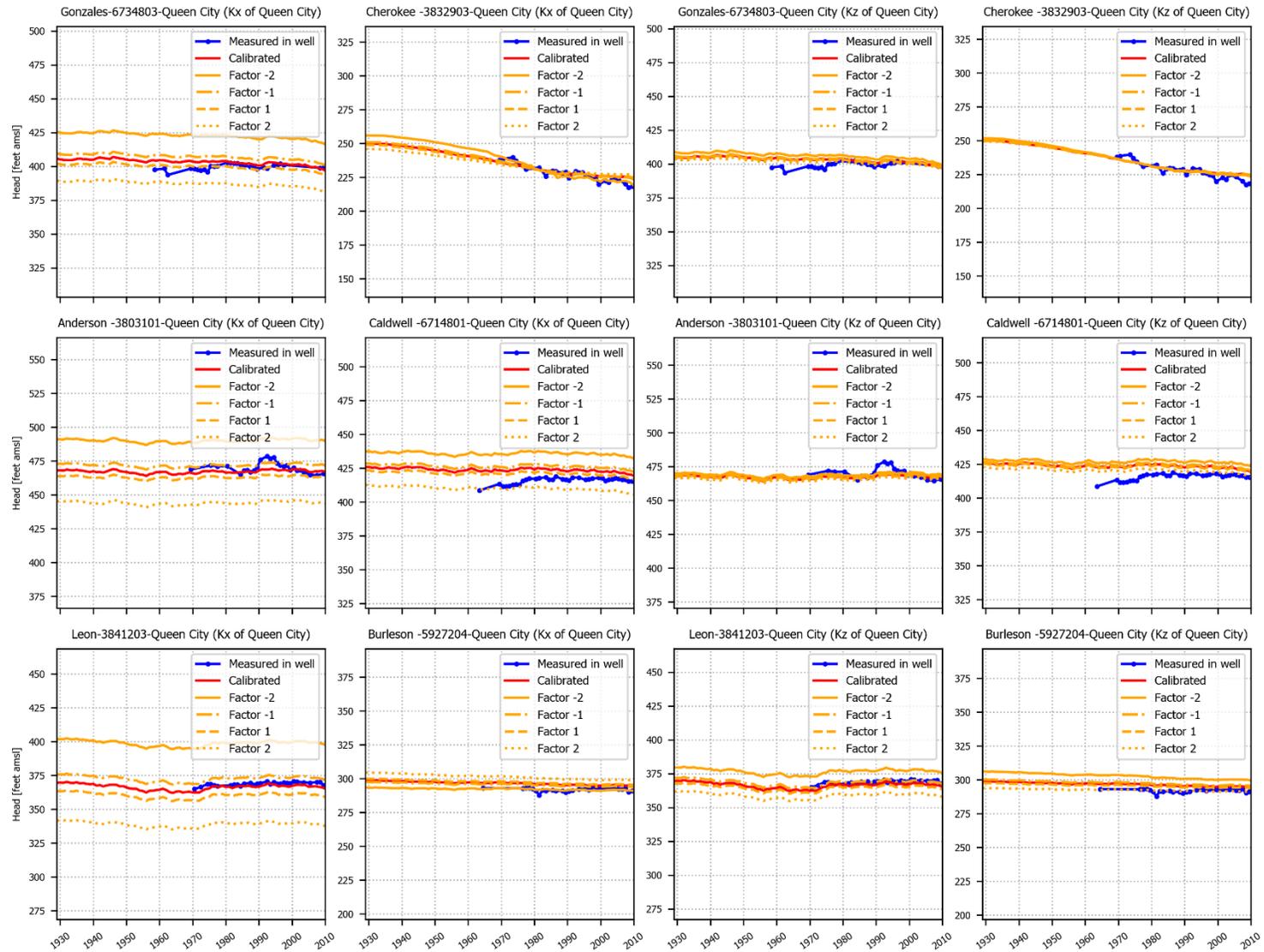
Figure 6.2.2v. **Hydrographs showing sensitivity of heads (in feet above mean sea level) to changes in the horizontal and vertical hydraulic conductivity of the Queen City Aquifer for select wells completed in the Queen City Aquifer.**

Note: Kx = horizontal hydraulic conductivity; Kz = vertical hydraulic conductivity
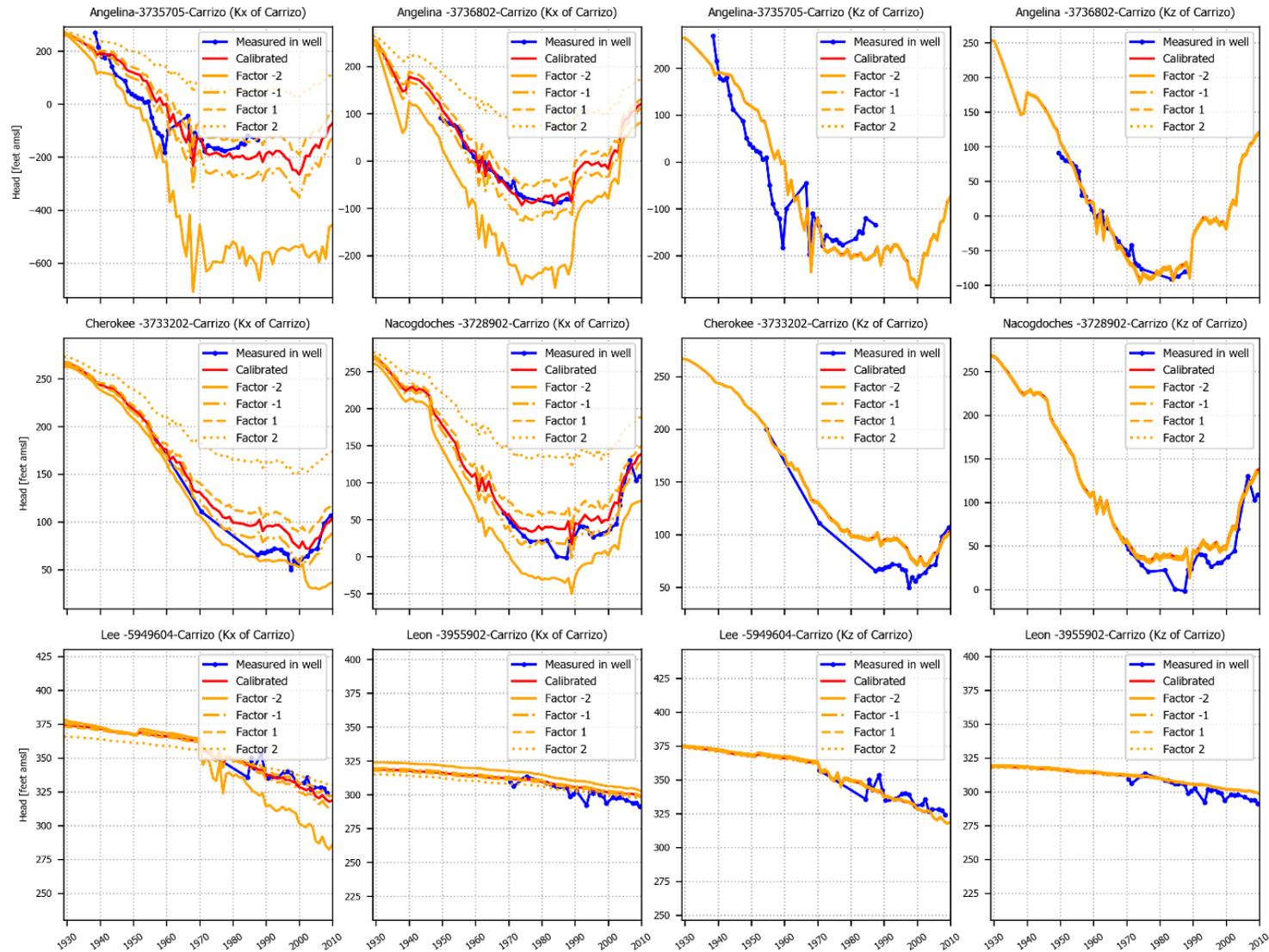
Figure 6.2.2w. **Hydrographs showing sensitivity of heads (in feet above mean sea level) to changes in the horizontal and vertical hydraulic conductivity of the Carrizo Aquifer for select wells completed in the Carrizo Aquifer.**

Note: Kx = horizontal hydraulic conductivity; Kz = vertical hydraulic conductivity
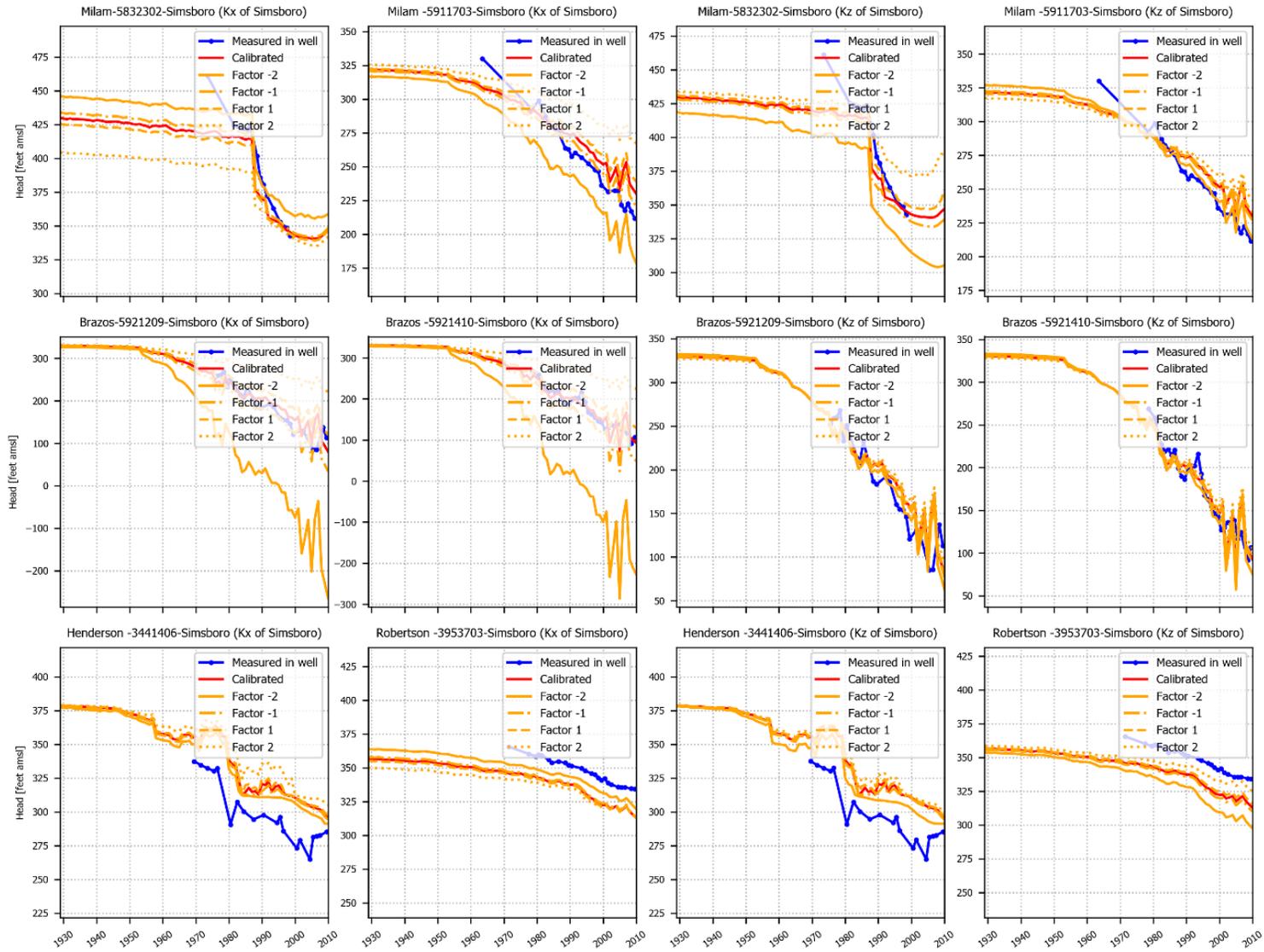
Figure 6.2.2x. **Hydrographs showing sensitivity of heads (in feet above mean sea level) to changes in the horizontal and vertical hydraulic conductivity of the Simsboro Formation for select wells completed in the Simsboro Formation.**

Note: Kx = horizontal hydraulic conductivity; Kz = vertical hydraulic conductivity.

This page is intentionally blank.

7   Model Limitations

A model can be defined as a representation of reality that attempts to explain the behavior of some aspect of it but is always less complex than the real system it represents (Domenico, 1972). As a result, limitations are intrinsic to models. Model limitations can be grouped into several categories including: (1) limitations in the data supporting a model, (2) limitations in the implementation of a model, which may include assumptions inherent to the model application, and (3) limitations regarding model applicability. The limitations of this modeling study are discussed in the following paragraphs consistent with these groupings.

7.1   Limitations of Supporting Data

Developing the supporting database for a large regional model with numerous grid cells is a challenge because the information available does not, and never will, sufficiently satisfy the model's data requirements. There are limitations in all of the varying types of data needed to develop a model representing such a large geographic area and extended time period. The following data limitations merit special attention and require discussion:

- Measured head data in the Colorado River alluvium
- Location and timing of historical pumping
- Measurements of vertical hydraulic conductivity
- Measurements of specific storage
- Measurements of sand and clay percentages and thicknesses
- Direct measurements of recharge rates
- Direct measurements of surface water–groundwater exchange

Each of these data limitations is discussed briefly below.

Inclusion of the alluvium associated with the Colorado River is an addition to this updated model. Although wells are completed in the alluvium, none have a hydraulic head measurement prior to 1950 and all have only one or two total hydraulic head measurements. Therefore, calibration targets for the Colorado River alluvium are lacking.

Pumping is the primary model input parameter that causes changes in hydraulic heads. If there are large errors in prescribing the timing and location of pumping, then those errors will inevitably be transmitted into the model as either incorrect hydrogeologic unit properties or as misfits to measured hydraulic heads. Because of the paramount importance of historical pumping to development of groundwater models, considerable resources were focused on using available data to develop as good a historical pumping record as possible. To maximize the utility of our resources, we prioritized our data searches with regard to location and time. For location, we primarily emphasized Groundwater Management Area 12 and secondarily emphasized Groundwater Management Areas 11 and 13. For time, we primarily emphasized post-1980 and secondarily emphasized pre-1980.

Vertical hydraulic conductivity is among the important properties that control cross-formational flow between hydrogeologic units. Vertical hydraulic conductivity is, however, also among the

most difficult to measure at the scale required for regional groundwater models. A lack of field measurements often makes vertical hydraulic conductivity one of the least constrained parameters during model calibration. To help constrain spatial variability in the vertical hydraulic conductivity values across the model domain, we guided the model calibration using two information sources. First, we used equations that account for the depth of burial on vertical hydraulic conductivity based on geomechanical considerations. Second, we used vertical hydraulic conductivity values for different hydrogeologic units utilized by previous groundwater models.

Specific storage is the primary hydrogeologic unit property that determines how much water will be released by a confined aquifer in response to a decline in hydraulic head. Field measurements of specific storage values are limited because they require the successful execution of aquifer pumping tests that include at least one observation well. Moreover, the representativeness of the specific storage value calculated from an aquifer pumping test is affected by the length and vertical placement of screened intervals for both the pumping well and observation well. To help overcome the limitations of the sparseness of specific storage values, we used a peer-reviewed and field-verified relationship for estimating specific storage that has been used in several regional groundwater models, including groundwater availability models of Texas aquifers.

A potentially useful indicator of the spatial variability in hydrogeologic unit parameters are vertical profiles of sand and clay sequences interpreted from geophysical logs. When analyzed collectively over large areas, maps of sand and clay thicknesses and/or percentages can be used as indicators of the relative transmissivity of a formation. During model development, we consulted the BRACs database of sand and clay picks and maps of sand thickness available from hydrogeologic studies, including several published by the TWDB and the Bureau of Economic Geology. Another source was hydrogeologic unit properties used by groundwater models previously developed for the hydrogeologic units of interest. However, we were not able to fuse these different data sources into a consistent set of information that had the resolution and coverage needed to generate a reliable set of indicators that could be used quantitively to constrain hydraulic conductivity values. Rather, the different data sources were used piecemeal and qualitatively to guide the application of pilot points for parameterizing the hydraulic conductivity fields.

Direct measurement of groundwater recharge is not possible at either the spatial or temporal granularity required to develop regional groundwater models. As a result, groundwater modelers must develop approaches to estimate historical recharge rates across the model that support the model calibration process. As part of this study, we spent considerable effort to improve on a method used by previous developers of groundwater availability models, which includes using base flow separation techniques to extract estimates of surface water-groundwater interaction. The specific improvement we incorporated was to account for the contribution of bank flow and basin flow to total base flow as part of the model calibration process. Despite our efforts to improve on recharge estimation, the lack of direct recharge measurements remains a major data limitation for the model development.

Despite the effort put forth to improve the numerical framework and capability of the groundwater availability model to simulate surface water-groundwater interactions, the full benefit of the improvements cannot be realized until substantial advancement occurs with direct measurements of surface water-groundwater interaction. These measurements would likely involve gain-loss studies on river reaches under a variety of stream flow conditions. As part of the update to the groundwater availability model for the central portion of the Carrizo-Wilcox, Queen City, and Sparta aquifers, an assessment was conducted to improve quantification of surface water-groundwater interaction in the Colorado River Basin (Young and others, 2017). Part of that assessment involved development of a work plan to conduct field studies to improve understanding of surface water-groundwater interaction in the lower part of the basin. Two sites were identified, one in Bastrop County and a second in either Matagorda or Wharton counties. The objective of the field study would be to answer questions that cannot be answered by traditional gain-loss studies and hydrograph-separation analyses. These questions include (1) what is the direction and magnitude of water exchange between the alluvium and stream under stable low-flow conditions, (2) what is the origin of water gained by the stream during low-flow conditions (the alluvium or from bank storage), and (3) how might pumping affect stream gains and losses over time?

7.2   Assessment of Assumptions

The model was constructed and calibrated with numerous assumptions inherent to the process of simplifying a groundwater flow system composed of multiple aquifers into a manageable set of equations and model input requirements. Many of these assumptions are not unique to this model and, though important in their own right, neither restrict nor impact the applicability of the model. However, there are several assumptions unique to this model and worthy of discussion. Among the limitations associated with the model assumptions are:

- Land use and its potential impact on recharge does not change over time
- Seasonal fluctuations are ignored by using annual time steps
- Assignment of ground surface elevation and drain locations
- Depth-decay relationships imposed on hydrogeologic unit hydraulic properties

Each of these assumption limitations is discussed briefly below.

The primary consideration used to adjust recharge spatially was surface geology. This criterion is reasonable and consistent with previous groundwater availability models. However, our model calibration period is 80 years and, over that duration, changes in land use in some areas would be sufficient to alter the recharge rate. These land use changes will be most important where agriculture or cities have expanded. If there were time and budget to gather and examine this level of data, we do not believe including the information into the calibration process would necessarily lead to improvement in either the calibration or application of the model because the groundwater model integrates recharge over large areas. Nonetheless, there are likely localized areas where changes to land use does affect the model's performance. If the model is to be applied to a localized region, then the modelers should investigate whether the model's spatial distribution of recharge should be modified to account for changes in land use.

The annual time step requires use of annual averages to represent all hydraulic boundary conditions in the model including recharge, pumping, groundwater-surface water interaction, and evapotranspiration. For the purpose of regional planning, which looks out over decades and focuses on the impacts of large groundwater projects on the availability of groundwater, the temporal discretization is reasonable. Across the majority of the model domain, the groundwater flow processes can be approximated as a linear response. As such, the averaging of pumping rates or recharge is a reasonable approximation.

Among the consequence of using grid cells that are 1 mile by 1 mile is that surface features that can affect groundwater flow are difficult to represent properly where there is considerable topographic variability. One measure of topographic variability is the standard deviation of the topography elevation from a digital elevation model for a grid cell. Across much of the northern half of the model domain, the standard deviation of ground surface in a single grid cell was 40 feet. For these grid cells, the average elevation generated by sampling the 10-meter digital elevation model was used to represent ground surface. In addition, we assigned the drain elevations equal to the ground surface elevation minus 20 percent of the thickness of model layer 2. This approach proved to work as well or better than other options we explored. We suspect that, at some locations, adjustments to our approach for setting the elevations for ground surface and the drains would be appropriate.

One major data gap in developing regional models is the lack of data for the downdip and deep regions of the aquifers. In these areas, there are no wells, so there is typically neither aquifer pumping test data nor hydraulic conductivity measurements. As shown by the model cross-sections in Section 4.2, most of the model layers extend to depths between 7,000 to 10,000 feet. To account for compressional forces that affect porosity and permeability, we used well-established equations to systematically reduce hydraulic conductivity values with depth. Because of the lack of hydraulic conductivity values measured at depths below a few thousand feet, we could not investigate the validity of our assumptions. However, our values are within the bounds of several of the studies we reviewed, indicating their reasonableness.

7.3   Limitations of Model Applicability

The purpose of the TWDB Groundwater Availability Modeling Program is the development of models to determine how regional water availability is affected on a large scale by water resource development. Except for the area near the Colorado and Brazos rivers alluvium, the model was developed at a grid scale of one square mile. At this scale, models are not capable of predicting aquifer responses at specific points, such as at a particular well. The groundwater availability models are accurate at the scale of tens of miles, which is adequate for understanding groundwater availability at the regional scale. Drawdowns that are observable at the regional scale should be reproducible by the model. Questions regarding local drawdown to a well should be based upon analytical solutions, such as TTim (Bakker, 2013), or a modification of the groundwater availability model that includes a refined numerical grid.

Although considerable effort focused on inclusion of a shallow groundwater flow system as model layer 2 to improve the capability of the model to simulate surface water-groundwater interaction, the model still represents a first-order approach to coupling surface water to

groundwater. The inclusion of the shallow groundwater flow system primarily serves to eliminate direct hydraulic connection between surface water and the intermediate or deep groundwater flow system. The addition of the shallow groundwater flow system did not include the appropriate equations to provide a physics-based rigorous solution to surface water–groundwater interaction. In addition to lacking the necessary physics, the current model also lacks the appropriate geometry for representing streams where detailed surface water-groundwater simulations are required.

The predictive capability of the model is tied not only to the availability of spatial data but also to that of temporal data. The lack of data over short time periods for use in developing model boundary conditions means that stress periods of less than one year were not warranted. Use of annual stress periods precludes the ability of the model to predict seasonal hydraulic head or flow variability. Temporal variability at a scale of less than one year is likely not important to regional water planning and groundwater management. However, if modifications to the model would be necessary to investigate processes that vary over a time scale less than one year, such as seasonal variability in base flow, the length of the model stress periods would have to be decreased. An example application requiring refined temporal resolution is coupling the model to a monthly surface water availability model.

The numerous figures in the report that compare simulated and observed heads provide a good opportunity to identify potential biases in the updated groundwater availability model. A review of the predictions of water levels in Brazos County suggests that the updated model provides good matches to the observed drawdowns in the downdip and confined regions of the Simsboro Formation. However, updip of Brazos County in Robertson County, the simulated and observed hydrographs for the Simsboro Formation indicate that there may be a small bias in underpredicting the drawdown in the Simsboro Formation. The observed bias could be caused by a under representation of pumping for the region but, in the event that it is not, users of the model should be aware that the updip migration of drawdown caused by downdip pumping in the confined Simsboro Formation may be underestimated in the updated model.

This page intentionally blank.

8   Summary and Conclusions

This report documents development of an update to the groundwater availability model for the central portion of the Carrizo-Wilcox, Queen City, and Sparta aquifers. Development of the numerical model documented in this report was based on the conceptual models described by Dutton and others (2003) and Kelley and others (2004). The numerical model is based on the groundwater availability model developed by Kelley and others (2004). The purpose of the model is to provide a tool for groundwater planning and management in the state of Texas. The project work included updates to both the conceptual and numerical models.

8.1   Updates to the Conceptual Model

The updates to the conceptual model for the groundwater availability model for the central portion of the Carrizo-Wilcox, Queen City, and Sparta aquifers included revisions to:

- The Milano Fault Zone
- Historical pumping
- Recharge
- Surface water and groundwater interaction

Each of these updates is summarized briefly in the following subsections.

8.1.1   Milano Fault Zone

The hydrogeologic assessment of the Milano Fault Zone consisted of three investigations: (1) a geologic investigation to map faults associated with the Milano Fault Zone and to estimate their vertical offset; (2) an investigation to identify evidence that faults impacted groundwater flow by analyzing aquifer pumping tests; and (3) a modeling investigation to evaluate the sensitivity of predicted water levels to the conceptualization of faults in the Milano Fault Zone. The results of the fault analysis led to a revised representation of the faults in the Milano Fault Zone in the updated model relative to those in the model of Kelley and others (2004).

Faults in the Milano Fault Zone were mapped using a combination of geophysical logs, existing fault traces based on seismic and outcrop data, and expert knowledge of fault structure and geometry. The fault traces shown at surface on the Geologic Atlas of Texas (Barnes, 1970, 1979, 1981; Stoeser and others 2007) were considered the best indicators of probable fault locations. Using the previously mapped fault traces as a guide, 656 geophysical logs were reviewed in the vicinity of the Milano Fault Zone to identify fault locations and estimate fault offsets. Our evaluations of fault offsets were based primarily on picks for the top of the Cretaceous Navarro Group and, secondarily, on picks for the Simsboro Formation. The top of the Navarro Group was used as our signature pick because the marine clays that comprise this formation provide a relatively clean and identifiable signature on geophysical logs. Our detailed review of geophysical logs indicates that the Milano Fault Zone consists of a series of connected grabens.

After the faults were mapped, data for 113 aquifer pumping tests were assembled and analyzed for evidence that a reduction in aquifer transmissivity, such as might be caused by a fault, occurs within a few miles of the pumping well. For each of the aquifer pumping tests, the drawdown

data were analyzed using the Cooper-Jacob approximation to the Theis nonequilibrium well equation. A Cooper-Jacob analysis relies on the fact that the slope of a semi-log plot of time-drawdown data for a constant-rate pumping test can be used to calculate aquifer transmissivity if the pumping rate is known (Cooper and Jacob, 1946). Butler (1990), Streltsova (1988), and Young (1998) show that the Cooper-Jacobs analysis method can be used to analyze different time periods of a time-drawdown curve to determine whether the aquifer's transmissivity field away from the pumping well is different than the aquifer's transmissivity field close to the pumping well. The results of the Cooper-Jacob analysis indicate that faults with vertical offsets greater than 200 feet were very likely to reduce the aquifer transmissivity and, thereby, impact groundwater flow.

The groundwater modeling investigation was performed with the analytical element code TTim (Bakker, 2013). TTim is a three-dimensional analytical element model capable of simulating groundwater flow and representing faults as vertical planes with low conductance. The application of the TTim approach reproduced the time-drawn data from the aquifer tests reasonably well and, thereby, confirmed that the faults identified as part of this study can be modeled as planes of low conductance.

8.1.2 Historical pumping

The groundwater availability model developed by Kelley and others (2004) included a transient period from 1980 to 1999. As part of this project, the transient period was expanded to 1930 to 2010. The majority of the historical pumping data were obtained from water use survey data and groundwater pumping estimates available from the TWDB and from historical reports. Additional pumping data were gathered by contacting groundwater conservation districts and municipalities. Assigning pumping to the model grid cells was a two-part process. First, a dataset of annual pumping by water user groups (for example, cities, water supply companies, industries, irrigation, livestock) and for rural domestic pumping was created. Second, a well dataset was compiled to guide the placement of pumping spatially as well as temporally.

The well-specific pumping from the groundwater conservation districts and associated with lignite mining were assigned to the model grid based on the node in which the wells are completed. For the remainder of the municipal, manufacturing, mining, and power pumping, wells associated with the pumping entity were identified based on the name of the pumping entity and the name of the well owner, and the pumping for that entity was assigned to the nodes in which the wells are completed.

8.1.3 Recharge

The approach used to update recharge rates was based on a hydrograph separation method similar to that used by Dutton and others (2003) in that average recharge rates for a watershed are estimated by dividing a watershed's annual base flow by the area of the watershed. The key distinguishing aspect of our approach was that the recharge rates were adjusted to account for two effects; the impact of surface geology on the spatial distribution of recharge and the impact of bank flow on base flow. Bank flow is groundwater from bank storage that leaves the alluvium

adjacent to a stream to become streamflow. Bank flow is groundwater that originates from stream water that infiltrates the river alluvium during periods of high stream water levels.

The approach to separate base flow values calculated for a river gage into a bank flow component and a basin flow component involved applying two adjustment factors. One factor accounted for the bank storage potential for river alluvium and was based on the amount of alluvium in a watershed. The other factor accounted for the occurrence of high water or flooding conditions and was based on the amount of annual precipitation received by a watershed. The recharge predicted from base flow estimates through hydrograph separation analyses was reduced by up to 70 percent based on the combined effect of these two adjustment factors. Without these two adjustment factors, recharge rates higher than 10 inches per year were estimated based solely on the results from the hydrograph separation analyses for watersheds with high annual rainfalls. For steady-state conditions, the revised approach generates an average recharge rate of 2 inches per year for the entire model domain. This is a factor of two increase over the average rate of 1 inch per year used by Kelley and others (2004).

8.1.4 Surface Water-Groundwater Interaction

One of the main problems with accurately representing surface water-groundwater interaction in groundwater availability models is concisely stated by Mace and others (2007):

> "One of the difficulties in accurately representing surface water-groundwater interaction is the vertical resolution in the groundwater availability model…. In many cases, the current groundwater availability models are too coarse, both laterally and vertically, to accurately represent surface water-groundwater interaction."

To help remedy the coarse vertical resolution with the groundwater availability model developed by Kelley and others (2004), two model layers were added to the updated model. One of the additional model layers was constructed to represent only the Colorado and Brazos rivers alluvium. Beneath this model layer, a second shallow model layer was added to represent the shallow groundwater flow system. This second model layer, which extends across the entire outcrop area of the simulated hydrogeologic units, was created by setting its top surface at ground surface or the base of the alluvium layer (where it exists) and setting its bottom surface at approximately 25 to 75 feet below the anticipated elevation of the predevelopment water table.

To help remedy the coarse lateral resolution for the two major rivers in Groundwater Management Area 12, the 1-mile by 1-mile numerical grids in the vicinity of the Colorado and Brazos rivers in the 2004 groundwater availability model were replaced with smaller grid cells. In the vicinity of the Colorado River and its major tributaries, the grid cells in the updated model were reduced to 0.25 mile by 0.25 mile. In the vicinity of the Brazos River and its major tributaries, the grid cells are reduced to 0.5 mile by 0.5 mile in the updated model. The increased refinement provided for improved resolution for representing horizontal hydraulic gradients between streams and the aquifer.

8.2   Updates to Numerical Model

8.2.1   Model Construction

The code used to implement the update to the groundwater availability model for the central portion of the Carrizo-Wilcox, Queen City, and Sparta aquifers is MODFLOW-USG (Panday and others, 2015). The numerical grid for the model was generated by refining the numerical grid developed by Kelley and others (2004) and by adding two additional model layers. Because the updated model was developed using MODFLOW-USG, the grid cells are no longer referred to by row and columns but rather by the unique node number assigned to each grid cell. Each model layer represents a different hydrogeologic units and different areal coverages. Table 8.2.1a lists the number of nodes and hydrogeologic units associated with each model layer.

Table 8.2.1a.   Number of nodes representing each model layer.

Model Layer	Hydrogeologic Unit	Number of Nodes
1	Colorado River and Brazos River Alluvium	2,221
2	Shallow Flow System	19,089
3	Sparta Aquifer	16,185
4	Weches Formation	17,218
5	Queen City Aquifer	21,941
6	Reklaw Formation	23,315
7	Carrizo Aquifer	24,786
8	Calvert Bluff Formation	29,084
9	Simsboro Formation	30,954
10	Hooper Formation	34,123

The updated model has 82 annual stress periods (see Table 4.2.2a). The steady-state period is the first stress period and represents predevelopment. Stress periods 2 through 82 represents 1930 through 2010.

8.2.2   Hydrogeologic Unit Hydraulic Properties and Hydraulic Boundary Conditions

The hydraulic properties for the model layers were determined as part of the calibration process using the parameter estimation software PEST (Doherty, 2018) to adjust and constrain groundwater parameters using a combination of pilot points and equations. The pilot points were primarily used to set the upper and lower boundaries of the allowable values for the hydraulic properties. The equations were used to adjust hydraulic properties based on theoretical and semi-empirical relationships that account for how increased compressibility forces and reduced porosity decrease hydraulic conductivity and specific storage values with increasing depth of burial. In addition, an equation was used to modify hydraulic conductivity based on the effect of groundwater temperature changes with depth. The hydraulic conductivities for the Brazos River Alluvium Aquifer were not determined as part of the calibration process; rather, they were

mapped from the Brazos River Alluvium Aquifer groundwater availability model (Ewing and Jigmond, 2016).

Recharge and evapotranspiration were simulated using the MODFLOW Recharge and Evapotranspiration packages, respectively. Surface water-groundwater interaction was simulated using river cells and drain cells. The MODFLOW River Package was used to represent groundwater exchange with major rivers and perennial streams. The locations of the river cells associated with the Brazos and Colorado rivers were mapped onto the refined numerical grid in the vicinity of those two rivers using the United States Geological Survey national hydrograph dataset of rivers and streams. The MODFLOW Drain package was used to simulate outflow from ephemeral streams, intermittent streams, and seeps.

8.3   Model Calibration

As previously mentioned, PEST (Doherty, 2018) was used to calibrate the model. PEST was applied using a series of programs linked together through a batch file that was execute on a computer cluster. PEST was applied first to help achieve a reasonable calibration for the steady-state condition and then used to calibrate the transient simulation from 1930 to 2010. A total of 522 measured hydraulic heads with a range of 400 feet were used for steady-state calibration targets. In addition, estimated surface water and groundwater fluxes at five watersheds were used as calibration targets. The steady-state calibration produced a mean error, mean absolute error, and a root-mean square error of 1.9, 18.9, and 22.9 feet, respectively. For the 190 measured hydraulic head values in Groundwater Management Area 12, the state calibration produced a mean error, mean absolute error, and a root-mean square error of 6.3, 19.3, and 24.1 feet, respectively.

For the entire model domain, 11,378 observed hydraulic heads from 647 wells were used to calibrate the model over the time period from 1930 to 2010. Analysis of the transient model data shows that, despite doubling the measurement range compared to steady-state conditions, the mean error, mean absolute error, and root mean square error are smaller than the values obtained for the steady-state conditions. The transient calibration statistics are nearly identical whether they are based on equal weights for each hydraulic head measurement or equal weights for the average hydraulic head at each well. Based on weighting the average hydraulic head at each well the same, the range of measurements is 743 feet and the transient calibration produced a mean error, mean absolute error, and a root-mean square error of -4.3, 14.4, and 21.3 feet, respectively.

8.4   Model Sensitivity Analysis

A sensitivity analysis was performed on the steady-state and transient model to determine the impact of changes in calibrated parameters on the predictions of the calibrated model. Four simulations were completed for each parameter sensitivity using factors of 0.5, 0.9, 1.1, and 1.5. Twenty-four parameters were varied for the steady-state sensitivity analysis and 20 were varied for the transient sensitivity analysis. Sensitivity of the steady-state model was assessed for the metrics average hydraulic head in each hydrogeologic unit, hydraulic boundary fluxes, number of additional flooded cells, and model calibration statistics. Sensitivity of the transient model was assessed for the metrics 2010 drawdown in the Sparta, Queen City, and Carrizo aquifers and the

Simsboro Formation, river and drain boundary fluxes, and model calibration statistics. To distill the results into a meaningful understanding of model sensitivity, a systematic methodology was developed based on ranking the impact on the metrics as a result of the change in parameter value.

For the steady-state model, all metrics are most sensitive to changes in recharge and are also sensitive to the horizontal hydraulic conductivity of the Queen City Aquifer. The top three parameters to which the steady-state model is most sensitive for the four metrics are summarized in Table 8.4a.

Table 8.4a   **Top two parameters to which the steady-state model is most sensitive.**

Average Hydraulic Head in Hydrogeologic Units	Hydraulic Boundary Fluxes[a]	Number of Additional Flooded Cells	Calibration Statistics
recharge	recharge	recharge	recharge
Kx Queen City	Kx Queen City	drain conductance	Kx Calvert Bluff
Kv Reklaw	Kx Sparta	river conductance	Kx Queen City

[a] general-head boundary, drain, and river boundary fluxes
Kx = horizontal hydraulic conductivity; Kv = vertical hydraulic conductivity

For the transient model, all metrics are sensitive to pumping and the horizontal hydraulic conductivity of the Queen City and Carrizo aquifers. The top five parameters to which the transient model is most sensitive for the three metrics are summarized in Table 8.4b. Based on all three metrics, the transient model is insensitive to changes in the specific storage and specific yield of the Sparta, Queen City, and Carrizo aquifers and the Simsboro Formation.

Table 8.4b   **Top five parameters to which the transient model is most sensitive.**

2010 Drawdown in Sparta, Queen City, and Carrizo Aquifers and Simsboro Formation	Hydraulic Boundary Fluxes[a]	Model Calibration Statistics
pumping	recharge	Kx Carrizo
Kx Carrizo	Kx Queen City	pumping
Kx Queen City	Kx Sparta	Kx Simsboro
Kx Sparta	Kx Carrizo	recharge
Kx Simsboro	pumping	Kx Queen City

[a] drain and river boundary fluxes
Kx = horizontal hydraulic conductivity

9 Future Model Implementation Improvements

Considering future model recalibration as new data are collected and/or new understanding of the central portion of the Carrizo-Wilcox, Queen City, and Sparta aquifers is achieved is recommended. To use models to predict future conditions requires a commitment to improve the models as new data become available or when modeling assumptions or implementation issues change. This groundwater availability model is no different. Through the modeling process, one generally learns what can be done to improve the model's performance or what data would help better constrain the model calibration. Future improvements to the model, beyond the scope of the current groundwater availability model, are discussed below.

9.1 Additional Supporting Data

Several types of data could be collected to better support future enhancement of the groundwater availability model. These include temporal hydraulic head data for wells completed in the Colorado River alluvium and a more refined vertical coverage of hydraulic head measurements, which would be helpful in improving understanding of cross-formational flow and the spatial variability of hydraulic heads where the aquifers are more than 200 feet thick. In addition, additional aquifer pumping tests and measurements of hydraulic heads in the deep portions of the aquifers where data are absent are needed to guide how these confined regions are represented in the models.

Performing aquifer pumping tests in areas where property estimates are lacking would be beneficial for validating the aquifer properties in the current model and for supporting future model recalibration. Aquifer pumping tests should be conducted for at least 8 hours and, if possible, nearby wells should be monitored for water-level changes during the test. Properly designed and implemented multi-well aquifer pumping tests would provide information from which vertical hydraulic conductivity and storage properties could be calculated at a scale useful for validating the aquifer parameters used in the model.

Among the studies that could prove to be very cost effective is assembling existing geophysical logs and identifying sand and clay sequences so that sand and clay percentage and thickness maps could be made using the existing stratigraphy. These maps would be useful in estimating spatial patterns for both horizontal and vertical hydraulic conductivity, as well as specific storage values. In addition, there is a need to modify the stratigraphic framework used to define the Carrizo Aquifer and the formations in the Wilcox Aquifer so that formations that comprise the Wilcox Aquifer are aligned across the different groundwater availability models used by Groundwater Management Areas 11, 12, and 13 to model the Wilcox Aquifer.

Additional studies of base flow in the Colorado and Brazos rivers are needed. These studies need to be more comprehensive in scope than previous studies and are needed to help quantify the impact of bank flow on total base flow and determine what climatic and hydrogeologic factors control groundwater-surface water interaction. A field study in the lower Colorado River Basin was recommended by Young and others (2017) to improve quantification of surface water-groundwater interactions between the Colorado River and groundwater in the alluvium. They developed a work plan for such a study designed to obtain data for understanding (1) the

direction and magnitude of water exchange between the alluvium and stream under stable low-flow conditions, (2) the origin of water gained by the stream during low-flow conditions (the alluvium or from bank storage), and (3) how pumping might affect stream gains and losses over time. The result from the analysis of river gages in Section 3 shows that there needs to be a standardized approach for performing base flow separation for the purpose of estimating average recharge rates for a watershed.

9.2 Additional Model Improvements

Because of the flexibility that MODFLOW-USG provides with respect to both horizontal and vertical grid refinement, there is opportunity to selectively improve model refinement where it may improve the models' ability to represent the real physical world. In areas near large well fields, whose pumping affects drawdown for tens of miles, more accurate placement of the vertical interval being pumped in the aquifer may help assess the impact of that pumping on groundwater resources.

Despite the robust refinement capability with MODFLOW-USG, that capability is not easily implemented or visualized with either Groundwater Vistas or Groundwater Modeling System by Aquaveo. And, even if such refinement can be made easily, the use of groundwater availability models by groundwater conservation districts to address local-scale problems would benefit by coupling MODFLOW-USG with an analytical solution to better incorporate pumping into the model. Current investigations are underway to couple the new Analytical Element Model code called TTim (Bakker, 2013) with numerical codes such as MODFLOW-USG. The Analytical Element Model code provides an exact solution to the groundwater flow equation enabling simulation of drawdown in the near vicinity (1 foot) of a pumping well. Such a coupling would greatly improve the ability of the groundwater availability model to simulate pumping impacts from a single pumping well at distances less than a mile away. This type of enhancement could make the state groundwater availability models a viable tool for assessing individual well permits and spacing rules commonly considered by groundwater conservation districts.

10   Acknowledgements

This page is intentionally blank.

11 References

Anaya, R., 2001, Using GIS Projection Parameters for GAM: TWDB groundwater availability model technical memo 01-01.

Anderson, M.P., and Woessner, W.W., 1992, *Applied Groundwater Modeling*: Academic Press, San Diego, CA, 381 p.

Ayers, W.B., Jr., and Lewis, A.H., 1985, The Wilcox Group and Carrizo Sand (Paleogene) in East-Central Texas: depositional systems and deep-basin lignite: The University of Texas at Austin, Bureau of Economic Geology, Geologic Folio No. 1, 19 p., 30 plates.

Arnold, J.G., and Allen., P.M., 1999, Automated methods for estimating baseflow and ground water recharge from streamflow records: Journal of the American Water Resources Association, v. 35, no. 2, p. 411–424.

Arnold, J.G., Allen, P.M., Muttiah, R., and Bernhardt, G., 1995, Automated base flow separation and recession analysis techniques: Groundwater, v.35, no. 2, p. 1010-1018.

Arnold, J.G., Kiniry, J.R., Srinivasan, R., Williams, J.R., Haney, E.B., and Neitsch, S.L., 2012, Soil & water assessment tool, Input/output documentation, Version 2012: Texas Water Resources Institute, TR-439.

Baker, E.T., Jr., Follett, C.R., McAdoo, G.D., and Bonnet, C.W., 1974, Ground-water resources of Grimes County, Texas: TWDB Report 186.

Bakker, M., 2013, Semi-analytic modeling of transient multi-layer flow with TTim: Hydrogeology Journal 21: 935-943

Bakker, M., and Strack, O.D.L., 2003, Analytic elements for multiaquifer flow: Journal of Hydrology, v. 271, n. 1, p. 119-129.

Barnes, V.E., 1970, Waco sheet: Bureau of Economic Geology, Geologic Atlas of Texas, scale 1:250,000.

Barnes, V.E., 1979, Seguin sheet: Bureau of Economic Geology, Geologic Atlas of Texas, scale 1:250,000.

Barnes, V.E., 1981, Austin sheet: Bureau of Economic Geology, Geologic Atlas of Texas, scale 1:250,000.

Bristone Municipal WSD, 2016, Total annual production 2005 – 2013: personal communication via email from Brent Locke with the Bristone Municipal WSD to Shannon George with INTERA, dated May 2, 2016.

Broadhurst, W.L., Sundstrom, R.W., and Rowley, J.H., 1950, Public water supplies in southern Texas: United States Geological Survey, Water-Supply Paper 1070.

Budge, T., Young, S.C., Kelley, V., Deeds, N., and Ewing, J., 2007, Importance of a properly conceptualized shallow flow system on ground water availability estimates for regional flow systems near coastlines with dipping stratigraphy: Program and Abstract Book, 2007 Ground Water Summit, National Ground Water Association, Albuquerque, New Mexico, April 29–May 3, 2007, p. 2.

Butler, J.J., 1990, The role of pumping tests in site characterization: some theoretical considerations: Ground Water, v. 28, n. 3, p 394-402.

Certes, C., and de Marsily, G., 1991, Application of the pilot-points method to the identification of aquifer transmissivities: Advances in Water Resources, v. 14, no. 5, p. 284-300.

Chow, V.T., Maidment, D.R., and Mays, L.W., 1988, Applied hydrology: McGraw-Hill, Inc.

Chowdhury, A. Wade, S., Mace, R.E., and Ridgeway, C., 2004, Groundwater availability of the central Gulf Coast Aquifer System: Numerical simulations through 1999: TWDB.

City of Giddings, 2016, Production pumpage in gallons 1993-2015: personal communication via email from Angie Stanfield with the City of Giddings to Shannon George with INTERA, dated May 10, 2016.

Cooper, H.H., and Jacob, C.E., 1946, A generalized graphical method for evaluating formation constants and summarizing well-field history: Transactions of the American Geophysical Union, v. 217, p. 626-634.

Day, A., 2016, BVGCD permitted production 2008-2015, file Intera PIA Request.xlsx: Personal communication from Alan Day with the Brazos Valley Groundwater Conservation District to Toya Jones with INTERA, dated May 9, 2016.

de Marsily, G., Lavedan, C., Boucher, M., and Fasanino, G., 1984, Interpretation of interference tests in a well field using geostatistical techniques to fit the permeability distribution in a reservoir model: in Geostatistics for Natural Resources Characterization, edited by G. Verly, M. David, A.G. Journal and A. Marechal. NATO ASI, Ser. C. 182. 831-849

Deeds, N., Kelley, V., Fryar, D., Jones, T., Whellan, A. J., and Dean, K. E., 2003, Groundwater availability model for the Southern Carrizo-Wilcox Aquifer: prepared for the TWDB.

Deeds, N.E., Yam. T., Singh, A., Jones, T., Kelley, V., Knox, P., and Young, S., 2010, Groundwater availability model for the Yegua-Jackson Aquifer: prepared for the TWDB.

Doherty, J., 2003. Ground-water model calibration using Pilot-points and Regularization. Ground Water. Vol 41 (2): 170-177

Doherty, J., 2018, Model-Independent parameter estimation user manual Part I: PEST, SENSAN, and global optimisers: 7th Edition: Brisbane, Australia, Watermark Numerical Computing.

Domenico, P.A., 1972, Concepts and Models in Groundwater Hydrology: McGraw-Hill, New York.

Dutton, A.R., Harden, R.W., Nicot, J.P., and O'Rourke, D., 2003, Groundwater availability model for the central part of the Carrizo-Wilcox Aquifer in Texas: The University of Texas at Austin, Bureau of Economic Geology, prepared for the TWDB.

Eckhardt, K., 2005, How to construct recursive digital filters for baseflow separation: Hydrological Processes, v. 19, p. 507–515.

Ewing, J.E, and Jigmond, M., 2016, Final numerical model report for the Brazos River Alluvium Aquifer groundwater availability model: prepared for the TWDB.

Ewing, J.E., Harding, J.J., and Jones, T.L., 2016, Final conceptual model report for the Brazos River Alluvium Aquifer groundwater availability model: prepared for the TWDB.

Ewing, T.E., Budnik, R.T., Ames, J.T., Ridner, D.M, and Dillon, R.L., 1990, Tectonic map of Texas: The University of Texas at Austin, Bureau of Economic Geology.

Fogg, G.E., Seni, S.J., and Kreitler, C.W., 1983, Three-dimensional ground-water modeling in depositional systems, Wilcox, Group, Oakwood Salt Dome area, east Texas: The University of Texas at Austin, Bureau of Economic Geology, Report of Investigations No. 133. and others, 1983

Follett, C.R., 1966, Ground-water resources of Caldwell County, Texas: TWDB Report 12.

Follett, C.R., 1970, Ground-water resources of Bastrop County, Texas: TWDB Report 109.

Follett, C.R., 1974, Ground-water resources of Brazos and Burleson Counties, Texas: TWDB Report 185.

Freeze, R.A., and Cherry, J.A., 1979, Groundwater: Englewood Cliffs, N.J. Prentice Hall, 604 pp.

Fryar, D., Senger, R., Deeds, N., Pickens, J., Whallon, A., and Dean, K., 2003, Groundwater availability model for the northern Carrizo-Wilcox Aquifer: prepared for the TWDB.

Galloway, W.E., 1982, Depositional architecture of Cenozoic Gulf Coastal Plain fluvial systems: The University of Texas at Austin, Bureau of Economic Geology Geological Circular 82-5, 29 p.

Galloway, W.E., Ganey-Curry, P.E., Li, X., and Buffler, R.T., 2000, Cenozoic depositional history of the Gulf of Mexico basin: American Association of Petroleum Geologists Bulletin, vol. 84, p. 1743–1774.

Grubb, H.F., 1997, Summary of hydrology of the regional aquifer systems, Gulf Coastal Plain, south-central United States; United States Geological Survey, Professional Paper 1416-A.

Guevara, E.H., and Garcia, R., 1972, Depositional systems and oil-gas reservoirs in the Queen City Formation (Eocene): Texas: Gulf Coast Association of Geological Societies Transactions, v. 22.

Gustard, A., Bullock, A., and Dixon, J.M., 1992, Low flow estimation in the United Kingdom: Institute of Hydrology.

Guyton & Associates, 1970, Ground-water conditions in Angelina and Nacogdoches counties, Texas: TWDB Report 110.

Guyton & Associates, 1972, Ground-water conditions in Anderson, Cherokee, Freestone, and Henderson counties, Texas: TWDB Report 150.

Harbaugh, A.W., 2005, MODFLOW-2005. The U.S. geological survey modular ground-water model – the ground-water flow process, Techniques and methods 6-A16: United States Geological Survey.

Harbaugh, A.W., and M.G. McDonald, 1996. User's Documentation for MODFLOW-96, an update to the U.S. Geological Survey modular finite-difference ground-water flow model: United States Geological Survey, Open-File Report 96-485, 56 p.

Harbaugh, A.W., Banta, E.R., Hill, M.C., and McDonald, M.G., 2000, MODFLOW-2000, the
U.S. Geological Survey modular groundwater model—User guide to modularization
concepts and the groundwater flow process: United States Geological Survey, Open-File
Report 00–92, 121 p.

Harden & Associates, Inc., 1976, Records for Texas A&M University Well A-7: prepared for
Riewe & Wischmeyer, Inc.

Harden & Associates, Inc., 1979a, Results of testing Texas A&M University Well 7: prepared
for Riewe & Wischmeyer, Inc., the City of College Station, Texas.

Harden & Associates, Inc., 1979b, Results of testing – City of College Station Simsboro Well 1:
prepared for Riewe & Wischmeyer, Inc., The City of College Station, Texas.

Harden & Associates, Inc., 1979c, Results of testing – City of College Station Simsboro Well 2:
prepared for Riewe & Wischmeyer, Inc., The City of College Station, Texas.

Harden & Associates, Inc., 1980, North Rockdale production well test results: prepared for Shell
Oil Company Houston, Texas.

Harden & Associates, Inc., 1982, South Milam Production Well B-35 test results appendices:
prepared for Shell Oil Company Houston, Texas.

Harden & Associates, Inc., 1984, North Camp Swift Project – Preliminary Ground-Water
Testing, prepared for Shell Mining Company Houston, Texas.

Harden & Associates, Inc., 1987, Groundwater Investigation for Calvert Lignite Mine, Robertson
County, Texas Volume 2, prepared for Phillips Coal Company, Richardson, Texas.

Harden & Associates, Inc., 1991, Groundwater information section 779.128 Permit No. 27B
permit renewal/revision application Calvert Mine Robertson County: Texas prepared for
Walnut Creek Mining Company.

Harden & Associates, Inc., 2001, Response to Section 12.139A Groundwater Control Plan,
Alcoa Sandow Mine Permit 1E Mine Permit Revision No. 1: prepared for Alcoa Inc.,
Rockdale, Texas.

Harden & Associates, Inc., 2007, Availability of groundwater Carrizo-Wilcox Aquifer - 130
Project: prepared for Blue Water Systems L.P.

Harden and Associates, Inc., 2016a, Depressurization Pumping for Walnut Creek Mine: personal
communication via email from Bob Harden to Toya Jones (INTERA) on June 7, 2016.

Harden & Associates, Inc., 2016b, TCEQ PW-2 Interim Approval Submittal: submitted on
behalf of 130 Regional Water Supply Corporation.

Harden & Associates, Inc., 2016c, Vista Ridge Regional Supply Project hydrogeologic report:
prepared for Central Texas Regional Water Supply Corporation

Hunter, J. D., 2007. Matplotlib: A 2D Graphics Environment: Computing in Science &
Engineering, v. 9, no. 3, p. 90-95, DOI:10.1109/MCSE.2007.55

Hsieh, P.A., and Freckleton, J.R., 1993, Documentation of a computer program to simulate
horizontal-flow barriers using the U.S. Geological Survey modular three-dimensional finite-
difference ground-water flow model: United States Geological Survey, Open-File Report 92-
477, 32 p.

Institute of Hydrology, 1980a, Research report, v. 1 of Low flow studies: Wallingford, United Kingdom, Institute of Hydrology, 42 p.

Institute of Hydrology, 1980b, Catchment characteristic estimation manual, v. 3 of Low flow studies: Wallingford, United Kingdom, Institute of Hydrology, 27 p.

Jacob, C.E., 1940, On the flow of water in an elastic artesian aquifer: Trans-American Geophysical Union 21: 574-586.

Jackson, M.P.A., 1982, Fault tectonics of the East Texas Basin: The University of Texas at Austin, Bureau of Economic Geology Geological Circular 84-2, 31 p.

Jackson, M.P.A., Rowan, M.G., and Trudgill, B.D., 2003, Salt-related fault families and fault welds in the northern Gulf of Mexico: The University of Texas at Austin, Bureau of Economic Geology, Report of Investigations No. 268.

Jones, N., 2014, 1998-1992 and 2005-2016 historical production for Texas A & M University, files TAMU_HistoricProductionbyWell-INTERA-May 2016.xls and TAMU_HistoricProductionbyWell-INTERA (2)-May 2016.xls: Personal communication from Nathan Jones with Texas A & M University to Toya Jones with INTERA, dated May 9, 2016.

Jones E., Oliphant T.E., and Peterson P.,2001. SciPy: Open Source Scientific Tools for Python, http://www.scipy.org/

Kelley, V.A., Deeds, N.E., Fryar, D.G., and Nicot, J-P, 2004, Groundwater availability models for the Queen City and Sparta aquifers: prepared for the TWDB.

Kelley, V.A., Ewing, J., Jones, T.A., Young, S.C., Deeds, N., and Hamlin, eds, S., 2014, FINAL REPORT Updated groundwater availability model of the Northern Trinity and Woodbine aquifers: prepared by INTERA for North Texas GCD, Northern Trinity GCD, Prairielands GCD, and Upper Trinity GCD, August 2014. http://www.twdb.texas.gov/groundwater/models/gam/trnt_n/Final_NTGAM_Vol%20I%20Aug%202014_Report.pdf

Kuiper, L. K., 1994, Nonlinear-Regression Flow Model of the Gulf Coast Aquifer Systems in the South-Central United States: United States Geological Survey, Water-Resources Investigations Report 93-4020.

Kunkle, G.R., 1962, The base flow duration curve: A technique for study of groundwater discharge from a drainage basin: Journal of Geophysical Research, v. 67, no. 4, p. 1543-1554.

Lavenue, A.M., and Pickens, J.F., 1992, Application of a coupled adjoint sensitivity and kriging approach to calibrate a ground-water flow model: Water Resources Research, v. 28, no. 6, p. 1543-1569.

Lim, K.J., Engel, B.A., Zhenxu, T., Choi, J.C., Kim, K.S., Muthukrishnan, S., and Tripathy, D., 2005, Automated WEB GIS based hydrograph analysis tool, WHAT: Journal of the American Water Resources Association, v. 41, no. 6, p. 1407–1416.

Lost Pines Groundwater Conservation District, 2017, Historical pumpage for the southern overlap counties: personal communication from Andy Donnelly with Danial B. Stephens & Associates to Toya Jones with INTERA, dated April 6, 2017.

Loucks, R.G., Dodge, M. M., and Galloway, W.E., 1986, Controls on porosity and permeability of hydrocarbon reservoirs in Lower Tertiary sandstones along the Texas Gulf Coast: The University of Texas at Austin, Bureau of Economic Geology Report of Investigations No. 149, 78 p.

Mace, R.E. and A.R. Dutton. 1994, Hydrogeologic controls on contaminant transport in weathered and fractured chalk: Toxic Substances and the Hydrologic Sciences, American Institute of Hydrology, p. 535-546.

Mace, R.E., Chowdhury, A.H., Anaya, R., and Way, S.C., 2000, Groundwater availability of the Trinity Aquifer, Hill Country Area, Texas: numerical simulations through 2050: TWDB Report 353, 117 p.

Mace, R.E., Austin, B.E., Angle, E.S., and Batchelder, R., 2007, Surface water and groundwater – Together again?: Proceedings for 8th Annual Changing Face of Water Rights in Texas, State Bar of Texas, San Antonio, TX. June 28-29.

Magara, K., 1978, Compaction and fluid migration – Practical petroleum geology: Elsevier Scientific Publishing Company, New York. 350 pages.

McDonald, M.G., and Harbaugh, A.W., 1988, A modular three-dimensional finite-difference ground-water flow model: United States Geological Survey: Techniques of Water-Resources Investigations, Book 6, chapter A1.

McKinney, W., 2010. Pandas: Data Structures for Statistical Computing in Python: Proceedings of the 9th Python in Science Conference, p. 51-56

Nathan, R.J., and McMahon., T.A., 1990, Evaluation of automated techniques for baseflow and recession analysis: Water Resources Research, v. 26, no. 7, p. 1465-1473.

National Weather Service, 1999, Major roads in the United States.

Neglia, S. 1979, Migration of fluids in sedimentary basins: in AAPG Bulletin, v. 63, p. 573-597, The American Association of Petroleum Geologists.

Neitsch, S., Arnold, J., Kiniry, R. Srinivasan, and J. R. Williams, 2002. Soil and Water Assessment Tool. User Manual Version 2000. Blackland Research Center Texas Agricultural Experiment Station 720 East Blackland Road ○ Temple, Texas 76502

Nicot, J-P, Hebel, A.K., Ritter, S.M., Walden, S., Baier, R., Galusky, P., Beach, J., Kyle, R., Symank, L., and Breton, C., 2011, Current and projected water use in the Texas mining and oil and gas industry: Bureau of Economic Geology, The University of Texas at Austin.

Niswonger, R.G., Panday, S., and Ibaraki, M., 2011, MODFLOW-NWT, A Newton formulation for MODFLOW-2005: U.S. Geological Survey Techniques and Methods 6-A37, 44 p.

Oliphant. T., 2006. A guide to NumPy, USA: Trelgol Publishing.
http://web.mit.edu/dvp/Public/numpybook.pdf

Panday, S., Langevin, C.D., Niswonger, R.G., Ibaraki, M., and Hughes, J.D., 2013, MODFLOW-USG version 1: An unstructured grid version of MODFLOW for simulating groundwater flow and tightly coupled processes using a control volume finite-difference formulation: U.S. Geological Survey Techniques and Methods, book 6, chap. A45, 66 p.

Panday, Sorab, Langevin, C.D., Niswonger, R.G., Ibaraki, Motomu, and Hughes, J.D., 2015, MODFLOW-USG version 1.3.00: An unstructured grid version of MODFLOW for simulating groundwater flow and tightly coupled processes using a control volume finite-difference formulation: U.S. Geological Survey Software Release, 01 December 2015, http://dx.doi.org/10.5066/F7R20ZFJ

Peckham, R.C., 1965, Availability and quality of ground water in Leon County, Texas: Texas Water Commission Bulletin 6513

Pettyjohn, W.A., and Henning., R., 1979, Preliminary esti-mate of ground-water recharge rates, related streamflow and water quality in Ohio: Columbus, Ohio State University, Water Resources

Piggott, A.R., Moin, S., and Southam, C., 2005, A revised approach to the UKIH method for the calculation of baseflow: Hydrological Sciences, v. 50, no. 5, p. 911–920.

PRISM Climate Group, 2012, Monthly precipitation raster data, Oregon State University website: http://prism.oregonstate.edu/, access January 2015.

PRISM Climate Group, 2015, 30-Year Normals: Oregon State University website: http://prism.oregonstate.edu/, access July 2015.

Proske, M., 2016, Production pumping for the city of Giddings in gallons 1993-2015, file Giddings_1993-2015_DOC030.PDF: Personal communication from Michael Proske with the city of Giddings to Shannon George with INTERA, dated May 10, 2016.

Prudic, D.E., 1991. Estimates of Hydraulic Conductivity from Aquifer-Test Analyses and Specific Capacity Data, Gulf Coast Regional Aquifer Systems, South-Central United States. U.S. Geological Survey, Water- Resources Investigation Report 90-4121.

Rettman, P.L., 1987, Ground-water resources of Limestone County, Texas: TWDB Report 299.

Rhodes, K.A., Proffitt, T., Rowley, T., Knappett, P.S.K., Montiel, D., Dimova, N., and Miller, G. R., 2017, Theimportance of bank storage in supplying baseflow to rivers flowing through compartmentalized, alluvial aquifers. Water Resources Research, 53. https://doi.org/10.1002/2017WR021619

Rogers, L.T., 1967, Availability and quality of ground water in Fayette County, Texas: TWDB Report 56.

Rutledge, A.T., 1998, Computer programs for describing the recession of ground-water discharge and for estimating mean ground-water recharge and discharge from streamflow records--update: USGS, Water- Resources Investigations Report 98-4148.

Ryder, P.D., and A.F. Ardis, 1991. Hydrology of the Texas Gulf Coast Aquifer Systems. U.S. Geological Survey, Open-File Report 91-64.

Saunders, G.P., 2005, Low flow gain-loss study, Task 1 – Water year 2000 historical data analysis: Lower Colorado River Authority, interim report, 10 pp.

Saunders, G.P., 2006, Low flow gain-loss study of the Colorado River in Texas: in Mace, R.E., Davidson, S.C., Angle, E.S., and Mullican, W.F., III, eds., Aquifers of the Gulf Coast of Texas, TWDB Report 365, p. 293-297.

Saunders, G.P., 2009, Low flow gain-loss study of the Colorado River in Bastrop County, Texas: in Hutchison, W.R., Davidson, S.C., Brown, B.J., and Mace, R.E., eds., Aquifers of the Upper Coastal Plains of Texas, TWDB Report 374, p. 161-165.

Scanlon, B.R., Reedy, R., Strassberg, G., Huang, Y., and Senay, Y.G., 2012, Estimation of Groundwater Recharge to the Gulf Coast Aquifer System in Texas, USA: TWDB Unnumbered Report.

Scanlon, B.F., Reedy, R.C., Stonestrom, D.A., Prudic, D.W., and Dennehy, K.F., 2005. Impact of land use and land cover change on groundwater recharge and quality in the southwestern USA: Global Change Biology, v.11, p. 1577-1593.

Schreüder, W. A., 2009. BeoPest Programmer's Documentation: http://www.prinmath. com/pest/RunBeoPEST.pdf Potomac, Maryland

Shafer, GH., 1965, Ground-water resources of Gonzales County, Texas: TWDB Report 4.

Shestakov, V. 2002. "Development of relationship between specific storage and depth of sandy and clay formations", Environmental Geology, v. 42, n. 2-3, pp. 127-130.

Slade, R.M., Jr., J.T. Bentley, and D. Michaud, 2002. Results of streamflow gain-loss studies in Texas, with emphasis on gains from and losses to major and minor aquifers, Texas, 2000. U.S. Geological Survey, Open-File Report 02-068.

Sloto, R.A., and Crouse., M.Y., 1996, HYSEP—A computer program for streamflow hydrograph separation and analysis: U.S. Geological Survey Water-Resources Investigations Report 96–4040, 46 p., http://pubs.er.usgs.gov/publication/wri964040.

Stoeser, D.B., Green, G.N., Morath, L.C., Heran, W.D., Wilson, A.B., Moore, D.W., and Van Gosen, B.S., 2007, Preliminary integrated geologic map databases for the United States: Central States: Montana, Wyoming, Colorado, New Mexico, North Dakota, South Dakota, Nebraska, Kansas, Oklahoma, Texas, Iowa, Missouri, Arkansas, and Louisiana, Version 1.2: United States Geological Society, Open-File Report 2005-1351, websites https://pubs.usgs.gov/of/2005/1351/ (report) and https://mrdata.usgs.gov/geology/state/state.php?state=TX (digital data).

Streltsova, T., D., 1988, Well Testing in Heterogeneous Formations, An Exxon Monograph, John Wiley and Sons, New York, New York, pg. 411

Sundstrom, R.W., Hastings, W.W., and Broadhurst, W.L., 1948, Public water supplies in eastern Texas: United States Geological Survey, Water-Supply Paper 1047.

Texas A&M University, 2016, Historical productivity Texas A&M University: personal communication via email from Nathan Jones with Texas A&M University to Toya Jones with INTERA.

Texas Natural Resources Information System, 2016, Political boundaries: Website: https://tnris.org/data-download/#!/statewide, accessed March 2016.

Texas Natural Resources Information System, 2017, Texas roads: Website: https://tnris.org/data-download/#!/statewide, accessed February 2017.

Tarver, G.E., 1966, Ground-water resources of Houston County, Texas: TWDB Report 18.

Toth, J. 1962, A theory of groundwater motion in small drainage basins in Central Alberta: Journal of Geophysical Research, v. 67, no. 11, p. 4375-4387.

Toth, J., 1963, A theoretical analysis of groundwater flow in small drainage basins: Journal of Geophysical Research, v. 68, no. 16, p. 475-4812.

Thompson, G.L., 1966, Ground-water resources of Lee County, Texas: TWDB Report 20.

Thornhill Group, Inc., 2009, Data and Analyses Derived from Drilling and Testing Programs to Verify Production and Water Quality in the Simsboro Aquifer, Prepared for EndOp, LP, Elgin, Texas.

Thornhill Group, Inc., 2014a, Letter Report, prepared for Lower Colorado River Authority

Thornhill Group, Inc., 2014b, Simsboro Production Well No. 5 – LPGCD Well No: 5933412 – Draft Well Completion Report, Prepared for Forestar USA, Austin, Texas.

Thornhill Group, Inc., 2014c, Simsboro Production Well No. 7 – LPGCD Well No: 5933123 – Draft Well Completion Report, Prepared for Forestar USA, Austin, Texas.

Thornhill Group, Inc., 2014d, Simsboro Production Well No. 8 – LPGCD Well No: 5933413 – Draft Well Completion Report, Prepared for Forestar USA, Austin, Texas.

Thornhill Group, Inc., 2014e, Hydrogeologic Evaluation of Well Completion and Testing Results Simsboro Production Well No. 1 and Well No. 2 — Lee County, Texas, Prepared for Heart of Texas Suppliers, LP, Houston, Texas.

Turner, S.F., Ground water in the vicinity of Bryan and College Station, Texas: Texas State Board of Water Engineers, Miscellaneous Report 024.

TWDB, 2001, Surveys of irrigation in Texas 1958, 1964, 1969, 1974, 1979, 1984, 1989, 1944 and 2000: TWDB Report 347.

TWDB, 2006, GIS data, Major aquifers shapefile, updated December 2006: TWDB website: http://www.twdb.texas.gov/mapping/gisdata.asp.

TWDB, 2009, GIS data, Major rivers shapefile, October 2009: TWDB website: http://www.twdb.texas.gov/mapping/gisdata.asp.

TWDB, 2014a, GIS data, Groundwater management areas, approved January 2014: TWDB website: http://www.twdb.texas.gov/mapping/gisdata.asp.

TWDB, 2014b, GIS data, Existing rivers shapefile, updated November 2014: TWDB website: http://www.twdb.texas.gov/mapping/gisdata.asp.

TWDB, 2014c, GIS data, Major river basins: TWDB website: http://www.twdb.texas.gov/mapping/gisdata.asp, accessed 2014.

TWDB, 2016a, Historical water use estimates, Other water use related reports, Historical surveyed municipal water intake, by water planning region and Historical surveyed industrial water intake, by water planning region: TWDB website http://www.twdb.texas.gov/waterplanning/waterusesurvey/estimates/index.asp, accessed April 2016

TWDB, 2016b, Historical groundwater pumpage, Groundwater pumpage estimates, Historical groundwater pumpage estimates and Pumpage detail, 2000 and later: TWDB website

http://www.twdb.texas.gov/waterplanning/waterusesurvey/historical-pumpage.asp, accessed April 2016.

TWDB, 2017a, GIS data, Minor aquifers shapefile, updated December 2017: TWDB website: http://www.twdb.texas.gov/mapping/gisdata.asp.

TWDB, 2017b, GIS Data, Groundwater conservation districts, updated December 2017: TWDB website: http://www.twdb.texas.gov/mapping/gisdata.asp.

TWDB, 2018, Precipitation & Lake Evaporation Data: website http://www.twdb.texas.gov/surfacewater/conditions/evaporation/index.asp, accessed February 2018.

United States Environmental Protection Agency (EPA), 2016, https://www.law.cornell.edu/cfr/text/40/part-136 .

United States Geological Survey, 2014, Map, National elevation dataset, 10-m digital elevation model: website http://datagateway.nrcs.usda.gov, accessed September 2014.

Wahl, K.L., and Wahl., T.L., 1995, Determining the Flow of Comal Springs at New Braunfels, Texas, Texas Water '95, American Society of Civil Engineers, August 16-17, 1995, San Antonio, Texas, pp. 77-86.

Williamson, A.K., H.F. Grubb, and J.S. Weiss, 1990. Ground-Water Flow in the Gulf Coast Aquifer Systems, South Central United States – A Preliminary Analysis. U.S. Geological Survey, Water-Resources Investigations Report 89-4071.

Williamson, A.K., and H.F. Grubb. 2001 *Ground-Water Flow in the Gulf Coast Aquifer Systems, South-Central United States,* USGS Professional Paper 1416-F. Denver, CO: U.S. Geological Survey.

Winter, T. C., Harvey, J. W., Franke, O.L., and Alley, W. M., 1999, Ground water and surface water – A single resource: U.S. Geological Survey Circular 1139,

Young, S. C., 1998, Impacts of positive skin effects in borehole flowmeter tests in a granular aquifer: Ground Water, v.36 no.1, p. 67-75.

Young, S.C., Kelley, V., Budge, T., Deeds, N., and Knox, P., 2009, Development of the LCRB Groundwater Flow Model for the Chicot and Evangeline aquifers in Colorado, Wharton, and Matagorda counties: LSWP Report Prepared by the URS Corporation, prepared for the Lower Colorado River Authority, Austin, TX.

Young, S. C., Doherty, J., Budge, T., Deeds, N., 2010. Application of PEST to Recalibrate the Groundwater Availability Model for the Edwards-Trinity (Plateau) and Pecos Valley Aquifers, prepared for the TWDB, Austin, TX.

Young, S., Jigmond, M., De, eds., N., Blainey, J., Ewing, T., and Banjeri, 2016. Identification of Potential Brackish Groundwater Production Area – Gulf Coast Aquifer System, prepared for the TWDB, unpublished report, September 2016.

Young, S. C., Jones, T., and M. Jigmond. 2017. Final Report: Field Studies and Updates to the Central Carrizo-Wilcox City, and Sparta GAM to Improve the Quantification of Surface Water-Groundwater Interaction in the Colorado Basin. Prepared for the TWDB, Austin, Texas.